WORKING PAPER

COPIES OF PAPERS PRESENTED AT WOOD'S HOLE CONFERENCE ON SEISMIC DISCRIMINATION

VOLUME 2

SPONSORED BY ADVANCED RESEARCH PROJECTS AGENCY

20 - 23 JULY 1970

This document contains unedited copies of papers presented at the conference. Any views expressed in the papers of this conference are those of the authors and are not to be construed as reflecting the official opinions or policy of the Department of Defense or any agency of the Federal Government.

WORKING PAPER

DISCLAIMER NOTICE

THIS DOCUMENT IS THE BEST QUALITY AVAILABLE.

COPY FURNISHED CONTAINED A SIGNIFICANT NUMBER OF PAGES WHICH DO NOT REPRODUCE LEGIBLY.

TABLE OF CONTENTS

TABLE OF CONTENTS (Cont'd.)

SIMULATION OF DISCRIMINATION ANALYSIS

By

Robert Shumway
Robert Blandford

Seismic Data Laboratory

In practical applications discrimination analysis is applied by deducing a discriminant from a data sample. The error rate on the data sample is often taken as a measure of the quality of the discriminant. However, there is no guarantee that the error rate on new test data will be the same as on the sample data. There are no known results from statistical theory bearing on this question; therefore the only way to discuss the question is by simulation.

A method has been developed to generate data vectors with any desired mean and covariance structure. Thus a discriminant may be designed on a data sample, and tested on test data drawn from the same population. In this report we consider only the linear Fisher discriminant applied to populations with equal covariance matrices.

Figure 1a shows a set of actual M_s-m_b observations, consisting of 38 explosions and 46 earthquakes. Note that, surprisingly, the explosions show the greater scatter. The covariance structure of these data were calculated, and the new data with the same covariance structures were generated. Two samples are shown in Figure 1b and 1c.

Table 1 shows the results of designing M_s-m_b discriminant lines on varying numbers of earthquakes and explosions. We see that the average error rates on new test data are somewhat greater than on the sample data. We note also, however, that there is a substantial probability of two-four times the error rate on the new test data as on the sample data. We note also that the error rate is somewhat larger if fewer points are used in the sample set. These results are as would be expected from simple intuitive arguments.

Table II shows the result if normal random numbers are added as a third discrimination variable. The two-dimensional discrimination ability is apparently not at all degraded.

Table III shows the result of adding in the third dimension a normal random distribution with different means for the earthquakes and explosions. We see again that the error rate is greater if there are fewer points in the sample set, and that, for the 10 earthqukes and 10 explosions case, the error rate on the sample is much less than on the test data.

Table IV shows analogous results for the 7-dimensional data of Booker and Mitronovas. Again the error rate is greater for the new data and for the cases with fewer sample points.

Table V presents a further breakdown of some of the Booker-Mitronovas results, and we see that if we ask for the 90% confidence level for the error rate on new data, given a sample of 20 earthquakes and 20 explosions; then the answer must be 35-40%

The main object of this exercise is to illustrate a method which can be used to analyze the stability of discriminants which are proposed by future workers.

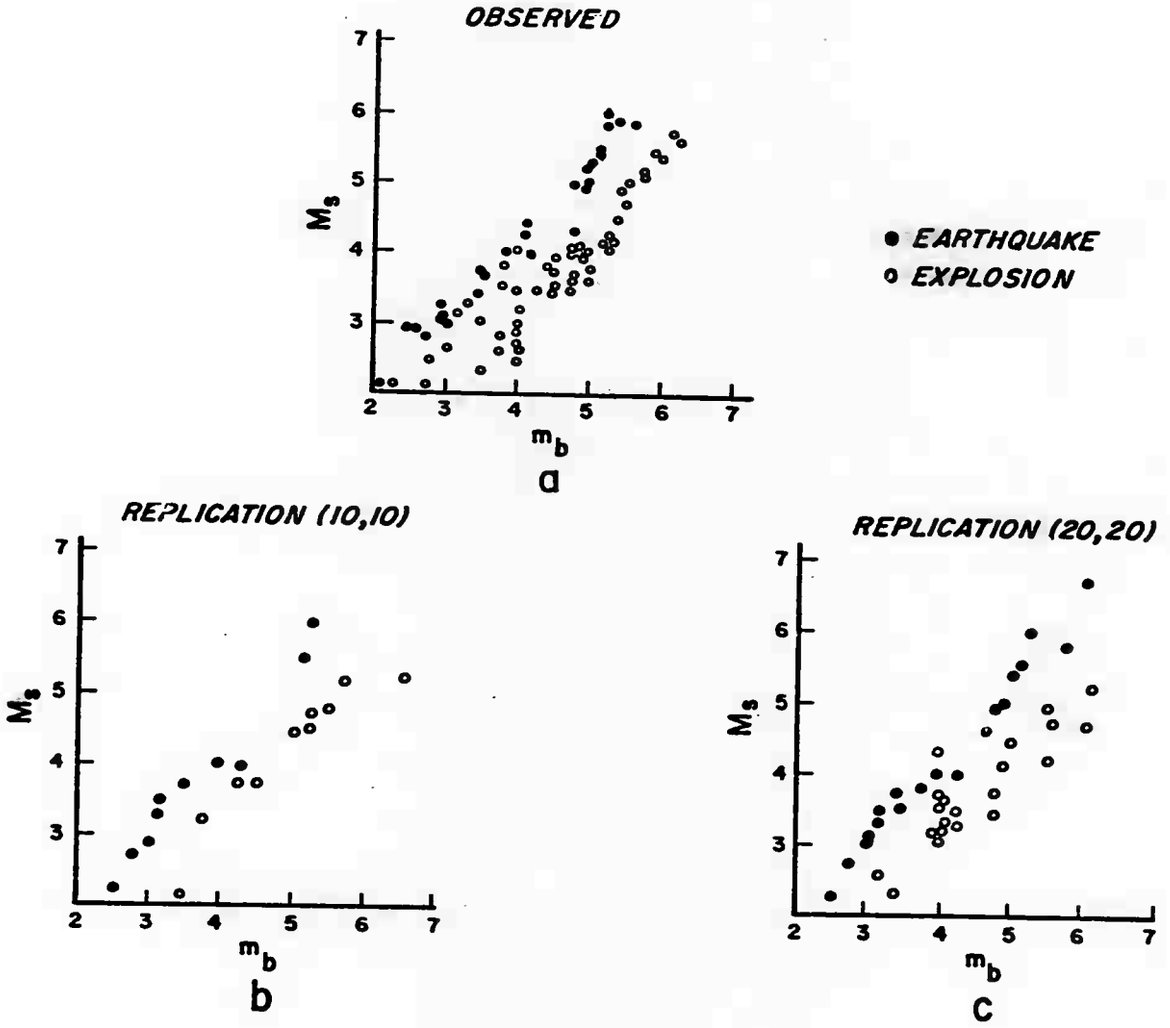
OBSERVED
EARTHQUAKE
EXPLOSION
M_s
m_b
a
REPLICATION (10,10)
b
REPLICATION (20,20)
c

Figure 1.

	Discriminant Line m_b-M_s	CT	Errors (Sample) EQ	EXP	Errors (New Data) EQ	EXP	DSQ
	-13.5,10.8	-14.7	0-10	0-10	6-100	10-100	6.5
	- 9.3, 8.3	- 5.3	0-10	1-10	12-100	5-100	3.7
	-12.6,10.6	-11.3	1-10	1-10	4-100	12-100	5.1
10 EQ	- 5.6, 4.6	- 5.6	0-10	2-10	2-100	8-100	2.3
10 EXP	-12.1,10.1	-11.3	0-10	1-10	6-100	18-100	6.4
	-7.40,6.92	- 4.8	0-10	1-10	2-100	17-100	3.2
	- 6.5, 5.8	- 4.4	0-10	3-10	2-100	12-100	3.0
	-12.3, 8.7	-19.2	0-10	0-10	4-100	26-100	5.0
	- 8.9, 8.1	- 6.1	0-10	1-10	2-100	13-100	4.0
	- 7.4, 6.6	- 5.4	0-10	1-10	4-100	18-100	3.5
			.01	.11	.04	.14	4.3
	Plus 30 more		.012	.097	.038	.134	
	- 9.3, 8.2	- 7.2	0-20	2-20	2-100	14-100	4.1
	- 7.3, 6.3	- 6.1	1-20	4-20	2-100	9-100	2.8
	-10.1, 9.0	- 7.3	1-20	3-20	3-100	10-100	4.1
20 EQ	-10.1, 9.1	- 7.1	1-20	2-20	1-100	7-100	3.9
20 EXP	- 6.9, 5.4	- 7.4	1-20	1-20	19-100	8-100	3.0
	- 9.8, 8.5	- 7.7	1-20	2-20	2-100	6-100	4.0
	- 6.3, 5.0	- 6.9	0-20	4-20	11-100	11-100	2.7
	- 8.8, 7.3	- 8.7	0-20	2-20	1-100	14-100	4.3
	-11.6, 9.4	-12.6	0-20	1-20	3-100	20-100	5.8
	- 5.9, 5.2	- 4.7	1-20	5-20	1-100	11-100	2.7
			.03	.13	.04	.11	3.8
	Plus 30 more		.022	.11	.032	.112	

TABLE 1. Simulation m_b-M_s (Parameters derived from 30 EQ, 46 EXP). Theoretical error rate 0.074.

	Discriminant Plane m_b	M_s	N(0,1)	CT	Errors (Sample) EQ	EXP	Errors (New) EQ	EXP	DSQ
	-16.6,	14.9	-1.8	-19.1	0-10	0-10	2-100	16-100	8.3
	- 7.6,	6.2	.1	- 6.9	1-10	1-10	6-100	5-100	2.7
	-20.8,	17.5	.6	-17.0	0-10	0-10	4-100	10-100	11.9
	- 9.7,	8.3	-.4	-10.6	0-10	1-10	2-100	14-100	3.4
10 EQ	-16.1,	13.3	-1.72	-23.5	0-10	0-10	2-100	19-100	9.1
10 EXP	-15.7,	12.1	- 11	-19.8	0-10	1-10	1-100	20-100	7.7
	-23.8,	20.5	- .1	-19.4	0-10	0-10	2-100	6-100	11.5
	-18.4,	17.0,	3.2	3.9	0-10	1-10	16-100	9-100	5.9
	-11.6,	9.2,	-1.8	-19.1	0-10	1-10	8-100	13-100	3.9
	- 8.4,	6.9,	.57	- 6.4	0-10	1-10	1-100	9-100	4.9
					.01	.06	.04	.12	6.9
	Plus 30 more				.012	.082	.054	.120	
					0-20	2-20	7-100	17-100	5.6
					0-20	0-20	2-100	9-100	9.3
20 EQ					1-20	2-20	5-100	15-100	5.6
20 EXP					0-20	1-20	4-100	13-100	3.9
					0-20	2-20	3-100	9-100	4.3
					0-20	3-20	3-100	12-100	3.0
					0-20	1-20	0-100	14-100	5.8
					1-20	5-20	2-100	12-100	2.6
					2-20	3-20	0-100	7-100	3.0
					0-20	1-20	1-100	13-100	5.6
					.02	.10	.03	.12	
	Plus 30 more				.017	.096	.029	.126	

TABLE 2. Simulation m_b-M_s-N(4,1) $\begin{matrix}\text{EQ}\\\text{EXP}\end{matrix}$

Theoretical error rate 0.074

	Errors (Sample)		Errors (New)		
	EQ	EXP	EQ	EXP	DSQ
	0-10	0-10	2-100	9-100	15.8
	0-10	1-10	5-100	2-100	5.7
	0-10	0-10	0-100	8-100	16.3
	0-10	0-10	1-100	11-100	6.8
10 EQ	0-10	0-10	0-100	7-100	16.5
10 EXP	0-10	0-10	2-100	11-100	11.7
	0-10	0-10	2-100	2-100	15.4
	0-10	0-10	10-100	10-100	8.6
	0-10	0-10	5-100	4-100	12.2
	1-10	0-10	0-100	6-100	5.9
Plus 30 more	.01 .018	.01 .030	.03 .024	.07 .063	
	0-20	0-20	2-100	8-100	7.62
	0-20	0-20	0-100	2-100	14.1
	1-20	1-20	0-100	4-100	7.8
20 EQ	0-20	1-20	3-100	5-100	6.0
20 EXP	0-20	1-20	3-100	2-100	6.2
	1-20	1-20	1-100	5-100	6.5
	0-20	0-20	2-100	8-100	9.5
	0-20	2-20	2-100	5-100	4.7
	1-20	0-20	2-100	2-100	7.4
	0-20	1-20	0-100	5-100	9.0
Plus 30 more	.02 .015	.035 .065	.01 .014	.05 .050	

TABLE 3. Simulation $m_b - M_s$ EQ N(4.0,1) EXP N(6.5,1)

Theoretical error rate 0.026

	Errors (Sample)		Errors (New)		
	EQ	EXP	EQ	EXP	DSQ
	0-10	1-10	19-100	23-100	2.82
	1-10	1-10	36-100	20-100	2.70
10 EQ	0-10	2-10	17-100	20-100	5.03
10 EXP	2-10	2-10	19-100	36-100	2.04
	0-10	0-10	12-100	34-100	3.87
	.06	.12	.21	.27	
Plus 35 more	.043	.092	.192	.266	
	1-20	4-20	14-100	24-100	1.63
	0-20	5-20	18-100	28-100	2.17
	3-20	1-20	40-100	16-100	3.29
20 EQ	1-20	3-20	6-100	21-100	3.35
20 EXP	2-20	2-20	9-100	22-100	3.53
	3-20	2-20	20-100	20-100	1.67
	2-20	4-20	17-100	20-100	1.76
	0-20	2-20	10-100	20-100	4.12
	0-20	2-20	12-100	14-100	3.94
	1-20	3-20	14-100	25-100	3.04
	.06	.14	.16	.21	P_{max} = .18, P_{min} = .075
Repeat	.045	.15	.14	.23	(200 instead of 100 in each test)

Table 4. Booker and Mitronovas data 20 EQ, 27 EXP, 7 dimensions, error on original sample data: EQ, .05, EXP, .037. DSQ = 2.20, Theor. error, 0.15.

EQ errors/20	EXP errors/20
3,0,0,1,1,2,0,2,1,2	11,9,8,5,6,11,9,7,7,4
2,1,1,0,0,1,0,0,0,1	7,6,4,7,3,2,5,8,4,5
5,3,2,2,4,2,6,4,2,3	2,1,9,4,5,3,5,5,5,4
1,0,1,0,1,2,1,0,0,0	7,4,4,7,4,3,4,4,4,4
5,5,3,3,2,2,5,2,3,1	6,1,4,6,7,3,4,2,5,7
3,6,5,4,6,7,0,7,4,1	4,3,5,5,4,1,5,4,1,2
7,5,4,6,8,3,4,7,7,9	4,2,2,2,2,5,2,5,1,0
2,2,4,1,0,1,2,2,2,3	6,6,5,3,5,5,3,3,5,3
5,2,2,4,5,2,1,4,3,2	5,6,6,5,3,7,4,4,5,3
5,5,4,4,9,5,3,4,4,8	10,7,5,4,6,5,8,9,3,5

Errors out of 20	6	7	8	9
Number of cases	4	5	2	1

One chance in 10 of missing 7 or more out of 20 or 0.35 error rate.

Errors out of 20	6	7	8	9	10	11
Number of cases	10	8	3	4	1	2

One chance in 10 of missing 8 or more out of 20 or 0.40 error rate.

Table 5. Booker and Mitronovas data 20 EQ, 27 EXP, 7 dimensions, error on sample data; EQ, .05; EXP, .037, DSQ = 2.20, Theoretical error rate 0.15, Average simulated error rate 0.19. Sample of 20 EQ and 20 EXP used to determine each discrimination line. A different discrimination line is used in each row of these tables.

THEORY OF THE SEISMIC SOURCE

By

C. B. Archambeau

California Institute of Technology
Division of Geological Sciences,
Seismological Laboratory
Pasadena, California 91109

Contribution No. 1902

THEORY OF THE SEISMIC SOURCE

By

C. B. Archambeau

California Institute of Technology
Division of Geological Sciences,
Seismological Laboratory
Pasadena, California 91109

Contribution No. 1902

ABSTRACT

A summary of seismic source representation theory can be most economically given in terms of the Green's function solution to the equations of motion for an elastic medium. In this paper, the equations of motion are reduced to wave equations containing source terms. Their integral solutions are seen to be composed of a sum of three integrals. In the context of seismic source theory, the first of the integrals can be used to represent applied forces or force equivalents of a tectonic source, the second for tractions applied at the boundaries of the medium and for dislocation equivalents of a seismic source, and the third for initial value or relaxation sources corresponding to the spontaneous release of stored potential energy. Either of the first two representation integrals can be used to obtain the radiated field from an explosion, while the third gives the field due to a tectonic or earthquake source. Both the body force and dislocation equivalents can be used to represent a tectonic source, but require an assumption of the source time function while the initial value solution inherently contains this information. Thus the latter solution can be used to predict the spectral and spatial properties of the field from various kinds of tectonic sources. Predictions of these properties of the field from a tectonic source are given using the initial value theory and lead, upon comparison with similar spectral and spatial properties of explosive sources, to criteria for the discrimination of earthquakes from explosions.

BLANK PAGE

INTRODUCTION

The plan of this short paper is to present in abbreviated form the theory of seismic sources as it applies to the problem of discriminating earthquakes from explosions. Very detailed discussions of source theory have been given by numerous authors, and the reader is referred to Archambeau (1968, 1970a, b) for reviews of past work and extensive references, as well as a more detailed discussion of some of the results to be presented in this discussion.

Basic theory

It is not difficult to show (e.g., Archambeau, 1970b) that the equations of motion for a homogeneous elastic medium can be represented by wave equations involving potentials χ_α, $\alpha = 1, 2, 3, 4$, such that

$$\nabla^2 \chi_\alpha - \frac{1}{v_\alpha^2} \frac{\partial^2}{\partial t^2} \chi_\alpha = -4\pi q_\alpha \ . \ . \ . \qquad (1)$$

The displacement field is connected to these potentials by the equation of motion itself, and in regions in which the source functions q_α are identically zero (a confined source), we have

$$\frac{\partial^2}{\partial t^2} u_i = v_4^2 \frac{\partial \chi 4}{\partial \chi_i} - 2v_k^2 \delta_{ijk} \frac{\partial}{\partial \chi_i} \chi_k \ . \ . \ . \qquad (2)$$

Here u_i is the displacement, χ_4 is the dilatation, and χ_k, $k = 1, 2, 3$ are the three cartesian components of rotation. Also v_4 is the compressional velocity and all the v_k are equal to the shear velocity. The summation convention applies to repeated roman indices throughout this discussion, while greek indices, when employed, are not subject to the summation convention.

We are concerned here with the representation of the radiation field from basically two kinds of seismic sources, applied forces over a finite region such as a pressure pulse over an internal boundary of the medium, and stress relaxation sources associated with the spontaneous reduction of strain energy in the region surrounding a zone of failure. In the latter case, we will assume that the nonlinear zone is bounded by a continuous surface outside of which the medium behaves elastically (at least to first order) and that the usual continuity conditions apply across this surface. We shall denote this boundary surface by Σ. Further, even while the medium is prestressed, we will neglect finite strain effects involving the prestress and radiation field stress since these effects involve products of the prestrain and the strain wave amplitudes which are both small (less than 10^{-3} certainly), so that such products are negligible. Similar statements apply to the applied force sources.

In addition to equation (1), we note that it is necessary to specify the equilibrium value of the potentials χ_α. In the case of a spontaneous rupture, in which a new boundary surface Σ is in effect introduced, the equilibrium value of the field must clearly be different before the rupture than after. In fact, if we start with the basic equations of elastic equilibrium in a prestressed medium, we find that the difference between the equilibrium potential $\chi_\alpha^{(0)}$ existent before introduction of Σ and that after introduction of Σ, call this $\chi_\alpha^{(1)}$, is given by (Archambeau, 1968)

$$\nabla^2 \chi_\alpha^* = 0 \quad . \quad . \quad . \tag{3}$$

where $\chi_\alpha^* = \chi_\alpha^{(0)} - \chi_\alpha^{(1)}$ is the difference in the potentials. Thus χ_α^* is harmonic. This potential serves as an initial value for χ_α, since initially χ_α must have the value $\chi_\alpha^{(0)}$, but finally (after a long time) it must reach the value $\chi_\alpha^{(1)}$. Thus we have what is nearly the classical initial value problem, in one dimension analogous to the mass on a spring initially displaced from equilibrium, except here the initial displacement is not arbitrary but must satisfy (3) since we are not supplying an external force to the medium. In all cases, we can solve such initial value problems by a Green's function method and simultaneously obtain the applied force solution.

In particular, the general solution to (1) is (e.g., Morse and Feshbach, 1953)

$$\chi_\alpha(\underline{r},t) = \int^{t+} dt_o \int_V G_\alpha(\underline{r},t;\, r_o,\, t_o)\, q_\alpha(\underline{r}_o,\, t_o)\, d\underline{r}_o$$

$$+ \frac{1}{4\pi} \int_o^{t+} dt_o \int_S \{G_\alpha[\nabla_o \chi_\alpha] - [\chi_\alpha]\nabla_o G_\alpha\} \cdot d\underline{S} \tag{4}$$

$$+ \frac{1}{4\pi v_\alpha^2} \int_o^{t+} dt_o \int_V \frac{\partial}{\partial t_o} \{\chi_\alpha \frac{\partial G_\alpha}{\partial t_o} - G_\alpha \frac{\partial \chi_\alpha}{\partial t_o}\}\, d\underline{r}_o \quad . \quad .$$

where $G_\alpha(\underline{r},\, t;\, \underline{r}_o,\, t_o)$ is the Green's function given by

$$\nabla_o^2 G_\alpha - \frac{1}{v_\alpha^2} \frac{\partial^2}{\partial t_o^2} G_\alpha = 4\pi\delta(\underline{r} - \underline{r}_o)\, \delta(t - t_o)$$

This solution contains the entire representation theory for seismic sources. Since we are interested in the source itself and not in the effects of any layering (internal boundaries), etc., we can take G_α to be the infinite space Green's function whose form we know immediately. Reflections and so on from internal and external boundaries may be treated separately once we have the solution of (4) with the infinite space Green's function (Archambeau, 1968). The terms in brackets, such as $[\chi_\alpha]$, appearing in the surface integrals over S denote the changes in the bracketed quantity across any boundary. Thus $[\chi_\alpha] = \chi_\alpha(\Sigma^-)$, for example, denotes the change in χ_α in going from the inside of Σ, denoted Σ^+, to the outside, denoted Σ^-. The coordinates $\underline{r}$ and t are the observer's space-time coordinates while $\underline{r}_o$ and t_o are the source space-time coordinates. The solution (4) essentially expresses the idea of superpositions.

We can interpret each of the integrals in terms of source representations. The first integral in (4) can be used to represent the effects of any force distribution imposed upon the medium by some external agent. Or it can be used to represent, by appropriate choice of q_α, a force system equivalent to an earthquake, if by some other means we determine what force system is appropriate. We have found from observations, for example, that at long periods the radiation from an earthquake is quadrapole in form so that for low-frequency radiation we can use a q_α appropriate to a double couple to obtain an equivalent spatial pattern for the field. At higher frequencies, observations suggest that a moving or propagating double couple point or line source provides a spatial pattern which is close to that observed (Ben Menahem, 1961). Furthermore, this latter equivalent reduces to a quadrapole field at low frequencies. Thus it is possible to obtain a representation which provides a field in reasonable agreement with the observations of the field's spatial characteristics. In addition, some of the high-frequency spectral properties of the radiation field associated with rupture propagation can be approximated. Nevertheless, we are required to rather arbitrarily assign a temporal behavior to the source term q_α and are consequently without a predictive capability when using this approach.

The second integral can be used in an interesting fashion to represent a tectonic source, as well as for representations of the radiation field due to a distribution of applied forces or tractions along a boundary of the medium. In the case of a tectonic source, we can use the concept of a dislocation (Love, 1944). In this case, we define a surface, which again can be Σ, across which either χ_α or $\nabla_o\chi_\alpha$ are discontinuous so that $[\chi_\alpha]$ or $[\nabla_o\chi_\alpha]$ are non-zero. We can allow this discontinuity to form along Σ in any manner we please, specifically with any time or space variation we may wish to choose. Clearly if this is the case, the integral in (4) over the surface Σ, will be non-zero, and by this means we can produce a radiation field. Then by choice of the kind of dislocation and its space and time dependence. It should be possible to obtain a fit to the observed radiation from a tectonic source. This is clearly again an equivalent type of source, although one with great intuitive appeal. In any case, we must go to the

observed radiation field from earthquakes in order to determine the proper "jump conditions" on the dislocation and the time dependence to be used. Considerable effort has gone into both the theory and its fit to observations (e.g., Haskell, 1964; Maruyama, 1963, 1964). The result is that many of the observed properties of earthquake radiation fields can be approximated using rather plausible and simple assumptions for the jump conditions. Again, however, the theory lacks a strong predictive capability since the representation requires specification of the entire functional form for $[\chi_\alpha]$, for example, and a large class of functions will fit the limited observations available. Therefore, we cannot predict well outside the range of observation.

The third integral represents contributions from "initial values" of χ_α. As we will illustrate below, this integral specifies both the spatial and temporal dependence of the radiation field in terms of a few parameters. Hence, we need only specify the geometry and dimensions of the rupture surface Σ, the prestress field, and the rupture velocity in order to obtain the complete radiation field and are not required to assume the form of an equivalent time function for the source in addition.

As was previously noted, if the medium is prestressed and failure occurs along a region enclosed by Σ, then necessarily χ_α must have an "initial value". Thus the third integral intrinsically represents a tectonic source. We will develop this concept in somewhat greater detail.

First, consider the simple case of the instantaneous fracture. This example will illustrate the idea and also give us the solution to the problem of a spherical rupture created at a rate greater than the intrinsic speed of wave propagation in the medium. Specifically, an explosive generated shock wave from a "point" source in a stressed medium would give rise to a roughly spherically symmetric fracture zone and if failure is totally controlled by the shock, created at a speed greater than the compressional velocity. Thus the rupture would, in effect, be instantaneous since no relaxation effects could occur until after its complete formation.

We have from equation (4) and our previous discussion, the following initial value problem for the instantaneous fracture

$$\chi_\alpha^{(1)}(\underline{r},t) = \frac{1}{4\pi v_\alpha^2} \int_o^{t+} \frac{d}{dt_o} \left[\int_V \left(\chi_\alpha \frac{\partial G_\alpha}{\partial t_o} - G_\alpha \frac{\partial \chi_\alpha}{\partial t_o} \right) d\underline{r}_o \right] dt_o \quad . \quad . \quad . \quad (5)$$

with

$$\chi_\alpha(\underline{r},0) = \chi_\alpha^*(\underline{r})$$

$$\left.\frac{\partial \chi_\alpha}{\partial t_o}\right|_{t_o=0} = 0$$

Here we only consider the relaxation or initial value part of the solution in (4) and denote it by $\chi_\alpha^{(1)}$, and use an infinite space Green's function for G_α. Since the fracture is instantaneous, say at time $t_o = 0$, then the equilibrium field must change, the change being by an amount $\chi_\alpha^*(\underline{r})$, and this is the initial value for the dynamic field at $t_o = 0$. The actual details of how the dynamic field changes for all time is given by the solution of equation (5), where $\chi_\alpha^{(1)}$ will be measured relative to the final state of equilibrium. Now, in view of (5) and the associated initial conditions,

$$\chi_\alpha^{(1)}(\underline{r},t) = -\frac{1}{4\pi v_\alpha^2}\int_V \chi_\alpha^*(\underline{r}_o)\left.\frac{\partial G_\alpha(\underline{r},\, t;\underline{r}_o,t_o)}{\partial t_o}\right|_{t_o=0} d\underline{r}_o \quad . \quad . \quad . \quad (6)$$

The evaluation of this integral solution for shock induced rupture in a prestressed medium will be given in the paper on tectonic release.

It is an easy generalization to the case of a rupture proceeding at some finite rate, or for the general case in which $v_R < v_\alpha$. A detailed treatment is given by Archambeau (1970b). However, we can see that if we consider a superposition of processes like that just described separated by small time intervals, then we can simulate a continuous process of rupture over a finite time interval. In particular, we treat the initial value integral in (4) as a Stieltjis integral and express it as

$$\chi_\alpha^{(1)}(\underline{r},t) = \frac{1}{4\pi v_\alpha^2}\lim_{\varepsilon\to 0}\Big\{\int_V \Big(\chi_\alpha\frac{\partial G_\alpha}{\partial t_o} - G_\alpha\frac{\partial \chi_\alpha}{\partial t_o}\Big)\, d\underline{r}_o\Big|_o^{\tau_1-\varepsilon}$$

$$+\int_V \Big(\chi_\alpha\frac{\partial G_\alpha}{\partial t_o} - G_\alpha\frac{\partial \chi_\alpha}{\partial t_o}\Big)\, d\underline{r}_o\Big|_{\tau_1+\varepsilon}^{\tau_2-\varepsilon}$$

$$+ \ldots + \int_V \Big(\chi_\alpha\frac{\partial G_\alpha}{\partial t_o} - G_\alpha\frac{\partial \chi_\alpha}{\partial t_o}\, d\underline{r}_o\Big|_{\tau_n+\varepsilon}^{t+}\Big\}$$

Here we have in effect broken the range of integration up into intervals (τ_k, τ_{k+1}) in which the integrand is continuous and evaluated each of the time integrals. We have required that the integrand be discontinuous at the times τ_k, $k = 1,\ldots, n$ and these times correspond to the instants of discrete growth in the rupture. Thus we require that the χ_α appearing in the integrands be such that

$$\lim_{\varepsilon\to 0}[\chi_\alpha(\tau_k-\varepsilon) - \chi_\alpha(\tau_k+\varepsilon)] = \delta\chi_\alpha^* \neq 0$$

which gives discontinuities in the field corresponding to changes in the equilibrium potential appropriate to a new, slightly changed, rupture dimension. This is then just a sum of instantaneous events separated by times $\delta\tau_k = \tau_k - \tau_{k+1}$. We note that for each such event no "velocity" is imparted to the system (pure relaxation), so that $(\partial\chi_\alpha/\partial t_o)$ is continuous at all times. The previous result can now be written as

$$\chi_\alpha^{(1)}(\underline{r},t) = \frac{1}{4\pi v_\alpha^2} \sum_{k=1}^{n} \delta\tau_k \int_V \left(\frac{\delta\chi_\alpha^*}{\delta}\right.$$

where we have multiplied and divided by $\delta\tau_k$. In the limit as $\delta\tau_k \to 0$, that is when the rupture process is continuous, we have

$$\chi_\alpha^{(1)}(\underline{r},t) = \int_o^t U(\tau_o - t_o)\, dt_o \int_V \left(\frac{\partial\chi_\alpha^*}{\partial t_o}\right)\left(\frac{\partial G_\alpha}{\partial t_o}\right) d\underline{r}_o \quad . \quad . \quad . \qquad (7)$$

where $U(\tau_o - t_o)$ is a step function and τ_o is the time interval of rupturing. The step function merely defines the time interval for the completion of the rupture process.

The relaxation effects can be obtained from (7) (or from (5) when $v_R > v_\alpha$) once we obtain χ_α^* from an appropriate solution of (3). Many such solutions exist in the literature (e.g., Landau and Lifshitz, 1959).

Seismic source fields

The simplest and often most convenient way of evaluating the source field integrals (5) or (7) is in the form of a multipole expansion in the frequency domain. Using the result for the equilibrium displacements for a cavity in a medium under pure shear, given by Landau and Lifshitz, 1959, we can consider the radiation due to relaxation around a moving spherical rupture zone which translates as it grows from a point to some maximum radius and then, as it continues to translate, decreases in radius to a point again, marking the end of a spheroidal rupture zone. Expressing the displacement field in terms of the potentials χ_α^*, with coordinates at the center of the moving sphere, allowing the radius appearing in the result to be an appropriate function of time, expanding χ_α^* in spherical harmonics and finally expressing the spherical harmonics in coordinates fixed in space at the point of first rupture (i.e. allowing thereby for the rupture propagation effect), one has (Archambeau, 1964, 1968)

$$\tilde{\chi}_\alpha^{(1)}(\underline{r},\omega) = \sum_{\ell=2}^{\infty} h_\ell^{(2)}(k_\alpha r) \sum_{m=0}^{2} [A_{\ell m}^\alpha(\omega)\cos m\phi + B_{\ell m}^\alpha(\omega)\sin m\phi]$$

$$P_\ell^m(\cos\theta) \ldots \tag{8}$$

with

$$A_{\ell m}^\alpha(\omega) = (-1)^\ell \frac{(\ell-m)!}{(\ell-2)!(2-m)!} G_\ell^{(\alpha)}(\omega)$$

$$\begin{matrix} 3\sigma_{23}^{(0)} & \sigma_{12}^{(0)} & \sigma_{23}^{(0)}/2 \\ -3\sigma_{13}^{(0)} & 0 & \sigma_{13}^{(0)}/2 \\ 0 & -\sigma_{23}^{(0)} & -\sigma_{12}^{(0)} \\ 0 & \sigma_{13}^{(0)} & 0 \end{matrix}$$

$$B_{\ell m}^\alpha(\omega) = (-1)^\ell \frac{(\ell-m)!}{(\ell-2)!(2-m)!} H_\ell^{(\alpha)}(\omega)$$

$$\begin{matrix} 0 & 0 & -\sigma_{13}^{(0)}/2 \\ 0 & -\sigma_{12}^{(0)} & -\sigma_{13}^{(0)}/2 \\ 0 & \sigma_{13}^{(0)} & 0 \\ 0 & \sigma_{23}^{(0)} & \sigma_{12}^{(0)}/2 \end{matrix}$$

where the matrices are indexed on $\alpha = 1, 2, 3, 4$, and $m = 0, 1, 2$, while $G_\ell^{(\alpha)}(\omega)$ and $H_\ell^{(\alpha)}(\ell)$ are series of hypergeometric functions.

If we use the same basic solution for a spherical cavity, in this case requiring that it grow symmetrically without translating, we can obtain the radiation effects due to shock induced rupture in a prestressed medium. This solution and its properties have been discussed in detail by Archambeau (1970 a, b) and are summarized in the paper: "Tectonic release from explosions and earthquakes",

by C. Archambeau, in these proceedings. The solution has the same form as does (8), with $\ell = 2$ the only non-zero term so that it is a pure quadrapole field.

We can summarize the properities of the radiation field for the tectonic source given by (8) as follows:

1. At low frequencies, the $\ell = 2$ term dominates, i.e., for $\omega L < 1$ with L the rupture length.

2. At high frequencies, $\omega L > 1$, higher ℓ value terms are important, and the summed (interference) effect is due to rupture propagation.

3. The spatial radiation pattern is controlled entirely by the prestress when $\omega L < 1$ and by the prestress <u>and</u> the propagation effects when $\omega L > 1$.

4. P-type displacement is approximately two orders of magnitude less than S-type displacements for tectonic sources at shallow depths.

5. The displacement (or velocity and energy density) spectrum has an absolute maximum with the peak frequency f_{max} depending on fault lenght L and to a lesser extent on rupture velocity v_R. The magnitude of the displacement spectrum at the peak is dependent primarily on the prestress level in the failure region.

6. Other (lesser) maxima and minima occur at higher frequencies and are due to rupture growth effects. Asymptotically the displacement spectrum approaches $1/\omega^2$ at high frequencies and a constant for very low frequencies.

It is of considerable importance to the problem of earthquake-explosion discrimination that these properities be contrasted with the corresponding properities of an explosive source in a prestressed medium. In the paper on tectonic release from explosions and earthquakes (Archambeau, in these proceedings), the details of the explosive radiation field will be discussed and, on the basis of the properties of that field compared to those listed above, a number of discrimination criteria are given. In this discussion, we will first illustrate some of the properties of (8) obtained from computations, and then supply evidence from observations that earthquake radiation fields do in fact have these properties.

Figure 1 shows the computed radiation pattern at a distance of $\rho = 301.5$ km for the translating sphere model. Both the phase and the amplitude as functions of azimuth are shown at a period $T = 1.25$ sec. This period corresponds to a wavelength about equal to the rupture length used, so the patterns show the asymmetric radiation due to rupture propagation effects. Note that both the phase and amplitudes are distorted. The initial strains are shown in the figure.

Figure 2 shows the patterns under the same conditions as apply to Figure 1, except that the initial strain field is different. Hence the pattern shape is seen to be very different. This, of course,

is entirely as expected. It is worth pointing out that the dilatation amplitudes in both Figures 1 and 2 are much smaller than the largest of the rotation amplitudes. These two figures illustrate the smaller P-wave amplitudes compared to S-wave amplitudes and the asymmetry introduced by rupture propagation at frequencies such that $\omega L \simeq 1$.

Figure 3 shows the radiation pattern due to rupture of the same kind as in Figure 2, but in this case at longer period. Now we see that the asymmetry introduced into the pattern shape by rupture propagation has effectively disappeared, and the pattern is essentially pure quadrapole. The period used is such that $\omega L >> 1$, and the first term in equation (8), $\ell = 2$, dominates. Thus as noted, the patterns become simple quadrapole at long periods, and we see that the pattern shape is frequency dependent.

On the other hand, Figure 4 shows the patterns at short period such that $\omega L \simeq 1$, but, because we have taken the rupture to propagate into the plane of the figure ("dip-slip" case), there is no observed effect on the pattern symmetry due to rupture growth effects. Therefore, we see that the projection of the field into planes normal to the direction of rupture propagation does not give a pattern showing the asymmetry of rupturing. This is clearly what would be expected, although could possibly be overlooked, since the effects of rupture growth on the field pattern is such as to keep the propagation direction an axis of symmetry. Naturally, observations of the field in the real earth could reveal the pattern asymmetry which exists through observations of those waves emerging in the direction of rupture propagation, but this would require observations at great distances such that the least time paths starting from the near vertical at the source were observed.

Figure 5 shows the patterns for an explosive source in the prestrain field of Figure 4, and we see that the patterns at the roughly 300 km distances are of the same form. The direct pressure wave monopole component has been omitted here. Hence we cannot expect to see any pattern differences between the anomalous field from an explosion in a prestressed medium and the field from a "dip-slip" earthquake at these distances, and only at great distances would differences due to rupture propagation appear. Of course, differences in the dilatational or P-wave field would occur at all distances due to the monopole component of the total field from the explosion. This would also be true for the Rayleigh-type surface waves.

The spectral properties of the field observed at a given distance can be illustrated through computations based on a somewhat simpler model than the propagating rupture model so far employed. In particular, for a spherical rupture developed at a rate $v_R < v_\alpha$ (Archambeau, 1968), we obtain the essential features of the spectrum for tectonic sources.

Figure 6 illustrates spectra computed from such a model. We show the spectra of displacement, velocity and energy all normalized

to unity. The features of these spectra which are especially important are the asymptotic behavior, the displacement going to a constant in the low-frequency limit and to zero like $1/\omega^2$ at high frequencies, and the peak in the spectrum. Thus we note, contrary to some of the previous models used for tectonic or earthquake sources, that the spectrum is not flat to zero frequency beyond some critical frequency, but is peaked and decreases quite rapidly beyond the peak frequency. The details of the frequency dependence of this model are given by Archambeau (1968). In a later section of this paper, we will show examples of observed earthquake spectra which have the predicted peaked spectrum behavior. In view of these results, as well as others, there appears to be little reason to believe that earthquakes produce the flat spectral character often used. One consequence of the fact that the assumption of a flat spectrum to zero frequency does not hold is that calculations of earthquake moments based on this assumption of flatness will be in error. The error introduced will always be such as to give too large a moment.

The peak frequency point, f_{max}, depends on the rupture dimensions (in particular L) and the rupture velocity, the latter to a lesser extent. Thus it is an important means of determining rupture length, and this in turn is an important means of discrimination since observations indicate that shallow earthquake mechanisms are such that the rupture length for an earthquake of given energy will be much larger than the source dimension for an explosion of the same seismic energy. Figure 7 shows the nature of the variation of f_{max} with the rupture dimension R_o. It is important to note that the location of this curve depends upon R_S/R_o as well, where R_S is the radius of the zone in which most of the relaxation of stress occurs. Archambeau, in these proceedings on tectonic release from explosions and earthquakes, discusses the interpretation and effect of R_S in greater detail.

Observations from seismic sources

In order to illustrate the verification of these predictions, we will present a few observations, emphasizing those that bear most directly on the discrimination problem.

Consider first the observed properties of the radiation patterns from an earthquake. We will consider the Love and Rayleigh surface waves from the Fallon earthquake, m_b = 4.4; these patterns should show the predicted properties of asymmetry at high frequencies, even though these predictions were made on the basis of the body wave field from the source. Figure 8 shows the Love wave radiation patterns from Fallon at four different frequencies. This data is from a paper by Lambert et al, 1970. At a period T = 9 sec, we see that the amplitudes to the northeast are larger than those to the southwest by a factor of 3 or 4. We also note, however, that the amplitudes on the northwest lobe are much smaller than those to the southeast and in fact smaller than on either of the other two lobes as well. We interpret this latter asymmetry to be due to scattering by lateral changes in

structure, since the Sierra Nevada lies across the path to the northwest, while the former asymmetry is interpreted as due to rupture propagation effects. The validity of this interpretation is strongly supported by the behavior of the pattern as the period becomes larger since we see that the small amplitude on the Sierra side remains while the asymmetry in the northeast-southwest lobes decreases steadily for longer periods, as is predicted for rupture propagation effects. The very efficient propagation of the surface wave energy across the interior of the continent to the east coast is a structural effect. Once the waves pass beyond the Rocky Mountains, they are not severely scattered and appear to be controlled first by a crustal wave guide (short periods) and then by a mantle wave guide at longer periods. The theoretical pattern is shown for reference and corresponds to a simple double couple at a depth h = 20 km. It has the same form for all periods since no rupture propagation effects were taken into account. Even so, the agreement is quite good, especially, of course, at the longer periods.

Figure 9 shows that similar effects occur for the Rayleigh waves from Fallon, although the patterns are more sensitive to fault orientation and structure. Thus the theoretical double couple patterns computed using the fault parameters shown (λ = slip angle, δ = dip angle and ϕ = strike angle) show a frequency dependence due to the rupture orientation and the local sturcture at the source. This frequency dependence is mild compared to the variation with frequency due to propagation effects. Again this shows up best through comparison of the pattern at T = 9 sec with that at T = 12 or 16 seconds. Thus we again see the propagational effect as predicted. In spite of this effect, however, the fit of a simple double couple, oriented as indicated, is quite good. The structural wave guide effects east of the Rocky Mountains are again apparent from the pattern variations shown.

These observations may be contrasted with those of Figure 10, the Love and Rayleigh wave radiation patterns from the underground explosion Bilby (m = 5.8). The patterns appear to be much more symmetric and to show little if any rupture propagation effects. In this case the Love waves are totally due to tectonic effects, while the Rayleigh wave is a superpostion of the monopole contribution to the dilatational field from the explosion itself, plus a quadrapole contribution from tectonic release. In this case, the patterns are fit very well by the theoretical model. These observations and the fit are consistent with the theoretical predictions of the relaxation effects due to a spherical rupture controlled by the explosive shock wave.

The details of earthquake spectra have been difficult to obtain reliably since most instrumentation has been very band limited relative to the spectrum from the larger earthquakes. However, broad band, high-frequency instrumentation has been used to observed microearthquakes, and it has been possible to obtain nearly the whole spectrum for such small sources. This offers us the opportunity of checking the spectrum of these sources with the predictions of a

relaxation source theory. Figure 11 shows the spectra of three micro-earthquakes in Anza, California, obtained by Sammis and Smith, 1970. Only at the very high frequencies is the instrument response such that there is some uncertainty in the spectrum. However, all the lower frequencies are well recorded, and these spectra show the predicted decrease in amplitude for longer periods and the associated spectral peak.

Using these spectral peaks, we can obtain an estimate of rupture dimension from the relaxation theory. A graph such as is shown in Figure 7 can be used and for the cases $R_S/R_o = 2$ and $R_S/R_o = 10$, with $v_R = 3$ km/sec, we can obtain bounds on the rupture dimensions. These bounds represent the required dimensions for these sources under the conditions that the failure is associated with a limited stress concentration ($R_S/R_o = 2$) or under the condition that the stress was regional and quite uniform before rupture ($R_S/R_o = 10$). Table 1 shows the rupture dimension limits obtained in this way.

In addition to rupture dimension, the energy partition between P, SV and SH can be computed from the spectra for htese phases. These values are given in the table and show that, as predicted, the P-wave energy is roughly two orders of magnitude below the S-type energy.

Thus we have observational support for the predicted properties of the tectonic source. In addition these properties suggest a number of methods of discrimination between earthquake-explosion events.

Summary, with implications for discrimination

The theory discussed in this paper appears to fit the rather limited observations of spectra and radiation patterns for earthquakes and explosions quite well. By way of summary, we will consider some of the consequences for discrimination between such events.

Figure 12 shows event magnitude versus characteristic source dimension. This data was gathered from a number of sources and has been discussed by Liebermann and Pomeroy, 1970, and by Liebermann in these proceedings. The single point near m = .6, L = .05 km represents the three determinations of rupture dimension obtained from the spectra of Figure 11. This distribution of observations suggests, at least at this stage, that there are both high stress, small rupture dimension events and low stress, large rupture dimension earthquake events. In spite of this, it appears that small magnitude explosions and earthquakes differ sufficiently in their magnitude-dimension relationship so that discrimination is possible in the range around $3 < m < 5$. Above $m = 5$, this discrimination criteria is already well established. Below $m \simeq 3$, we have no indications from this data at least, but it appears possible that the differences may extend below this level as well.

In addition to this approach, however, we have several other criteria which can be used. First we might point out that a simpler

and probably more meaningful criteria related to m vs L (or m_S, the surface wave magnitude) is a criteria based on f_{max} (spectral peak frequency) vs E (energy of the phase with spectral peak at f_{max}). Since we have seen that f_{max} is simply related to L and E to the magnitude, then we expect a similar earthquake-explosion source separation as is evidenced for m vs L. Actually if E is plotted (on the ordinate) against $T_{max} = 1/f_{max}$, we would obtain a plot very similar to that in Figure 12 if E and T_{max} were obtained for one of the S phases, one would expect the explosions to be lower than the earthquakes, that is just inverted from that for a P phase.

In view of the differences in radiation patterns between earthquakes and explosions as evidenced in Figures 8 through 10, we can use strong "high" frequency asymmetries in the Love and Rayleigh wave patterns and differences in the shape of the Rayleigh pattern at all frequencies as discriminants. Further, due to the relatively high excitation of S motion by earthquakes relative to P and similar excitation of P and S for explosions, we can see the Love to Rayleigh wave spectral ratio as a function of frequency to discriminante. For L/R vs frequency, we should see a much larger ratio for earthquakes than for explosions at long periods. This approach is also, of course, applicable to the S/P body wave spectral ratio. These criteria are investigated in more detail in the paper on tectonic release from earthquakes and explosions in these proceedings.

REFERENCES

Archambeau, C.B., 1964, Elastodynamic source theory, Ph.D. Thesis, California Institue of Technology, Pasadena.

Archambeau, C.B., 1968, General theory of elastodynamic source fields, Rev. Geophys., v. 6, p. 241-288.

Archambeau, C.B., and Sammis, C., 1970a, Seismic radiation from explosions in prestressed media and the measurement of tectonic stress in the earth, Rev. Geophys., August.

Archambeau, C.B., 1970b, The theory of stress wave radiation from explosions in prestressed media, to be submitted to Geophys. J.

Ben-Menahem, A., 1961, Radiation of seismic surface waves from finite moving sources, Bull. Seism. Soc. Am., v. 51, 3, p. 401-435.

Haskell, N.A., 1964, Total energy and energy spectral density of elastic wave radiation from propagating faults, Bull. Seism. Soc. Am., v. 56, 6, p. 1811-1841.

Lambert, D.G., Flinn, E.A., and Archambeau, C.B., 1970, Seismic radiation and source parameters for earthquakes and underground explosions, in preparation.

Lambert, D.G., Flinn, E. A., and Archambeau, C.B., 1970, Seismic radiation and source parameters for earthquakes and underground explosions, in preparation.

Landau, L.D., and Lifshitz, E.M., 1959, Theory of Elasticity, Pergamon Press.

Liebermann, R.C., and Pomeroy, P.W., 1970, Source dimensions of small earthquakes in the western U.S. as determined by the size of the aftershock zone, Bull. Seism. Soc. Am., v. 60, p. 879-890.

Love, A.E.H., 1944, A treatise on the mathematical theory of elasticity, Dover.

Maruyama, T., 1964, Statistical elastic dislocations in an infinite and semi-infinite medium, Bull. Earthquake Res. Inst. v. 42, p. 289-368.

Maruyama, T., 1963, On the force equivalents of dynamical elastic dislocations with reference to the earthquake mechanism, Bull. Earthquake Res. Inst., v. 41, p. 467-486.

Morse, P.M., and Feshbach, H., 1963, Methods of theoretical physics, McGraw-Hill.

Sammis, C., and Smith, S.W., 1970, personal communication.

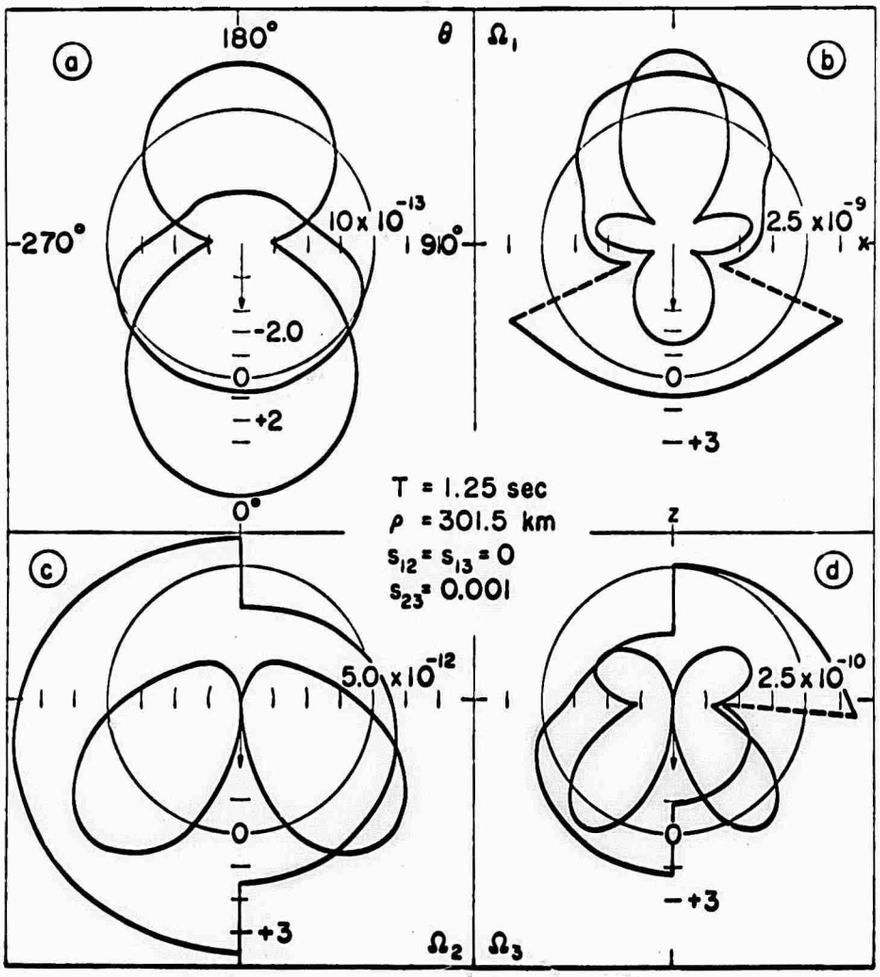

Figure 1. Radiation patterns for a propagating spherical rupture with final rupture dimensions L = 1.5 km, W = .2 km (width). (a) Dilatation amplitude and phase versus azimuth. (b)-(d) Rotation components, amplitude and phase versus azimuth. Arrow in the figures indicates direction of rupture propagation. Asymmetries in the patterns are due to rupture propagation or growth effects. Patterns correspond to radiation wavelengths λ_p = 4 km and λ_s = 2 km as compared with L = 1.5 km. The asymmetries increase for shorter wavelengths and decrease (to pure quadrapole) at long wavelengths. The patterns shown are typical for $\lambda/L \approx 1$. The patterns therefore change shape as functions of frequency (Archambeau, 1968).

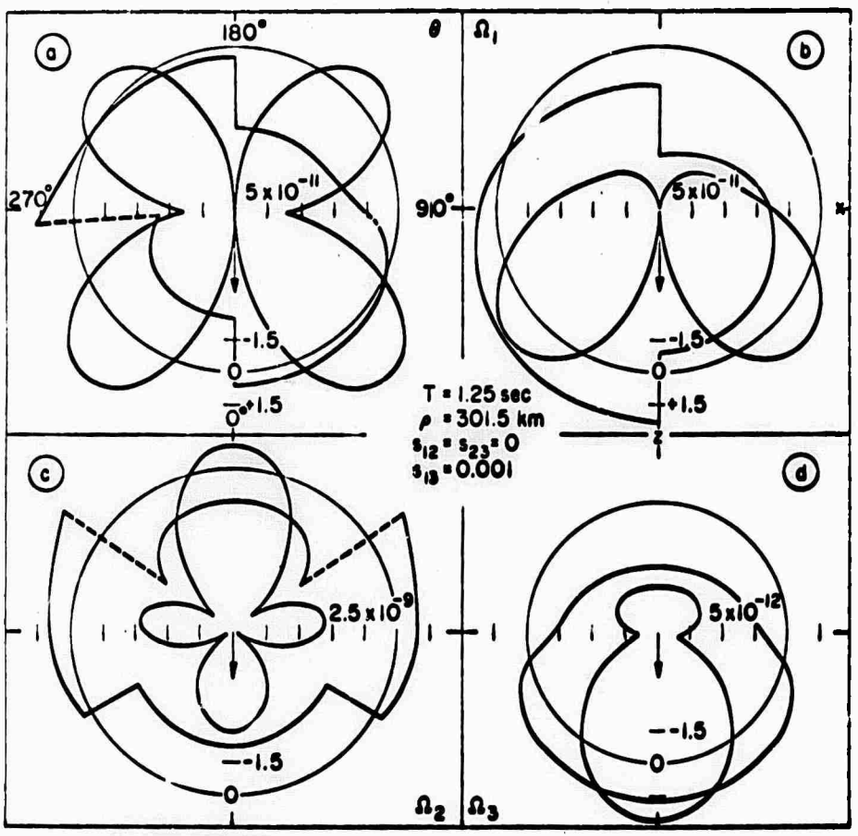

Figure 2. Radiation patterns for the same propagating rupture model used in Figure 1 but with a different initial strain field. Note that the dilatation amplitude is much smaller than the largest of the rotation amplitudes here and also for the case shown in Figure 1 (Archambeau, 1968).

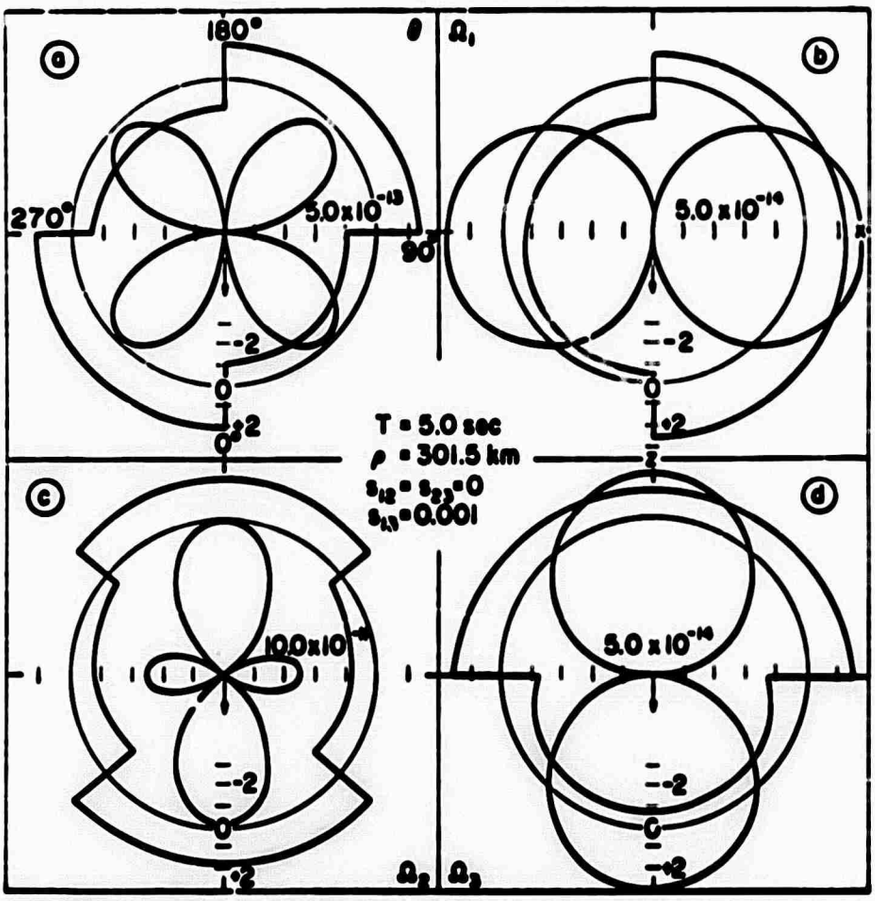

Figure 3. Radiation patterns for the same propagationg rupture model of Figure 2, but at a longer period. In this case the pattern is nearly pure quadrapole in form and the effects of rupture propagation are small. In this example $\lambda/L \approx 10$ for all components (Archambeau, 1968).

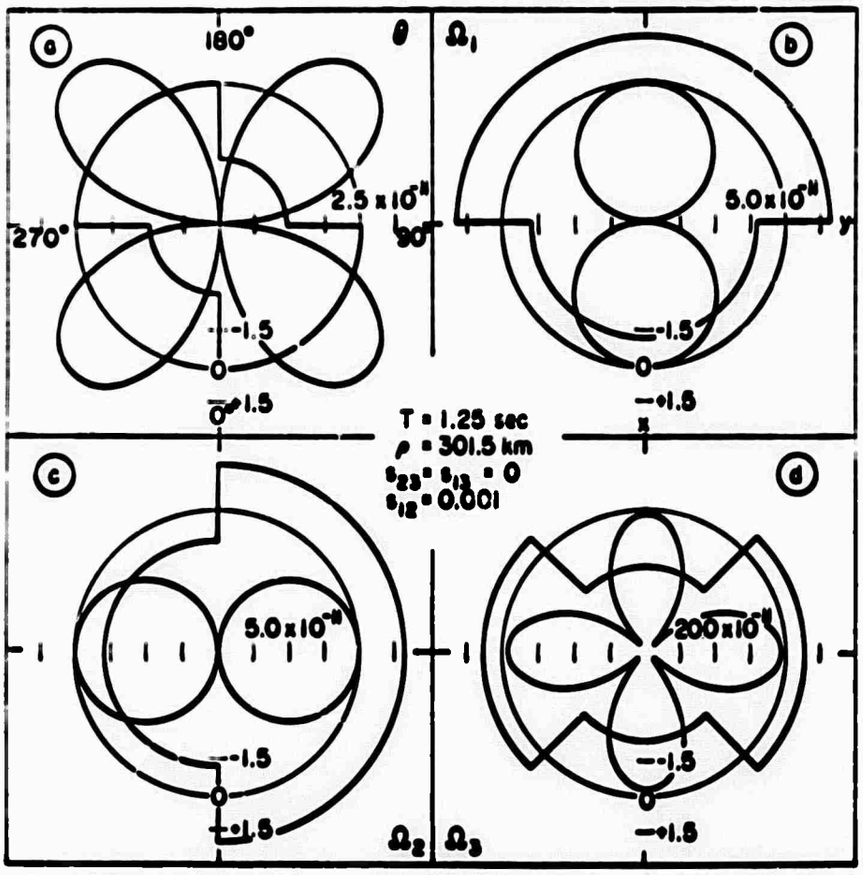

Figure 4. Radiation patterns for rupture propagation into the plane of the figure. In this case projection of the field onto the plane normal to the rupture propagation direction (symmetry axis of the field) does not show rupture propagation effects at the distance $\rho = 301.5$ km even though $\lambda/L \sim 1$. This corresponds to a "dip slip" fault configuration (Archambeau, 1964).

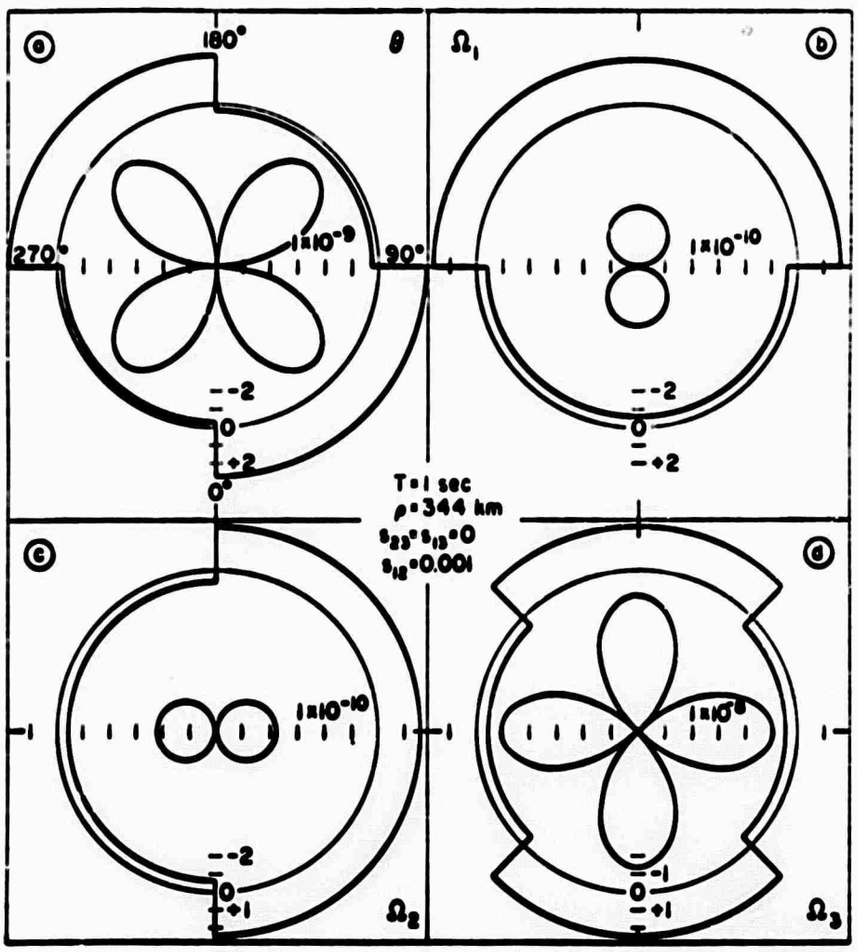

Figure 5. Radiation patterns due to tectonic release associated with shock controlled rupture ($v_R > v_\alpha$) in a medium having a pre-strain field the same as in Figure 4. The monopole component (pure dilatational) due to the explosive pressure wave itself has been omitted so that only the anomalous field is shown. The patterns are seen to be the same as for the dip slip configuration illustrated in Figure 4 (Archambeau, 1964).

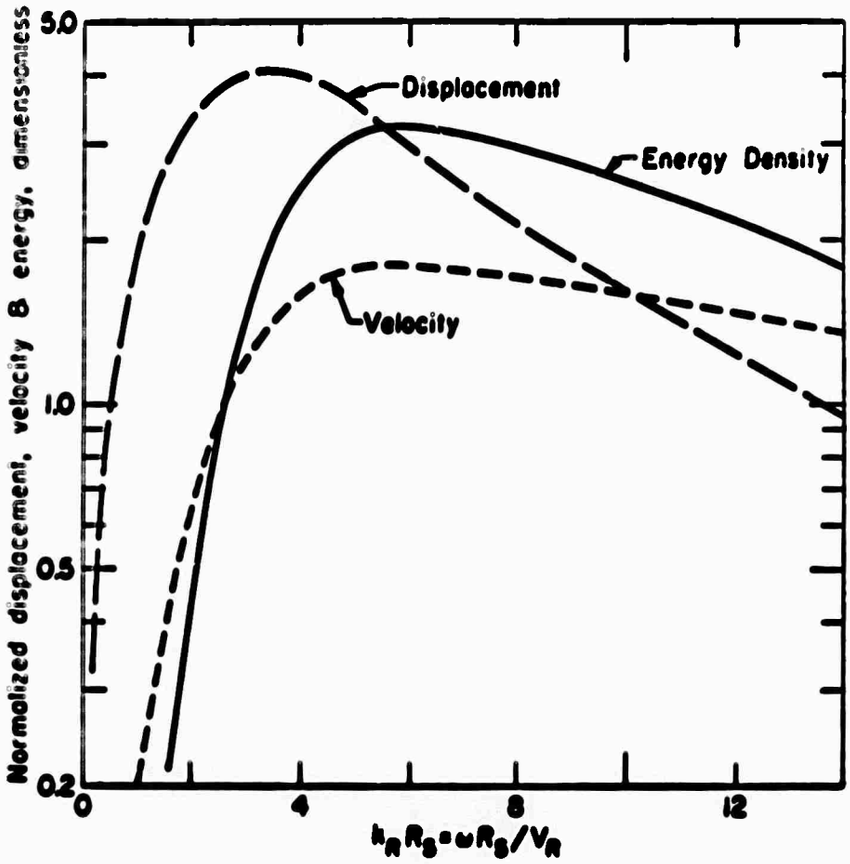

Figure 6. Displacement, velocity and energy versus frequency for an equilateral spherical rupture. Rupture paranoters are chosen so that $v_R/v_p = 1/2$, $R_s/R_o = 2$, with R_s the effective radius of strain relaxation and R_o the fixed rupture zone radius. Spectra for this simple model have one maximum, unilateral propagating rupture models have many maxima, with the largest corresponding to the maximum illustrated here. The spectruns correspond to the radiated field to be observed at distances such that $kr > 1$, with k the wave number and r the distance from the source origin (Archanbeau, 1968).

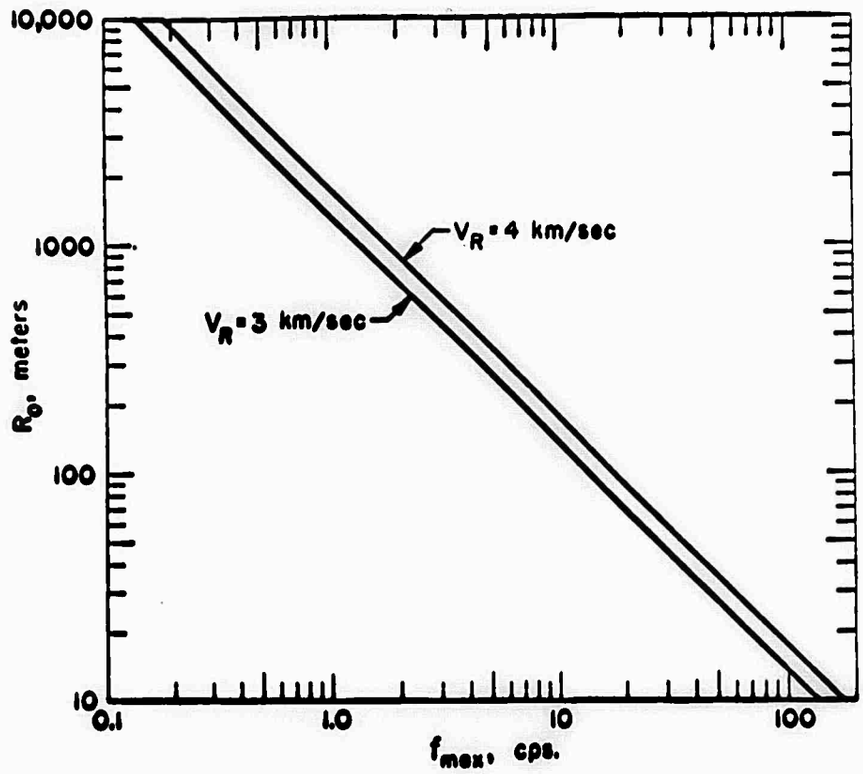

Figure 7. Plot of frequency at the maximum in the velocity spectrum for the simple equilateral spherical rupture as a function of rupture radius R_o, with rupture velocity as a parameter. Here $v_R/v_p = 1/2$ and $R_s/R_o = 2$. For larger ratios of R_s/R_o the curves move in parallel to the left, that is to lower frequencies. For R_s/R_o infinite, a limit point is reached. For $R_s/R_o > 3$ there is very little change in the position of the curves with increases in this ratio. If the pre-strained region is uniform over a large region around the rupture, large values of R_s/R_o are appropriate. If the rupture is in response to a localized stress concentration then lower values of R_s/R_o would be expected (Archambeau, 1968).

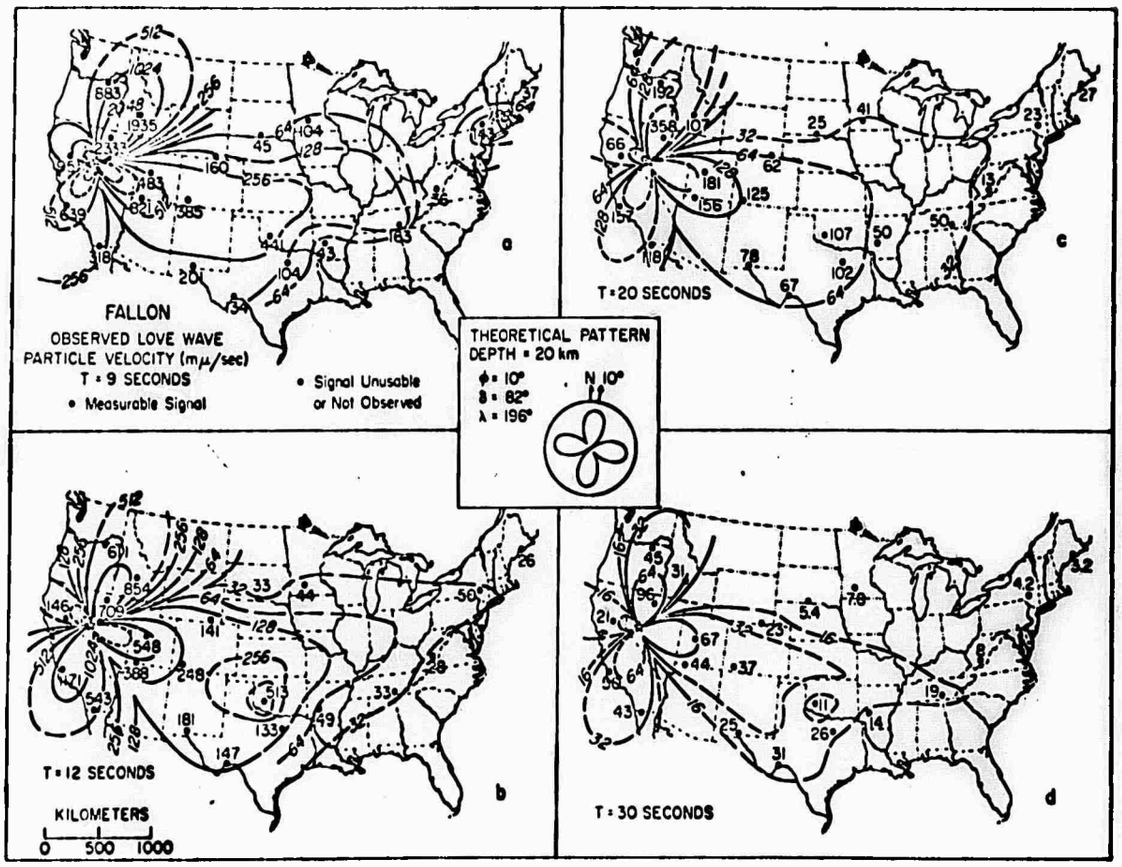

Figure 8. Love wave radiation patterns observed from the Fallon earthquake, m_b = 4.4, with period as a parameter. The pattern shapes are affected by rupture propagation and lateral variations in earth structure. The large amplitudes to the northeast at short periods are due to rupture propagation; the small amplitudes to the northwest at all periods are the result of scattering produced by lateral variations in structure in going from the Basin and Range structural province into and across the Sierra Nevada. Theoretical pattern for a simple double couple at depth h = 20 km, λ = slip angle with λ = 0 horizontal, δ = dip angle and ϕ = azimuth angle (data from Lambert et al, 1970)

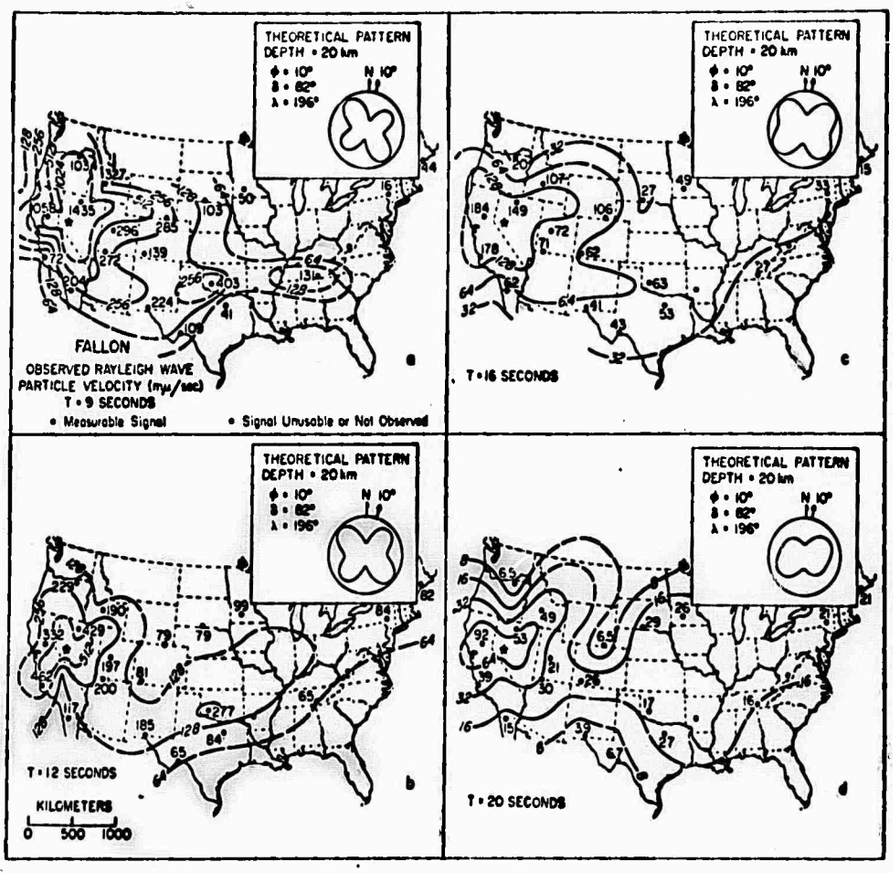

Figure 9. Fallon Rayleigh waves as a function of azimuth with period a parameter. These patterns show basically the same behavior as do the Love waves of Figure 8, with somewhat greater complications due to fault orientation and structure effects. The theoretical patterns shown are for a simple double couple at h = 20 km and change shape slightly with period. The asymmetry associated with the north-south lobes at T = 9 sec again appears to be due to rupture propagation. The eastern U.S. again appears to have period dependent wave guide characteristics (data from Lambert et al, 1970).

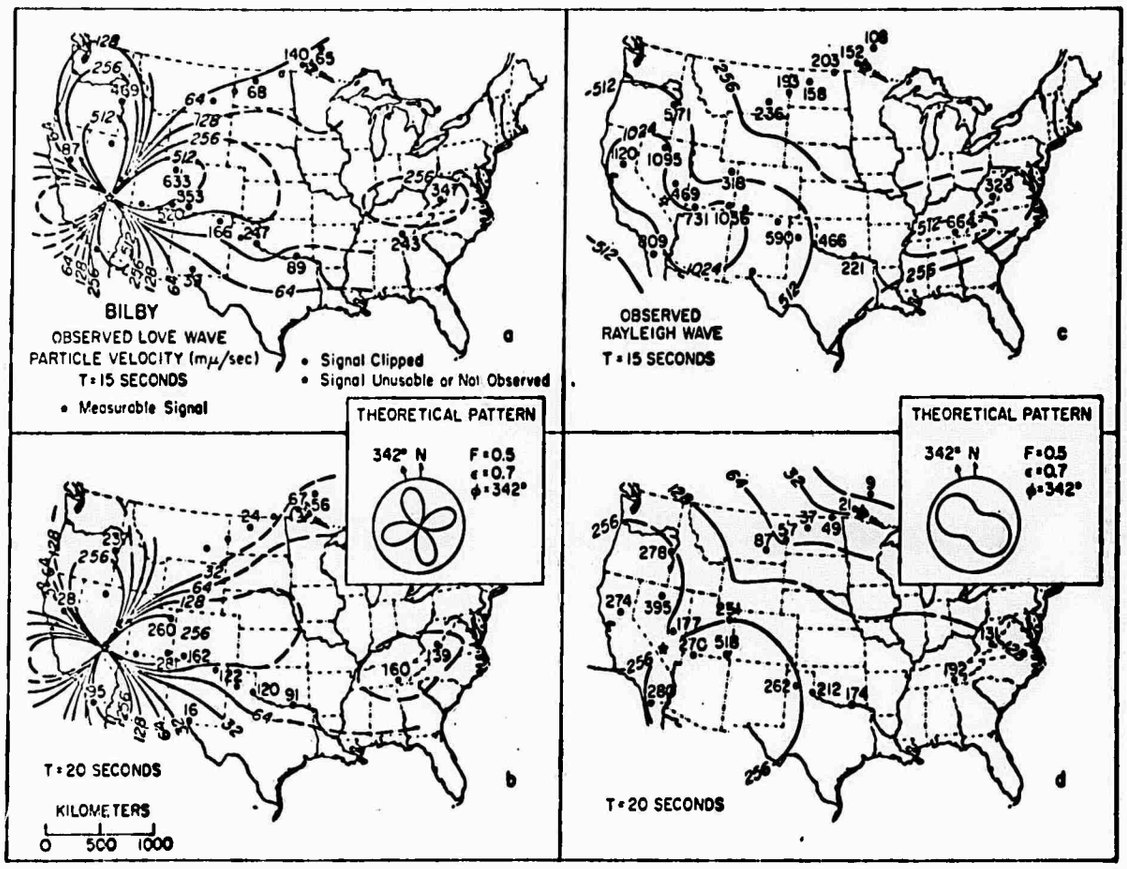

Figure 10. Love and Rayleigh wave radiation patterns from the underground explosion Bilby (m_b = 5.8) at periods T = 15 and 20 seconds. The patterns show rather strong symmetry at all periods and conform to the theoretical predictions of a simple quadrapole source for the anomalous radiation due to tectonic release. The theoretical patterns are from a simple quadrapole or double couple source superposed on a pure dilatational monopole and agree quite well with the observed patterns. The factor F represents the ratio of double couple to monopole source excitation (data from Lambert et al, 1970).

THREE CALIFORNIA MICRO-EARTHQUAKE P WAVE SPECTRA (Sammis & Smith, 1967)

Event	m_b	f_{max}
5	0.6	24 cps
9	0.6	25 cps
11	0.8	23 cps

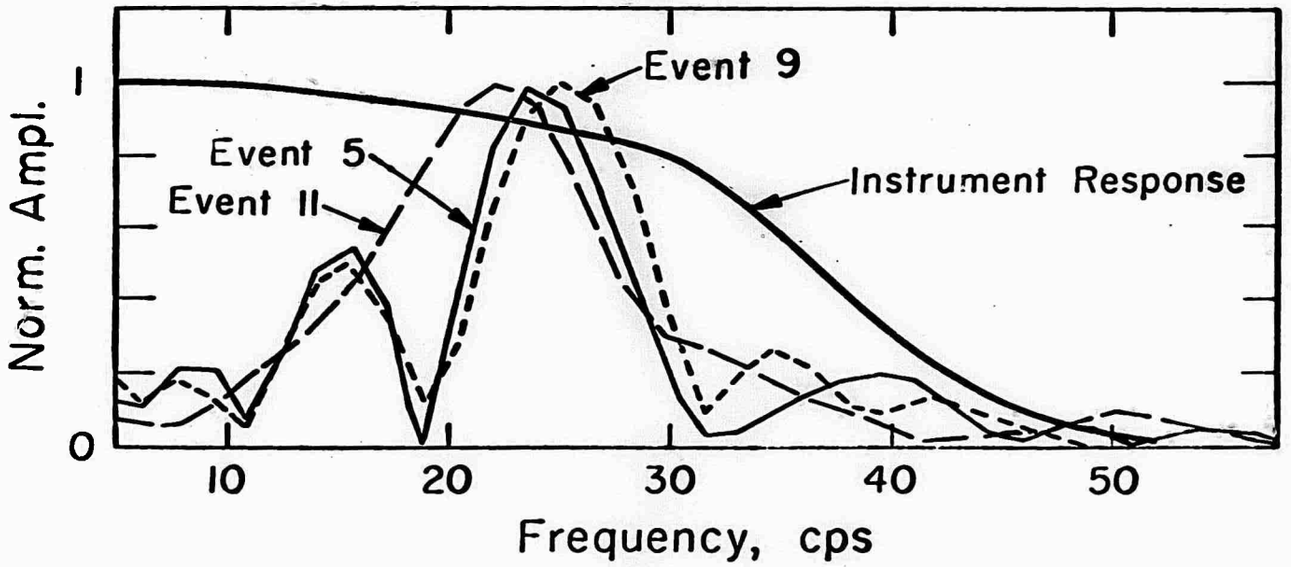

Figure 11. Spectra from three microearthquakes (Anza, California area) recorded on a broad band seismometer. The spectra show the predicted peak for a tectonic source. The spectral peaks are used to compute rupture length (Sammis and Smith, 1970).

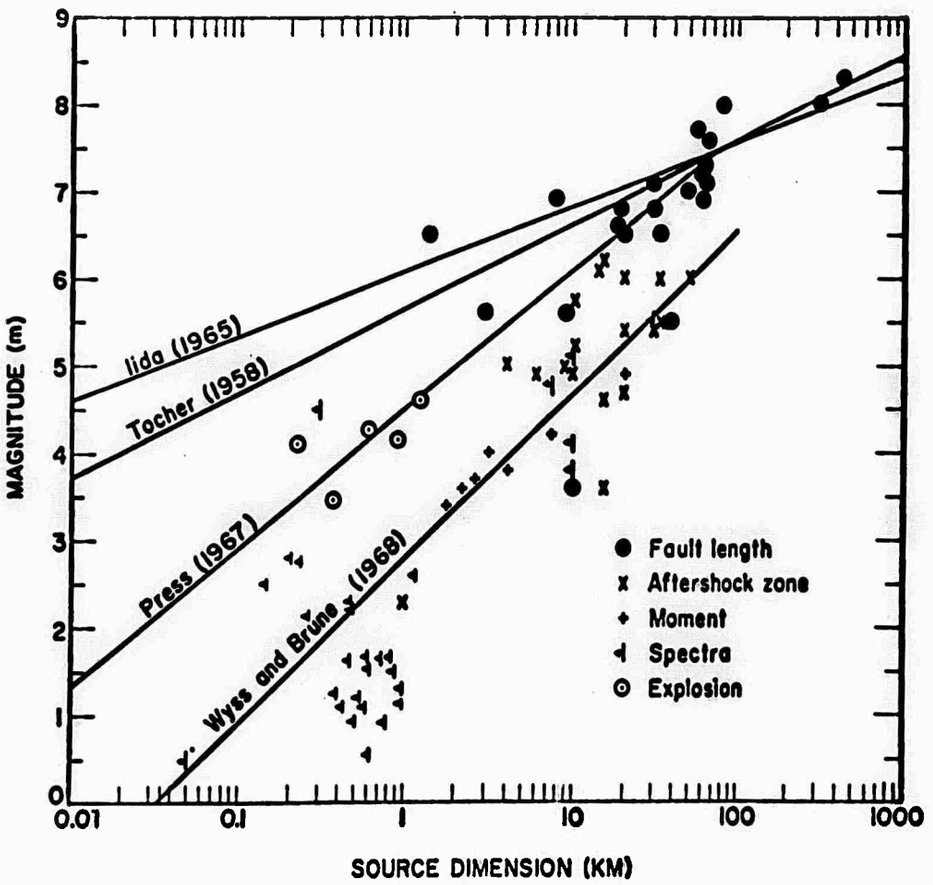

Figure 12. Body wave magnitude m versus fault length L determined by a variety of methods and investigators. The point at m ≃ .6 and L ≃ .05 km corresponds to the magnitudes and fault lengths determined from the microearthquake spectra of Figure 11. The point established by these observations is in agreement with the Wyss-Brune curve and is the smallest magnitude for which accurate fault length has been determined. The data suggest both high and low stress earthquakes in the low magnitude range (m<4.5) with shorter faults for high stress events when both types have the same observed magnitude. The relatively few observations of explosions suggest that the source dimension is small relative to an earthquake of the same magnitude, even for magnitudes m < 4.5, although clear separation between explosions and earthquakes below m ≃ 3 may become less clear in view of the observations of high stress microearthquakes (Liebermann and Pomeroy, 1970; Liebermann, these proceedings, 1970).

TABLE I

Energy distribution, magnitude and peak frequency for the three micro-earthquakes of Figure 11. The fault length is obtained using the relaxation source theory described in this paper, where the observed spectral peak frequency is related to fault dimension by a curve like that of Figure 7. Specifically the curve for v_R = 3 km/sec with R_S/R_o = 2 for the upper bound and R_S/R_o = 10 (i.e. $R_S/R_o >> 1$) for the lower bound on the source dimension R_o. The energy partition in P and S waves is obtained from spectra and shows the predicted two orders of magnitude difference between P and S wave excitation by a tectonic source (Sammis and Smith, 1970).

Energy Distribution in the Band 7-34 cps

Event	m_b	P Wave Peak Frequency	Fault Length	Energy (ergs)			Energy Total
				P	SV	SH	
# 5	0.6	24 cps	50 - 115 m.	1.1×10^8	7.3×10^9	1.0×10^{10}	1.7×10^{10}
# 9	0.6	25 cps	48 - 110 m.	4.2×10^7	2.5×10^9	9.5×10^9	1.2×10^{10}
# 11	0.8	23 cps	52 - 120 m.	9.1×10^8	4.5×10^{10}	2.5×10^{10}	7.0×10^{10}

DEDUCTION OF SEISMIC SOURCE PARAMETERS FROM LONG PERIOD WAVES

By

James N. Brune

The deduction of source parameters of seismic events from long period waves is here discussed in connection with the problem of detecting underground nuclear explosions and discriminating earthquakes from explosions.

Several fundamental assumptions may be taken as valid for the purposes of this discussion. The first is that underground explosions and naturally occurring seismic events are distinctly different as seismic sources. Hence, if all seismic waves generated by the two sources could be clearly recorded, there would be no difficulty in distinguishing them. It is a generally accepted and experimentally supported result that explosive seismic sources may be approximated by a more or less symmetric pressure pulse, whereas, earthquakes may be approximated by a more or less complicated superposition of shear couples. Thus explosions cause relatively symmetric radiation of seismic waves, whereas earthquakes cause very asymmetric radiation with many nodes and changes in phase. In addition explosions generate seismic waves with much greater relative high frequency and compressional energy than do earthquakes.

Given large numbers of high quality seismographs operating at close distances to seismic sources, there would be no difficulty in detecting and identifying explosions as small as a fraction of a kiloton in yield. In practice detection and identification of small underground explosions is made very difficult by constraints imposed on the available data. The main constraint is the combined effect of seismic noise level in the earth and political and economic limitations on the locations and number of seismographs. A typical problem is posed by the condition that for some possible underground explosions, no seismographs may be located nearer than 30°. Other limitations might be caused by difficulties in recording in the oceans. In the presence of seismic noise and such constraints there will be some lower yield limit below which explosions cannot be detected or identified. Special arrays and special processing will allow a significant increase in signal-to-noise ratio but it is probable that even a large investment in arrays of instruments and sophisticated processing will not increase the signal-to-noise ratio by more than a factor of 10.

To orient the discussion toward the role of long period observations in the problem of detecting and discriminating earthquakes from explosions, consider Figure 1. This is a figure comparing amplitude of ground noise with amplitudes of surface waves and body waves corresponding to certain magnitude siesmic events.

The ground noise measurements are from Brune and Oliver (1958), Haubrich (1967), and Haubrich (1970). They show a sharp peak in ground noise at periods near 6-8 seconds (storm microseisms) with noise sharply decreasing to longer and shorter periods. There is a minimum in noise near 25-40 seconds period and then a sharp rise to longer periods. Beyond periods of 20 seconds these ground amplitudes were computed from the noise spectral density curves of Haubrich (1970) assuming arecording band width of 172 cph, the approximate

bandwidth of the instruments first used to study the noise in this period range (Pomeroy, et al, 1969). This longer period noise is apparently not of the propagating wave type (as for periods less than 21 seconds), but is presumably related to atmospheric effects (Haubrich, 1970). Superimposed on the noise figure are ground amplitudes for various magnitude events at $\Delta = 30°$ as defined by the m_b and M_S magnitude definitions (Richter, 1958). Also shown is the average fundamental mode surface-wave-ground amplitude expected at $\Delta = 30°$ for a double couple strike slip point source located at depths of 0 and 10 km with a moment of 10^{22} dyne cm (corresponding to $M_S \sim 2.5$). This curve was estimated using the numerical surface wave excitation results of Harkrider (1970) for a shield structure.

The main point of interest in Figure 1 is the minimum in seismic noise which occurs at a period of about 30 seconds. Because ground amplitudes of seismic waves from events with depth ~ 10 km do not vary as rapidly with period, the minimum is also a maximum in signal-to-noise ratio for these events. For very shallow events the amplitudes near 20 seconds period are higher and signal-to-noise ratio is nearly constant between 20 and 40 seconds.

Given 50 good long period stations distributed around the world, what sort of detection and identification capability might we ultimately expect? As a result of previous studies three possible discrimination criteria are suggested:

1. Use of the complex radiation pattern expected for earthquakes.

2. Use of the excitation of long period waves relative to waves of about 1 second period (which also have a high signal-to-noise ratio, see Figure 1), e.g., M_s versus m_b, AR versus m_b.

3. Use of the slope of the surface-wave spectrum in the period range 20-50 seconds.

To make use of the complex radiation pattern of earthquakes, surface waves or body waves have to be clearly recorded at least 2 separate azimuths to verify the existence of a node in the radiation pattern or a shift in phase. In practice several more observations would generally be necessary to confirm that an event did not have explosion-like symmetry. From Figure 1, we see that for distances $\Delta > 30°$ events of magnitude M_S less than about 2.5 would not be recorded above noise level. Thus with a large number of stations near 30° distance covering a large azimuth range around the source it would be possible to identify earthquake like radiation patterns for events as small as $M_S \sim 3.0$. If large arrays are used this limit might be lowered to $M_S < 2.5$.

The second criteria listed above, namely the ratio of long period waves to short period waves (M_S vs m_b, AR vs m_b) could also be applied to these small magnitudes.

The third criteria listed above, the slope of the spectrum near

30 seconds period, requires reliable above-noise recording over a wide enough frequency range to establish a characteristic slope; this might be difficult to apply for events with M_S ~ 3.0.

With this brief general discussion of the situation, I will list a few special problems which need further study.

Time function for explosions

It is remarkable that after so many years of research under the Vela Uniform program, there is still uncertainty about the source time function for explosions. Should explosions be represented by a step function of pressure on a cavity? an exponential? an impulse? a combination step function with exponential? Good broad-band high dynamic range recorders (digital) operated at varying distances from explosive sources should quickly provide concrete information. This has relevance to explaining the spectral shapes at long periods (20-50 sec) and to explaining the relatively low excitation of long-period waves (especially surface waves) by explosions.

Spectral shapes between 20 and 50 seconds

Molnar et al (1970) have suggested that the ratio of 20 second to 50 second amplitudes of fundamental mode Rayleigh waves is a discriminant. This needs to be tested using more data and an adequate explanation of this spectral ratio needs to be confirmed. Special study needs to be made of the source time function and of the effect of source depth on this ratio.

Regional and depth variations in surface wave excitation, source dimensions, stress, stress drop, and source mechanism

In certain regions or at certain depths earthquakes excite only very low amplitude long period waves (particularly surface waves) and discrimination of earthquakes may be difficult. In such regions stress or stress drops may be relatively large or source conditions may be different. A detailed study of the near-source spectra of such earthquakes needs to be made so that the nature of regional variations in spectra is understood.

Propagation effects, attenuation, scattering

One of the main difficulties in using the complex radiation patterns of earthquakes as a discriminant is the complex effects of propagation on surface waves. Diffraction, reflection, scattering and multiple travel paths lead to complicated surface wave trains. In principle these effects may be taken into account; in practice the necessary detailed knowledge of variation in crustal structure may be difficult to achieve.

CONCLUSION

Given a world-wide array of long period seismographs operating at near teleseismic distances and capable of taking full advantage of the ground noise minimum near 40 seconds, it should be possible to discriminate earthquakes from explosions at magnitudes $M_S = 3.0$. Discrimination would involve identification of an earthquake-like radiation pattern, using phase, amplitude, and spectral shape. With techniques to reduce long period noise the limit might be extended to $M_S < 2.5$.

REFERENCES

Brune, J. and Oliver, J., 1959, The seismic noise of the earth's surface, Bull. Seism. Soc. Amer., v. 49, 4, p. 349.

Harkrider, D.G., (in press), Surface waves in multi-layered elastic media No. 2; higher mode spectra and spectral ratios from point sources in plane-layered earth models, Bull. Seism. Soc.

Haubrich, R., 1967, Microseisms, Intern. Dictionary of Geophysics, Pergamon Press Ltd., London, England.

Haubrich, R., 1970, Seismic noise between 2.5 and 200 cycles per hour, Air Force Office of Scientific Research report.

Molner, et al, 1969, Small earthquakes and explosions in western North America recorded by new high gain, long period seismographs, Nature, v. 224, p. 1268.

Pomeroy, P.W., Hade, G., Savino, J., and Chander, R., 1969, Preliminary results from high-gain wide-band long-period electromagnetic seismograph systems. Journ. Geoph. Res., v. 74, 12, p. 3295.

Richter, C.F., 1958, Elementary seismology, W.H. Freeman and Co., San Francisco.

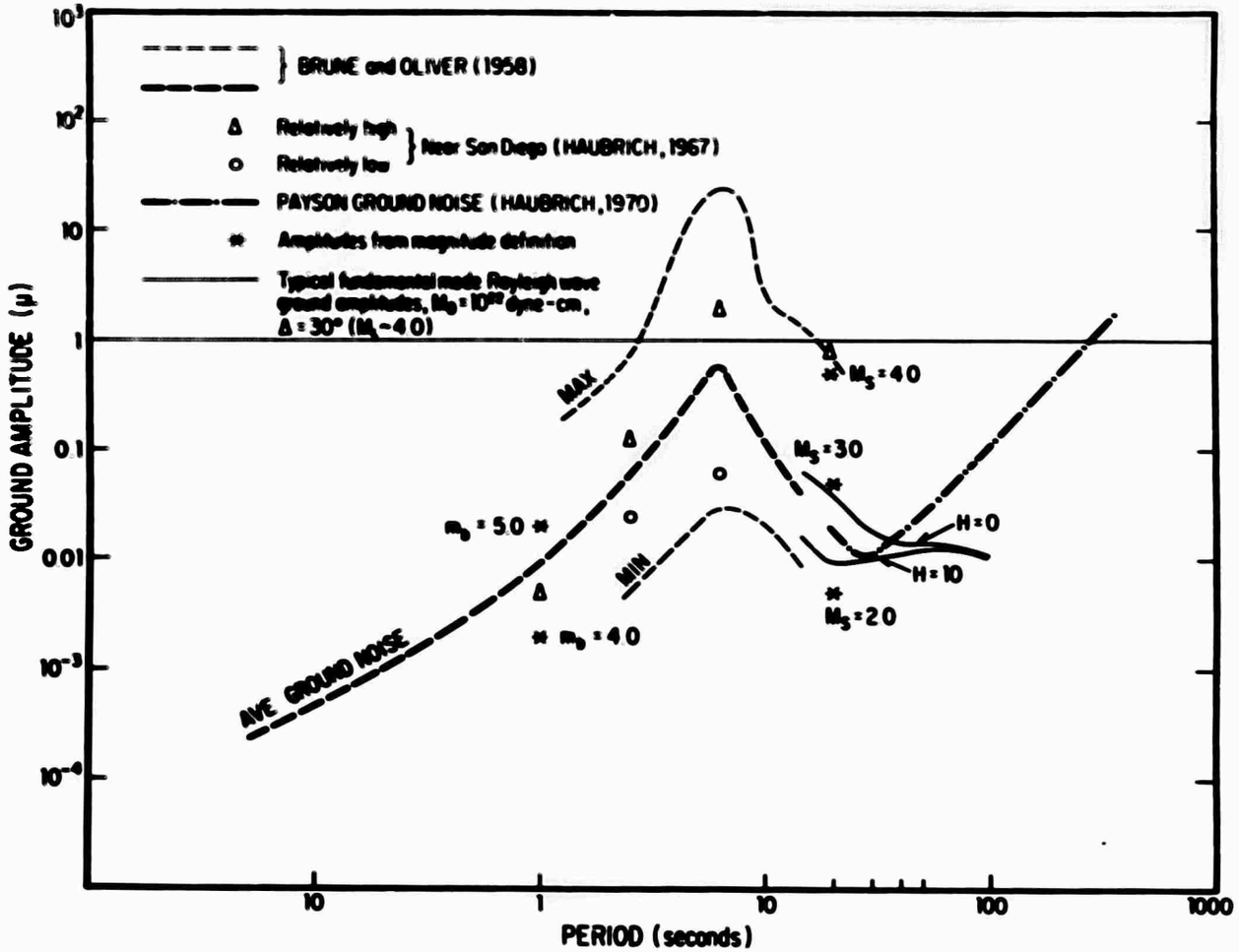

Figure 1. Seismic wave and ground-noise amplitudes plotted versus period.

SOURCE DIMENSIONS OF NUCLEAR EXPLOSIONS AND SMALL SHALLOW EARTHQUAKES

By

M. Wyss[1]
J. N. Brune[1]
T. C. Hanks[2]
B. E. Tucker[1]

[1]Institute of Geophysics and Planetary Physics,
La Jolla, California

[2]California Institute of Technology,
Pasadena, California

ABSTRACT

Recent studies indicate that source dimensions of small earthquakes are about ten times larger than those of explosions of the same local magnitude. Since this difference is associated with differences in the seismic spectra, explosions and earthquakes within the magnitude range studied can in principle be discriminated on the basis of seismic recordings.

INTRODUCTION

It is difficult to measure the source dimensions of small earthquakes since they usually do not produce obvious surface breaks. Recently, the surface breaks of two relatively small magnitude earthquakes, the Parkfield (Brown and Vedder, 1967) and the Imperial (Brune and Allen, 1967) earthquake, have been documented. Both events were associated with the San Andreas fault system and had larger source dimensions than would have been expected on the basis of extrapolations from larger magnitude data. Combining field observations with analysis of seismic waves Wyss and Brune (1968) suggested relatively large source dimensions for seven Parkfield aftershocks with local magnitudes, M_L, between 3 and 5.

For earthquakes which do not rupture the surface but are large enough to produce a distinct aftershock sequence, the source dimensions can be estimated from the aftershock distribution. Liebermann and Pomeroy (1970) have summarized this kind of data for $M_L > 4.5$. They found that between magnitudes 4.5 and 6.0, the fault dimensions fell between the earlier curves for large magnitudes and the curve of Wyss and Brune (1968).

For explosions and earthquakes alike, the source dimensions can be estimated by relating the peak or corner frequency to the source dimensions (e.g. Sharp, 1942; Kasahara, 1957). Smith et al (1967) and Schick (1968) have estimated the dimensions of earthquakes with $M_L \approx 0.75$ and $M_L \approx 2.5$ respectively, using the amplitude spectra of body waves. The dimensions they found agree with the length-magnitude relation for small earthquakes obtained by Wyss and Brune (1968). Many investigators have deducted equivalent source dimensions for explosions from the shape of amplitude spectra, their results collected from the literature are given in Table I.

The best way to see the difference in the amplitude spectra of explosions and earthquakes is of course to compare the spectra. The spectra are not generally available but two parameters that approximately describe the spectra are available, the magnitude and the source dimension or corner frequency. If we plot source dimensions against magnitude, we essentially compare the turn (or peak) frequency as a function of the level of the amplitude spectrum at the frequency at which the magnitude is obtained.

DATA

In this summary, we collected existing data on source dimensions of earthquakes and underground nuclear explosions and added 32 new fault lengths for earthquakes with $0.75 < M_L < 5.2$. Almost all of these source dimensions were estimated from the corner frequency of S-wave amplitude spectra. The way the data were obtain will be described in detail in three shortly forthcoming publications.

It should be emphasized that we have not assumed that the local magnitude, M_L, of a seismic event is on the average, equal to any of the body wave magnitudes, m_b, m_b' or m_{sr} (Evernden, 1967). Liebermann and Pomeroy (1970) have assumed that $M_L = m_b'$ for earthquakes. We have preferred to keep our data homogeneous by using only M_L magnitudes. For explosions M_L was obtained from the California Institute of Technology seismic array except for the two explosions outside of Nevada for which m_b' was converted to M_L using the formula $M_L = 0.76\, m_b' + 1.38$. This equation was obtained from a comparison of Evernden's (1967) m_b' with M_L measured on the Caltech array for 47 Nevada explosions.

CONCLUSION

Recent studies suggest that source dimensions of small earthquakes are larger than those of explosions (Wyss and Brune, 1968; Brune, 1968; Liebermann and Pomeroy, 1970). In an earlier study, Press (1967) estimated that earthquakes and explosions had approximately equal source dimensions. His estimate was based on assumptions about the strain-energy in the source region, -- in particular, he assumed a 100 percent stress drop. Recently, however, it has been suggested by King and Knopoff (1968) and substantiated by Wyss (1970) that stress drop is an increasing function of magnitude and can be very small for small earthquakes. The overestimate of the stress drop at small magnitudes leads to an underestimate of the fault dimensions.

In Figure 1, all the presently available source dimensions of seismic events with known $M_L < 6$ are plotted. All these small shallow earthquakes have larger source dimensions than explosions of the same local magnitude M_L. The earthquakes with the shortest dimensions (Hanks and Brune, 1970; and Ryall et al, 1968) were located in regions which characteristically exhibit relatively great high frequency excitation and might be inferred to be under comparatively high stress (Wyss, 1970). Some of the shocks with small dimensions (Hanks and Brune, 1970; McEvilly, 1966) were located at depths between 10 and 20 km and could possibly be excluded as nuclear blasts on these grounds. For some other shocks with small dimensions, no depth determination was available. It is possible that particular regions could produce high stress or high stress drop earthquakes with dimensions of the size Press's (1967) theoretical curve predicts, i.e., comparable to explosions. More detailed regional studies of earthquake source dimensions are needed to clarify this possibility.

We conclude that recent data indicate explosions and small shallow earthquakes of the same magnitude in general differ in source dimensions by approximately a factor of 10 and can therefore, in principle, be discriminated on the basis of seismic spectra as well as radiation pattern. The actual feasibility of such discrimination of course depends on the conditions imposed on the data available.

REFERENCES

Archambeau, C.B., 1964, Elastodynamic source theory, Ph.D. Thesis, Calif. Inst. Tech.

Archambeau, C.B. and Sammis, C.G., 1970, in preparation, Seismic radiation from explosions in prestressed media and the measurement of tectonic stress in the earth.

Brown, R.D. and Vedder, J.D., 1967, Surface tectonic fractures along the San Andreas fault, the Parkfield-Cholame, California Earthquakes of June-August 1966, U.S. Geol. Surv. Profess. Paper, 579, 2-22.

Brune, J.N., 1969, Source dimensions of earthquakes and underground explosions of magnitude near 4.0, Earthquake Notes, v. XL, No. 2.

Brune, J.N., 1970, Tectonic stress and the spectra of seismic shear waves from earthquakes, J. Geophys. Res., in press.

Brune, J.N., Espinosa, A., and Oliver, J., 1968, Relative excitation of surface waves by earthquakes and underground explosions in the California-Nevada region, J. Geophys. Res., v. 68, p. 3501.

Brune, J.N. and Allen, C.R., 1967, A low-stress-drop low-magnitude earthquake with surface faulting: The Imperial, California earthquake of March 4, 1966, B.S.S.A., v. 57, p. 501-514.

Davies, J.B. and Smith, S.W., 1968, Source parameters of earthquakes and discrimination between earthquakes and nuclear explosions, Bull. Seis. Soc. Am., v. 58, p. 1503.

Evernden, J.F., 1967, Magnitude determination at regional and near-regional distances in the United States, Bull. Seis..Soc. Am., v. 57, p. 591.

Hanks, T.C. and Brune, J.N., 1970, Seismicity of the San Gorgonio Pass (abstract) Trans. Am. Geophys. Union, v. 51.

Kasahara, K., 1957, The nature of seismic origins as inferred from seismological and geodetic observations, Bull. Earthquake Res. Inst., Tokyo Univ., v. 35, p. 473-532.

King, Chi-Yu and Knopoff, L., 1968, Stress drop in earthquakes, Bull. Seis. Soc. Am., v. 58, No. 1, p. 249.

Liebermann, Robert C. and Pomeroy, Paul W., 1970, Source dimensions of small earthquakes as determined from the size of the aftershock zone, Bull. Seis. Soc. Am., v. 60, p. 879.

McEvilly, T.V., 1966, The earthquake sequence of November 1964 near Corralitos, California, Bull. Seis. Soc. Am., v. 56, p. 755.

McEvilly, T.V. and Cassaday, K.B., 1967, The earthquake sequence of September 1965, near Antioch, California, Bull. Seis. Soc. Am., v. 57, p. 113.

Press, F., 1967, Dimensions of the source region for small shallow earthquakes, Proceedings of the VESIAC Conference on the Current Status of Future Progress for Understanding the Source Mechanism of Shallow Seismic Events in the 3 to 5 Magnitude Range, VESIAC Rept. 7885-1-X, p. 155.

Romney, C., 1959, Amplitudes of seismic body waves from underground nuclear explosions, J. Geophys. Res., v. 68, p. 1489.

Ryall, A.T., Van Worner, J.D. and Jones, A.E., 1968, Triggering of microearthquakes by earth tides, and other features of the Truckee, California earthquake sequence of September 1966, Bull. Seis. Soc. Am., v. 58, p. 215.

Sharpe, J.A., 1942, The production of elastic waves by explosive pressures. I. Theory and empirical field observations, Geophysics, v. 7, p. 144-154.

Shick, R., 1968, Untersuchungen über die Bruchausdehnung and Bruchgeschwindigkeit bei Erdbeben mit kleinen Magnituden (M < 4), Zeitschrift für Geophysik, v. 34, p. 267.

Smith, S.W., Sammis, C.G. and Jackson, W.H., 1967, Microearthquake source dimensions and energy release (abstract), Trans. Am. Geophys. Union, v. 48, p. 201.

Thirlaway, H.I.S. and Carpenter, E.W., 1966, Seismic signal anomalies, travel times, amplitudes and pulse shapes, Proceedings of the VESIAC Special Study Conference on Seismic Signal Anomalies, Travel Times, Amplitudes and Pulse Shapes, VESIAC Rept. 4410-99-X, p. 119.

Toksöz, M.N., Ben-Menahem, Harkrider, D.G., 1964, Determinations of source parameters of explosions and earthquakes by amplitude equalization of seismic surface waves, 1. Underground nuclear explosions, J. Geophys. Res., v. 69, No. 43, p. 4365.

Toksöz, M.N., Harkrider, D.G. and Ben-Menahem, A., 1965, Determination of source parameters by amplitude equalization of seismic surface waves, 2. Release of tectonic strain by underground nuclear explosions and mechanisms of earthquakes, J. Geophys. Res., v. 70, p. 907.

Udian, A. S., 1965, A study of the aftershocks and focal mechanism of the Salinas-Watsonville earthquakes of August 31 and September 14, 1963, Bull. Geol. Soc. Am., v. 55, p. 85.

Werth, G.C and Herbst, R.F., 1963, Comparison of amplitudes of seismic waves from nuclear explosions in four mediums, J. Geophys. Res., v. 68, p. 1463.

Werth, G.C. and Randolph, P., 1966, The Salmon seismic experiment, J. Geophys. Res., v. 71, p. 3405.

Wideman, C.T. and Major, M.W., 1967, Strain steps associated with earthquakes, Bull. Seis. Soc. Am., v. 57, p. 1429.

Wyss, M. and Brune, J.N., 1968, Seismic moment, stress and source dimensions for earthquakes in the California-Nevada region, J. Geophys. Res., v. 74, p. 4681.

Wyss, Max, 1970, Observation and interpretation of tectonic strain release mechanisms, Ph.D. Thesis, Calif. Inst. Tech.

Wyss, M., Hanks, T.C., and Liebermann, R.C., 1971, in preparation, A comparison of P-wave spectra of earthquakes and nuclear explosions.

ACKNOWLEDGEMENT

This work was supported by National Science Foundation grant NSF-GA-19473.

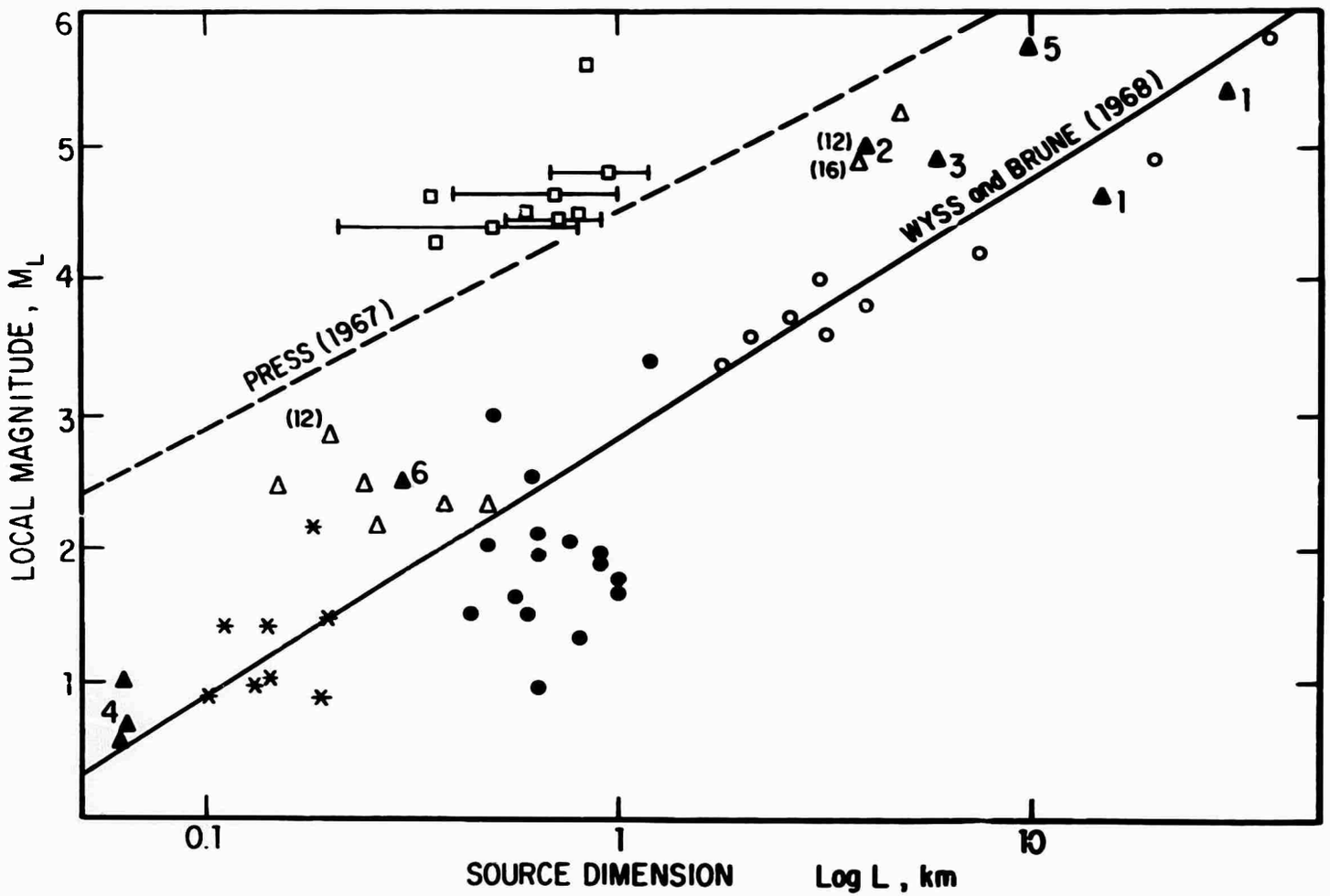

Figure 1. Estimated source dimensions of nuclear explosions (squares) and earthquakes (all other symbols) are compared on the basis of local magnitude. References are: o = Wyss (1970), ● = Wyss and Brune (1968), Δ = Hanks and Brune (1971), ▲1 = Udias (1965), ▲2 = McEvilly (1966), ▲3 McEvilly and Cassaday (1967), ▲4 = Smith et al (1967), ▲5 = Ryall et al (1968), ▲6 = Schick (1968), * = Tucker and Brune (in preparation). Numbers in parenthesis indicate source depth in km.

TABLE 1

SOURCE DIMENSIONS OF UNDERGROUND EXPLOSIONS

Event	m_b^1	M_L	L = 2r (km)
Milrow	6.3	—	2.5[12]
Bilby	5.61[2]	5.6	0.84[9]
Shoal	4.6[2]	4.8	0.7[7] - 1.2[8]
Haymaker	4.52[2]	4.49[4]	0.8[7]
Salmon	4.35[15]	4.68	0.35[6], >0.3[14]
Gnome	4.27[2]	4.58	0.6[3]
Sedan (crater)	4.15[2]	4.6	0.4 - 1.0[5]
Hardhat	4.15[2]	4.45[4]	0.54[7] - 0.91[3]
Rainier	4.1[1]	4.4	0.22[3], 0.6[10], 0.8[13]
Fisher	3.45[2]	4.27[4]	0.36[3]

1 Romney (1959)

2 Evernden (1967)

3 Werth and Herbst (1963)

4 Bruns et al (1963)

5 Toksöz et al (1964)

6 Healy et al (1970)

7 Toksöz et al (1965)

8 Davies and Smith (1968)

9 Archambeau and Sammis (1970)

10 Press (1967)

12 Wyss et al (1971)

13 Archambeau (1965)

14 Wideman and Major (1967)

15 Werth and Randolph (1966)

DEDUCTION OF SEISMIC SOURCE PARAMETERS FROM LONG PERIOD WAVES

By

W. Stauder

The remarks which I have to make in commenting on or enlarging upon the presentation by the Chairman pertain to two applications of data from long period waves in deducing seismic source parameters. The first of these refers to the use of P wave amplitude data, and is readily applicable to data from WWSSN or other conventional stations. The second refers to the application of spectral ratios of direct surface waves at pairs of stations, and is particularly appropriate for the use of digital data from a world array of 10-12 long period stations. These topics are taken up in turn in the pages which follow.

BLANK PAGE

An application of P wave stationary phase approximation in determining source parameters by equalization procedures

A stimulus for the use of P wave amplitude data in determining source parameters arises from the personal observation of similarity of wave-form of the P wave from station to station for a given earthquake and of the diminishing of amplitude of the initial P wave at stations which after analysis and comparison of all the data are shown to be near nodal lines. This personal experience was made more objective in a study by Nuttli (Nuttli and Gudaitis, 1966).

Nuttli measured the amplitude of the first half-cycle of the P wave at numerous stations for the Kodiak Island earthquake of February 6, 1964. These amplitude data, corrected only for instrumental response, are shown in Figure 1. The scatter in the data is considerable.

The fault plane solution of the particular earthquake is known (Stauder and Bollinger, 1966). The theoretical P wave amplitude radiated by a double couple point source in a homogeneous medium is given by the relation

$$u_p = \frac{2}{4\pi\rho} \frac{xy}{\alpha^3 R^3} K'(t-\frac{R}{\alpha}) \qquad (1)$$

where ρ is the density, α the P wave velocity, R distance along the ray, K(t) the source time function, and x and y the space coordinates of an observing point with respect to the mechanism axes. Nuttli corrected the observed amplitudes by dividing by the factor xy appropriate to each station.

The results are shown in Figure 2. The character of the symbols in the figure is related to the distance of a point from a nodal line, or, equivalently, to the magnitude of the factor xy. It is noted that the scatter is considerably reduced, with the exception of a few points for which values of xy are less than 0.1, i.e., points near nodal lines. By perturbing the mechanism solution by only a few degress in the dip and dip directions of the nodal planes, a solution was obtained for which even these exceptions disappeared and for which the residuals in observed versus calculated amplitudes were a minimum.

The final solution obtained in this way is shown in Figure 3. The line drawn on the figure is the amplitude variation expected from geometric spreading only, based on the Jeffrey-Bullen P wave travel time curve for 0.00R. The correspondence between the observed amplitudes corrected for focal mechanism and the theoretical amplitudes is good. One may conclude that the chief factor in the scatter of P wave amplitude data is the effect of the radiation pattern at the source.

These observations suggest the possibility of seeking a focal mechanism solution for which some quantity, say the variance, S, of the observed versus computed amplitudes is a minimum, where

$$S = \frac{\sum_{i=1}^{N} (A_{iobs} - A_{icalc})^2}{N} \qquad (2)$$

In principle this is, of course, a well established technique, that of the body-wave equalization procedure which was proposed by Ben-Menahem et al (1965) and has been applied to a number of earthquakes (Teng and Ben-Menahem, 1965; Ben-Menahem et al, 1968; Khattri, 1969). In a recent paper Chandra (1970) has further applied the method of equalization of P wave spectral amplitudes to determine the focal mechanism of five earthquakes, and has compared the results with solutions from the first motion of P and from the polarization of the S wave. He found close agreement in the solutions determined independently by the three procedures.

In the application here proposed, however, there is question not so much of the spectral amplitudes of P equalized to the source as of the amplitude of the first half-cycle of the P wave observed in the time domain. That is, the amplitude of the first half-cycle of the P wave is considered to represent the spectrum of the wave at the predominant period of the P wave. This is a stationary phase approximation. Teng and Ben-Menahem first used the term in this connection and applied the stationary phase approximation technique to the SH waves of the Banda Sea earthquake (Teng and Ben-Menahem, 1965). Chandra (Teng and Ben-Menahem, 1965). Chandra (1970b) has applied the same technique systematically to the P waves for a group of eight earthquakes. He found that the stationary phase solutions agreed with solutions previously determined by equalization of the P wave spectra.

A stationary phase approximation, since it utilizes only the first half-cycle, or event the first quarter cycle (P wave onset to first peak or trough) may be considered to sample the direct P arrival, uncontaminated by converted waves in the crust beneath the stations or in the neighborhood of the source. It is potentially applicable, therefore, to shallow focus earthquakes as well as to the isolated signals of P waves from deep focus shocks.

Even after equalization to the source, P wave amplitudes will vary in absolute value depending upon the magnitude of the earthquake In order to compare equalized amplitudes to calculated amplitudes a normalizing factor must be introduced. For this, following

(3)

Jarosch (1968), we let

$$A_{iobs} = k\, A_{icalc} + e_i \qquad (3)$$

where A_{iobs} is the observed amplitude at the ith station

A_{icalc} is the calculated amplitude as given by equation (1)

k is a constant to be determined

e_i is the error in the ith observation.

In order to minimize the sum of the squares of the errors, e_i, we choose k so that

$$k = \frac{\sum A_{iobs}\, A_{icalc}}{\sum A_{icalc}\, A_{icalc}} \qquad (4)$$

A value of k may be so obtained for any orientation of the source axes. But a search program is introduced in order to seek that orientation of the source axes for which

$$\frac{\sum \left(\frac{1}{k} A_{iobs} - A_{icalc}\right)^2}{N} \qquad (5)$$

is a minimum. A best fitting solution is thus obtained in a manner quite analogous to the procedure proposed by Ben Menahem et al (1965) in the equalization and comparison of spectral amplitudes.

An illustrative example, and a presentation of the results in a plane other than the geographic plane, may help to summarize both the method and a limitation common to all equalization techniques. Figure 4 presents the conventional P wave first motion and S wave polarization mechanism solutions for a Hokkaido earthquake of October 25, 1965. It is noted that the azimuthal coverage of stations about the epicenter is rather good, and that one nodal plane is well determined by the P wave first motion. The positions of both nodal planes may be fixed by a best fit to the S wave polarization data.

In order to apply the equalization of the amplitudes to the focal sphere by the stationary phase approximation, the amplitudes and periods of the first half-cycle of the P wave were determined at 25 stations. These observations were then equalized to the source by taking into account the effect of the instrument and of the crust,

and by compensating for geometric spreading and absorption in the mantle. The results of the search program are displayed in Figure 5. The observed equalized amplitudes are presented on the left, the calculated amplitudes for the best fitting orientation of the focal axes on the right.

As has been pointed out by users of this technique, the graphs of Figure 5 are a two dimensional presentation of what in reality is a three dimensional figures; the irregularities of the amplitude diagrams are a function not of azimuthal dependence but of difference in the take-off angle at the source. For example, Figure 6 shows the variation in amplitude as a function of azimuth corresponding to the greatest and to the least take-off angle for the particular observations used in the examination of this earthquake. While either curve is smooth, it is readily seen that if rays corresponding to different take-off angles are plotted on a polar graph a quite irregular figure can result. Hence the star-like shape of the observed and calculated amplitude plots.

While for surface waves it is necessary to present a radiation pattern in a geographic plane, this does not seem to be necessary, or even of particular advantage, for the reduction and presentation of body wave amplitude data. A presentation in terms of the focal axes may be more instructive.

In terms of spherical coordinates referred to the source axes, the amplitude of the P wave on the surface of a sphere of radius R equation (1) is given by

$$u_p = \frac{\sin^2\theta \sin 2\phi}{4\pi\rho\alpha^3 R} K'\left(t - \frac{R}{\alpha}\right) \qquad (6)$$

where ϕ is measured in the xy plane, or in the plane of the forces, and θ is measured from the Z or B (null) axis. The variation with ϕ is the familiar four-lobed P wave radiation pattern. Both ϕ and θ are readily related to the azimuth and take-off angles of a given ray through the direction cosines of the mechanism axes relative to the geographic axes. The amplitude along a ray making an angle θ may in turn be reduced to the amplitude of a ray leaving a source of the same strength at an angle $\theta = \pi/2$ by dividing the observed amplitude by $\sin^2\theta$. In this way the radiation pattern is reduced to the xy plane or plane of the forces. Or, equivalently, one view the radiation pattern from the B axis, looking toward the xy plane.

Figure 7 presents the amplitude data of the Hokkaido earthquake in this fashion. One sees immediately the effect of the nodal line and the degree of closeness of fit of the observed P wave amplitudes with the calculated amplitudes for the orientation of the focus selected. One sees as well, and more graphically than in other presentations, the limitation in the distribution of data over the focal

sphere. Even with good geographic distribution of observations, the data points are spread over barely a quarter of the xy plane covers several quadrants (strike slip faulting in a vertical plane) a presentation as in Figure 7 may serve to identify the plane of faulting and the direction rupture propagation; the lobes will be asymmetric, enlarged in the direction of the rupture.

A final reference to the quantity k determined above (equation (4)). If we let $\bar{A}$ be an average value of the amplitude on the focal sphere, then

$$\bar{A}_{obs} = k \bar{A}_{calc}$$

and since

$$M \propto \log \bar{A}_{obs}$$

we have

$$M \propto \log (k\bar{A}_{calc})$$

or

$$M \propto \log k + \log \bar{A}_{calc}.$$

The value of $\bar{A}_{calc}$ is obtained by the relation

$$\bar{A}_{calc} = \frac{\int 2xy \, dS}{\int dS} = .424$$

Thus the value of k may be used to determine a magnitude derived simultaneously from many observations of the P wave amplitude and corrected for the effect of the radiation pattern of the source.

REFERENCES

Ben-Menahem, A., Smith, S.W., and Teng, T.L., 1965, A procedure for source studies from spectrums of long-period seismic body waves, BSSA, v. 55, p. 203-235.

Ben-Menahem, A., Jarosch, H., and Rosenmen, M., 1968, Large scale processing of seismic data in search of regional and global stress patterns, BSSA, v. 58, p. 1899-1932.

Chandra, U., 1970a, Comparison of focal mechanism solutions obtained from P and S wave data, JGR, v. 75, p. 3411-3420.

Chandra, U., 1970b, Stationary phase approximation in focal mechanism determination, BSSA, v. 60, (in press).

Jarosch, H.S., 1968, Body wave magnitude and source mechanism, Seismic Data Laboratory Report No. 225, Teledyne Geotech, Inc.

Khattri, K. N., 1969, Focal mechanism of the Brazil deep-focus earthquake of November 3, 1965, from the amplitude spectra of isolated P waves, BSSA, v. 59, p. 691-704.

Nuttli, O.W., and Gudaitis, V.V., 1966, On the amplitude of long period P waves (Abstract), Earthquake Notes, v. 37, p. 24.

Stauder, W., and Bollinger, G.A., 1966, The focal mechanism of the Alaska earthquake of March 28, 1964, and of its aftershock sequence, JGR, v. 71, p. 5283-5296.

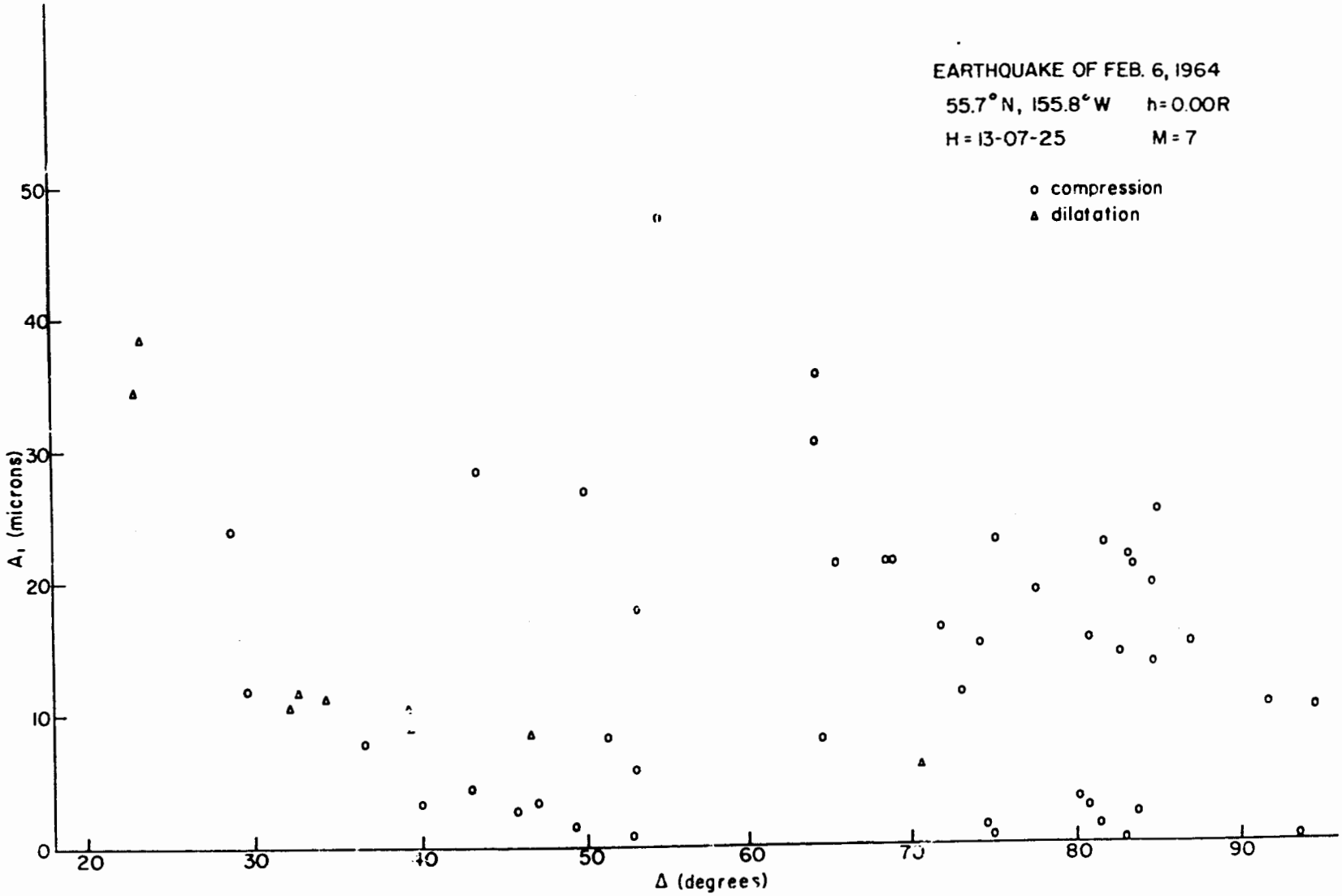

Figure 1. Amplitudes of first half-cycle of the P wave, corrected only for instrumental response, Kodiak Island earthquake of 6 February 1964.

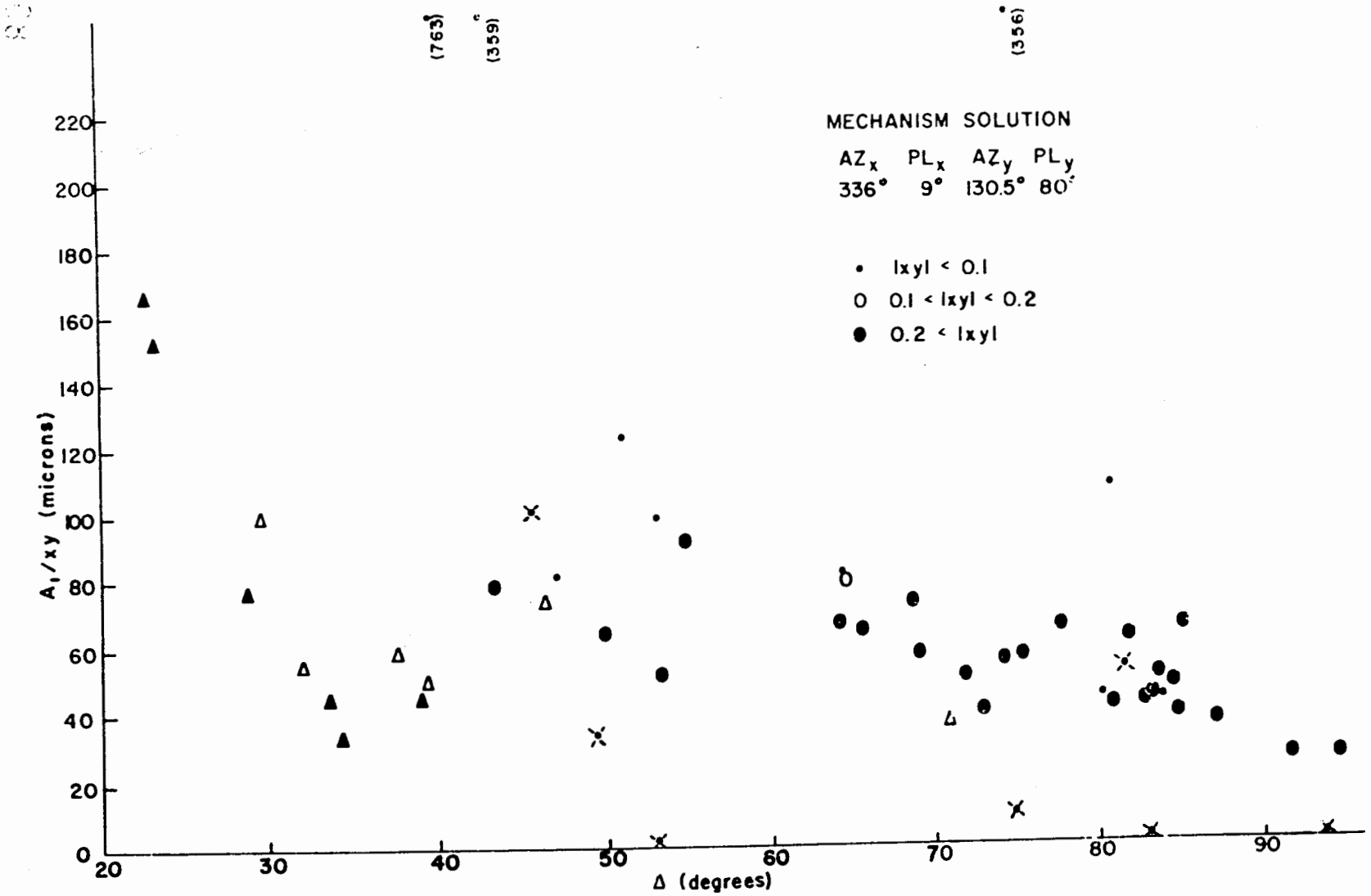

Figure 2. Amplitudes of first half-cycle of the P wave corrected for focal mechanism as determined by Stauder (1965).

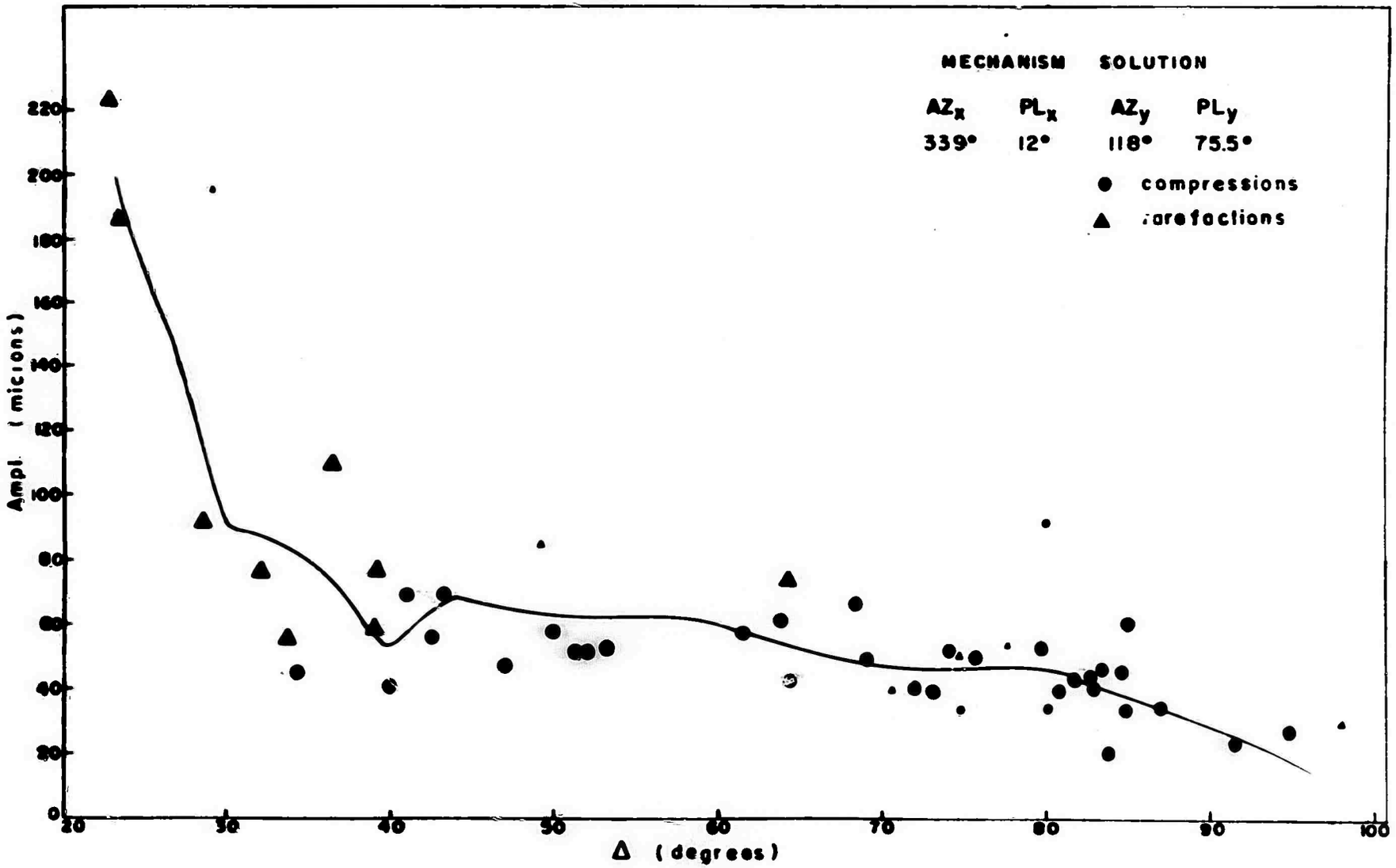

Figure 3. Amplitude of first half-cycle of the P wave corrected for adjusted focal mechanism. Solid line is the amplitude expected on the basis of the Jeffreys-Bullen travel time tables.

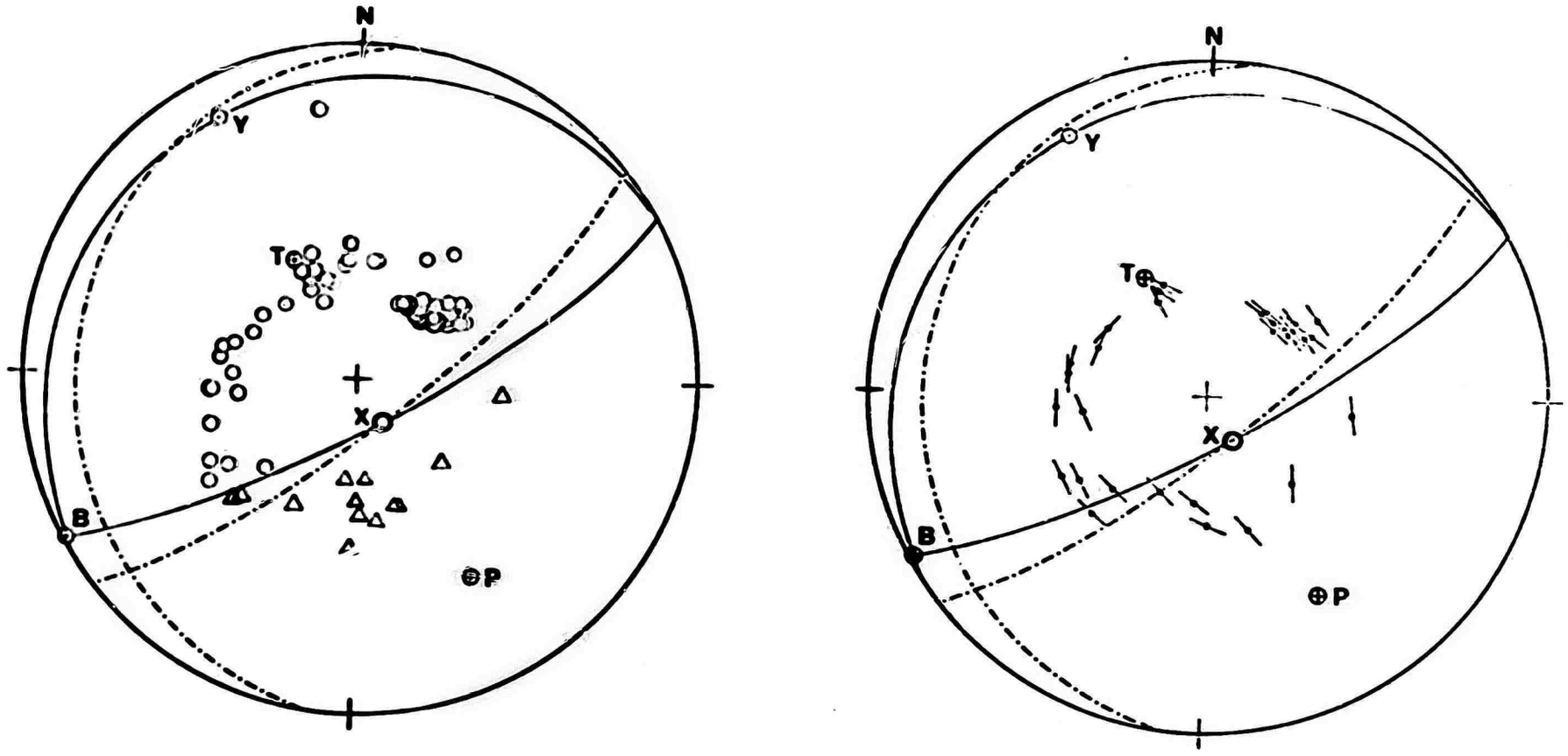

Figure 4. Conventional first motion of P and polarization of S mechanism solution for the Hokkaido earthquake of 25 October 1965.

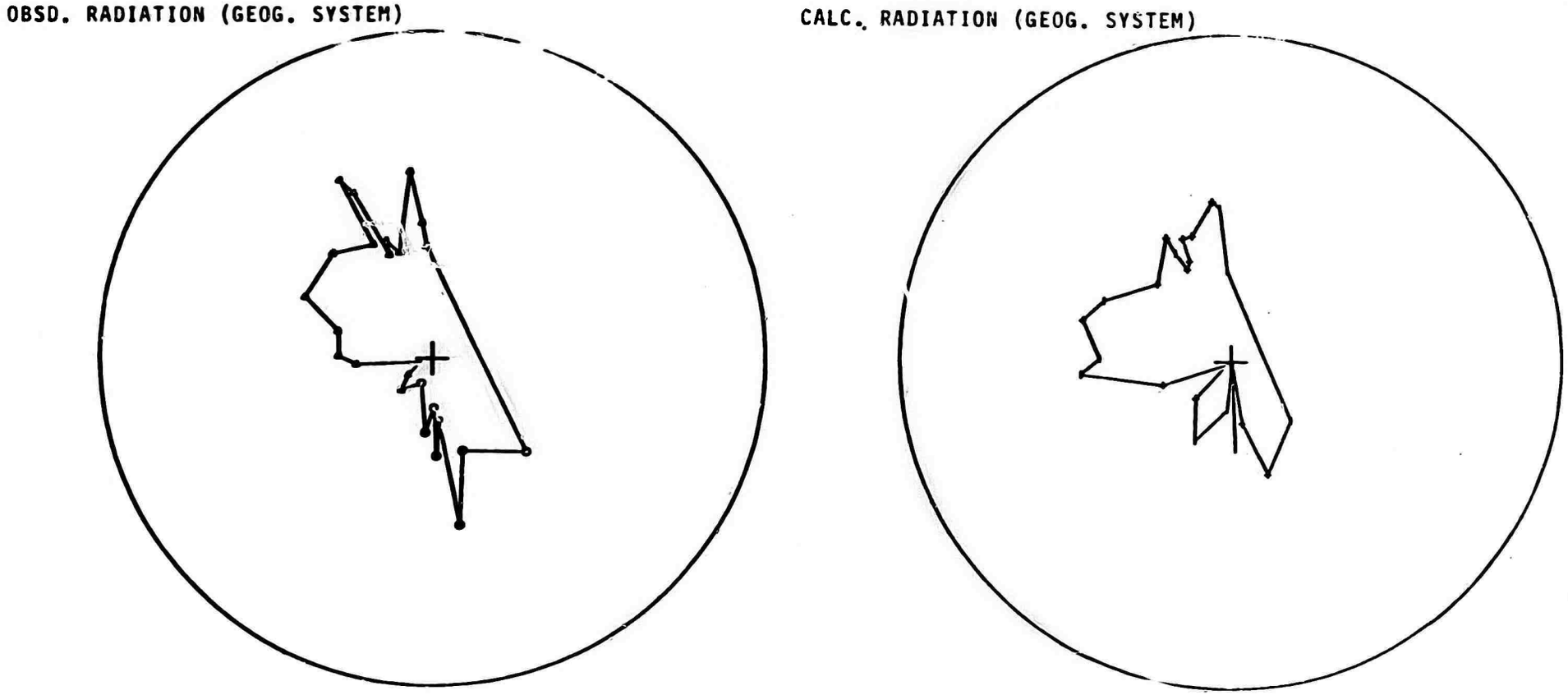

Figure 5. Observed amplitudes (left figure) equalized to the source, and the calculated P amplitudes (right figure) for best fitting double couple source, earthquake of 25 October 1965.

CONTINUOUS RADIATION (GEOG. SYSTEM)

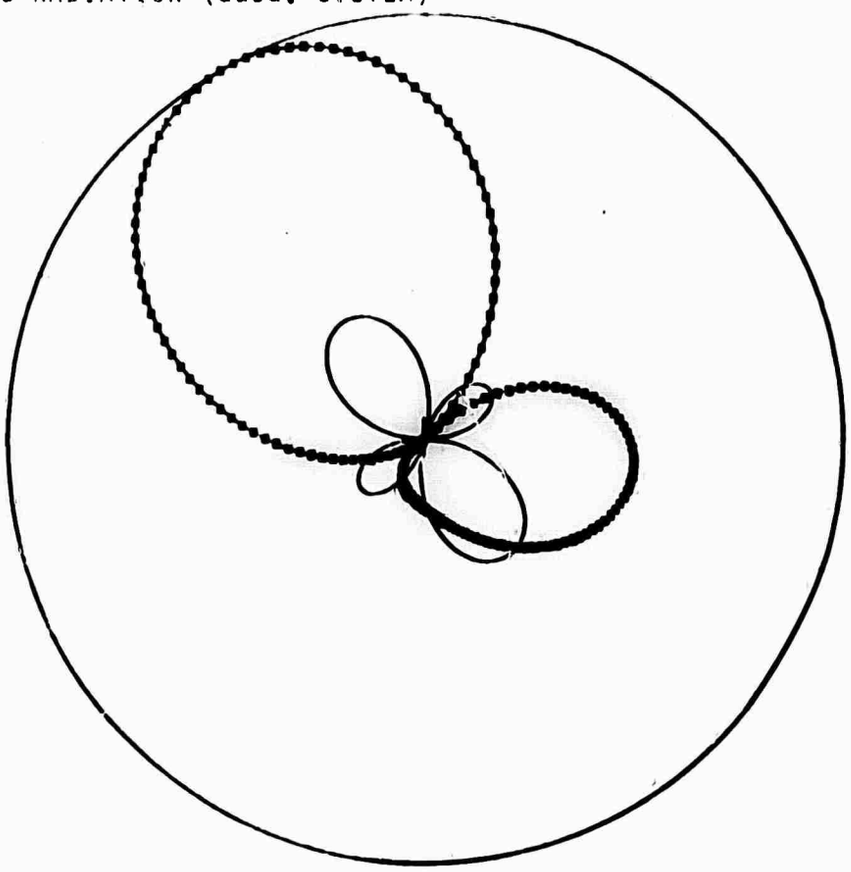

Figure 6. Variation in calculated P wave amplitude for take-off angles corresponding to the greatest and least value of i_h for stations represented in Figure 5.

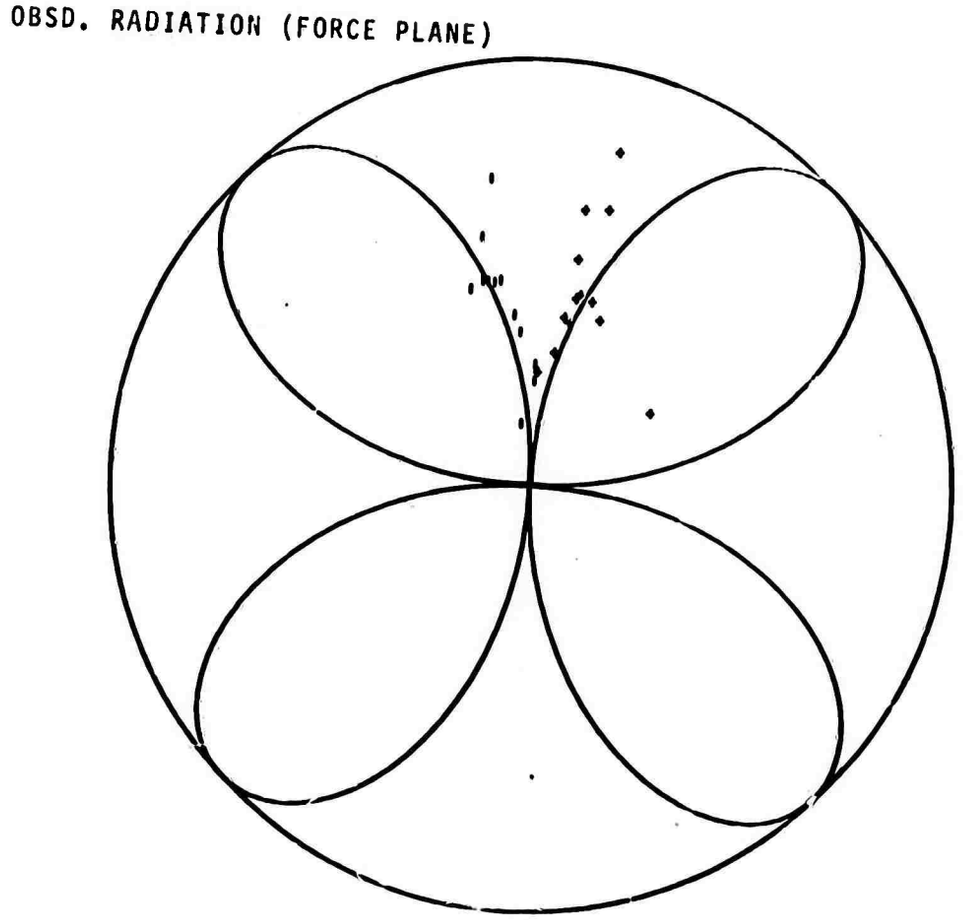

Figure 7. Amplitude data for the Hokkaido earthquake reduced to the xy plane.

SOURCE PARAMETERS OF EARTHQUAKES FROM SPECTRA OF RAYLEIGH WAVES

By
A. Udias

Saint Louis University

LENGTH OF FAULT AND VELOCITY OF RUPTURE

Ben-Menahem (1961) has developed the expressions for the far field displacements of Rayleigh waves radiating from a propagating fault of finite dimensions. The model of the fault is a surface of length b and width d. The propagating fracture is represented by a point source propagating along the b dimension with a velocity v and radiating energy as it propagates. For a vertical strike-slip fault and a propagating double couple the displacement of the vertical component of the Rayleigh wave is given by

$$U_z^R(\omega) = \frac{\sin 2}{\sqrt{v}}\, g_z(\omega)\, \sqrt{k_\beta}\, \frac{\sin X_R}{X_R}\, e^{i(\phi_R + \frac{3\pi}{4})} \qquad (1)$$

where

$$X_R = \frac{\pi b f}{C_R}\left(\frac{C_R}{v} - \cos\theta\right) \qquad (2)$$

The effect of the finite dimensions is included in the factor $X_R(\omega,\theta)$. To isolate this factor Ben-Menahem defined the directivity function, D, as the ratio of the spectral amplitudes of the surface waves corresponding to waves leaving the source in opposite directions.

$$D = \frac{U_z^R(\theta)}{U_z^R(\theta+\pi)} = \frac{\sin Z_R(\theta)\; X_R(\theta+\pi)}{\sin X_R(\theta+\pi)\; X_R(\theta)} \qquad (3)$$

Since the only factors which depend on θ in equation (1) are $\sin X_R/X_R$ and $\sin\theta$, we can generalize the expression for the directivity to be the ratio of the spectral amplitudes at two stations corresponding to rays leaving the source with an arbitrary angle, α, between them. Thus

$$D_\alpha = \frac{U_z^R(\theta)}{U_z^R(\theta+\alpha)} = \frac{\sin\{\frac{\pi b f}{C_R}(\frac{C_R}{v} - \cos\theta)\}(\frac{C_R}{v} - \cos(\theta+\alpha))\sin 2\theta}{\sin\{\frac{\pi b f}{C_R}(\frac{C_R}{v} - \cos(\theta+\alpha))\}(\frac{C_R}{v} - \cos\theta)\sin 2(\theta+\pi)} \qquad (4)$$

Minima in this function occur at zeros of the numerator, that is, at values of the argument of the sine function

$$\frac{\pi bf}{C_R}\left(\frac{C_R}{v} - \cos\theta\right) = n\pi, \quad n = 0, 1, 2, \ldots.$$

Maxima occur at zeros of the denominator, or for

$$\frac{\pi bf}{C_R}\left[\frac{C_R}{v} - \cos(\theta+\alpha)\right] = n\pi, \quad n = 0, 1, 2, \ldots.$$

The values of the frequency at which either maxima or minima occur can be used to determine the fault length b. For example, for the first order extrema

$$b = \frac{C_R}{f_{max}\left[\frac{C_R}{v} - \cos(\theta+\alpha)\right]} = \frac{C_R}{f_{min}\left(\frac{C_R}{v} - \cos\theta\right)} \tag{5}$$

The directivity function, D, as defined originally (equation (1)) was used with R or G waves of consecutive order recorded at the same station. This procedure minimizes the sources of error, but reduces the use of the method to earthquakes sufficiently large to generate return surface waves or waves which circle the earth more than once. In theory nothing prevents using direct Rayleigh or Love waves recorded at different stations distributed at arbitrary but differing azimuths about the epicenter. In this event the more general directivity function, D_α, (equation (4)) applies. Allowance must be made, of course, for differences in epicentral distance, path of propagation, etc. This procedure makes it possible to apply the method to earthquakes smaller than M = 7.

The advantage of applying the more generalized expression for the directivity is that stations can be selected at which the Rayleigh waves are well recorded without the constraint of being 180° apart in azimuth. Since the directivity function is normalized, the amplitudes in the spectral ratios must be reduced to a common distance. This is done through the equation

$$\bar{A}_2 = A_2 \left(\frac{\sin\Delta_1}{\sin\Delta_2}\right)^{1/2} e^{-(\Delta_1-\Delta_2)\gamma} \tag{6}$$

As an example, the method here proposed is applied to the Aleutian Island earthquake of July 4, 1966. The two nodal planes of P are assumed to be known, and are taken from Stauder (1968). Figure 1 shows the orientations, AA' and BB', of these planes and also indicates the stations and their distribution about the source at which the direct Rayleigh waves were used in the analysis. The Rayleigh waves at these stations were digitized and a Fourier analysis made of the digitized data. In this process care must be taken to select a suitable time window, for it is important to exclude from the analysis any interference from later arrivals, lateral refractions, etc.

Given the spectra, as many combinations as possible of spectral ratios are formed. By application of equation (5), repeated from above

$$b = \frac{C_R}{f_{max}\left[\frac{C_R}{v} - \cos(\theta+\alpha)\right]} = \frac{C_R}{f_{min}\left(\frac{C_R}{v} - \cos\theta\right)} \qquad (5)$$

a value of b can be obtained from the first maximum or first minimum of any one of these spectral ratios. In so doing it is necessary to assume a value of v, the velocity of rupture. In fact, when using only the amplitude portion of the spectra there is no independent way of determining the fracture velocity, v. However, if many ratios are used for the calculation of b, we may assume different values of v and from these select that v which gives the least standard error for the mean value of b. In this manner we obtain a simultaneous estimate of both b and v.

A by-product of the method when a sufficient number of stations around the epicenter are used is the determination, through the proper choice of θ of the plane of faulting from the two nodal planes and the direction of fracture.

Figures 2 and 3 show two examples of the spectral ratios for the earthquake of July 4, 1966. The points in the figures are observational values of the spectral ratio for the pairs of stations indicated. The solid lines are the computed directivity function for the fault length, fracture velocity, and direction of fracture assumed for the best fit to the data. While there is some variation in the observed from the computed spectral ratio, the minima and maxima are well defined. For this Aleutian Island earthquake the NS striking plane is selected as the plane of faulting, with the fracture propagating southward. This is in keeping with the interpretation of this earthquake as an arc-arc transform fault.

Figure 4 shows a similar application to an earthquake in the Azores. The focal mechanism was determined by Sykes (1967). The

earthquake is strike-slip, with epicenter on a fracture zone.

Seismic moment

The seismic moment is calculated following the work of Aki (1966) and the theoretical results of Ben-Menahem and Harkrider (1964) from the spectral amplitudes of the vertical component of the Rayleigh waves at periods sufficiently large that the point source approximation of the source is valid.

Assuming a step function for the source time function the value of the moment is given by

$$M_o = \frac{|U(\omega)|(2\pi r)^{1/2} C_R \, e^{\gamma r}}{N_{rz}|\chi(\theta)|} \tag{7}$$

$U(\omega)$ is the spectral amplitude, r the distance, γ the attenuation coefficient, C_R the phase velocity, N_{rz} the Rayleigh wave singlet transfer function and $\chi(\theta)$ the radiation pattern function as defined by Ben-Menahem and Harkrider.

For the earthquakes studied here we calculated the moment at two values of the period, 100 and 50 seconds. For these periods the uncertainties in the assumed phase velocity and attenuation coefficient are small. The results are given in Table I.

Stress drop, seismic energy, and average dislocation

Values for the stress drop, σ, and average dislocation, $\bar{w}$, have been found from the above determined values of the moment and fault length using the relations

$$\bar{\omega} = \frac{M_o}{\mu A} = \frac{M_o}{\mu b d} \tag{8}$$

$$\sigma = \frac{1}{2} \frac{\omega_m \mu}{d} \tag{9}$$

where

$$\omega_m = \frac{4}{3} \bar{\omega} \tag{10}$$

The value of μ was taken as 3.3×10^{11} and the fault width equal to 10 km for the Aleutian earthquake and 5 km for that in the Azores. The results, again, are given in Table I.

REFERENCES

Aki, K., 1966, Generation and propagation of G waves from the Niigata earthquake of June 16, 1964, 2. Estimation of earthquake moment, released energy, and stress-strain drop from the G wave spectrum, Bull. Earthquake Res. Inst., Tokyo Univ., v. 44, p. 73-88.

Ben-Menahem, A., 1961, Radiation of seismic surface-waves from finite moving sources, BSSA, v. 51, p. 401-435.

Ben-Menahem, A., and Harkrider, D.G., 1964, Radiation patterns of seismic surface waves from buried dipolar point sources in a flat stratified earth, JGR, v. 69, p. 2605-2620.

Stauder, W., 1968, Mechanism of the Rat Island earthquake sequence of 4 February 1965 with relation to island arcs and sea-floor spreading, JGR, v. 73, p. 3847-3858.

Sykes, L.R., 1967, Mechanism of earthquakes and nature of faulting on the mid-oceanic ridges, JGR, v. 72, p. 2131-2153.

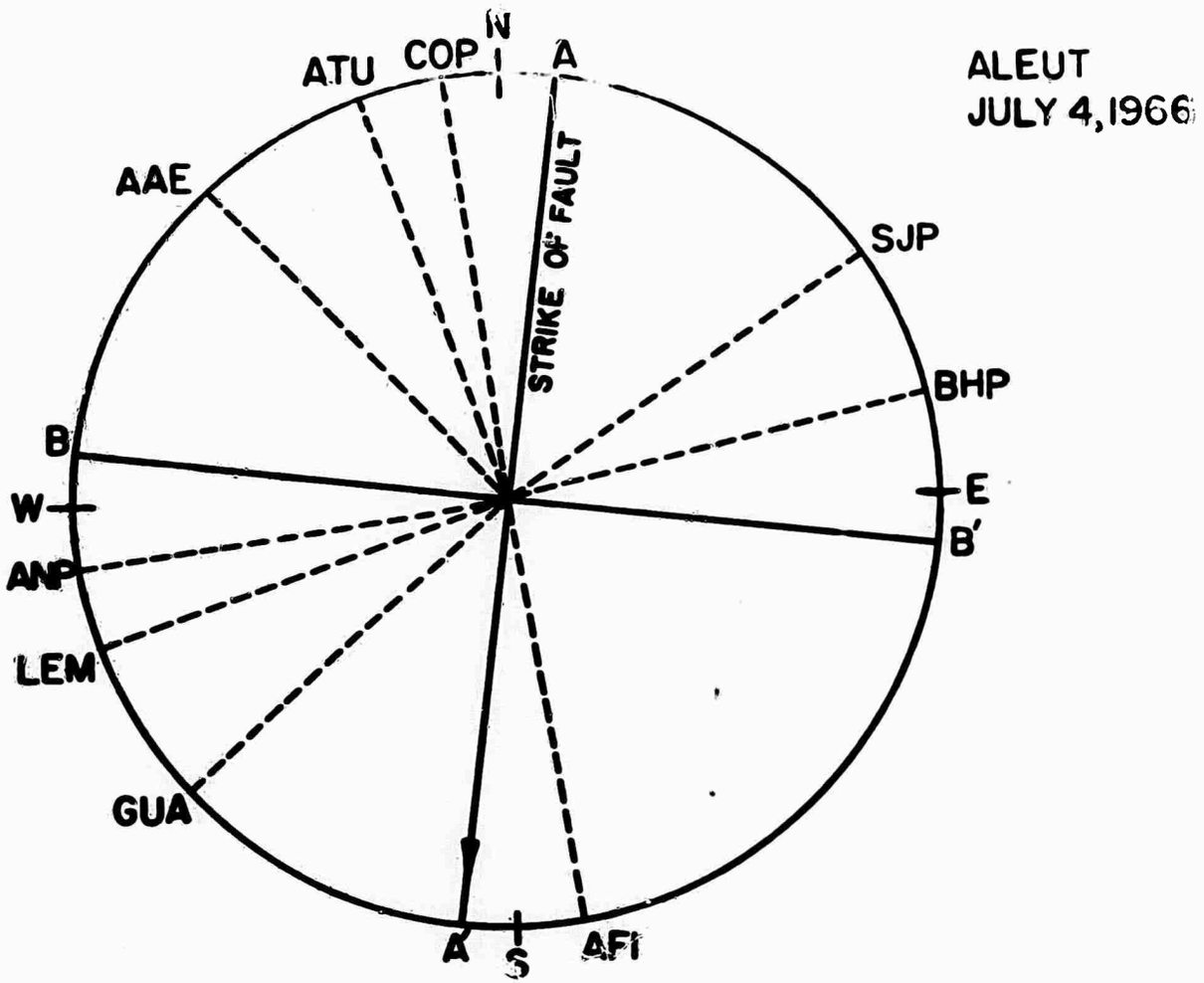

Figure 1. Orientation of nodal planes, AA', BB' and azimuthal relation of stations selected for surface wave analysis, Aleutian Island earthquake of July 4, 1966.

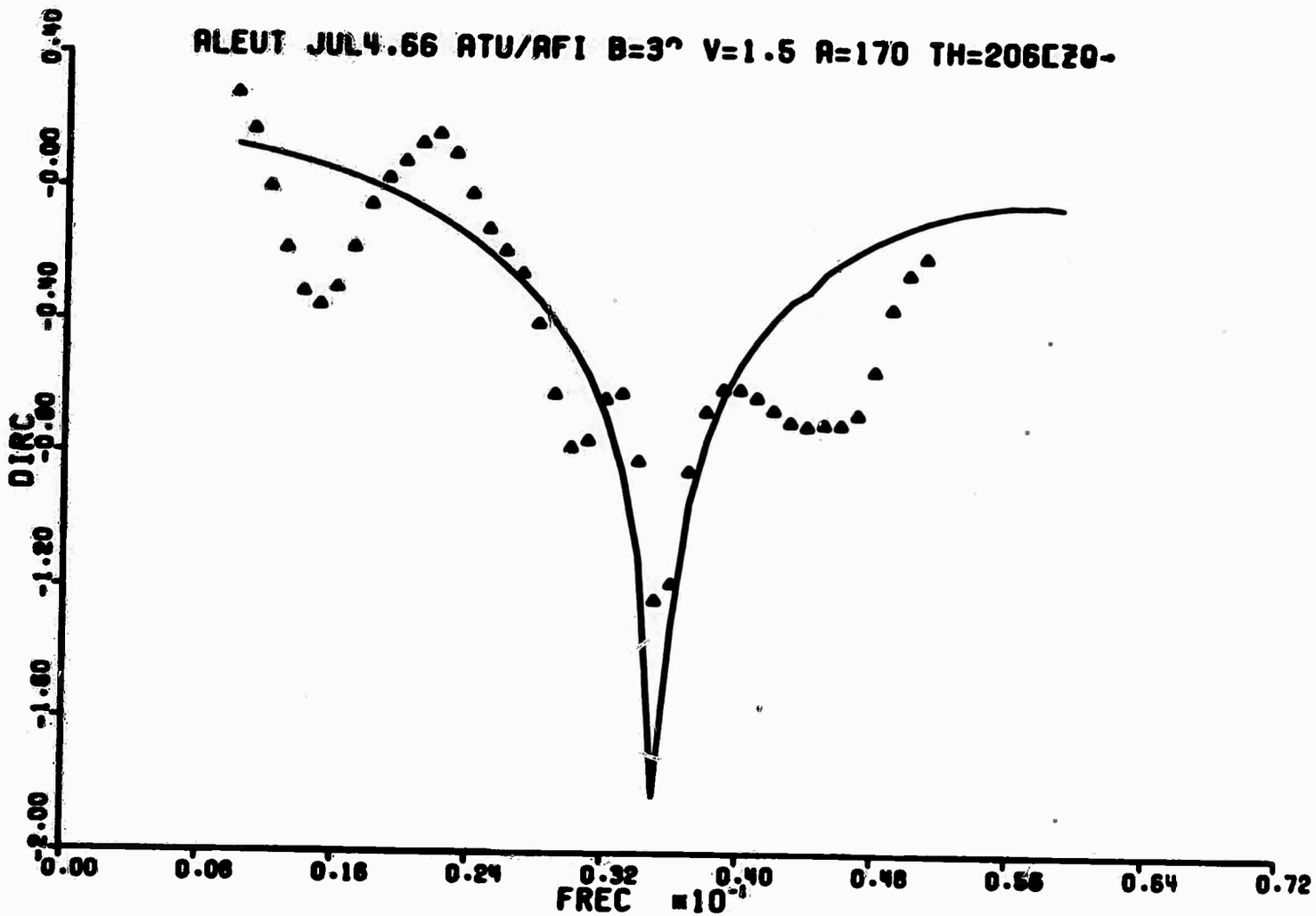

Figure 2. Spectral ratio for station pair ATU/AFI. Plotted points correspond to observational values, solid line to the theoretical spectral ratio for the values of b and v indicated, Aleutian Island earthquake of July 4, 1966.

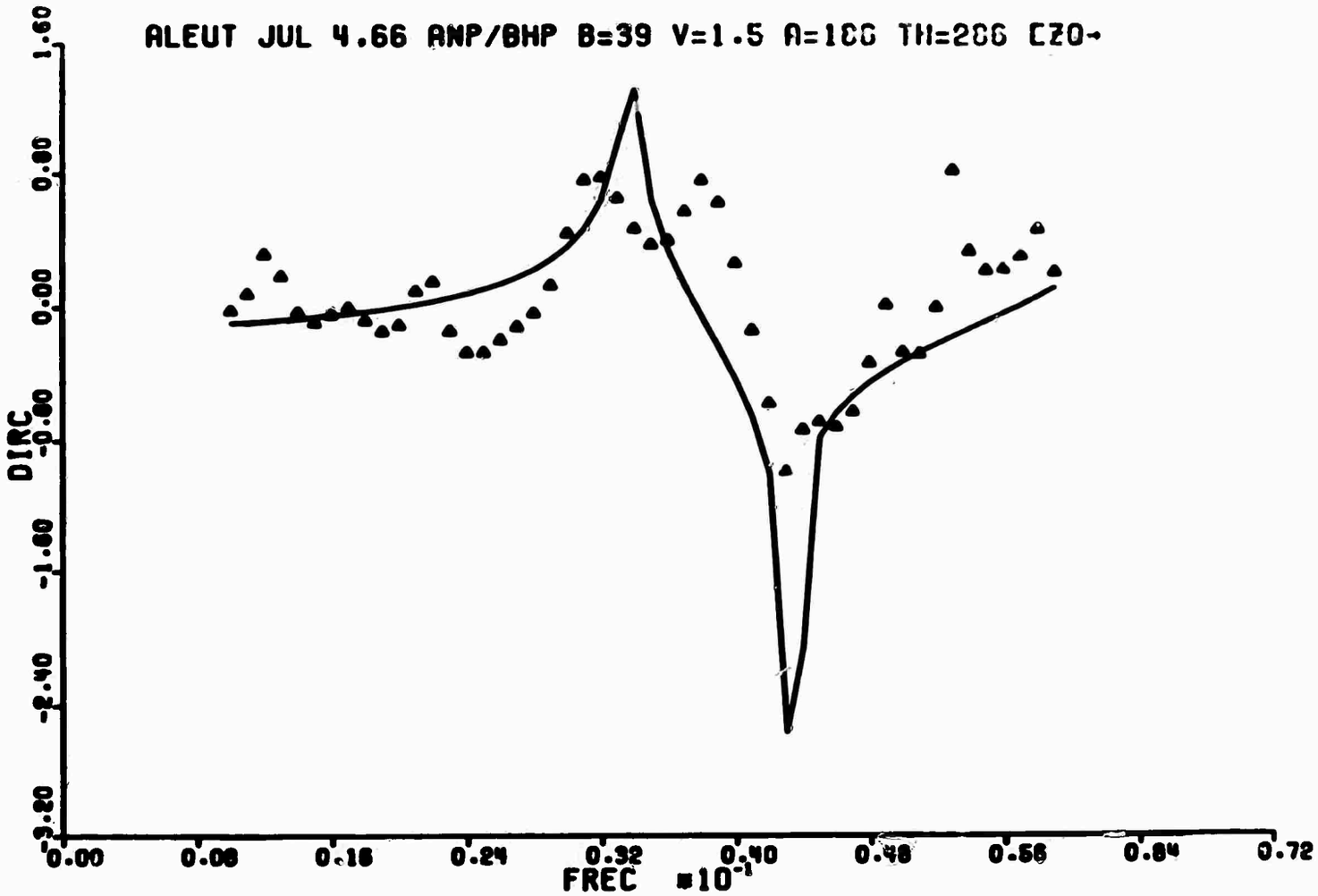

Figure 3. Spectral ratio for station pair ANP/BHP, Aleutian Island earthquake of July 4, 1966.

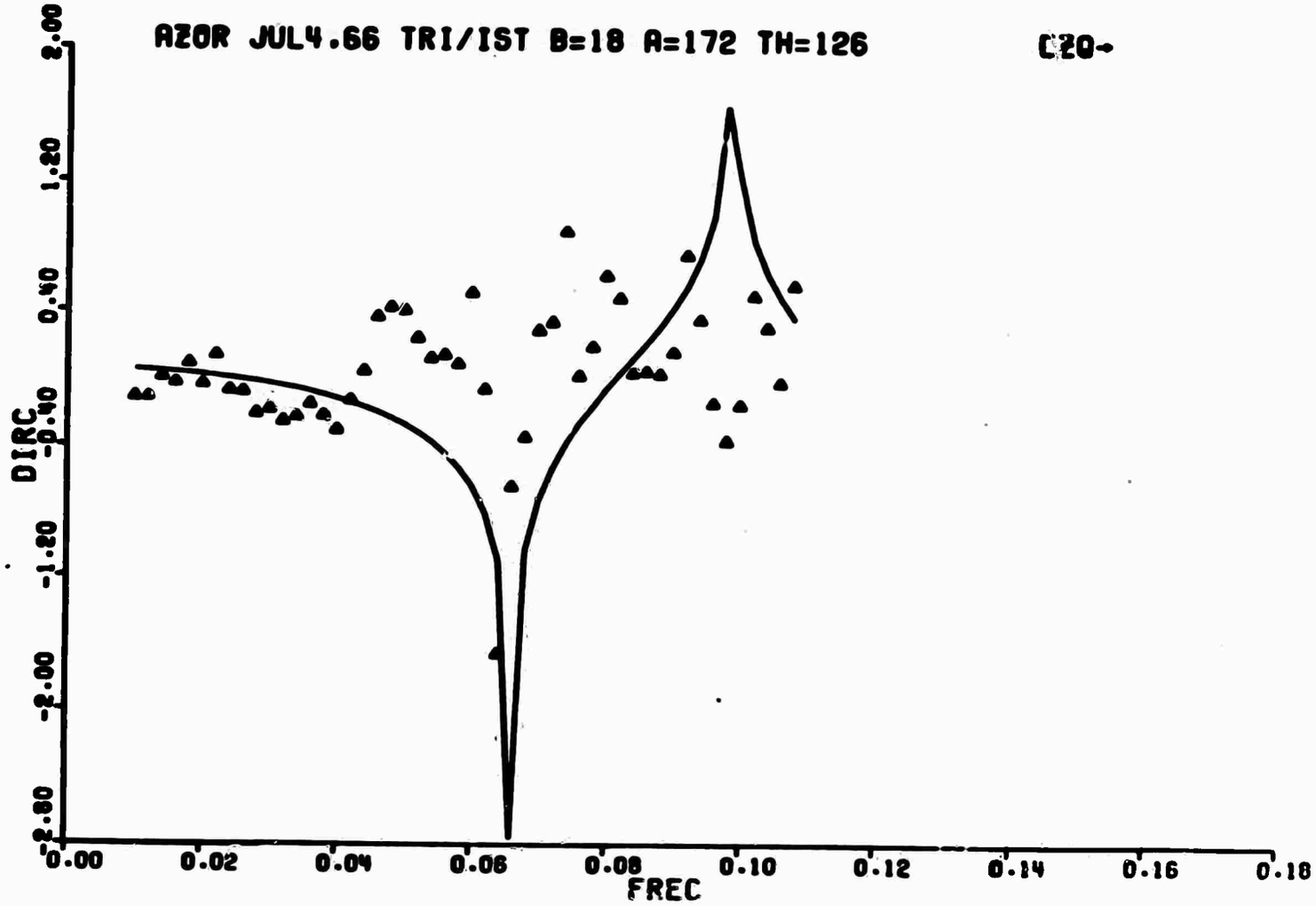

Figure 4. Spectral ratio for station pair TRI/IST, Azores earthquake of July 4, 1966.

TABLE I.

		JULY 4, 1966 18^h ALEUT	JULY 4, 1966 12^h AZORES
m_b		6.5 ±0.4	5.7 ±0.3
M_o	10^{25} dyne cm	14 ± 3.7	0.24±0.09
b	km	35 ±0.4	18 ± 1.8
d	km	10	5
v	km/sec	1.5	1.5
$\bar{w}$	cm	120	6.6
σ	bars	43	2.8

DIMENSIONS OF NUCLEAR EXPLOSIONS AND SMALL SHALLOW EARTHQUAKES

By

Max Wyss

James N. Brune

ABSTRACT

It is shown that source dimensions of small shallow earthquakes are an order of magnitude larger than those of explosions.

Explosions and earthquakes can be discriminated on the basis of seismic recordings if their source dimensions or source time functions are significantly different. If we can demonstrate that the source dimensions are different for equal magnitude events between magnitude 1 and 5, we have shown that in principal discrimination on the basis of spectral shapes is possible for such events. For two reasons such a possibility was doubted. Press (1967) estimated the source dimensions of small earthquakes and explosions to be of the same size. His estimate was based on reasonable assumptions about the strain-energy in the source region and in elastic waves. However, Press has assumed a 100 percent stress drop. Recently it has been found that stress drop is a function of magnitude and can be very small for small earthquakes (King and Knopoff 1968, Wyss 1970). The overestimate of the stress drop leads to an underestimate of the fault dimensions. The second reason to doubt that discrimation for small explosions was possible on the basis of spectral differences, came from the observation that it appeared as if the $M_S - m_b$, values of small explosions and earthquakes converged (Thirlaway and Carpenter 1966, Liebermann and Pomeroy, 1969). More recently, however, it was found that no such convergence took place (Pasechnik 1968, Basham 1969, Molnar et al 1969, Lacoss 1969). Equivalent source dimensions for explosions collected from the literature are given in Table 1. The local magnitude M_L is not equal to the body wave magnitude m_b or m_b^g. M_L for explosions was obtained from Pasadena records or estimated on the basis of m_b^g and m_{sr} (Evernden 1967) in order to compare the explosions with earthquakes for which only local magnitudes are available.

On this basis the source dimensions were compared in Figure 1. Most of the source dimensions were obtained from the peak or turn frequency of seismic spectra. Figure 1 therefore corresponds to a comparison of seismic spectra. For some of the larger earthquakes the dimensions were based on field observations or aftershock zones. A more complete summary of the latter approach including shocks with m_b and M_L magnitudes, is given by Liebermann and Pomeroy (1970).

Figure 1 shows clearly that all studied small shallow earthquakes have larger source dimensions than explosions in accordance with Wyss and Brune (1968) and Liebermann and Pomeroy (1970). The earthquakes with the shortest dimensions determined by Hanks and Brune (1970) and Ryall et al (1968) were located in regions under comparatively high stress (Wyss 1970). Some of the shocks with small dimensions by Hanks and Brune (1970) and McEvilly (1966) were located at depths between 10 and 20 km and could possibly be excluded as nuclear blasts on these grounds. For some other shocks with small dimensions no depth determination was available. It is possible that particular regions could produce high stress or high stressdrop earthquakes with dimensions like the ones surmised by Press (1967), i.e. with dimensions comparable to explosions. More detailed regional studies of earthquake source dimensions are needed to clarify this possibility.

The smallest nuclear explosion for which a source dimension was available, Sterling, was a decoupled event. It was exploded in the cavity produced by Salmon. The magnitude of Sterling is approximate only. However, it appears that it would be possible to confuse this event with an earthquake if as criterion only the relative source dimension is considered. It is possible that the source time function may still provide a discriminant for Sterling.

It is concluded that explosions and small shallow earthquakes differ in source dimensions by approximately an order of magnitude and can be discriminated on the basis of their seismic spectra.

TABLE I

SOURCE DIMENSIONS OF UNDERGROUND EXPLOSIONS

Event	m_b'	M_L	L = 2r (km)
Milrow	6.3	---	2.5[12]
Bilby	5.61[2]	5.6	0.84[9]
Shoal	4.6[2]	4.8	0.7[7] - 1.2[8]
Haymaker	4.52[2]	4.49[4]	0.8[7]
Salmon	4.35[15]	4.6	0.35[6], > 0.3[14]
Gnome	4.27[2]	4.5[2]	0.6[3]
Sedan (crater)	4.15[2]	4.6	0.4 - 1.0[5]
Hardhat	4.15[2]	4.45[4]	0.54[7] - 0.91[3]
Rainier	4.1[1]	4.4	0.22[3], 0.6[10], 0.8[13]
Fisher	3.45[2]	4.27[4]	0.36[3]
Sterling (decoupled)	1.3[11]	1.8	0.06[6]

1 Romney (1959)
2 Evernden (1967)
3 Werth and Herbst (1963)
4 Brune et al (1963)
5 Toksöz et al (1964)
6 Healy et al (1970)
7 Toksöz et al (1965)
8 Davies and Smith (1968)
9 Archambeau and Sammis (1970)
10 Press (1967)
11 Evernden personal communication
12 Wyss et al (1971)
13 Archambeau (1965)
14 Wideman and Major (1967)
15 Werth and Randolph (1966)

REFERENCES

Archambeau, C.B., 1964, Elastodynamic source theory, Ph.D. Thesis, California Institute of Technology.

Archambeau, C.B., and C.G. Sammis, 1970, Seismic radiation from explosions in prestressed media and the measurement of tectonic stress in the earth, in preparation.

Basham, P.W., 1969, Canadian magnitudes of earthquakes and nuclear explosions in south-western North America, Geophys. J. R. Astr. Soc., v. 17, p. 1.

Brune, J.N., Espinosa, A., and Oliver J., 1963, Relative excitation of surface waves by earthquakes and underground explosions in the California-Nevada region, J. Geophys. Res., v. 68, p. 3501, 1963.

Davies, J.B., and Smith, S.W., 1968, Source parameters of earthquakes and discrimination between earthquakes and nuclear explosions, Bull. Seism. Soc. Am., v. 58, p. 1503.

Evernden, J.F., 1967, Magnitude determination at regional and near-regional distances in the United States, Bull. Seism. Soc. Am. v. 57, p. 591.

Hanks, T.C., and Brune, J.N., 1970, Seismicity of the San Gorgonio Pass (abstract), Trans. Am. Geophys. Union, v. 51.

Healy, J.H., King, Chi-Yu, and O'Neill, M.E., 1970, Source parameters of Salmon and Sterling nuclear explosions, (abstract), Trans. Am. Geophys. Union, v. 51.

King, Chi-Yu, and Knopoff, L., 1968, Stress drop in earthquakes, Bull. Seism. Soc. Am., v. 58, 1, p. 249.

Lacoss, R.T., 1969, A large-population LASA discrimination experiment, Technical Note 1969-24, Lincoln Laboratory, MIT.

Liebermann, Robert C., and Pomeroy, Paul W., 1969, Relative excitation of surface waves by earthquakes and underground nuclear explosions, J. Geophys. Res., v. 74, p. 1575.

Liebermann, Robert C., and Pomeroy, Paul W., 1970, Source dimensions of small earthquakes as determined from the size of the after-shock zone, Bull. Seism. Soc. Am., v. 60, p. 879.

McEvilly, T.V., 1966, The earthquake sequence of November 1964 near Corralitos, California, Bull. Seism. Soc. Am., v. 56, p. 755.

McEvilly, T.V., and Cassaday, K.B., 1967, The earthquake sequence of September 1965, near Antioch, California, Bull. Seism. Soc. Am., v. 57, p. 113.

Molnar, Peter, Savino, John, Sykes, Lynn R., Liebermann, Robert C., Hade, Gorge, and Pomeroy, Paul W., 1969, Small earthquakes and explosions in western North America recorded by new high gain, long period seismographs, Nature, v. 224, p. 1268.

Pasechnik, I., 1968, In seismic methods for monitoring underground explosions, International Inst. for Peace and Conflict Research, Stockholm.

Press, F., 1967, Dimensions of the source region for small shallow earthquakes, Proceedings of the VESIAC Conference on the Current Status and Future Progress for Understanding the Source Mechanism of Shallow Seismic Events in the 3 to 5 Magnitude Range, VESIAC Rept. 7885-1-X, 155.

Romney, C., 1959, Amplitudes of seismic body waves from underground nuclear explosions, J. Geophys. Res., v. 68, p. 1489.

Ryall, A.T., Van Worner, J.D., and Jones, A.E., 1968, Triggering of microearthquakes by earth tides, and other features of the Truckee, California earthquake sequence of September 1966, Bull. Seism. Soc. Am., v. 58, p. 215.

Schick, R., 1968, Untersuchungen über die Bruchausdehnung and Bruchgeschwindigkeit bei Erdbeben mit kleinen Magnituden (M<4), Zeitschrift für Geophysik, v. 34, p. 267.

Smith, S.W., Sammis, C.G., and Jackson, W.H., 1967, Microearthquake source dimensions and energy release (abstract), Trans. Am. Geophys. Union, v. 48, p. 201.

Thirlaway, H.I.S., and Carpenter, E.W., 1966, Seismic signal anomalies, travel times, amplitudes and pulse shapes, Proceedings of the VESIAC Special Study Conference on Seismic Signal Anomalies, Travel Times, Amplitudes and Pulse Shapes, VESIAC Rept. 4410-99-X, p. 119.

Toksöz, M.N., Ben-Menahem, A., and Harkrider, D.G., 1964, Determinations of source parameters of explosions and earthquakes by amplitude equalization of seismic surface waves, 1. Underground nuclear explosions, J. Geophys. Res., v. 69, 43, p. 4365.

Toksöz, M.N., Harkrider, D.G., and Ben-Menahem, A., 1965, Determination of source parameters by amplitude equalization of seismic surface waves, 2. Release of tectonic strain by underground nuclear explosions and mechanisms of earthquakes, J. Geophys. Res., v. 70, p. 907.

Udias, A.S., 1965, A study of the aftershocks and focal mechanism of the Salinas-Watsonville earthquakes of August 31 and September 14, 1963, Bull. Geol. Soc. Am., v. 55, p. 85.

Werth, G.C., and Herbst, R.F., 1963, Comparison of amplitudes of seismic waves from nuclear explosions in four mediums, J. Geophys. Res. v. 68, p. 1463.

Werth, G.C., and Randolph, P., 1966, The Salmon seismic experiment, J. Geophys. Res., v. 71, p. 3405.

Wideman, C.T., and Major, M.W., 1967, Strain steps associated with earthquakes, Bull. Seismol. Soc. Am., v. 57, p. 1429.

Wyss, M., and Brune, J.N., 1968, Seismic moment, stress and source dimensions for earthquakes in the California-Nevada region, J. Geophys. Res., v. 74, p. 4681.

Wyss, Max, 1970, Observation and interpretation of tectonic strain release mechanisms, Ph.D. Thesis, Calif. Inst. Tech..

Wyss, M., Hanks, T.C., and Liebermann, R.C., 1971, A comparison of P-wave spectra of earthquakes and nuclear explosions, in preparation.

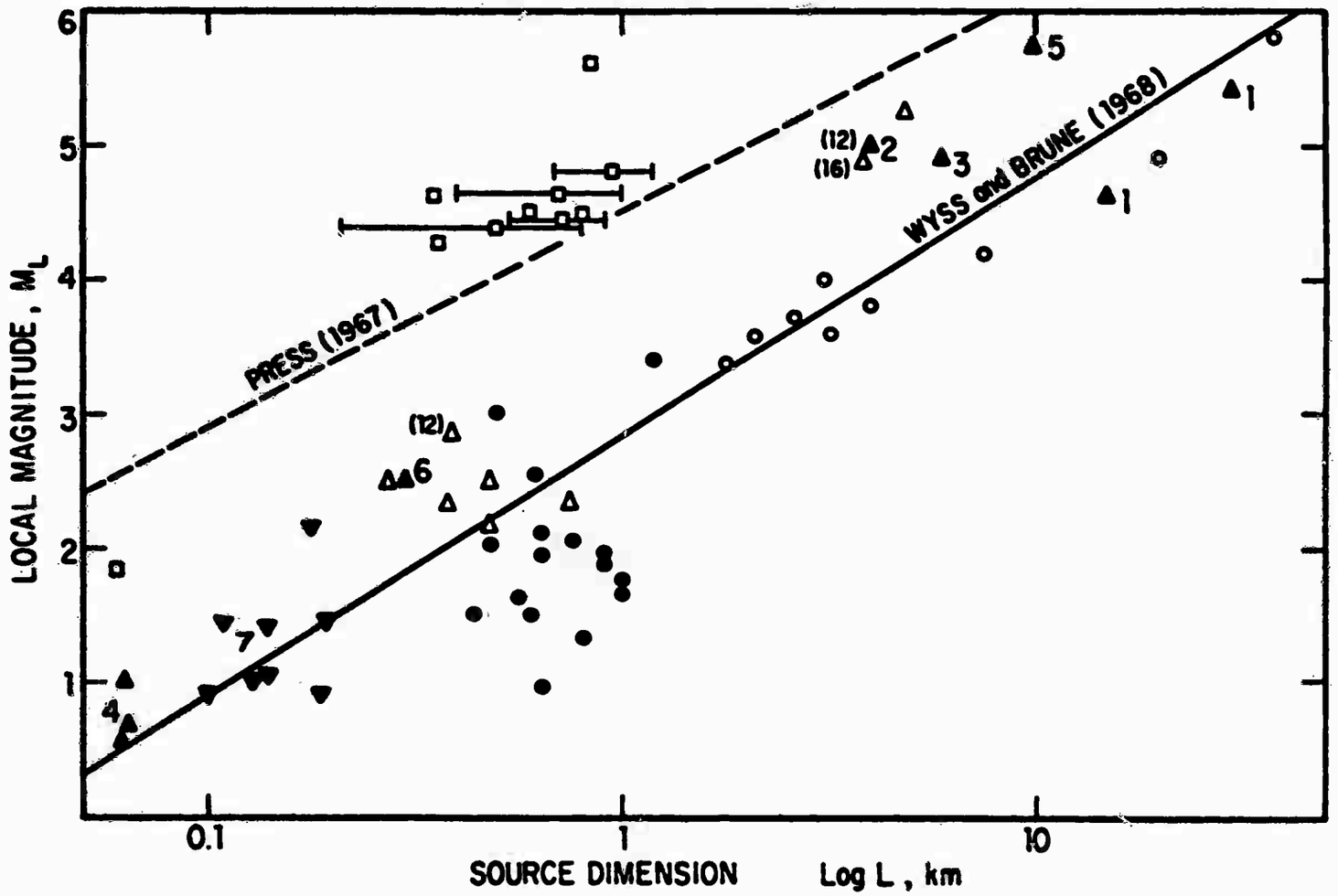

Figure 1. Source dimensions of nuclear explosions (squares) and earthquakes (all other symbols) are compared on the basis of local magnitude. References are: O = Wyss (1970), O - Wyss and Brune (1968), Δ = Hanks and Brune (1971), Δ1 = Udias (1965), Δ2 = McEvilly (1966), Δ3 = McEvilly and Cassaday (1967), Δ4 = Smith et al (1967), Δ5 = Ryall et al (1968), Δ6 = Schick (1968), Δ7 = Tucker and Brune (in preparation).

SOURCE DEPTHS FROM SURFACE WAVE SPECTRAL RATIOS

By

David G. Harkrider

Using arguments based on the reciprocity theorems of Knopoff and Gangi (1959), Aki (personal communications, 1961) realized that the vertical surface displacement spectrum of fundamental Rayleigh waves should possess a zero which was dependent on the depth of a horizontal force. This phenomenon was investigated in a series of modal experiments (Aki and Healy, personal communications, 1962). Harkrider and Anderson (1966) noted that the higher mode Rayleigh and Love waves possess depth dependent spectral zeros for vertical as well as horizontal forces.

One of the difficulties encountered in using amplitude spectra for depth determination has been the time-space source function. This function will in general have zeros associated with the fault displacement-time function, fault dimensions and rupture velocity. For stationary point sources, the source factor can be eliminated by dividing the spectra of different arrivals. This division eliminates all of the effects of distance except the difference in anelastic absorption. For more realistic sources complications arise which will be discussed later.

For small earthquakes, the departure from point source theory is usually negligible for periods greater than 20 seconds. Tsai (1969) found that the assumption that the source is a point in space and a step function in time was adequate for determining the focal depths of earthquakes in the mid-ocean ridges with magnitudes 6.0 or smaller. The depths were determined from the shapes of the Rayleigh wave spectra by comparing with theoretical spectra from a vertical strike slip fault with a step function rupture in time. The depth estimates were confirmed by observation of P and pP phases.

In order to investigate the use of spectral ratios as a possible measure of source depth, we have evaluated the ratio of various surface wave modes as a function of period and depth. The calculations are for a double couple source with an oceanic propagation path. The orientation of the double couple was chosen in order to represent the far field spectra from a vertical strike slip fault. The station azimuth is 22.5° from the fault plane.

The ratio zeros and infinities for this double couple orientation are determined by the nodal periods in horizontal displacement at the source depth. Thus the spectra of each higher mode has one more zero than the next lower mode. For a given mode the displacement zeros migrate downward in depth with increasing period. Therefore successively deeper sources have spectral zeros at successively longer periods.

Even though all the spectral ratios have nodes and infinities which are sensitive to the source depth, the most promising is the fundamental Rayleigh to Love ratio. The easily identified large amplitudes of fundamental surface waves in the time domain are important to taking meaningful spectral ratios. The interference of similar signals can cause spectral holes which along with spectral zeros due to source time history and finiteness make identification of the source depth minimum improbable. If there is enough energy in

the observed fundamental Love wave, the minimums in Love spectra will be due to interferences, such as multipath arrivals, and source time and finiteness functions. Thus ratios should not be formed at periods for which there is a low power level in the Love wave spectrum.

The ratio minima are dependent on the fault orientation parameters of dip, δ and slip, λ, as well as source depth. The ratio of fundamental Rayleigh to Love has a true node at all azimuths only for fault models, (δ, λ) of (90°, 0°) and (90°, 180°). The (45°, 90°) and (45°, 270°) faults can have true nodes at azimuthal angles from the strike of θ = 45°, 135°, 225°, and 315°.

The nodal period as a function of source depth for the vertical pure strike slip fault model, (90°, 0°), is shown in Figure 1. For the oceanic and shield earth structures, the relation between period and source depth is almost linear down to depths of 150 km. A rough estimate of the source depth can be obtained by equating the depth in kilometers to the nodal period in seconds. For a homogeneous Poisson solid half space, the relation between source depth, h, and the nodal period is given by

$$h = (0.19) \times (CT)$$

(Ben-Menahem and Toksöz, 1963). The ratio of source depth to this critical wavelength, $\lambda_c = CT$, versus source depth is shown in Figure 2 for the two models.

Figure 3 illustrates the effects of varying the fault geometry parameters (δ,λ). For changes in dip and slip of less than 10° from the vertical pure strike slip fault (90°, 0°), the minimum near 60 seconds is recognizable and essentially stable. But at an observer azimuth of θ = 22.5° a change of 15° in δ or λ can virtually eliminate the minimum. On the other hand, at an azimuth of 30°, the spectral ratio has an easily identified minimum at 60 seconds for the (75°, 15°) model. Another complicating factor then is that the minimums are sensitive to azimuth. It should also be remembered that these are spectral ratio minimums. Except for geometries where the minima are near zero, their presence may not be evident in either the Rayleigh or the Love spectra until the ratio has been formed.

The complications inherent in these spectral techniques can be demonstrated by considering the Fallon earthquake of 20 July 1962 (Toksöz et al 1964). The fundamental Rayleigh and Love spectra measure at Ruth, Nevada, are shown in Figure 4. Taking their spectral ratio, R_z/L we obtain a minimum near 26 seconds which corresponds to focal depth of 20 km for a vertical strike slip fault (90°, 0°) and a Fallon to Ruth propagation path (Figure 5). The minimum is also apparent in the observed R_z.

The depth is the same as that obtained in Toksöz et al (1965)

by comparing the observed and theoretical spectra for the surface waves at Ruth, Pasadena and Jamestown. As in Tsai (1969), the assumed source time variation was a step function. In order to fit the observed spectra at these stations, they required a fault orientation of (76°, 230°) and a strike azimuth of 355°. This corresponds to an azimuthal angle from the strike of $\theta = 100°$ at Ruth. The (90°, 0°) faults at a depth of 20 and 26 km require a $\theta = 50° - 55°$ or $\theta = 125° - 130°$ at Ruth in order to obtain a reasonable spectral ratio (Figure 5). This results in an unacceptable theoretical spectral ratio at Jamestown which is two orders of magnitude less than observed there. The spectral ratios for their (76°, 230°) fault have barely perceptable minima only at θ near 40° and 145°. There are no minima in R_z at any azimuth for periods less than 40 seconds.

The fault orientation was determined from a three station fit of a radiation pattern of the Love to Rayleigh wave peak amplitudes (T = 16 sec). Flinn, Lambert and Archambeau (1970) using the Fallon earthquake Rayleigh and Love waves recorded at 17 LRSM stations found that the radiation pattern for the 16 second ratio could be fit best by a 20 km depth (82°, 196°) fault plane with a strike azimuth of 10°. Since the radiation pattern of the ratio at a given period is relatively insensitive to source depth, the 20 km source depth was determined from the individual Love and Rayleigh radiation patterns at various frequencies. The shapes of these individual patterns also admit a fault orientation of (82°, 174°) (Flinn et al, 1970).

The spectral ratios at selected azimuths for the two LRSM determined fault solutions are shown in Figure 6 with the observed Ruth ratio. Again we cannot fit the Ruth data ($\theta = 85°$) without violating the strike azimuth. The range of azimuth in which there is a detectable minimum in the R_z/L ratio and in R_z for a step function source are shown in Figure 7 for the LRSM fault solutions. In the same figure we show the 16 second Love to Rayleigh radiation patterns.

Another piece of evidence that the fault strike azimuth is within 15° of North as in Toksöz et al (1965) and Flinn et al (1970) can be found in the small dips in the absolute spectra of the Jamestown and Pasadena stations (Figure 4). Assuming that the Fallon event was due to a rupture moving to the North with a uniform velocity of 2.2 km/sec along a fault segment of length 20 km, these dips can be explained as the first minimums of the source propagation factor (Ben-Menahem, 1960). This factor would cause a minimum in the Rayleigh and Love wave spectra at just below 10 seconds period at Ruth, at 14 seconds at Pasadena, and at 12 to 14 seconds at Jamestown. The minimum necessary length of 20 km is considered large for an earthquake of this magnitude (King and Knopoff, 1968). On the other hand, the shallowness of the minima can be explained by the rupture strength being much smaller at the tends of the fault relative to the center (Ben-Menahem and Toksöz, 1962). Thus the effective length contributing most of the seismic energy could be much smaller and the spectra would

still have the same minima locations found in Figure 4.

Unless the solutions obtained from the three Caltech and the 17 LRSM stations are incorrect or can be shifted in strike azimuth a minimum of 25° to the east, the dip in the Ruth, Nevada, Rayleigh spectrum and the Rayleigh to Love spectra ratio at 26 seconds must be due to mechanisms other than source depth (Toksöz et al, 1965).

Considering the difficulties and the sources of possible spectral contamination it is hard to visualize spectral ratios playing an important role in the determination of focal mechanisms except for events where there is consistent and adequate station coverage, high signal to noise levels, and some supplementary information on the fault and propagation path.

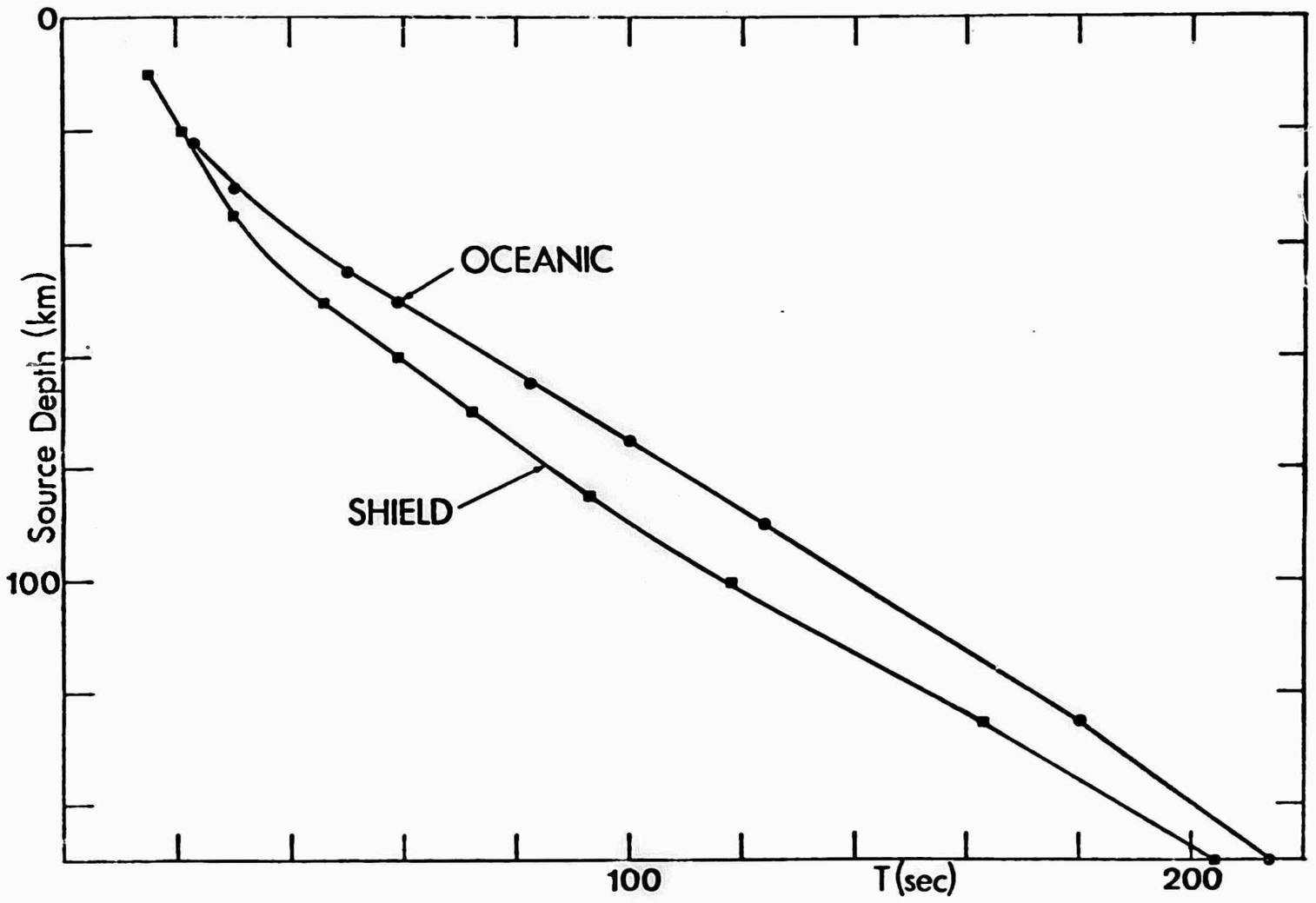

Figure 1.

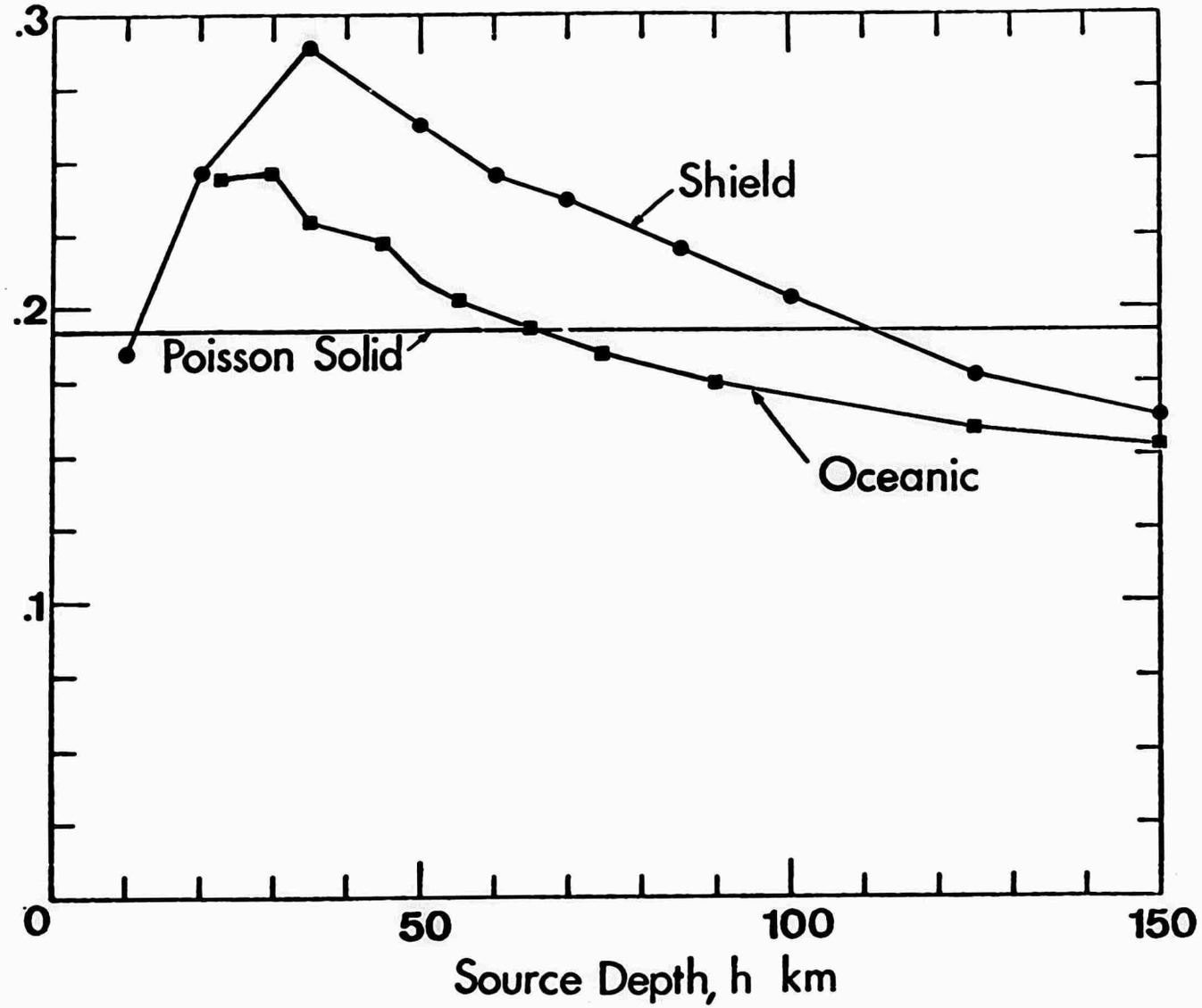
.3
.2
.1
0
50
100
150
Shield
Poisson Solid
Oceanic
Source Depth, h km

Figure 2.

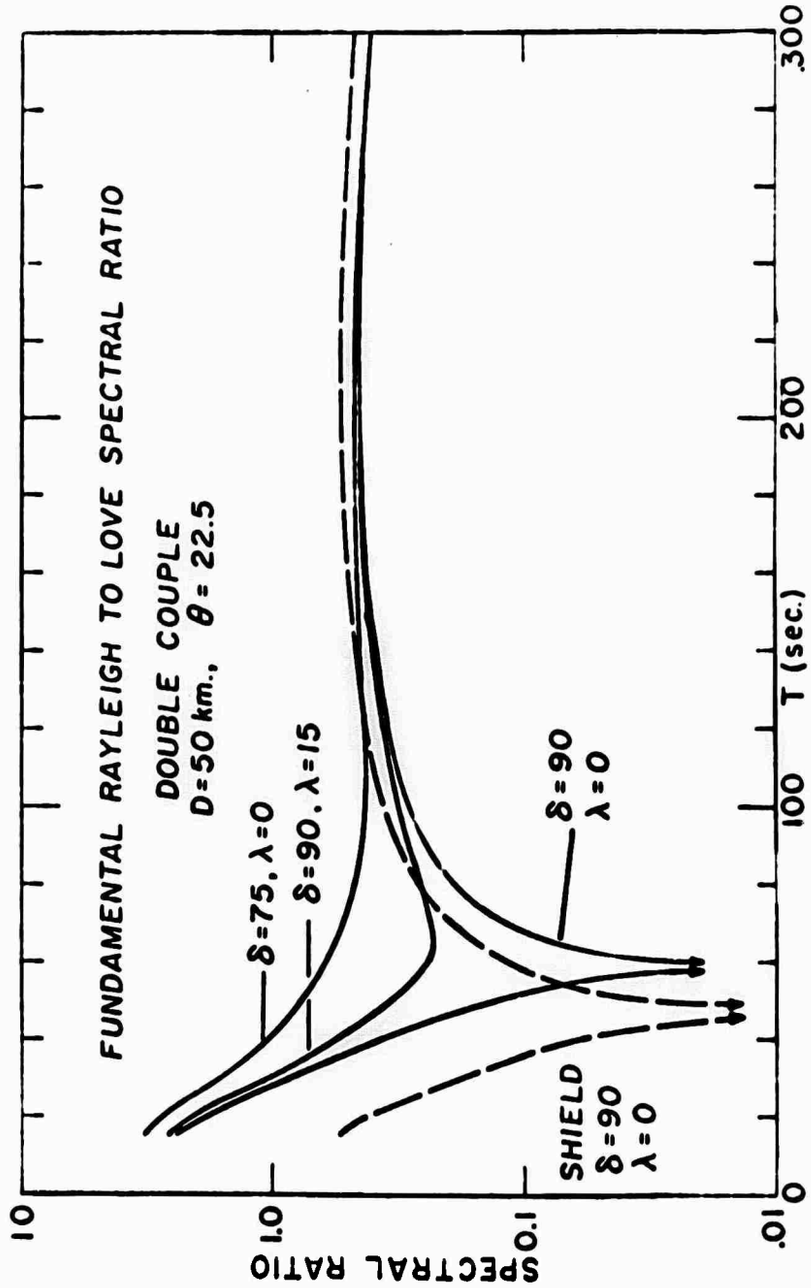
FUNDAMENTAL RAYLEIGH TO LOVE SPECTRAL RATIO
DOUBLE COUPLE
D=50 km., θ= 22.5
δ=75, λ=0
δ=90, λ=15
δ=90
λ=0
SHIELD
δ=90
λ=0
SPECTRAL RATIO
10
1.0
.1
.01
0
100
200
300
T (sec.)

Figure 3.

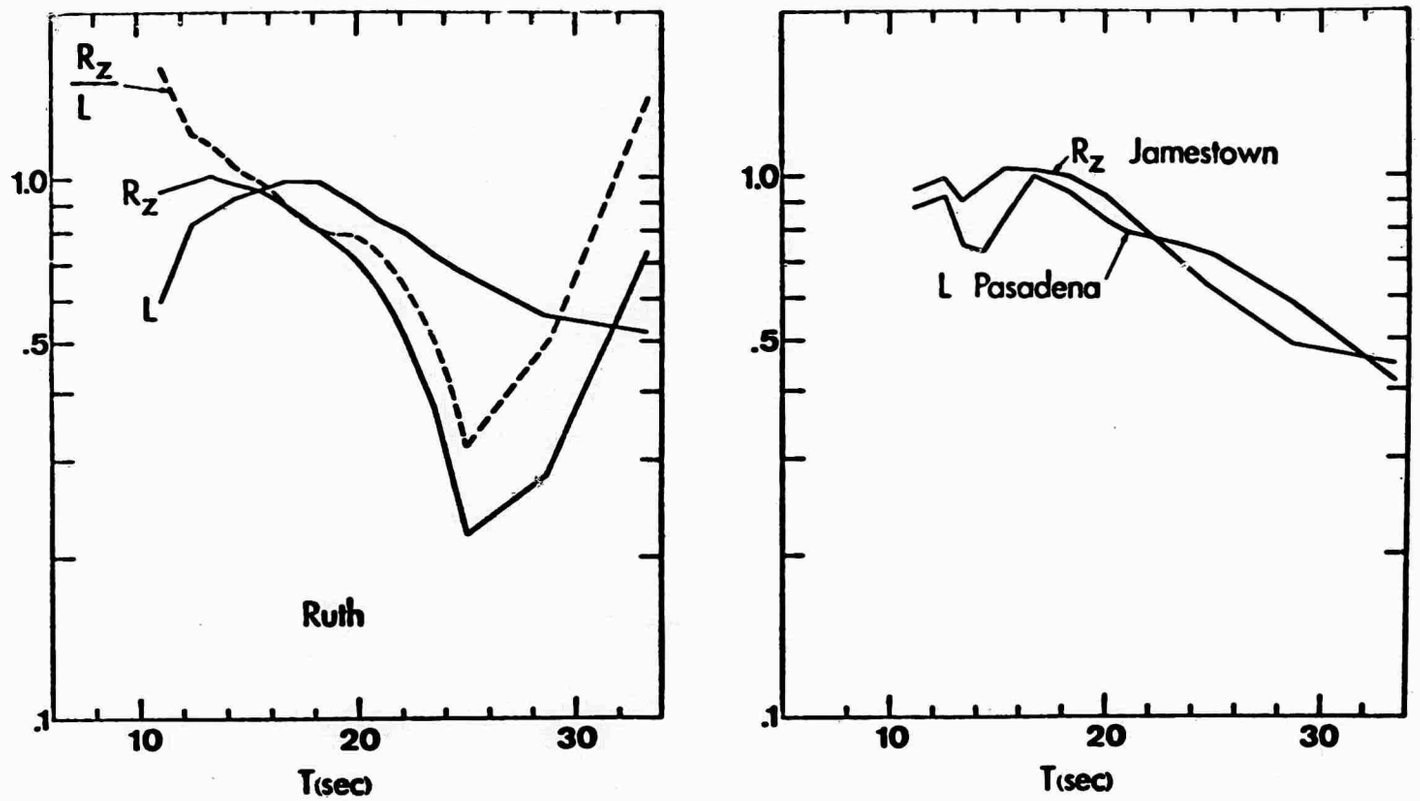
R_Z
L
R_Z
L
1.0
.5
.1
Ruth
10
20
30
T(sec)
R_Z Jamestown
L Pasadena
1.0
.5
.1
10
20
30
T(sec)

Figure 4.

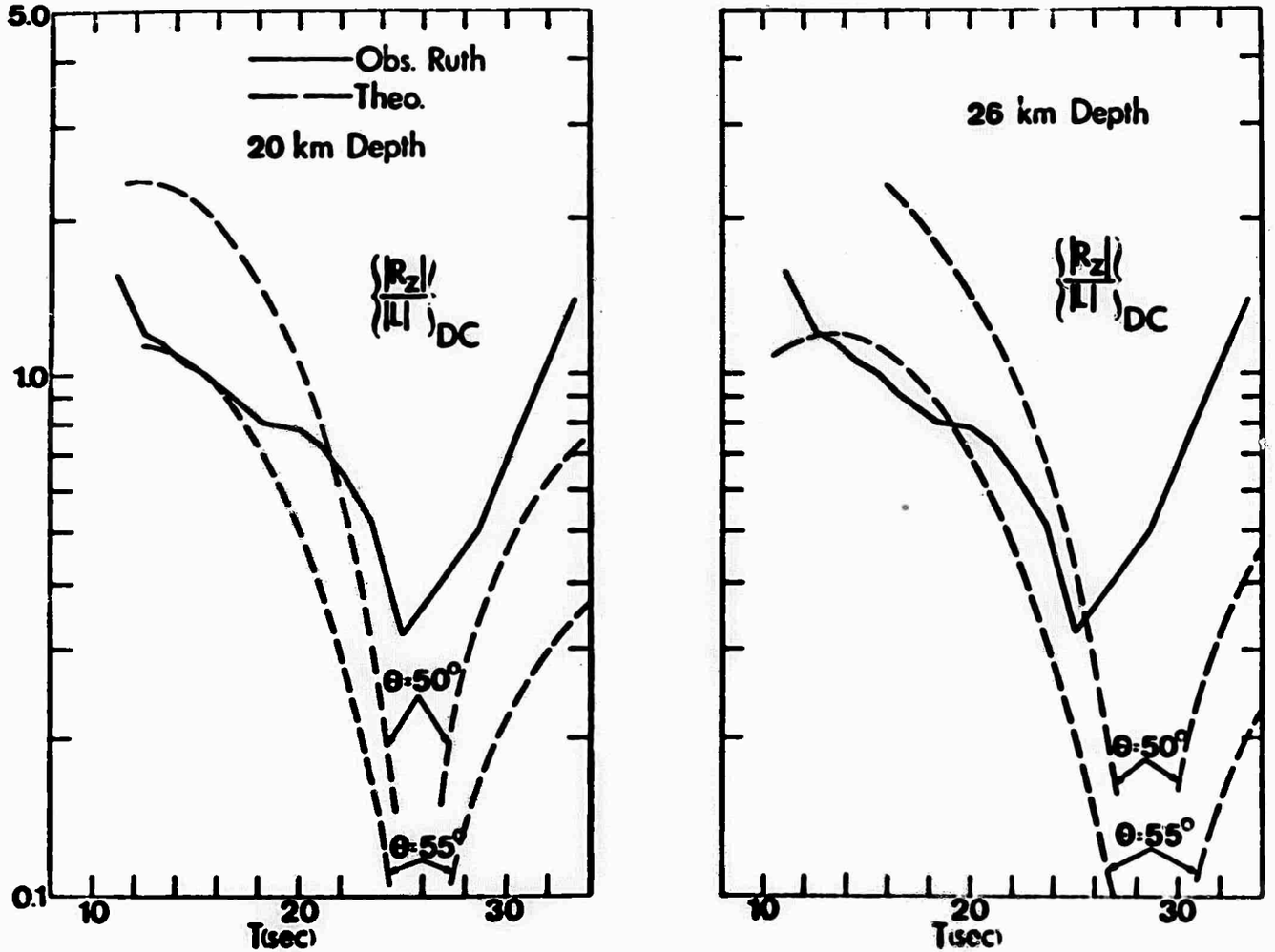
5.0
1.0
0.1
Obs. Ruth
Theo.
20 km Depth
26 km Depth
$\left(\frac{|R_z|}{|L|}\right)_{DC}$
θ=50°
θ=55°
10
20
30
T(sec)

Figure 5.

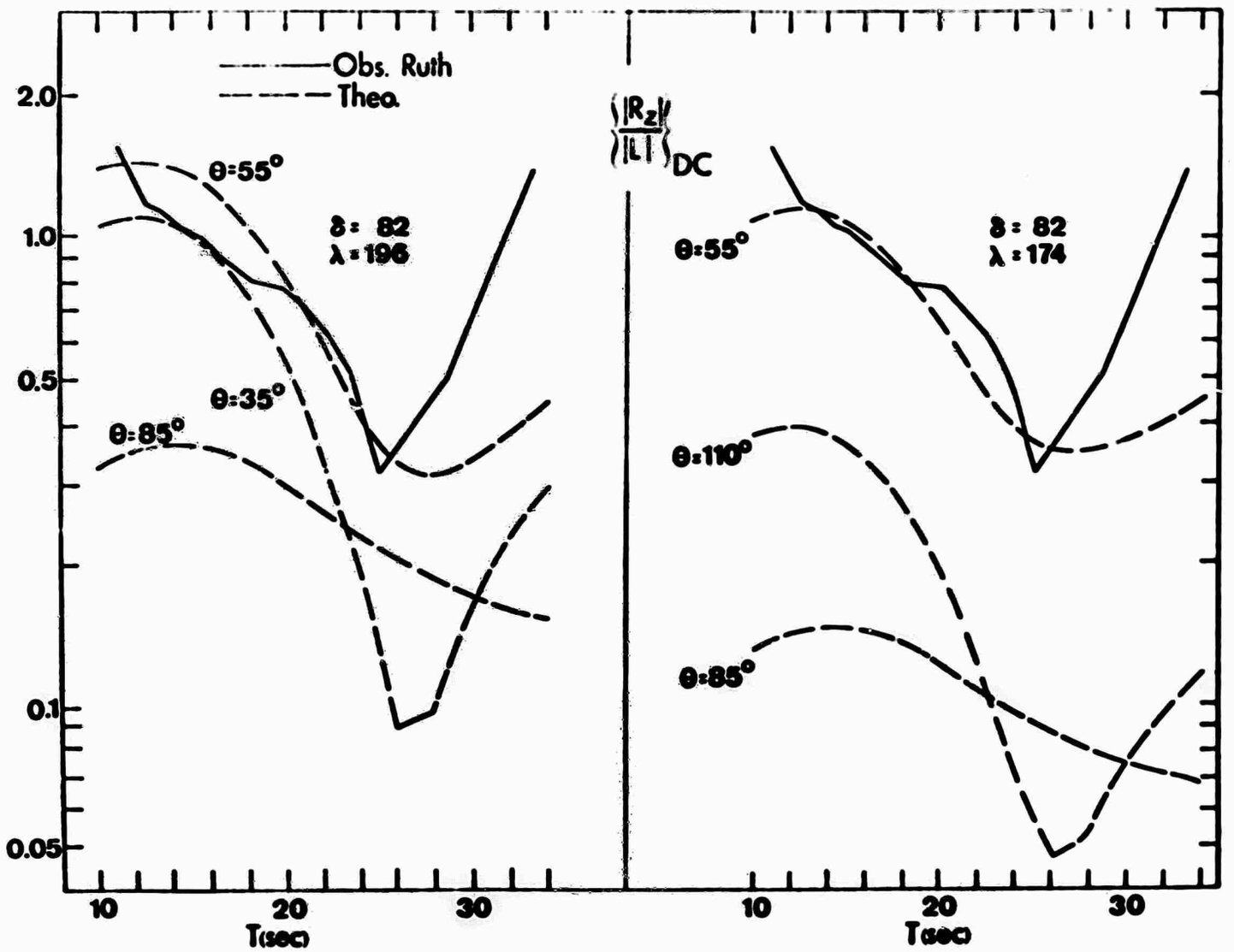
Obs. Ruth
Theo.
$\left\langle \frac{|R_z|}{|L|} \right\rangle_{DC}$
2.0
1.0
0.5
0.1
0.05
θ=55°
θ=35°
θ=85°
δ = 82
λ = 196
θ=55°
θ=110°
θ=85°
δ = 82
λ = 174
10
20
30
T(sec)
10
20
30
T(sec)

Figure 6.

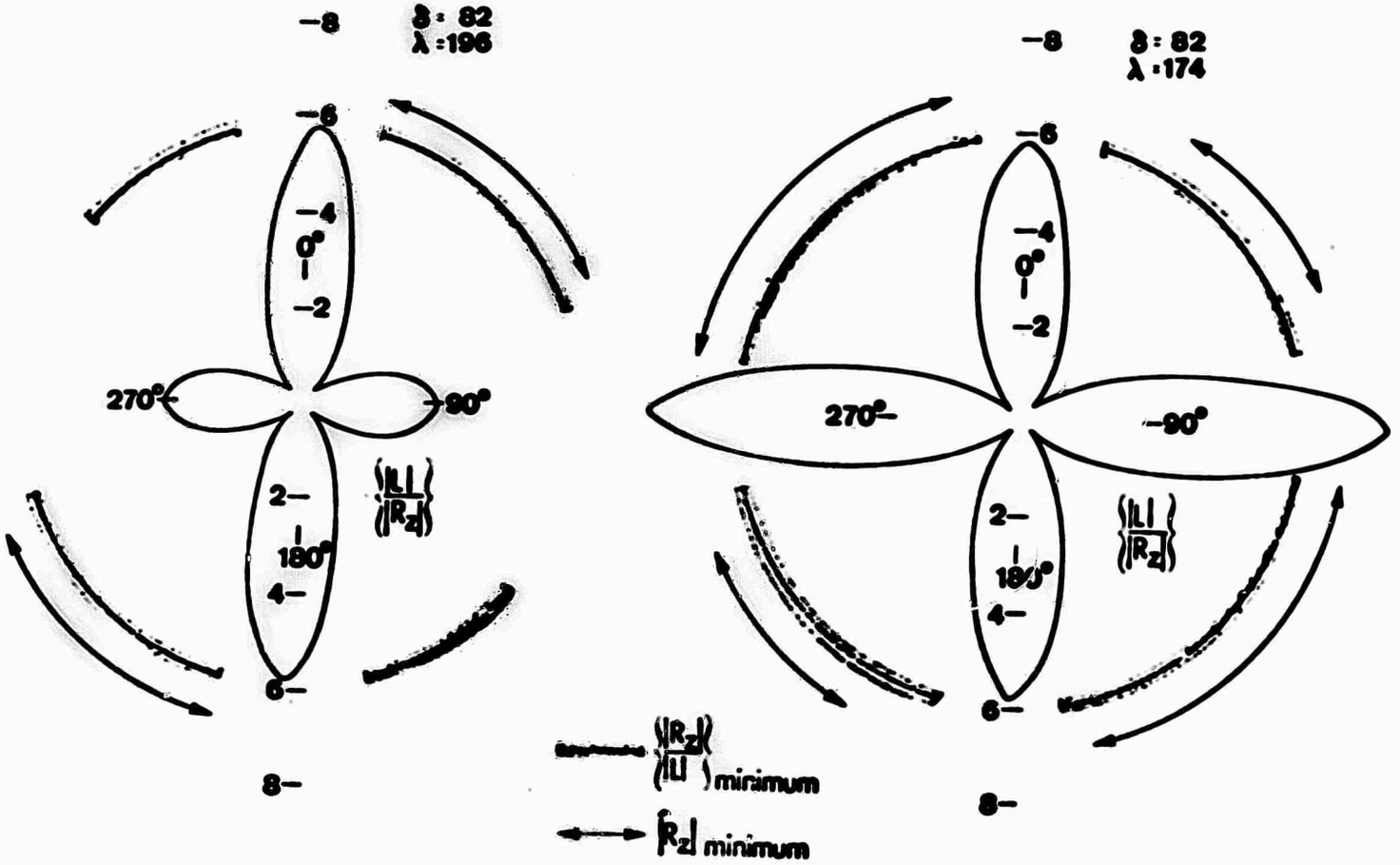

Figure 7.

EXCITATION OF THE NORMAL MODES OF THE EARTH BY EARTHQUAKE SOURCES

By

Freeman Gilbert

Institute of Geophysics and Planetary Physics
and Scripps Institution of Oceanography
University of California, San Diego
La Jolla, California 92037

ABSTRACT

Some century old results, due to Rayleigh and Routh, are used to derive a very compact and simple representation for the transient response of the Earth to earthquakes. In particular, it is shown how the residual static displacement field is naturally represented in terms of the normal mode eigenfunctions.

BLANK PAGE

If one can calcuate the excitation of the normal modes of the Earth due to a particular earthquake source, one can use such calculations in an attempt to infer the earthquake mechanism and total moment. Some general results in normal mode theory, due to Rayleigh and Routh about a century ago, make the excitation calculations remarkably simple. First we treat a system of N particles and then pass to the continuum limit.

Consider a conservative system of N particles in small oscillation about a state of stable equilibrium. Let the α^{th} particle, $\alpha = 1,\ldots, N$ have mass m_α, displacement u_α, and let a force $f_{m\alpha}$ be applied to it. Then, if $V_{m\alpha\beta}$ is the symmetric, positive definite potential energy matrix, the linearized equation for the conservation of linear momentum is

$$m_\alpha \frac{d^2 u_{m\alpha}}{dt^2} + \sum_{\beta=1}^{N} V_{m\alpha\beta} \cdot u_{m\beta} = f_{m\alpha} \tag{1}$$

The Laplace transform of (1) is

$$m_\alpha p^2 \bar{u}_{m\alpha} + \sum_{\beta} V_{m\alpha\beta} \cdot \bar{u}_{m\beta} = \bar{f}_{m\alpha} \tag{2}$$

where

$$\bar{u}_{m\alpha}(p) = \int_0^\infty u_{m\alpha}(t)\, e^{-pt}\, dt; \quad \mathrm{Re}\, p > 0 \tag{3}$$

and

$$u_{m\alpha}(0) = \frac{d}{dt} u_{m\alpha}(0) = 0$$

We recall that there are 3N eigenfrequencies ω_n; $n = 1,\ldots, 3N$, and 3N eigenvectors, or normal modes, $s_{m\alpha,n} e^{i\omega_n t}$ for the dynamical system. The normal modes can be orthonormalized (* denotes complex conjugate)

$$\sum_\alpha m_\alpha s^*_{m\alpha,n} \cdot s_{m\alpha,\ell} = \delta_{n,\ell} \tag{4}$$

and, since there are 3N degrees of freedom, they form a complete basis for the system. Consequently, $\bar{u}_{m\alpha}$ has the representation

$$\bar{u}_{m\alpha} = \sum_n a_n s_{m\alpha,n} \tag{5}$$

and the use of (4) gives

$$a_n = \sum_{\alpha} m_{\alpha} \, s^*_{m\alpha,n} \cdot \bar{u}_{m\alpha} \tag{6}$$

If we take the scalar product of (2) with $s^*_{m\alpha,n}$ and sum over α we get

$$p^2 a_n + \sum_{\alpha\beta} s^*_{m\alpha,n} \cdot V_{m\alpha\beta} \cdot \left(\sum_{\ell} a_{\ell} \, s_{m\beta\ell}\right) = \sum_{\alpha} s_{m\alpha,n} \cdot \bar{f}_{m\alpha} \tag{7}$$

We can simplify (7) by using a form of Rayleigh's principle. The normal mode $s_{m\alpha,n}$ is a solution to

$$-\omega_n^2 \, m_{\alpha} \, s_{m\alpha,n} + \sum_{\beta} V_{m_{\alpha\beta}} \cdot s_{m\beta,n} = 0 \tag{8}$$

Taking the scalar product of (8) with $s_{m\alpha,\ell}$, summing over α, and using (4) gives

$$\sum_{\alpha\beta} s^*_{m\alpha,\ell} \cdot V_{m\alpha\beta} \cdot s_{m\beta,n} = \omega_n^2 \, \delta_{n\ell} \tag{9}$$

Since, $V_{m\alpha\beta}$ is symmtric we can interchange α and β, as well as n and ℓ, in (9). Thus, using (9) in (7) gives

$$(p^2 + \omega_n^2) a_n = \sum_{\alpha} s^*_{m\alpha,n} \cdot \bar{f}_{m\alpha} \tag{10}$$

and we can write (5) as

$$\bar{u}_{m\alpha} = \sum_{n} s_{\alpha,n} \left[\frac{\sum_{\beta} s^*_{m\beta,n} \cdot \bar{f}_{m\beta}}{(p^2 + \omega_n^2)} \right] \tag{11}$$

Most earthquake sources are modeled as step functions so that $\bar{f}_m = p^{-1} f_m$, then the Laplace inversion of (11), for $t > o$, is

$$u_{m\alpha}(t) \sum_{n} s_{m\alpha,n} \left(\sum_{\beta} s^*_{m\beta,n} \cdot f_{m\beta}\right) \frac{1-\cos\omega_n t}{\omega_n^2} \tag{12}$$

When there is a small amount of dissipation (Q>>1) we modify (12)

$$u_{m\alpha}(t) = \sum_n s_{m\alpha,n} \left(\sum_\beta s^*_{m\beta,n} \cdot f_{m\beta}\right) \frac{1-\cos\omega_n t e^{-\omega_n t/2Q_n}}{\omega_n^2} \qquad (13)$$

All that remains after a long time is the static displacement

$$\lim_{t\to\infty} u_{m\alpha}(t) = \sum_n s_{m\alpha,n} \left(\sum_\beta s^*_{m\beta,n} \cdot f_{m\beta}\right) \frac{1}{\omega_n^2} \qquad (14)$$

It appears to be unappreciated by many geophysicists that the static response of a mechanical system can be expressed in terms of the normal modes of that system. Thus, the statical or dynamical theory of bodily tides, all Love number calculations, the excitation of the chandlerian nutation are all expressible in terms of the Earth's normal mode eigenfunctions, as is the static displacement field caused by an earthquake.

For the Earth, which we approximate as a classical continuum, a particle sum, such as

$$\sum_{\beta=1}^{N} s^*_{m\beta,n} \cdot f_{m\beta} \ ,$$

becomes a volume integral, such as $\int dV s^*_{mn}(r) \cdot f_m(r)_m$. The body force $f_{m\beta}$ is replaced by the body force per unit volume $f_m(r)_m$. For (13) we have

$$u(r_m,t) = \sum_n s_{mn}(r)_m \left(\int dV_o s_{mn}(r_{mo}) \cdot f_m(r_{mo})\right) x \qquad (15)$$

$$x \frac{1-\cos\omega_n t e^{-\omega_n t/2Q_n}}{\omega_n^2}$$

The sum in (15) is now an infinite sum but, as shown by Rayleigh, it converges as ω_n^{-2}. The normal modes $s_{mn}(r)_m$ in (15) are normalized (4),

$$\int dV_\rho(r)_m \ s^*_{mn}(r)_m \cdot s_{mn}(r)_m = 1 \qquad (16)$$

and ρ is the density. In many applications the body force $f_m(r)_m$ is represented by δ-functions so that the evaluation of the volume integral in (15) is particularly simple.

For earthquake sources, a commonly used concept is that of a stress release mechanism. Let the difference between the initial static stress, before the earthquake, and the final static stress, after the earthquake, be T_m so that the static stress field, T_m, has the representation

$$T_m = T_{mo} = T_m H(t) \tag{17}$$

and let the source region be confined to a volume V_S. Then the action tensor, M_m, for the source is

$$M_m = \int dV_S \; T_m \tag{18}$$

When the source dimensions are small compared to wavelengths of interest

$$T_m = M_m \delta(r_m - r_{mS}) \tag{19}$$

where r_{mS} is in the source volume V_S.

The body force caused by the stress drop, T_m, is $f_m = -\nabla \cdot T_m$ and the volume integral in (15) becomes

$$\int dV_o s^*_{mn}(r_{mo}) \cdot f_m(r_{mo}) = - \int dV_o s^*_{mn}(r_{mo}) \cdot (\nabla_o \cdot T_m) \tag{20}$$

integrating (2) by parts, using Gauss' divergence theorem plus the symmetry of T_m gives

$$\int dV_o s^*_{mn}(r_{mo}) \cdot (\nabla_o \cdot T_m) = \int dA_o \hat{n}_m \cdot (T_m \cdot s^*_{mn}) \tag{21}$$

$$- \int dV_o T_m : \varepsilon^*_{mn}$$

111

where ε_m is the strain tensor for the displacement vector s_{mn}, Λ_o is the surface of V_o, and $\hat{n}_m$ is the outward unit normal to V_o. For sources within V_o, the surface integral in (21) vanishes. Substituting (19) into the remaining volume integral in (21) gives

$$\int dV_o \; s^*_{mn}(r_o) \cdot (\nabla_o \cdot T_m) = -M_m : \varepsilon^*_{mn}(r_{mS}) \tag{22}$$

where

$$M_m : \varepsilon_m = \sum_{i=1}^{3} \sum_{j=1}^{3} M_{ij} \; \varepsilon_{ij}$$

With the aid of (22) we can write (15) as

$$u_m(r_m,t) = \sum_n s_{mn}(r_m) \; (M_m : \varepsilon^*_{mn} \; (r_{mS})) \; \frac{1-\cos\omega_n t \, e^{-\omega_n t/2Q_n}}{\omega_n^2} \tag{23}$$

A special kind of action tensor is the one that represents a shear dislocation, or fault plane model. Let the unit normal to the fault plane be $\hat{p}_m$ and let the slip direction be $\hat{d}_m$. Then $\hat{p}_m \cdot \hat{d}_m = 0$ and

$$M_m = M(\hat{p}_m \, \hat{d}_m + \hat{d}_m \hat{p}_m)$$

for a shear dislocation. The symmetry of the action tensor is a consequence of the conservation of angular momentum.

The normal modes of the earth are of two kinds: spheroidal, $s_m = \sigma_{nm\ell}{}^m$

$$\sigma^m_{nm\ell} = \hat{r}_m \; U_{n\ell}(r) \; Y^m_\ell(\theta,\phi) + V_{n\ell}(r) \; \nabla_1 \; Y^m_\ell(\theta,\phi) \tag{25}$$

and toroidal, $s_m = \tau^m_{nm\ell}$

$$ {}_n\tau^m_{m\ell} = - {}_nW_\ell(r)\ \hat{r}_m \times \nabla_1\ Y^m_\ell\ (\theta,\phi) \qquad (26) $$

in (25) and (26)

$$ \nabla_1 = \hat{\theta}_m \frac{\partial}{\partial\theta} + \hat{\phi}_m \csc\theta \frac{\partial}{\partial\phi} $$

and

$Y^m_\ell(\theta,\phi)$ is a normalized surface harmonic

$$ Y^m_\ell(\theta,\phi) = (-1)^m \left(\frac{2\ell+1}{4\pi}\right)^{1/2} \left(\frac{(\ell-m)!}{(\ell+m)!}\right)^{1/2} P^m_\ell\ (\cos\theta)e^{im\phi} $$

The scalars U, V, W are solutions to the ordinary differential equations that represent the stress-strain relations and the conservation of linear momentum. Once the scalars U, V, W, have been obtained, and this is, by far, the most time consuming part of the numerical calculations, they can be stored for repeated retrieval, so that the evaluation of (23) for a particular M_m, r_{mS}, and r_m can be extremely rapid and inexpensive.

Several applications of the techniques presented here will be published elsewhere.

REFERENCE

Rayleigh, Lord, 1877, The theory of sound, I, chapters IV and V, MacMillan, London.

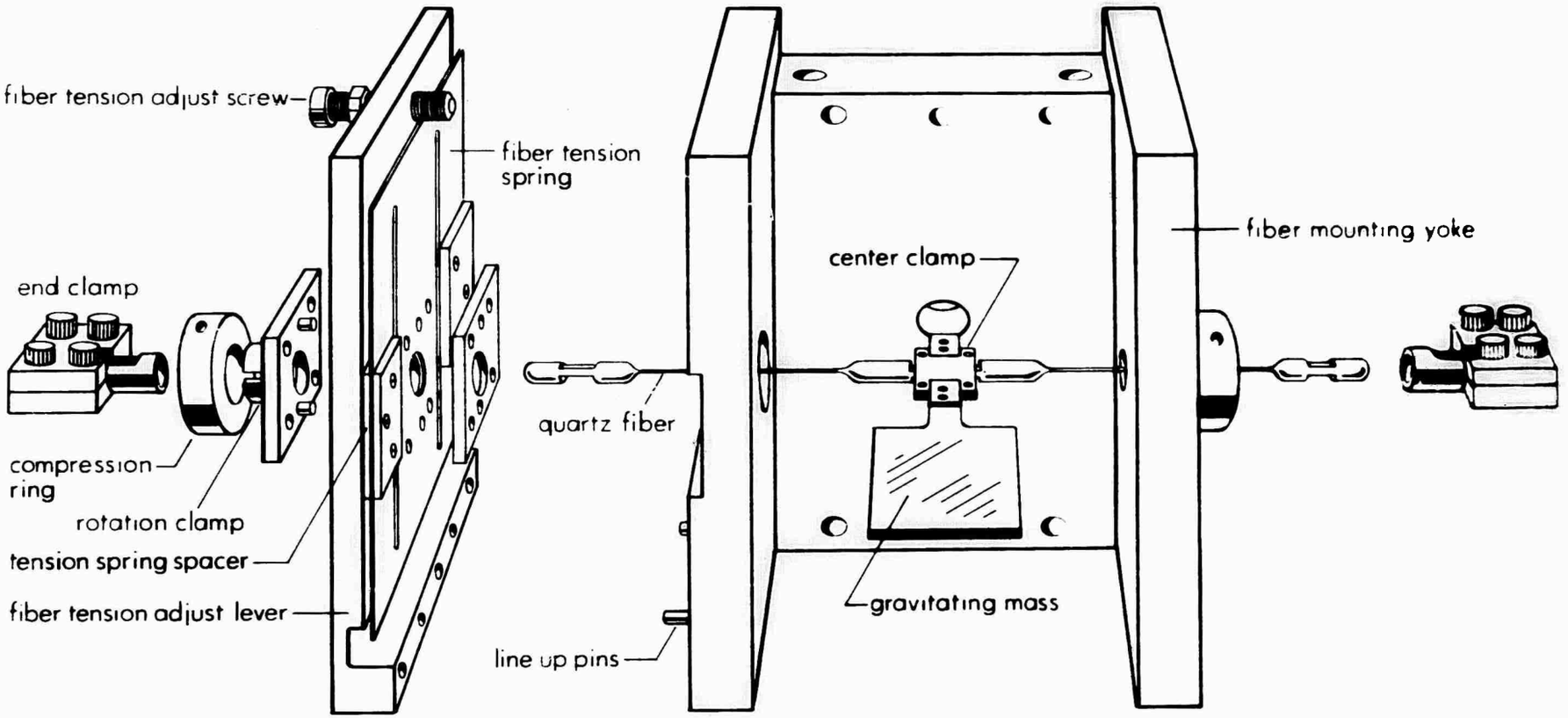

Figure 1. Exploded view of torsion spring system.

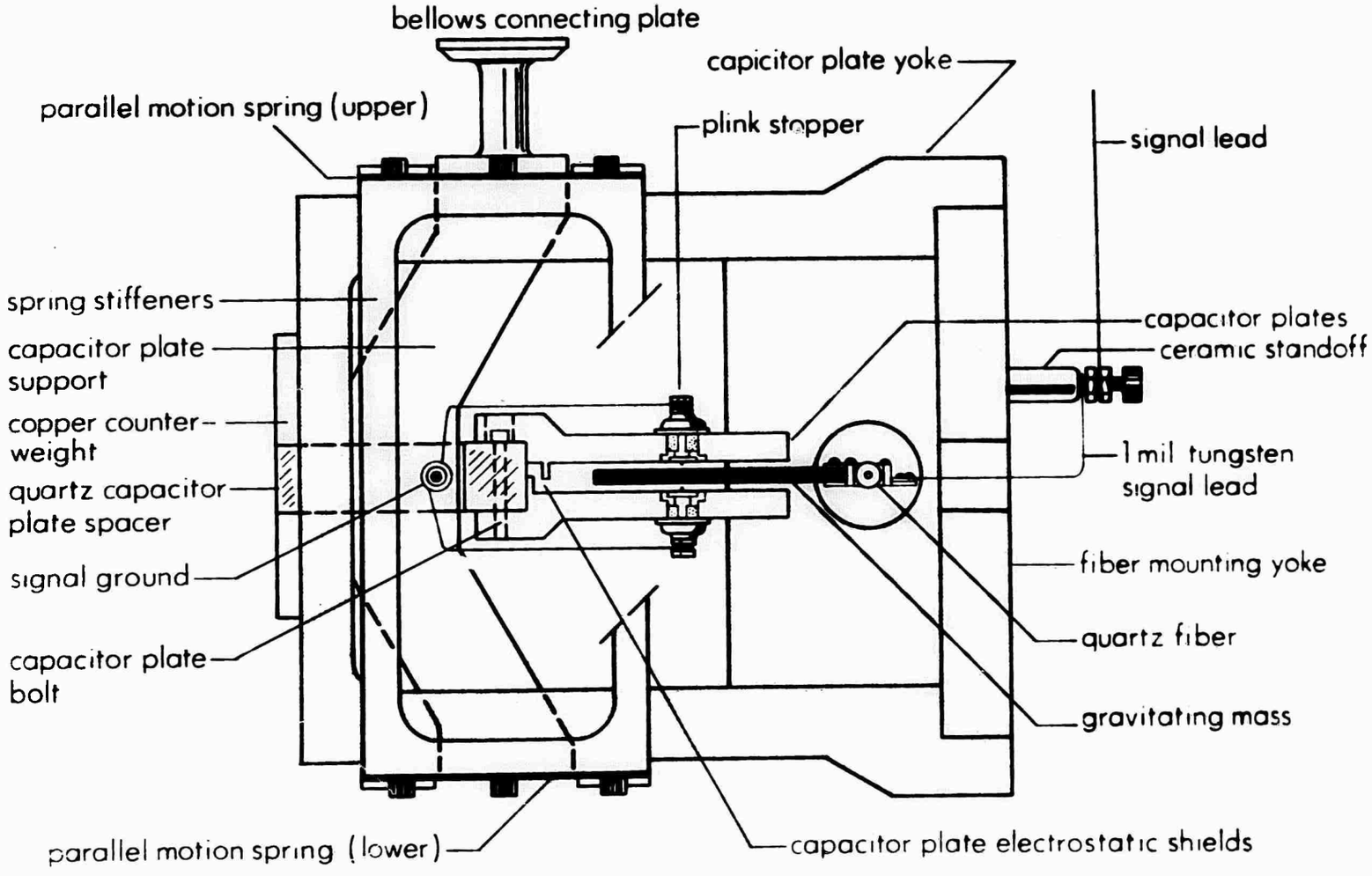

Figure 2. Side view of capacitor position sensor and torsion spring system.

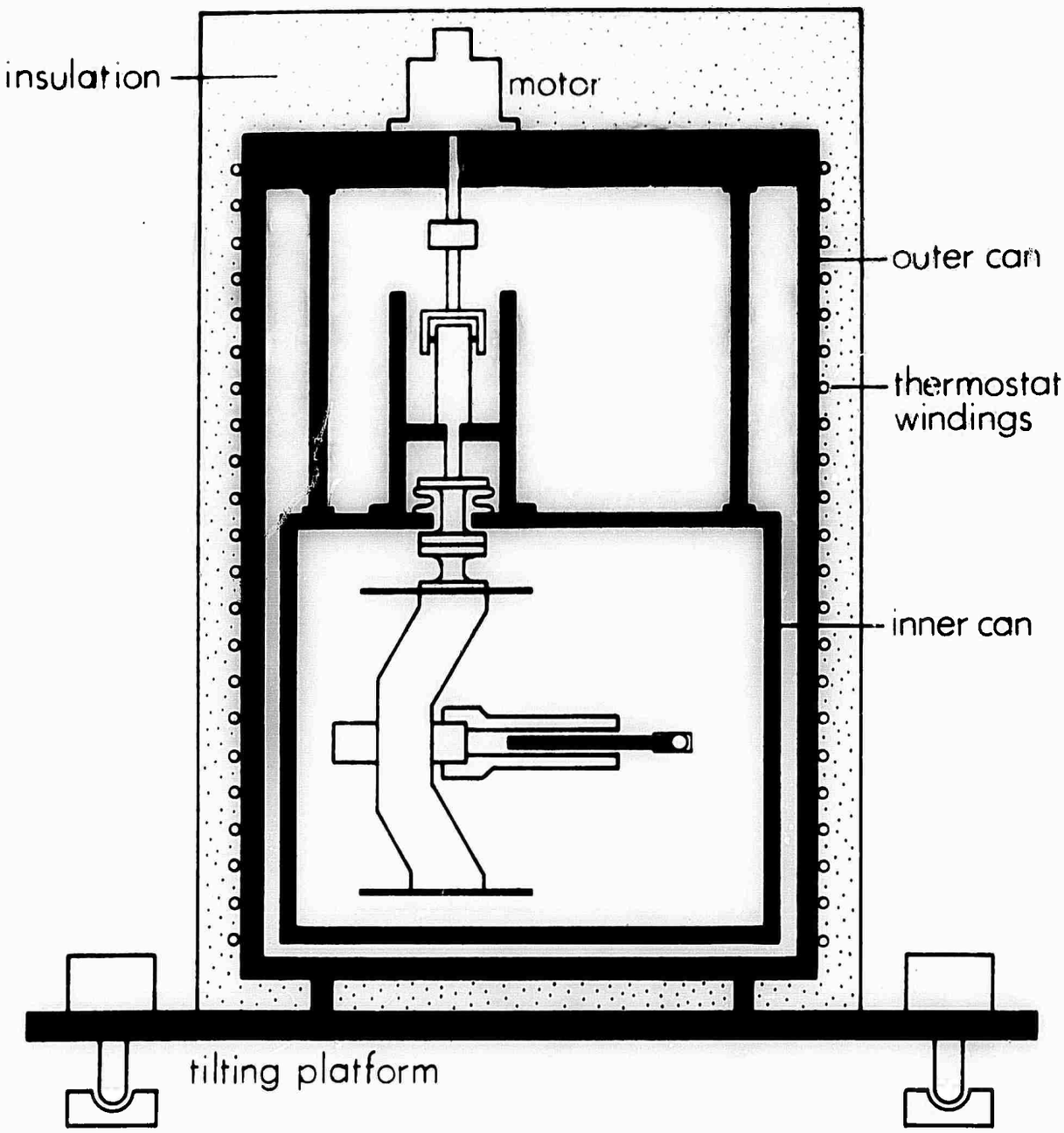

Figure 3. Double vacuum can assembly and tilting platform.

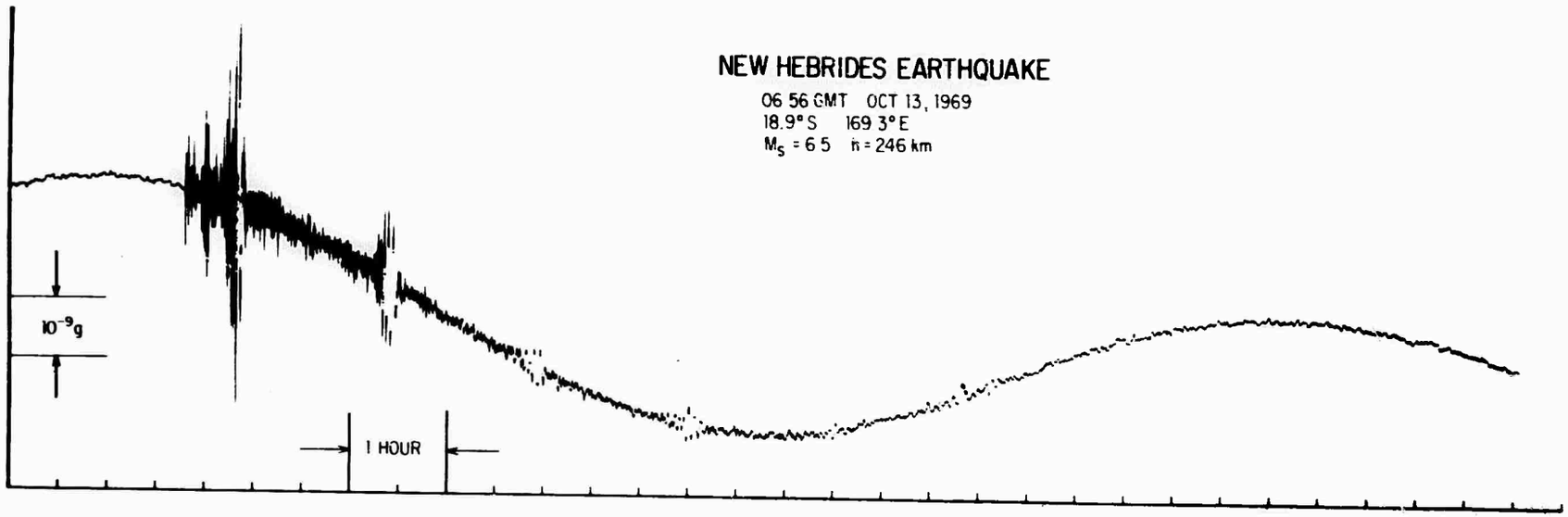

Figure 4. Filter output for New Hebrides earthquake M_S = 6.5, h = 246 km at 06:56 GMT, October 13, 1969; 18.9°S, 169.3°E.

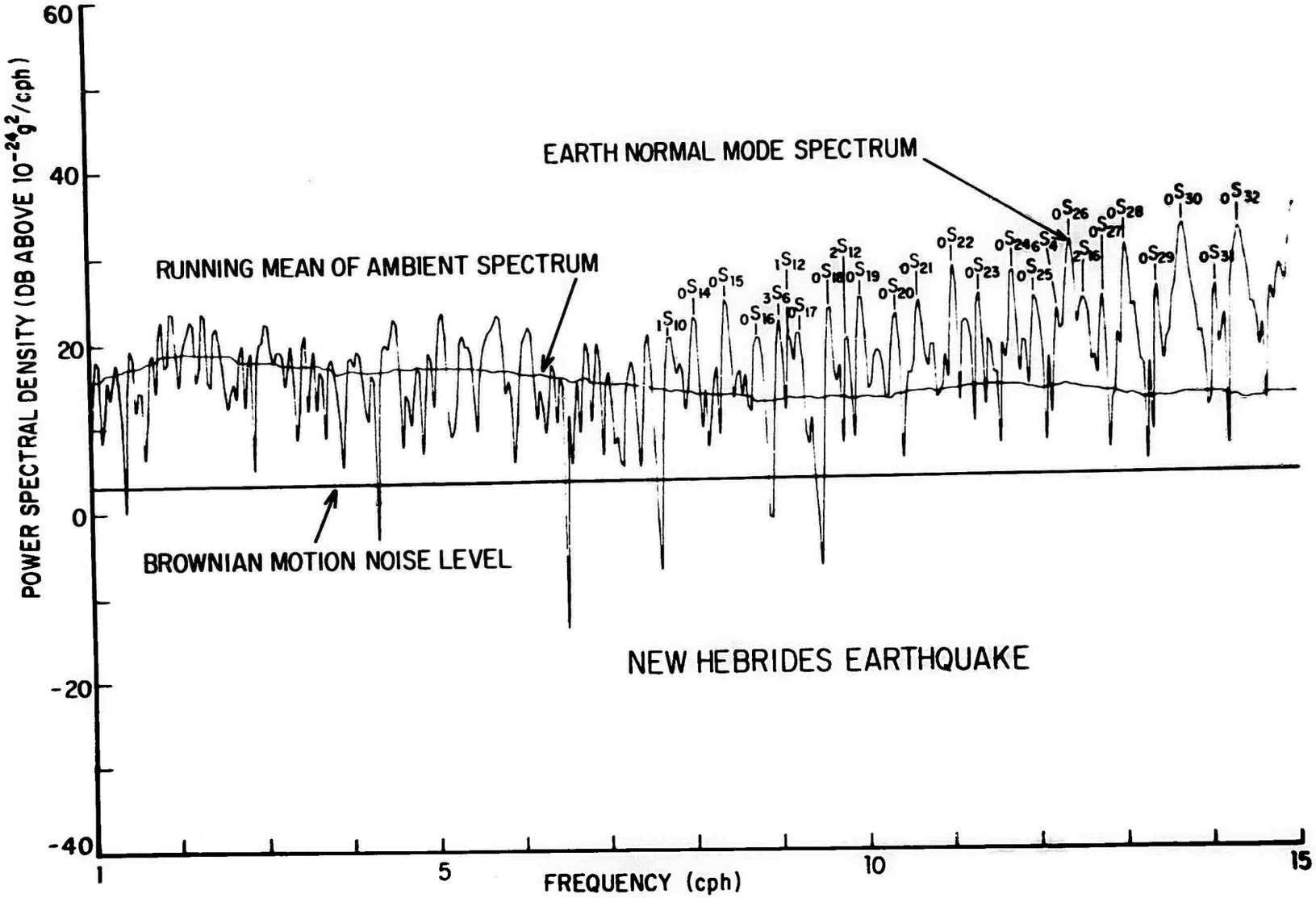

Figure 5. Power spectral density for New Hebrides earthquake of Figure 4 from 1 - 15 cph. 0 DB on Figure is 1 x 10^{-24} g^2/cph.

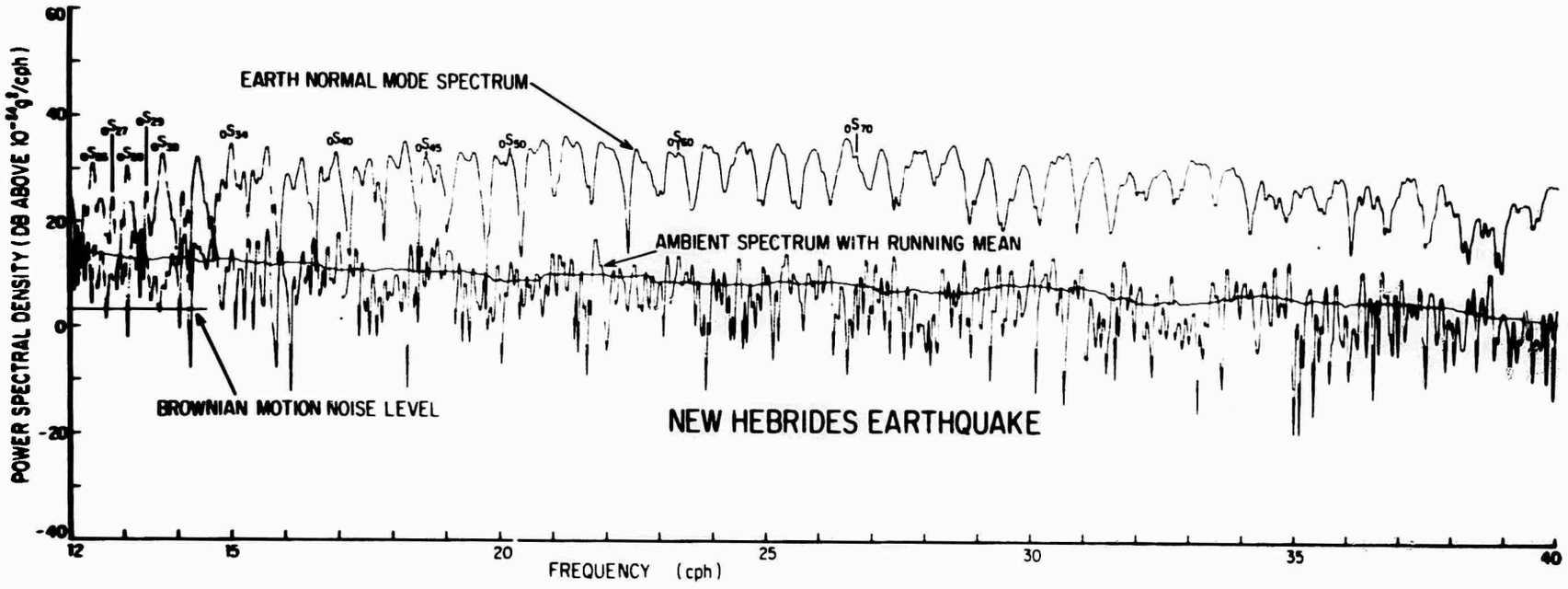

Figure 6. Continuation of Figure 5 from 12 - 40 cph.

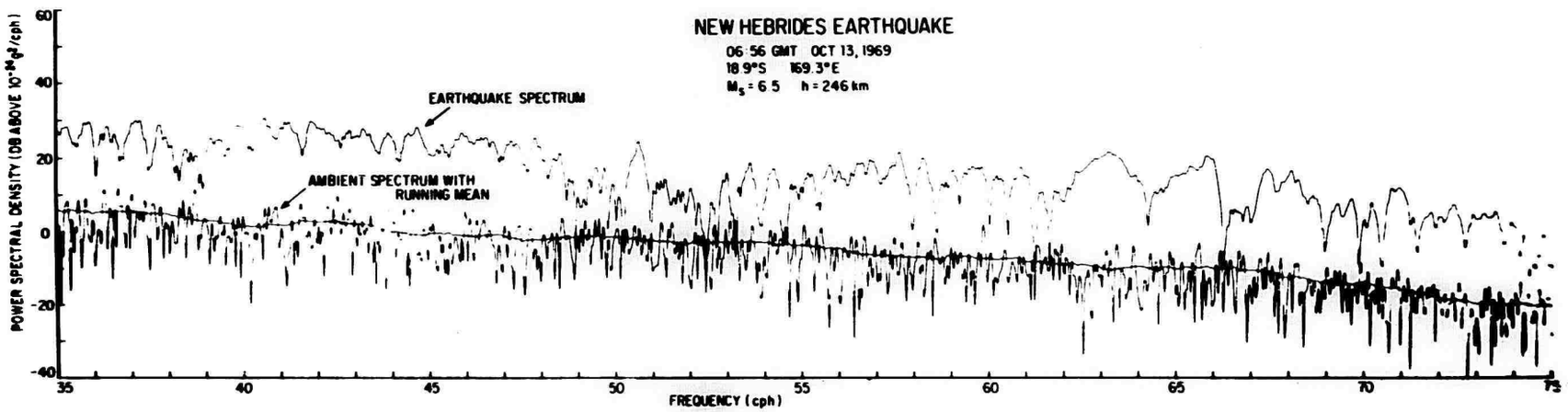

Figure 7. Continuation of Figure 6 from 35 - 75 cph.

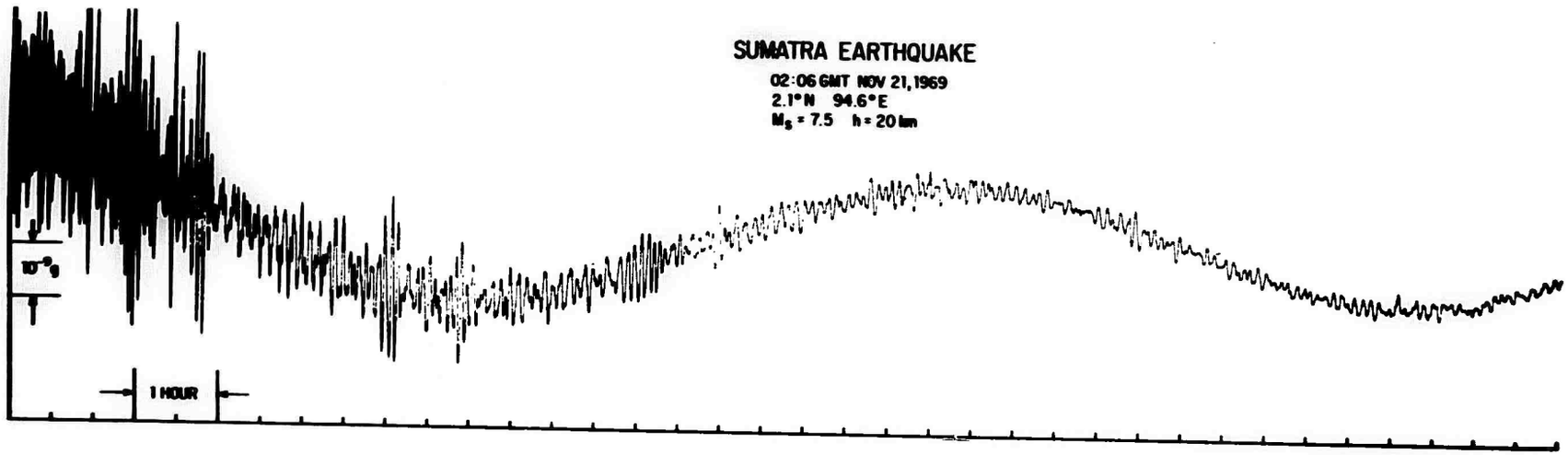

Figure 8. Filter output for Sumatra earthquake, M_S = 7.5, h = 20 km at 02:06 GMT, November 21, 1969; 2.1°N, 94.6°E.

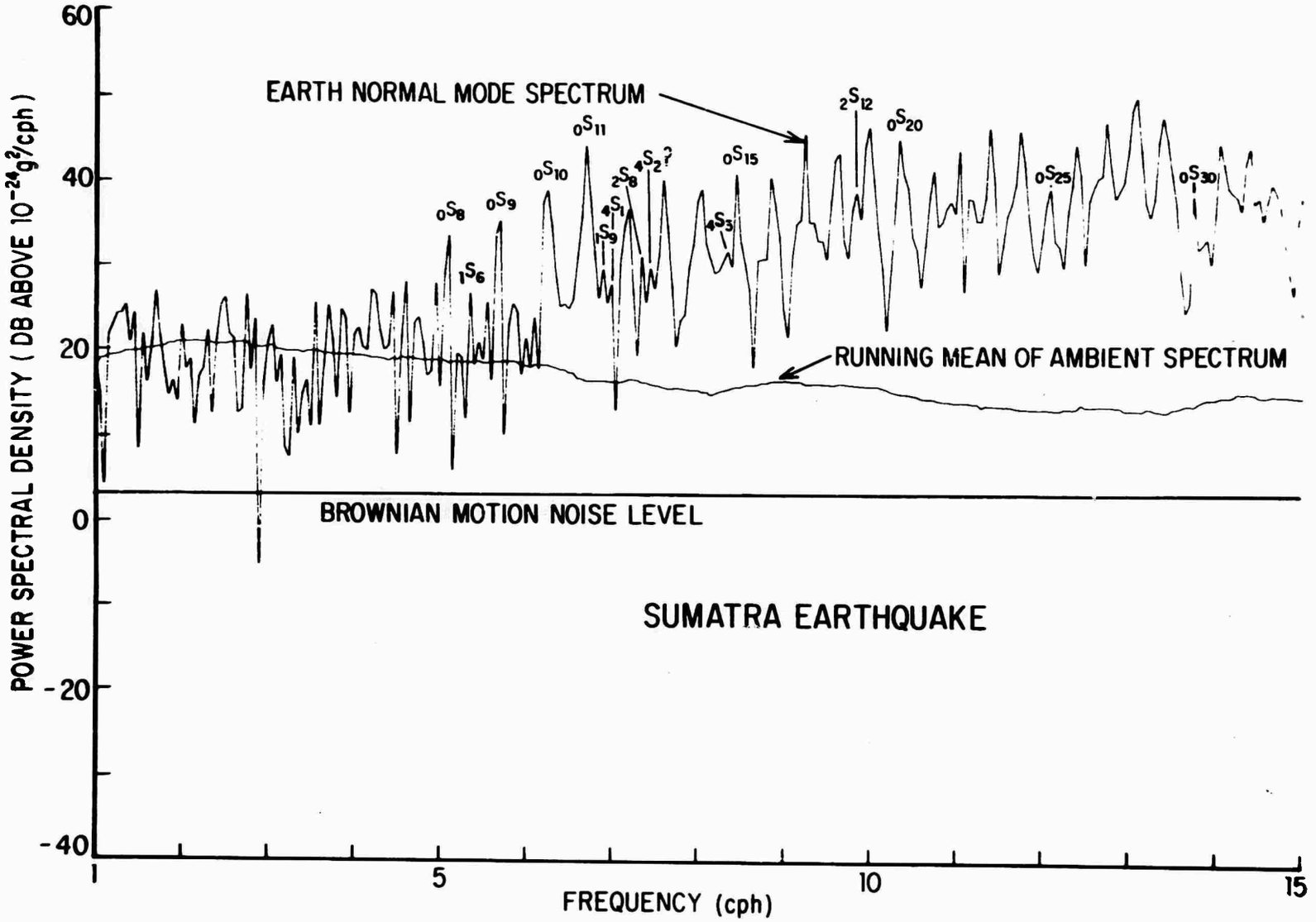

Figure 9. Power spectral density for Sumatra earthquake of Figure 8 from 1 - 15 cph. 0 DB on Figure is 1 x 10^{-24} g2/cph.

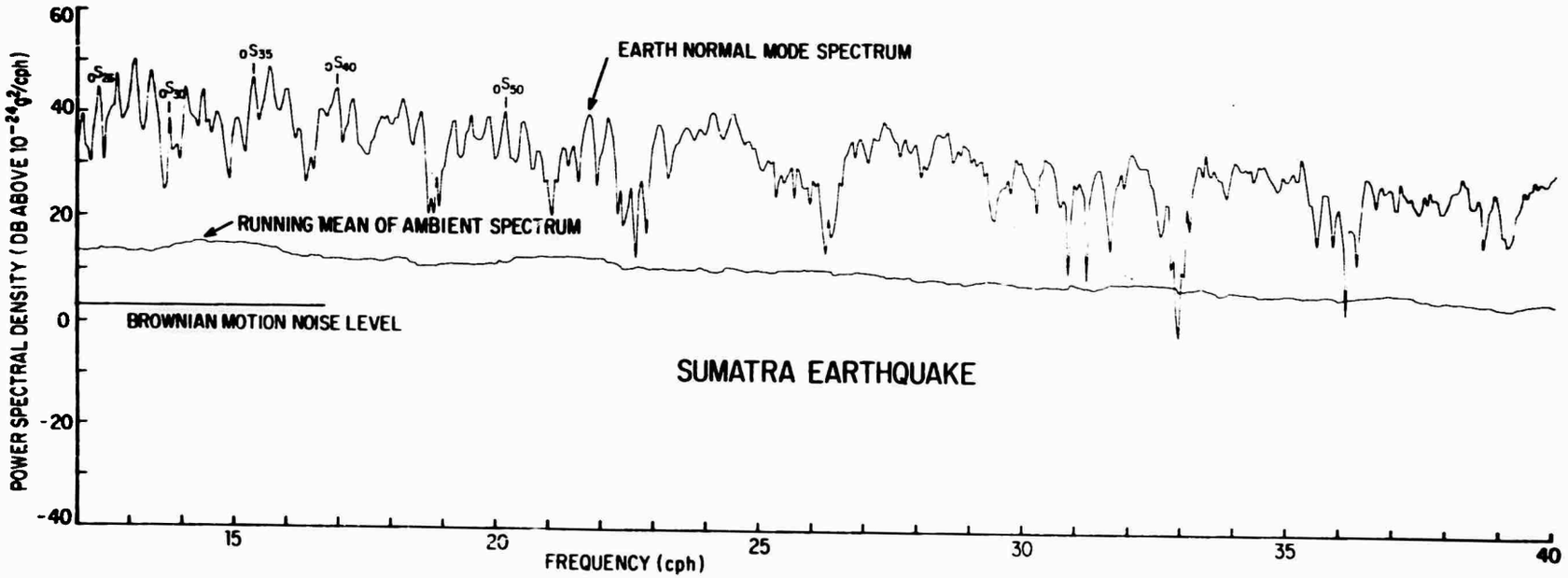

Figure 10. Continuation of Figure 8 from 12 - 40 cph.

SHORT PERIOD SPECTRAL DISCRIMINANTS FOR EXPLOSIONS

By

William H. Bakun
Lane R. Johnson

Seismographic Station
Department of Geology and Geophysics
University of California
Berkeley, California

SUMMARY

Spectra (0-5 Hz) of the Pg phase at JAS, California (Δ = 250-500 km), for 69 events (M = 2.8-4.5) located within 100 km of NTS are used to investigate source differences between the short period spectra of nuclear explosions and 'natural' earthquakes. The Pg spectral ratio (0.6-1.25 Hz)/(1.35-2.0 Hz) of ground displacement satisfactorily discriminates NTS explosions from 'natural' earthquakes for a threshold magnitude at least as low as M = 3.2. The explosion spectra are relatively richer in the high frequency band (1.35 - 2.0 Hz) than are the natural earthquake spectra. An interesting result suggested by this study is that the short period P-wave spectra of 'afterevents' of large NTS explosions resemble the spectra of explosions rather than that of 'natural' earthquakes.

BLANK PAGE

INTRODUCTION

The problem of identifying underground nuclear explosions has received the close attention of many seismologists in the last ten years. Of the many proposed explosion discriminants, the body wave-surface wave magnitude (m:M) criteria seems the most promising. The SIPRI report (1968) concluded that the m:M criteria is a "positive identifier" for m≥4 3/4.

Using the m:M criteria with Canadian stations for western North America events, Basham (1969) demonstrated a separation of the earthquake and explosion populations for m>4.5. Basham noted that due to continental margin and/or propagation path effects on the surface wave amplitudes, the m:M detection threshold for intercontinental distances may be at best about m=4.7.

Using data from the Berkeley (BRK) broad band system at a distance of 500 km from NTS, McEvilly and Peppin (personal communication, 1970) have found a separation of the NTS explosion and Nevada earthquake populations down to a threshold magnitude at least as low as m = 3.7. Surface waves for smaller events are lost in the background noise.

The new high-gain long-period seismometers (Molnar et al, 1969) are capable of recording events with M_S possibly as low as 2.7 (~m = 3.7 for explosions) at epicentral distances of 30° or more. Data are thus becoming available to test even lower thresholds of the m:M criteria for intracontinental discrimination.

Discrimination criteria based solely on direct P-waves have also received considerable attention. The SIPRI report (1968) indicates that P-wave spectra are a diagnostic aid and a possible "positive identifier" for events with m>5.25. Using the LASA short period instruments, Lacoss (1968) has evaluated a spectral ratio criteria that discriminates between earthquakes and explosions if decision rules based on noise analyses are employed. Unfortunately the probability of making any decision falls from unity at m=4.5 to near zero at m≃4.1.

Since earthquakes and explosions have different source time histories, one might expect a systematic difference in their high frequency asymptotic behavior. With respect to earthquakes, Haskell (1966) and Aki (1967) have considered theoretical models of a dislocation across a fault imbedded in an infinite elastic medium. Haskell assumed a particular time history for the dislocation which resulted in a $1/\omega^3$ high frequency spectral asymptote for the body wave spectrum while Aki assumed a different time history which resulted in a $1/\omega^2$ spectral asymptote.

In this paper we report an attempt to evaluate P-wave spectral discriminants at small epicentral distances (Δ~2-4°); the hope was that encouraging results might be extended for stations at larger epicentral distances. The demonstration that spectral differences between earthquakes and explosions do exist down to low magnitude 3 events should lend impetus to research on spectral discriminants at

teleseismic distances and improvement in detection methods required for operations at this level. Because there is no continental margin effect on teleseismic P-wave propagation, a successful intracontinental P-wave spectral discriminant might easily be extended to an intercontinental discriminant.

Data

The data used in this study have been restricted to the output of a single high-gain (600 K at 1 Hz, background noise ~ 1 mμ at 1 Hz) vertical short period seismograph at Jamestown, California (JAS), located 340-410 km from explosion epicenters at the Nevada Test Site (NTS) (Figure 1). JAS (37°56!8 N., 120°26!3 W., elev. = 457 m) lies in the Sierra foothills and is part of the Berkeley seismographic net. Since October, 1965, the output of a 14 kgm vertical Benioff (T_0 = 1 sec, T_g = 0.2 sec) seismometer at JAS has been telemetered to Berkeley and recorded on magnetic tape. (The tape system at Berkeley is described in detail by Rodgers et al, 1965.)

This magnetic tape library was searched for events with hypocenters within 100 km of NTS. Sixty-nine events (Table 1) with equivalent Wood-Anderson magnitudes ranging from 2 3/4 to 5 were selected. The lower magnitude limit corresponds to a P_g signal-to-noise ratio of about 2. The upper magnitude limit corresponds to P clipping for distances of about 500 km from JAS.

Table 1 includes the following types of events: (a) announced underground nuclear explosions at NTS, (b) 'natural' earthquakes, (c) 'afterevents' of the large underground nuclear explosions BOXCAR, BENHAM, and JORUM, (d) subsidence of craters (collapses) of underground nuclear explosions, and (e) unidentified events with epicenters on NTS. An example of types (a), (b), (e) and (c) is shown in Figure 2. The type (b) 'natural' earthquake category is limited to earthquakes with accurate epicenters at least 30 km outside the NTS boundary. The type (c) 'afterevent' category is reserved for events with epicenters within about 20 km of the explosion shotpoint and occurring in a time span similar to that of aftershocks in an earthquake aftershock sequence. The last type, (e), consists of all events with epicenters on NTS which were not included in types (a), (c) or (d) and presumably contains some 'natural' earthquakes in addition to 'afterevents' or collapses of nuclear explosions which we have failed to identify. No claim is made for completeness of the event population of Table 1 in the epicentral area and magnitude range listed.

The most frustrating part of this study was the unavailability of more events that could be classified as known 'natural' earthquakes. All recent studies of discriminants (i.e., the SIPRI report, 1968) have stressed the necessity of examining events on a regional basis. In order to limit propagation effects this study was restricted to events having a small azimuth range (Figure 1). The propagation path JAS for NTS events crosses the Basin and Range Province, White

Mountains and the Sierra Nevada. Propagation along other azimuths to JAS could introduce serious unknown propagation path effects.

In the distance range 250-500 km P_n is the first arrival with an apparent velocity of about 7.9 km/sec. Arriving 8-10 sec after P_n with an apparent velocity of about 6.1 km/sec is the prominent phase which we have identified as P_g. In general we have attempted to carry out a dual analysis of both the P_n and P_g phases. However, for the data considered in this report the results have been inconclusive, which probably reflects the fact that the signal-to-noise ratio for P_n was small (Figure 2). Thus most of this report will be concerned with the analysis of the P_g phase.

The magnitudes quoted in Table 1 are based on both P_n and P_g amplitudes at JAS, using a scale calibrated by Wood-Anderson magnitudes at BRK for larger events. Magnitudes computed separately from the P_n and P_g amplitudes consistently agree to 0.1 to 0.2 units. We feel that the magnitudes used are self-consistent to an accuracy of 1/4 magnitude unit.

The data were digitized (12-bit resolution) at 50 samples/sec with a tolerance of 0.5% in the sampling rate. The minute of record preceding the P_n-wave onset was also digitized for purposes of noise analysis. The data were Fourier transformed using an 8 sec window with a cosine taper applied to the final 2 sec. The 8 sec window length was selected because this is the minimum P_g-P_n time at JAS for the event population used. Numerical experiments with shorter window lengths indicate that the result of this study are not altered by reasonable changes in the window length. A typical signal and the resultant spectra are shown in Figure 3.

Noise analyses indicate that for the epicentral distances involved (250-500 km) signal amplitudes are lost in the background noise for frequencies greater than about 5 Hz. For events in the magnitude range 3-5, signal amplitudes for frequencies less than about 0.6 Hz are generally near the microseism level. Thus, all analyses discussed in this paper have been restricted to the 0.6 - 5.0 Hz band.

The spectral moduli were corrected for instrument response and attenuation. A value of 400 was assumed for Q for both P_n and P_g. Numerical experiments indicated that reasonable variations in this assumed value would not change the conclusions of this paper.

Spectral asymptotes

Haskell's (1966) and Aki's (1967) earthquake source models predict high frequency spectral asymptotes in the far-field of $1/\omega^3$ and $1/\omega^2$, respectively. By assuming various dislocation time histories, one could predict a range of asymptotic behavior. Although explosion source obviously do not fit the source geometries assumed by Haskell and Aki, appropriate models and source time histories presumably would yield characteristic asymptotic behavior, which might be different than that predicted for earthquakes.

Least-squares regression lines were computed for both the P_n and P_g log displacement vs log frequency data. The slopes showed no recognizable pattern that could be used to discriminate between earthquakes and explosions. The notches in the spectral moduli (scalloping) introduce large uncertainties in the computed slopes. An unsuccessful attempt was made to alleviate this difficulty by computing the least-squares regression lines to the relative maxima in the log-log spectral data.

Although our attempts to use the spectral asymptotes as a discriminant were unsuccessful, we are not convinced that this approach is without promise. The spectral scalloping can be explained by the arrival of secondary pulses (Pilant and Knopoff, 1964) due to near source and/or near receiver reverberations. A more elaborate analysis which takes account of these secondary arrivals might possibly demonstrate spectral asymptotes to be a useful discriminant.

Spectral ratio

A preliminary examination of the spectra of the large earthquakes and announced explosions in our event population indicated that 0.6-2.0 Hz was the most promising spectral band for discrimination at JAS for NTS events. As noted previously, the spectral amplitude for frequencies less than about 0.6 Hz is near the microseism level at JAS for the magnitudes and distances considered in this study. Other P-wave spectral discriminant schemes that rely on spectral information below about 0.6 Hz might also suffer from serious noise contamination. The fact that the LASA spectral ratio incorporates information at frequencies down to 0.35 Hz might explain the serious noise contamination noted for lower magnitude events (Lacoss, 1968).

A spectral ratio which compares the average ground displacement in the 0.6 - 1.25 Hz band to that in the 1.35 - 2.0 Hz band for P was found to be a satisfactory discriminant. The spectral ratio was defined as:

$$R = \frac{\sum_{i=7}^{14} C_i S_i}{\sum_{i=15}^{22} C_i S_i}$$

where Ci are the instrument response and attenuation corrections to the spectral moduli S_i. The frequency increment is .09766 Hz.

The computed values of this spectral ratio for the P_g phase are shown in Figure 4. Standard errors of the computed spectral ratios for the smaller events are indicated by error bars. Noise spectra were computed using the same data window and computational procedure as in the signal analysis for 5 segments of the record in the minute

preceding the P_n onset. The variance of the noise at each spectral point was then used in computing the spectral ratio standard errors. The noise was assumed to be stationary and the only source of error in the estimated spectral ratio.

Two areas in Figure 4 have been delineated: 1) 'natural' earthquake, and 2) explosion. All known 'natural' earthquakes and no announced explosions lie in 1; no known 'natural' earthquakes and all announced NTS explosions lie in 2. Most of the unidentified type (3) events fall in field II. Collapses follow no pattern as might be expected in light of their highly variable source time histories. Presumably collapses can be identified by other means.

It is interesting to note that all the 'afterevents' associated with the large underground NTS explosions BOXCAR, BENHAM and JORUM lie in II, the explosion field, rather than in 1, the earthquake field. Basham et al (1970), using the Lacoss (1968) spectral ratio for teleseismic P-waves recorded at Canadian stations, found that three BENHAM 'afterevents' separated from three NTS explosions. Of the six events used in their study, only the 19 December 1968 BENHAM 'afterevent' at 2223 GMT (No. 58, Table 1) did not clip on the P_g phase at JAS, so that a meaningful comparison of their result to the work reported in this paper is not possible.

The spectral ratio frequency bands chosen in this work were selected because they seemed appropriate for the JAS instrument response, the magnitude range and the epicentral distance to the events studied. Different spectral bands might be chosen for various other combinations of these factors.

In Figure 5, representative P_g spectra are shown, corrected for attenuation, over a range of magnitudes for announced explosions and 'natural' earthquakes, respectively. In a discriminant it is desirable to select the frequency band least contaminated by background noise in which spectral differences exist. As magnitude decreases, progressively less energy is generated at the lower frequencies relative to the higher frequencies. This shift in dominant frequency with magnitude suggests that it might be advisable to choose spectral bands as a function of magnitude. For example, a better separation of the explosion and 'natural' earthquake populations for $M>3.6$ would possibly result if the smaller magnitude events ($M<3.5$) were analyzed by a second spectral ratio with bands shifted to higher frequencies.

For epicentral distances of 250-500 km, hypocenter location becomes a very critical factor. For example the event on April 28, 1967 (No. 15) is poorly located. A possible error in the location of 100 km would increase the magnitude from 2.9 to 3.2, putting the event inside II, the explosion field. Possible errors in the analysis of this event lead us to hesitate to make any discriminant decision. This event gives some idea of the threshold magnitude of the JAS P_g spectral ratio discriminant in the frequency range used. As another example, if the White Mountain earthquake of October 27, 1967 (No. 30), which is well

located, were to be mislocated at Pahute Mesa, 100 km further from JAS, the magnitude would increase from 2.8 to 3.0. This would move the event from field I, the earthquake field, into field II, the explosion field. Of course a hypocenter error of 100 km at teleseismic distances would not present the serious errors in magnitude determination discussed here. The error in the attenuation correction introduced by a mislocation of 100 km does not alter the computed spectral ratios to any significant degree.

Explosion 'afterevents'

The explosion-like character of the 'afterevents' of BOXCAR, BENHAM, and JORUM indicated in Figure 4 was further investigated by forming a composite spectra of these events. All 'afterevents' in the magnitude range 3.4-4.3 that are not thought to be collapse events are included. The individual spectra were corrected for attenuation and normalized to their maximum amplitude before being summed at each frequency to form the composite. The BOXCAR, BENHAM, and JORUM composites are similar.

In Figure 6 the BENHAM composite (including events No. 55, 56, 57, 59, 62, 63, and 64) is plotted together with similarly constructed composites for 18 announced explosions, and all events in the earthquake field (I) in the magnitude range 3.4-4.3. The spectral similarity between explosions and their afterevents is evident. The demonstrated P_g spectral differences between 'natural' earthquakes and explosions for epicentral distances of a few hundred km might be detectable for teleseismic P-waves if sensitive enough instruments and careful analysis are employed.

Discussion

According to the P_g spectral ratio criteria, events fall into two separate populations. The announced explosions in field II are located over lateral distances of 60 km (Yucca Flat and Pahute Mesa) in the geologically complex NTS region. Unidentified events within NTS fall in both fields I and II. Known 'natural' earthquakes on the near (No. 30) and on the far (No. 4, 16, 17) sides of the NTS from JAS lie in field I. These facts lead us to believe that the differences noted between earthquake and explosion spectra are real and not merely a reflection of the source region geology.

It is important to point out that the discrimination displayed in Figure 4 could possibly be due to the effect of focal depth. It may be that all of the type (a) and (e) events in field I have appreciably greater focal depths than the type (b), (c) and (e) events in field II. We have been unable to obtain reliable estimates for the focal depths of the 'natural' earthquakes. The explosions are shallow focus and available information on the BENHAM 'afterevents' (Hamilton et al, 1969) indicates that they have focal depths of less than 10 km. Thus, the effect of focal depth cannot be eliminated as a possible explanation of the spectral differences.

The result that short period P-wave spectra of 'afterevents' of large explosions resemble explosions rather than earthquakes is puzzling. Although these 'afterevents' are not capable of being separated from explosion by P-wave spectra, the analysis has identified them as explosion-related events. McEvilly and Peppin (personal communciation, 1970) find that these 'afterevents' are identified as earthquakes by the m:M criteria. Apparently the explosion 'afterevents' generate explosion-like short period P-wave spectra and earthquake-like surface waves. We do not have a convincing explanation of this phenomenon. In some way the short time strain field of the explosion is expressed in the short period P-wave spectra, yet the 'afterevent' surface wave generation is indicative of the large source regions associated with 'natural' earthquakes. By using the short period P_g-wave spectral ratio in conjunction with the m:M criteria, it appears that the 'afterevents' of large explosions can be separated from 'natural' earthquakes and explosions and defined as a third type of event.

Events No. 18, 19, 20, and 21, which are located near Pahute Mesa and are the only events on NTS that were identified as 'natural' earthquakes by the spectral ratio criteria, occur 2-6 hours after the underground nuclear explosion SCOTCH on May 23, 1967, at Pahute Mesa (OT = 14 00 00.0 GMT; shot-point coordinates = 37°16'30"N, 116°22'12"W; BRK Wood-Anderson magnitude = 5.6). We have classified these events as unidentified, but it is clear that in accordance with our classification cirteria for type (c) events they might also be considered as 'afterevents' of the explosion SCOTCH. If these four events actually are SCOTCH 'afterevents', then their spectral behavior is different from that of the 'afterevents' of the larger NTS explosions BOXCAR, BENHAM, and JORUM which all had magnitudes of about 6 1/4.

This uncertainty about the events No. 18, 19, 20, and 21 has led us to consider them in a little more detail. The largest of these events, No. 21, has a magnitude of 3.7 and is thus near the detection threshold of the body wave-surface wave (m:M) criteria. Although the surface wave signal-to-noise ratio at BRK is quite small for this event, McEvilly and Peppin (personal communication, 1970) find that according to their body wave-surface wave generation criteria (m:M), this event would not be identified as an explosion. McEvilly and Peppin also find that, in terms of the relative Love to Rayleigh wave generation and the phase relation of the Rayleigh wave to the Rayleigh wave generated by the explosion SCOTCH, this event is not a collapse following SCOTCH, but that it closely resembles, in these characteristics, the dipslip 'afterevents' of the BENHAM explosion that they have studied. A couple of other points are worth noting. To our knowledge, 'afterevents' have previously been observed only for explosions with magnitudes greater than 6. Thus the occurrence of 'afterevents' of a magnitude 5.6 explosion is anomalous in itself. It is also interesting to note that according to McKeown and Dickey (1969) the SCOTCH event was accompanied by fracturing on nearby faults for a distance of about 1 1/2 km.

CONCLUSIONS

1. A P_g spectral ratio which compares the average ground displacement in the 0.6 - 1.25 Hz band to that in the 1.35-2.0 Hz band at JAS appears to be successful in discriminating NTS explosions from 'natural' earthquakes for $M \gtrsim 3.2$. The magnitude threshold may be substantially lower, particularly if the frequency bands used to define the spectral ratio are chosen to be a function of magnitude.

2. The short period (0.6-5.0 Hz) P_g-wave spectra of the 'after-events' of the large NTS explosions BOXCAR, BENHAM and JORUM resemble the spectra of NTS explosions rather than that of 'natural' earthquakes with epicenters near NTS.

3. As a general observation, details of the spectra we have studied are quite variable even for announced explosions with shot-points separated only by a few kilometers. These differences in the spectral detail might be explained by delayed secondary pulses due to near source reflections.

ACKNOWLEDGEMENTS

We wish to express our appreciation to Professors B.A. Bolt, P. Byerly, and T.V. McEvilly for their critical review of the manuscript. The California State Department of Water Resources provides funds for the maintenance of the Jamestown station. This research was sponsored by the Air Force Office of Scientific Research, Office of Aerospace Research, United States Air Force under AFOSR Grant No. 69-1783.

REFERENCES

Aki, K., 1967, Scaling law of seismic spectrum, J. Geophys. Res., v. 72, p. 1217-1231.

Basham, P.W., 1969, Canadian magnitudes of earthquakes and nuclear explosions in south-western North America, Geophys. J., v. 17, No. 1, p. 1-13.

Basham, P.W., Weichert, D.H., Anglin, F.M., 1970, An analysis of the 'Benham' aftershock sequence using Canadian recordings, J. Geophys. Res., v. 75, p. 1545-1556.

Hamilton, R.M., and Healy, J.H., 1969, Aftershocks of the BENHAM nuclear explosion, Bull. Seism. Soc. Am., v. 59, p. 2271-2281.

Haskell, N.A., 1966, Total energy and energy spectral density of elastic wave radiation from propagating faults: Part II, Bull. Seism. Soc. Am., v. 56, p. 125-140.

Lacoss, R.T., 1968, Semiannual technical summary report to the Advanced Research Projects Agency on seismic discrimination, Lincoln Laboratory, MIT, 31 December 1968, sec. 1, 1-20.

McKeown, F.A., and Dickey, D.D., 1969, Fault displacements and motion related to nuclear explosions, Bull. Seism. Soc. Am., v. 59, p. 2253-2269.

Molnar, P., Savino, J., Sykes, L.R., Lieberman, R.C., Wade, G., and Pomeroy, P.W., 1969, Small earthquakes and explosions in western N. America recorded by new high gain, long period seismographs, Nature, v. 224, p. 1268-1273.

Pilant, W.L., Knopoff, L., 1964, Observations of multiple seismic events, Bull. Seism. Soc. Am., v. 54, p. 13-39.

Rodgers, P., Marion, W., Sell, R., and Lomnitz, C., 1965, Magnetic-tape data-acquisition system, final report to the Advanced Research Projects Agency - a study of focal mechanisms and aftershock characteristics of small earthquakes, Seismographic Station, Univ. of California, Berkeley, p. 15-42.

SIPRI, 1968, Seismic methods for monitoring underground nuclear explosions - an assessment of the status and outlook, International Institute for Peace and Conflict Research, rapporteur - D. Davies, Stockholm, p. 130.

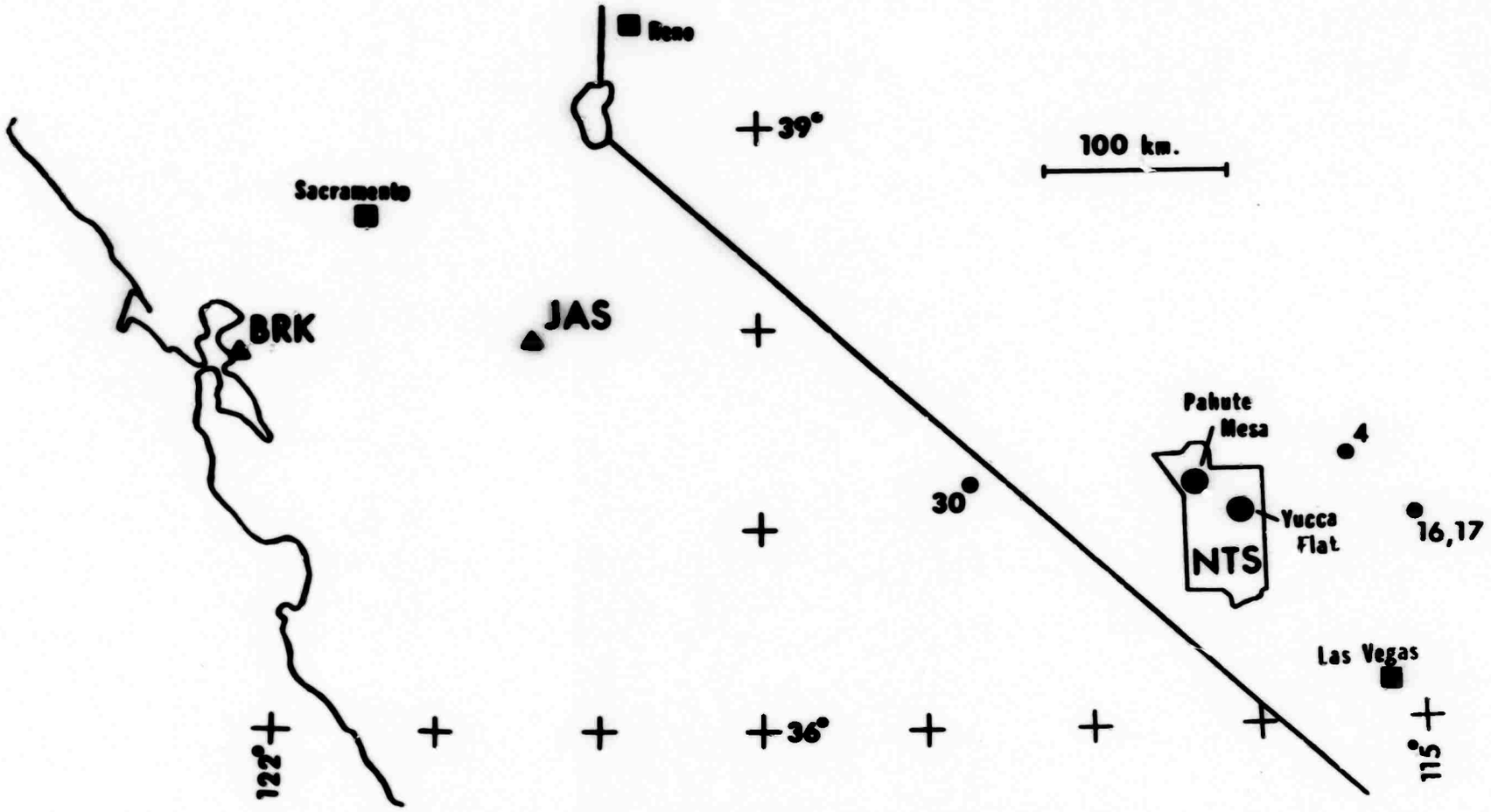

Figure 1. Map of the California-Nevada region showing the relationship of Jamestown (JAS), the Nevada Test Site (NTS), and the 'natural' earthquakes, plotted as small circles, used in this study. The earthquake numbering corresponds to the listing in Table 1.

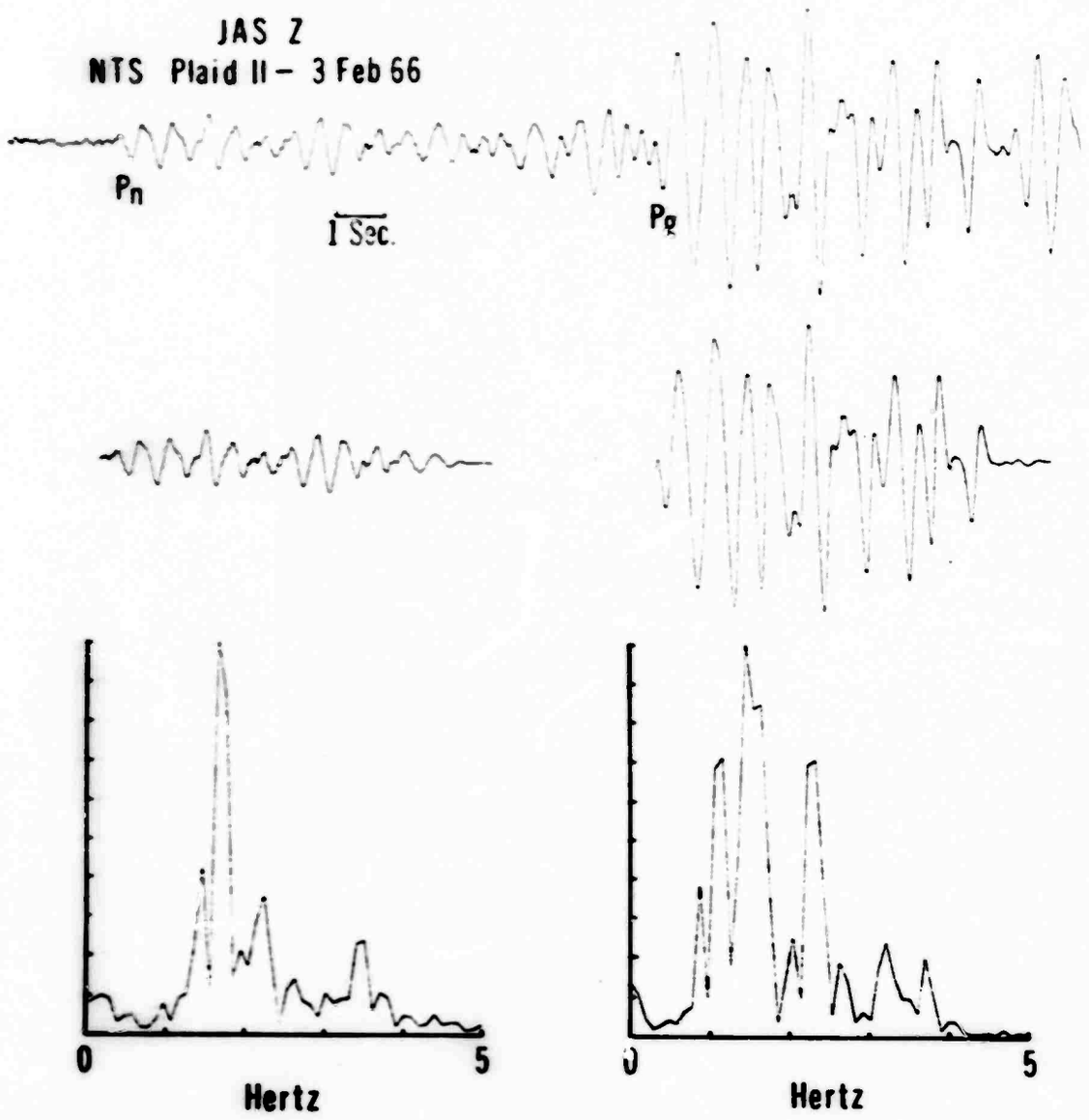

Figure 2. Seismograms recorded on the vertical Benioff at JAS. The traces from top to bottom are an announced NTS explosion, a 'natural' earthquake, an unidentified source, and a BENHAM 'afterevent', respectively. All of the traces have been normalized to the same maximum amplitude. The numbers refer to the listing in Table 1.

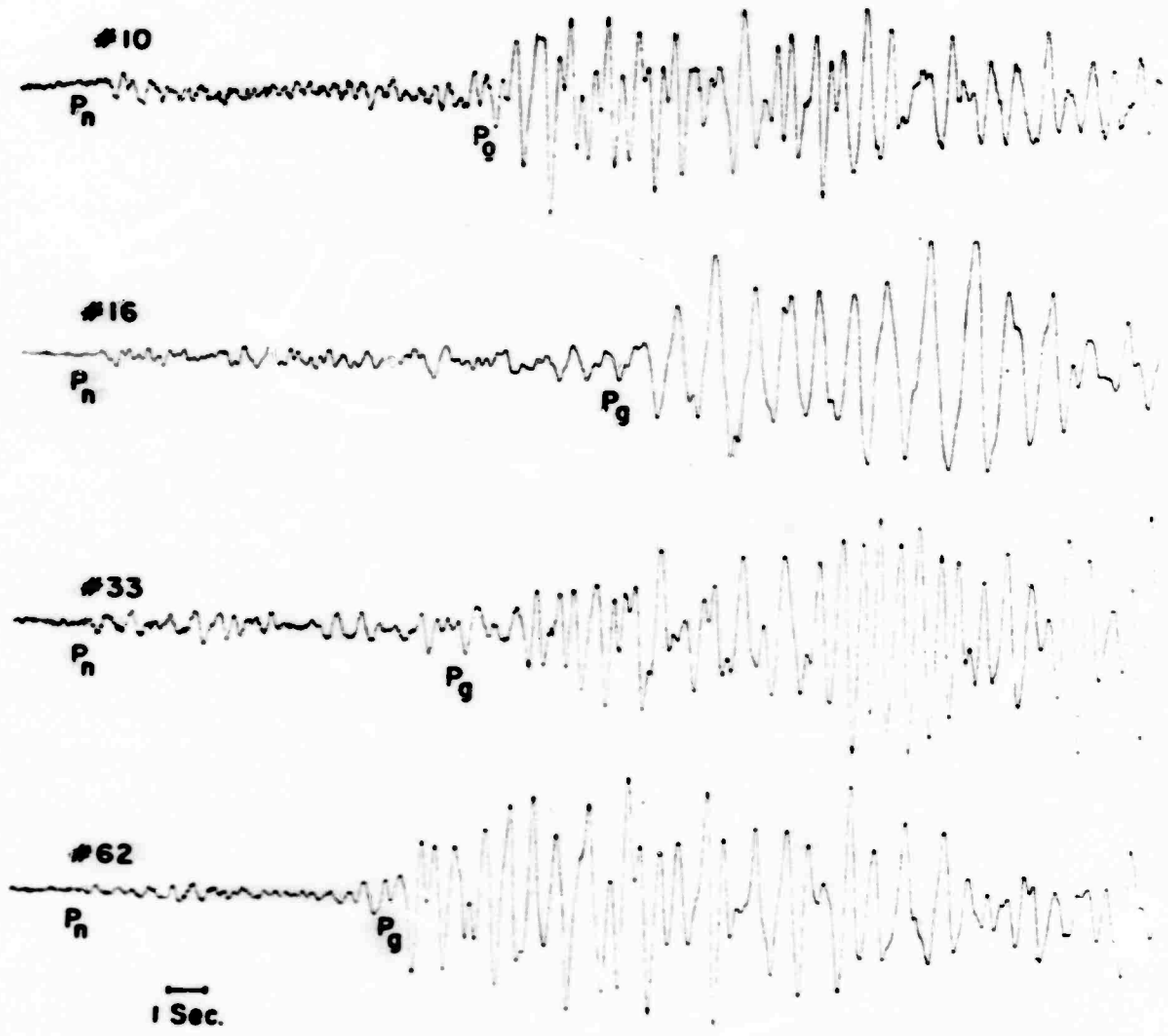

Figure 3. Digitized data of a typical time signal (top); P_n and P_g phases with the 8-second window used (middle); resultant spectral moduli normalized to 1 and plotted on a linear-linear scale (bottom). Spectra have not been corrected for attenuation or instrument response.

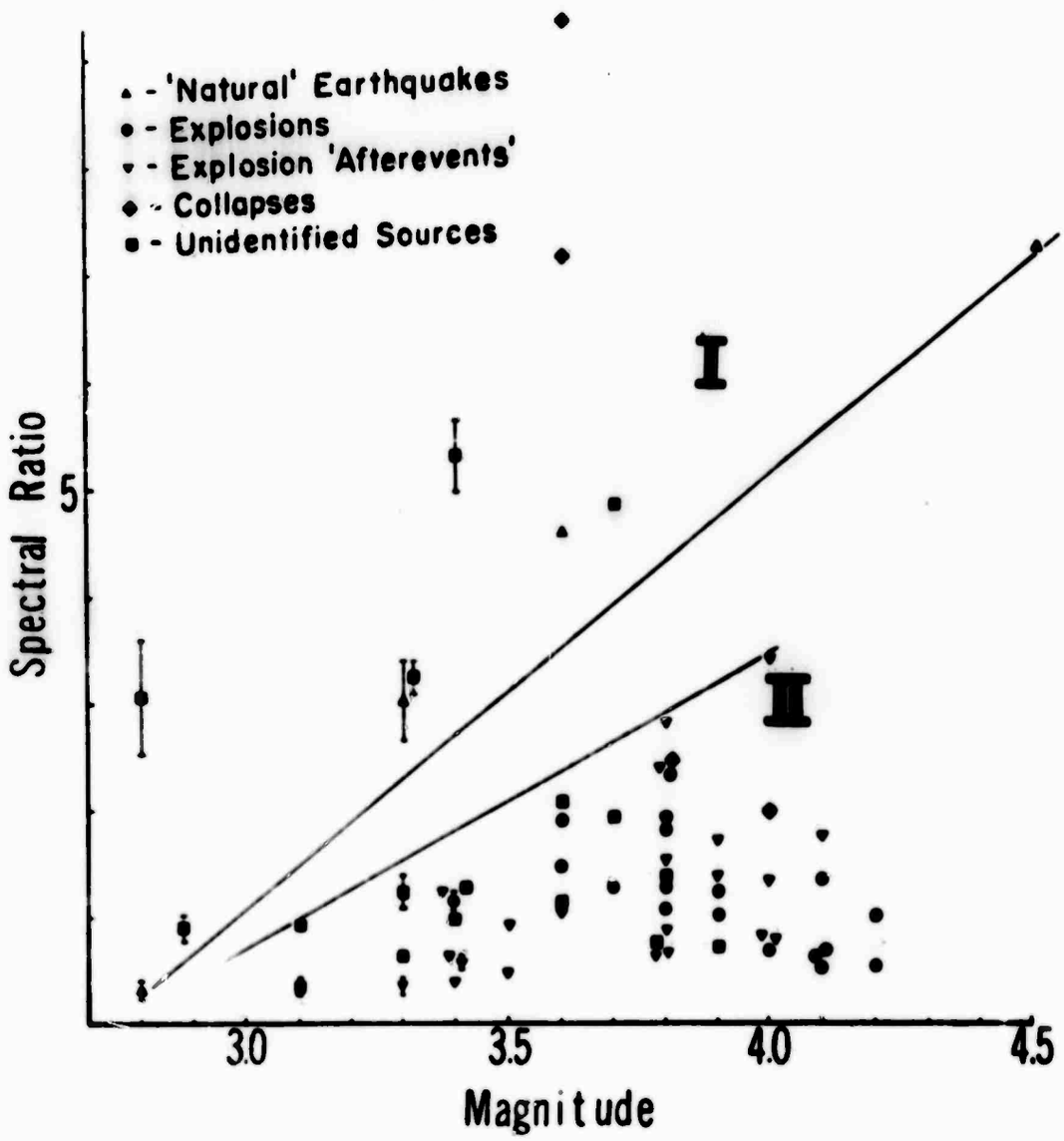

Figure 4. P_g spectral ratio of vertical surface displacement, corrected for attenuation with Q = 400, at JAS for events within 100 km of NTS. 1 and 2 denote the earthquake and explosion fields, respectively.

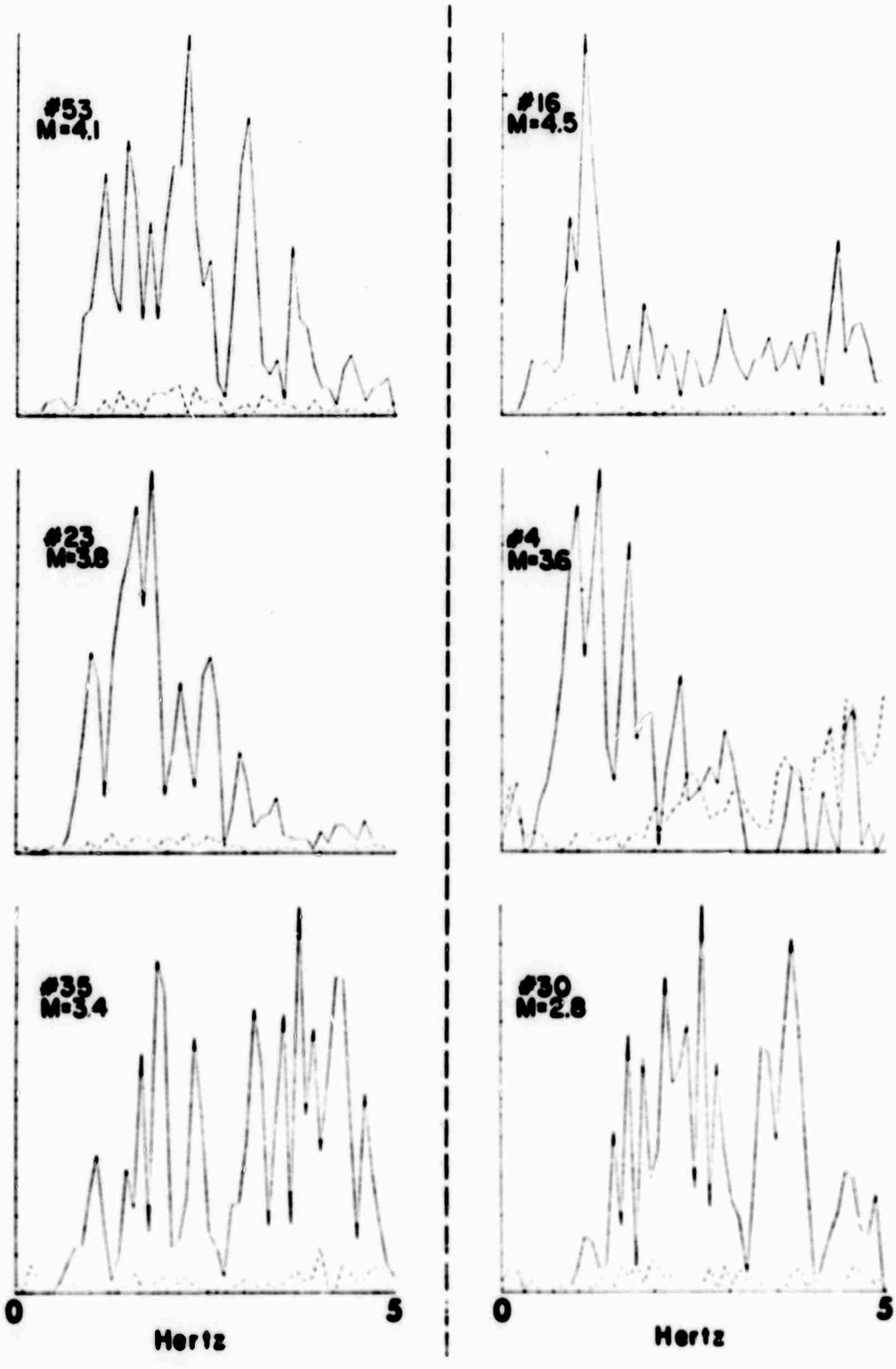

Figure 5. Spectral moduli of NTS explosions (left) and 'natural' earthquakes (right). Average spectral moduli of background noise are indicated by broken lines. Both signal and noise spectra have been corrected for attenuation (Q = 400). The ordinate and abscissa scales are both linear.

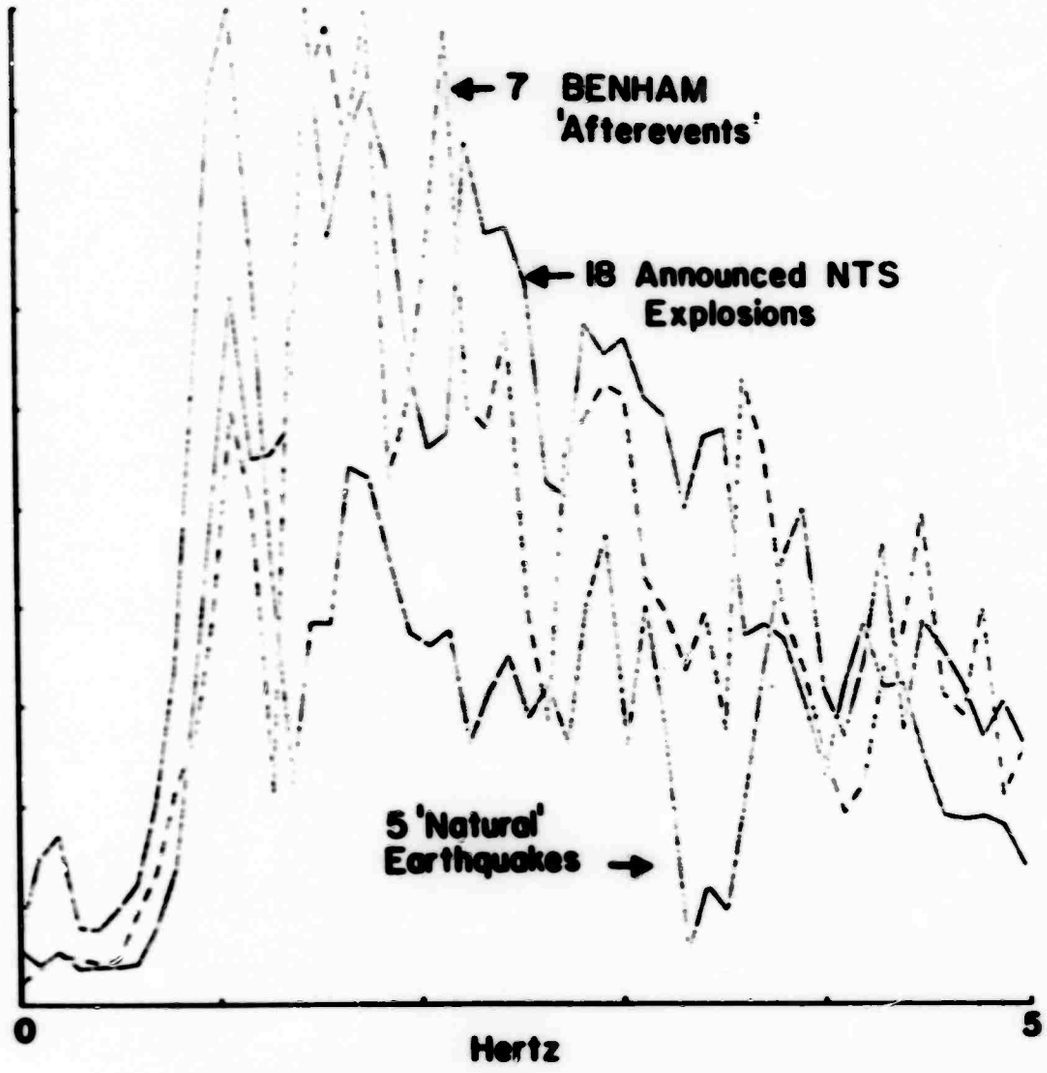

Figure 6. P_g composite spectra at JAS of announced NTS explosions, 'natural' earthquakes, and BENHAM 'afterevents'. Spectra have been corrected for attenuation (Q = 400).

Table 1. Event characteristics

#	Type	Date	OT (GMT)	Lat. (N)	Long. (W)	Δ (km) from GTA	M(L)	Spectral Ratio (P_g)	Comments
1	a	25 Feb. 66	18-17-27.1	37°07'34.7"	116°04'10.1"	387	4.8	1.00	FLACO II (Y), in alluvium[1]
2	a	01 Apr. 66	13-40-00	37 06 09.7	116 01 11.8	395	3.6	1.90	LUNE (Y), in alluvium[2]
3	a	26 Apr. 66	13-37-17.1	37 08 22.3	116 06 27.1	385	4.1	-	STUTZ (Y), in tuff[2]
4	b	06 Apr. 66	17-56-31.7	37.3	116.4	430	3.6	4.60	(3)
5	d	19 May 66	15-37-18	37 06 40.1	116 03 28.5	390	3.8	2.43	DUMONT Collapse (Y)[2]
6	d	1 July 66	01-33-40	37 18 36.9	116 17 56.3	390	4.0	1.99	HALFBEAK Collapse (Y)[2]
7	a	12 Sept.66	13-30-00.5	36 58 37.0	115 57 02.2	410	3.9	1.04	DERRINGER (Y)[2]
8	a	05 Jan. 67	23-15-23.1	37.3	116.5	360	3.6	1.15	(3)
9	d	20 Feb. 67	21-21-35	37 07 36.7	116 03 59.0	392	3.6	7.17	AGILE Collapse (Y)[2]
10	a	02 Mar. 67	03-00-00.0	37 09 37	116 02 50	395	3.6	1.49	ZUNI III (Y), in alluvium[2]
11	a	03 Mar. 67	15-19-00	(37.3)	(116.4)	(360)	3.4	1.58	(4)
12	a	07 Apr. 67	15-00-00.0	37 03 15.3	116 01 22	420	3.9	1.91	PAHUTE (Y), in alluvium[2]
13	a	21 Apr. 67	13-09-01.0	37 01 09.1	116 02 14.7	420	3.7	1.28	CHOCOLATE (Y), in alluvium[2]
14	a	27 Apr. 67	14-45-00.0	37 08 19.6	116 03 47.5	395	4.0	0.69	ERMINI (Y), in alluvium[2]
15	a	28 Apr. 67	19-22-58	37.1	116.0	(390)	2.9	0.91	(4)
16	b	27 May 67	16-31-36.1	37.0	116.0	400	4.5	7.22	(3)
17	b	30 May 67	03-43-01.0	37.0	116.0	400	3.3	3.01	(3)
18	a	13 May 67	13-37-47	(37.2)	(116.4)	(360)	3.4	5.24	Assume hypocenter of event at [illegible]
19	a	23 May 67	16-22-03	(37.2)	(116.4)	(360)	2.8	3.07	

Table --cont. 2

	Type	Date	OT (GMT)	Lat. (N)	Long. (W)	Depth from DTS	M(1)	Energy/Moment Ratio (2)	Comments
21	e	23 May 67	17-52-[illegible].1	37.3	116.4	360	3.3	3.26	(3)
24	e	23 May 67	20-1[illegible]-06.5	37.2	116.4	360	3.7	4.88	(3)
22	e	22 June 67	13-10-00.0	37°02'32"	116°01'43"	400	3.8	2.34	SATCH (Y), in tuff(2)
24	e	23 June 67	11-25-00.[illegible]	37 01 43	116 01 24	400	3.8	1.08	[illegible]ER (Y), in alluvium(2)
26	e	27 July 67	13-00-00	37 05 55.4	116 02 54.7	395	4.3	-	STANLEY (Y), in tuff(2)
25	e	03 Aug. 67	17-52-13.8	37.2	116.5	360	3.3	1.24	(3)
26	e	09 Aug. 67	06-45-05.3	37.2	116.7	340	3.4	1.24	(3)
27	e	10 Aug. 67	14-10-00.0	37 09 24.1	116 02 50.2	395	3.9	1.23	WASHER (Y), in tuff(2)
28	e	24 Aug. 67	13-30-00	(37.3)	(116.4)	(360)	3.9	0.70	(4)
29	d	07 Sept.67	14-24-50	37 09 11.4	116 03 10.0	380	3.6	9.37	ZARD Collapse (Y)(2)
30	b	27 Oct. 67	01-42-26	(37.2)	(117.7)	(260)	2.8	0.31	White Mountains Earthquake
31	e	15 Jan. 68	15-30-00.0	37 03 44.1	116 03 56.4	385	4.2	0.55	[illegible]MOPILE (Y)(2)
32	e	26 Jan. 68	16-00-00.1	37 16 51.1	116 30 52	350	3.8	1.80	CABRIOLET (F), in rhyolite(2)
33	e	31 Jan. 68	13-30-00	(37.3)	(116.4)	(360)	3.7	1.92	(4)
34	e	12 Mar. 68	17-04-00.1	37 00 27	116 02 11.9	350	4.1	0.66	[illegible]ESSY (R), in basalt(2)
35	e	14 Mar. 68	15-19-00.1	37 02 51.8	116 00 38.9	400	3.4	1.15	FONZARD (Y), in alluvium(2)
36	e	23 Apr. 68	17-01-30.0	37 20 15.8	116 22 32.1	345	4.1	0.54	SCROLL (F), in tuff(2)
37	e	26 Apr. 68	15-14-52.0	37.1	116.2	(360)	4.0	0.82	(3)-BOXCAR 'Aftershock' in Rayleigh wave
38	e	"	15-24-00	(37.2)	(116.4)	(360)	4.0	0.78	BOXCAR 'Aftershock'
39	e	"	15-32-21.0	37.2	116.5	360	4.3	0.93	(3)-BOXCAR 'Aftershock' (collapse?)

Table 1--page 3

#	Type	Date	OT (GMT)	Lat. (N)	Long (W)	Δ (km) from GTS	M(1)	Spectral Ratio (P_L)	Comments
-1	e	26 Apr. 68	16-08-00	(37.2)	(116.4)	(360)	3.5	0.93	BOXCAR 'Afterevent'
-2	e	"	16-12-30	(37.2)	(116.4)	(360)	3.4	0.65	"
-3	e	"	16-35-17.1	37.3	116.4	360	4.1	1.77	(3)-BOXCAR 'Afterevent'
-4	e	"	16--5-30	(37.2)	(116.4)	(360)	4.0	1.35	BOXCAR 'Afterevent'
-5	e	"	20-42-19.0	37.2	116.4	360	3.4	0.68	(3)-BOXCAR 'Afterevent'
-6	e	"	21-50-15	(37.2)	(116.4)	(360)	3.3	0.37	BOXCAR 'Afterevent'
46	e	27 Apr. 68	09-06-33	(37.2)	(116.4)	(360)	3.8	0.66	"
47	e	04 May 68	23-28-45.0	37.2	116.4	360	3.1	0.35	(3)
-8	e	15 May 68	16-01-11.0	37.2	116.3	360	3.3	0.63	(3)
-9	e	30 June 68	21-21-22.0	37.2	116.6	360	3.1	0.93	(3)
50	e	30 July 68	13-00-00.0	37°08'00"	116°04'56"	390	4.1	0.46	TANYA (Y)(2)
51	e	15 Nov. 68	15-30-00	(37.1)	(116.0)	(390)	3.6	2.09	(4)
1	a	15 Nov. 68	18-45-00.4	37 01 34	116 02 00	400	3.8	1.27	KNIFE B (Y)(2)
52	a	22 Nov. 68	16-19-00.2	37 08 24	116 02 32	395	4.1	1.35	TINDERBOX (Y)(2)
54	e	12 Dec. 68	15-20-00	(37.1)	(116.0)	(390)	3.8	1.36	(4)
55	e	19 Dec. 68	17-30-22.8	37.2	116.5	360	3.4	1.24	(3)-BENHAM 'Afterevent'
56	e	"	19-18-19.6	37.3	116.4	360	3.5	0.48	"
57	e	"	19-54-01.2	37.2	116.5	360	3.4	0.39	"
58	e	"	22-23-26.3	37.2	116.5	360	3.6	1.06	" (collapse?)

#	Type	Date	OT (GMT)	Lat. (N)	Long. (W)	Δ (km) from JAS	M(1)	Spectral Ratio (P_g)	Comments
59	c	20 Dec. 68	20-08-20.4	37.2	116.5	360	3.8	0.61	(3)-BENHAM 'Afterevent'
60	c	21 Dec. 68	00-14-25.2	37.3	116.5	360	4.3	-	"
61	c	06 Jan. 69	06-34-14.5	37.3	116.5	360	4.2	-	"
62	c	10 Jan. 69	09-41-21.5	37.2	116.5	360	3.9	1.72	"
63	c	"	17-01-44.5	37.2	116.5	360	3.8	2.82	"
64	c	"	17-14-17.2	37.2	116.5	360	3.8	0.88	"
65	c	18 Mar. 69	14-40-02.7	37.2	116.0	400	3.8	0.69	(3)
66	c	16 Sept.69	15-43-39.2	37.3	116.5	360	3.8	2.38	(3)-JORUM 'afterevent'
67	c	"	16-23-53.8	37.3	116.5	360	3.9	1.39	"
68	c	"	17-31-14.7	37.3	116.5	360	4.0	3.44	"
69	c	"	18-15-39.3	37.3	116.5	360	3.8	1.52	"

(1) Magnitudes based on P_n and P_g amplitudes at JAS. The scale is based on Wood-Anderson magnitudes at BRK for larger events.

(2) Personal communication, Don Springer, 1970. The letter designations (Y) and (P) indicate the test areas Yucca Flat and Pahute Mesa, respectively; (A5) indicates the explosion was detonated in alluvium; (R) indicates an elongated explosive charge was detonated as a "row shot" at Buckboard Mesa.

(3) U. S. C. G. S. hypocenter.

(4) Arrival times at the Berkeley net indicate NTS hypocenter. Δ = 360 or 390 km is assumed for purposes of attenuation and magnitude calculations.

* Arrival times available for this event are inconsistent so that the epicentral distance is uncertain. The magnitude thus may be as large as 3.2 if the epicenter is 500 km from JAS. The error in the attenuation correction due to the epicentral uncertainty is not significant.

SOME REMARKS ON SHORT PERIOD DISCRIMINATION

By

D. Davies

Lincoln Laboratory
Massachusetts Institute of Technology

BLANK PAGE

I would like to discuss very briefly some aspects of short period discrimination which seem to be developing at the moment. One advantage of short period work is the lower threshold for detection of P waves and hence the prospect that some characteristic will reveal itself routinely at m4.5, say.

Spectral ratio

Thus far a short period spectral discriminant 'spectral ratio' has proved valuable for LASA studies. The spectral ratio, defined as the ratio of the power in the bands 0.35 to 0.85 Hz and 1.45 to 1.95 Hz, has been studied extensively by Kelly (1968) and Lacoss (1969). It was demonstrated that the high frequency content of explosions is markedly higher than that of earthquakes for shallow quakes and that this criterion appeared to be effective above m4.8 and maybe useful if not conclusive below that magnitude.

The question of NORSAR's capability in the spectral ratio test is important. There is no reason to believe that a site in Scandinavia should have as good a teleseismic window on the Asian continent as is possible. The shield-like characteristics of the Scandinavian area and the Russian and Siberian platforms strongly suggests poorly developed, if present at all, low velocity zones. We thus expect low Q zones also to be much less important practically anywhere in the Sino-Soviet bloc. Hence we would predict (a) that a broader frequency window is available to us at NORSAR and (b) that there should not be gross variations in spectral character for explosions anywhere in the Sino-Soviet region, with the possible exception of the Kuriles.

The first results from NORSAR look promising in this respect. We may well be able to take advantage of the greater excitation of high frequencies by explosions by means of the broader frequency window. Figure 1 shows the mean spectrum of a small population of earthquakes and events at the Eastern Kazakh test site presumed to be explosions. This is, of course, a very meagre sample on which to base any conclusions, but it is clear that some attempt to tailor a discriminant to take advantage of the clear peaks and troughs in the two spectra may be profitably made. Such a discriminant, based on this population, has been constructed and is defined as

$$S_{12} = \frac{S_1 + 2\,S_3}{S_2}$$

where S_1, S_2 and S_3 are sums of spectral components in the bands: 0.63 to 1.06 Hz, 1.22 to 1.65 Hz and 1.88 to 2.31 Hz, respectively.

Figure 2 shows some results of this discriminant where the population extends beyond that of the events shown in Figure 1. It is important to note that such a discriminant would be ineffectual for Nevada Test Site explosions which are, it is widely believed, fired over a region of the upper mantle in which a low Q zone exists.

Complexity

The question of complexity has been widely argued since the Novaya Zemlya events showed high complexity. It is obviously important to understand what is meant by high and low complexity and the definitions that have been used in the past have been of the form of power ratios, energy in the first thirty seconds divided by energy in the first five seconds or some such figure. This ratio is, of course, strongly dependent on what happens in the first five seconds. A much better measure of complexity would be the energy between 5 and 30 seconds scaled by the Gutenberg B-factor and related to a good teleseismic magnitude estimate. I think we can too easily be deceived by high relative coda levels into thinking that the coda is much more important than it actually is. We have recently done a survey of the Novaya Zemlya data in order to try and find out what causes complexity and also whether it is predictable.

The first thing one discovers is that the complexity of signal varies dramatically from place to place on the globe. A particularly striking example of this was shown by Key of UKAEA when two stations in the UK with Δ's differing negligibly but azimuth differing by 8° showed wildly different records. That this is a function of source rather than receiver is obvious when one compares complexity distributions for other explosions in other regions -- the pattern does not repeat.

There is something very subtle about the source phenomenon because it yields different repeatable signals at different stations relatively close together. I think this completely rules out any explanation in terms of Rayleigh wave to P-wave conversion near source since we have no reason whatsoever to believe that this latter phenomenon is other than very isotropic in its radiation pattern.

If complexity were generated simply by rattling around in upper mantle heterogeneities of various sorts we would expect the radiation to be fairly isotropic and this we do not see. So I think that too is ruled out as would be, for instance, also triggering of tectonic strain. If we rule out this form of complexity generation we are left with, in my opinion, only one alternative and that is deeper structure beneath Novaya Zemlya producing lateral constrasts in seismic velocity.

The emphasis on the coda is probably illusory. All underground explosions have substantial codas lasting for at least a minute and if we were to remove the first five seconds of the P-wave we would always be confronted with a very complex event whose magnitude might not be more than half a unit less than that of the explosion itself. We are beginning to understand the structure of this coda now in terms of a variety of mechanisms and we know that a certain amount of it is suppressed by array processing and thus must be locally generated. However, what remains is still substantial even for explosions from other regions. I would like to suggest that what appears to be complexity is no more than an absence of the primary P wave.

This is akin to the shadowing process that produces low amplitude signals in the range $10° < \Delta < 20°$ except that we now have lateral rather than vertical variations in velocity. At this stage it is appropriate to look at Long Shot. We know that this was fired in a region of strong lateral heterogeneity in seismic velocity and the waveforms were accordingly very variable in character. For example, I show some LASA waveforms from Long Shot which are fairly confused and very incoherent (Figure 3). The same event however produced a relatively simple PcP (Figure 4). A careful examination of the waveforms available shows a strong dependence of 'complexity' on angle of emergence from the source. Figure 5 shows this very dramatically. I have taken a slice through the focal hemisphere at the location of Long Shot and marked on it the angle of emergence to get to various stations, including one PcP phase. I have also traced the waveforms at these stations. The large arrow shows the believed dip angle of the plate at this point in the Aleutians. The results are most interesting in that the first five seconds amplitudes vary by a factor of about 30 and yet the post-signal coda is fairly constant. I can only interpret this in terms of shadowing due to the presence of the plate. Figure 6 shows the relationship between reported magnitude and complexity for Long Shot and Figure 7 shows the same for a Novaya Zemlya event. Both clearly show the relationship between an apparent complexity and a diminution in the first P-wave amplitude.

What evidence do we have to make such a plate postulate for Novaya Zemlya? One particularly cogent argument is the wide existence of ultra-basic rocks along the Urals - Novaya Zemlya fold system, and the presence of ophiolite complexes along the Urals. This makes it, by analogy with the Mediterranean for instance, very probably a locus of compressive orogeny at the close of a plate consumption period when the Siberian platform and the Russian platform became jammed together Himalayan-style. All the reliable information we have on this suggests the orogeny was Permo-Carboniferous. This leaves many puzzles -- one being that of explaining how a plate can maintain its identity for at least 200 My in the Upper Mantle. However this problem is not insoluble and we are still at a relatively early stage in understanding fossil plate behavior.

If my assertion that lateral velocity structure is the explanation for signal variability is correct, two things follow. The first is that we might be able to map simplicity and complexity on a focal sphere and get a picture of the broad structure under Novaya Zemlya. So far we have not obtained results significant enough to display, or it may be that the structure is so complicated that no clear focal sphere picture will emerge.

The second point is that in determining a magnitude for Novaya Zemlya events, only observations from stations giving simple records ought to be included, as these are probably not in the shadow. Thus it is probable that P-wave magnitudes of Novaya Zemlya explosions are consistently underestimated.

REFERENCES

Kelly, E.J., 1968-8, A study of two short-period discriminants, Lincoln Laboratory Technical Note.

Lacoss, R.T., 1969-24, A large-population LASA discrimination experiment, Lincoln Laboratory Technical Note.

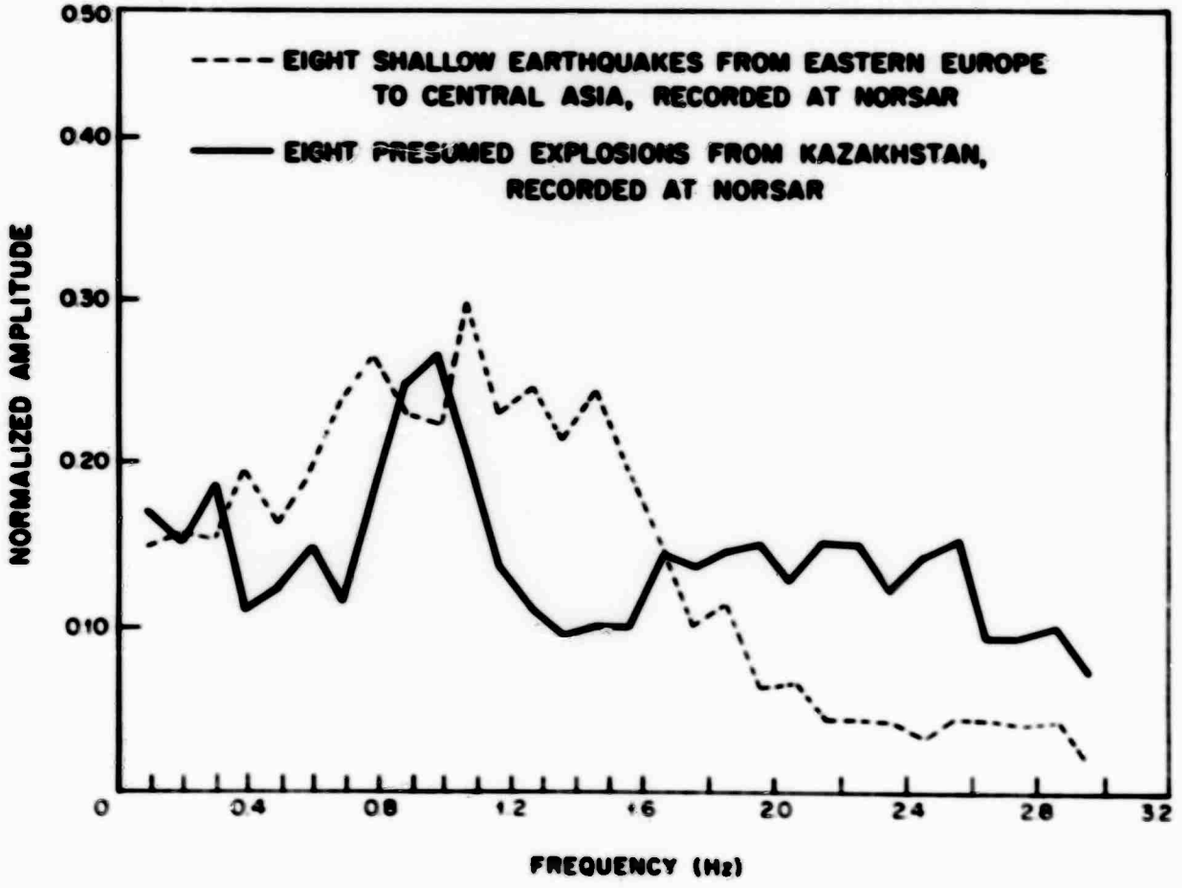

Figure 1. Spectral characteristics of earthquakes and explosions recorded at NORSAR (during the early stages of construction).

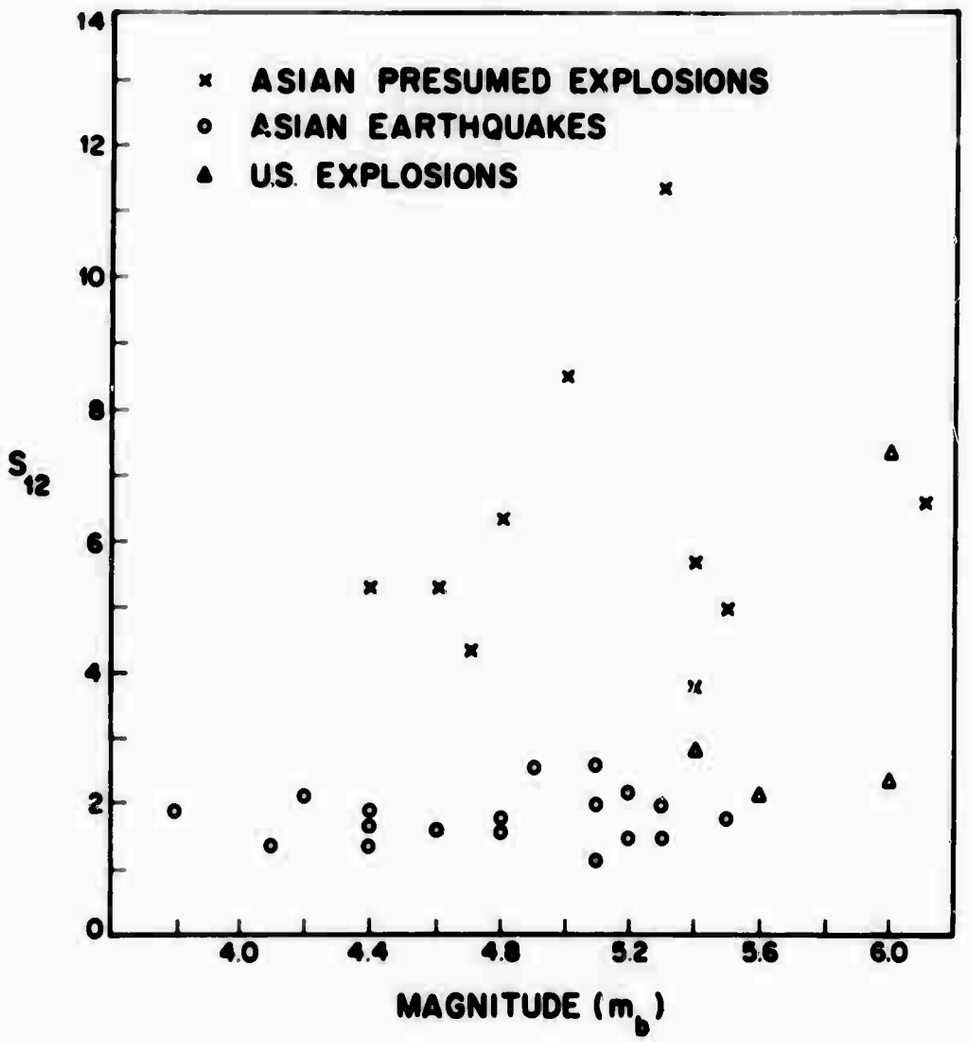

Figure 2. Discrimination based on a modified spectral ratio S_{12} at NORSAR.

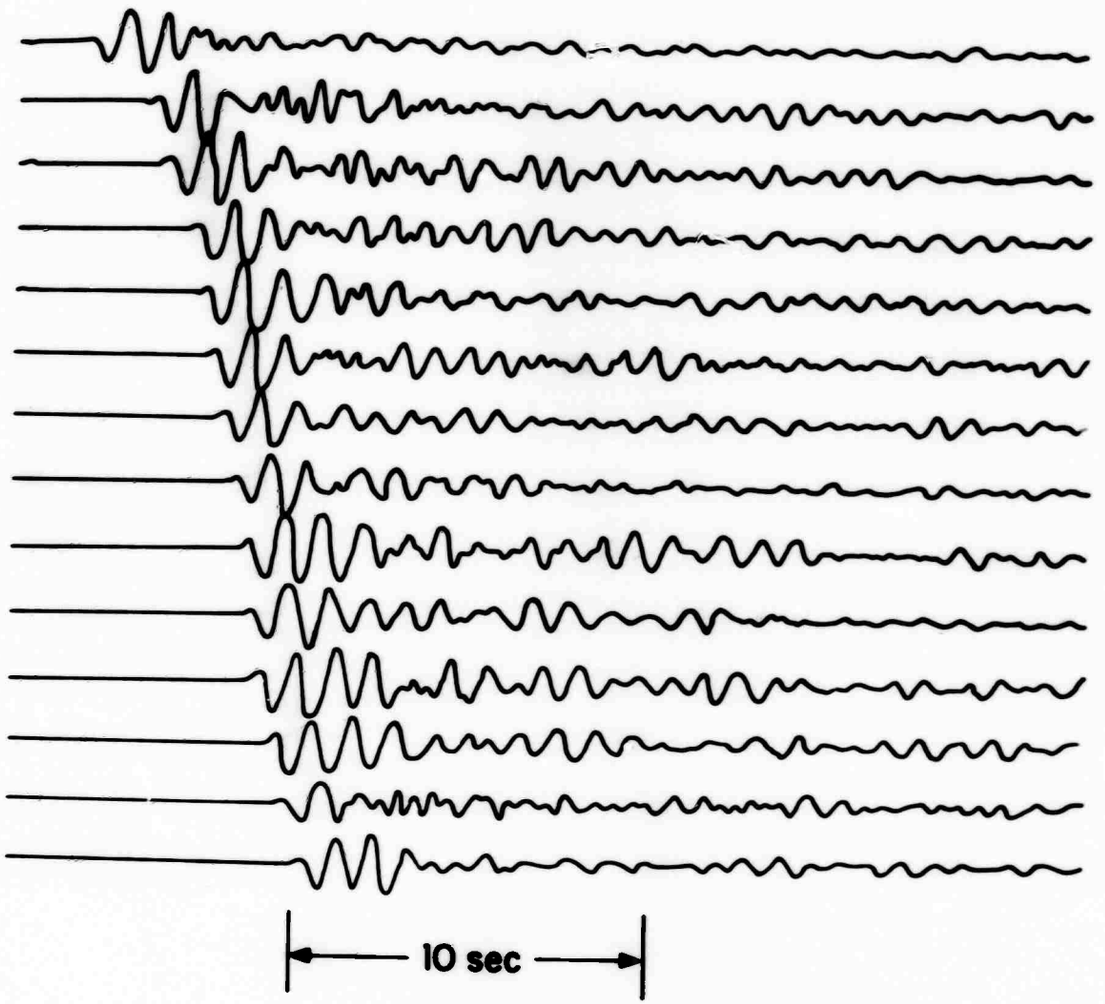

Figure 3. A set of P-waveforms of LONG SHOT recorded across the aperture of LASA.

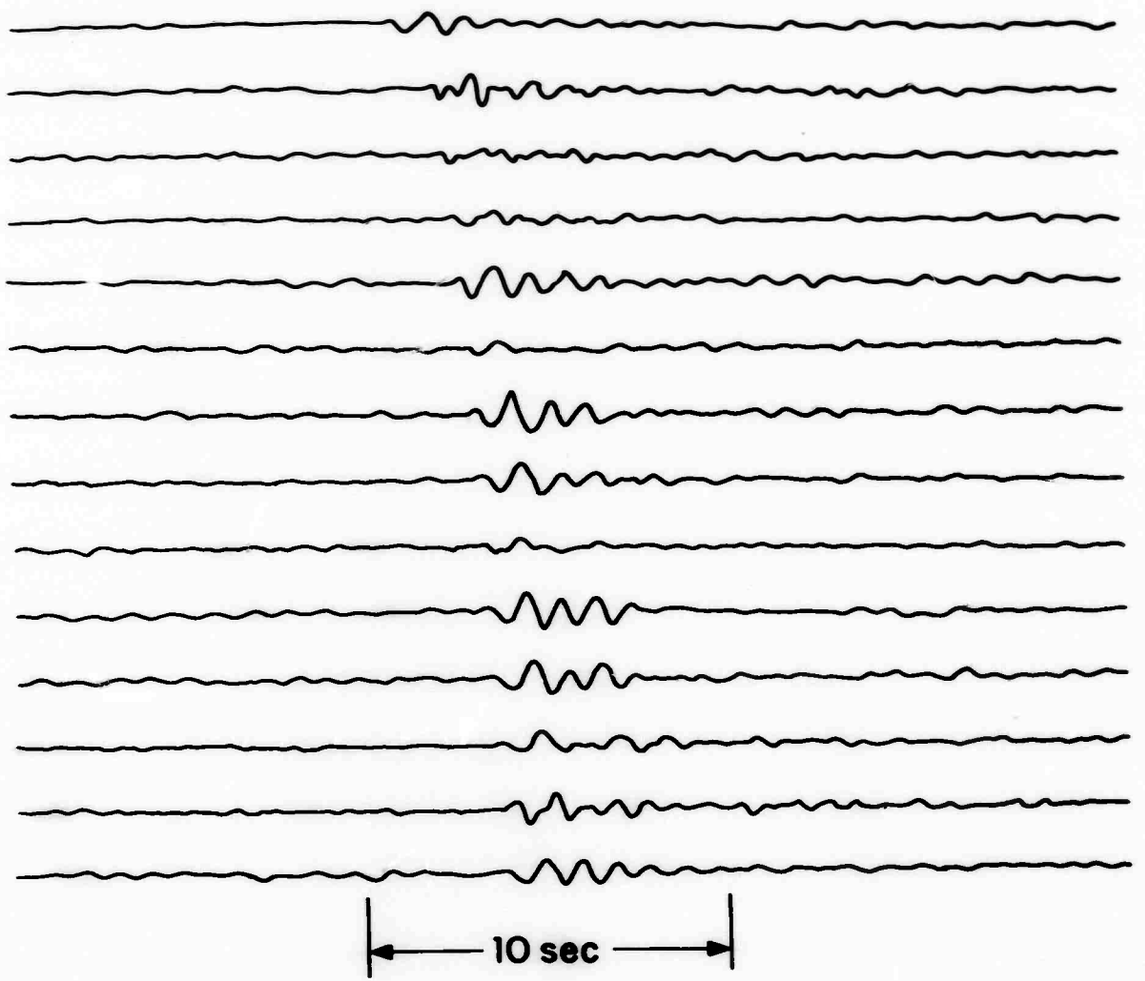

Figure 4. PcP waveforms recorded from LONG SHOT at LASA (at the same gain).

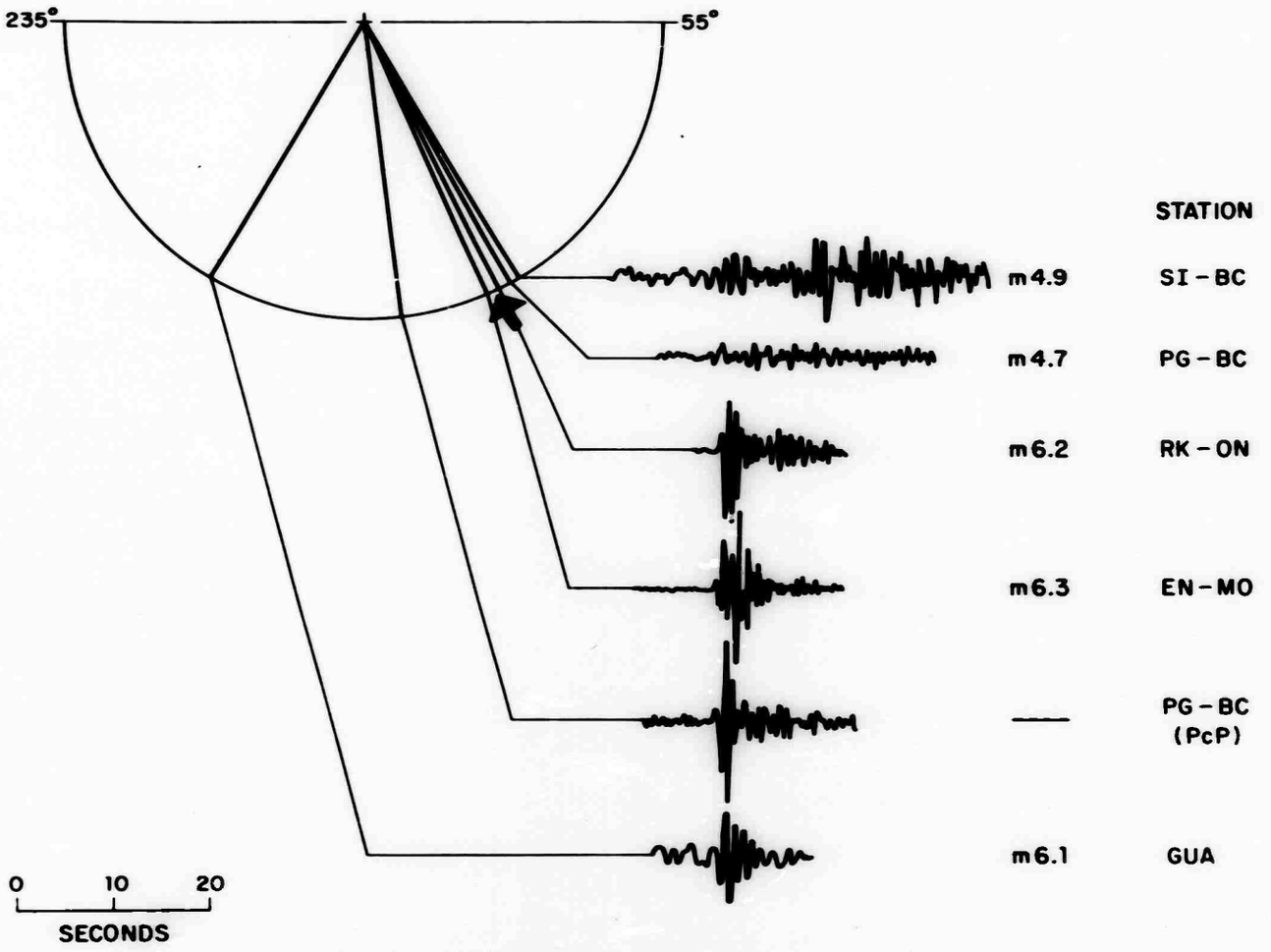

Figure 5. A section through the focal hemisphere at LONG SHOT striking 55° - 235°. The calculated dip of the plate is shown by a bold arrow. Waveforms for P and PcP from several stations show the clear shadowing effect of the plate.

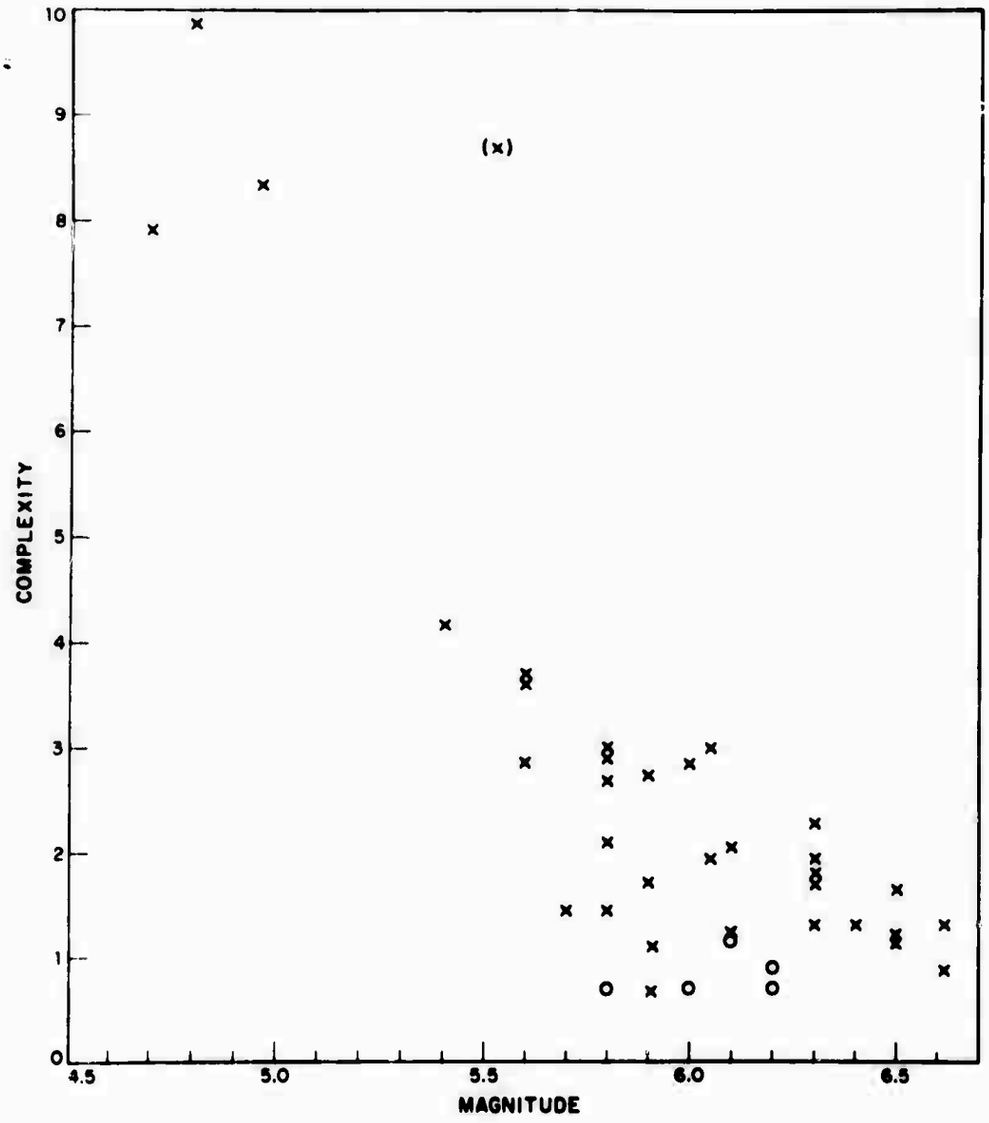

Figure 6. A plot of complexity against reported magnitude for LONG SHOT from a set of stations.

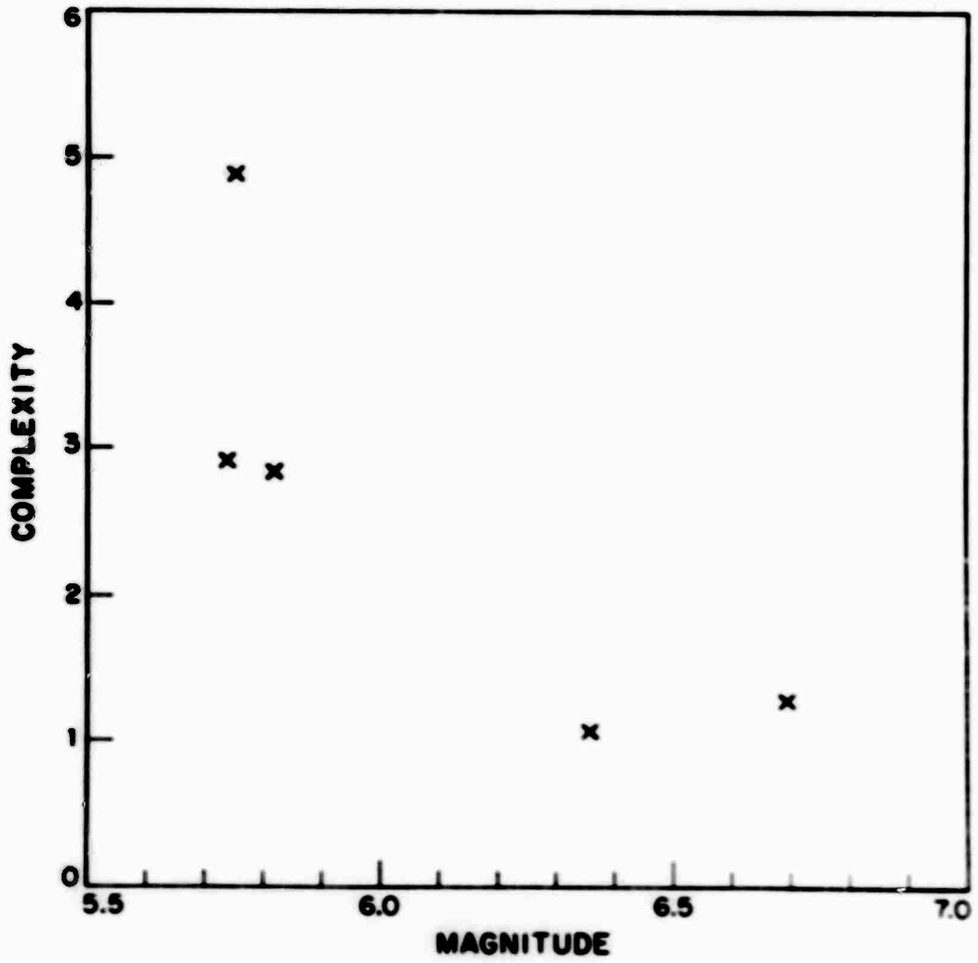

Figure 7. A plot of complexity against reported magnitude for a Novaya Zemlya event from a set of stations.

DISCUSSION OF DEPTH DETERMINATION USING SP DATA

By

R. Lacoss

We wish to touch upon several different topics related to short period depth determination and the role it can play in the discrimination area. These are:

A. pP or sP detection using a continental array

B. pP or sP detection using LASA

C. pP or sP detection using LASA and NORSAR jointly

D. Use of depth phases in conjunction with other criteria for discrimination

E. Use of phases other than pP, sP for depth determination

F. Very shallow depth determination using spectral information.

In general we believe that short period depth phases cannot be neglected since it appears that perhaps 50% of natural events can be so identified without incorrectly dismissing any underground explosions. This may be particularly significant since depth phases may be used to correctly identify events which are troublesome for other criteria. For example a deep event may have weak surface waves. Also, depth phases can be observed for many events in the low magnitude range m_b = 4.0 to 5.0.

A. pP or sP determination using a continental array

The suggestion has often been made that short period data from stations spanning an aperture of thousands of kilometers might be coherently combined to significantly aid in the detection of phases, particularly pP and sP. Lincoln undertook a limited study to investigate this suggestion using LASA data and digitized LRSM data. Data was visually aligned on P arrivals, scaled to correct for distances, and beams were formed for trial depths from 10 to 200 km in 2 km increments. Beams were compared for a one second interval around the predicted arrival time for pP. Data was normalized in such a way that depth determination was essentially based upon coherence. The depth was determined correctly for only one of the four earthquakes processed. That event is shown on the first figure. An event for which the processing failed is shown in Figure 2. It is worth mentioning that all four earthquakes had depths restricted by USC&GS based upon depth phase observations at some of their stations.

There is no doubt that the performance of a continental array could be somewhat improved. For example the general energy level as well as coherence could be utilized. However we have not pursued this course. It seems to us that one can probably be as successful as one might be using a coherent continental array by searching through LASA, NORSAR, smaller arrays, and single instrument sites for phases and using the different sites to corroborate each other's data. If this is true then the analysis can be accomplished without introducing an

excessive computational load. One might even argue the radiation pattern problems also mitigate against a continental array unless only stations favorably located for a specific event are included. For example it would appear that the stations used in Figure 2 are just poorly located.

B. pP or sP detection using LASA

A discrimination experiment using only LASA data from 156 Eurasian earthquakes and 35 presumed explosions was completed at Lincoln and has been discussed in various reports. We wish to review the results of that experiment with respect to depth determination using pP and sP.

All events in the population were examined by an analyst for possible depth phases (sP or pP). The analyst operated as follows. First the best LASA beam waveforms were examined for any possible arrivals after the initial P wave onset. Picks corresponding to PcP times were discarded. The time corresponding to the largest amplitude of any remaining picks was then accepted as a candidate for sP or pP. The analyst accepted picks associated with amplitudes less than 25% of the P amplitude only if he felt the arrival very clearly rose above the coda or noise level.

The above procedure was scrupulously executed for presumed explosions as well as for earthquakes. As a result erroneous depth phases were attributed to three explosions in the population. Two of these were complex Novaya Zemlya events with many apparent secondary arrivals, some as large as 0.8 of the initial P amplitude. The third event was quite simple and will be shown subsequently. The danger of accepting apparent depth phases at LASA as unequivocal evidence of depth for discrimination is obvious. Corroborating evidence from other sources should be required in order to avoid the incorrect classification of an explosion as an earthquake.

The analyst accepted depth phases for 58% of all the earthquakes in our data base. This is just slightly less than the acceptance rate for the 55% of all earthquakes in the data base which were also reported by USC&GS. For that subset of earthquakes depth phases were attributed to 63% of the events by the analyst.

If events restrained to 33 km by USC&GS are excluded from consideration there are 41 earthquakes in our population to which we attributed depth phases and which were reported by USC&GS. Given the available data it is difficult to precisely evaluate the success of the depth determinations made using LASA beams. There were only two cases (LASA pP depth = 29 km, USC&GS depth = 87 km; LASA pP depth = 80; USC&GS depth = 10) in which there is virtually no doubt that the LASA phase was neither pP nor sP. There are about 30 cases in which it is most reasonable to assume that the LASA phase was either pP or sP. The remaining events are ambiguous at best. Thus, for earthquakes, between 70% and 95% of the possible depth phases picked on SPLP beams corresponded to either sP or pP. This implies that sP or pP was

correctly picked for between 42% and 57% of all the earthquakes in our population.

C. pP and sP detection using LASA and NORSAR jointly

Short period NORSAR data from eleven elements distributed over a 20 km aperture was available for a number of the events included in our previously mentioned LASA discrimination experiment. The NORSAR data from a total of 41 earthquakes and six presumed Soviet explosions which had previously been processed at LASA have been considered to estimate the degree to which two large arrays can be used jointly for depth determinations. Beams were formed using the eleven available sensors at NORSAR and an analyst identified possible depth phases on those beams. The presumed explosion which showed a possible depth phase at LASA was not in this population. However, a different presumed explosion showed a possible depth phase at NORSAR which was not corroborated at LASA.

The following table is a summary of depths implied by depth phase picks for the 37 earthquakes for which either site showed a provisional depth phase. The depth shown is that which follows from assuming that the phase was pP. If the phase were sP, the depth would be reduced by a factor of roughly 2/3. A zero entry indicates no depth phase was picked by the analyst. Events in the table have been identified as showing good, fair, or poor agreement between the LASA and NORSAR depths. Good or fair agreement was obtained for 54 percent of the events. Comparison with USC&GS events indicate that some events with poor agreement probably have a correct depth phase picked at one or both sites. In passing we might note that for this population provisional depth phases were picked at LASA for 73% of the earthquakes and for 83% at NORSAR. This is significantly higher than the 60% at LASA for the parent population of 156 earthquakes.

Extrapolating to a system using two large sP arrays and several smaller arrays or high quality single sensor sites our estimate is that 50 percent or more of earthquakes can be identified by depth phases without erroneously classifying any explosions. This could be very significant, particularly at small magnitudes, since many earthquakes identified in this way might be troublesome events for other criteria.

D. Use of depth phases in conjunction with other criteria for discrimination

Figure 3 shows a suite of 10 earthquakes and three explosions in the LASA discrimination experiment which were incorrectly or were the most marginally identified events as judged by the short period spectral ratio discriminant. Our evaluation was that earthquakes C, G, and I were incorrectly identified and that, although all presumed explosions were identified correctly that only event 3 was strongly in the explosion region. Our objective in discussing these specific events is to

DEPTH DATA FOR USCGS AND LASA-NORSAR BASED UPON POSSIBLE pP PICKS

Events with Good LASA-NORSAR Agreement			Events with Fair LASA-NORSAR Agreement			Events with Poor LASA-NORSAR Agreement		
LASA	NORSAR	USCGS	LASA	NORSAR	USCGS	LASA	NORSAR	USCGS
150	160	155	34	40	50	0	90	-
580	580	582	30	55	33R	15	90	-
450	470	463	23	30		140	40	161
510	510	511	15	20		0	8	-
20	25	21	55	30		0	15	-
120	110	118	30	50		150	15	134
15	15	33R	50	33		0	15	20
170	170	160	17	11		110	0	113
30	25	-				0	80	16
20	17	-				20	100	33R
46	44	-				33	10	50
45	50	-				115	15	10
						50	0	-
						75	0	94
						0	21	33R
						70	20	33R
						0	160	-

demonstrate the value of utilizing more than one discriminant, and in particular sP depth phases.

Events, A, B, C, D, G, H, and 2 were probably identified by LASA M_S - m_b. Event E was incorrectly identified. Surface waves could not be used for the remaining five events. First motion, not a currently popular discriminant, might well be used to correctly identify some of the earthquakes. Complexity might also be considered although this criteria, which might be quite powerful, must be utilized with considerable understanding and probably requires a network rather than a single station.

This brings us to the potentially powerful role of depth phases in discrimination. All of the earthquakes have possible depth phases and several give evidence of both pP and sP. In our opinion corroboration by one or more other stations would probably identify all or most of the earthquakes.

Unfortunately event 2 shows evidence of both pP and sP at about 18 and 27 seconds respectively. In fact these are probably peg-leg reflections from the Mahorovic discontinuity in the source region. Even other receivers might lead one to believe these to be depth phases. Event 2 probably represents about the largest reflections from an explosion, relative to P, that one can obtain from discontinuity in the crust and upper mantle. Thus, convincing apparent phases less than 10 db down from the peak of P at more than one receiver are excellent evidence that the event is an earthquake. This assumes that no multiple explosions are being considered.

E. Use of phases other than pP, sP for depth determination

The preceding discussions dealt only with P, pP and sP. However, there are many other phases available for discrimination and, in particular, to act as aids to depth determination. Figures 4 and 5 show a striking example of this. Figure 4 shows a LASA beam and three individual sensors for a P wave from an Aleutian earthquake. No distinctive pP or sP is to be seen on that data. However, Figure 5 shows the beam for PcP and the same individual sensors. A depth phase, with a reversal in polarity, is very clear on this data. We have seen many other examples where secondary phases can be of considerable value although we have not yet completed any systematic study. Other phases such as sScP or pPKKP can often be detected and used.

We are just beginning to utilize some of these other phases but the prospects are quite exciting. These other phases allow one to see the event from more than one angle even at a single large array. In a sense the power of the array is multiplied in this way. The cumulative evidence from phases can be extremely valuable in the same way that the cumulative evidence of discriminants and other sites is greater than the sum of the parts.

F. Very shallow depth determination using spectral information

Finally we wish to comment upon the prospects of depth determination in the range 0 to a few kilometers using short period spectral information. An experiment has been performed using cepstral analysis for four presumed explosions recorded at five different global array sites. The raw spectra, for beams, is shown in Figure 6. The variability of the data between sites is considerable. Various notches in the spectra were reconfirmed by cepstral analysis. Delays inferred from this analysis are shown in the following table.

DELAYS INFERRED FROM MAXIMA IN COMPUTED CEPSTRA

LASA m_b	Norway	Australia	India	Canada	LASA
5.3	No data	0.4	0.6	0.4	0.5
5.4	0.6	0.5	0.4, 0.8	0.7	0.4, 0.9
5.6	0.6	0.4	No data	0.7	0.5
6.1	0.5	0.4, 0.9	0.5	0.6	0.5

The cepstral results do not appear to be definitive. Although the values obtained are reasonable, the variation between sites is greater than can be accounted for by the variation of the angle of incidence. Also, assuming the overburden velocity to be unchanged, an increase of τ with magnitude might be expected, since increased magnitude usually means increased depth, but is not evident from these data. Finally, at Norway, Australia, and LASA the values of τ seem to remain rather constant, indicating a possible array site effect, while at Canada and India such constancy is not observed.

It is our general feeling that such work may be of scientific or intellectual value but is not likely to be important to discrimination. Notches in spectra are so common that the presence of one in the range which implies a reasonable burial depth for an explosion is not good evidence that the event is an explosion. Also, we would like to comment that the physics of waves in the source region is very poorly understood and it is not clear that a simplistic ray theory view of a surface reflection from explosions is justifiable.

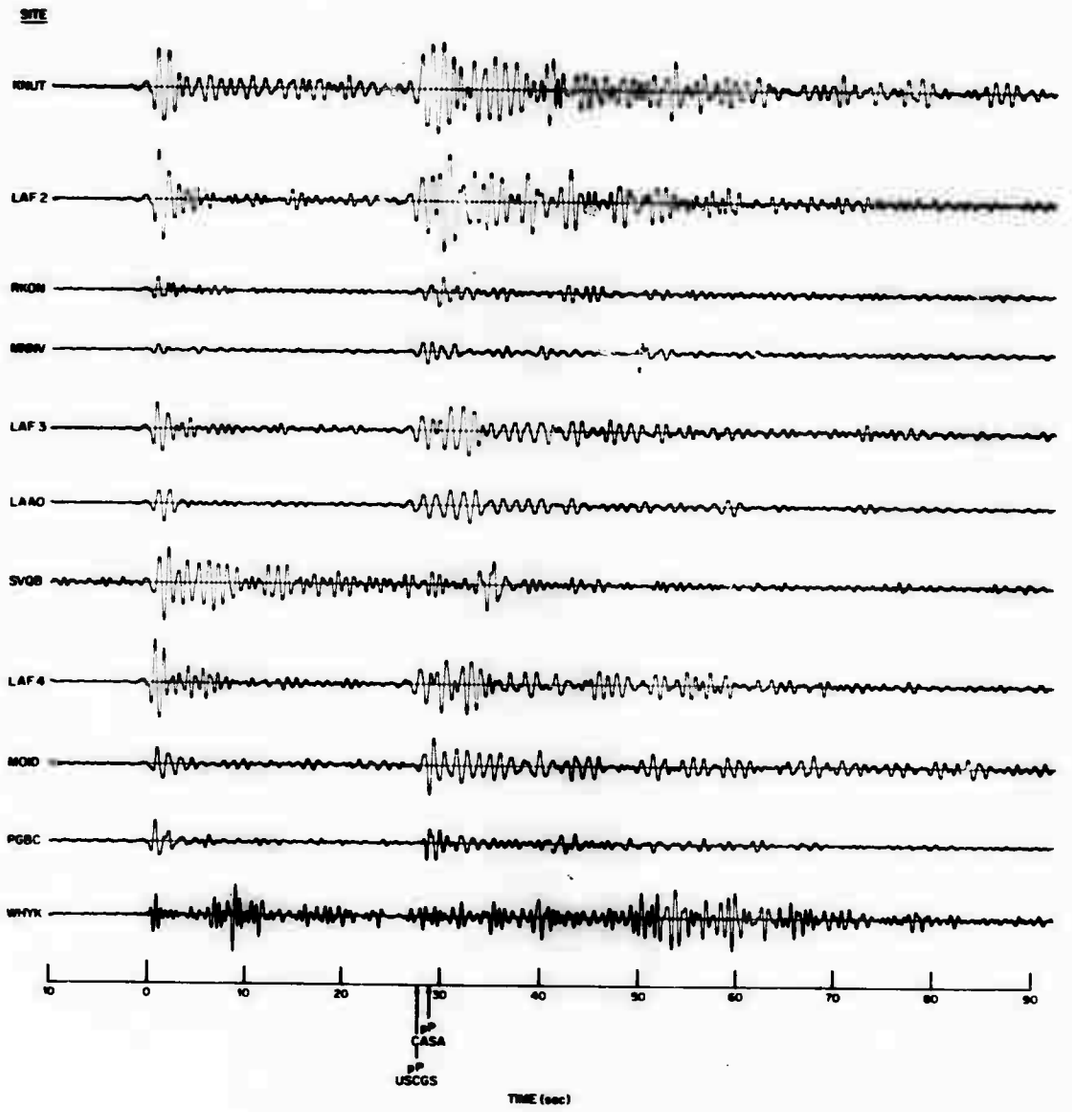
SITE
KSUT
LAF 2
RKON
MBBV
LAF 3
LAAO
SVQB
LAF 4
MOID
PGBC
WHYK
10
0
10
20
30
40
50
60
70
80
90
pP
CASA
pP
USCGS
TIME (sec)

Figure 1.

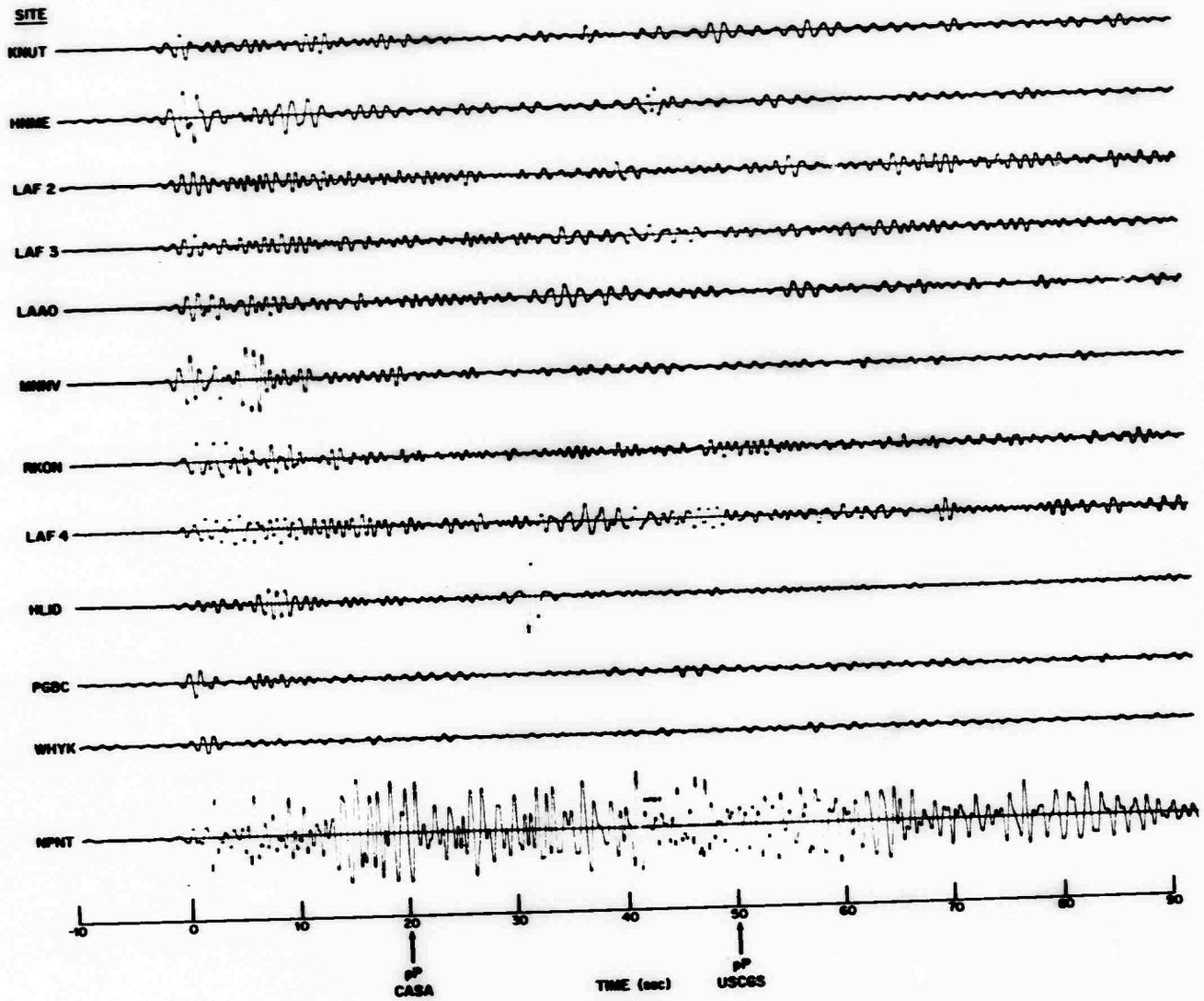
SITE
KNUT
HIME
LAF 2
LAF 3
LAAO
MMNV
RKON
LAF 4
HLID
PGBC
WHYK
NPNT
-10
0
10
20
30
40
50
60
70
80
90
pP
CASA
TIME (sec)
pP
USCGS

Figure 2.

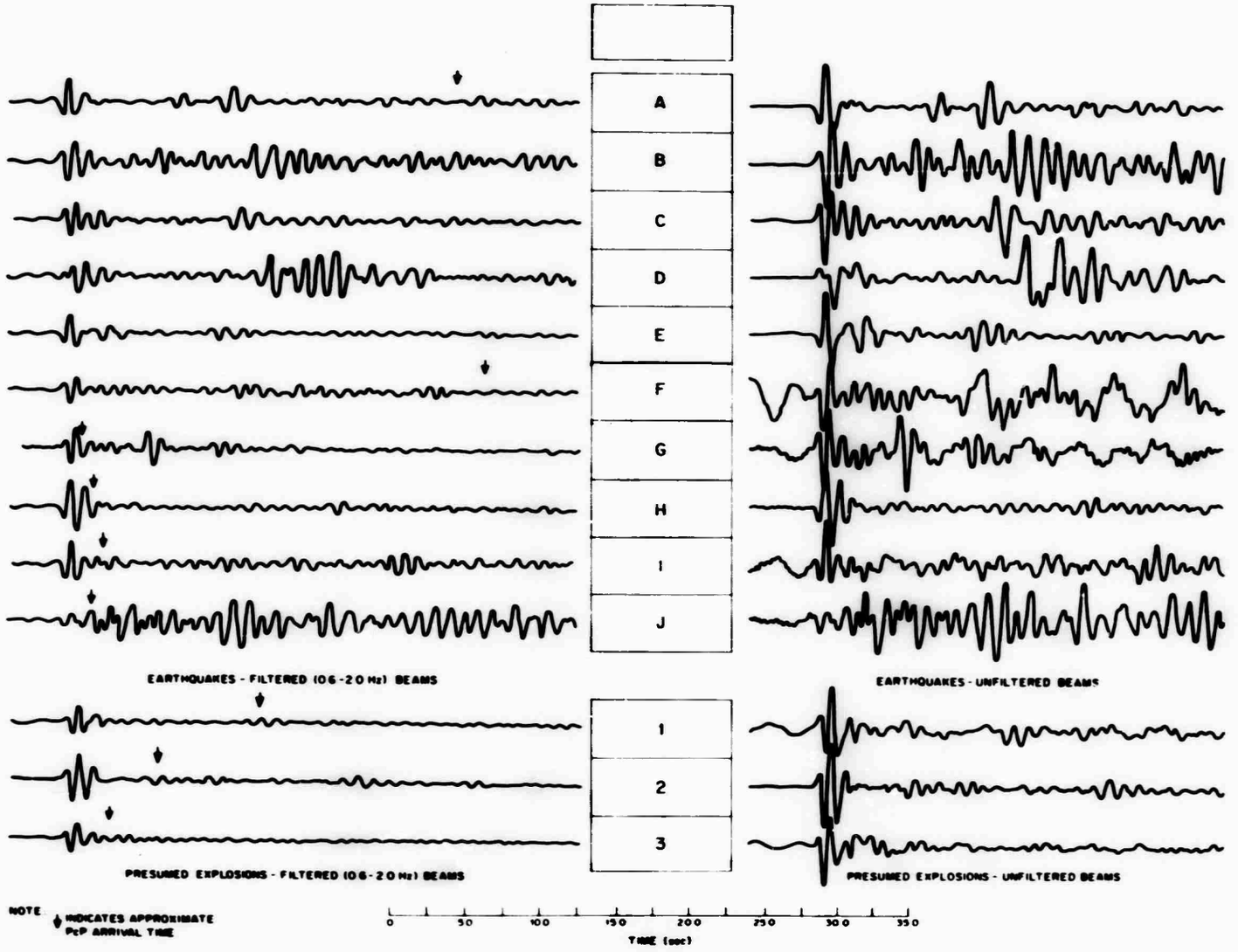
A
B
C
D
E
F
G
H
I
J
EARTHQUAKES - FILTERED (0.6 - 2.0 Hz) BEAMS
EARTHQUAKES - UNFILTERED BEAMS
1
2
3
PRESUMED EXPLOSIONS - FILTERED (0.6 - 2.0 Hz) BEAMS
PRESUMED EXPLOSIONS - UNFILTERED BEAMS
NOTE ↓ INDICATES APPROXIMATE PcP ARRIVAL TIME
0
50
100
150
200
250
300
350
TIME (sec)

Figure 3.

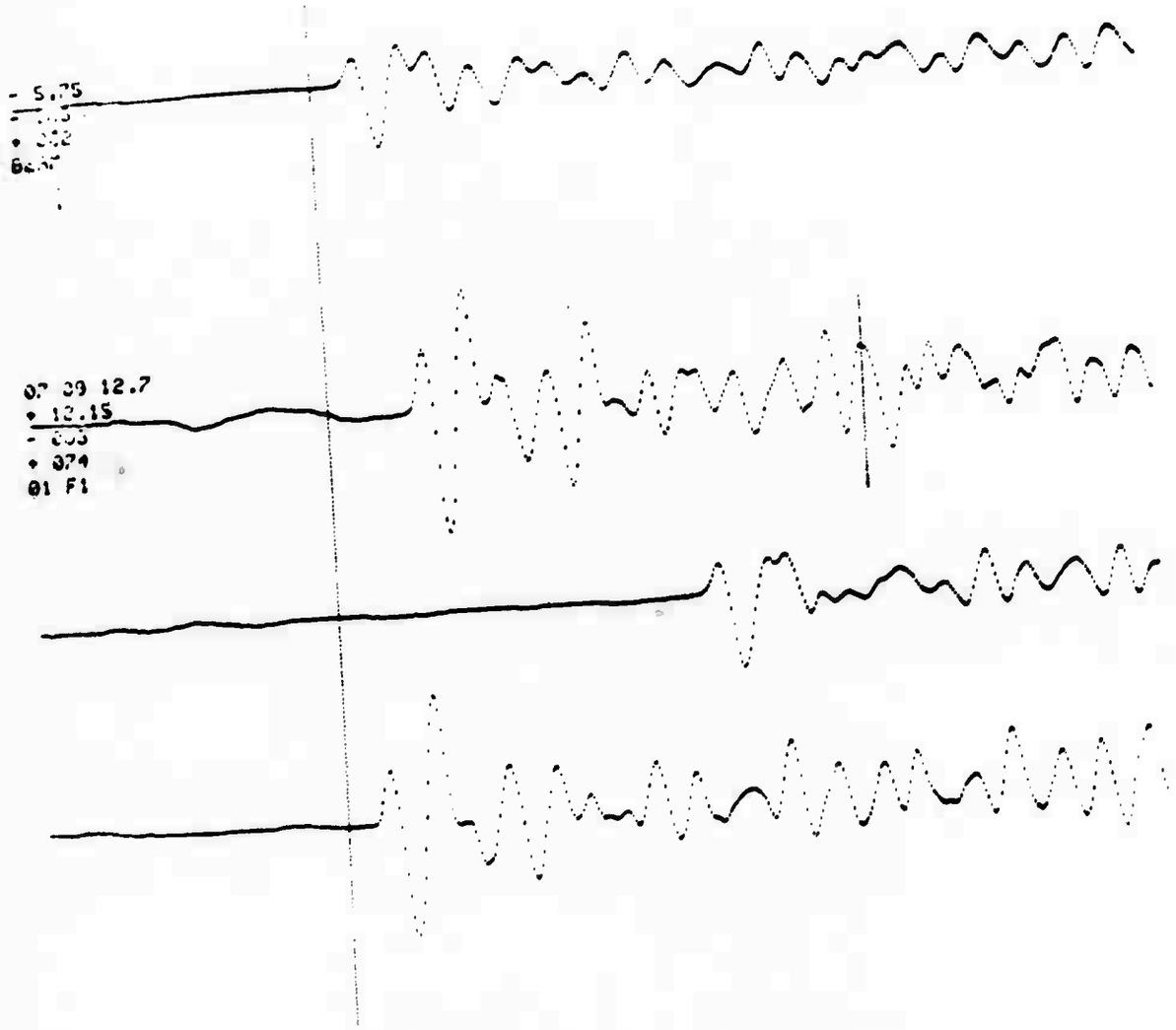

Figure 4.

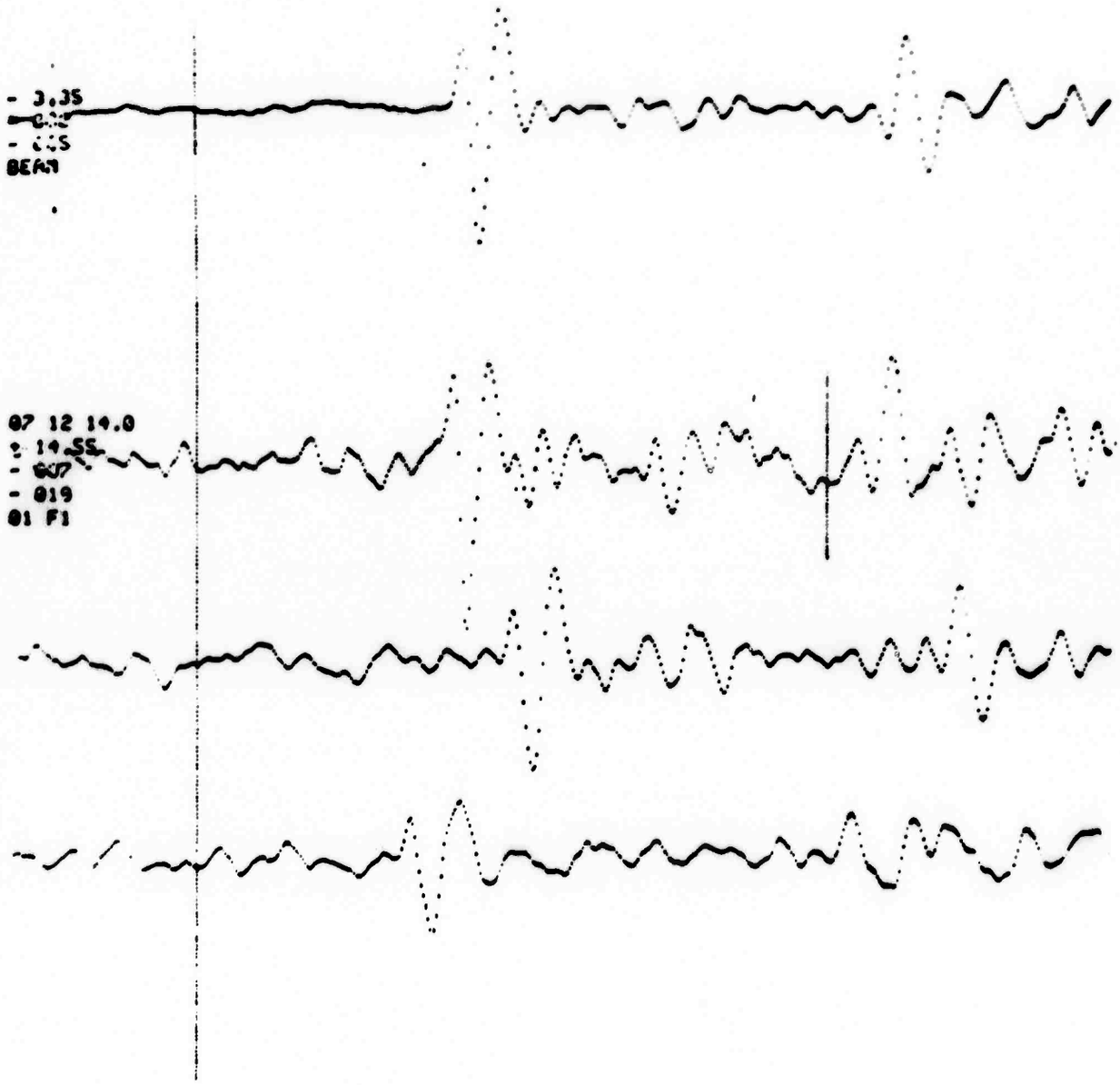

Figure 5.

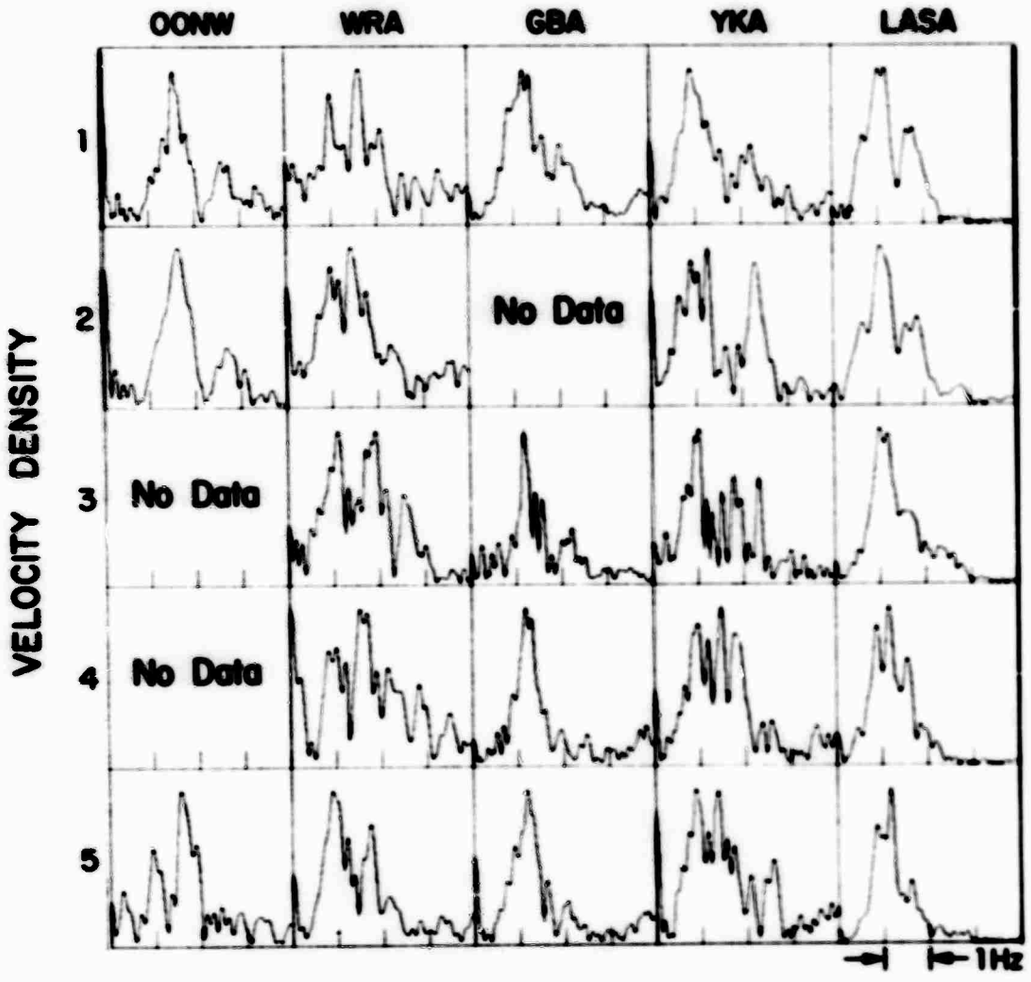
OONW
WRA
GBA
YKA
LASA
1
2
3
4
5
No Data
No Data
No Data
VELOCITY DENSITY
1Hz

Figure 6.

COMPARISON OF P-WAVE SPECTRA OF UNDERGROUND EXPLOSIONS AND EARTHQUAKES

By
Max Wyss[1]
Thomas C. Hanks[2]
Robert C. Liebermann[2]

[1]Institue of Geophysics and Planetary Physics
University of California
San Diego, California
Present address Lamont Doherty Geological Observatory
Palisades, New York

[2]Seismological Laboratory
California Institute of Technology
Pasadena, California

ABSTRACT

The P-wave displacement spectra of the underground explosion MILROW and LONG SHOT are compared to those of four shallow earthquakes of comparable body-wave magnitude (m_b) in the Aleutian Islands. The spectral data ($0.4 \leq T \leq 40$ sec) have been obtained from three vertical instruments at Pasadena, approximately 50° from the epicentral region common to six events. A Novaya Zemlya explosion of comparable m_b was also analyzed. The peak spectral amplitude for the earthquakes occurs at periods approximately ten times larger than for equal m_b explosions, indicating that earthquakes have source dimensions roughly ten times larger than explosions. For $T \leq 1.5$ sec the spectra for both types of events are comparable, with respect to both absolute level and rate of decay (ω^{-2}) with increasing frequency. The explosion spectra peak sharply in the interval 2 sec $> T \geq 1$ sec and decay as ω for longer periods. The earthquake spectra, however, continue to increase to a long-period level. This spectral behavior at long periods suggests that for explosions an exponentially decaying pulse may be a better approximation for the source time function than a step. The greatest differences in spectral amplitudes occur at periods longer than 3 sec. The observed differences in the P-wave spectra provide a diagnostic method for discriminating between earthquakes and underground explosions.

INTRODUCTION

A characteristic feature of the P-wave displacement spectrum for a seismic event is the frequency at which the amplitude spectral density is largest. This peak frequency (ν_o), which marks the center of the band of useful seismic information, varies with magnitude and ranges for earthquakes from 2 Hz at magnitude 1 (Wyss, 1970a) to 0.033 Hz at magnitude 8 (Kasahara, 1957). ν_o can be related to the source dimension through the equation $\nu_o = c \frac{v}{r}$, where v is elastic wave velocity, r is source radius and c is a constant of order 1 and depends on the particular source model assumed (e.g. Sharpe, 1942; Kasahara, 1957; Archambeau, 1964; Berchkhemer and Jacob, 1968; Brune, 1970). Most of the seismic energy is contained in frequencies near ν_o.

For frequencies larger than ν_o, the amplitude spectral density must decay at least as fast as $\omega^{-\gamma}$, $\gamma>1$, so that the energy integral is bounded. Typically the spectra of seismic events fall off as ω^{-2}. This portion of the spectrum gives information only about the rise time of the source time function.

At low frequencies, the amplitude spectrum depends strongly on the source time function. For a step function which may be taken to represent an earthquake source time function, the long-period spectral amplitude level is flat and can be related to the stress drop τ or moment M_o (Aki, 1966). For an explosion, a more realistic pressure source time function may be $p = p_o e^{-\alpha t}$ (Sharpe, 1942); for $t >> \alpha^{-1}$, the pressure on the surface of the equivalent cavity should return to zero unless a permanent change of elastic stress in the medium occurred. The spectra resulting from sources with the above time functions are given in Figure 1. In the limit of $\alpha = 0$, the spectrum will be that of a step function source.

On the basis of the preceding discussion, the spectral differences between earthquakes and explosions should be greatest in the frequency range $\nu < \nu_o$. For $\nu > \nu_o$, the spectra may be expected to be similar, reflecting only minor differences in the rise time of the source time function. For earthquakes of $m_b > 5$, ν_o may be expected to be less than 0.3 Hz (Wyss and Brune, 1968; Liebermann and Pomeroy, 1970). Therefore, in this study we have concentrated our attention on the frequency band 0.04 to 1.0 Hz. Traditionally, little interest has been directed towards body waves in this band. Previous efforts have concentrated on frequencies higher than 0.3 Hz (e.g. Matumoto and Boucher, 1966; Lacoss, 1969; Bakun and Johnson, 1970). The only studies of the spectra of shallow earthquakes with frequencies smaller than 0.3 cps have been Kasahara (1957), Wu (1968), Wyss (1970b, c). The only information available to us for underground explosions in this frequency range is a short remark and Figure 2.7 in the SIPRI (1968) report, where Pasechnik suggested that marked spectral differences exist between earthquakes and explosions in the frequency range 0.2 to 0.5 Hz. The reason for the small interest in

the long periods was ground noise and instrument noise. The ground noise has a strong peak at frequencies around 0.16 Hz (Brune and Oliver, 1959; Brune, in preparation), the region in which the peak frequency of a magnitude 4 to 5 earthquake is expected to fall. At longer periods the ground noise is smaller but instrument noise has been a problem. New long period instruments remove this obstacle (Pomeroy et al, 1969; Block and Moore, 1970) and allow us to study surface waves as well as body waves with 10 to 100 sec periods.

Data

Four Aleutian earthquakes of comparable m_b to LONG SHOT and MILROW were selected for comparison of P-wave spectra. Their epicenters are within 160 km to 400 km of the shot points of LONG SHOT and MILROW (Table 1). The seismic recordings used were obtained at Pasadena and Tinemaha, California. Spectral differences of the P-pulse should reflect differencies associated with the source, since the wave paths are the same for all events.

The P-wave spectra for the explosions and earthquakes were obtained from three vertical instruments with different response curves operated at Pasadena. The magnification curves of these instruments are given in Figure 2. Each instrument furnished a spectrum in a frequency band close to its peak magnification and containing only periods that could be resolved with the standard paper speed. The analysis would be facilitated if broad band instruments of the Kirnos type (Figure 1) or Block and Moore (1970) type were available. The characteristics of the different instruments used and the data parameters are given in Table 2.

The spectra of the three different instruments have been combined on one graph to show the composite P-wave spectrum for periods between 0.4 and 40 sec. The data (uncorrected for attenuation) for MILROW and LONG SHOT are given in Figures 3 and 4, and for earthquakes in Figures 5 to 8. The spectral densities match well in regions of instrument overlap. As well as indicating good instrumental calibration, the matching indicates that problems arising from finite sample lengths are not adversely affecting the spectral analysis. The spectra of a Novaya Zemlya explosion recorded at Pasadena (distance approximately 73°) is given in Figure 9 for comparison.

For the earthquake of 20 February 1958, the long period vertical component at Pasadena was off scale. The NS component was analyzed instead. The spectral densities obtained from this record have been corrected for the angle of emergence. For the explosions the long period portion of the signal was smaller or equal to the noise. The spectral density of the noise is indicated by arrows in Figure 4. For LONG SHOT the spectrum was obtained from recordings at Tinemaha, California. The absolute magnifications at this station are not known. Therefore an arbitrary scale was used in Figure 4.

Discussion

The spectra (not corrected for attenuation) of four analyzed earthquakes are compared to the spectrum of MILROW in Figures 5 to 8. It is evident that the peak frequencies are different by approximately an order of magnitude. The difference shows up clearly in the seismic recordings of the long-period Benioff instruments also shown in these figures. The different positioning of the peak frequencies constitutes a major spectral difference between the two sets of data, suggesting source dimensions an order of magnitude larger for earthquakes than for explosions. In Figure 10, the attentuation corrected spectra of the earthquakes are compared to the MILROW spectrum. The dimensions of the sources were estimated from the peak frequencies of the Q-corrected spectra and are given in Table 3. For MILROW this estimate was obtained from Sharpe's (1942) model. For the earthquakes Brune's (1970) relation of turn-frequency to source size was used after substituting P-wave velocity for S-wave velocity. The same differences in source dimensions between earthquakes and explosions have been noted previously by Wyss and Brune (1968), Liebermann and Pomeroy (1970), and Wyss (1970d).

The shape of the earthquake spectra are very similar to each other but markedly different from the explosion spectrum. At the high frequency end the uncorrected spectra look more or less alike. After the Q-correction (following Julian and Anderson, 1968) was made (Figure 10) the larger high frequency content of the explosion is more obvious, but all spectra fall off as ω^{-2} towards higher frequencies. This indicates that all the sources have time functions that rise from zero to the peak value, in times small compared to the shortest periods analyzed. At low frequencies the earthquake spectra are more or less flat to 0.02 Hz, except the smallest of the earthquakes, June 2, 1966. This spectral behavior with a flat long period part corresponds to a step function at the source. The explosion spectrum behaves differently. It decays rapidly, at least as ω, from the peak value towards lower frequencies. In the band 0.1 to 1 Hz, the earthquake and explosion spectra differ completely, the first drops as ω^{-2} whereas, the second increases linearly with increasing frequency. The pronounced drop-off of the P-wave spectra for explosions at frequencies less than the peak frequency constitutes a second major difference between the spectra of explosions and earthquakes.

The fact that the explosion spectrum is poor in low frequency spectral amplitudes compared to earthquakes has to be explained by a difference in the source function. The simplest approximation is to follow Sharpe (1942) and consider the source time function

$$p = p_o e^{-\alpha t} \qquad (1)$$

acting at the surface of an equivalent cavity with an infinite elastic

medium. It can, however, be expected that the free surface and perhaps "ringing" of the equivalent cavity will enhance the spectra near the peak frequency. A theoretical spectrum was fitted through the explosion data using Sharpe's (1942) result (Figure 3) the radius of the equivalent (elastic) cavity of MILROW is 1.25 km. α in (1) is approximately .4 sec-1. This value is larger, i.e. the time function is sharper, than values found by surface wave analysis for two smaller explosions (Toksöz et al, 1964).

Stress drops

From the estimated source dimensions and the seismic moments given for three events by Wyss (1970c), one can obtain the average dislocation and the stress drop associated with the three earthquakes. These parameters are given in Table 3. Since the stress drop is a lower bound of the acting stress in the source region it is of interest to compare these values with values from other regions. In view of pending nuclear tests in Amchitka it would be alarming if stress drops in this region should be unusually high, possibly indicating a large total stress in the region. The stress drops derived for the studied events, however, are comparable with values of equal magnitude events in other regions Wyss (1970b).

CONCLUSIONS

Discrimination of underground explosions and earthquakes

The data suggest that there are two potentially useful diagnostic features of the P-wave spectra for earthquakes and underground explosions of comparable m_b from the same geographic and tectonic region. The first criterion is that the peak frequency for the explosion is almost an order of magnitude greater than the corner frequency of the earthquake spectra. Equivalently, the source radius of an explosion, as determined from the spectral data, is approximately an order of magnitude less than the earthquake dimension. (See also Wyss, 1970d; Liebermann and Pomeroy, 1970). Since the peak frequency is not generally known beforehand, it is necessary to obtain as complete a spectral curve as possible. The ratio of amplitudes at any predetermined frequencies need not reflect the maximum spectral differences. One should also bear in mind that the peak frequency can be shifted by decoupling and/or lengthening the time duration over which the explosive pulse is operative.

The second diagnostic feature is the pronounced decay of the explosion spectra for frequencies less than the peak frequency, in contrast to the earthquake spectra which remains flat below ν_0. These spectral features at low frequencies are most readily interpretable in terms of different source time function for the two events -- a step function for earthquakes and an exponentially-decaying step for explosions.

The observed behavoir of the P-wave spectra at low frequencies agrees well with the data of Molnar et al (1969) on the spectra of surface waves between 20 and 50 sec for earthquakes and explosions in western United States. Their data show that the spectra for explosions decay more rapidly with decreasing frequency than do the earthquake spectra. Molnar et al (1969) also interpret the differences in the spectra as representing differences in the source time functions of the two types of events.

It is interesting to note from Table 1 that some of the earthquakes studied here may be as deep as 40 km. Tsai (1969) and Tsai and Aki (1970) have pointed out that earthquakes of these depths exhibit surface wave spectra with pronounced minima due to destructive interference (holes) in the period range studied by Molnar et al (1969). These holes can make it difficult, if not impossible, to apply the surface wave spectral ratio discriminant to all events. However, the criteria presented in this study of P-wave spectra enable us to discriminate between explosions and earthquakes of 40 km depth.

ACKNOWLEDGEMENTS

We wish to thank Paul G. Richards for helpful discussions.

This research was supported by National Science Foundation Grant NSF GA-19473 and by the Advanced Research Project Agency of the Department of Defense and was monitored by the Air Force Office of Scientific Research under Contract No. F44620-69-C-0067. Any views expressed in this paper are those of the authors and are not to be construed as reflecting official opinions or policy of the Department of Defense or any other agency of the U.S. Government.

REFERENCES

Aki, K., 1966, Generation and propagation of G-waves from the Niigata earthquake of June 16, 1964, 2, Estimation of earthquake moment, released energy, and stress-strain drop from the G-wave spectrum, Bull. Earthquake Res. Inst., Tokyo Univ., v. 44, p. 73-88.

Archambeau , C.B., 1964, Elastodynamic Source Theory, Ph.D. Thesis, Calif. Inst. of Tech., Pasadena, California.

Bakun, W.H., and Johnson, L.R., 1970, Short period spectral discriminants for explosions, (abstract), Trans. Am. Geophys. Union, v. 51.

Berchkhemer, H., and Jacob, K.H., 1968, Investigation of the dynamical process in earthquake foci by analyzing the pulse shape of body waves, Final Scientific Report, AF 61 (052)-801.

Block, B., and Moore, R.D., 1970, Tidal to seismic frequency investigations with a quartz accelerometer of new geometry, J. Geophys. Res., v. 75, p. 1493-1505.

Brune, J.N., 1970 (in press), Tectonic stress and the spectra of seismic shear waves from earthquakes.

Brune, J.N., Seismic noise and the detection problem (in preparation).

Brune, J.N., and Oliver, J., 1959, The seismic noise of the earth's surface, Bull. Seism. Soc. Am., v. 49, p. 349-353.

Julian, B.R., and Anderson, D.L., 1968, Travel times, apparent velocities and amplitudes of body waves, Bull. Seism. Soc. Am., v. 58, p. 339-366.

Kasahara, K., 1957, The nature of seismic origins as inferred from seismological and geodetic observations (1), Bull. Earth. Res. Inst., v. 35, p. 473-532.

Lacoss, R.T., 1969, A large-population LASA discrimination experiment Techncial Note 1969-24, Lincoln Laboratory, MIT.

Liebermann, R.C., and Pomeroy, P.W., 1969, Relative excitation of surface waves by earthquakes and underground explosions, J. Geophys. Res., v. 74, p. 1575-1590.

Liebermann, R.C., and Pomeroy, P.W., 1970, Source dimensions of small earthquakes as determined from the size of the aftershock zone, Bull. Seism. Soc. Am., v. 60, p. 879-890.

Matumoto, T., 1960, On the spectral sturcture of earthquake waves, Bull. Earth. Res. Inst., v. 38, p. 13-27.

Matumoto, T., and Boucher, G., 1966, Comparison of the initial motion of the Long Shot explosion and the Aleutian earthquake of December 22, 1965, (abstract), Trans. Am. Geophys. Union, v. 48, p. 165.

Molnar, P., Savino, J., Sykes, L.R., Liebermann, R.C., Hade, G., and Pomeroy, P.W., 1969, Small earthquakes and explosions in North America recorded by new high gain, long period seismographs, Nature, v. 224, p. 1268-1273.

Pomeroy, P.W., Hade, G., Savino, J., and Chander, R., 1969, Preliminary results from high-gain wide-band long-period electromagnetic seimsograph systems, J. Geophys. Res., v. 74, p. 3295-3298.

Sharpe, J.A., 1942, The production of elastic waves by explosive pressures. I. Theory and empircial field observations, Geophysics v. 7, p. 144-154.

SIPRI, 1968, Seismic methods for monitoring underground explosions. Report by a seismic study group, International Inst. for Peace and Conflict Research (SIPRI), Stockholm, p. 130.

Toksoz, M.N., Ben-Menahem, A., Harkrider, D.G., 1964, Determination of source parameters of explosions and earthquakes by amplitude equalization of seismic surface waves -- Pt. 1, Underground nuclear explosions, J. Geophys. Res., v. 69, p. 4355-4366.

Tsai, Y.B., 1969, Determination of focal depths of earthquakes in the mid-oceanic ridges from amplitude spectra of surface waves, Ph.D. Thesis, M.I.T.

Tsai, Y.B. and Aki, K., 1970, (in press), Precise focal depth determination from amplitude spectra of surface waves, J. Geophys. Res.

Wu, F.T., 1966, Lower limit of the total energy of earthquakes and partitioning of energy among seismic waves, Ph.D. Thesis, Calif. Inst. of Tech., Pasadena, California.

Wyss, M., 1970a, Observation and interpretation of tectonic strain release mechanisms, Ph.D., Thesis, Calif. Inst. of Tech., Pasadena, California.

Wyss, M., 1970b., Stress estimates of South American shallow and deep earthquakes, J. Geophys. Res., v. 75, p. 1529-1544.

Wyss, M., 1970c, A comparison of apparent stresses of earthquakes on ridges with earthquakes in trenches, Geophys. J. Roy. Astr. Soc.

Wyss, M., , 1970d., Dimensions of underground explosions and small shallow earthquakes, (in preparation).

Wyss, M., and Brune, J.N., 1968, Seismic moment, stress, and source dimensions for earthquakes in the California-Nevada region, J. Geophys. Res., v. 73, p. 4681-4694.

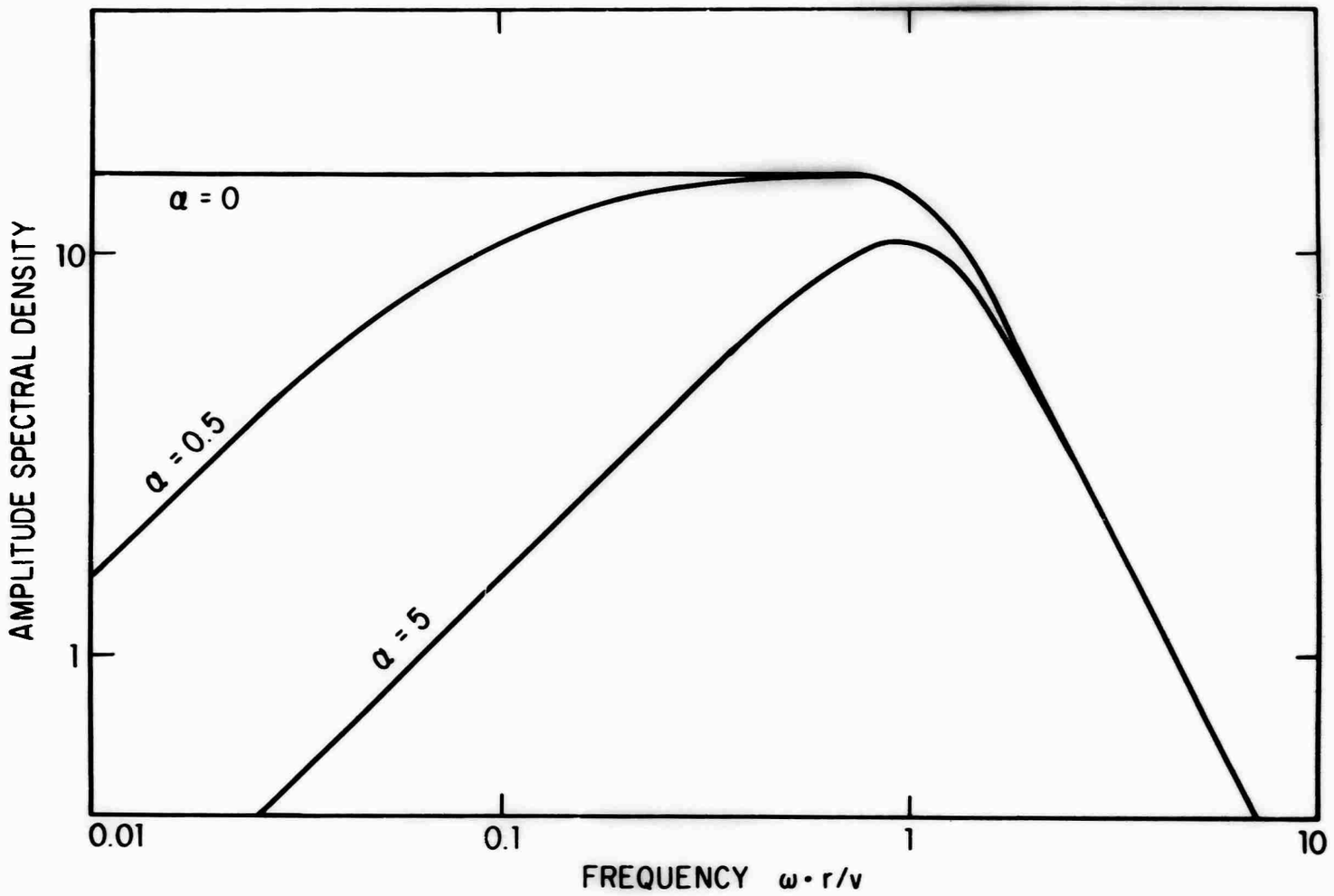

Figure 1. Displacement spectra corresponding to a source function $p = p_o e^{-\alpha t}$ following Sharpe (1942).

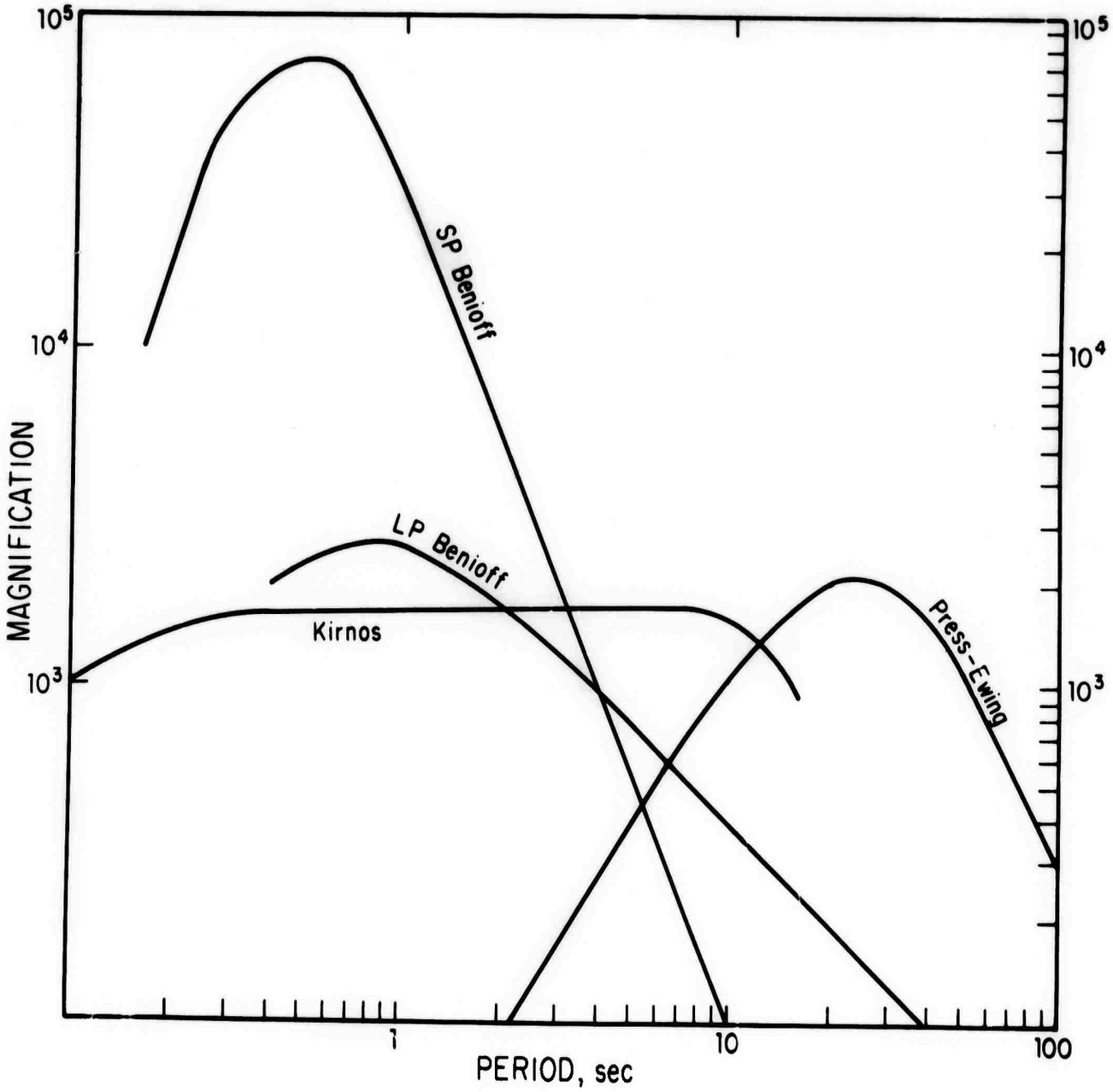

Figure 2. Instrument magnifications.

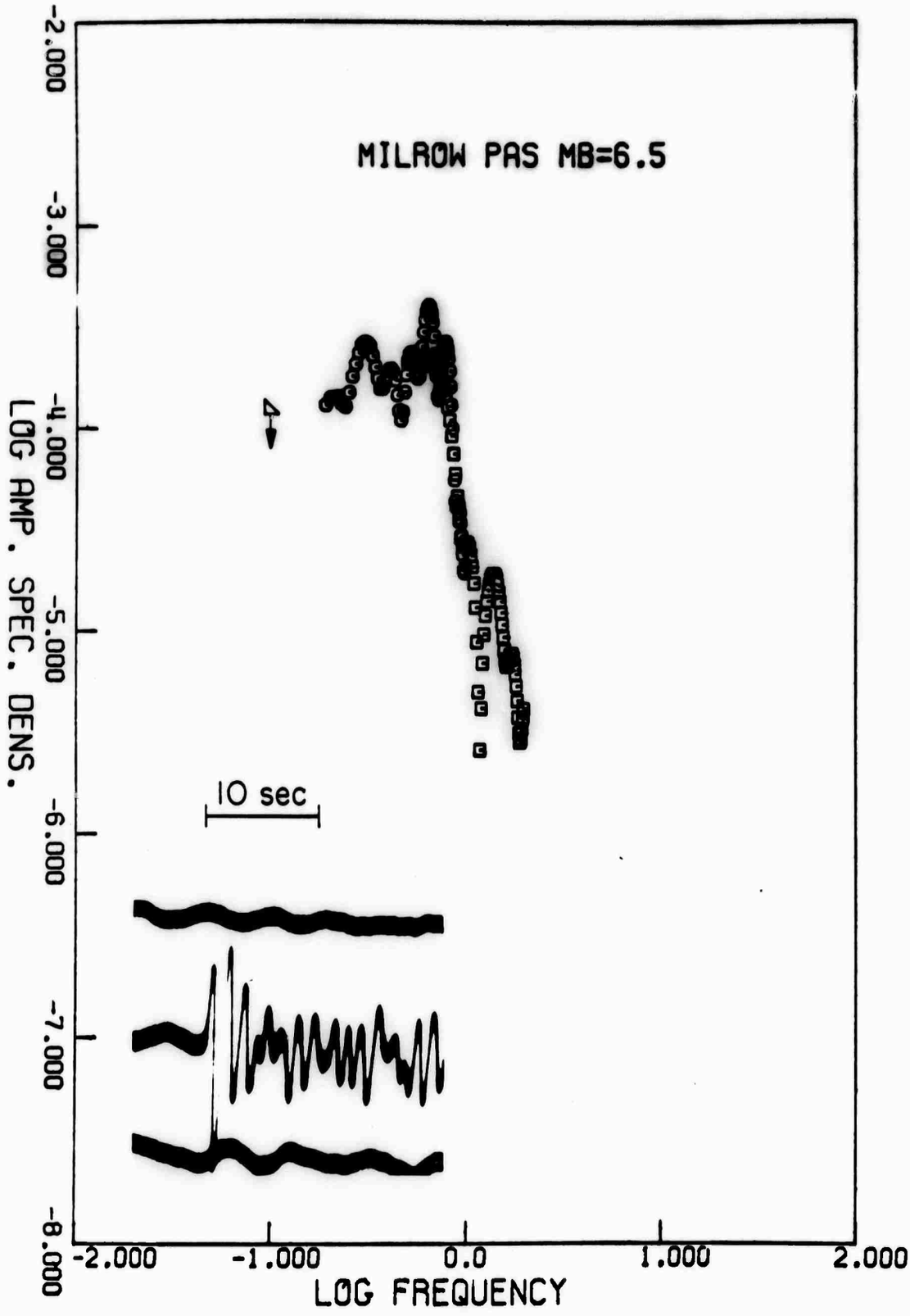

Figure 3a. Amplitude spectrum for MILROW recorded at Pasadena ($\Delta \approx 50°$).

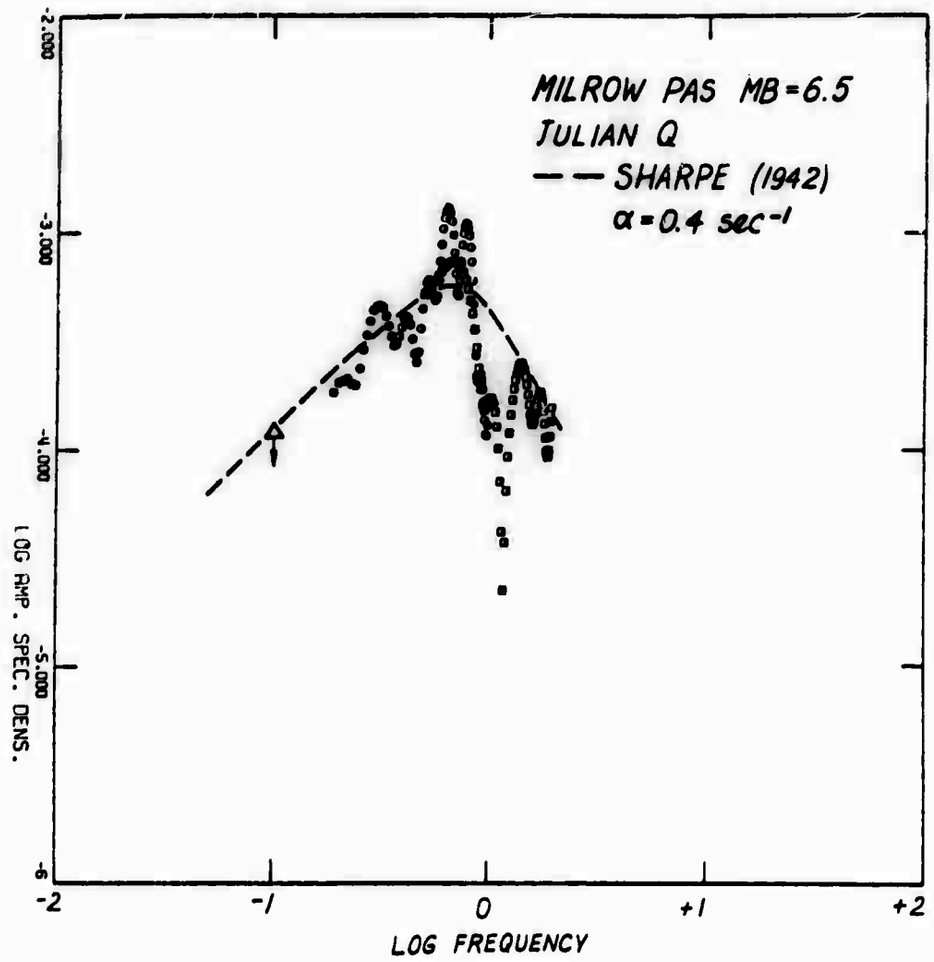

Figure 3b. Attenuation corrected amplitude spectrum for MILROW. The dashed curve is a fitted theoretical spectrum after Sharpe (1942) with $\alpha = 0.4$ sec^{-1}.

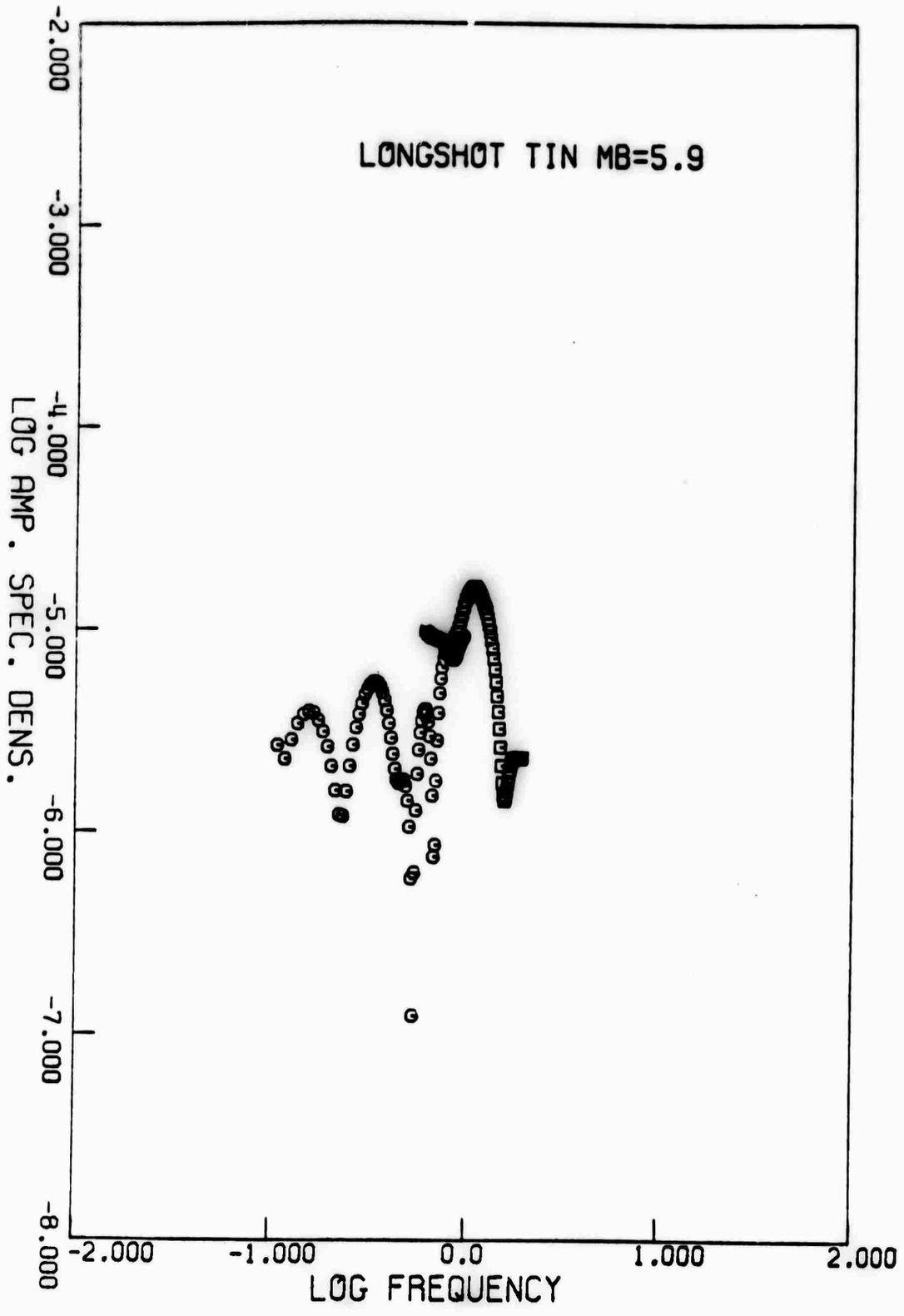

Figure 4. Amplitude spectrum for LONG SHOT recorded at Pasadena.

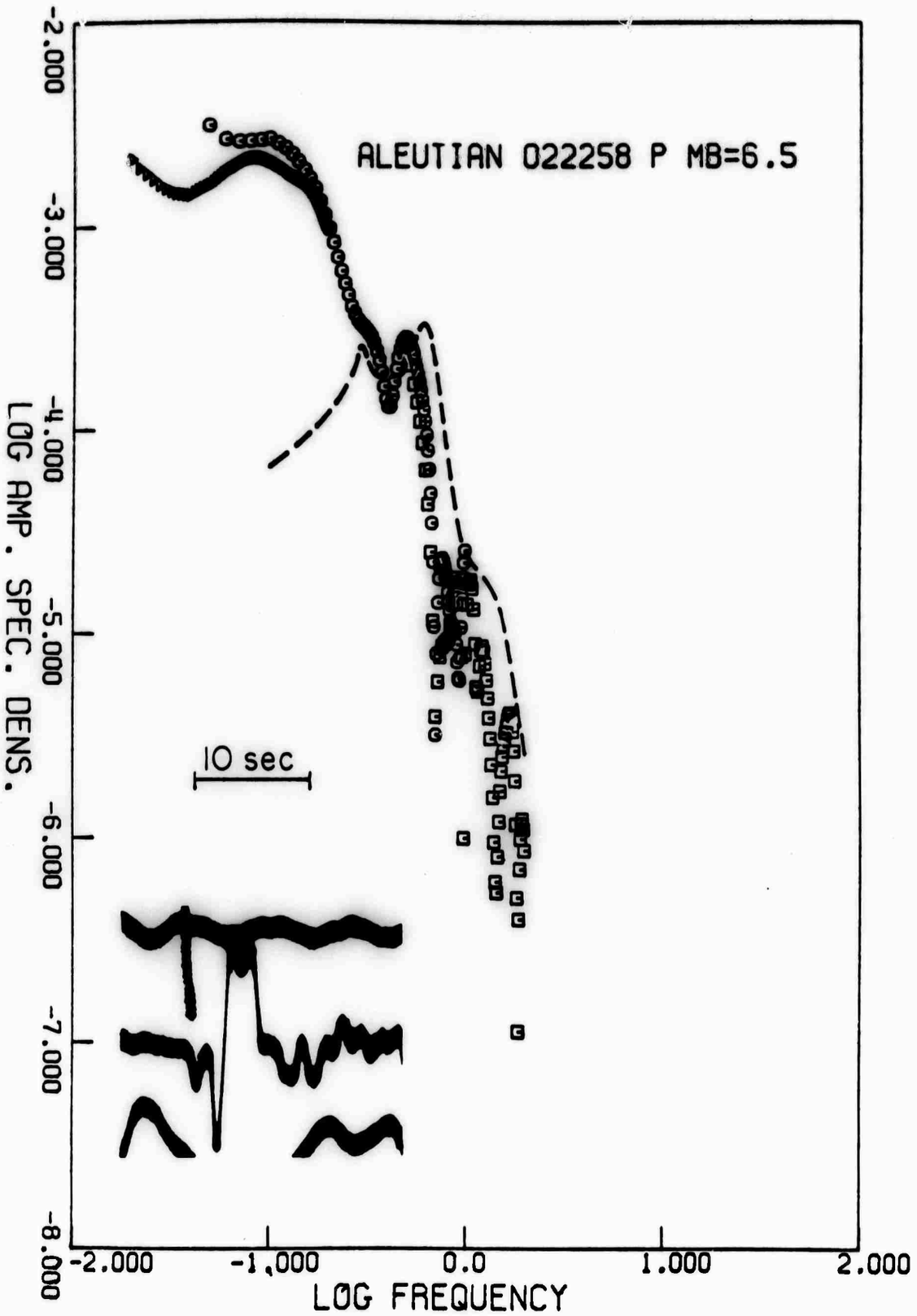

Figure 5. Amplitude spectrum of an Aleutian earthquake compared to the amplitude spectrum of MILROW, both recorded at Pasadena.

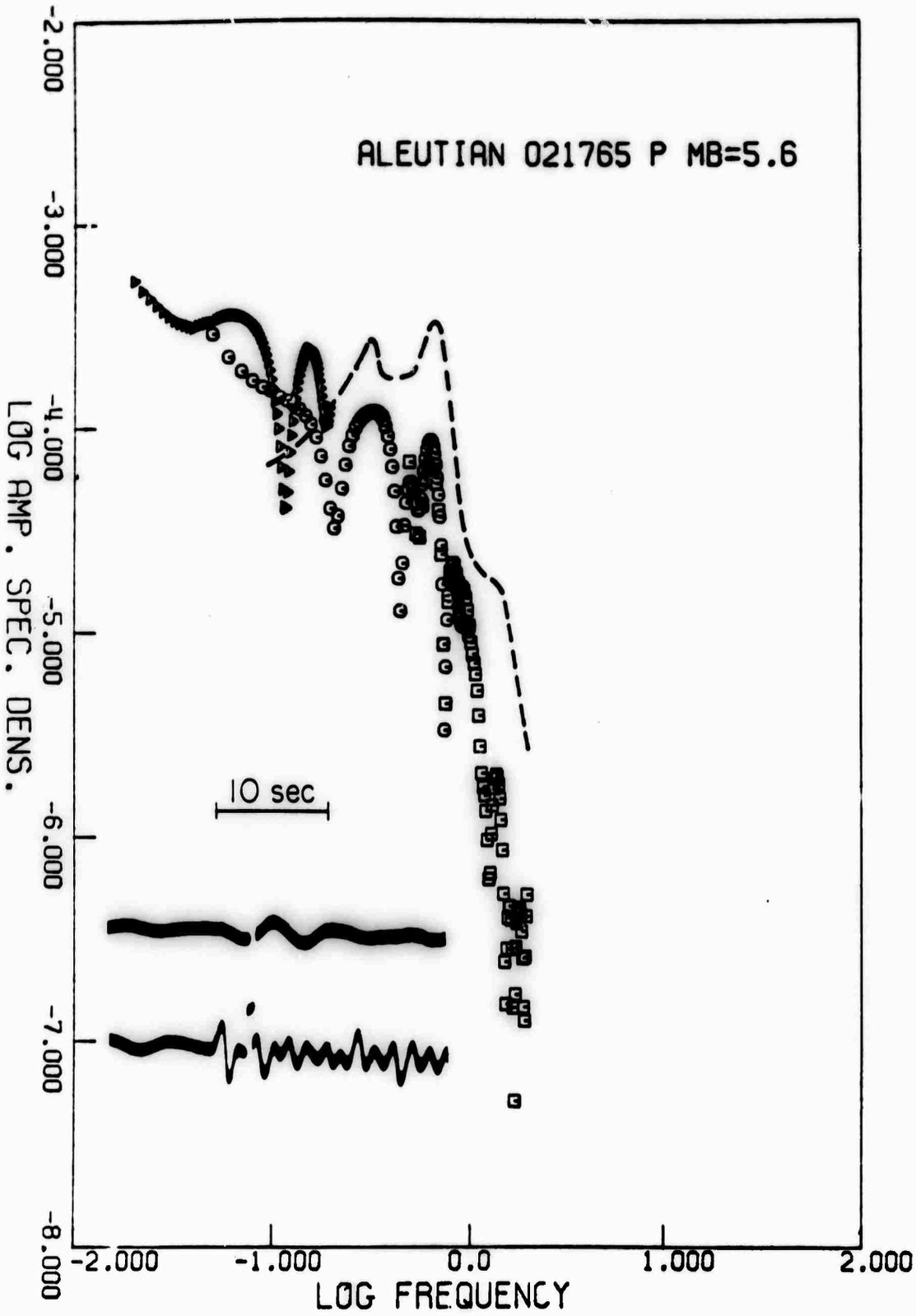

Figure 6. Amplitude spectrum of an Aleutian earthquake compared to the amplitude spectrum of MILROW, both recorded at Pasadena. (See Figure 5.)

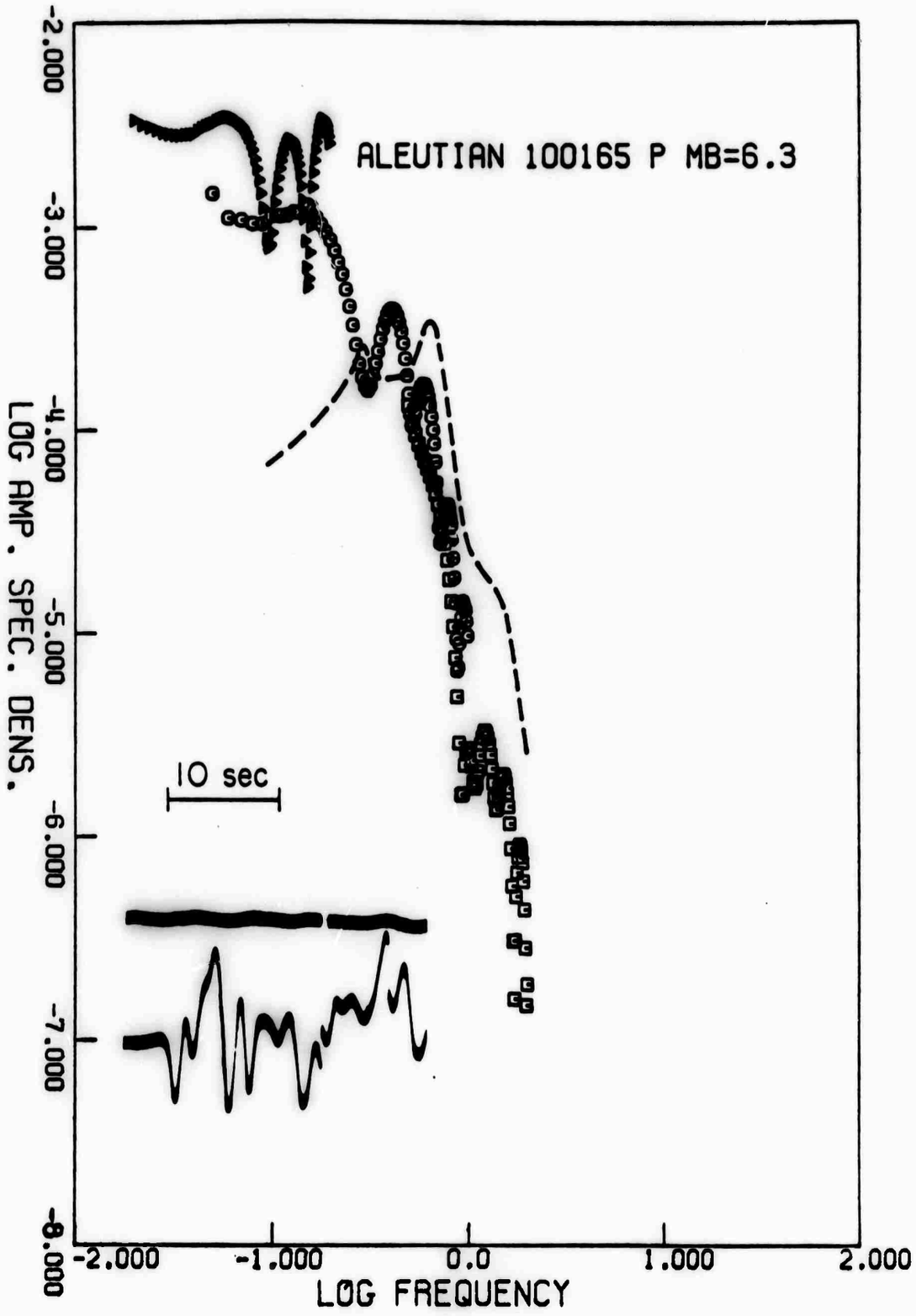

Figure 7. Amplitude spectrum of an Aleutian earthquake compared to the amplitude spectrum of MILROW, both recorded at Pasadena. (See Figure 6).

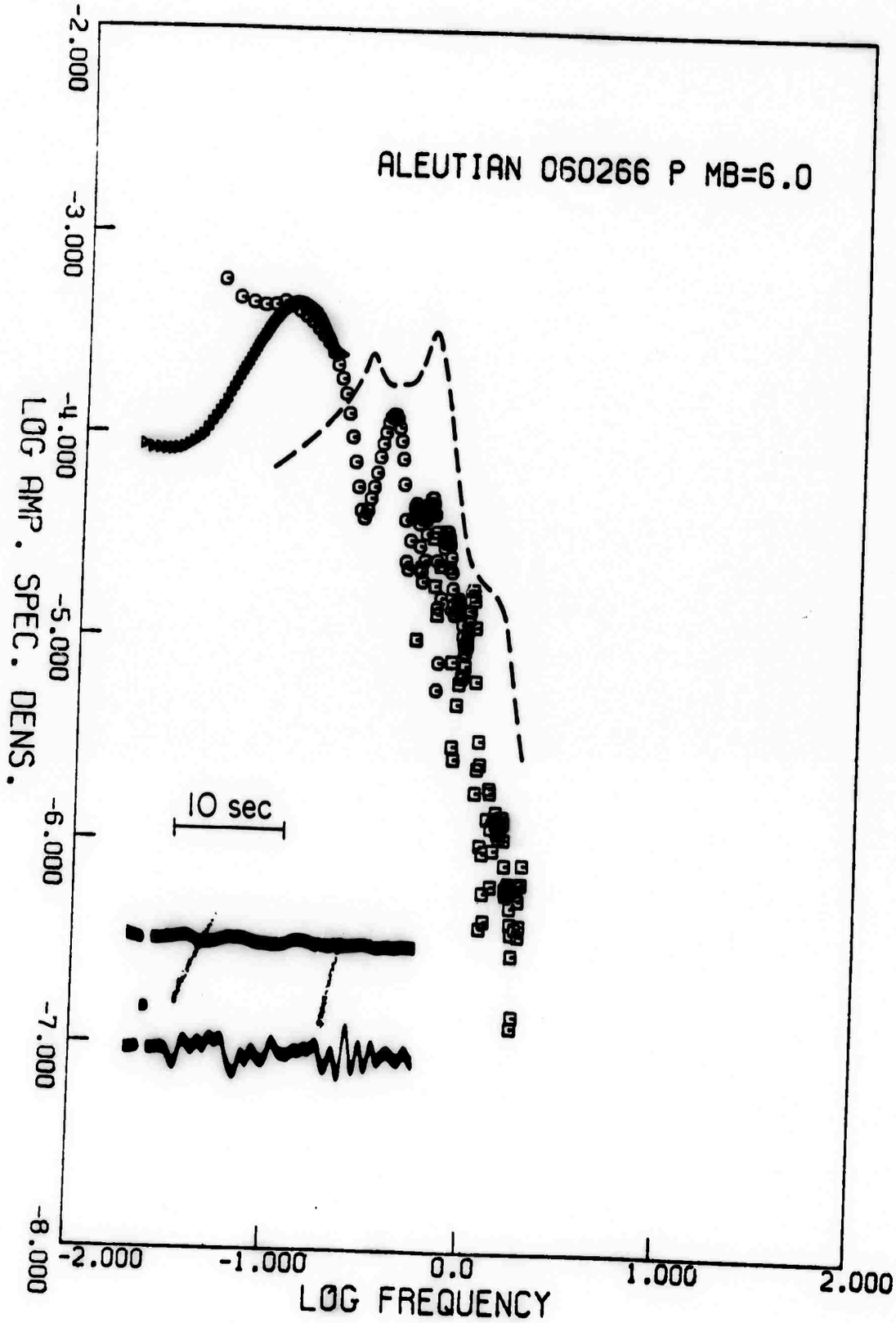

Figure 8. Amplitude spectrum of an Aleutian earthquake compared to the amplitude spectrum of MILROW, both recorded at Pasadena. (See Figure 5).

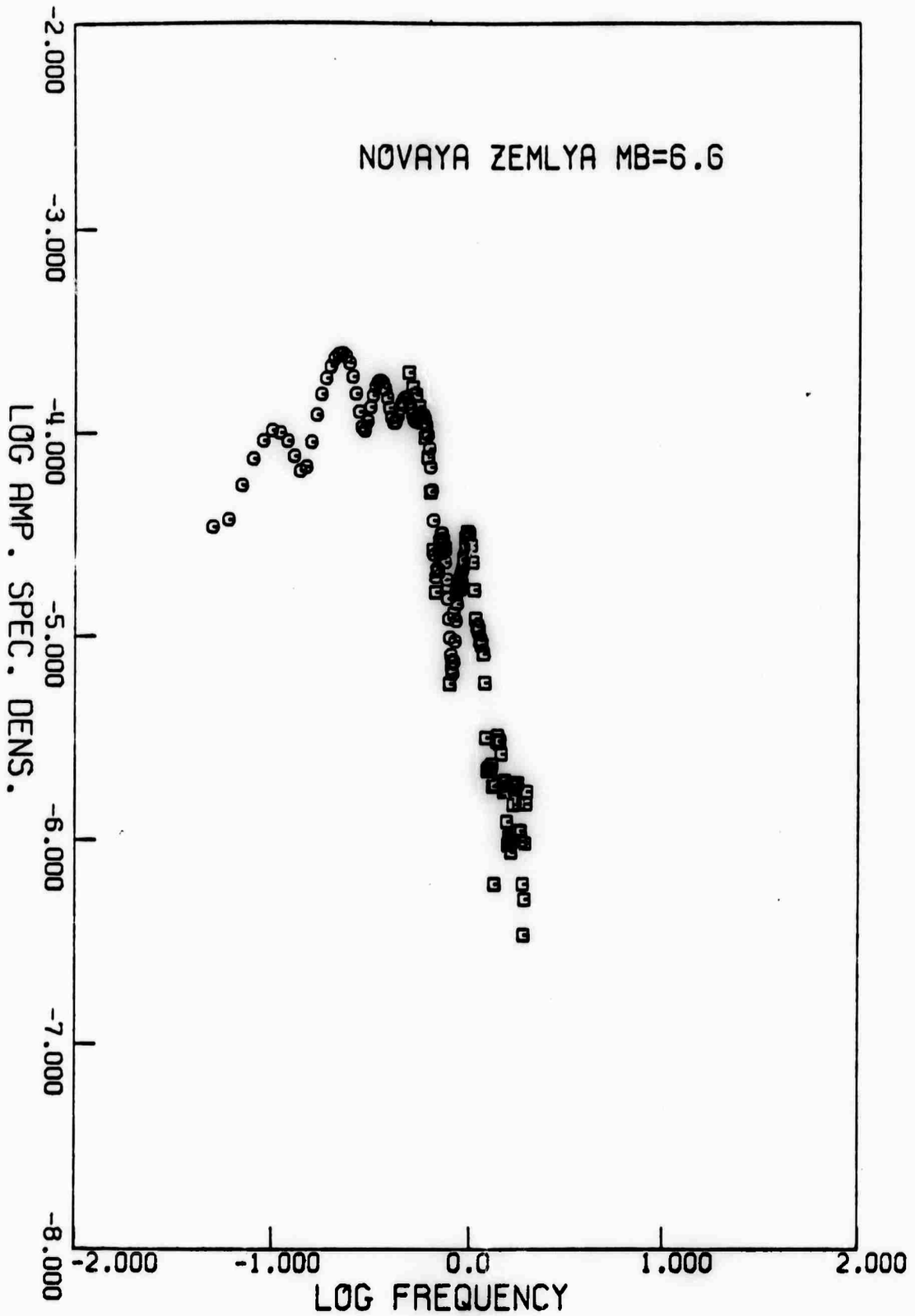

Figure 9. Amplitude spectrum of a NOVAYA ZEMLYA test recorded at Pasadena.

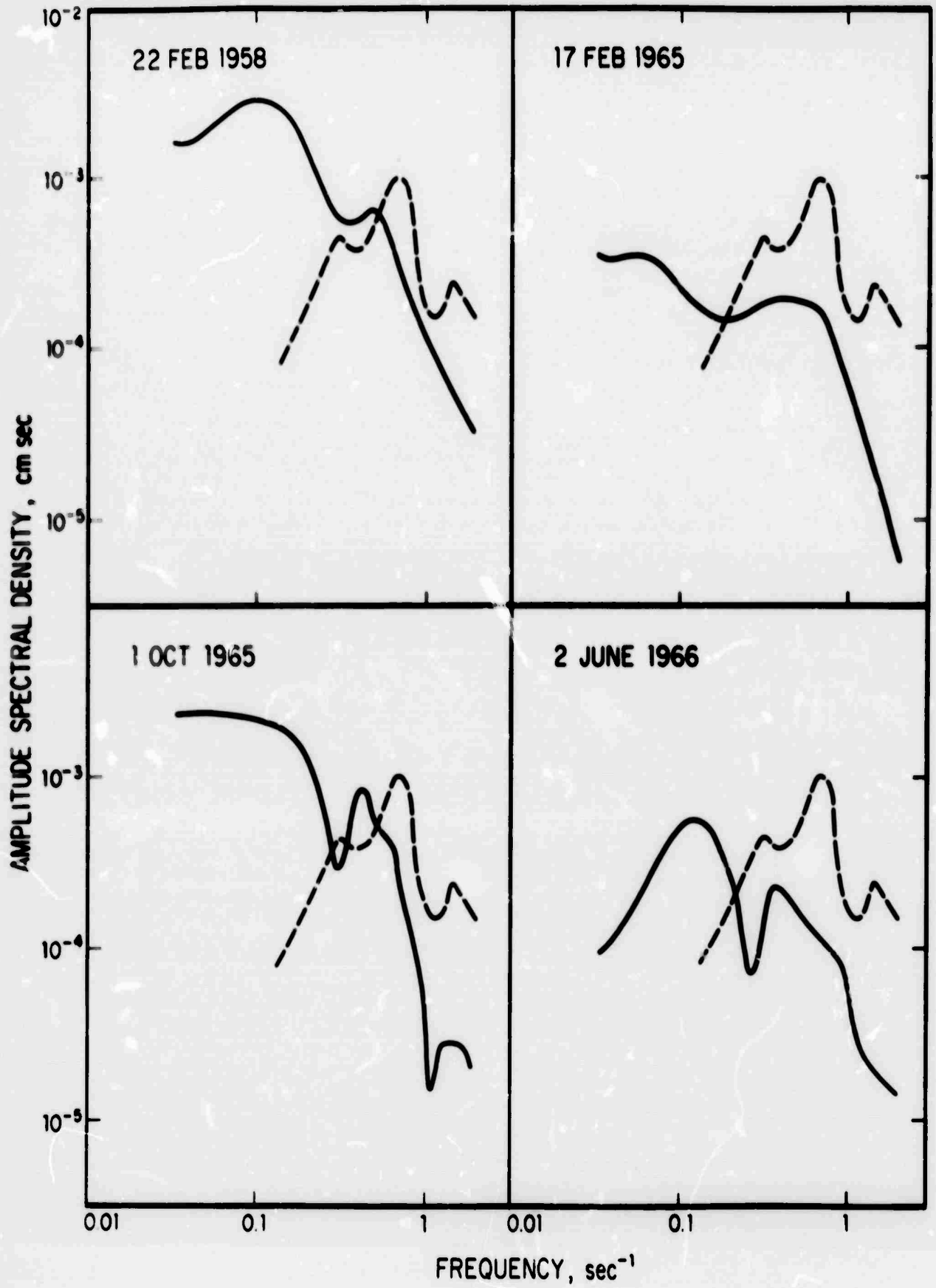

Figure 10. Attentuation corrected amplitude spectra of four Aleutian earthquakes compared to that of MILROW (dashed line).

TABLE 1. Selected Seismic Events

Event	Date	Origin Time (G.C.T.)	Latitude degrees	Longitude degrees	Depth h	m_b[1]
	d m y	h m s			km	
1	22 Feb 1958	10:50:23	50 1/2N	175W	33	6.5[2]
2	17 Feb 1965	10:18:51	51.8N	176.6E	44	5.6
3	01 Oct 1965	08:52:05	50.1N	178.3E	23	6.3
4	02 June 1966	03:27:53	51.1N	176.0E	41	6.0
MILROW	02 Oct 1969	21:00:00	51.4N	179.2E	1.2	6.5
LONGSHOT	29 Oct 1965	22:06:00	51.4N	179.2E	0.7	5.9
NOVAYA ZEMLYA[4]	27 Oct 1966	05:57:58	73.4N	54.8E	—	6.6[3]

1. U.S. Coast and Geodetic Survey reports
2. Determined from Pasadena seismograms
3. *Liebermann and Pomeroy* (1969)
4. Atomic Energy Commission press release of October 27, 1966, announcing Soviet test in northern testing area of NOVAYA ZEMLYA.

TABLE 2. Instrument Characteristics

	Short-period Benioff	Long-Period Benioff	Press-Ewing
Seismometer period (sec)	1.0	1.0	30
Galvanometer period (sec)	0.2	90	90
Bandwidth (sec)	0.4 to 2.0	1 to 10	6 to 40
Time window (sec)	10	10	25-30
Paper speed (cm/min)	6	3	1.5

TABLE 3

SOURCE PARAMETERS

Event No.	Peak Frequency cps	Dimension $2r$ km	Displacement $\bar{u}$ cm	Stressdrop τ bar
1	0.1	20.	130.	47.
2	0.1	13.	—	—
3	0.07	29.	45.	11.
4	0.12	14.	12.	10.
Milrow	0.64	2.5	—	—

EXPLOSIONS/AFTEREVENTS/EARTHQUAKES -- CHARACTERISTICS AT SHORT (500 - 600 km) AND VERY SHORT DISTANCES

By

T. V. McEvilly

University of California
Berkeley, California

Range of investigations under present contract

Four areas of study are in progress

1. P wave spectral discriminants at small magnitudes and short distances.

2. P wave structure synthesis including multiple arrivals at short distance.

3. P_n/Rayleigh ratios for small events at short distances

4. Close-in measurements of accelerations from large NTS shots and afterevents for source parameter studies.

BRK data for earthquakes, explosions, and aftershocks at 500-600 km

With nuclear tests of m_b = 6 the phenomena of associated aftershocks (as opposed to the common cavity collapse), faulting some 10+ km from the shot, and implied strain release (regional or shot-induced) became of interest. Berkeley (BRK) broadband seismic data, recorded some 500-600 km from NTS, with extensive tape library files of past events, were studied to make general comparisons of the various seismic events. Results can be stated through the accompanying suite of figures.

Figure 1 contrasts afterevent activity of the largest Pahute Mesa shots. Figure 2 shows their locations. Much discussion has centered around the relative "earthquake" component of these large sources.

Figures 3-6 compare events in various ways, presumably establishing a maximum time duration of "earthquake" components in the sources. Figure 3 compares explosion and collapse Rayleigh wave pairs at BRK for several shots. These are aligned on the P_n arrival, clearly recorded on our high gain JAS station. Note the clear 180 degree phase shift of the collapses and the excellent correlation, peak for peak, of both explosion-collapse pairs and among explosions in the same source region. This correlation extends for some 2+ minutes in the wave train, down to periods of 3 or 4 seconds. Figure 4 compares four events, vertical components, broadband data, as further illustration of the correlation for events near one another. The surface wave train, as expected, correlates much better than the body waves. Implications are that, to a time scale of about two seconds, the large events have identical source functions which are very similar to the collapse sources (presumably very localized). Figure 5 presents velocity spectra of the same events. Close events (e.g. Jorum and Boxcar) show marked similarity all the way to 1 Hz. (P spectra will be compared also.) Event Pipkin is less than 0.1 the size of Benham, yet these also compare well (Benham is lower frequency) to about 0.8 Hz.

Figure 6 shows discrimination parameters available in a sequence of afterevents (well documented) of the Benham explosion.

In an attempt to investigate the M_s - m_b discriminant at lower

magnitudes, P_g amplitude (at BRK or JAS, normalized) and Rayleigh wave peak amplitudes (at BRK, usually in the 10-15 second period range) for various events in the 500-600 km distance range from BRK were compared. Figure 7, the result, includes earthquakes in Oregon, Nevada (off NTS), and California, NTS explosions, collapses, and explosion-induced aftershocks to the limit of the BRK surface wave detection threshold.

Clearly, the basis for discrimination is indicated. It is interesting that collapses are also separated from explosions, probably due to their relatively weak P-wave generation and/or very shallow source depths.

Close-in measurements for Jorum and Handley:

Figure 8 shows accelerometer deployment for the Jorum and Handley tests. Instruments are 0.5g servoaccelerometers at 8 km recorded at dual gains (32 db separation), 0.02-50 Hz, on magnetic tape at NTS. Despite tape recorder malfunctions, a large amount of data are available for these events. The purpose of the experiment was observation of azimuthal variations related to source function asymmetry due to possible contributions from faulting in the explosion and to make comparisons with the aftershocks. The data here presented are preliminary with much analysis remaining.

Jorum

The tape recorder for sites, 1, 2, 3 on Jorum failed prior to shot time reducing azimuthal coverage to 45 degrees (Figure 9). Figure 10 shows the recorded vertical and transverse data. Site effects are severe in both amplitude and frequency content. Figures 11-12 present acceleration spectra to 10 Hz for Jorum. Differences are great. Some indications exist of a minimum in the transverse spectra from 1 to 2 Hz and of variations in the low 'frequency' ripple among sites. Implied source durations greater than 1-2 seconds, however, would seem impossible in light of the total signal duration of about 3-5 seconds.

Many aftershocks were recorded. Figure 13 compares Jorum with three large such events typical of the types observed. All originate at or very close to the shot point. Z4 (vertical, site 4) data are shown. Figure 14 compares spectra of these signals, showing the wide variations observed. The explosion is richer in lower frequencies than the afterevents (Magnitudes 4-4 3/4). Figures 15-18 show azimuthal variation for a high- and low-frequency afterevent, respectively. Note the wide variation in site effect (possible source mechanism differences, also), the generally higher frequency content than Jorum, and the much longer duration of the signals. Event 1928 is not unlike in appearance a low magnitude (0+) microearthquake as observed on the San Andreas system in California.

Handley

The experiment was repeated for Handley (Figure 19 with 9 stations and proportionately more failures. While sites 1-5 (100 degrees coverage) recorded the shot, only 1-3 functioned throughout the recording period to provide afterevent data. Figures 20-21 show accelerations recorded -- not unlike Jorum except for larger accelerations (site 1 exceeded 0.5g on alluvium in Gold Flat, sites 2 and 4 also reached 0.5g on the initial pulse). Figures 22-23 present acceleration spectra. Minima and ripple are again apparent, but systematic variations with azimuth are not obvious. Cepstrum analyses will be carried out, though strong signal duration of only about 3 seconds provides a clear constraint on the source time function.

Aftershock types are shown in Figure 24, spectra in Figure 25. Very high (2013) and very low (1818) frequency events are present, all with significantly longer duration than Handley; 1818 a truly remarkable collapse(?) with a long train of very slow (or late generated) surface waves. Figures 26-27 show the available azimuthal coverage on event 1818. The low frequency wave is clearly not simply a site effect, appearing uniformly at all three stations. The transverse arrival is oddly late.

Discussion

Large nuclear tests at Pahute Mesa, while responsible for aftershocks and displacements on existing faults at distances of several kilometers, appear to be very localized and impulsive sources when viewed from 8 km. While analyses are not yet complete, there seems to be no azimuthal spectral variations apparent corresponding to source time-space functions required for a significant "earthquake" type fault rupture component in the source. These implications are substantiated by similarity of Rayleigh wave signals recorded at BRK to periods as short as 4 seconds for shots near together at NTS, and by the similarity of explosion and collapse Rayleigh waves. A necessary conclusion from these preliminary data is that the shear generation (S- and Love waves) occurs in the same localized high stress source of compression and that regional strain is relatively unimportant except in providing a preferred orientation for failure in the source region.

Relative surface-to-body wave generation characteristics, differing for explosions and earthquakes at m_b = 5, are apparent for NTS events and regional earthquakes recorded at BRK (500-600 km) as low as detection allows observation (m_b in range 3.5 - 4.0) with conventional broadband tape recorded seismographs. It seems reasonable to assume that such differences exist at teleseismic distances.

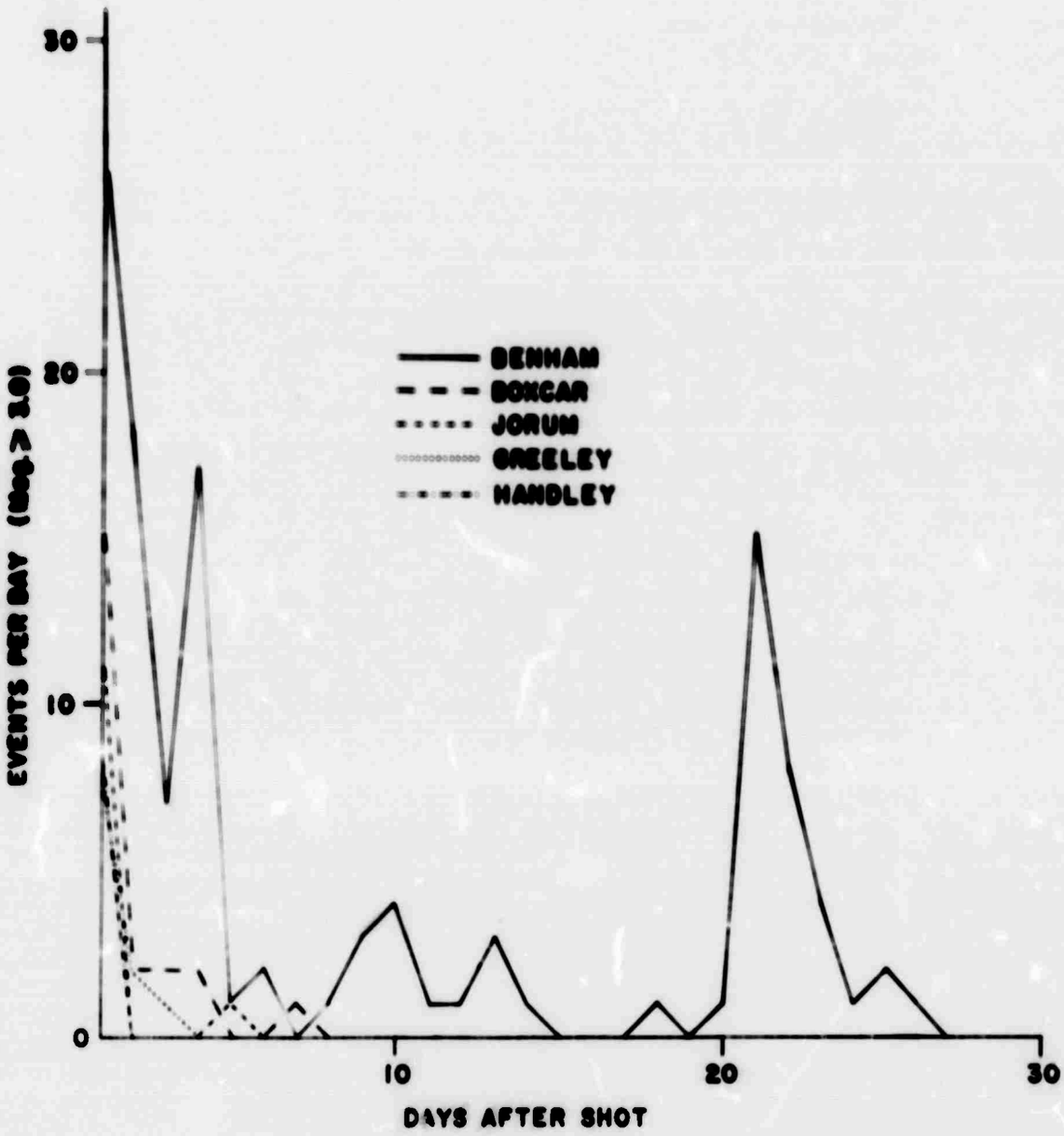

Figure 1. Afterevents from large Pahute Mesa shots.

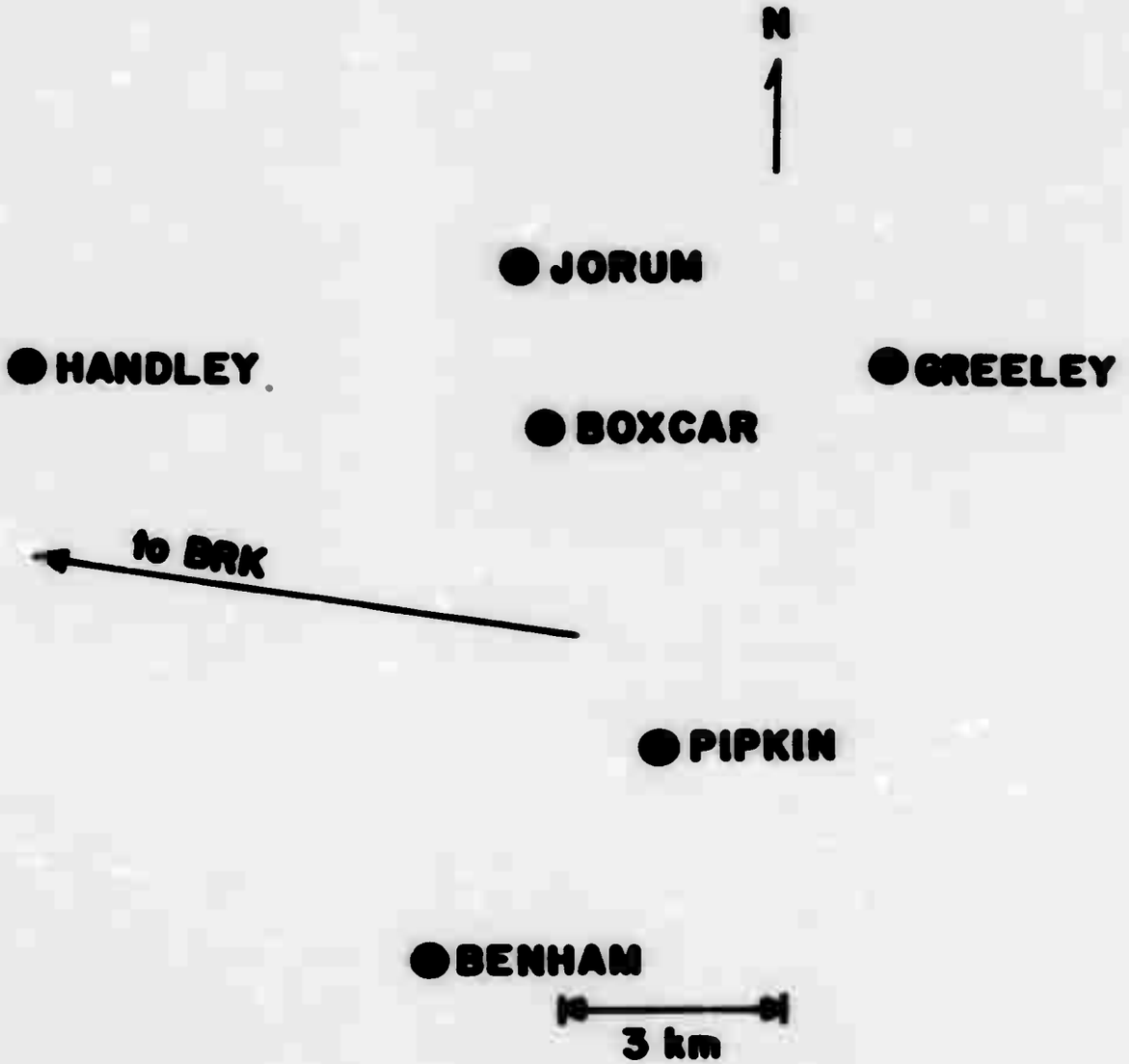

Figure 2. Pahute Mesa events compared in this study.

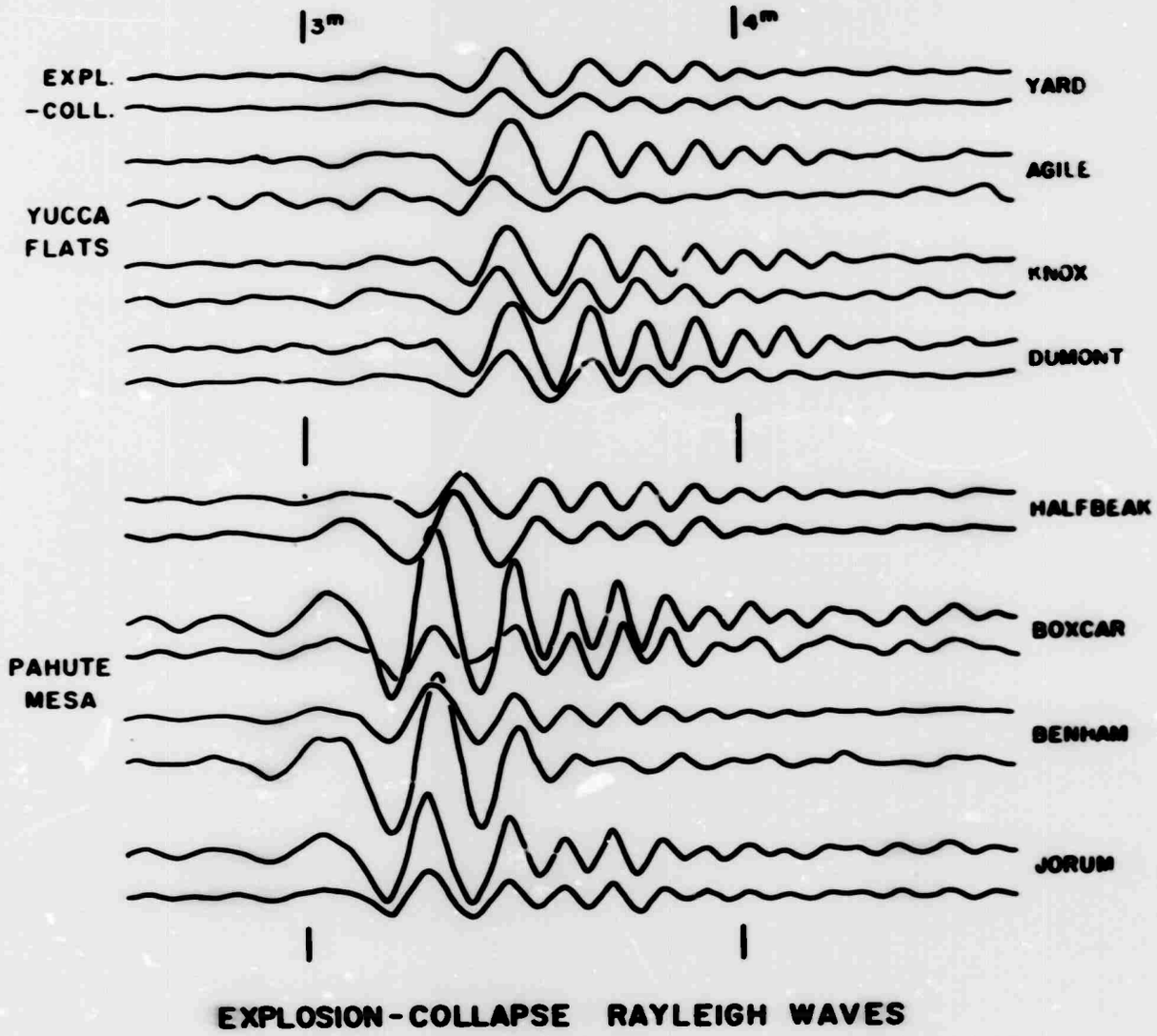

Figure 3. Comparison of explosion and inverted collapse Rayleigh waves for NTS events. Events aligned on P_n.

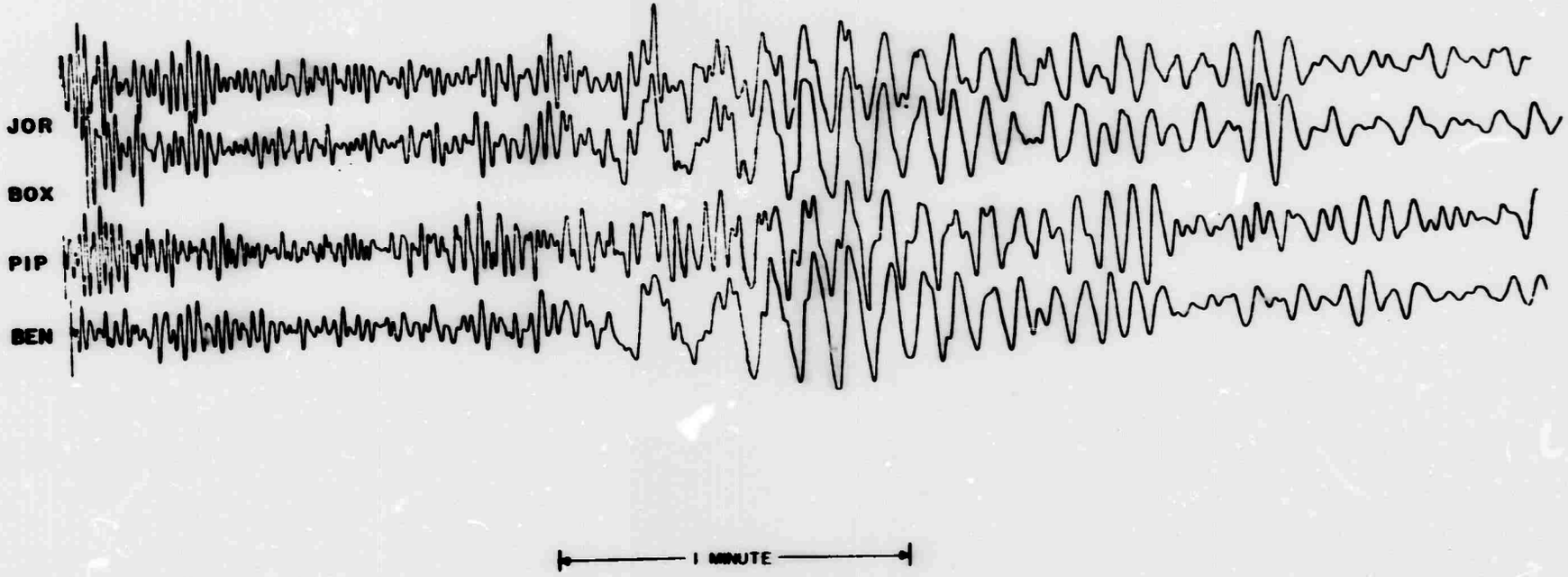

Figure 4. Comparison of BRK vertical broadband traces for Pahute Mesa events.

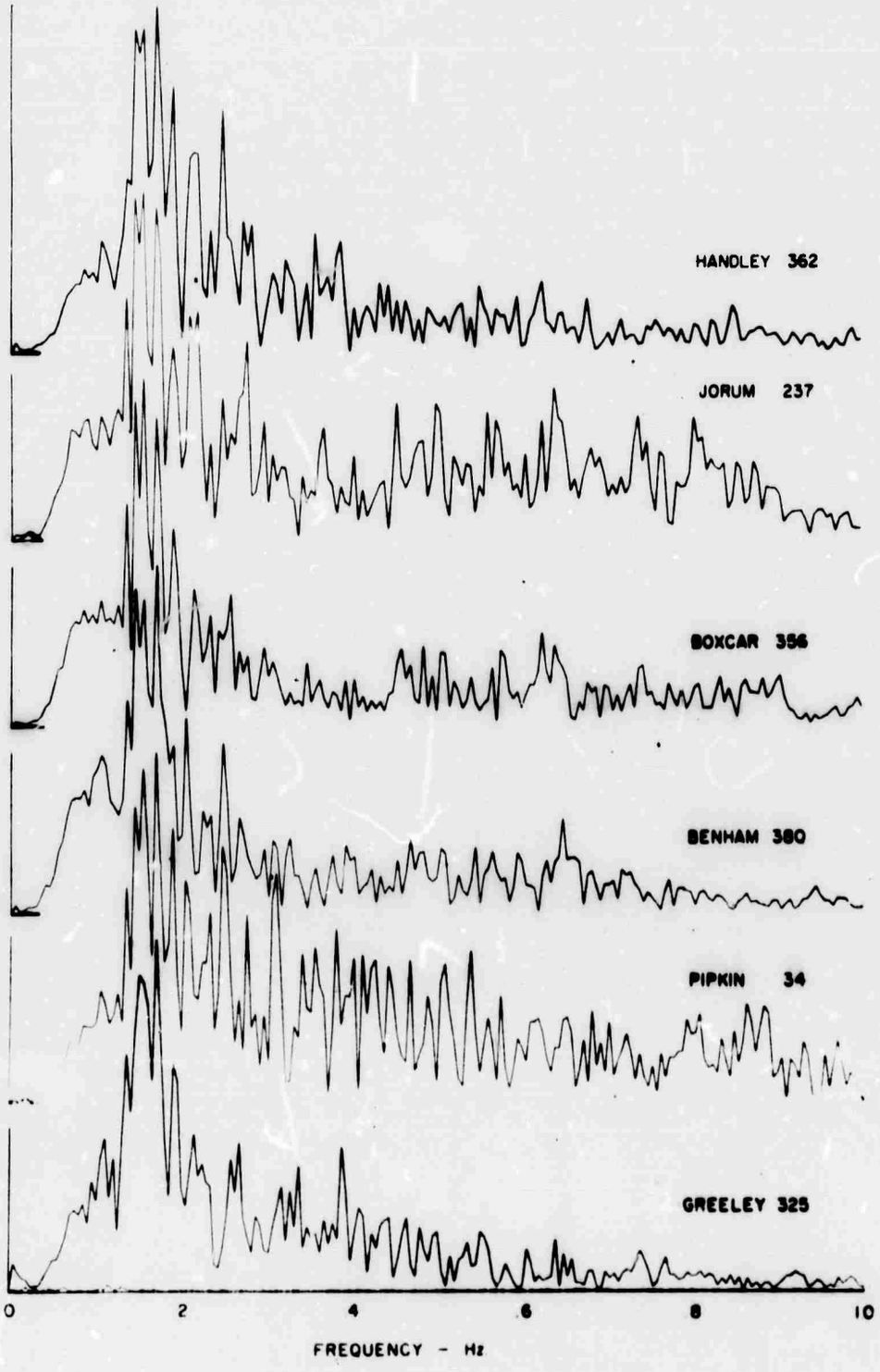

Figure 5a. Vertical spectra for Pahute Mesa events. Numbers give peak spectral values.

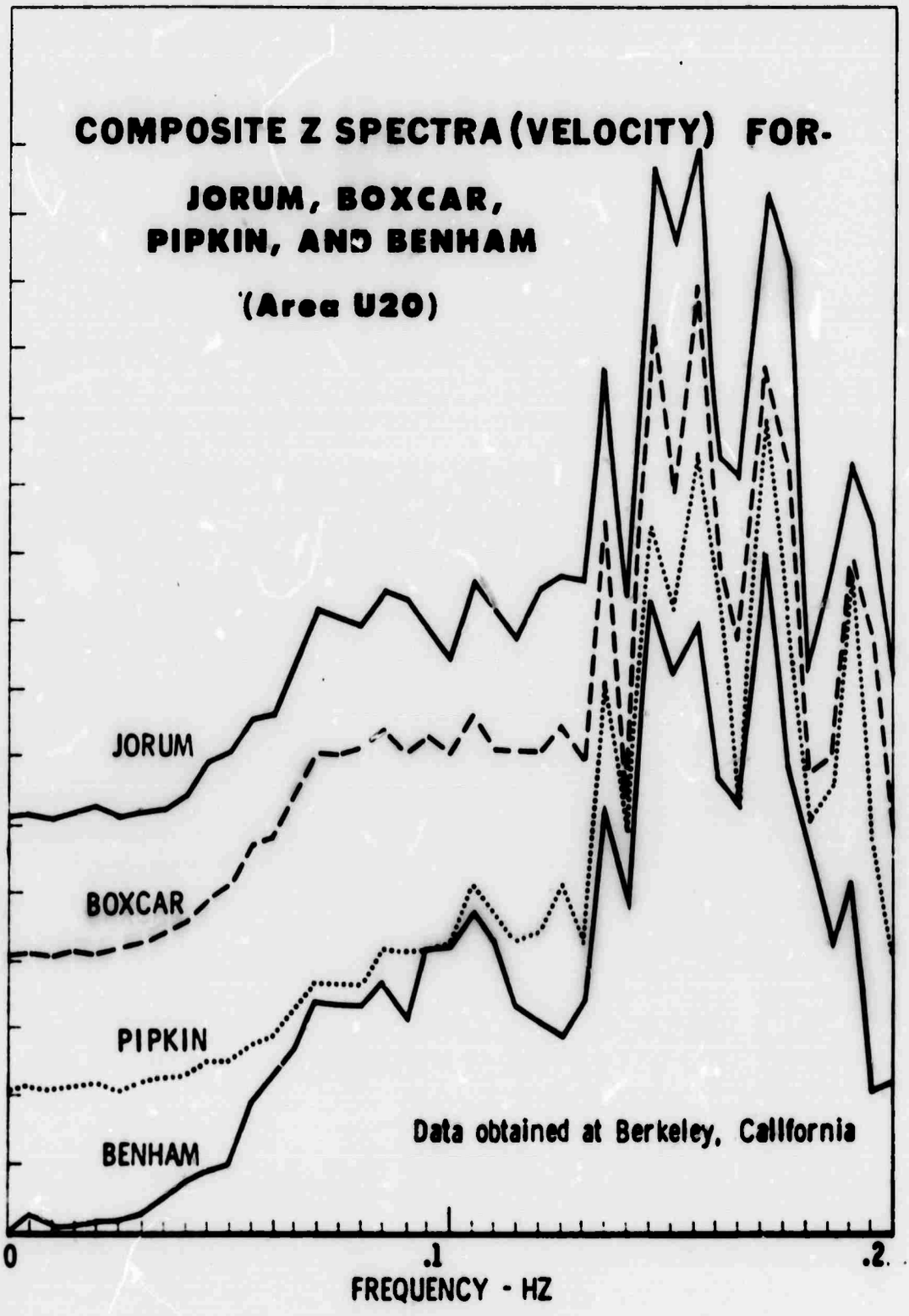

Figure 5b. 0-0.2 Hz Pahute Mesa events spectra.

EVENT	PHASE DIFF. FROM BENHAM .04-.06 Hz	LOVE / RAYLEIGH .04-.06 Hz	SOURCE TYPE
BENHAM	0	0.8	EXPLOSION
2224	0.9π	0.2	COLLAPSE
0014	0.2π	1.1	DIP SLIP
1810	0.2π	1.3	DIP SLIP
0634	0	2.5	STRIKE SLIP ?
0941	0	4.1	STRIKE SLIP
1701	0	3.4	STRIKE SLIP
1715	0	2.1	STRIKE SLIP

Figure 6. Summary of discriminants for Benham afterevent sequence events.

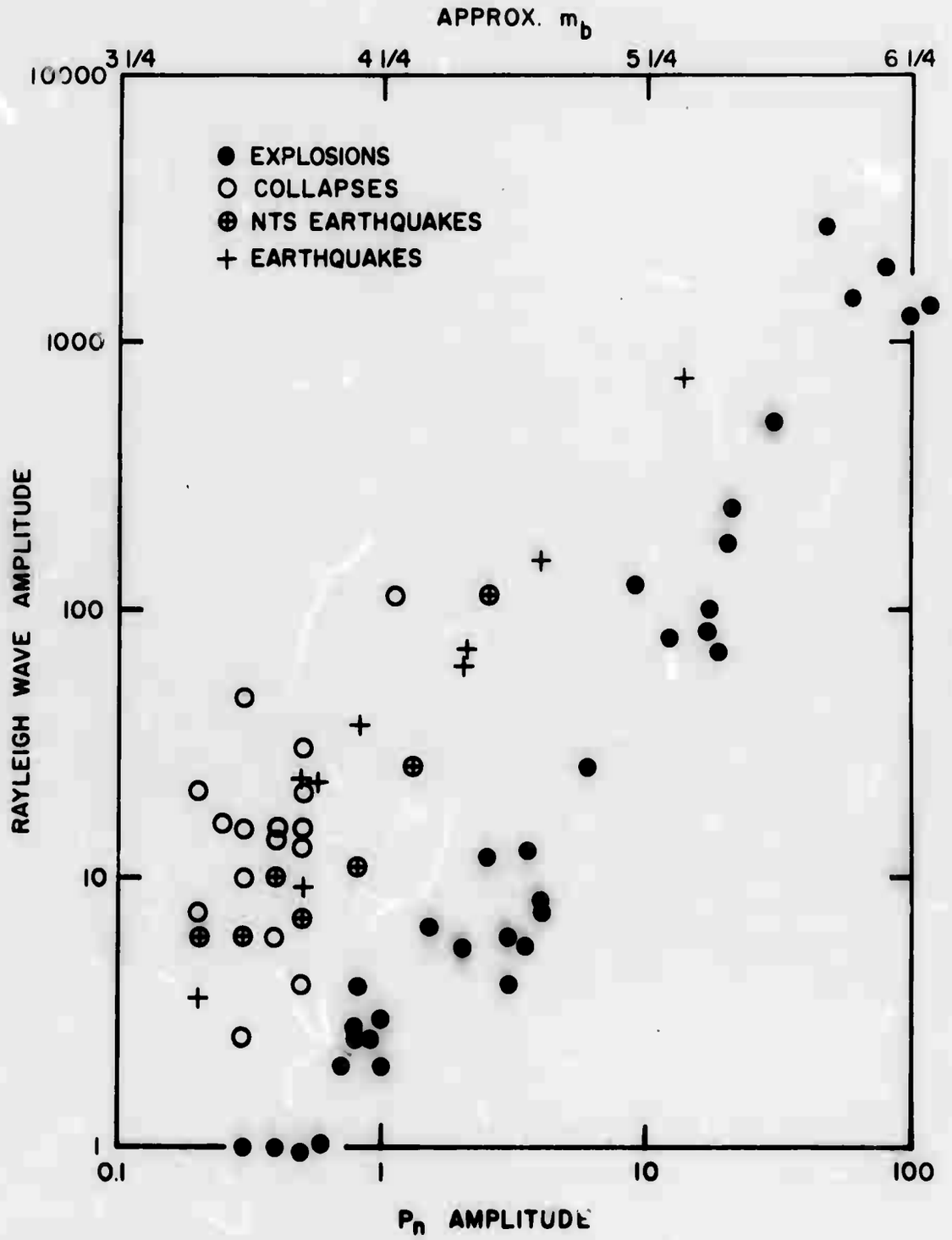

Figure 7. Rayleigh - P_n (M_s-m_b) relative for events 500-600 km from BRK.

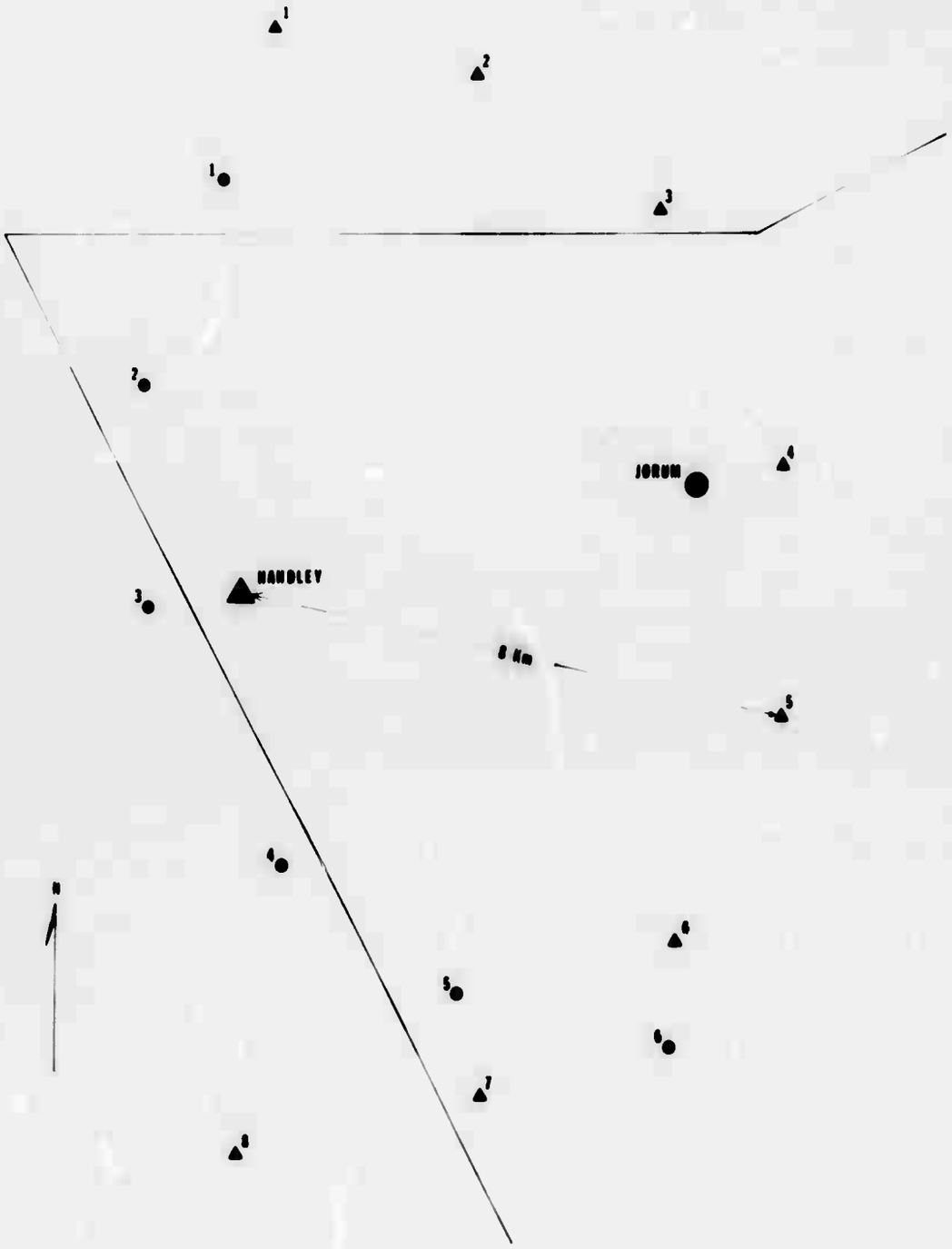

Figure 8. Accelerometer site designations for Jorum and Handley tests.

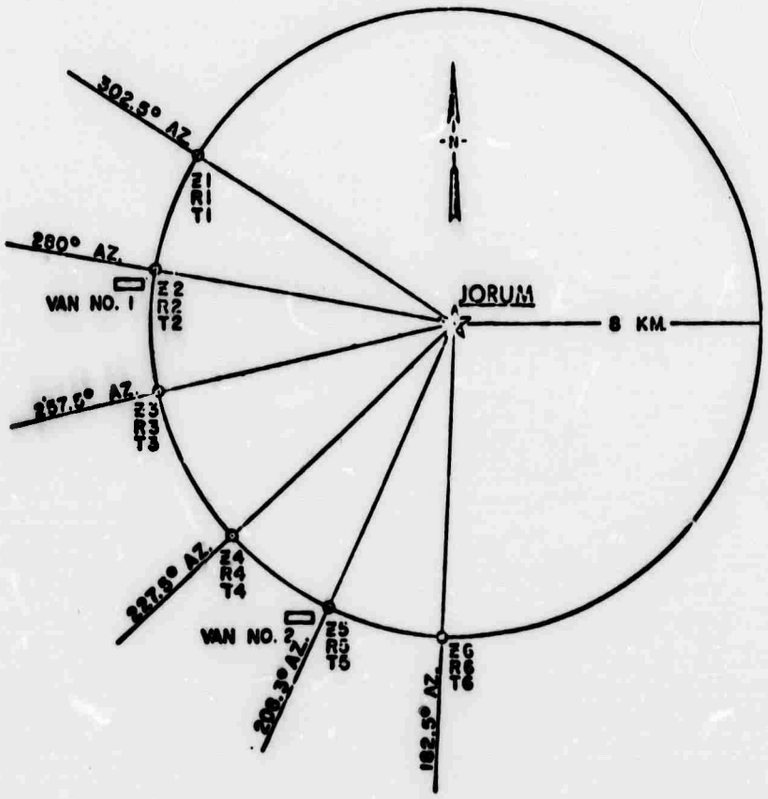

JORUM COORDINATES: 933,400.50 N 559,900.23 E

SITE COORDINATES:

SITE NO. 1.	947,344 N	537,813 E
SITE NO. 2.	937,813 N	534,167 E
SITE NO. 3.	927,604 N	534,479 E
SITE NO. 4.	915,625 N	540,729 E
SITE NO. 5	909,760 N	547,200 E
SITE NO. 6	907,031 N	558,802 E

Figure 9. Field plan for Jorum.

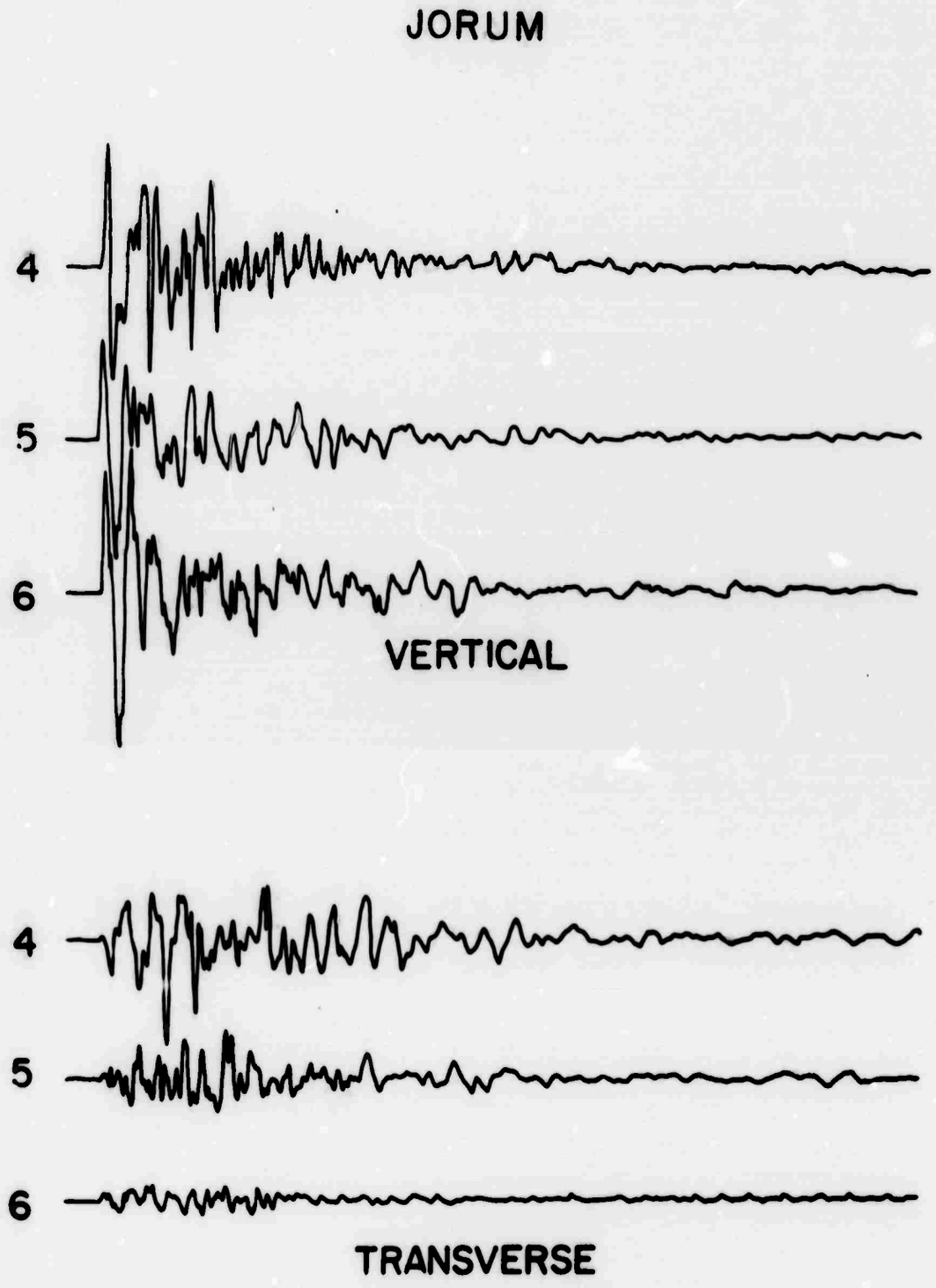

Figure 10. Jorum accelerations at 8 km.

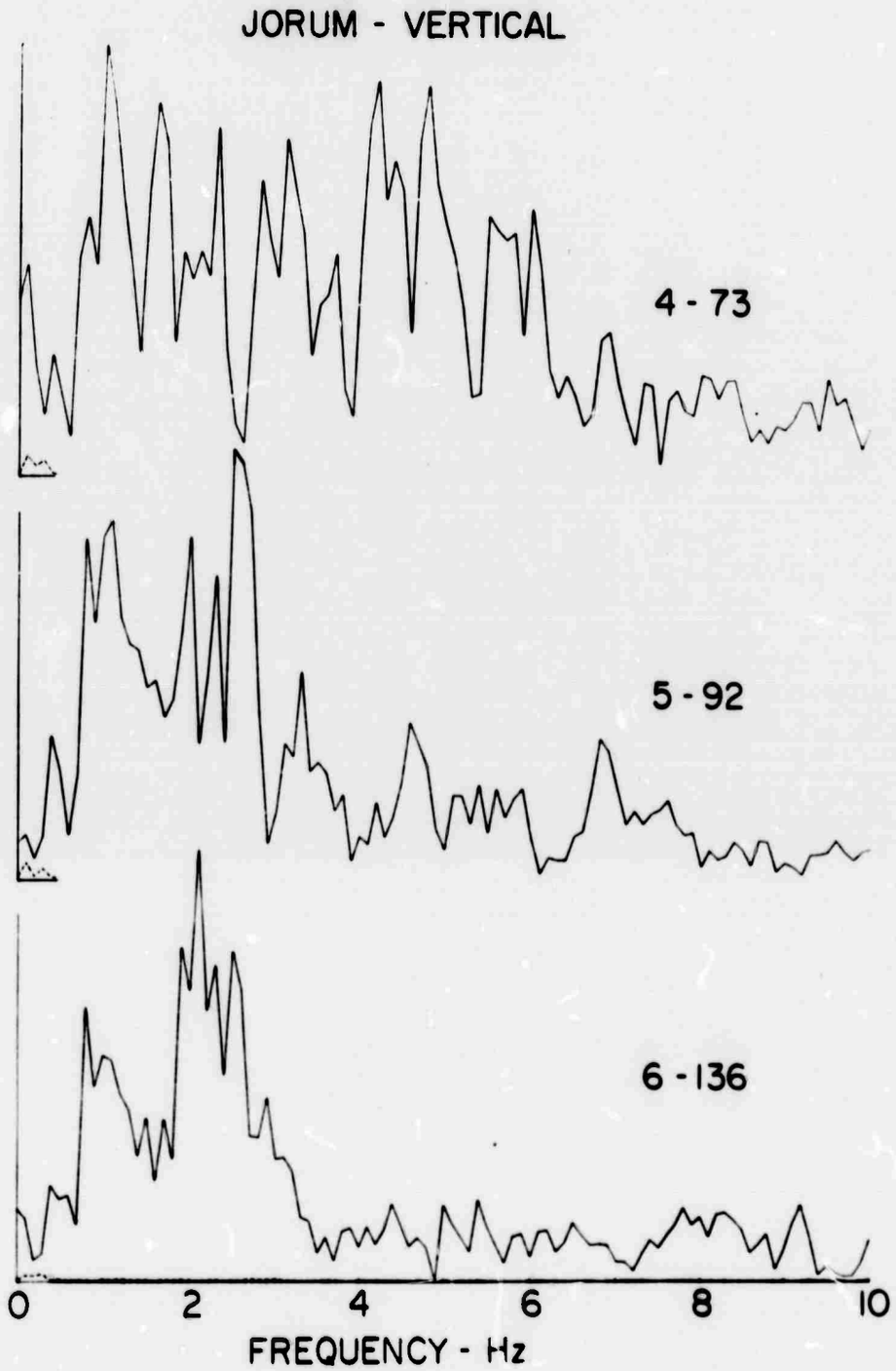

Figure 11. Jorum acceleration spectra at 8 km. Numbers give site-peak spectral amplitude.

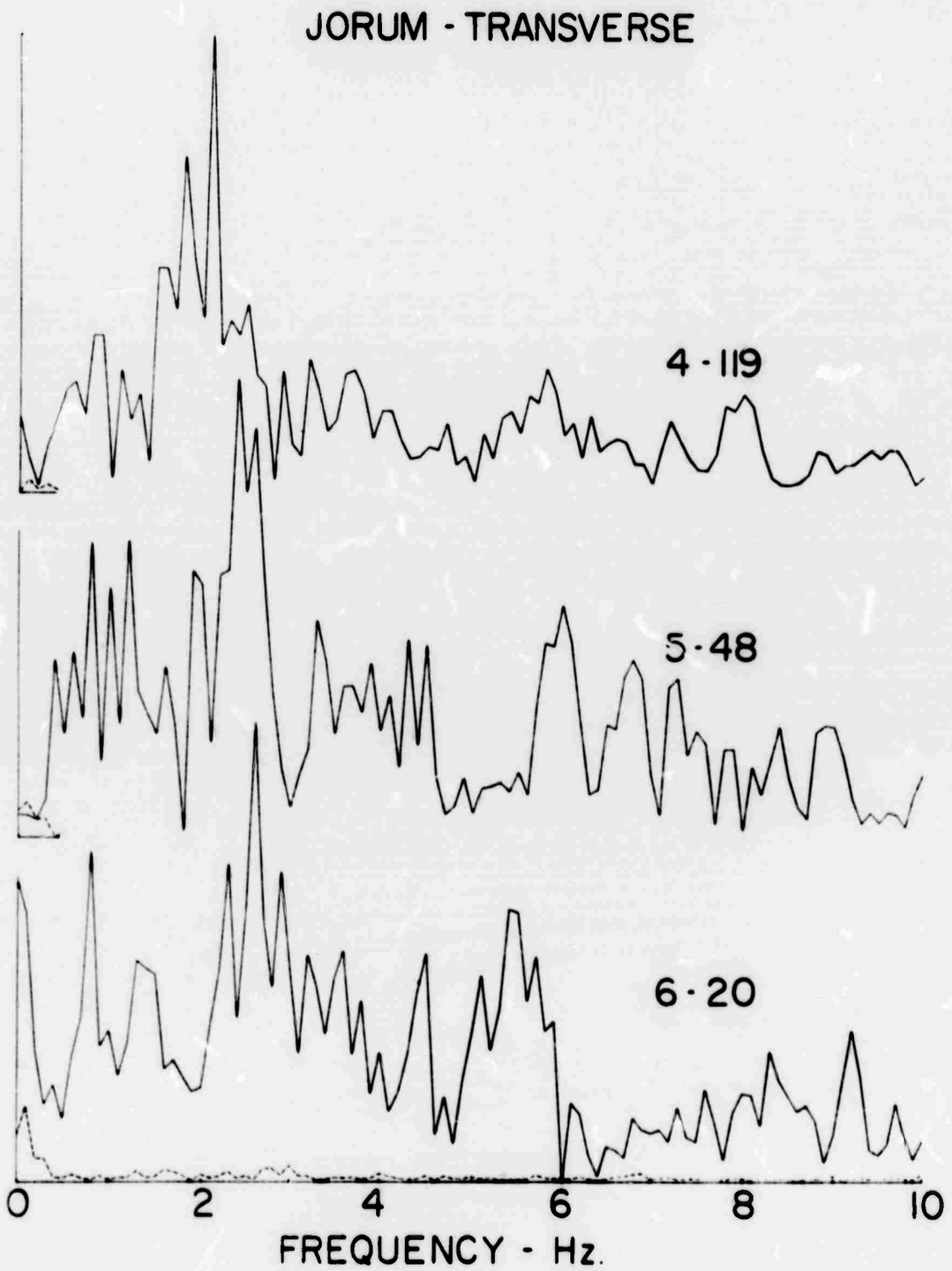

Figure 12. Jorum acceleration spectra at 8 km. Numbers give site - peak spectral amplitude.

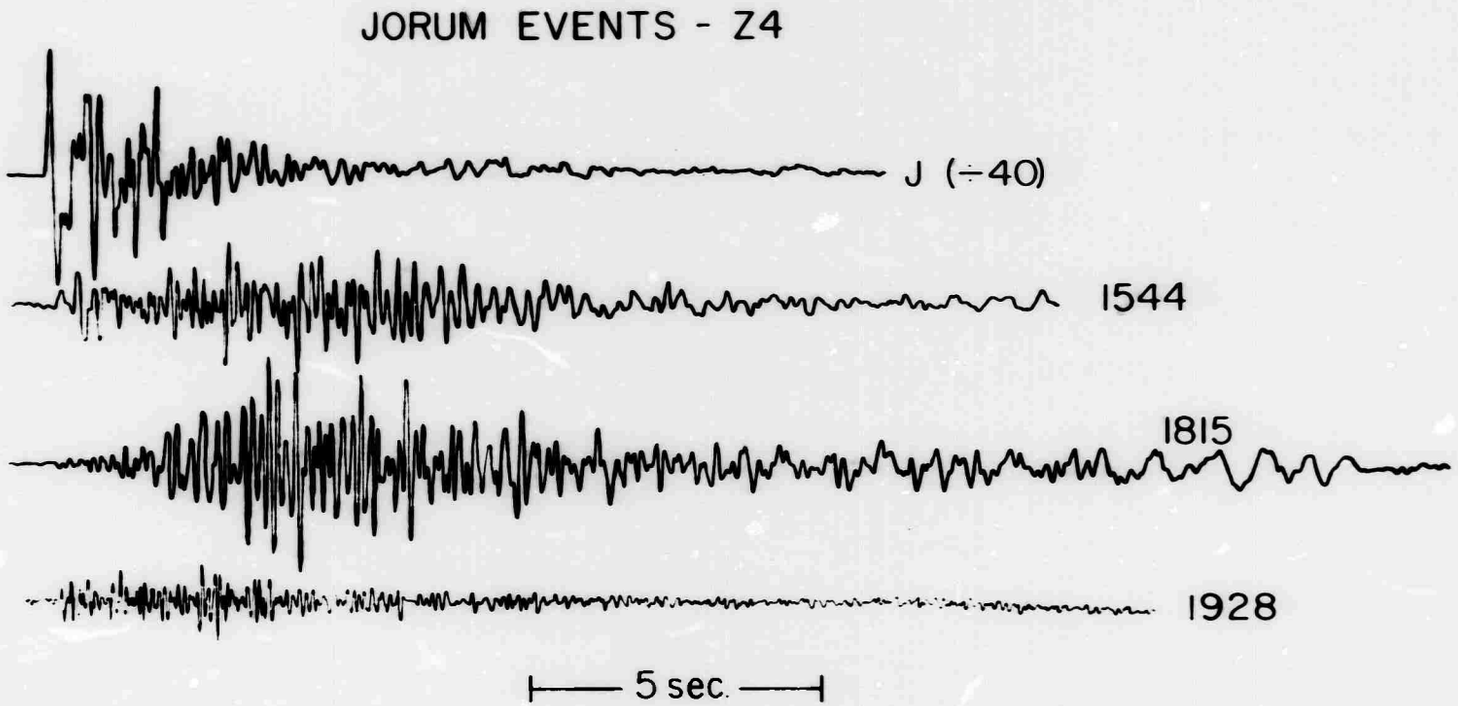

Figure 13. Sample Jorum afterevents. Numbers are origin times for afterevents.

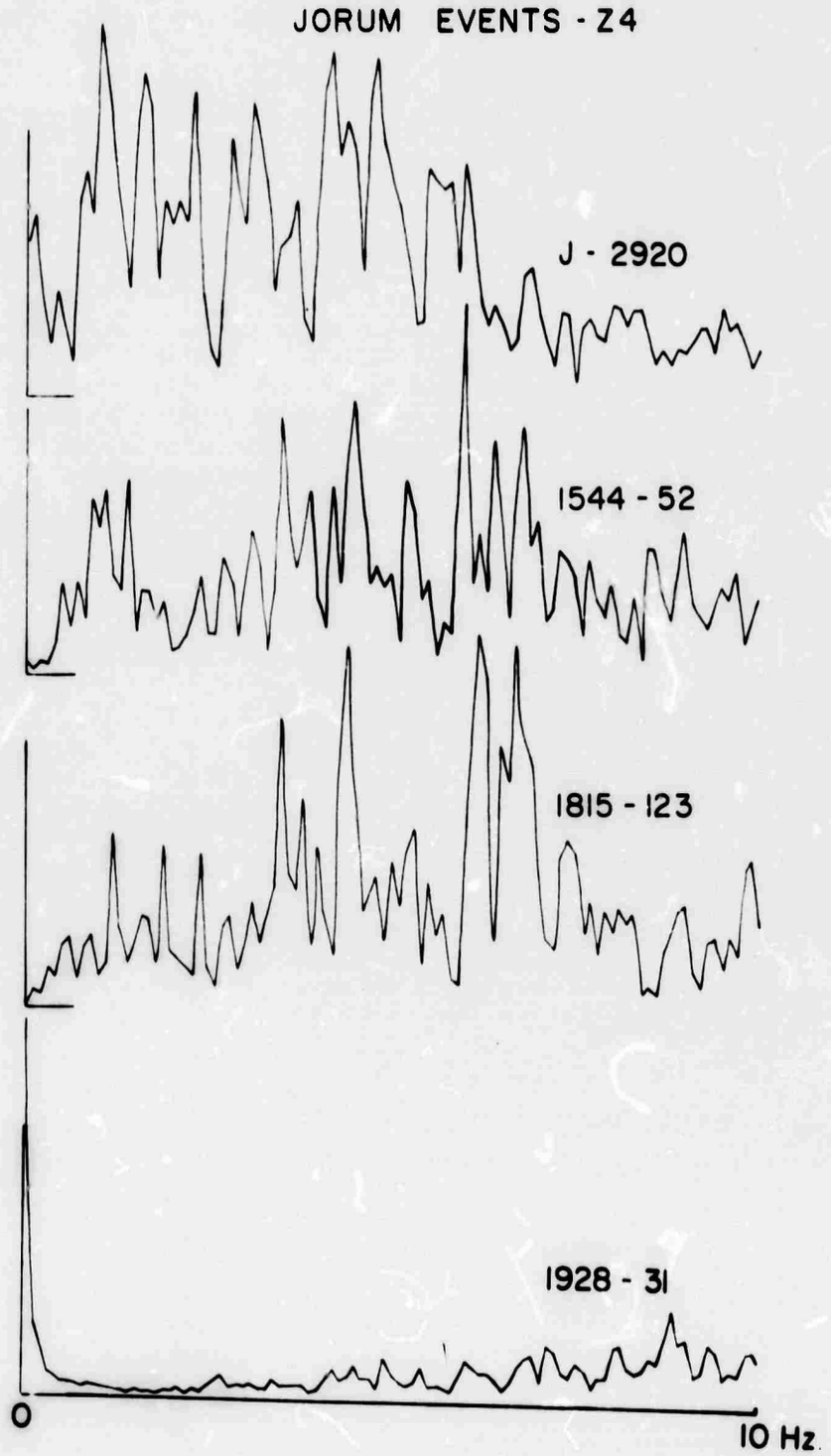

Figure 14. Jorum afterevents spectra. Numbers give origin time - peak spectral amplitudes.

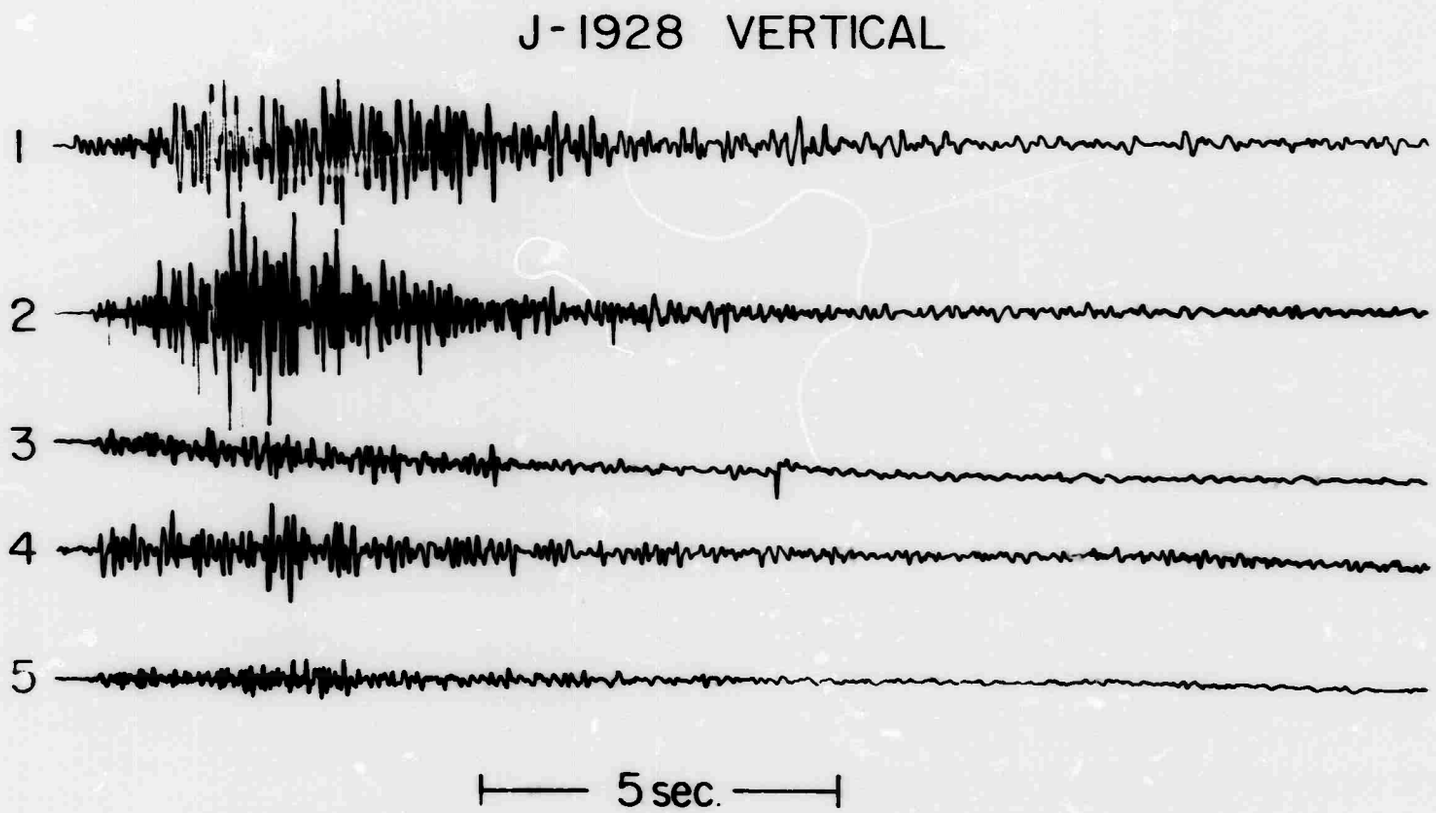

Figure 15. Azimuthal variation, event Jorum 1928.

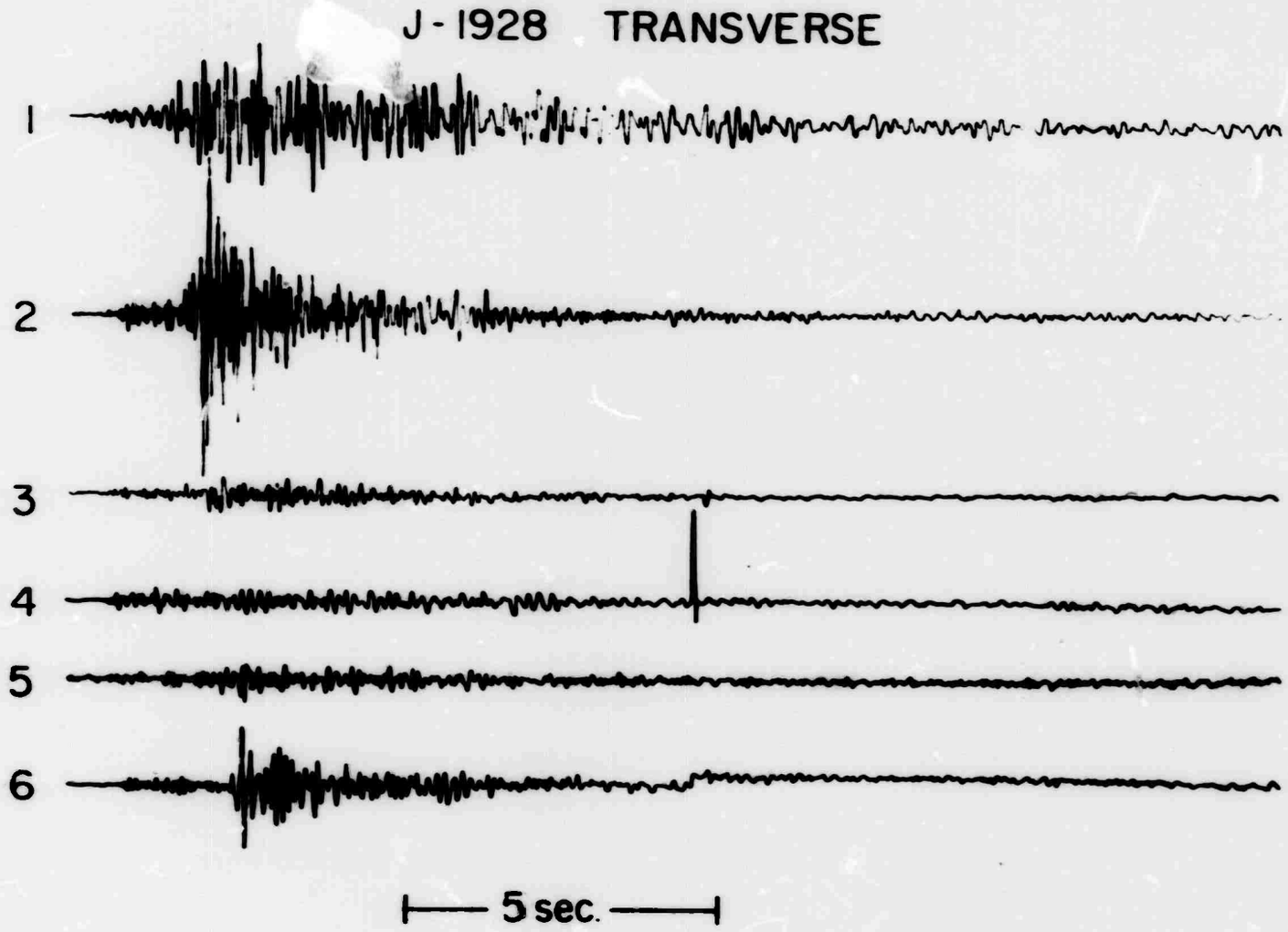

Figure 16. Azimuthal variation, event Jorum 1928.

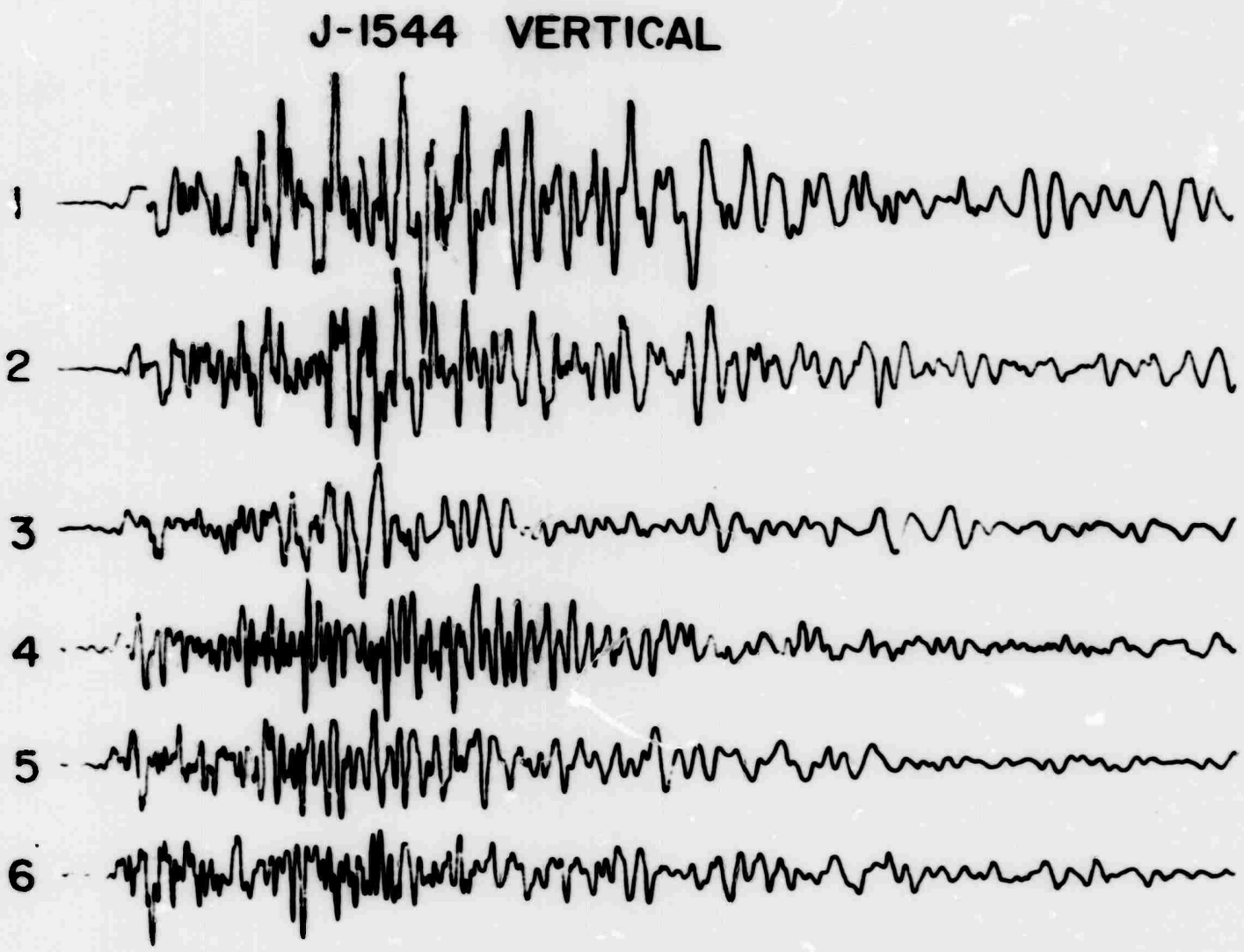

Figure 17. Azimuthal variation, event J1544.

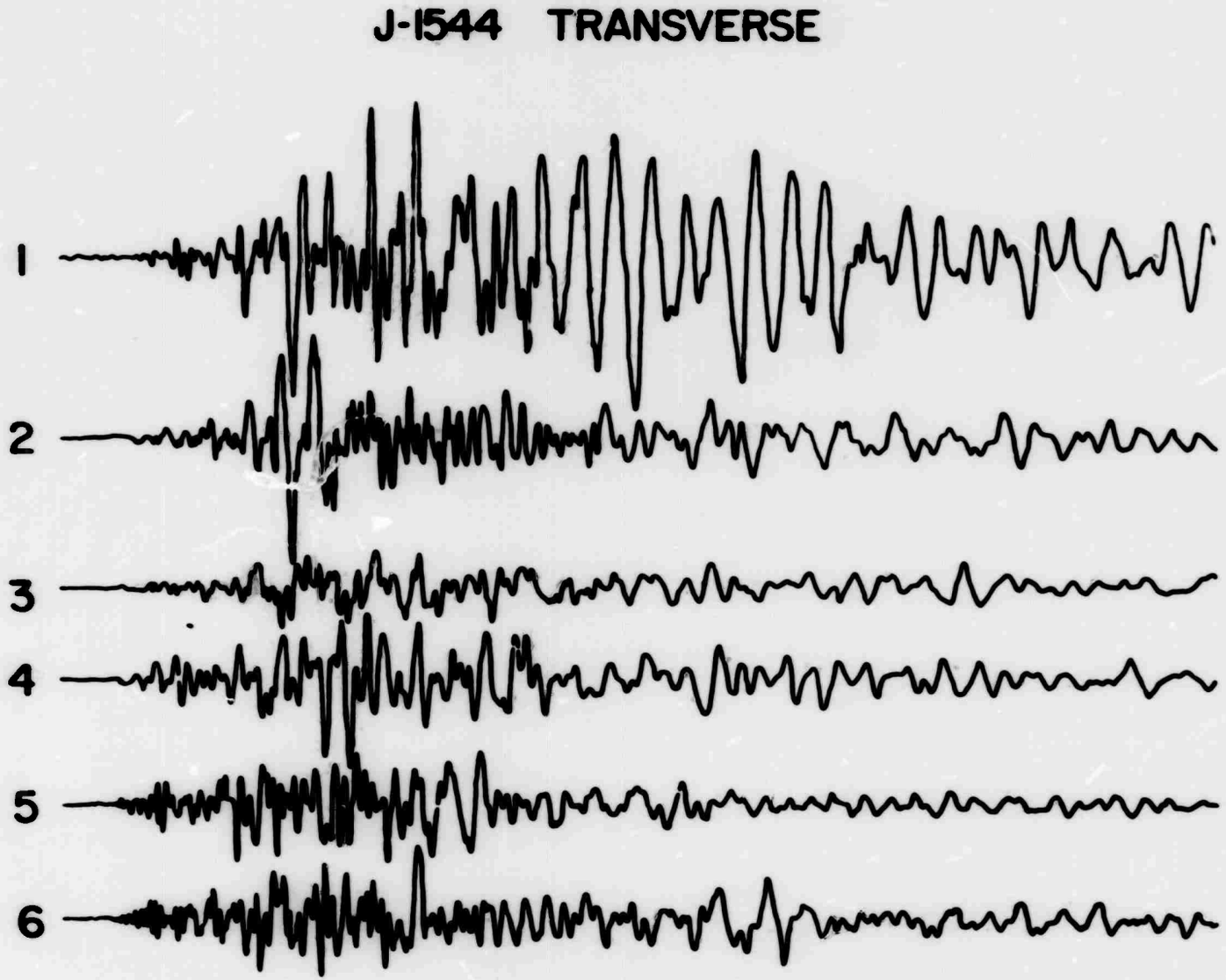

Figure 18. Azimuthal variation, event J1544.

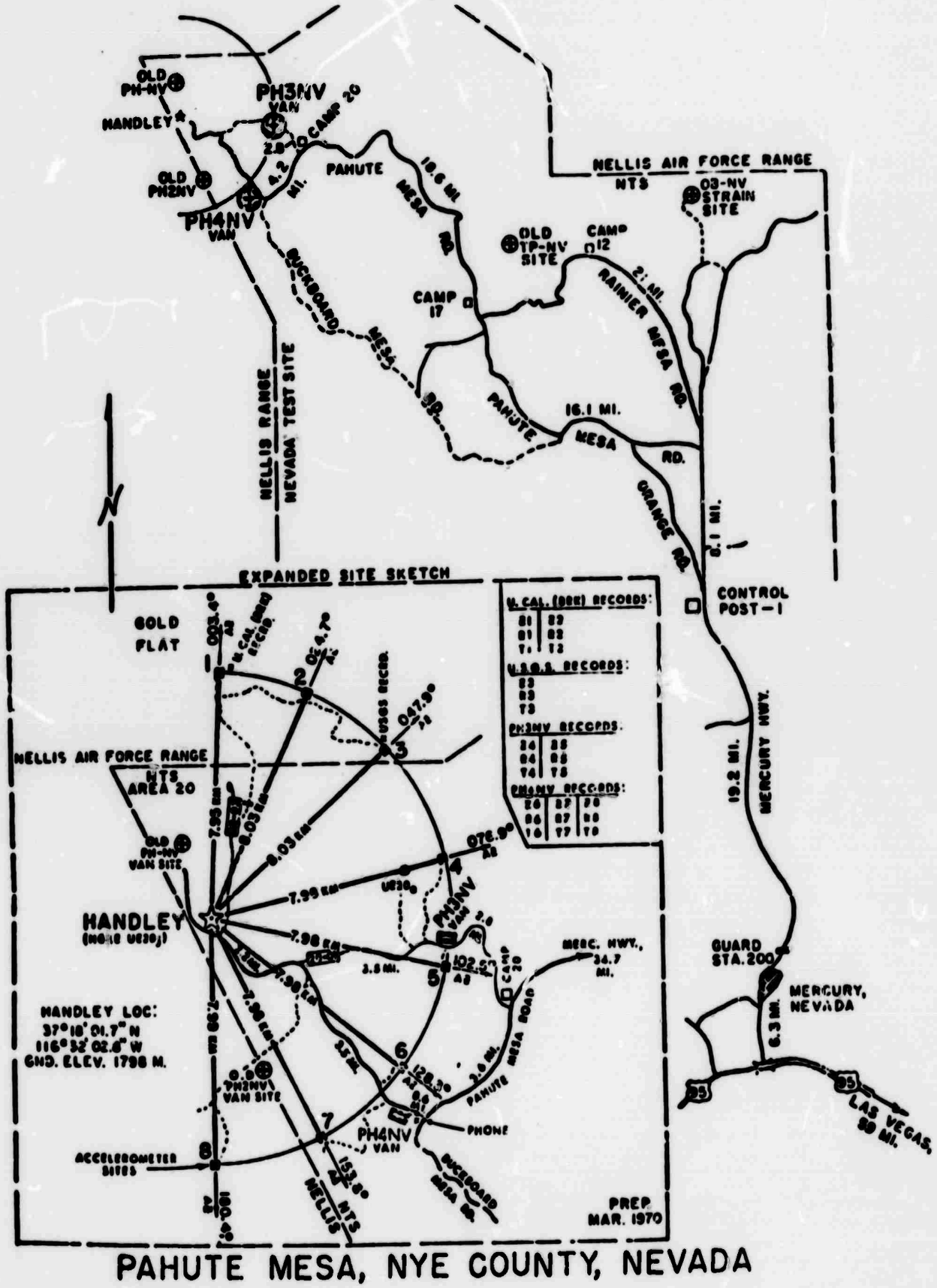

Figure 19. Field plan for Handley.

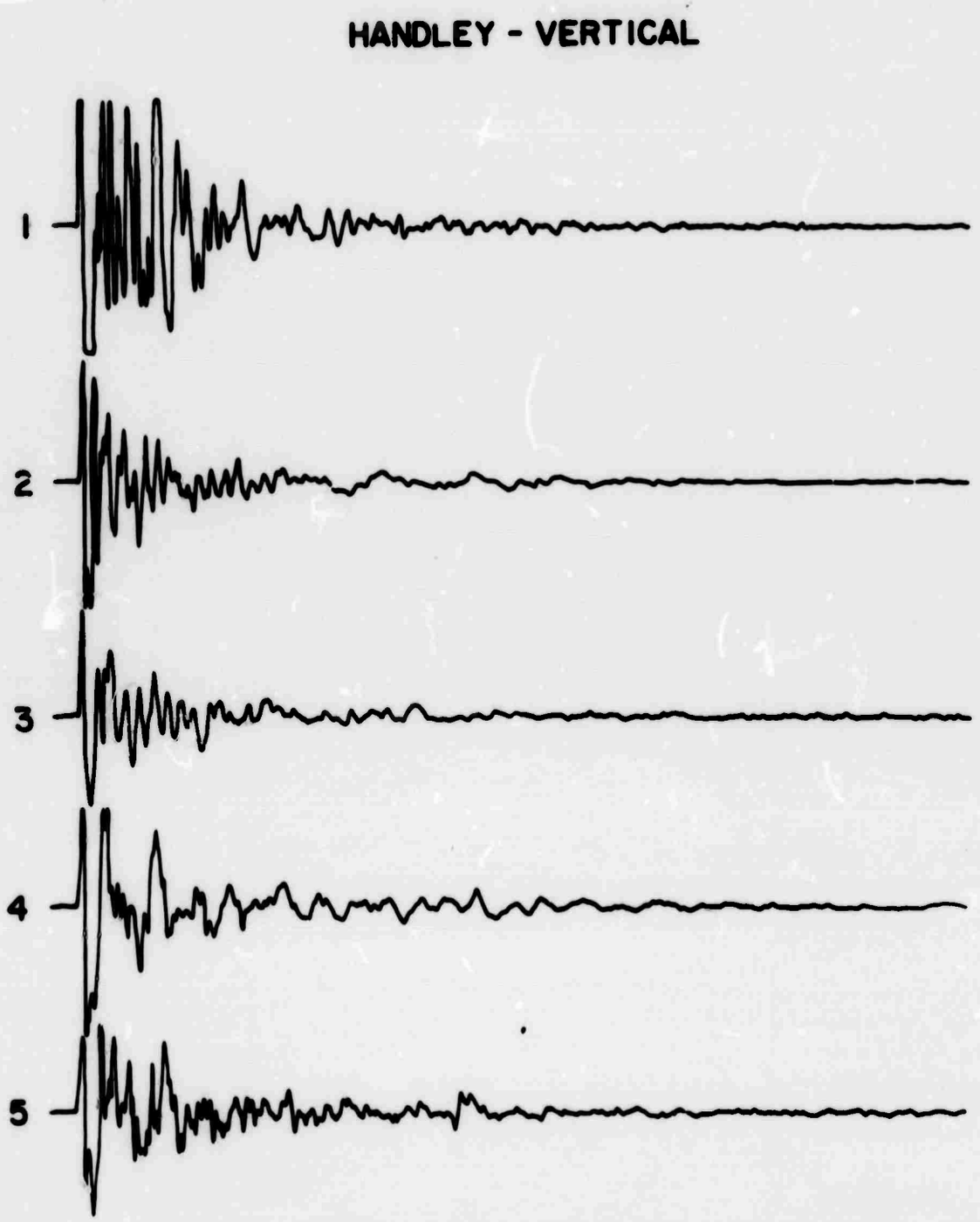

Figure 20. Handley vertical acceleration with azimuth.

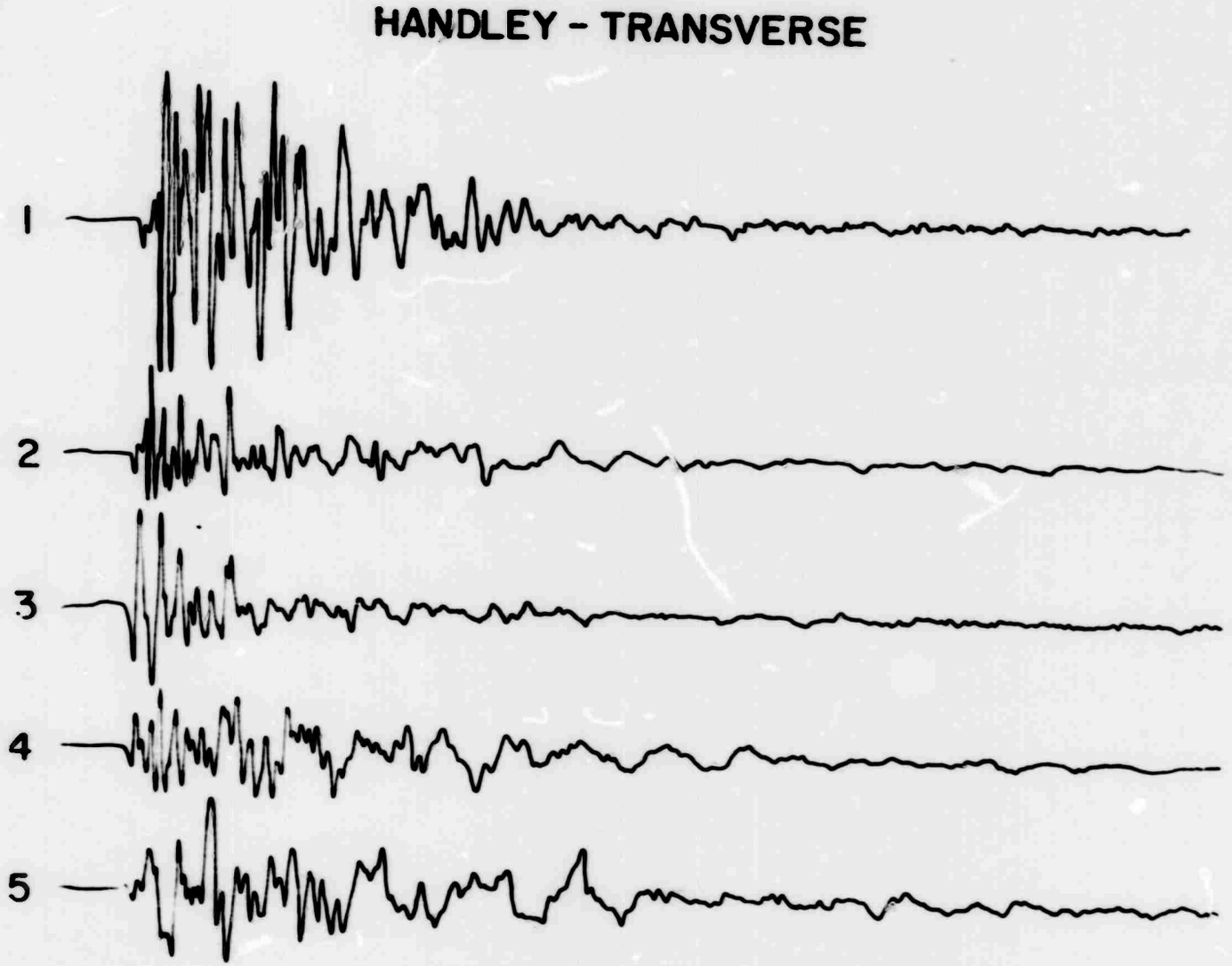

Figure 21. Handley transverse accelerations with azimuth.

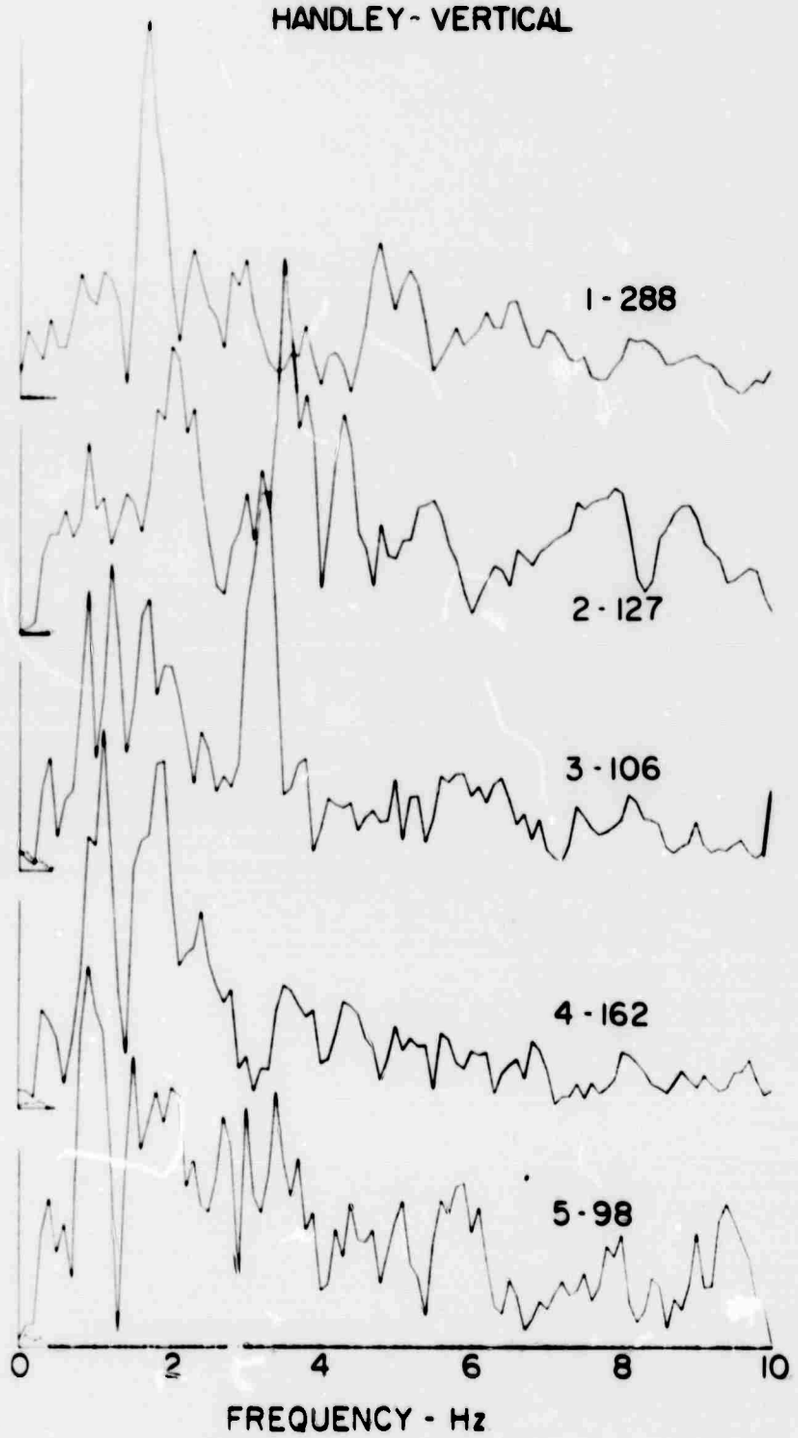

Figure 22. Handley vertical spectra, 8 km distance.

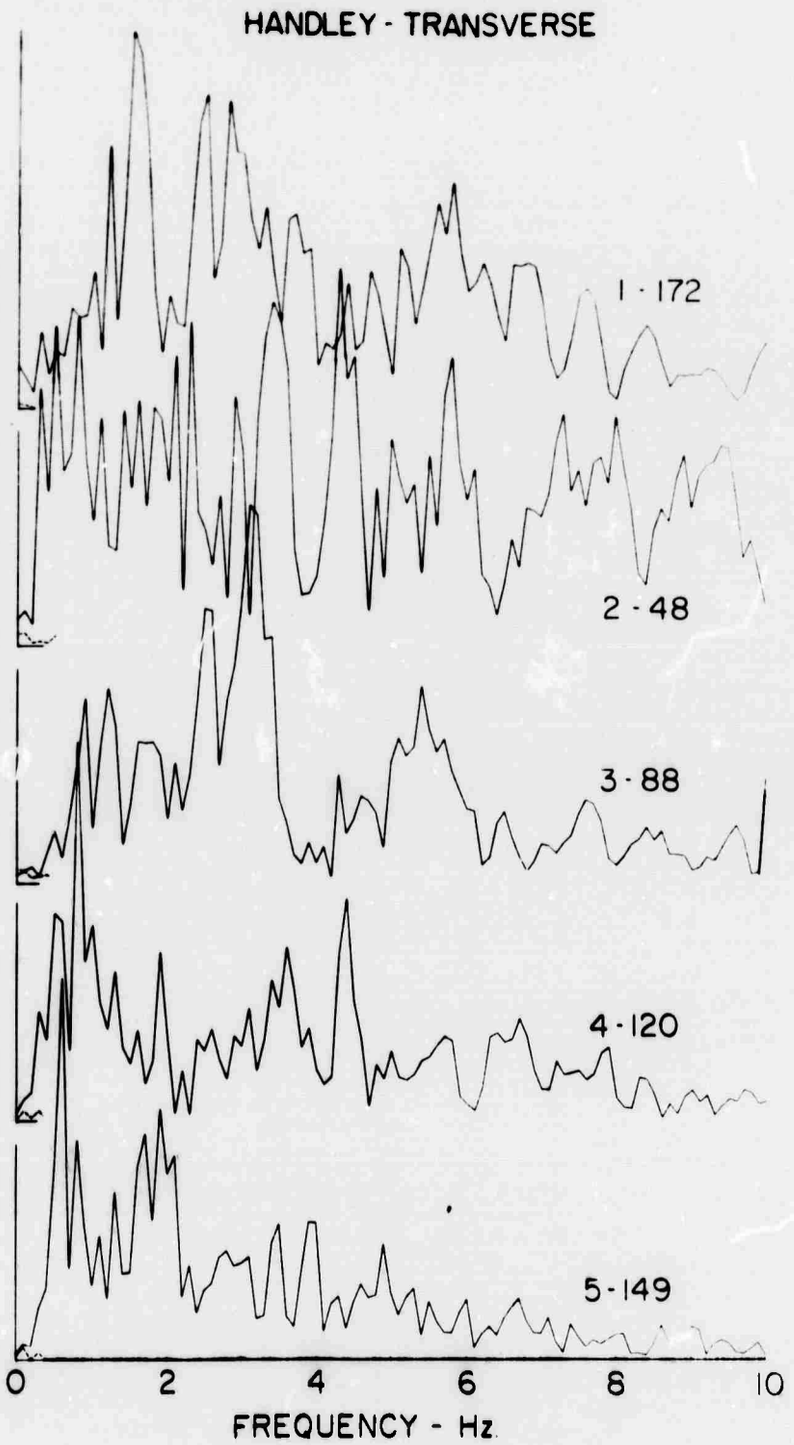

Figure 23. Handley horizontal spectra, 8 km distance.

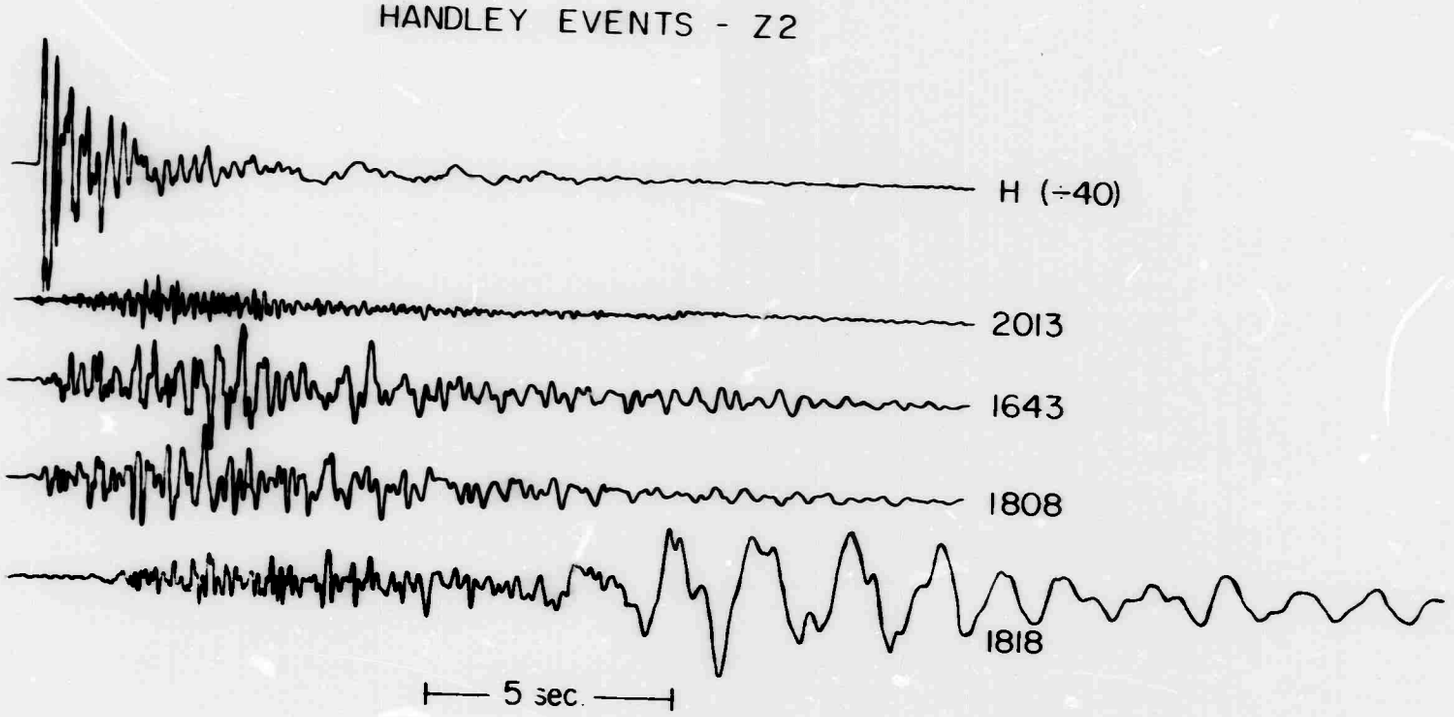

Figure 24. Sample Handley afterevents. Numbers are orgin time for afterevents.

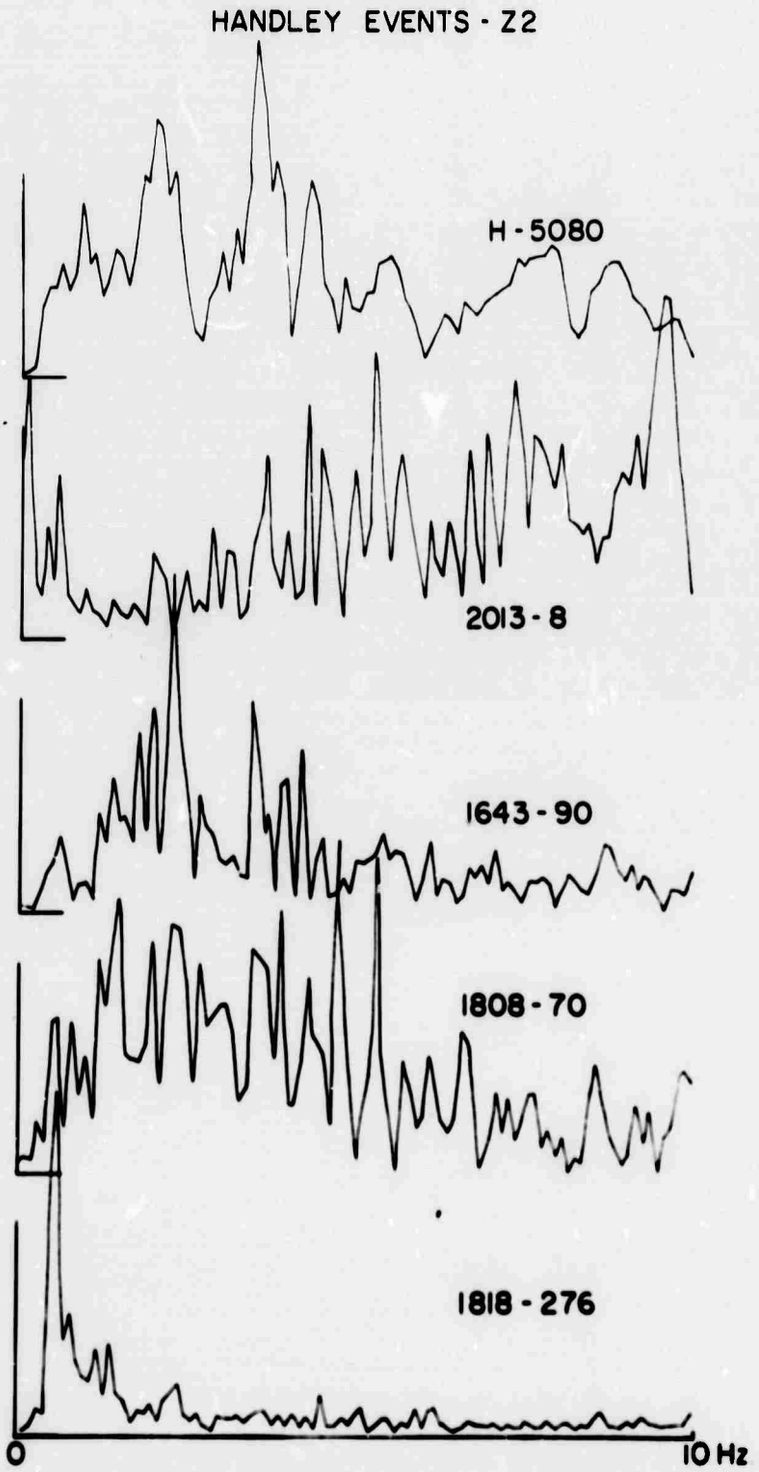

Figure 25. Handley afterevents spectra. Numbers give origin time - peak spectral amplitude.

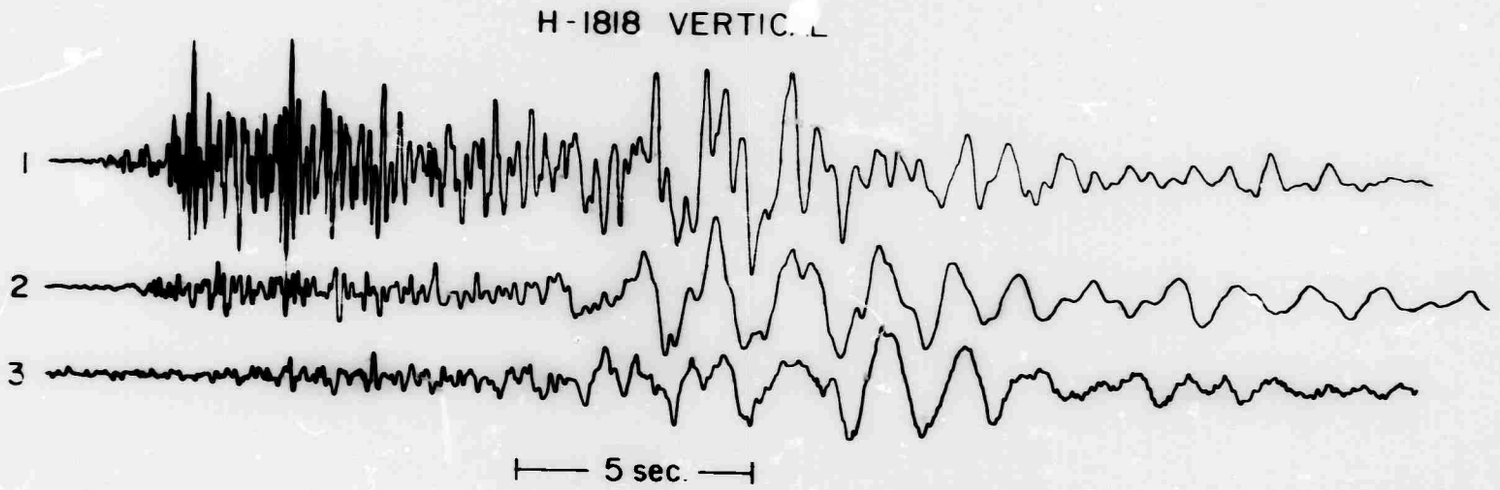

Figure 26. Azimuthal variation, event H1818, vertical.

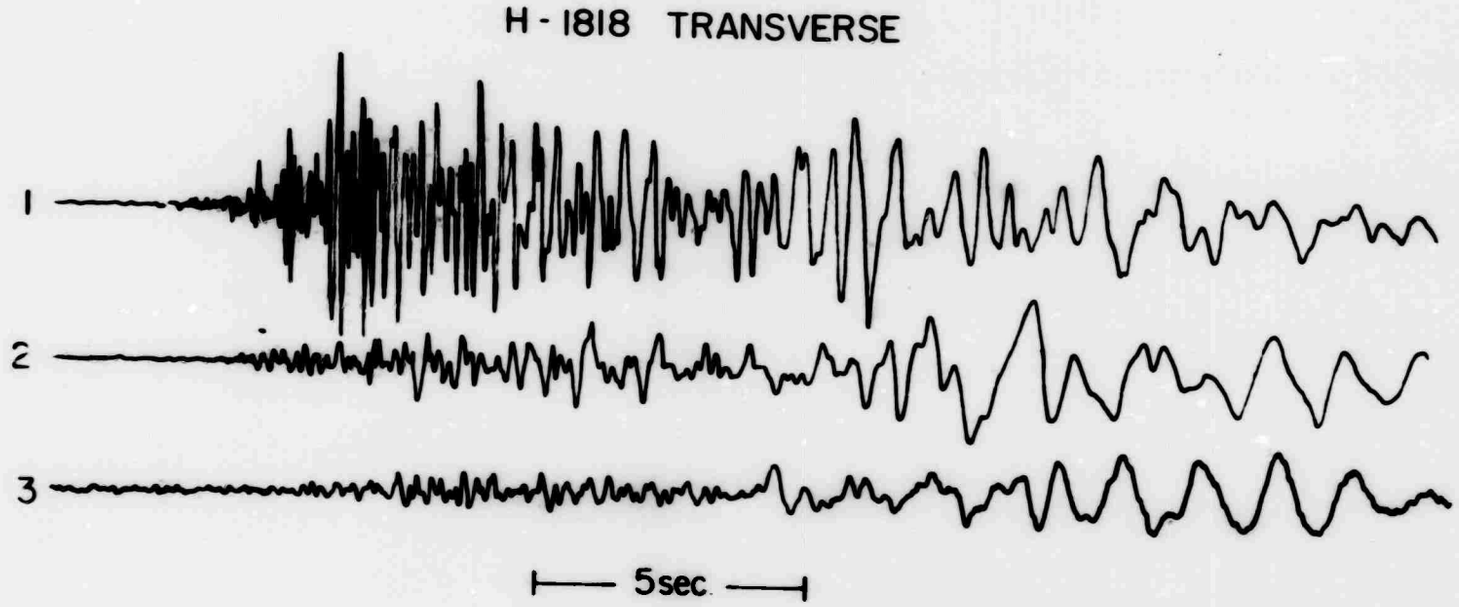

Figure 27. Azimuthal variation, event H1818 transverse.

TECTONIC STRAIN RELEASE AND THE MONITORING OF UNDERGROUND NUCLEAR EXPLOSIONS

By

Carl Kisslinger

It is known that when an explosion is fired in a solid medium under stress, the resulting seismic signal is altered from that produced by a similar explosion in an unstressed medium. With reference to the specific problem of monitoring underground explosions, the important question is whether this alteration of the signal can make the detection, location, or identification of the event more difficult. The principal concern is whether the concurrent release of tectonic strain energy at the time of the explosion can sufficiently alter the seismic signal to make application of identification criteria less certain. A closely related question is whether it might be possible to intentionally place an explosion in a tectonic environment in which a large release of tectonic strain by faulting would occur, i.e. a large earthquake would be triggered intentionally, as an evasion technique.

An ambient stress field will affect the seismic signal through several mechanisms. Of these, the least important for the present problem is the introduction of a small amount of velocity anisotropy because of the stress dependence of the elastic moduli. More important is the control exerted by the ambient stress on the generation of tensile fractures. In a homogeneous, isotropic unstressed material, the tensile fractures that mark the outer limits of non-elastic behavior will be distributed more or less uniformly around the shot cavity, with essentially the same length, so that the basic spherical symmetry of the source is not markedly disturbed. If, however, an appreciable prestress is present, tensile cracks in a few directions will grow to considerable length. Prestress is not the only condition that can result in preferential fracturing. Planes of weakness resulting from depositional processes will have a similar effect, especially in surficial materials.

A propagating tensile fracture is a source of seismic waves and these will be superimposed on the primary signal from the explosion. This is one mechanism by which S waves are generated directly by the explosion. The energy for these waves is derived from the expanding explosion products and the role of the ambient stress is primarily that of determining the direction of crack propagation.

Finally, prestress will result in the production of a seismic signal due to release of stored elastic strain energy in response to the shot. One way in which this will occur is as a result of the sudden creation of an enlarged cavity in the medium. Another, potentially more dramatic, is the occurrence of slip on fault surfaces in response to the explosion loading.

It is this last effect, the triggering of a tectonic earthquake by the explosion, that is most likely to cause difficulty in applying discrimination criteria. However, a concurrent earthquake can cause difficulty only if it generates seismic waves comparable in energy to those produced by the explosion itself. An earthquake with magnitude equal to or exceeding the seismic magnitude of the explosion has not

yet been triggered, but because earthquakes generate wave types and put energy in frequency bands that are not strongly excited by explosions, there is evidence from the seismic signals of earthquake generation.

Our interest has been directed to the question of the circumstances under which triggering will occur and the environmental factors that determine the extent of the faulting. The question of the mechanism of stimulation of after-shocks of explosions will be omitted here as not pertaining very much to the main question of the alteration of the explosion-generated signal. However, temporal and spatial distribution of aftershocks does convey important information about the state of stress in the vicinity of the shot that is important to understanding the prompt release of tectonic energy.

Of the numerous questions raised by the available field observations of explosion-induced faulting, one of the most interesting is whether the extent of faulting scales with the yield of the explosion. The alternative is that the action is one of triggering such that once the yield exceeds some threshold, rupture begins and its extent is determined by the ambient stress and strength of the material and is independent of the yield. McKeown and Dickey (1969) have published data for Pahute Mesa that shows a straightforward relation of fault length to yield. This dependence, when combined with the absence of aftershocks on these faults, indicates that the prestress is well below that at which slip would occur naturally and the slippage is driven by the stress pulse from the explosion. However, the occurrence of appreciable slip and of some aftershocks, especially after Benham, is evidence that a sizable tectonic stress field is present in the rocks of Pahute Mesa.

The fact that Boxcar, Benham, and Jorum all produced visible surface faulting of about the same extent, but only Benham produced large numbers of aftershocks has not been explained. A possible explanation is inherent in a model of the local structure that was suggested by Cummings (1968), Figure 1. He modelled the Timber Mountain caldera as a hole in a homogeneous elastic plate under uniform tension. He used this model to account for the orientation of the numerous faults that intersect the caldera boundary, including those in the neighborhood of the events under discussion. Though the model is undoubtedly too simple, it does account for the orientation of the faults fairly well and is a credible representation of the situation.

In this model, the large events on Pahute Mesa are located roughly along the line at right angles to the direction of regional tension. Benham is at about 1.3 caldera radii from the center, and the other shots, Boxcar, Jorum, Handley, and Greeley are at about 2 radii from the center. Because the effects of the hole in a prestressed plate are quite localized, this model calls for a maximum tensile stress and a maximum shear stress at Benham about 0.5 times that at the more northern sites, Figure 2. The gradients in stress

are greater at Benham than at the other places also. For each kilobar of regional tensile load, the maximum tensile stress is 1.82 kb at Benham (almost twice the applied load) and 1.22 kb at the northern site. The corresponding values of maximum shear stress are 0.73 kb and 0.47 kb, respectively. The stress gradients at Benham are, for the tensile stress 0.15 bar/meter per kilobar of regional stress, and for the maximum shear stress, 0.07 bar/meter. At the northern sites the corresponding gradients are about one-fifth the value of Benham. Of course, local inhomogeneities may cause localized stress gradients over short distances that are much greater than these.

A further point in support of the applicability of this model is the fact that the numerous Benham aftershocks are concentrated along a trajectory whose direction is predicted by Cumming, for which there was no surface fault, but which connected known segments of faults.

In the absence of more information about the in situ stress and the strength of the faults it is not possible to judge if a stress increase of fifty percent is enough to account for the difference in response at Benham and the other shots.

Further evidence of a difference in Benham and Boxcar related to tectonic strain release is found in the relative excitation of SV and SH waves by the two explosions. The horizontal component of SV as observed at 11 stations in the Western Hemisphere is close to the same for the two events. SH amplitudes, on the other hand, are uniformly three to four times larger for the Benham event than for Boxcar, with about the same period.

We are currently engaged in a model study in which a hole in a Plexiglas sheet simulates the caldera and small shots will be fired at points scaled to the positions of Benham and Jorum. A range of applied loads will be tested. The objective is to determine the pattern of fracturing that occurs and the effects on the seismic signal of the resulting strain release.

Milrow raised some interesting questions, in that it produced so few afterevents in a setting that is known to be highly seismic. The absence of aftershocks later than cavity collapse (Engdahl and Tarr, 1970) and evidence of the long-term tectonic stability of Amchitka Island (Morris, 1970; Anderson, 1970) indicate that the rocks of that island are under less stress than those of the Basin and Range Province. One inference is that the island is mechanically decoupled from the active seismic region in which it is embedded. Anderson interprets "the deformation of the surficial rocks of the central Aleutian Ridge as related to volcanism and plutonism, and as such the deformation does not reflect in a first order sense the regional compressional stress across the arc."

The strain energy released in the aftershock almost certainly came from the static strain field produced by the explosion and subsequently relieved by the collapse.

Thus, the prompt release of tectonic strain by an explosion is governed by a number of factors that can be evaluated in the field but have not been adequately treated yet. These include the magnitude and orientation of the regional stresses and the stress concentrations in the neighborhood of the shot caused by the local geology. The occurrence of an unstable rupture that would give rise to a large earthquake seems to require that the explosion take place near a fault that is stressed almost to the point of failure. In this event the identification of the signal as coming from an explosion might be very difficult.

It has been recognized that surface wave magnitudes from NTS events are systematically larger, relative to m_b, than those for explosions in Central Asia, Novaya Zemlya and the Sahara. For example, for a large Novaya Zemlya event, $m_b = 6.5$, the ratio m_b: M_s is 1.38. The average for two Central Asia events, $m_b = 6.0$ and 5.5, the ratio is 1.52. For one Sahara event, $m_b = 5.7$, the ratio is 1.32. For events Greeley and Boxcar the ratios are both 1.18. O. Nuttli has determined shear wave magnitudes and found for these events that the shear body wave magnitude is close to M_s for all sites, the ratios m_{shear}:M_s ranging from 1.02 to 1.13. The relatively high values for both M_s and m_{shear} for NTS events have been interpreted as due to the contribution of tectonic strain release. The contribution to the shear wave magnitude from the SII component is very small for most of the events examined. A detailed study of the Benham shear wave magnitude is still to be done.

REFERENCES

Anderson, R.E., 1970, Tectonic setting of Amchitka Island, Alaska, USGS-474-75, U.S. Geological Survey: Denver, Colorado.

Cummings, D., 1968, Mechanical analysis of the effect of the Timber Mountain caldera on basin and range faults, Jour. Geophys. Res., v. 73(8): 2787-2797.

Engdahl, E.R., and Tarr, A.C., 1970, Aleutian seismicity - Milrow seismic effects, CGS-746-102, U.S. Coast and Geodetic Survey: Rockville, Maryland.

McKeown, F.A., and Dickey, D.D., 1968, Fault displacements and motion related to nuclear explosions, Bull. Seis. Soc. Amer., v. 59(6): p. 2253-2270.

Morris, Robert H., 1970, A preliminary study of relict marine terraces of the western Aleutian Islands, Alaska, USGS-474-62, U.S. Geological Survey: Denver, Colorado.

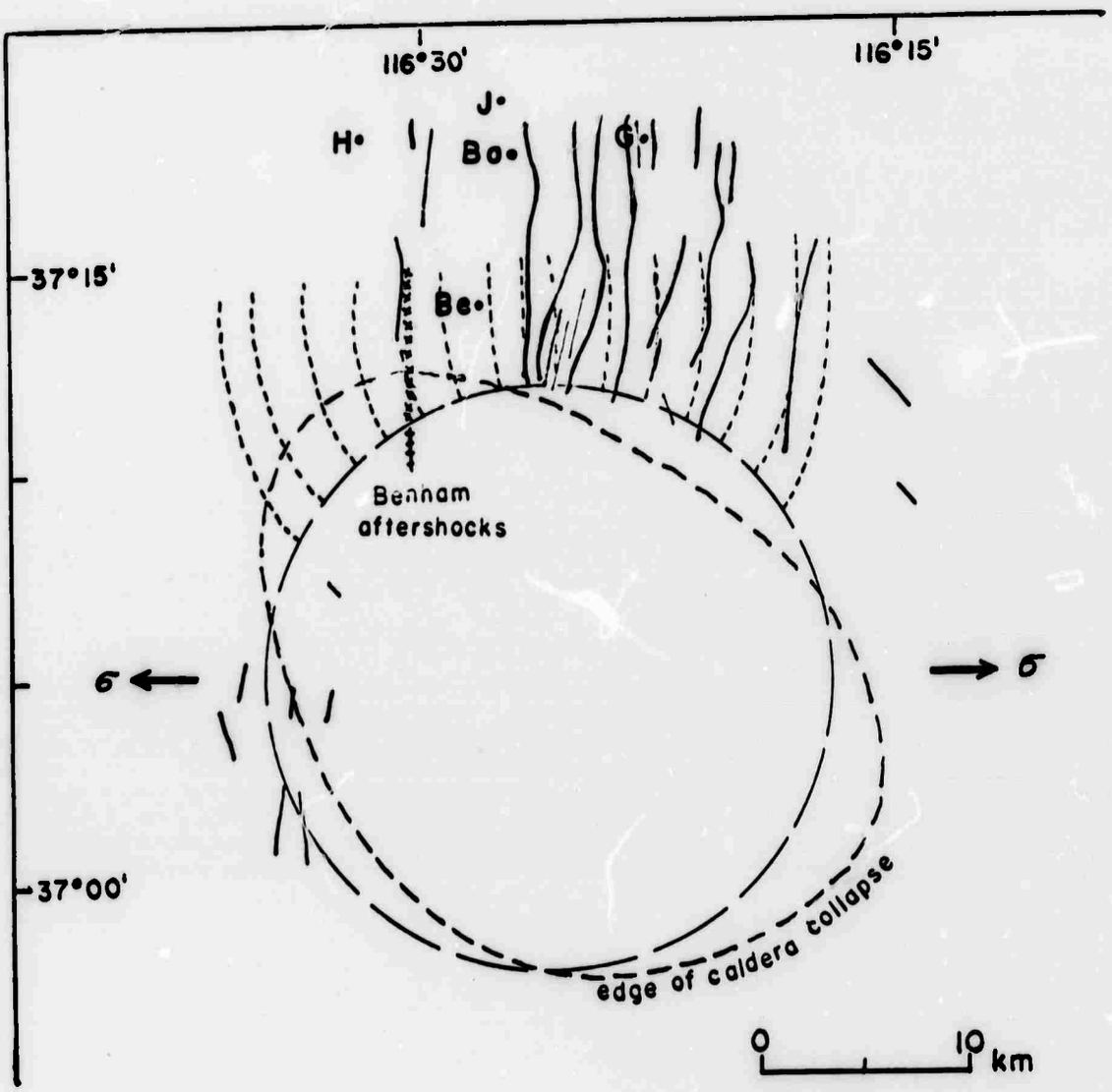

adapted from Cummings (1968)

Figure 1. Model of Pahute Mesa - Timber Mountain caldera tectonics after D. Cumming. σ is the regional tensile stress. Nuclear events are designated: H - Handley, J - Jorum, G - Greeley, Bo - Boxcar, Be - Benham. The dashed curves are predicted orientations of faults.

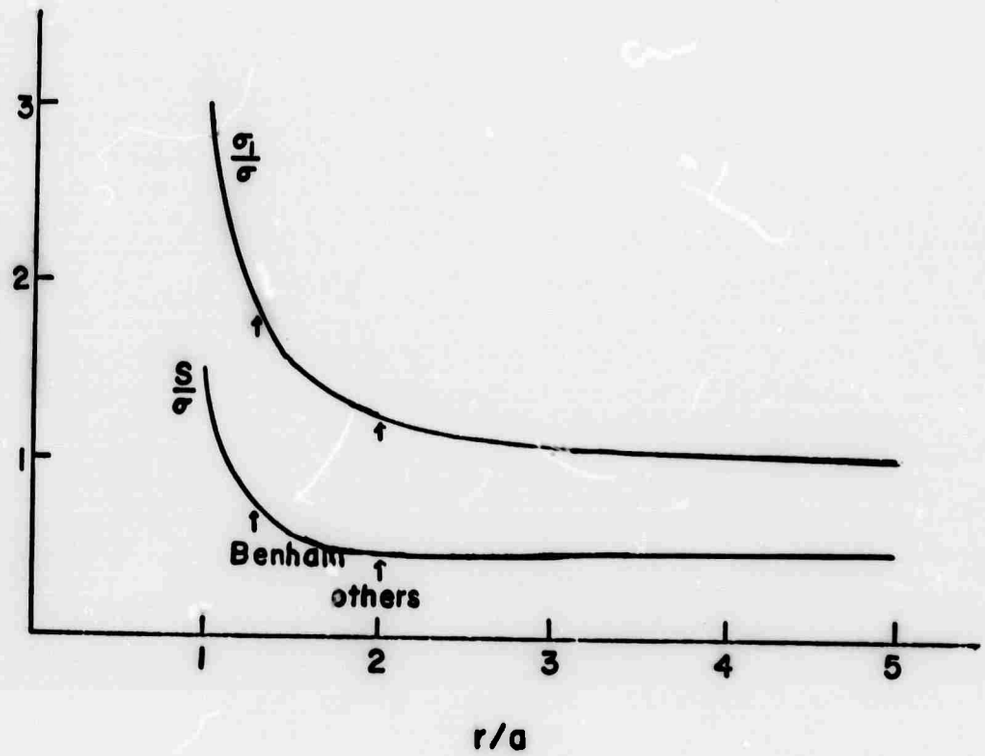

Figure 2. Variation of maximum tensile stress, σ_1, and maximum shear stress, S, with distance to the north from the caldera boundary. Distance is in terms of caldera radii.

THE RELATION OF THE P WAVE A_2/A_1 RATIO TO FOCAL MECHANISM

Nuttli and Gudaitis (1966) remarked a relationship which may be of advantage in multi-azimuth use of long period data in examining focal mechanisms. The decrease in amplitude of the first half-cycle of the P wave in the neighborhood of a nodal line has already been noted. However, for the earthquake of February 6, 1964, and for other earthquakes studied, Nuttli and Gudaitis found that the amplitude of the second half-cycle of the P wave remained relatively large at all stations, even those near nodal lines. More exactly, they found the ratio of the amplitude of the second to the first half-cycle of the P motion to be almost constant for all stations except those near a nodal line, where the ratio becomes very large.

This is illustrated by Figure 1, which shows examples of the P wave at selected stations. The value of xy, or relative expected first amplitude, is shown under each tracing of the P motion. The increase in A_1 as xy increases is evident. Also evident is the variation of A_2/A_1 with the value of xy. For xy small (HNR) this ratio is about 5; at other stations, as xy increases, A_2/A_1 has a constant value of about 2.

The plot of the amplitude ratios A_2/A_1 versus xy at all stations for the earthquake of February 6, 1964, is shown in Figure 2. One point is off the curve. At four stations the amplitude of the first half-cycle was less than the noise, and so the ratio A_2/A_1 is indeterminate but large. The amplitude ratios at those stations are represented by vertical bars, arbitrarily taken to have the value 5. The relation of the amplitude ratio A_2/A_1 to proximity to a nodal line is dramatic.

Several conclusions suggest themselves. First, the ratios A_2/A_1 might be used as a rapid reconnaissance tool in estimating the position of nodal lines. Or, this ratio might be used as a means of refining a preliminary focal mechanism solution, which was the application made by Nuttli and Gudaitis. Or routine observations of the ratio A_2/A_1 at stations of a world-array might be an auxiliary point of information or an identfication criterion.

REFERENCE

Nuttli, O.W., and Gudaitis, V.V., 1966, On the amplitudes of long period P waves (Abstract). Earthquakes Notes, v. 37, p. 24.

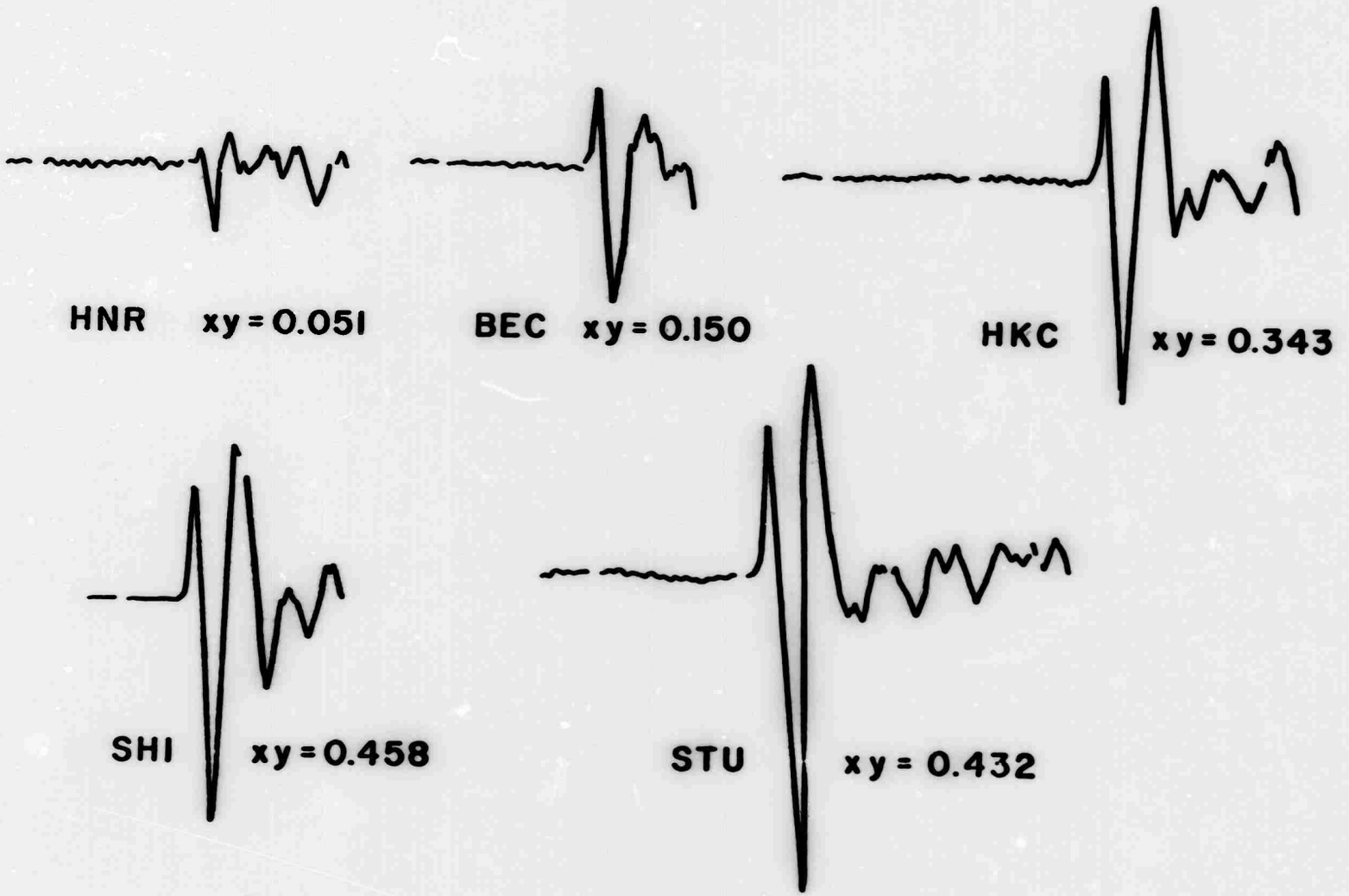

Figure 1. Examples of P wave arrivals illustrating the relation between the amplitude of the first half-cycle and the xy factor.

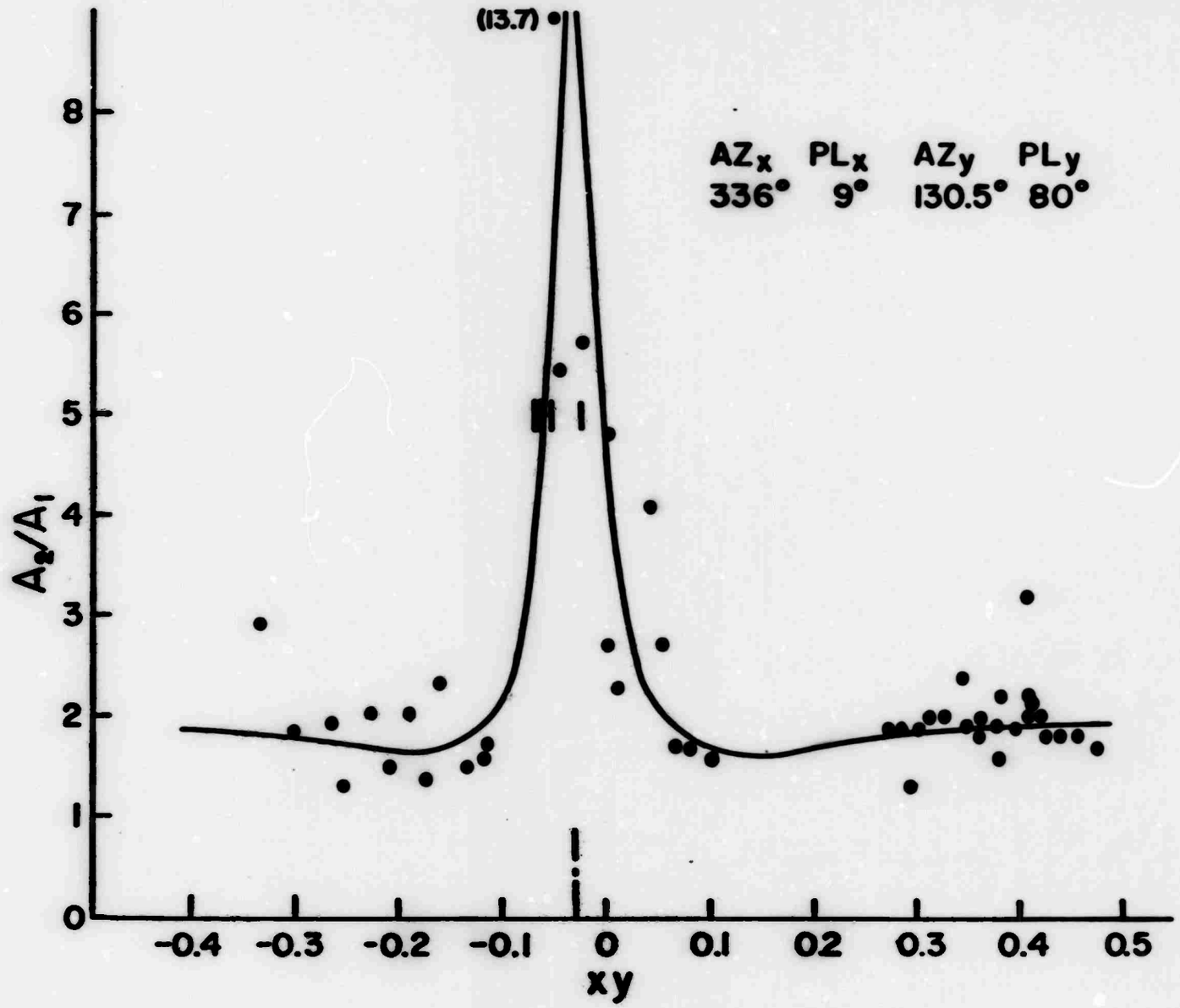

Figure 2. Plot of A_2/A_1 versus the xy factor, earthquake of February 6, 1964, Kodiak Island.

A THEORETICAL MODEL FOR EXPLOSION SPECTRA

By

Lane Johnson
William Bakun

BLANK PAGE

The objective of this study has been to construct a theoretical model which suitably explains the compressional body waves that are radiated from a contained explosion. The theoretical model contains a number of variable parameters which are presumably related to physical processes at the source and along the propagation path. For any given explosion the values of these parameters can be estimated by obtaining a least squares fit between the spectrum of an observed body waves and the spectrum of the theoretical model. Hopefully, the net result of this approach is that the seismic body wave can be completely characterized by these estimated parameters, which are considerably less in number than the points required to represent the signal in either the time domain or frequency domain and which are more directly related to physical processes at the source.

In this initial stage of the analysis we have considered a very simplified model of a contained explosion in an elastic medium. We represent the explosion as a pressure which is suddenly generated within a spherical cavity of radius r_o imbedded in an infinite elastic medium. The problem has spherical symmetry so that for outward propagating compressional waves the radial displacement at any distance r from the center of the cavity is

$$u_r(r,t) = \frac{\partial}{\partial r}\left(\frac{\phi(\tau)}{r}\right)$$

where ϕ is the reduced displacement potential, τ is the reduced time

$$\tau = t - \frac{r-r_o}{\alpha}$$

and α is the compressional body wave velocity in the medium. The only boundary condition to be satisfied is that the radial stress at r_o equal the pressure within the cavity. Following Favreau (J. Geophys. Res., v. 74, p. 4267-4280, 1969) we assume that at $t = 0$ the pressure within the cavity jumps to an initial value P. Thereafter the pressure within the cavity is related to the volume of the cavity (and thus the displacement u_r at r_o) by assuming that the explosion gases behave as an ideal adiabatic gas. With this assumption the boundary equation is easily solved, especially if the equation is first transformed into the frequency domain. The solution for the Fourier transform of $\phi(\tau)$ is

$$\Phi(\omega) = \frac{-c}{i\omega}\,\frac{1}{1 - \frac{1}{2a}\left(\frac{\omega}{b}\right)^2 + i\frac{\omega}{b}}$$

where

$$a = \frac{1-2b}{1-b} + \frac{3}{2}\frac{\gamma P}{\rho\alpha^2}$$

$$b = \frac{\alpha}{r_o}$$

$$c = \frac{r_o^3}{\rho\alpha^2}\ \frac{1}{2a}$$

and

P is the initial explosions pressure within the cavity

γ is the ratio of the specific heats of the explosion gases

α is the compressional velocity in the medium

ρ is the density in the medium

b is the Poisson's ratio in the medium

The Fourier transform of the far field part of the radial displacement is simply

$$U_r(r,\omega) = \frac{c}{1 - \frac{1}{2a}\left(\frac{\omega}{b}\right)^2 + i\,\frac{\omega}{b}}$$

If we consider the modulus of this, which is shown in Figure 1 for various values of a and b, we see that for $a \geq 1$ the spectrum will have its only maximum at $\omega = 0$ and decay monitonically as ω increases. But for $a < 1$ the spectrum will have a maximum value at some finite ω given by

$$\omega = b\sqrt{2a(1-a)}$$

In order to explain the observed spectra we must also take into account the effects of propagation. We have approximated the effect of frequency dependent attenuation along the propagation path by including the factor

$$\exp\left(\frac{-\omega T}{2Q}\right)$$

where T is the travel time and Q is the average quality factor along the path. In our calculations for P_n we have assumed a value of 400 for Q. The observed spectra are computed from a time window of 2 - 8 seconds and the signal generally consists of more than one simple pulse. We have assumed that it consists of an initial pulse followed by n secondary pulses which are identical to the initial pulse except for an amplitude factor d and a time delay Δt. The effect of these secondary pulses on the spectra is

$$1 + \sum_{i=1}^{n} d_i \exp(-\omega \Delta t_i)$$

Finally, the instrument response, $I(\omega)$, is also taken into account. The complete theoretical model for the spectrum is summarized in Figure 2.

Given the theoretical model with its variable parameters a, b, c, d_i, and Δt_i it is straightforward to obtain estimates of these parameters that minimize the squared difference between the theoretical spectrum and any particular observed spectrum. Figure 3 shows the fit obtained for the P_n phase of a particular explosion, PLAID II. We have taken P_n to be a head wave and thus have added an additional $1/\omega$ factor to the theoretical model. The fit both with and without secondary pulses is shown. It is clear that the secondary pulses must be included if one is to obtain a good fit and meaningful estimates of the unknown parameters. As a check upon the fit in the frequency domain we have computed the time trace corresponding to the theoretical spectrum and plotted it along with the observed time trace in Figure 4. Table 1 lists the values of the parameters a, b, and c that were obtained from the analysis of P_n from a number of events.

The question of how unique, reliable, and useful these estimated parameters actually are is still being studied. The problem of uniqueness or stability is present in any non-linear fitting process. The presence of noise and the limited frequency band in which we have useful data complicate this problem even more.

It may be that a combination of the parameters may be more stable or more useful than the individual parameters themselves. To illustrate such an approach we considered the quantity ab^2. Figure 5 shows this quantity plotted as a function of magnitude. Explosions are separated from earthquakes and there appears to be some separation between explosions in tuff and explosions in alluvium. However, more data are required to check out these suggestions.

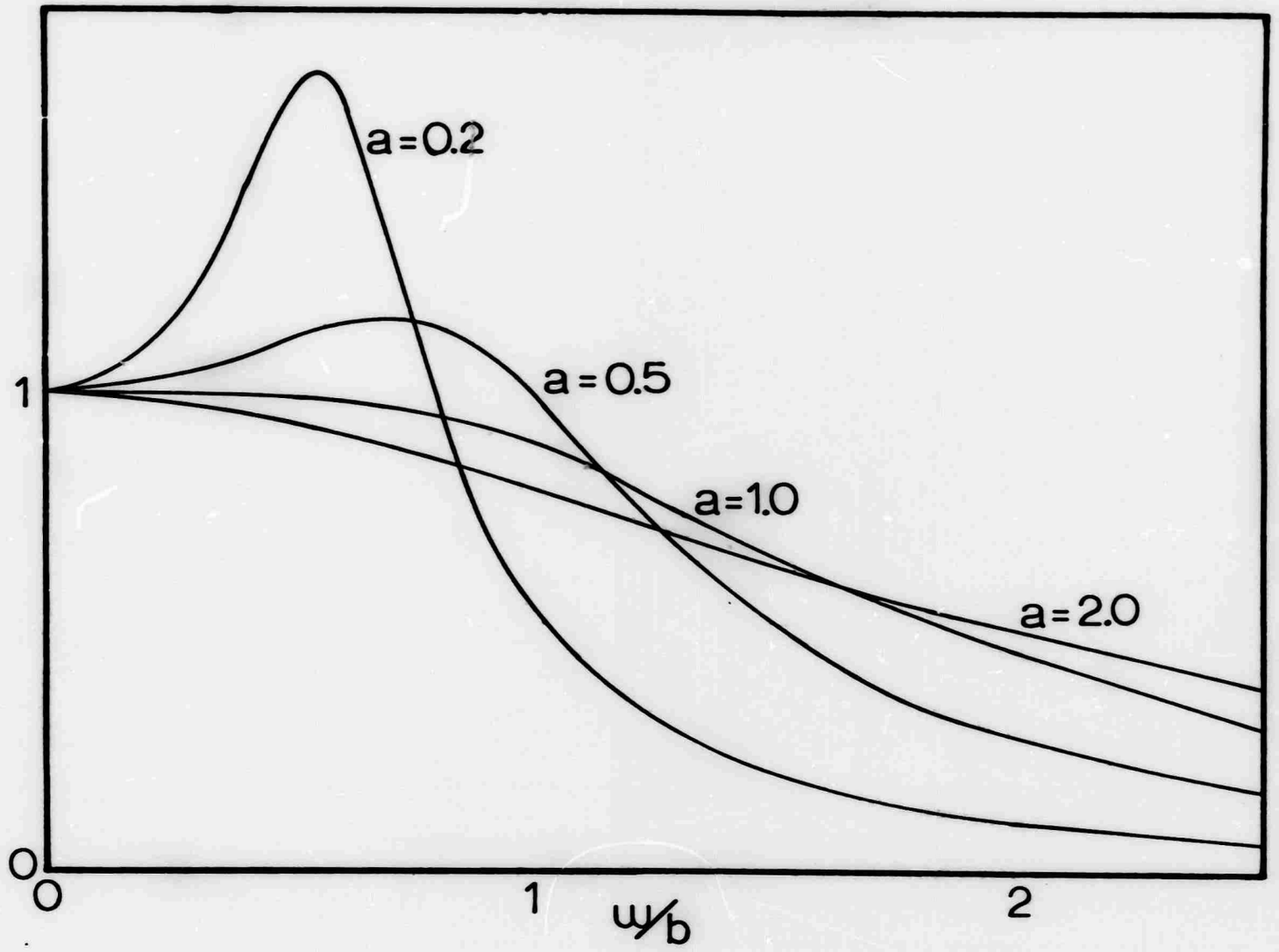

Figure 1. Spectral modulus of the radial displacement from a spherical cavity as a function of the two parameters a and b.

Spectrum

$$S(\omega) = F(\omega)\ E(\omega)\ R(\omega)\ I(\omega)$$

Source:

$$F(\omega) = c\ [1 - (\omega/b)^2/2a + i(\omega/b)]^{-1}$$

$$a = (1 - 2\sigma)/(1 - \sigma) + 3\gamma P/\rho\alpha^2$$

$$b = \alpha/r_o$$

$$c = Pr_o^{\ 3}/2a\rho\alpha^2$$

Attenuation:

$$E(\omega) = \exp\ (-\omega T/2Q)$$

Secondary Pulses:

$$R(\omega) = \sum_{i=1}^{n} [1 + d_i \cos(\omega\Delta t_i) - id_i \sin(\omega\Delta t_i)]$$

Instrument:

$$I(\omega)$$

Figure 2. Summary of the theoretical model used to characterize the spectra of compressional waves radiated by a contained explosion.

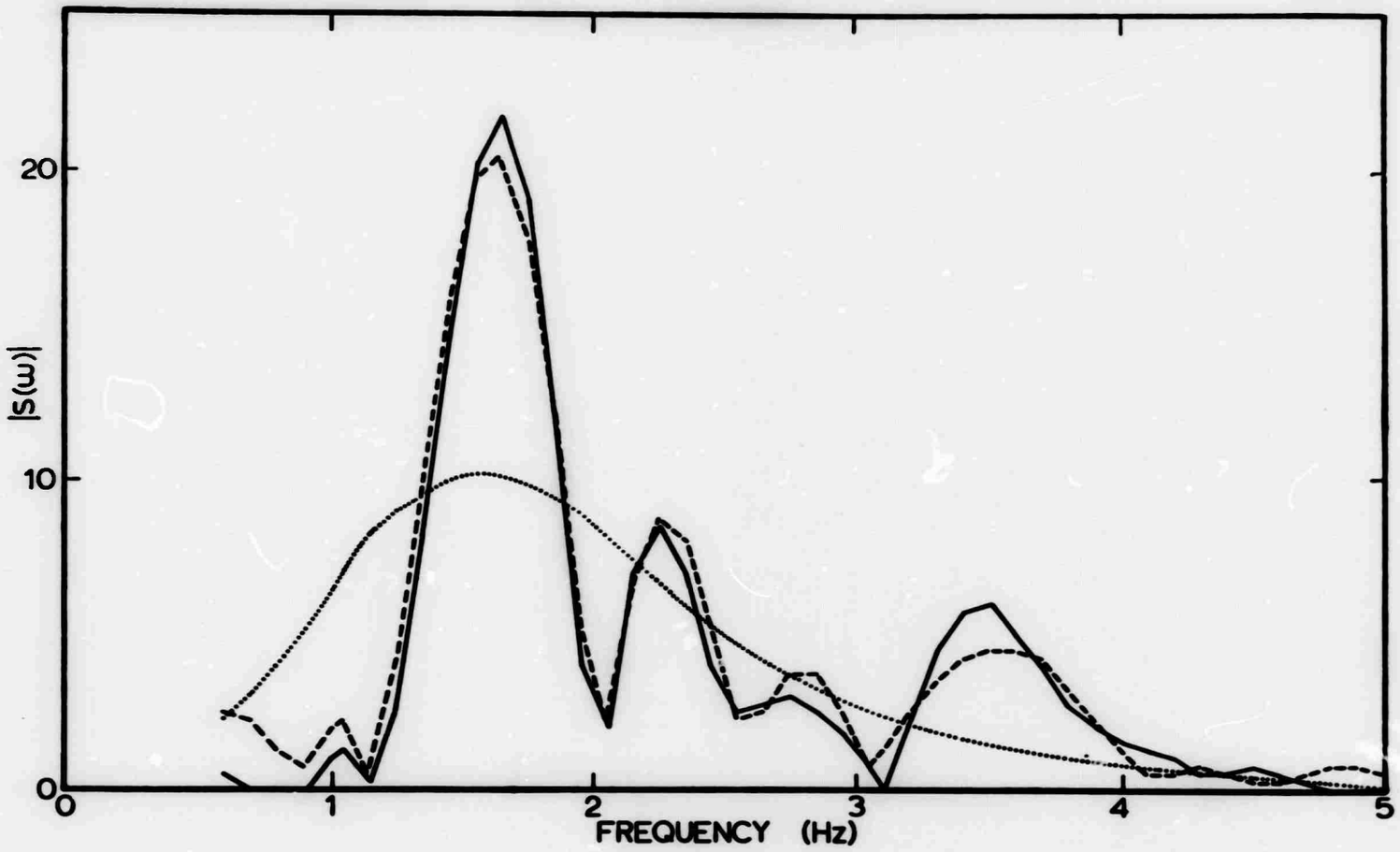

Figure 3. Spectral modulus of the P_n phase recorded at JAS from the underground explosion PLAID II on 3 February 1966 (magnitude = 4.2, distance = 380 km). The solid line is the observed spectra, the dotted line is a least squares fit assuming no secondary pulses, and the dashed line is a least squares fit assuming 4 secondary pulses.

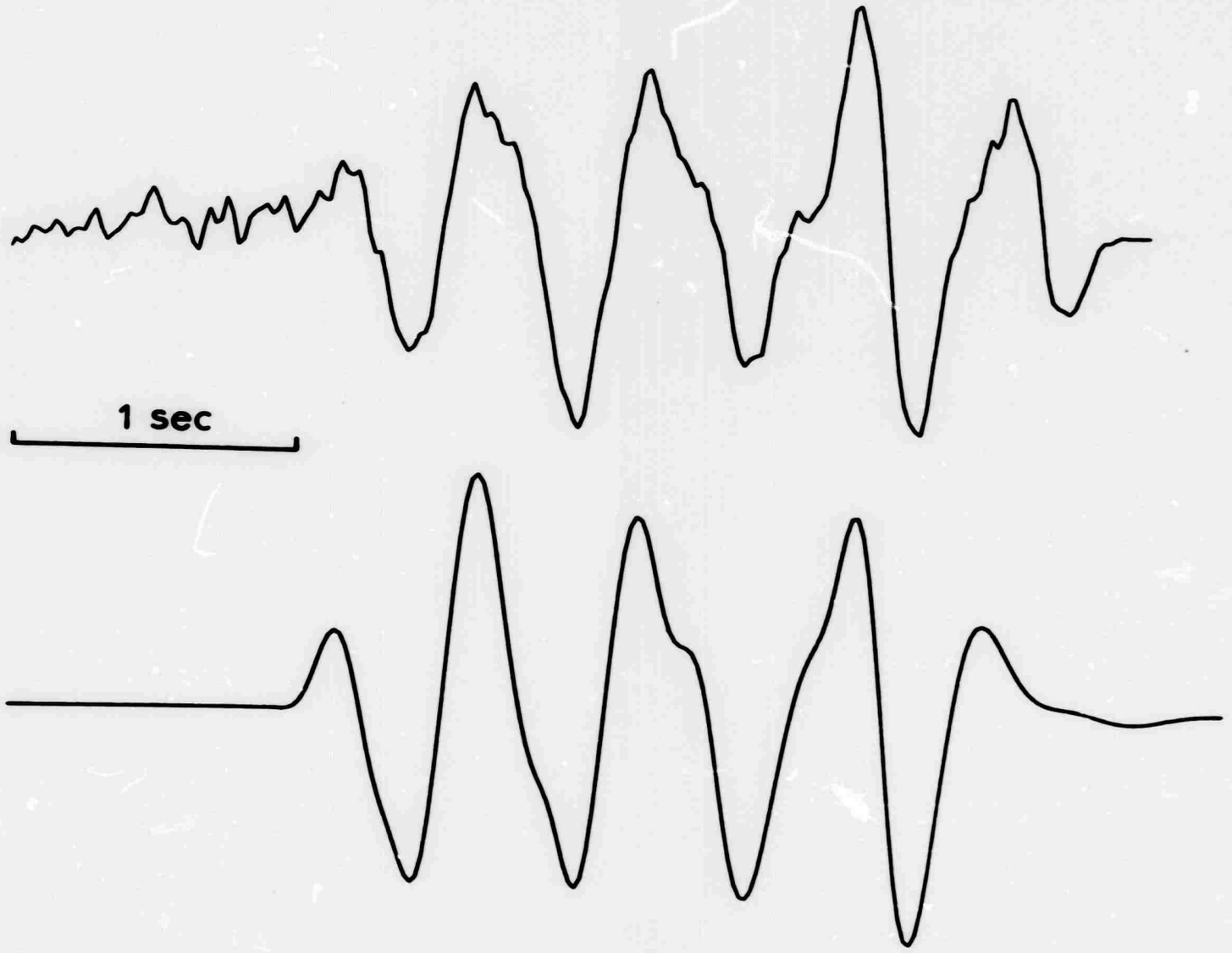

Figure 4. P_n phase recorded at JAS from the explosion PLAID II. The top trace is observed while the bottom trace is calculated on the basis of a least squares fit of a theoretical model to the spectral modulus of the top trace.

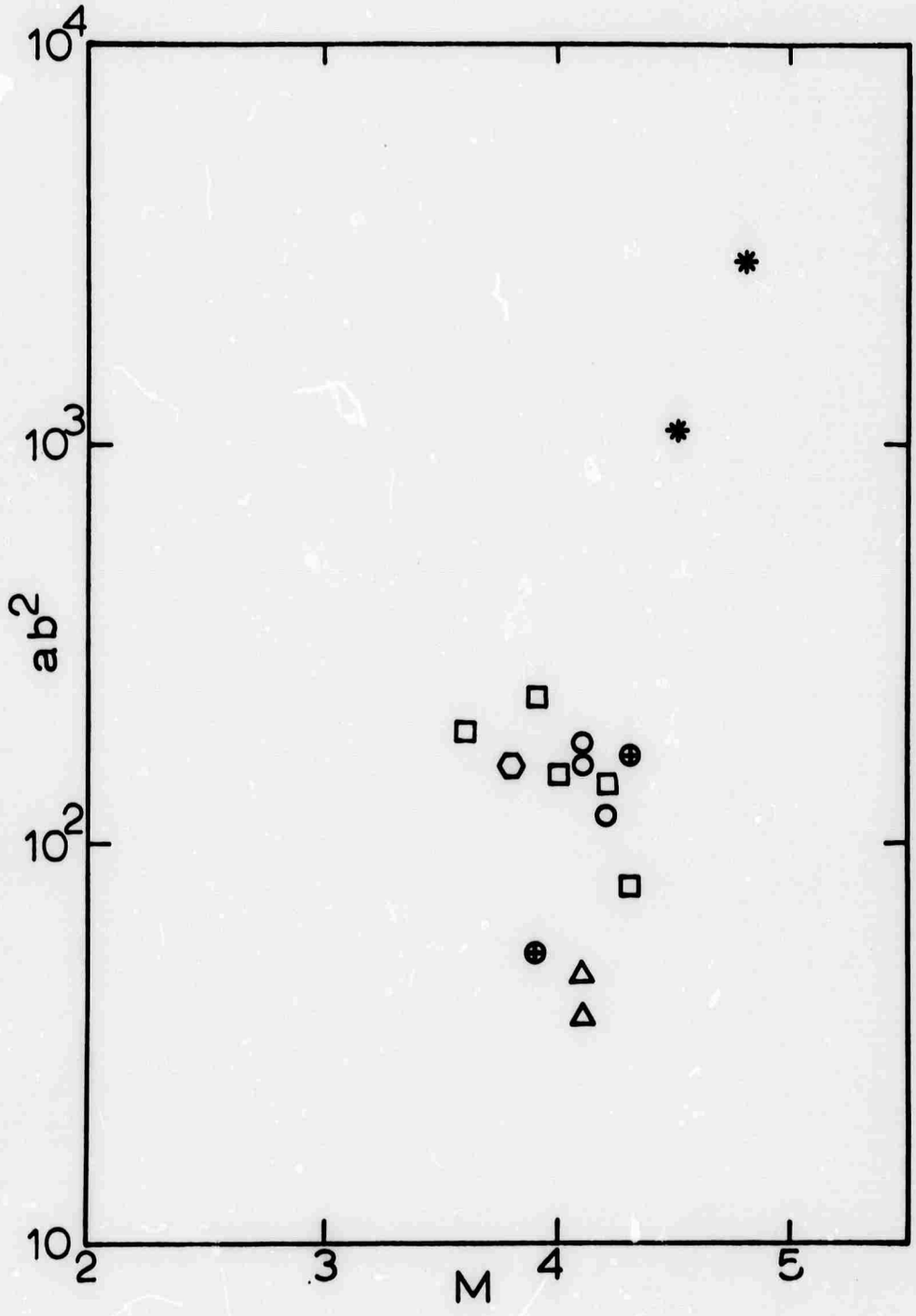

Figure 5. The measured values of ab^2 plotted as a function of magnitude. The open symbols denote explosions, the enclosed crosses are afterevents of explosions, and the asterisks are natural earthquakes. The media in which the explosion was detonated is denoted by a square for alluvium, a triangle for tuff, a hexagon for rhyolite, and a circle for unknown.

Table 1. Event characteristics

Date	Event	Magnitude	Distance	a	b	c
3 Feb 66	PLAID II	4.2	380	0.19	27.2	1.3
6 Apr 66	STUTZ	4.1	385	0.26	12.0	2.8
12 Sep 66	DERRINGER	3.9	410	0.13	42.1	0.9
2 Mar 67	RIVET III	3.6	395	0.23	28.7	0.7
27 Apr 67	EFFENDI	4.0	395	0.44	18.4	1.0
7 May 67	18 01 36	4.5	490	0.35	55.8	1.5
29 Jun 67	UMBER	4.3	400	0.12	25.5	0.7
18 Jan 68	HUPMOBILE	4.2	395	0.13	30.1	1.3
26 Jan 68	CABRIOLET	3.8	350	0.18	29.5	0.6
23 Apr 68	SCROLL	4.1	345	0.21	15.0	10.7
22 May 68	13 21 56	4.8	390	0.52	74.4	1.6
30 Jul 68	TANYA	4.1	390	0.13	37.1	1.7
22 Nov 68	TINDERBOX	4.1	395	0.40	19.9	1.0
21 Dec 68	00 14 25	4.3	360	0.68	15.6	4.0
16 Sep 69	16 23 54	3.9	360	0.12	21.1	1.0

CORE PHASE IDENTIFICATION OF EARTHQUAKES AND EXPLOSIONS

By

W. F. Isherwood
D. R. Grine

INTRODUCTION

Stanford Research Institute, with support from ARPA and NSF, installed a four element seismic array (BYA) at Byrd Station, beginning operation January 18, 1968. The system is described by Isherwood (1969). The site was selected to study core phase arrivals because PKP waves have a principal focus at an angular distance, Δ, of approximately 142° from the source (point B in Figure 1), and Byrd Station is close to 142° from several of the great seismic zones in the Northern Hemisphere as shown in Figure 2.

The tape records from the first two years, including approximately 1000 core phase arrivals, are being analyzed to enhance the core phases and to interpret them in terms of the source characteristics and the details of the earth's core. Ambient noise is being studied to relate it to oceanic and continental storms.

Part of the study of source characteristics has shown that core phases offer some promise in discriminating between earthquakes and explosions. PKP and PKIKP can be used in most of the same ways as teleseismic P. As pointed out by Bolt (1968), they have an advantage in that PKIKP has a sharp onset beyond $\Delta = 160°$. PKP has a large amplitude with a sharp onset for $142° < \Delta < 152°$ on the BC branch. Bolt also notes that the contrast in $dt/d\Delta$ between the AB and EF branches for $\Delta > 160°$ gives a PKP_2 - PKIKP interval more sensitive to changes in Δ than the S-P interval near $\Delta = 50°$. An error of 0.1° in Δ should be detectable.

This paper presents the preliminary results of our work on core phase discrimination between earthquakes and explosions. Examples are shown for earthquakes and Russian nuclear shots of first motion, determination of depth from BC branch travel times, and the sharpness of the PKP_2 - PKIKP interval.

RESULTS

General

PKP arrivals were observed at Byrd Station for the range of 110° to the antipode. The amount of energy transmitted, however, varies considerably over this range as pointed out by Shahidid (1968). This is seen in both the amplitudes of arrivals and the quality of the first motion seen.

Ray-paths associated with the GH branch transmit so little energy that arrivals are seen only on the largest of events and even then onsets are emergent. GH arrivals appear to be useless for discriminating earthquakes from explosions. The maximum sensitivity -- or lowest detection threshold -- appears to fall on the BC branch, at 142° $<\Delta<$ 152°. Within this range numerous events of (C&GS) magnitude, m_b, 4.5 and occasionally less are seen even on unenhanced records. Below 142°, there appears a gradual dropping off in amplitude and quality to ~ 110°. For example:

117° Nevada Test Site (Boxcar) m_b = 6.3 Yielded 15 mμ Poor onset

147.6° North-Atlantic earthquake m_b = 4.7 Yielded 40 mμ Good onset

Although data are sparse beyond 152° for the recording period observed, the first indication is of higher thresholds again at Δ greater than 160°, with AB arrivals containing more energy than DF ones. The gap between 152° and 160° will be discussed in more detail later.

The background noise qualitatively appraised at Byrd lies mostly at much higher frequencies and slightly lower frequencies than the PKP signals. Signals at ~ 1 Hz have least competition with background noise, which is generally < 1.5 mμ of ground motion. The main interference arises from longer period noise, which rises to ~ 30 mμ at 0.3 Hz and may be as high as ~ 10 mμ at 0.5 Hz (to which frequency the signal often extends). A higher amplitude noise is encountered when snow cats are in operation in the Byrd Station area, which occasionally renders the first playback useless. However, this noise is regularly near 5 Hz, well out of the signal band and therefore subject to more filtering.

First motion

As for P, the first motions of PKP events are possible distinguishing characteristics between explosions and natural earthquakes. Figure 3 shows onsets of arrivals of the BC branch. Trace 1 shows the common case in which explosions show a clearly compressional first motion. However, Trace 2 shows that these are not always clear-cut, especially if only one seismometer trace is examined. (In this case, comparison with traces from the other recording seismometers showed the true compressional onset.) Although none of the BC arrivals from

blasts examined showed clear dilation, such as shown on Trace 3 from a North Atlantic earthquake, onsets from events of $m_b < 5.0$ were unclear from preliminary examinations.

Depth determinations

The sharp onsets observed on the BC branch arrivals lead to another distinguishing criterion -- depth of hypocenter. Since PKP waves travel along paths nearly normal to the earth's surface, differences in arrival time vary more with hypocenter depth than for other wave paths. For example, if the true onset of a PKP wave could be determined to + 0.5 sec and compared with an accurate time prediction of a zero depth event, the hypocenter would be determined to about + 3 km. (In practice, effects of local geology cannot be completely discounted.) The feasibility of this is examined briefly.

Figure 4 shows the BC portion of the travel time curve. Each point plotted represents the travel time from a single event, corrected for the earth's ellipticity and USC&GS depth (using depth corrections based on Bolt, 1968). Circles are earthquakes, triangles are blasts (0 km depth by C&GS). No "station corrections" are introduced, since they would merely show up as a small constant on all points. From a total of 115 arrivals, a curve was computed by a least squares fit. The first order fit:

$$t = 19\text{ m }31.07726\text{ sec} + 3.00003\ (\Delta - 142^\circ)\text{ sec}$$

standard error = 0.746 sec.

is shown as the figure. Second and third order curves were also calculated and are given below:

$$t = 19\text{ m }30.749\text{ sec} + 3.2447\ (\Delta - 142^\circ)\text{ sec} - 0.0282003\ (\Delta - 142^\circ)$$

sec standard error = 0.726 sec.

$$t = 19\text{ m }30.885\text{ sec} + 2.988\ (\Delta - 142^\circ)\text{ sec} + 0.04730\ (\Delta - 142^\circ)^2\text{ sec} - 0.00573871\ (\Delta - 142^\circ)$$

sec

standard error = 0.724 sec.

Because of the small difference in standard errors, the second and third order fits are not justified at this time. The first order curve was used to predict travel times for surface focus events to Byrd Station.

In Table I, the results of subtracting these predicted times from the actual travel times without depth correction are shown. The time residual can be used with tables from Bolt (1968) to recalculate hypocenter depth. The depths determined from our

residuals are then compared with those depths given by the USC&GS. All those events, presumably explosions, listed at 0 km by the USC&GS also show times corresponding to depths within 5 km of the surface based on the Byrd Station arrival times. The only other event with such a shallow depth determination is an event at Lake Baikal (Δ=151°), which the USC&GS similarly lists as 4 km deep.

The small scatter in BC arrival times allows their use for depth determination. The steeper penetration of the crust and upper mantle may make this BC curve more valid as a world average than P travel time. The errors shown by Evernden (1969) in depth determination from average P travel time curves should be less for PKP.

Although some investigators have extended the BC branch to 155° or farther, the sparse BYA data do not confirm extension beyond 152°. The USC&GS shows few earthquakes at these distances; also the detection threshold appears to be higher for this range. At the least, the BC arrival has lost its preeminence and the other onsets seen are of poorer quality for precise time determinations.

At 157° (Ural Mountains), two surface events of m_b = 4.9 show arrivals on the AB branch, whereas neither the DF arrival nor BC arrival is seen. The DF arrival was not seen on any BYA records or events with $m_b < 5.0$.

Beyond 152° in Table I, there is no immediate attempt to determine hypocenter depth from arrival times because of differences between observed travel time and published values (Bolt, 1968) of several seconds. BYA data were too sparse to justify fitting a curve as done for the BC branch.

For $\Delta > 160°$, on larger events were DF and AB are both clearly observable, there is another way to determine hypocenter depth that is independent of the USC&GS origin time and epicenter solutions. Figure 5 shows the recording of an explosion at Novaya Zemlya, 173° from Byrd. The onsets of both DF and AB arrivals are clear on all four seismometers.

At $\Delta \leq 160°$, the slope of the AB branch is many times as steep as that of the DF branch. For example the interval between these branches is increasing at 4.0 sec/degree at 173°.

If the AB-DF interval can be picked accurately to 0.4 sec, the Δ is determined to 0.1 degree. Once this confidence can be gained in the true Δ, the depth can be determined by the absolute travel time and predicted time curves.

The records from events checked in Table I have been digitized by the Vela Digitizing Center at 50 samples per second. The first enhancement of PKP was by digital filtering with a bandpass of 0.33 to 2 Hz. The cutoff frequencies were chosen by visual inspection of the records. The improvement in arrival sharpness is shown for a surface event from East Kazakh (Δ = 149.2), in Figures 6 and 7.

CONCLUSIONS AND FUTURE WORK

Work with records for the first two years from BYA showed that the BC branch of PKP is sharp enough to be promising for depth determination on events with $m_b < 4.8$. A better determination of threshods as a function of Δ will be made by using digital techniques to enhance arrivals on more records.

The EF and AB branches offer possibilities in depth determination beyond $\Delta = 160°$. Arrays in South Africa, Malagasy, and Kerguelen could be used to monitor western U.S. earthquakes and nuclear shots over a range of Δ to establish any advantages over P depth determination. Arrays should be large enough to determine $dt/d\Delta$ as an aid in separating the various branches near BC.

Operating arrays covering Asia could be established in South America and New Zealand, event if only the BC branch should have a clear advantage over P in depth determination.

NOTES FOR TABLE I

O.T. - origin time as calculated by USC&GS

*Epicenter determination considered by USC&GS as less accurate than others.

Lat., Long. - as calculated by USC&GS.

m_b - body wave magnitude as calculated by USC&GS.

No. Sta. - number of stations used in C&GS computation.

$\Delta°$ - geocentric angle between seismometers and epicenter - average used when pick taken from more than one seismometer.

Compression/dilation - first motion where noted.

T.T. - absolute travel time. When two travel times are listed, the first is DF and the second is either BC or AB.

ε_{ij} - ellipticity correction - from Jeffreys and Bullen 1967.

Period - visual appraisement.

Amp. - peak amplitude based on instrument calibration (two place accuracy only).

Digitized - X indicates digital records were made (by Vela Digitizing Center, Alexandria, Virginia).

Residual for 0 depth. Predicted time minus travel time where predicted time is based on first order least squares fit for the BC arrivals (depth corrected using A. Qamar's tables Bolt, 1968 for Point B) and travel times have been corrected for earths ellipticity.

Depth from Res. using A. Qamar's tables (Bolt, 1968) for Point B C&GS depth - 33 km is used where C&GS considers "N" or normal depth.

No. of seismometers - the number of seismometers from which the BYA picks were made and averages taken. The 1970 records are generally only from 1; the helicorder record. Others, 2, 3, or 4 are functions of playback equipment used.

REFERENCES

Bolt, B.A., 1964, The velocity of seismic waves near the Earth's center, BSSA, v. 54, p. 191-208.

Bolt, B.A., 1968, Estimation of PKP travel times, B.S.S.A., v. 58, No. 4, p. 1305-1324.

Evernden, J.F., 1969, Identification of earthquakes and explosions by use of teleseismic data, J. Geophys. Res., v. 74, No. 14 p. 3828-3856.

Isherwood, W.F., 1969, Investigation of PKP seismic waves, SRI Report To AFOSR, Contract F44620-67-C-0080.

Shahidi, Mohammad, 1968, Variation of amplitude of PKP across the Caustic, Phys. Earth Planet. Interior, v. 1, p. 97-102.

BLANK PAGE

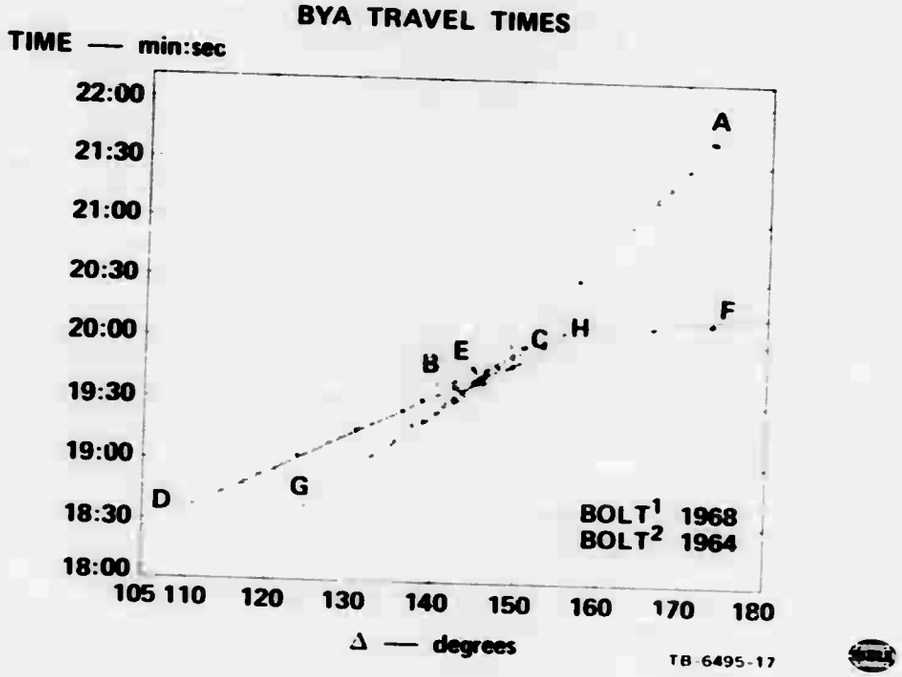

Figure 1. PKP travel time curve. Solid lines from Bolt (1968), dashed lines from Bolt (1964) Δ's are blasts, 0's are earthquakes.

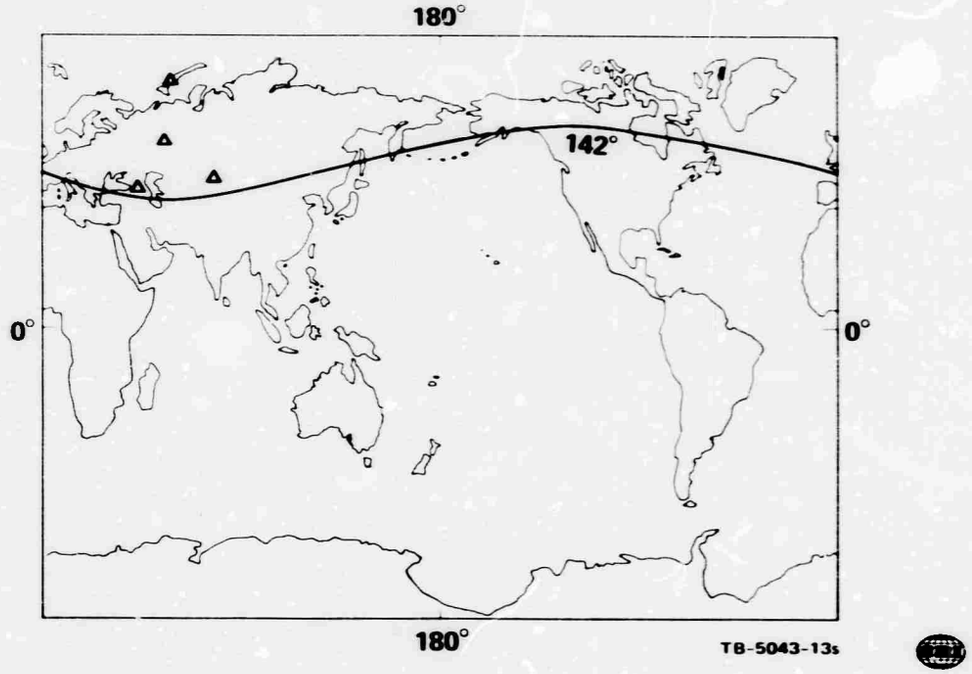

Figure 2. World map with line at 142° i.e., B, the beginning of BC branch. Approximate locations of Russian events in Eastern Kazakh SSR, Novaya Zemlya, Ural Mt. Region, and Sourthwestern Russia are indicated.

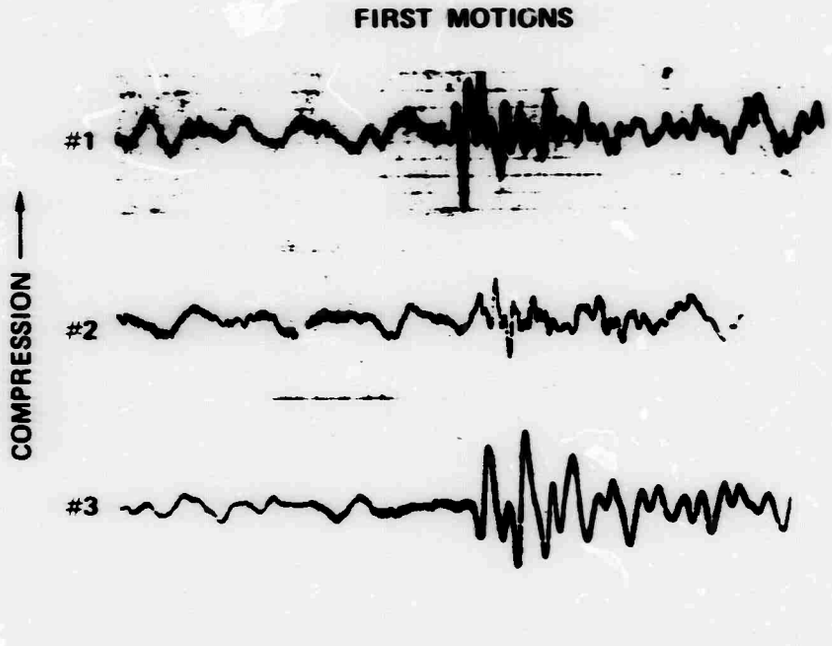

Figure 3. First motions - (BC Branch)

Trace	Date (1968)	Origin Time	Location	Blast or Earthquake	m_b	Δ
1	Jul 12	120757.2	E. Kazakh	Blast	5.4	148.9°
2	Apr 24	103557.1	E. Kazakh	Blast	5.0	149.1°
3	Jul 03	095527.0	N. Atlantic	Quake	4.7	147.6° (normal depth)

Trace 1 is a blast clearly showing compressional first motion.
Trace 2 is a blast where first motion is not clear.
Trace 3 is a natural earthquake with clear dilational first motion.
Compression is upward.

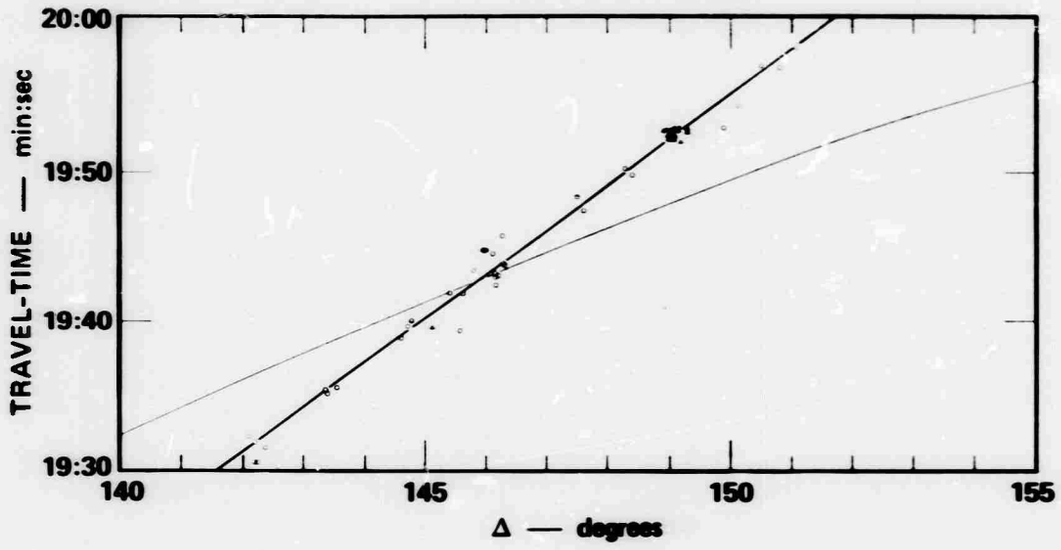

Figure 4. Travel time curve for BC Branch, 142° to 152°. Equation of least squares fits (from 115 arrivals). Shown: $t = 19m\ 31.07726\ sec + 3.00003 \cdot (\Delta - 142°)$ sec standard error 0.744. Also found: $t = 19m\ 30.749\ sec + 3.2447\ (\Delta - 142°)\ sec - 0.0282003\ (\Delta - 142°)\ sec - 0.0282003\ (\Delta - 142°)^2_{sec}$ standard error 0.726. $t = 19m\ 30.885\ sec + 2.988\ (\Delta - 142°)\ sec + 0.04730\ (\Delta - 142°)\ sec + 0.04730\ (\Delta - 142°)^2\ sec - 0.00573871\ (\Delta - 142°)^3_{sec}$ standard error 0.724. Note the low scatter of blasts. The scatter of earthquakes may be partially due to inaccurate depths by USC&GS.

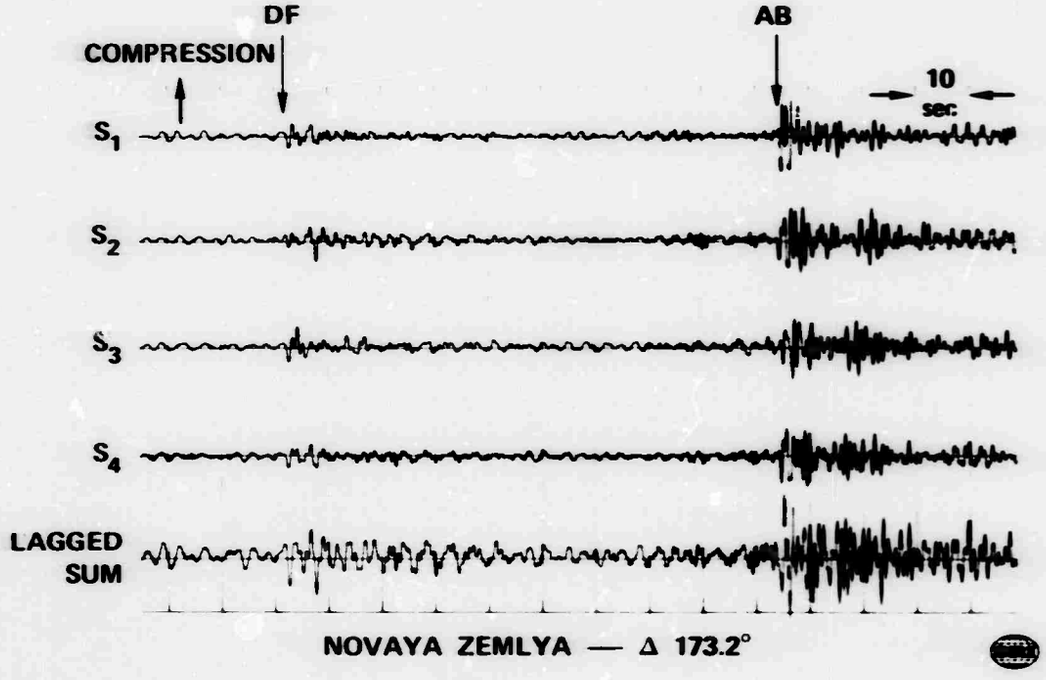

Figure 5. Event: Nov. 7, 1968 100205.3 Novaya Zemlya m_b = 6.0 Δ = 173.2° S_1, S_2, S_3, S_4 are the four seismometers at BYRD. Lagged Sum is formed by using theoretical relation (via Bolt's tables) between arrival times. No account taken for local geology or visually picked onset times. First arrival is PKIKP or DF branch C-P Deflection ~ 22 mμ. Second arrival is PKP_2 or AB branch C-P Deflection ~ 40 mμ. High frequency preceding AB arrival is also seen on the other event recorded from Novaya Zemlya, but is unreported in the literature. Compression is upward. Note -- both arrivals start with dilations. Spacing between timing lines is 10 sec. (Playout from digitized record).

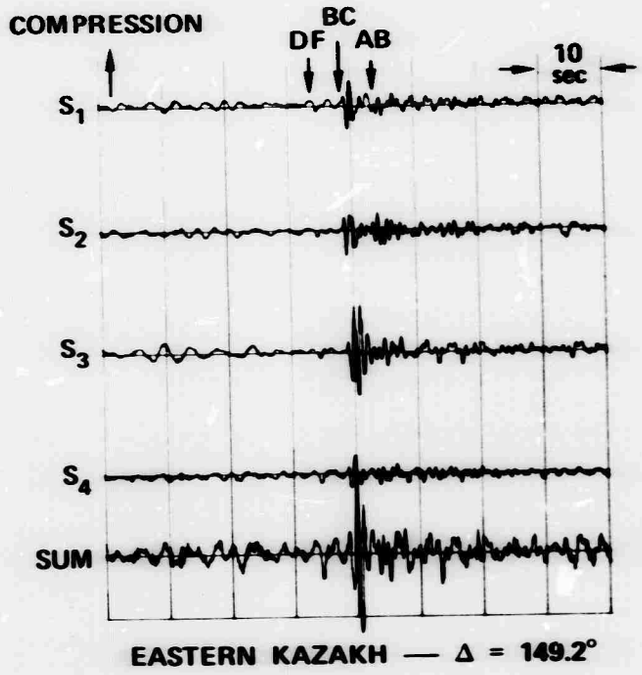

Figure 6. Event: June 19, 1968 - E. Kazakh Blast m_b = 5.5 Δ = 149.2 No. 6 shows S_1, S_2, S_3, S_4, and sum.

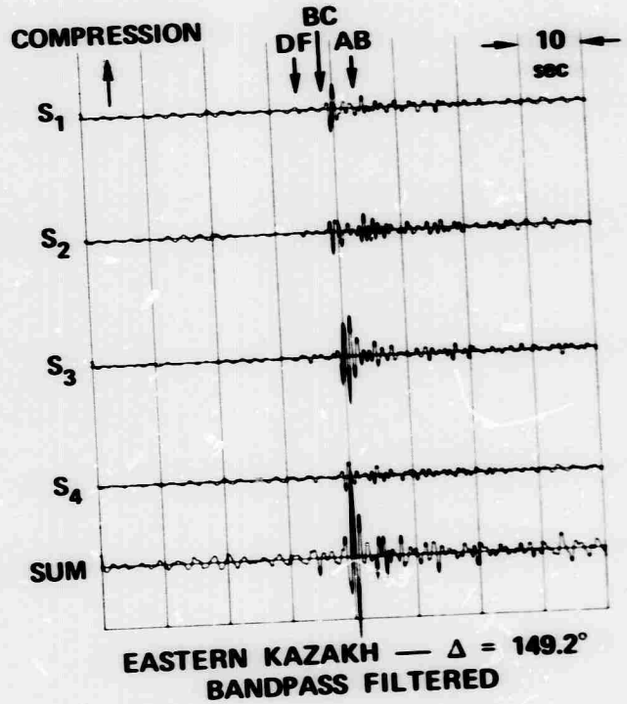

Figure 7. Event: June 19, 1968 - E. Kazakh Blast m_b = 5.5 Δ = 149.2. Band passed 0.33 Hz to 2 Hz (0.5 sec to 3 sec periods). Selected by qualitative guess. Three arrivals seen DF, BC, AB, PKIKP, PKP_1, PKP_2.

TABLE 1 - RESULTS

Date	O.T. Hr-Min-Sec	Lat.	Long.	Region	m_b	No. Sta.	Δ°	Compression/ Dilation	T.T. Min-Sec	ϵ_{ij} (Sec.)	Period (Sec.)	Amp. (m_μ)	Digitized	Res.for 0 Depth (Sec.)	Depth From Res. (km)	C & GS Depth (km)	No. of Seismometers
3/14/68	020836.6	42.3N	66.5E	C. Kazakh	5.4	17	112.112	C	19m 25.8	1.5	1.7	8.0	X	1.2	28	33	3
3/13/68	233848.9	42.4N	66.5E	C. Kazakh	5.2	18	112.212	C	19m 25.1	1.5	1.0	2.6	X	1.9	42	33	3
8/11/68	011315.2	55.6N	162.1E	E. Kamchatka	5.3	53	112.216	C	19m 19.4	1.9	1.0	2.5	X	10.5	89	70	1
1/26/69	150532.7	55.8N	162.9E	E. Kamchatka	5.5	71	112.246		19m 26.2	1.9				3.9	25	16	2
1/22/69	001230.0	55.9N	163.0E	E. Kamchatka	5.5	87	112.371		19m 21.6	2.0			X	5.7	38	33	2
5/ 1/69	040008.7	44.0N	77.9E	E. Kazakh	4.9	25	113.350		19m 26.2	1.5				7.5	53	53	1
2/ 9/68	142253.9	45.6N	26.4E	Rumania	4.6	9	113.388	D	19m 17.8	1.6	0.9	3.0		15.9	124	122	3
10/20/68	241501.0	45.7N	26.6E	Rumania	4.6	52	113.535		19m 18.1	1.6	0.9	2.4	X	16.0	125	123	1
7/17/69	205501.3	61.0N	147.3W	C. Alaska	4.5	17	111.635		19m 43.5	2.2				3.3	21	20	1
11/16/69	195740.3	61.1N	147.5W	C. Alaska	4.4	28	111.717		19m 42.8	2.2				3.4	29	30	1
7/17/69	205137.5	61.1N	147.6W	C. Alaska	4.9	35	111.753		19m 33.1	2.2				4.1	27	31	1
9/26/69	063955.8	45.9N	42.5E	S.W. Russia	5.6	82	115.143		19m 38.2	1.6				.8	5	0	1
9/ 8/68	162258.6	61.8N	147.6W	C. Alaska	4.5	21	115.420		19m 37.8	2.2	1.0	3.1	X	1.1	9	12	1
9/ 5/68	085715.3	46.7N	82.2E	Kazakh-Sinkiang	4.7	11	115.691		19m 35.3	1.6	0.9	1.9	X	5.4	35	33	1
7/31/69	120644.5	61.9N	151.2W	C. Alaska	4.4	32	115.789		19m 32.1	2.2				6.2	38	33	1
9/13/68	215126.5	57.9N	32.1W	N. Atlantic	4.5	18	115.829		19m 36.1	2.0	0.8	1.1		1.2	28	33	4
9/20/69	005651.3	58.1N	32.2W	N. Atlantic	5.0	39	115.987		19m 37.9	2.0				3.1	20	33	1
9/20/69	011301.6	58.1N	32.1W	N. Atlantic	5.2	25	116.001		19m 37.9	2.0				3.3	21	33	1
9/20/69	010738.4	58.2N	32.1W	N. Atlantic	5.0	16	116.099		19m 37.6	2.0				3.8	25	33	1
9/20/69	032428.8*	58.3N	32.3W	N. Atlantic	4.1	8	116.161		19m 36.3	2.0				5.3	35	33	1
11/13/68	120339.9	58.3N	32.7W	N. Atlantic	4.6	21	116.165		19m 35.5	2.0			X	6.1	41	33	2
9/20/69	050857.6	58.3N	32.2W	N. Atlantic	5.6	72	116.178		19m 36.0	2.0				5.7	38	33	1
10/29/68	221615.6	65.1N	150.1W	Alaska	6.0	105	116.209		19m 39.8	2.2	2.0	760.0	X	1.7	11	7	1
9/19/69	205112.1*	58.4N	32.3W	N. Atlantic	4.5	12	116.256		19m 38.8	2.0				3.2	20	33	1
9/19/69	232159.1*	58.4N	32.3W	N. Atlantic	4.6	10	116.256		19m 36.9	2.0				5.1	31	33	1
9/20/69	002050.1*	58.4N	32.1W	N. Atlantic	4.4	10	116.290		19m 36.8	2.0				5.2	31	33	1
7/ 1/68	010201.7	17.9N	48.0E	W. Kazakh	5.5	62	117.195	C	19m 11.7	1.7	1.0	11.0	X	4.2	28	33	4
7/ 3/68	095527.0*	59.4N	30.4W	N. Atlantic	4.7	11	117.607	D	19m 40.1	2.1	2.0	10.0	X	5.5	37	33	1
10/28/69	001600.5*	68.2N	136.5W	N. Yukon	4.2	8	118.278		19m 11.0	2.2				4.8	32	33	1
4/ 6/69	192239.1	50.3N	91.2E	USSR-Mongolia	4.8	28	118.110		19m 11.3	1.8				5.3	35	31	3
7/12/68	120757.2	49.7N	78.1E	E. Kazakh	5.1	51	118.959	C	19m 17.1	1.7	0.8	18.0	X			0	4
									51.0	1.7			X	-.7	-1	0	4
12/18/68	050157.0	49.7N	78.1E	E. Kazakh	5.2	55	118.984	C	19m 51.0	1.7				-.7	-4	0	2
7/ 4/69	021657.0	49.7N	78.2E	E. Kazakh	5.3	70	119.006	C	19m 50.1	1.7				0	0	0	1
9/11/69	010157.1	49.7N	78.1E	E. Kazakh	5.0	28	119.013	C	19m 50.9	1.7				-.5	-3	0	1
9/ 5/68	010557.1	49.8N	78.1E	E. Kazakh	5.5	68	119.031	D	19m 46.0	1.7	0.8	1.0	X			0	1
								C	50.5	1.7	0.8	40.0		-.1	-1	0	1
9/29/68	031257.5	49.8N	78.2E	E. Kazakh	5.8	90	119.043		19m 46.5	1.7	1.5	8.4	X			0	1
									50.7	1.7	0.9	110.0	X	-.3	-2	0	4

Date	O.T Hr-Min-Sec	Lat.	Long.	Region	m_b	No Sta	Δ°	Compression Dilation	T.T. Min-Sec	ϵ_{ij} (Sec.)	Period (Sec.)	Amp. (m_μ)	Digi-tized	Res for 0 Depth (Sec.)	Depth From Res. (km)	C & GS Depth (km)	No. of Seismometers

Date	O.T Hr-Min-Sec	Lat.	Long.	Region	m_b	No. Sta.	Δ^o	Compression Dilation	T.T. Min-Sec	ϵ_{11} (Sec.)	Period (Sec.)	Amp. (m_μ)	Digi-tized	Res.for 0 Depth (Sec.)	Depth From Res. (km)	C & GS Depth (km)	No. of Seismometers
11/ 9/68	025337.7	19.8N	78.0E	E. Kazakh	4.9	28	149.065		19m 51.1	1.7				-.6	-4	0	2
4/24/68	103557.1	49.8N	78.1E	E. Kazakh	5.0	34	149.079	C	19m 51.1	1.7	1.0	15.0	X	-.5	-3	0	3
3/ 7/69	082657.5	49.8N	78.2E	E. Kazakh	5.5	67	149.079	C	19m 46.1	1.7						0	4
									50.8	1.7				-.2	-1	0	4
10/ 1/69	040257.6	49.8N	78.2E	E. Kazakh	5.3	59	149.106	C	19m 50.1	1.7				-.2	-1	0	1
5/16/69	040257.1	49.8N	78.1E	E. Kazakh	5.3	83	149.112	C	19m 50.6	1.7				0	0	0	1
6/11/69	030557.8	49.8N	78.2E	E. Kazakh	5.3	53	149.115		19m 50.6	1.7	1.0	10.0	X	0	0	0	4
6/19/68	030557.3	50.0N	79.1E	E. Kazakh	5.5	45	149.170		19m 46.8	1.7	1.0	2.6	X			0	4
									51.2	1.7	1.0	19.0	X	-.1	-2	0	4
7/23/69	024658.1	49.9N	78.3E	E. Kazakh	5.5	56	149.199	C	19m 50.3	1.7				.6	+4	0	1
8/20/68	040558.1	50.0N	78.0E	E. Kazakh	4.8	22	149.318		19m 50.9	1.7	0.6	3.0		.1	2	0	1
5/31/69	050156.6	50.0N	77.7E	E. Kazakh	5.1	50	149.337	C	19m 51.1	1.7				.1	2	0	1
10/30/68	121722.3	52.3N	95.8E	C. Russia	4.8	35	149.897		19m 46.1	1.8				6.9	48	33	1
7/21/68	014119.5	55.2N	113.3E	E. Baikal	5.1	35	150.158		19m 47.5	1.9	2.1	27.0	X	6.2	42	33	1
4/21/69	171831.2	61.9N	26.7W	Iceland	4.6	24	150.501		19m 49.8	2.2				1.6	30	33	1
8/31/68	180635.7	56.3N	115.6E	E. Baikal	4.6	19	150.791		19m 51.1	2.0	1.8	10.0	X	4.3	28	25	1
11/26/68	183151.8	55.9N	111.4E	L. Baikal	5.1	56	151.091		19m 55.6	2.0			X	.7	8	1	2
12/ 5/68	094411.0	63.9N	21.7W	Iceland	5.5	99	153.340		19m 53.1	2.2			X			5	2
									20m 13.8	2.2			X			5	2
9/ 9/68	022057.9	66.1N	142.1E	E.Siberia	5.1	47	155.400	D	19m 57.6	2.2	1.2	4.0	X			33	1
5/ 5/69	214731.7	66.8N	18.2W	Iceland	5.2	52	156.470		20m 22.3	2.2						33	1
9/ 2/69	045957.1	57.4N	51.9E	W. Russia	4.9	31	157.215		20m 25.6	2.0						0	1
9/ 8/69	045956.1	57.4N	55.1E	Ural Mts.	4.9	27	157.220		20m 27.9	2.0						0	1
3/ 7/68	072742.7	71.6N	3.5W	Jan Mayen	4.9	28	163.299	D	20m 50.9	2.4	2.0	1.0				33	3
3/ 7/68	072106.5	71.7N	3.1W	Jan Mayen	4.6	27	163.452		21m 08.6	2.3	1.0	1.2				26	3
4/ 7/69	202629.9	76.5N	130.8E	Laptev Sea	5.5	82	166 113		19m 59.0	2.1						33	1
									21m 2.9	2.1						33	1
8/22/69	191056.1	76.9N	120.8E	Laptev Sea	4.6	20	166.471		21m 5.9	2.1						33	1
8/19/69	022655.1	74.4N	10.1E	Norwegian Sea	4.5	11	167.860		21m 9.6	2.1						33	1
12/30/68	102709.7	76.2N	7.5E	Svalbard	5.0	11	168.858		20m 9.7	2.1			X			33	2
									21m 27.0	2.1			X			33	2
4/ 7/68	051621.9	81.5N	3.9W	N.Svalbard	5.3	53	169.995	C	21m 20.2	2.1	0.8	1.3	X			34	3
10/11/69	070006.2	73.4N	54.8E	Novaya Zemlya	6.1	127	173.211		20m 6.8	2.1						0	1
							173.229		21m 38.8	2.1						0	1
11/ 7/68	100205.3	73.4N	54.9E	Novaya Zemlya	6.0	131	173.237		20m 7.4	2.1	1.0	22.0	X			0	4
									21m 39.0	2.1	1.0	38.0	X			0	1

Date	O.T Hr-Min-Sec	Lat.	Long.	Region	m_b	No. Sta.	Δ^o	Compression/ Dilation	T.T. Min-Sec	ϵ_{11} (Sec.)	Period (Sec.)	Amp. (m_μ)	Digi-tized	Res.for 0 Depth (Sec.)	Depth From Res. (km)	C & GS Depth (km)	No. of Seismometers

LONG PERIOD ARRAY PROCESSING DEVELOPMENT PROGRAM

By
T. Harley

The Long Period Array Processing Development program consists of two phases; a software development effort, which has been completed, and a long period array evaluation effort, which currently is in progress for the Alaskan Long Period Array (ALPA) and will be conducted for the Norwegian Long Period Array (NORSAR) beginning later this year. This presentation reviews the processing capability available at SAAC and discusses preliminary results from ALPA evaluation.

During software development an on-line data acquisition and display package and an off-line evaluation package were written. A simplified flow diagram of the ALPA on-line package is shown in Figure 2. This package, developed by Texas Instruments, has been operating at SAAC since 13 February 1970. Its primary functions are data acquisition, on-line beamforming and data display (on develocorders). Raw data, beams and status information are written on 9-track 1600 bpi library tapes for permanent retention at SAAC. Twenty-eight beams are currently being formed; one vertical straight summation, three 3-component S wave beams and six 3-component surface wave beams steered to areas of interest. All beams are rotated to a V, T, R orientation. The beams can be redeployed if desired.

Up to 18 data channels can be displayed on the two develocorders at SAAC. Any combination of the 57 raw data channels (in the triax orientation or rotated to V, E, N) and the 28 beams can be displayed. Channels to be displayed can be changed if desired.

On about 1 October 1970 the on-line data acquisition will expand as shown in Figure 3. The major difference in this system is that a long period library tape which contains data from ALPA, LASA (including microbarograph data) and NORSAR will be generated. The ALPA part of the system will perform the same functions that currently are being executed, the LASA part of the system will perform functions similar to those for ALPA, the NORSAR part of the system will record raw data only. NORSAR data may not be continuous, depending on how the Trans-Atlantic link is utilized. Both ALPA and LASA data will be displayed on the SAAC develocorders. This system is being developed by IBM, and uses a special purpose computer (SPS) in tandem with one of the SAAC S360/40's to perform the data acquisition, processing and display

The off-line processing system, developed by Texas Instruments, is capable of processing data from all three arrays. The software is designed so that many events can be processed on a given run. The analyst has control of the functions performed and can make processing decisions after the execution of any of the programs.

Figure 5 shows the general flow of the off-line package. The package consists of 13 programs; six mainline programs, 3 analysis programs and 4 utility programs. The basic functions performed by each program are shown in Figure 6. The mainline programs can be further subdivided into event selection and preparation (SELECT and QCEDIT), multi-channel processing (NOISE, MCFGEN, TDFILT) and single

channel processing and analysis (BEAMAN). All processing is by component (i.e., vertical from all sites, etc.), but output beams can be combined for additional signal enhancement in the program BEAMAN.

Note that all important intermediate outputs from the off-line package are saved on magnetic tape. This allows the analyst to recycle his processing for a given event with a minimum of effort and provides easily accessible input to the analysis programs (NOISAN and SIGNAN).

The off-line package was used to process a suite of ten events from the Southwestern United States $\Delta \sim 30°$ Azimuth ~130°). The events are listed in Figure 7. During the period covered nine ALPA sites were operational (designated by triangles in Figure 8), however only four or five of these sites could be used for processing. Figure 9 summarizes the processing that was performed for these events.

Of the ten events used six had identifiable surface wave arrivals at ALPA. For two of the four events missed body wave magnitudes were not assigned by USC&GS, the other two events had m_b values of 3.5 and 4.1. It is emphasized that the data presented here are very preliminary in nature and involve just 4 or 5 sites (the full array will have 19 sites). Thus these results should not be interpreted as a measure of ALPA's detection capability.

Figures 10 and 11 show average noise spectra at ALPA on three different days. Note that the horizontals have been rotated to an orientation transverse and radial to the direction of the single associated with these noise samples, so that the sensitive axis are not north and east. Two observations can be made from these spectra:

The "18-second" peak is quite variable with time.
The long period (50 second) noise level is quite high, and tends to be higher on the horizontals than on the vertical (the spectra are not corrected for system response).

The long period noise level is much lower (15 to 20 db) for these samples than it was in January and February of 1970, however it is still significant. It is variable from site to site, with sites 3-34, 2-2 and 1-1 having the highest levels. An explanation for the source of the noise has yet to be found.

Figure 12 shows the multiple coherences for four noise samples, using site 3-3 as reference. Note that the minimum separation of the sensors from site 3-3 was 35 km. The basic ALPA spacing is 20 km, so that higher coherences would be expected when close-in sensors are available. Later processing gave the expected higher coherences.

Figure 13 summarizes the results of Wiener filtering. The filters were designed using 4096 seconds of measured noise data and theoretical Rayleigh wave signal models. Noise data were equalized, 1% white noise was added prior to design, and a SNR of 4 was used. The filters gave 9 to 10 db noise rejection at the microseismic peak (design noise) and did not attenuate the signals, so that SNR improvement was the same as noise rejection. Wavenumber spectral analysis showed that

noise propagates from roughly the same direction as the signal azimuth so the MCF performance should be relatively poor for these events. A SNR improvement of 17 db was obtained for a North Atlantic ridge event (Azimuth = 42.7°), and similar results were obtained for later events from "off-noise" azimuths.

Figure 14 shows A/T values measured from the seismograms at 25 and 40 seconds respectively for the four largest events. A/T values at 25 seconds were 7 to 8 db higher than those at 40 seconds. However, unless the long period (40 + second) noise level can be reduced, utilization of long period signal data at ALPA does not appear promising.

Figures 15 to 18 summarize the results of matched filtering. First Handley was taken as a master waveform and matched against itself, and the results were compared with chirp filters (specified in the frequency domain) applied to Handley. The Handley spectrum was scaled so that the matched filter RMS noise was unchanged; thus the SNR improvement achieved could be measured by taking the ratio of the matched filter peak to the peak signal in the output beam. Two different bandpasses were used; .02 to .075 Hz and .025 to .05 Hz. It can be seen that the chirps gave 3 to 5 db less SNR improvement, probably because the NTS-ALPA travel path is complicated and the surface wave arrivals appear to be multipathed.

Handley was then applied to two other NTS events that were clearly visible on the surface wave beams. SNR improvement was very good (7 to 8 db) for the Rayleigh wave, but relatively poor for the Love wave. Since explosion-generated Love waves should be medium dependent the poorer results are not surprising. Figure 16 shows the vertical Rayleigh wave and matched filter output (using Handley) for one of the events (NTS02).

NTS02 and NTS05 were used to obtain a conversion factor from matched filter amplitude to trace amplitude. This factor was used to estimate magnitudes for two events which could not be seen on the Rayleigh wave beams, but could be picked from the matched filter outputs (Figure 17). NTS05 was especially weak; Figure 18 shows the matched filter outputs for both the vertical and radial components at two different bandpasses. The fact that a small peak occurs on all four outputs at the expected time for the signal gives the analyst confidence that it is a valid signal peak.

Figure 19 shows the M_S - m_b values for the six events detected. No conclusions can be drawn from this small sample, except to say that the data are not surprising.

Figure 1.

LONG PERIOD ARRAY PROCESSING
DEVELOPMENT PROGRAM

PURPOSES

- DEVELOP A GENERAL LONG PERIOD ARRAY PROCESSING SYSTEM AT SAAC.
- DETERMINE DETECTION AND DISCRIMINATION CAPABILITIES OF ALPA AND NORSAR LONG PERIOD ARRAYS.

SOFTWARE PACKAGES

- ON-LINE DATA ACQUISITION AND DISPLAY
  - ALPA INTERIM SYSTEM
  - THREE ARRAY SYSTEM
- OFF-LINE DATA PROCESSING AND EVALUATION

PRELIMINARY RESULTS FOR ALPA

Figure 2.

ALPA ON-LINE SYSTEM

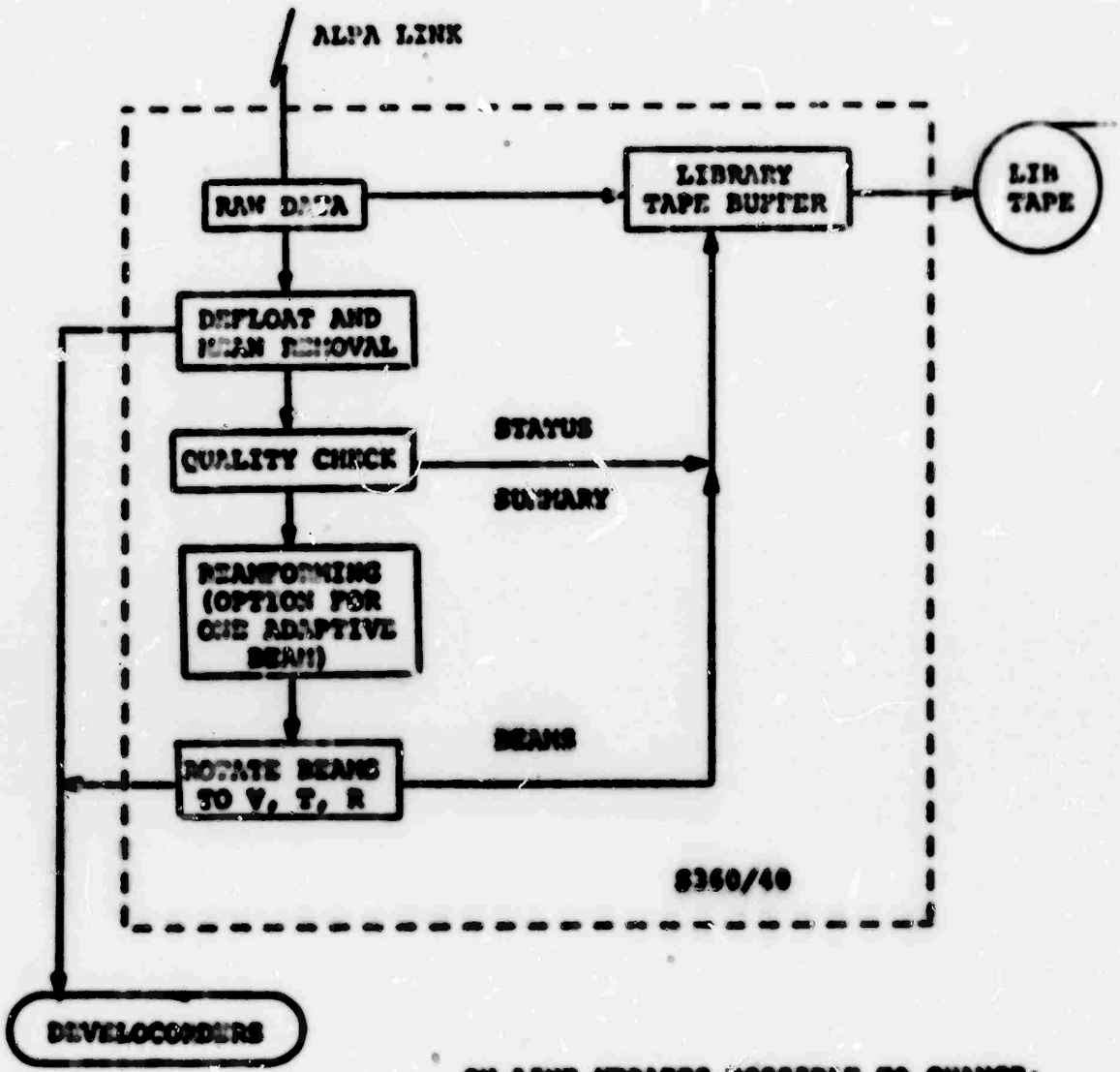

ON-LINE UPDATES POSSIBLE TO CHANGE:

- BIT SELECTION FOR PROCESSING
- QUALITY CHECK PARAMETERS
- BEAM DEPLOYMENT
- CHANNEL SELECTION FOR DEVELOCORDERS

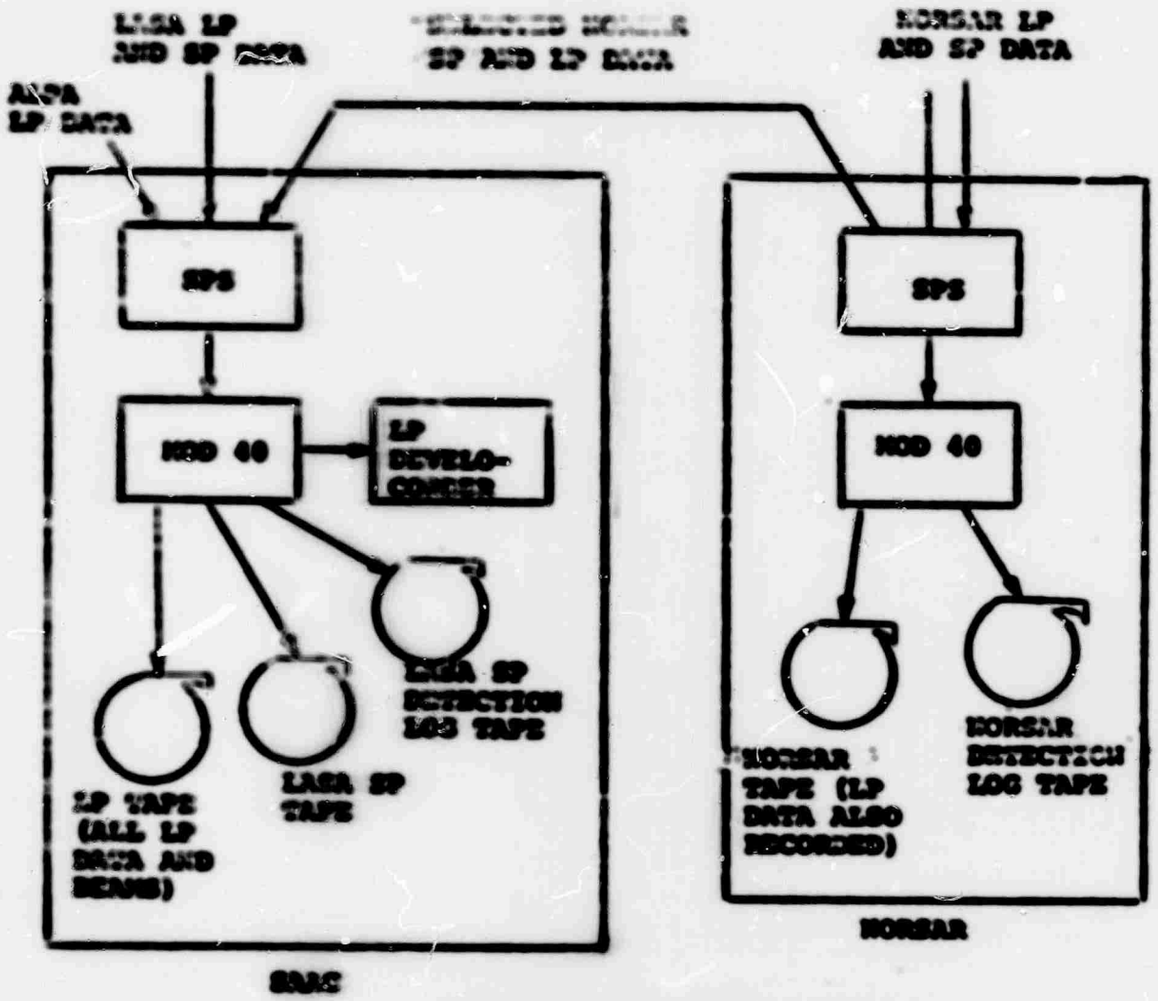

THREE ARRAY CM-LINE SYSTEM

Figure 3.

Figure 4.

OFF-LINE PACKAGE DESIGN APPROACH

- CAPABLE OF PROCESSING DATA FROM ALL THREE LONG-PERIOD ARRAYS
- BATCH PROCESSING OF EVENTS
- STEP-WISE PROCESSING WHICH IS ANALYST CONTROLLED
- IMPORTANT DATA WILL BE SAVED ON TAPE (CPS MATRICES, BEST BEAMS, SPECTRA, ETC.)

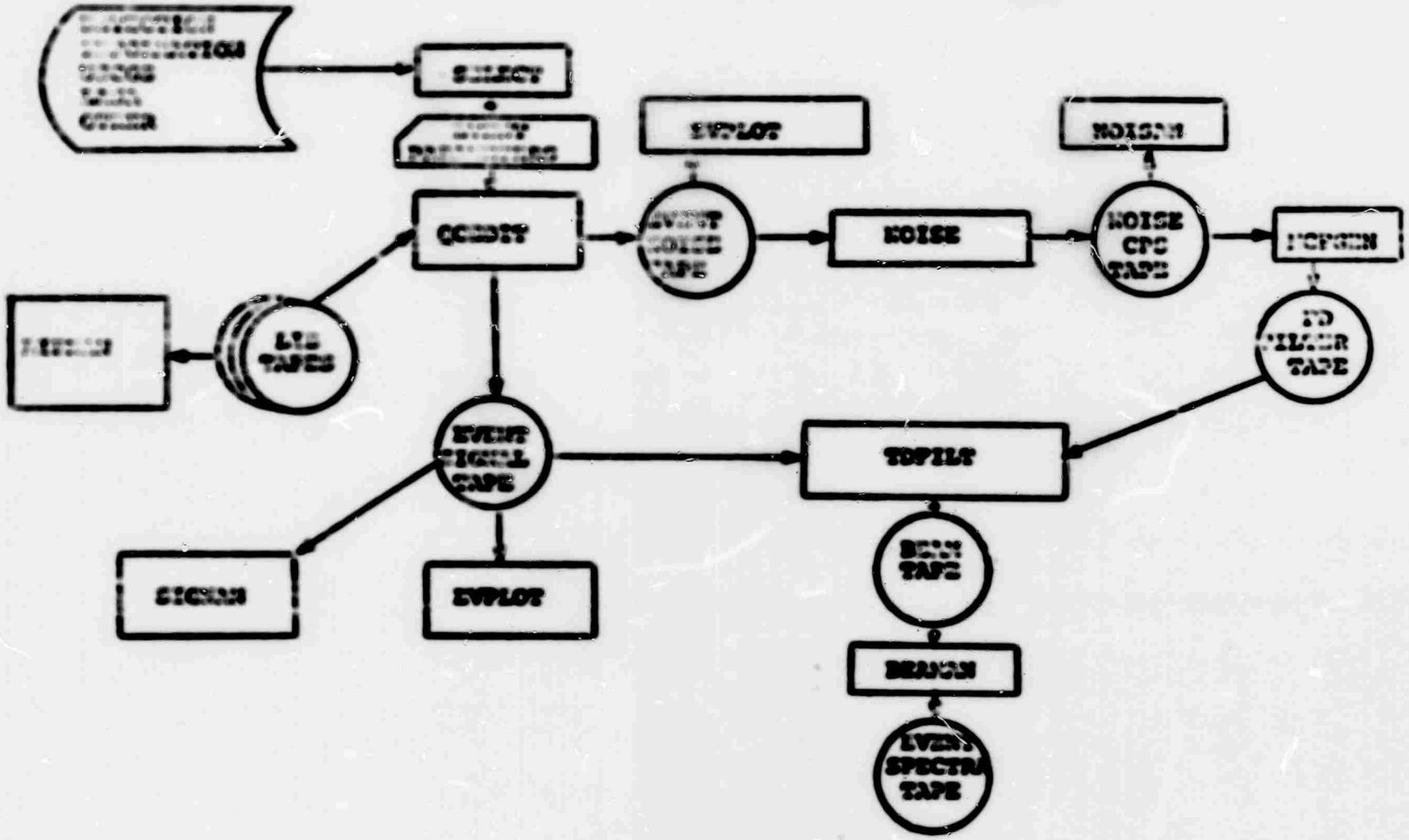

OFF-LINE PACKAGE
GENERAL FLOW
Figure 5.

Figure 6.

OFF-LINE PACKAGE PROGRAM SUMMARY

MAINLINE PROGRAMS

PROGRAMS	FUNCTION
SELECT	Calculate Event Parameters
QCEDIT	Edit and Quality Check Signal and Noise Data
NOISE	Generate Frequency Domain Cross Power Spectral Matrix
MCFGEN	Generate Frequency Domain Multichannel Filters
TDFILT	Inverse Transform Filters and Apply to Partitioned Time Domain Signal Data
REAMAN	Perform Single Channel Processing and Analyze Signal Data

ANALYSIS PROGRAMS

PROGRAMS	FUNCTION
LIBNAN	Access Library Tapes and Perform Spectral and Coherency Analysis (Signal or Noise)
NOISAN	Compute Power Spectra, Coherences and f-k Spectra (Signal or Noise)
SIGNAN	Analyze Signal Characteristics Across the Array

UTILITY PROGRAMS

PROGRAMS	FUNCTION
EVPLOT	Plot Time Domain Signal or Noise Data
DUMPLIB	Dump Contents of Library Tape
DUMPXXX	Dump Contents of Any Off-Line Tape
TAPE MERGE/COPY	Collect and Copy Information from Off-Line Tapes

Figure 7.

EVENTS PROCESSED

DATE	ORIGIN TIME	DELTA	AZIMUTH	m_b	DESIGNATION
20 MARCH	19:00:00.0	33.3	130.9	6.5	WTS03
21 MAY	11:16:22.0	33.7	121.8	-	S001
21 MAY	14:00:05.5	33.4	130.9	5.5	WTS04
21 MAY	14:15:00.1	33.0	131.1	5.1	WTS05
23 MAY	22:55:24.0	34.1	125.5	4.6	S003
23 MAY	08:55:12.3	34.7	114.7	4.1	S002
24 MAY	02:09:53.7	34.0	125.6	-	S004
25 MAY	14:16:05.5	33.4	131.4	5.0	WTS01
26 MAY	15:00:01.0	33.4	131.4	5.6	WTS02
7 JUNE	04:12:12.0	27.4	142.1	5.0	S005

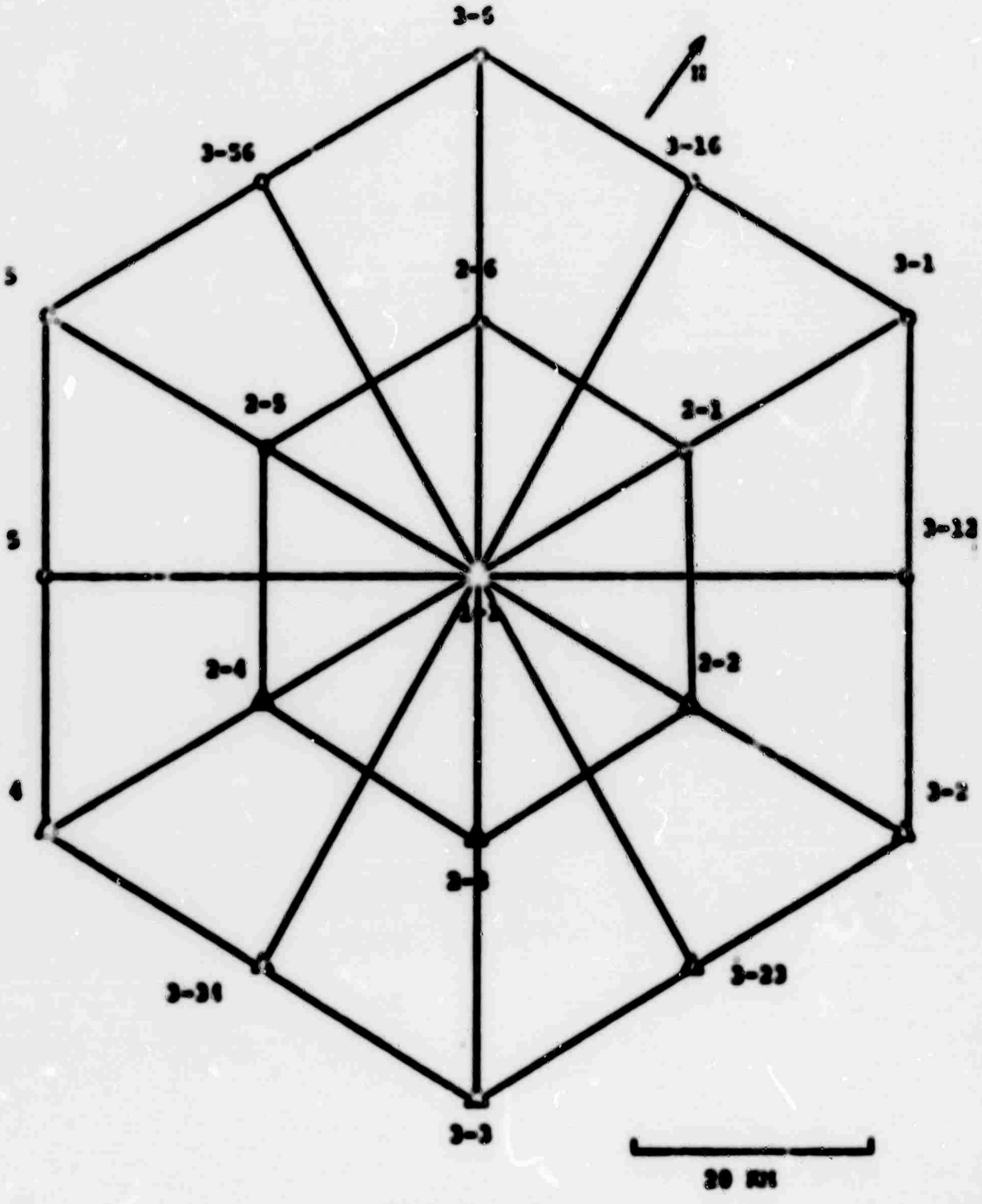

ALPA GEOMETRY

Figure 8.

Figure 9.

PROCESSING SEQUENCE

- EDIT AND QUALITY CHECK SIGNAL AND NOISE DATA
- CROSSFEED NOISE CUTS (STACK 16 256-SECOND RECORDS)
- DESIGN P, S LOVE AND REVERSED WAVE WIENER OCF'S (S/N = 4.0, 10 WHITE NOISE, 5 CROSSFEED) AND FOR CORRESPONDING BEAMS
- MEASURE SNR IMPROVEMENT (DESIGN NOISE) FOR OCF'S AND BEAMS
- COMPUTE HIGH RESOLUTION f-k SPECTRA, MULTIPLE COHERENCES OF NOISE
- APPLY MATCHED FILTERS (CHIRP AND MASTER WAVEFORM)
- CALCULATE M_b

Figure 10.

AVERAGE ALPA NOISE SPECTRA

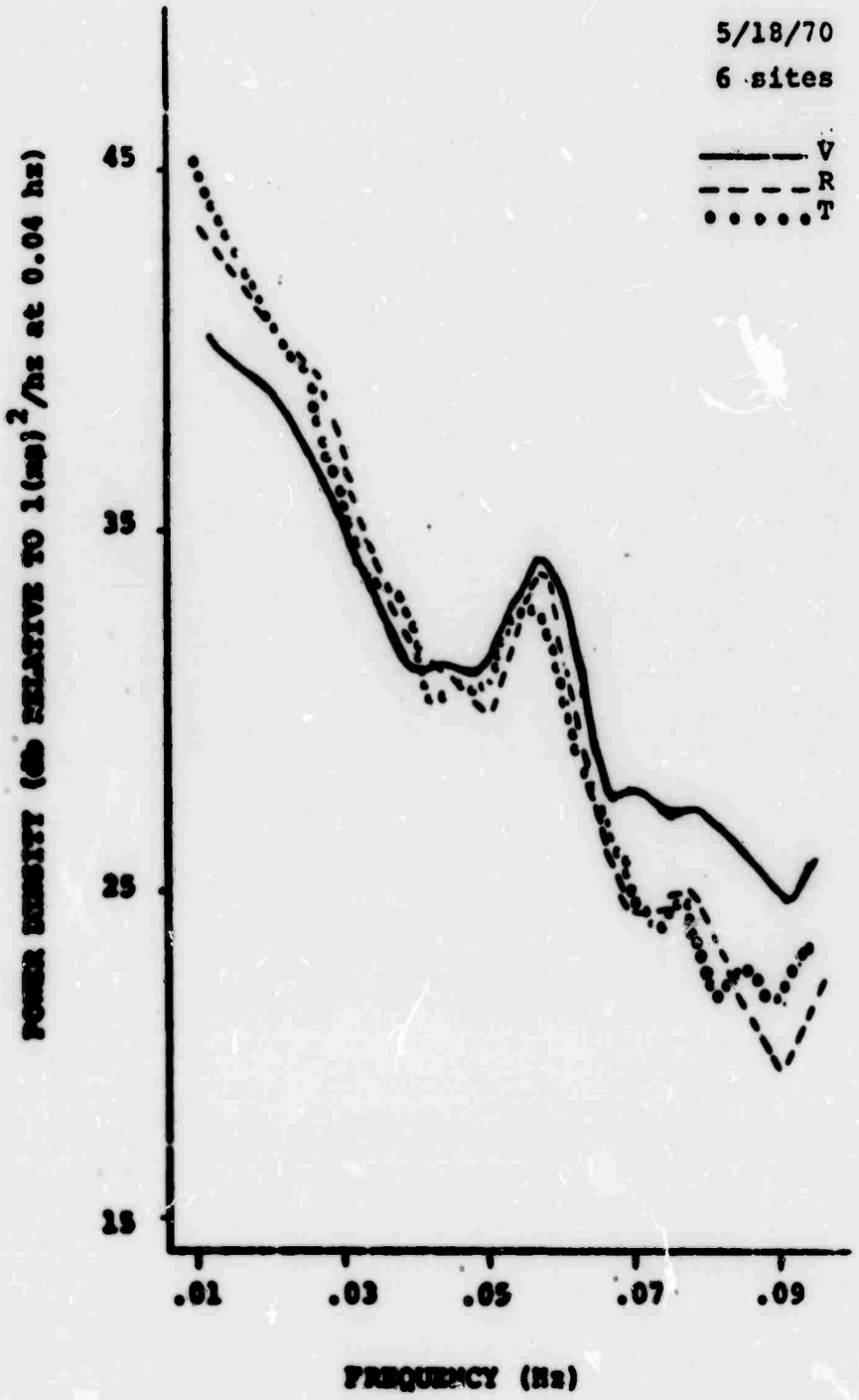

Figure 11

AVERAGE ALPA NOISE SPECTRA

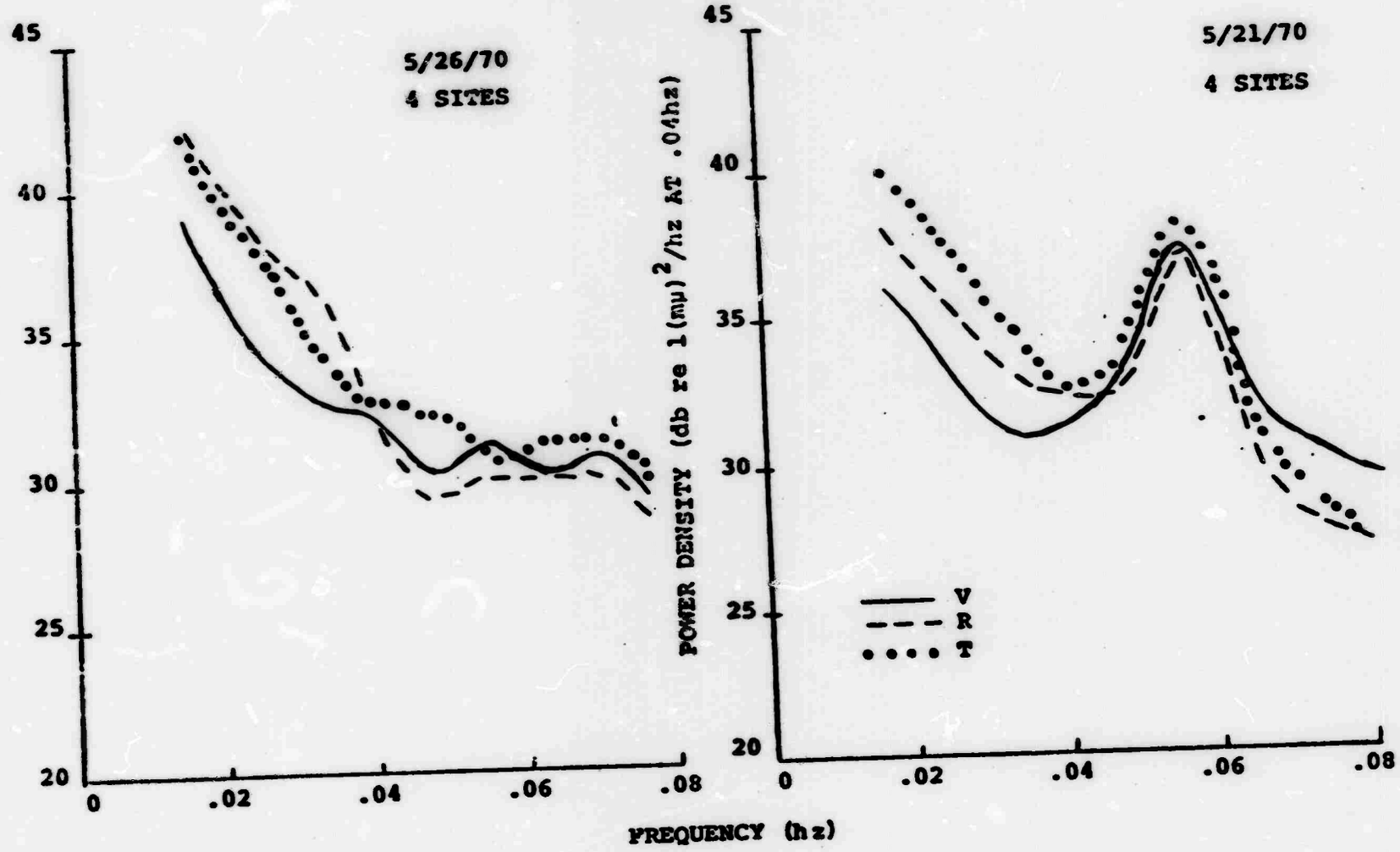

MULTIPLE COHERENCE VALUES

ALPA NOISE

NOISE STATION	CHANNEL PREDICTED	NO CHANNEL USED	MINIMUM SPACING (KM)	VERTICAL COH	VERTICAL PER	RADIAL COH	RADIAL PER	TRANSVERSE COH.	TRANSVERSE PER
5/21/70	3-3	4	35	.85	18	.84	18	.83	18
5/23/70	3-3	4	35	.92	16	.88	16	.84	16
5/24/70	3-3	4	35	.86	16	.80	16	.82	16
5/26/70	3-3	3	35	.82	14	.81	14	.74	14

Figure 12

Figure 13.

[illegible]

- [illegible] AT MICROSEISMIC [illegible] WAS 9 TO 10 DB (4 OR 5 SITES) FOR VERTICAL [illegible] SIGNAL [illegible] ($\sqrt{N}$ GIVES 6 TO 7 DB)

- [illegible] THIS IS CLOSE TO A [illegible] f-k [illegible] THAT NOISE [illegible] THE [illegible] (i.e., CLOSE TO SIGNAL [illegible])

- [illegible] FOR AN EVENT FROM THE NORTH ATLANTIC RIDGE (Δ = 42.7) WAS 17 DB VERSUS 12 DB FOR [illegible] (6 [illegible])

Figure 18.

A/T VALUES AT 25 AND 40 [illegible]

[illegible] NO.	A/T (25) ([illegible])	A/T (40) ([illegible])	RATIO ([illegible])
[illegible]	6.50	2.45	8.5
[illegible]	492.0	315.0	7.2
[illegible]	2.05	0.85	7.3
[illegible]	46.0	39.6	7.5

[illegible] FILTERING RESULTS

EVENT	CORRELATION (DB)					
	VERTICAL		RADIAL		TRANSVERSE	
	.02-.075 Hz	.025-.05 Hz	.02-.075 Hz	.025-.05 Hz	.02-.075 Hz	.025-.05 Hz
[illegible] (NV)	9.8	6.6	9.6	6.5	9.4	6.8
[illegible] (CB)	4.9	3.0	4.7	2.9	6.0	3.0
[illegible] (NM)	7.3	5.1	8.4	5.8	4.2	5.3
[illegible] (NM)	7.2	[illegible].8	8.0	6.2	1.7	3.7

NOTE: HANDLEY WAS USED AS MASTER WAVEFORM. TWO EVENTS NOT VISIBLE ON VERTICAL RAYLEIGH WAVE SCAN COULD BE IDENTIFIED AFTER MATCHED FILTERING WITH HANDLEY (INCLUDING ONE 4° EAST OF THE HANDLEY EPICENTER

Figure 15.

Figure 16.

[illegible] VERTICAL RAYLEIGH WAVE

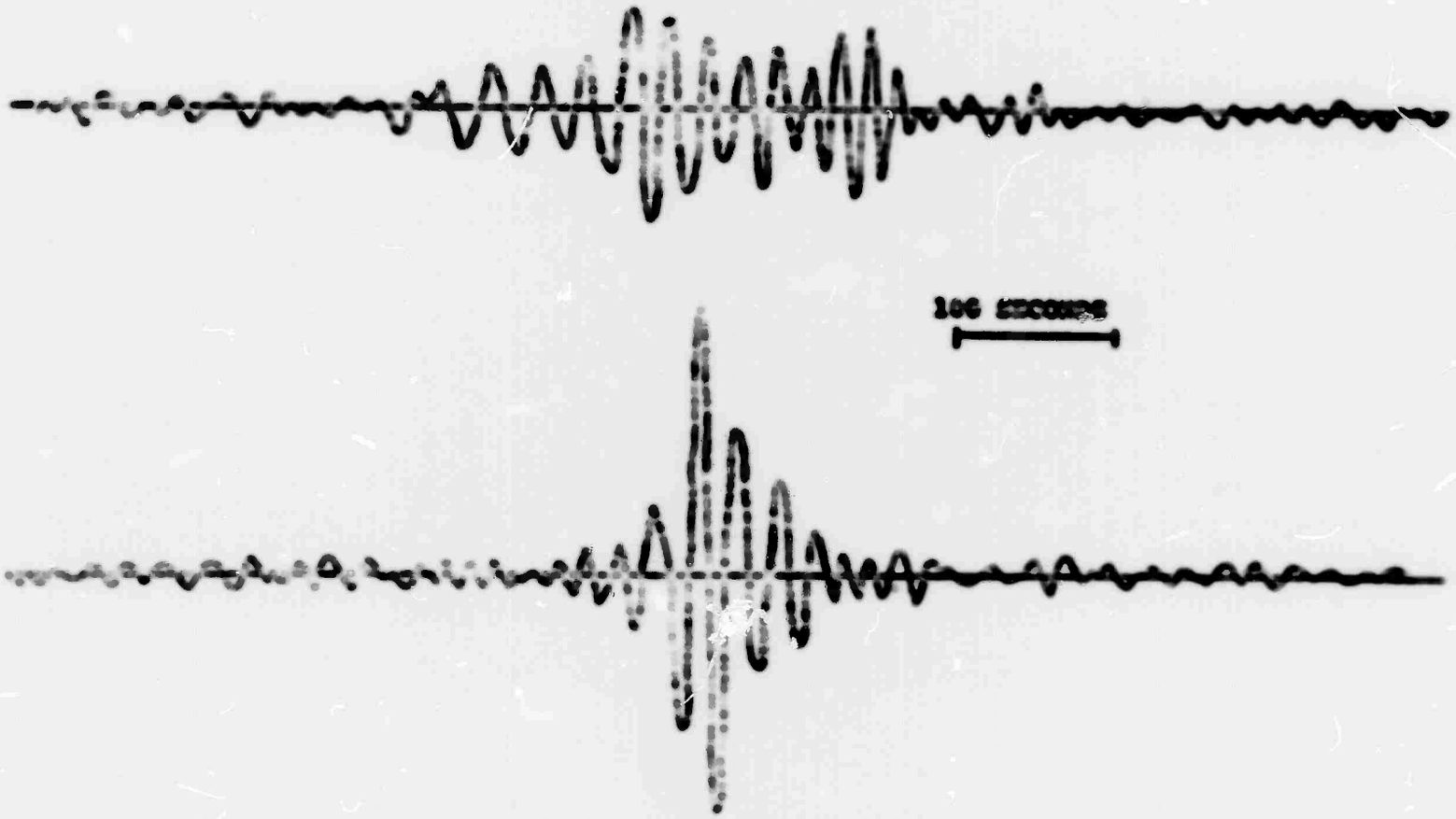

[illegible] ANGLE [illegible]

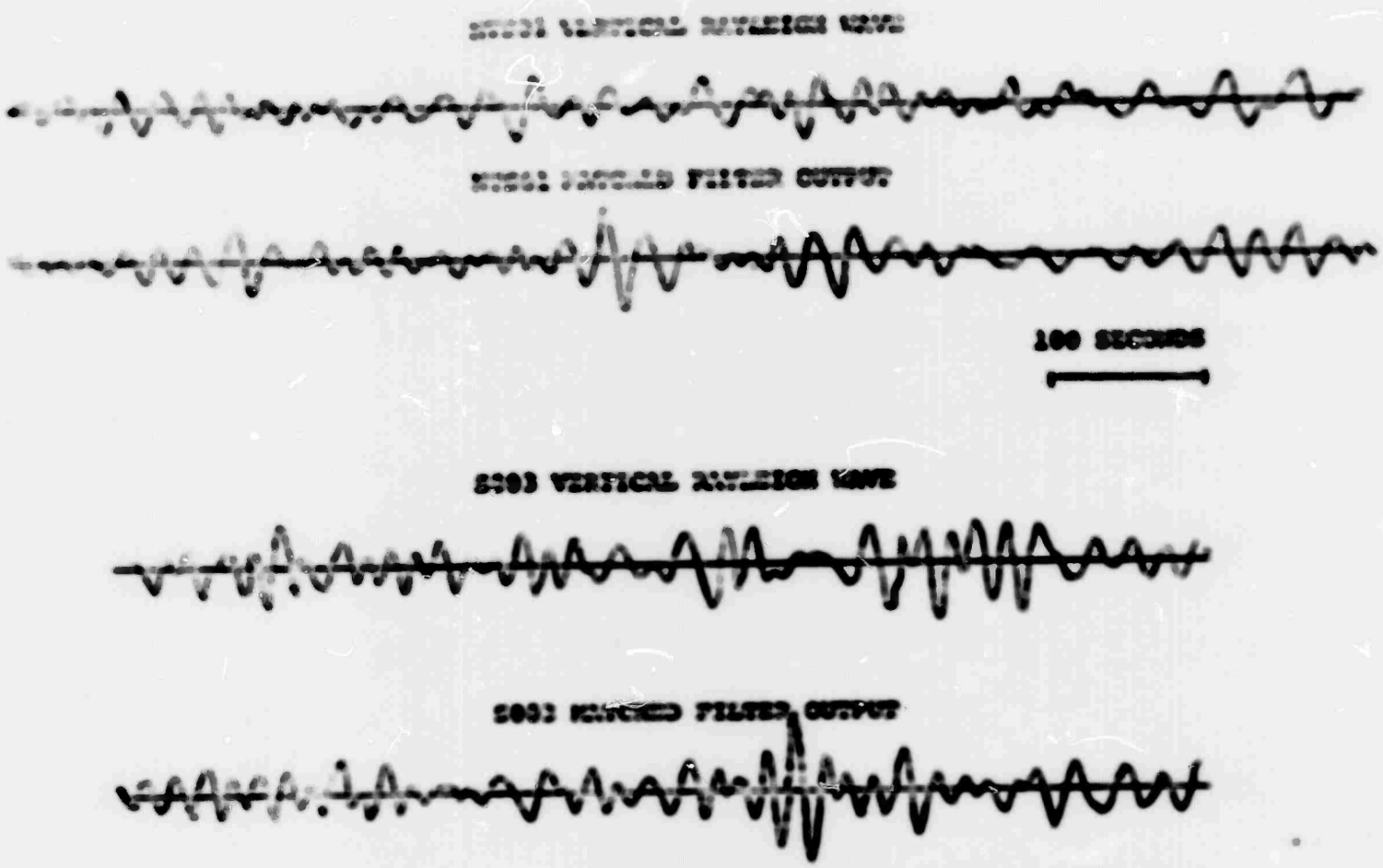

Figure 17.

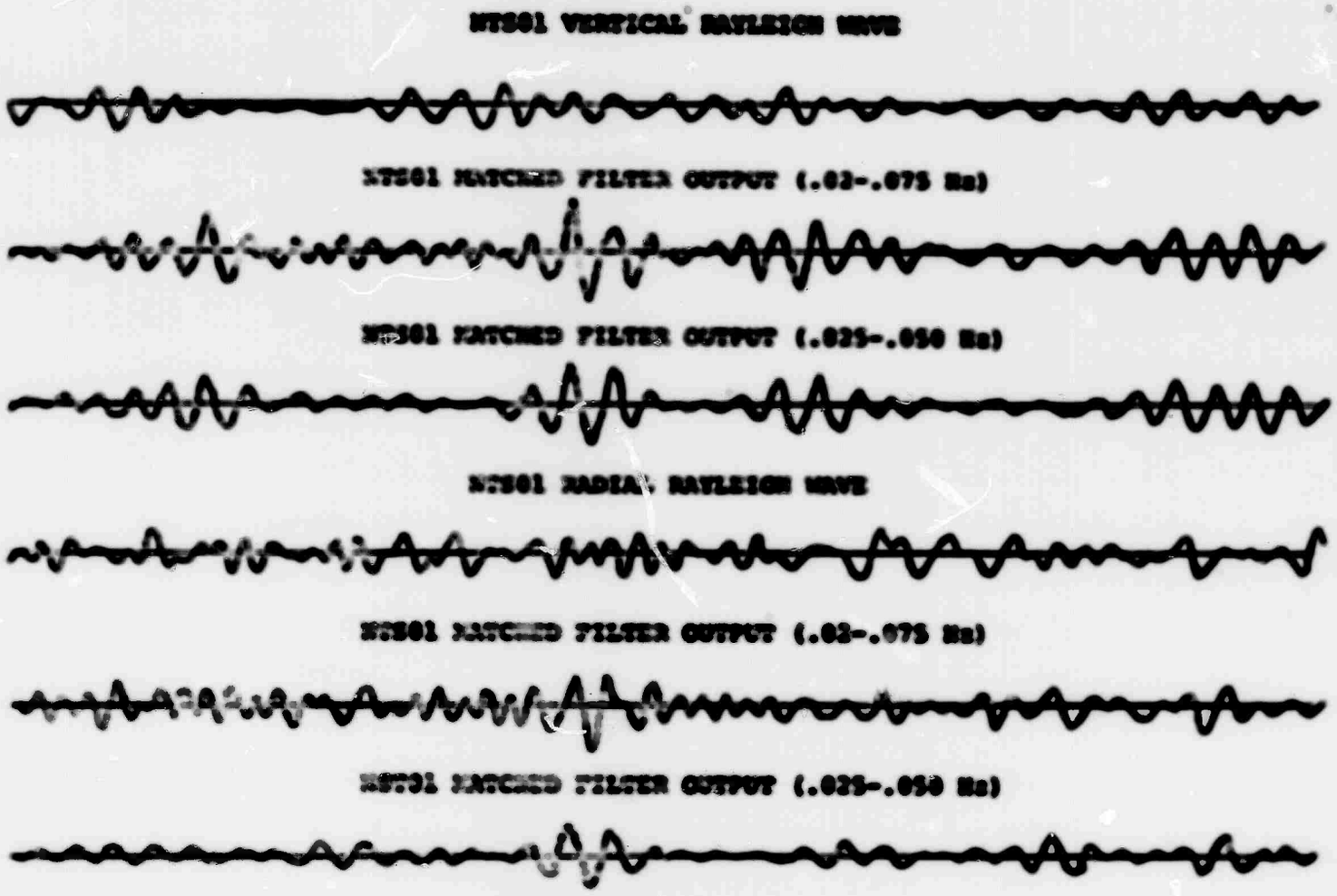
NTS01 VERTICAL RAYLEIGH WAVE
NTS01 MATCHED FILTER OUTPUT (.02-.075 Hz)
NTS01 MATCHED FILTER OUTPUT (.025-.050 Hz)
NTS01 RADIAL RAYLEIGH WAVE
NTS01 MATCHED FILTER OUTPUT (.02-.075 Hz)
NTS01 MATCHED FILTER OUTPUT (.025-.050 Hz)

Figure 15.

Figure 19.

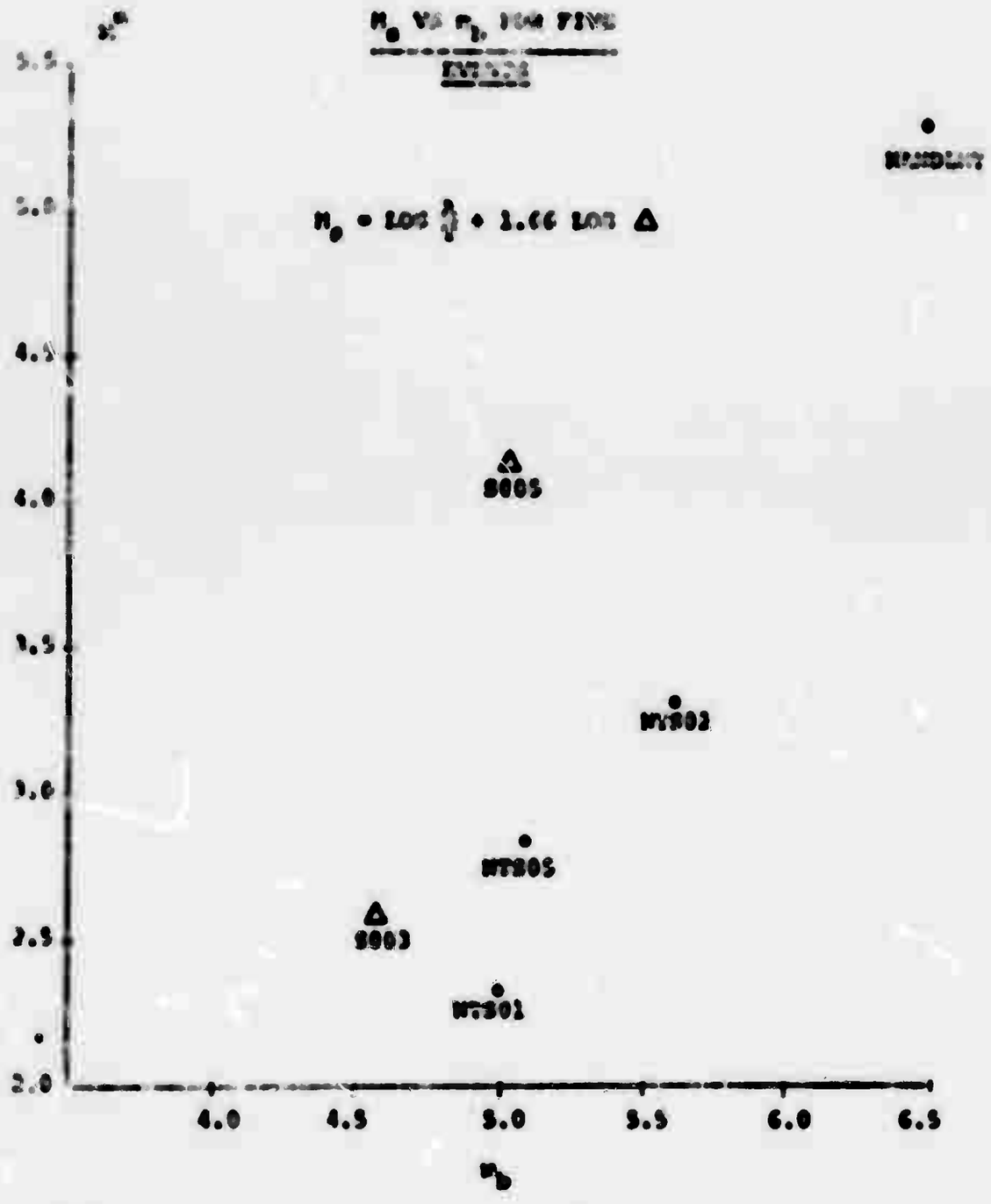

LONG PERIOD EXPERIMENT PROGRAM

By

T. Harley

BLANK PAGE

The Long Period Experiment Program consists of two phases; a software development effort and an evaluation effort. The software development effort currently is in progress; this presentation reviews the program design and processing capabilities that will be available at SAAC.

Figures 2 and 3 show the general data flow. The programming can be divided into four parts:

Data merge and display
Event selection and display
Single station processing and analysis
Multiple station processing and analysis

The functions performed by each part of the programming are summarized in Figures 4 to 7.

Data merge and display generates a composite library tape (9-track 1600 bpi) which contains data from all stations. All velocity data are stored on one set of tapes (at a 2-second sample rate), all displacement data on a second set of library tapes (at the field tape sample rate-expected to be 5 seconds). These tapes will be retained permanently in the SAAC library and can be duplicated for outside users on request.

The library tapes then are reformatted to 7-track 556 bpi tapes for input to the Texas Instruments playback system in Dallas, where 16mm films of the network data are generated (both the velocity and displacement data). The film format is:

Verticals from all stations on one film
N-S's from all stations on a second film
E-W's from all stations on a third film

GMT is of course encoded on the films. The 7-track 556 bpi input tapes will not generally be saved, but can be duplicated on request. Copies of the film also could be made available.

Using detection information from the USC&GS and other sources and the results of film analysis events are selected for processing. The event selection parameters (e.g., edit time, duration) are calculated and the velocity data for specified events are edited onto a processing tape. Noise data from the vicinity of the event can be included in the edit. During the edit the data are quality checked and bad data are deleted. Events can be Calcomp plotted and reformatted from the 9-track 1600 bpi processing tapes to 7-track 556 bpi tapes for film playback. Both of these tapes and the film can be duplicated on request.

Events then are input to the single station processing and analysis section of the programming. The software is designed so that any or all stations can be processed for a given event, and several events can be processed on a given run. The output from this section of the programming provides the basic data for evaluation.

This section consists of three program packages. The first (LXGEN) performs noise analysis (spectra and coherences) and performs multi-component processing for Rayleigh wave signal enhancement. The second program (LXTRAN) performs single channel processing (matched filtering and bandpass filtering), spectral analysis of the phase arrivals, and can compute discriminants such as AR, AL and long period spectral ratios. Either chirp or master waveform matched filtering (or both) can be performed. The third program (LXGRP) uses a high resolution running-gate spectral estimate technique to estimate group velocities and to search for higher order modes in the surface wave arrival (by identifying secondary peaks in the spectrum). This program would be used primarily for large events. Plots of all data generated (both frequency and time domain information) can be made at the discretion of the analyst. The output data will provide the basis for interpretation and for specifying the multiple station processing and analysis to be done.

The multiple station processing and analysis is not yet fully defined, but will consist of several programs which perform two types of functions. The first type utilizes data from several stations for a given event. Examples include stacking matched filter outputs from several stations to improve the signal-to-noise ratio for weak events and spectral analysis of surface wave data for source characterization (Tsai's Method). The second type will collect data from several events for a given station (or stations). Examples include analysis of noise variability with time and a definition of signal characteristics (spectral content) by region. Finally, all data will be combined to define the network detection threshold.

Figure 1

LONG PERIOD EXPERIMENT SYSTEM

PURPOSES

- BLOCK STATION DATA TO OBTAIN LIBRARY TAPE FOR PROCESSING RESTRICTED
- OBTAIN 16mm FILM DISPLAY OF ALL LPE DATA
- DETERMINE DETECTION AND DISCRIMINATION CAPABILITIES OF LP NETWORK

SOFTWARE PACKAGES

- DATA PLOT AND DISPLAY
- DATA EDIT
- SINGLE STATION PROCESSING AND ANALYSIS
- MULTIPLE STATION PROCESSING AND ANALYSIS

DATA AVAILABILITY

- TAPES
- FILM

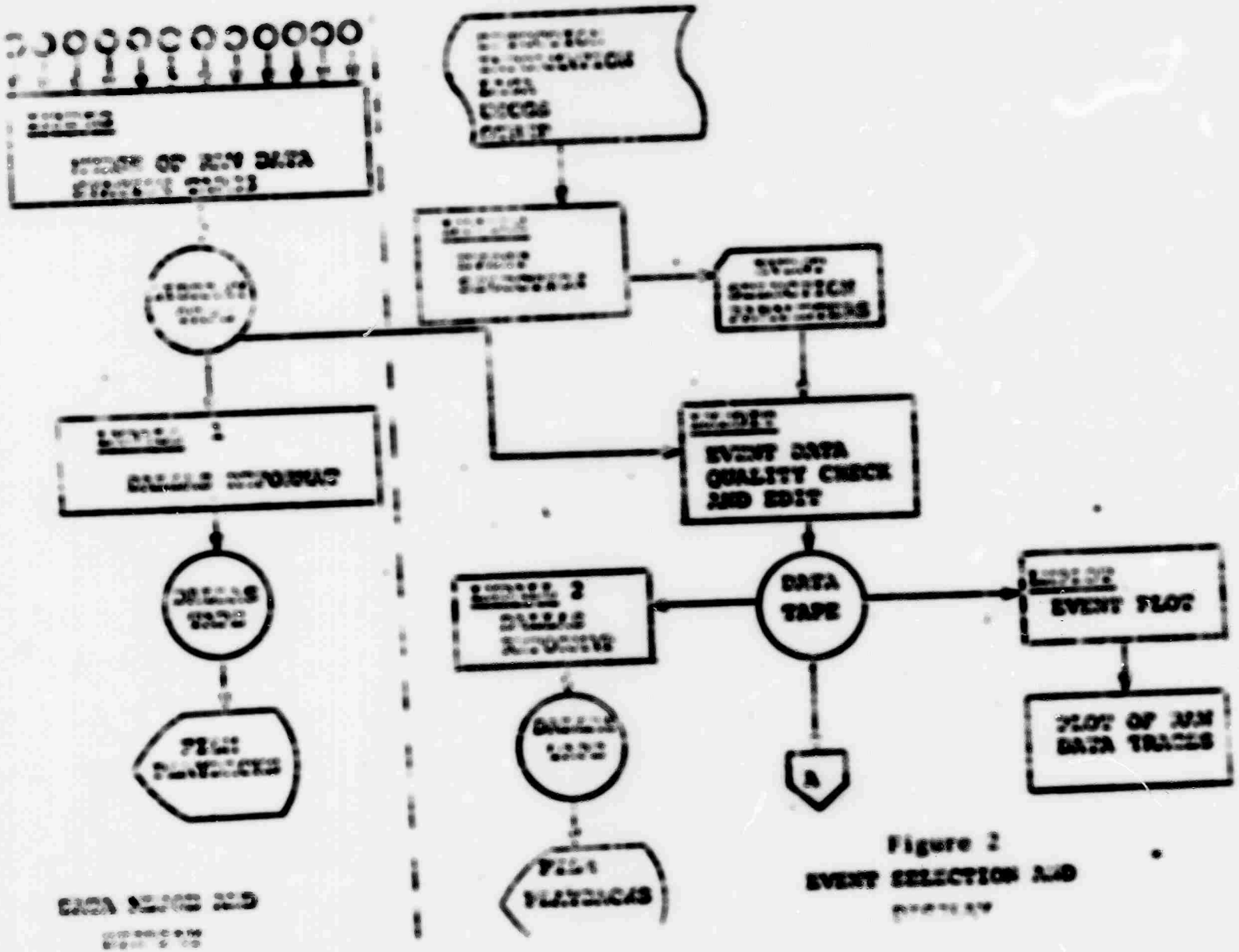

Figure 2
EVENT SELECTION AND

Figure 5

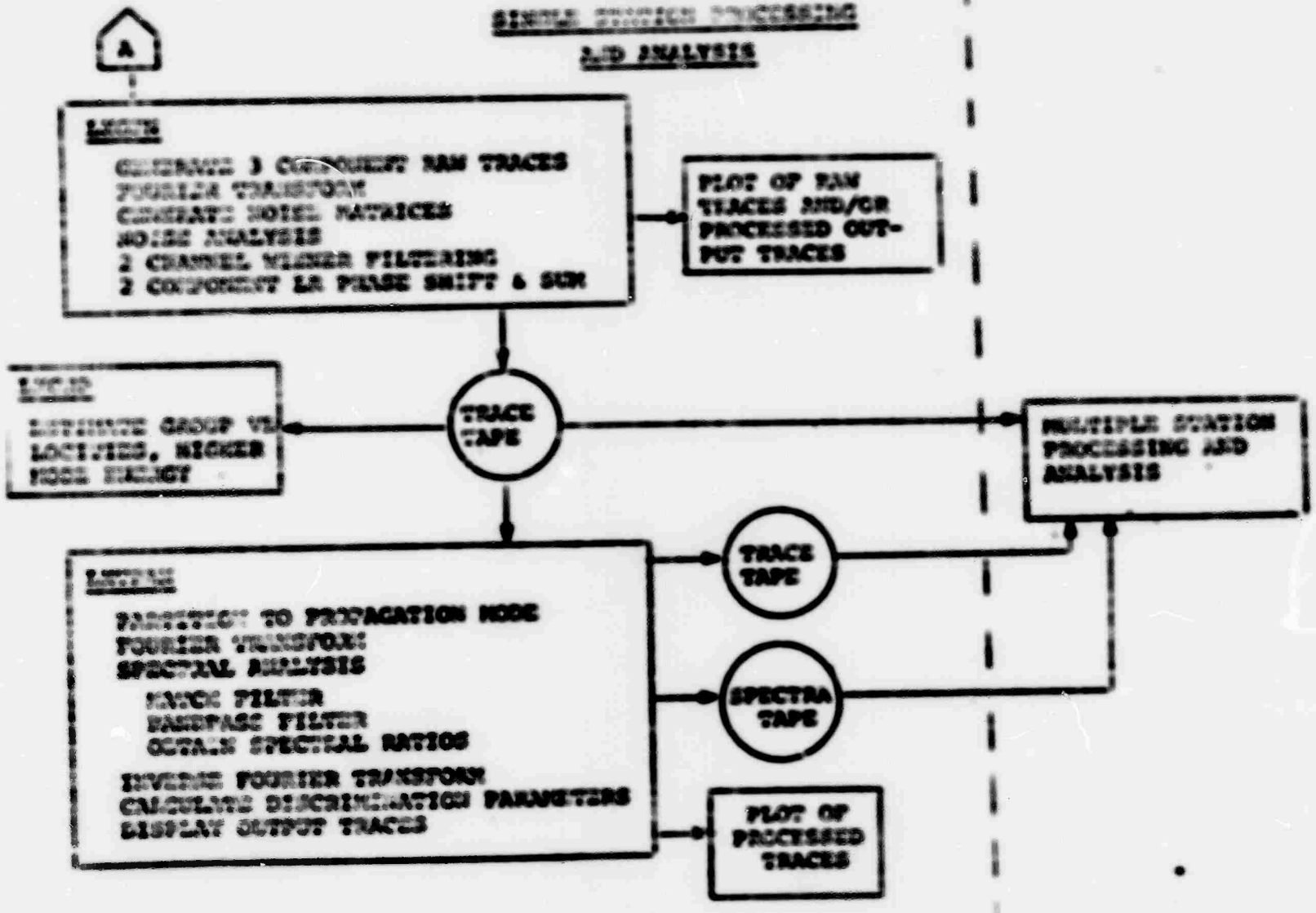
A
PLOT OF RAW TRACES AND/OR PROCESSED OUTPUT TRACES
TRACE TAPE
MULTIPLE STATION PROCESSING AND ANALYSIS
TRACE TAPE
SPECTRA TAPE
PLOT OF PROCESSED TRACES

Figure 4

DATA PRICE AND DISPLAY

- TIME-MULTIPLEX INDIVIDUAL STATION TAPES ONTO A LIBRARY TAPE FOR PERMANENT RETENTION. LIBRARY TAPES WILL BE 9-TRACK 1600 bpi. VELOCITY AND DISPLACEMENT DATA WILL BE RECORDED ON SEPARATE TAPES.
- REFORMAT 9-TRACK 1600 bpi LIBRARY TAPES TO 7-TRACK 556 bpi TAPES FOR FILM PLAYBACK. THESE DATA WILL NOT ROUTINELY BE SAVED, BUT CAN BE DUPLICATED ON REQUEST.
- PLAYBACK DATA ONTO 16-mm FILMS
  - VERTICALS FROM ALL STATIONS ON ONE FILM
  - NORTH-SOUTH FROM ALL STATIONS ON A SECOND FILM
  - EAST-WEST FROM ALL STATIONS ON A THIRD FILM

  ONE TIME WILL BE ENCODED ON THE FILMS. VELOCITY AND DISPLACEMENT DATA WILL BE RECORDED ON SEPARATE FILMS.

Figure 5

EVENT SELECTION AND DISPLAY

- CHOOSE EVENTS FOR PROCESSING AND ANALYSIS AND CALCULATE EVENT SELECTION PARAMETERS

- EDIT SIGNALS (AND NOISE) ONTO PROCESSING TAPES (9TRACK, 1600 bpi) AND CALCOMP PLOT

- REFORMAT TO 7 TRACK 556 bpi FOR FILM PLAYBACK IF DESIRED. THESE TAPES WILL NOT GENERALLY BE SAVED, BUT CAN BE COPIED ON REQUEST

- PLAYBACK DATA ONTO 16mm FILMS; FORMAT WILL BE THE SAME AS PREVIOUSLY DESCRIBED

Figure 6

SIGNAL [illegible]

AND ANALYSIS

- [illegible] WILL BE DIRECTED TOWARD DETERMINING DETECTION THRESHOLD OF EACH STATION AND BEHAVIOR OF DISCRIMINANTS

- NOISE ANALYSIS
  - SPECTRAL CONTENT (VARIABILITY WITH TIME)
  - INTER-COMPONENT COHERENCES

- SIGNAL PROCESSING (BY PHASE)
  - TWO-COMPONENT WIENER RAYLEIGH WAVE SIGNAL EXTRACTION
  - TWO-COMPONENT RAYLEIGH WAVE PHASE SHIFT AND SUM
  - MATCHED FILTERING
  - BANDPASS FILTERING

- SIGNAL ANALYSIS
  - SPECTRAL CONTENT
  - GROUP VELOCITY ESTIMATES
  - IDENTIFICATION OF HIGHER MODE ENERGY
  - [illegible] AMPLITUDE AS A FUNCTION OF FREQUENCY
  - DISCRIMINANTS (Ms, AR, AL,)

Figure 7

MULTIPLE STATION PROCESSING
AND ANALYSIS

- COMBINE SINGLE STATION RESULTS TO DEFINE NETWORK DETECTION THRESHOLD
- INVESTIGATE POSSIBILITY OF ACHIEVING ADDITIONAL SIGNAL-TO-NOISE RATIO IMPROVEMENT BY STACKING SELECTED MATCHED FILTER OUTPUTS (FOR SMALL EVENTS)
- UTILIZE COLLECTED SPECTRAL DATA FOR SOURCE CHARACTERIZATION

Figure 8

DATA AVAILABILITY

- LIBRARY TAPE
  - ALL DATA ON 9-TRACK 1600 bpi TAPES. VELOCITY AND DISPLACEMENT DATA SEPARATE
  - ALL DATA ALSO WILL BE TEMPORARILY ON 7-TRACK 556 bpi TAPES
- PROCESSING TAPES
  - SELECTED EVENTS AND NOISE WILL BE RETAINED ON 9-TRACK 1600 bpi TAPES. THE CAPABILITY TO TRANSCRIBE THESE TO 7-TRACK 556 bpi WILL EXIST (VELOCITY DATA ONLY)
- FILMS
  - 16mm FILM OF BOTH VELOCITY AND DISPLACEMENT DATA WILL BE MADE AND CAN BE DUPLICATED ON REQUEST
- PLOTS
  - CALCOMP PLOTS OF SIGNAL (OR NOISE) DATA AND PROCESSED TRACES

SURFACE-WAVE SPECTRAL SPLITTING AS A DISCRIMINANT

By

David von Seggern

Seismic Data Laboratory

BLANK PAGE

Theoretical computations of the transfer function of a layered media in the period range 15 to 50 seconds for force systems equivalent to earthquake mechanisms shows that their Rayleigh-wave spectra will be dependent on azimuth from the source, depth of the source, and orientation of the dip and slip vectors. The transfer function for an explosive force depends only on its depth but does not vary significantly for depths of practical concern. Figure 1 shows various earthquake transfer functions normalized to the transfer function of a near-surface explosion, both in the same Gutenberg continental structure. Limited knowledge of time and space dimensions for explosions and earthquakes indicates that the Fourier transform of the displacement-time function near the source for periods between 15 and 50 seconds may differ between these two seismic sources only when $M_S > 5.0$. Thus spectral discrimination capability in the 15-50 seconds' range is mainly due to the different response of the earth's structure to explosion and earthquake sources. We have calculated spectral ratios of the energy between periods of 22 to 48 seconds over the energy between periods of 15 to 48 seconds for 13 underground explosions and 19 earthquakes using several, not necessarily common, recording stations for each. Ratios and recording distances for each event were averaged and a plot of these average values is shown in Figure 2. The spectral ratio increases with distance due to frequency-dependent attenuation, and we select the explosion ratios (excluding one weak Kazahk event) as the sample on which to fit an exponential curve relating spectral ratio to distance, the result being

$$\bar{R}_1 = 4.29^{-3}\ \Delta^{-.456}$$

where $\bar{R}_1$ is the explosion ratio and Δ is the distance in kilometers. With this empirical relation, we normalize all the average ratios to 1000 km distance and plot them as a function of surface-wave magnitude M_S in Figure 3. The explosion ratios lie in a narrow band; this shows that the Fourier transform of the displacement-time function near the source for periods between 15 and 50 seconds is apparently invariant for a large magnitude range ($2 < M_S < 5$) and that the transfer function of the layered earth does not change much for these same periods since different source and recording sites are represented. The earthquake ratios are scattered about the explosions ratios with some falling in the band of explosions, as expected from theory.

We investigated the Nevada source region in detail since propagation paths to several of the stations were nearly the same for explosions and earthquakes. A more pronounced separation of the NTS shots and Nevada earthquakes is attained when energy between 10 and 15 seconds is included in the spectral ratio calculations. Spectra from explosions tended to be very similar at a given station while those of earthquakes were usually not. Figure 4 exemplifies this for recordings at TFO. Also, spectra for a given explosion among several stations tended to be more similar than spectra for a given earthquake, a result of the azimuthal dependency of the earth's layering response to force systems equivalent to earthquake mechanisms.

Spectral ratio may be applied in two steps to diagnose an explosion. First, by calculating the ratio itself, it can be determined whether an event lies within the band of explosions; and second, by calculating the ratios' variance among stations, it may be determined that no azimuthal dependence on spectra, characteristic of earthquakes, is present. The second criterion can be applied only when there is sufficient azimuthal coverage and would be a more useful diagnostic if a reference explosion from the same area as the event under investigation had already been recorded so that a normalization procedure could be carried out.

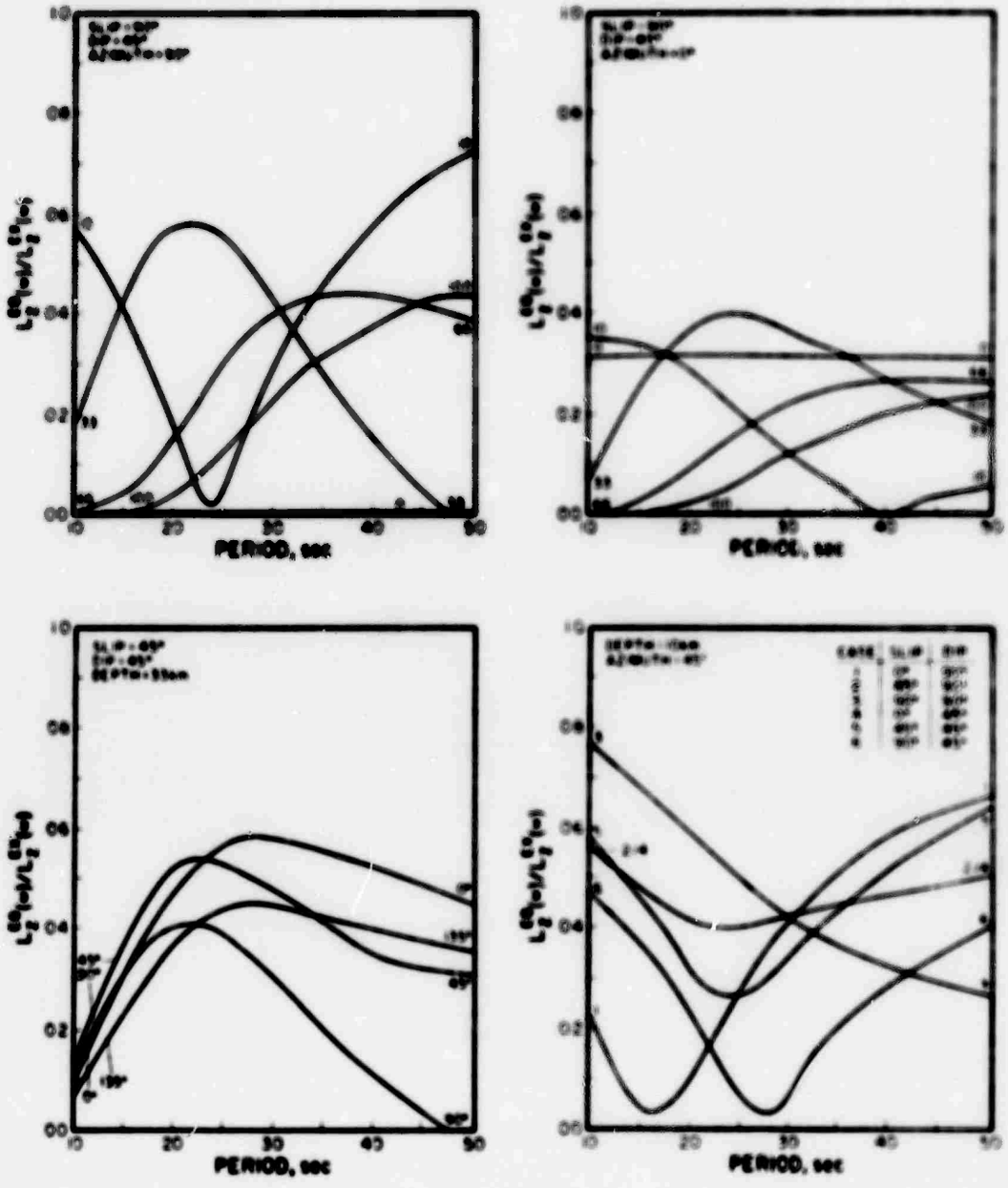

Figure 1.

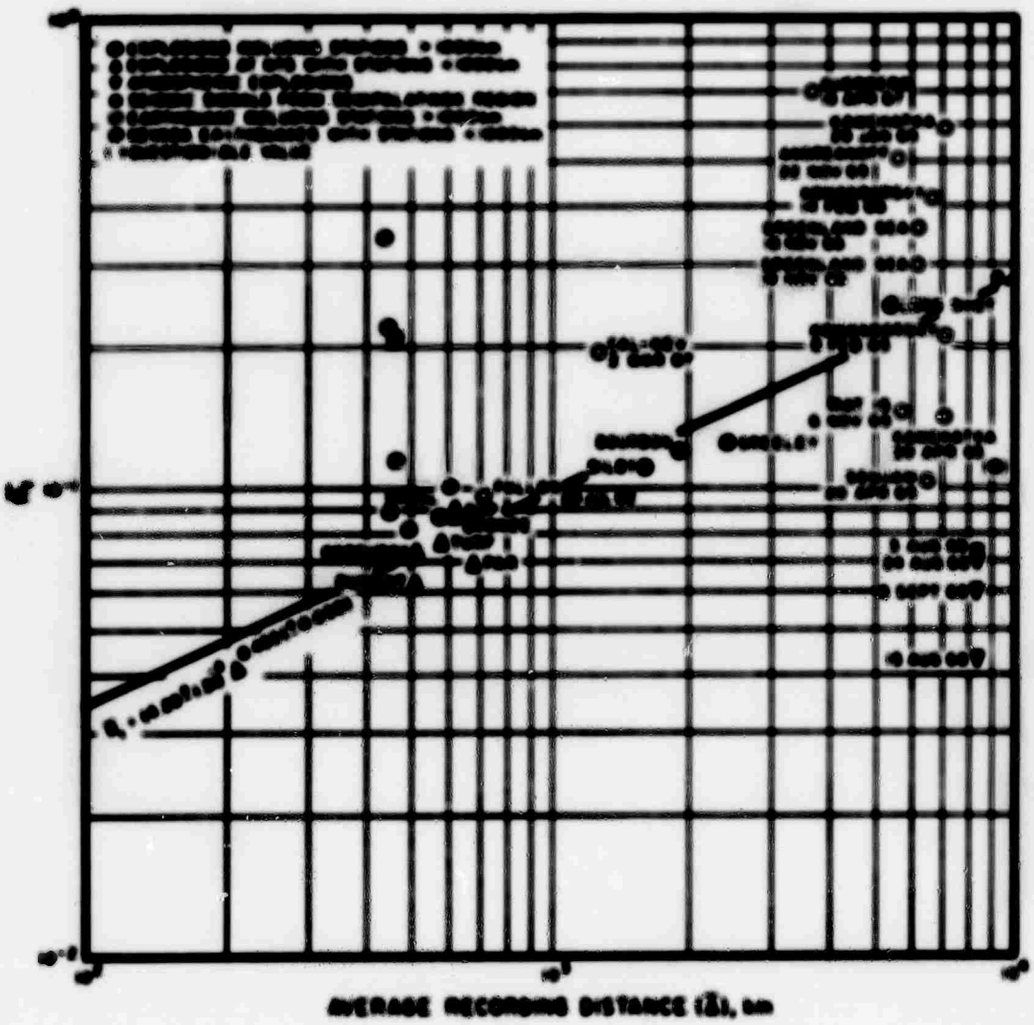

Figure 2.

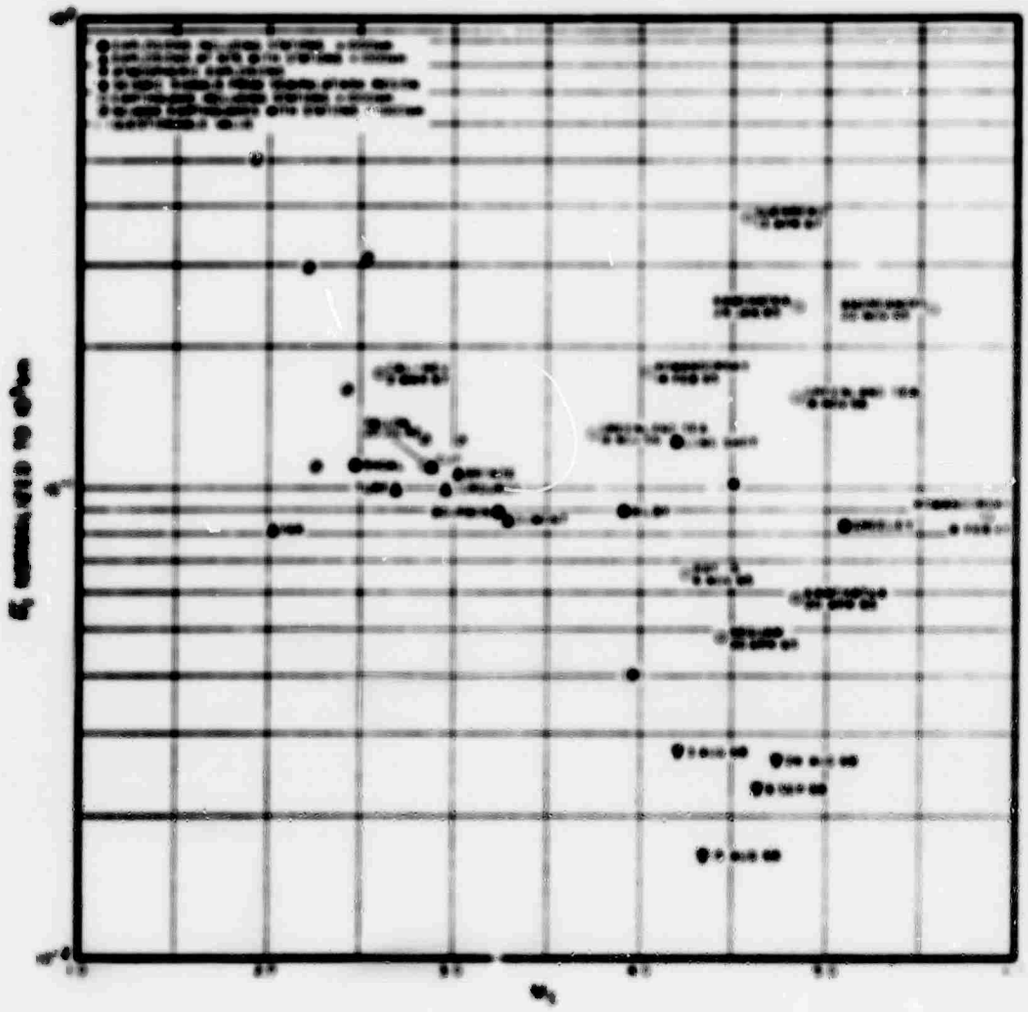

Figure 3.

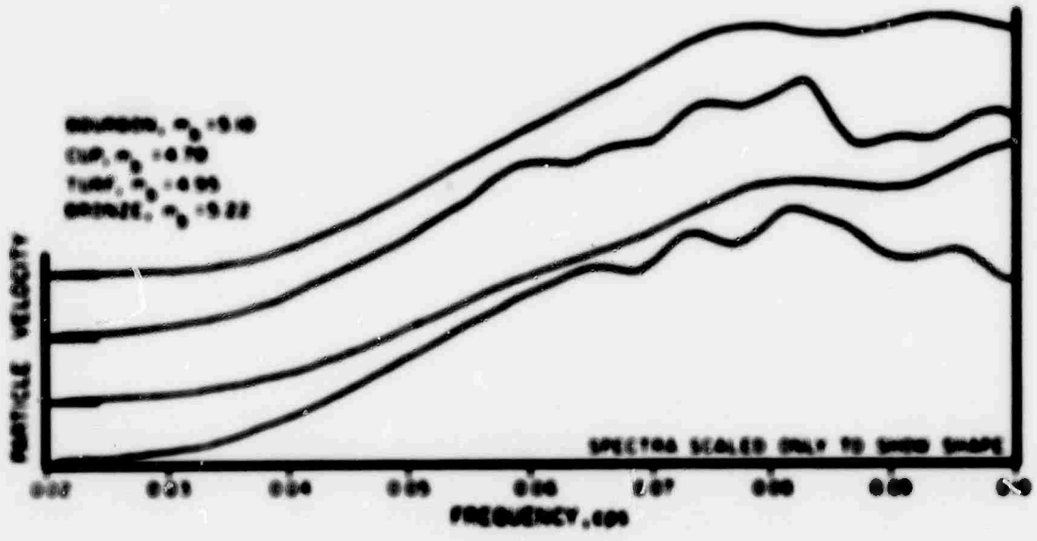
PARTICLE VELOCITY
SPECTRA SCALED ONLY TO SHOW SHAPE
FREQUENCY, cps

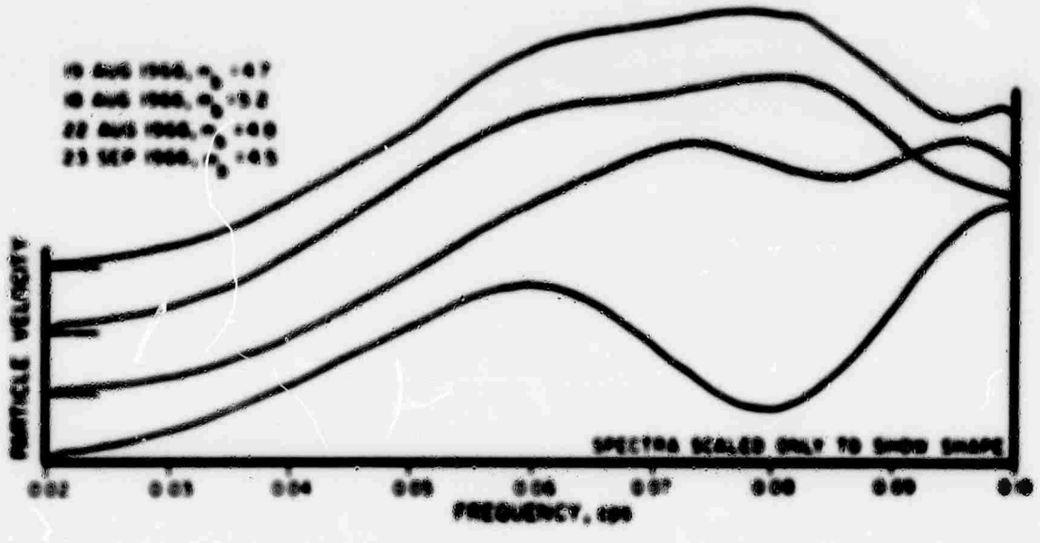
PARTICLE VELOCITY
SPECTRA SCALED ONLY TO SHOW SHAPE
FREQUENCY, cps

Figure 4.

DISTANCE CORRECTIONS FOR SURFACE WAVE MAGNITUDE IN THE WESTERN UNITED STATES

By

David von Seggern

Seismic Data Laboratory

BLANK PAGE

Use of the surface-wave magnitude formula,

$$M_s = \log_{10} (A_{max}/T) + 1.66 \log_{10} \Delta - 0.18$$

where A = peak-to-peak maximum amplitude on record,
T = period of maximum amplitude cycle,
Δ = distance in degrees,

(essentially that of Gutenberg) for explosions in Nevada from LRSM recordings results in systematically lower magnitudes for regional distances as compared to teleseismic distances. This fact is illustrated in Figure 1. For this reason surface-wave magnitudes for small shots, recorded only at regional distances, are about one-half unit too low. Retaining the usual procedure of measuring for and computing magnitude, the distance-correction factor for $\Delta<15°$, $1.66 \log_{10} \Delta - 0.18$, was revised for the NTS source region by a method that forced regional magnitudes to agree closely with teleseismic ones. Only events for which surface-waves were recorded out into the teleseismic range were used. This new correction factor is $1.16 \log_{10} \Delta + 0.74$. Magnitudes of many NTS events were recomputed employing the new correction at distances to 15° and the Gutenberg correction beyond 15°; in Figure 2 typical improvement in regional magnitudes is shown by the much closer agreement of CUP regional magnitudes with those at teleseismic distance when the new distance correction is applied. Due to the slope change in the regional correction (1.16 versus the former 1.66), the standard deviation of regional magnitudes is also reduced, as shown for 41 NTS events in Figure 3. For these same events, the standard deviation of body-wave magnitudes using Evernden's corrections at regional distances is compared in Figure 4 with that of the surface-wave magnitudes using the new correction at regional distances; evidently, surface-wave magnitude is much more consistent among stations.

Attenuation rates along different paths from NTS were significantly different, but not enough to make path-dependent distance corrections differ by more than one-tenth of a magnitude unit, a quantity which does not warrant the added effort involved in applying path-dependent corrections.

The new regional distance corrections factor was applied to the RULISON event in Colorado, and Figure 5 shows that its regional magnitude average then lies closer to the teleseismic average.

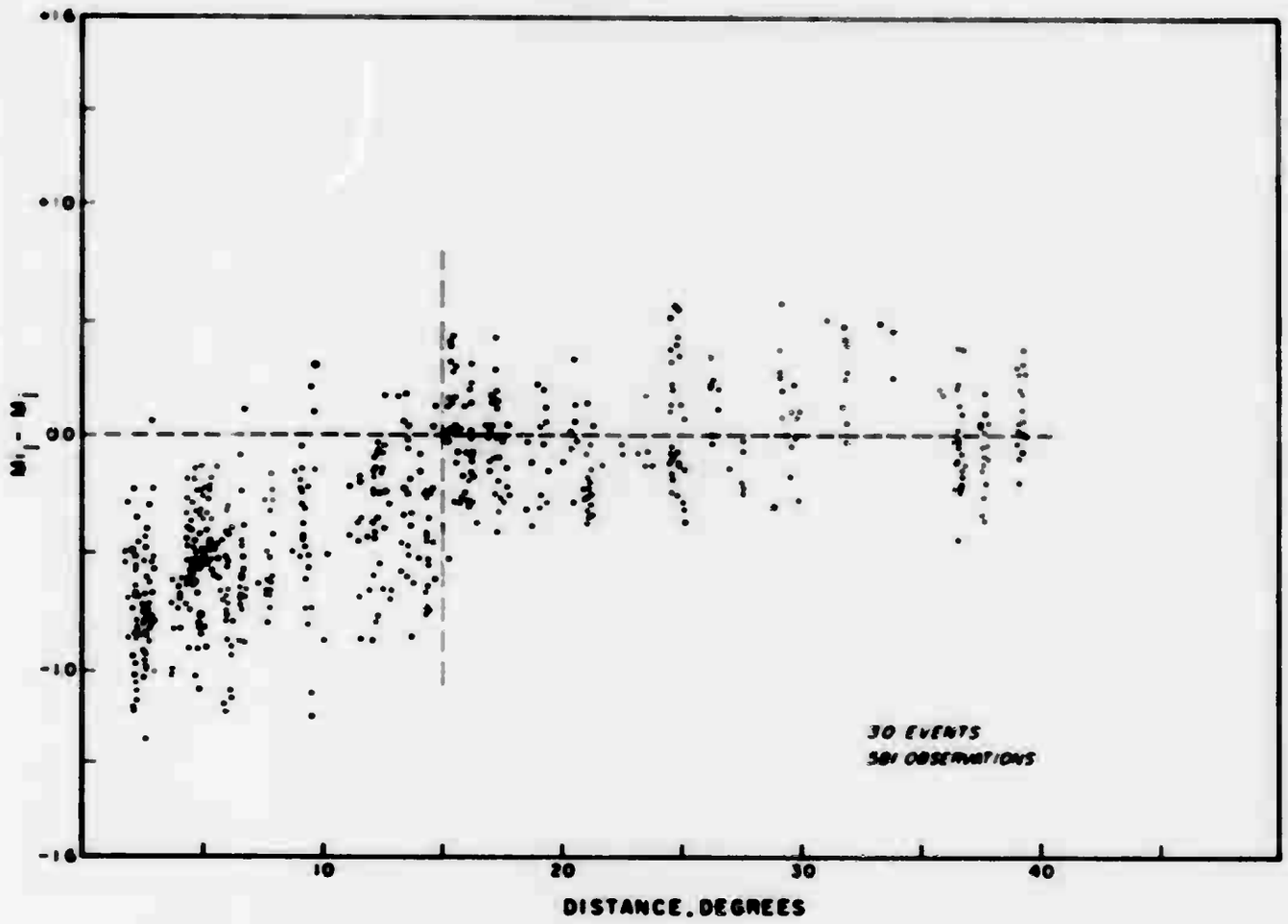

Figure 1. Individual magnitude deviations from the average for 31 Nevada Test Site explosions.

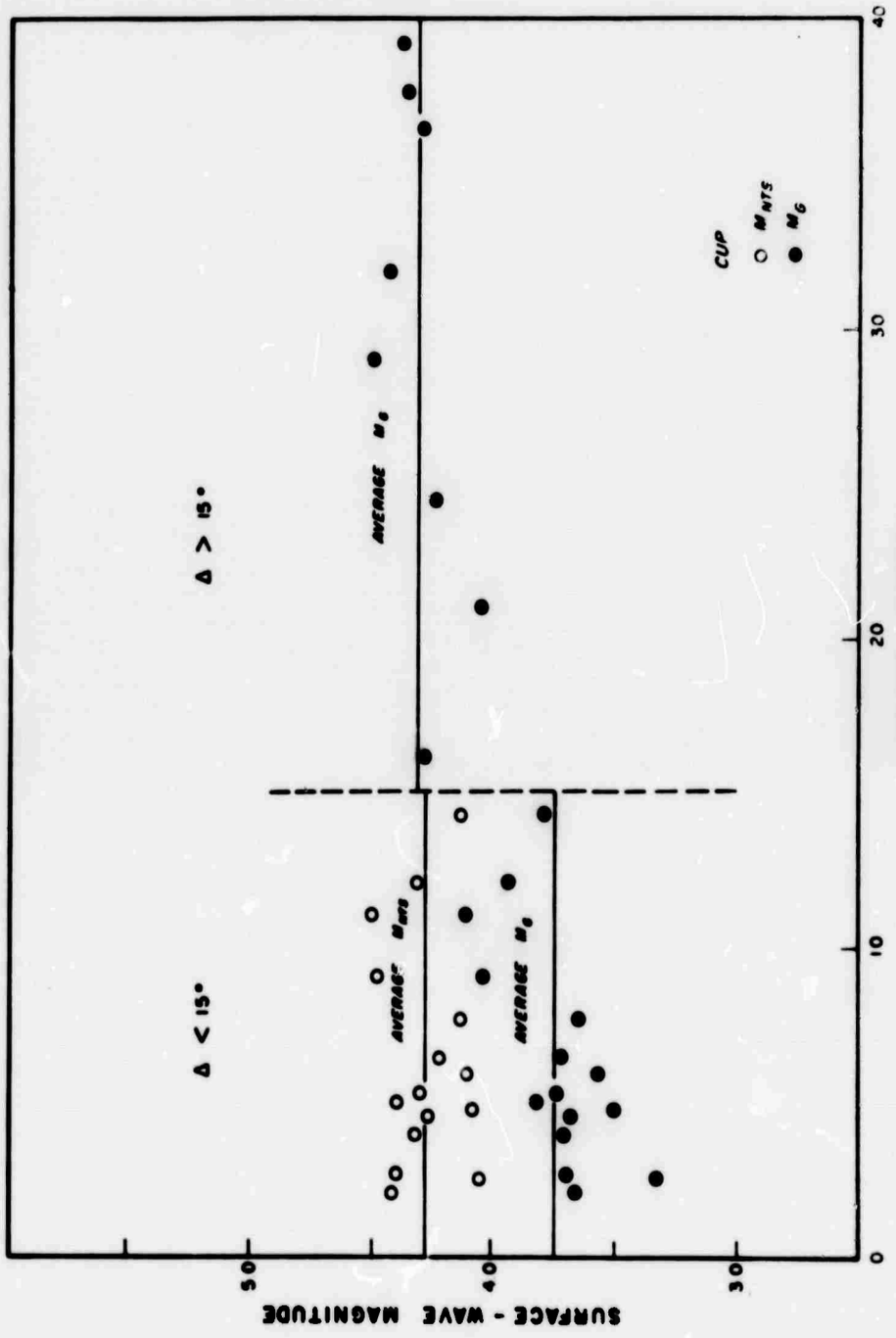

Figure 2. CUP - M_G and M_{NTS}.

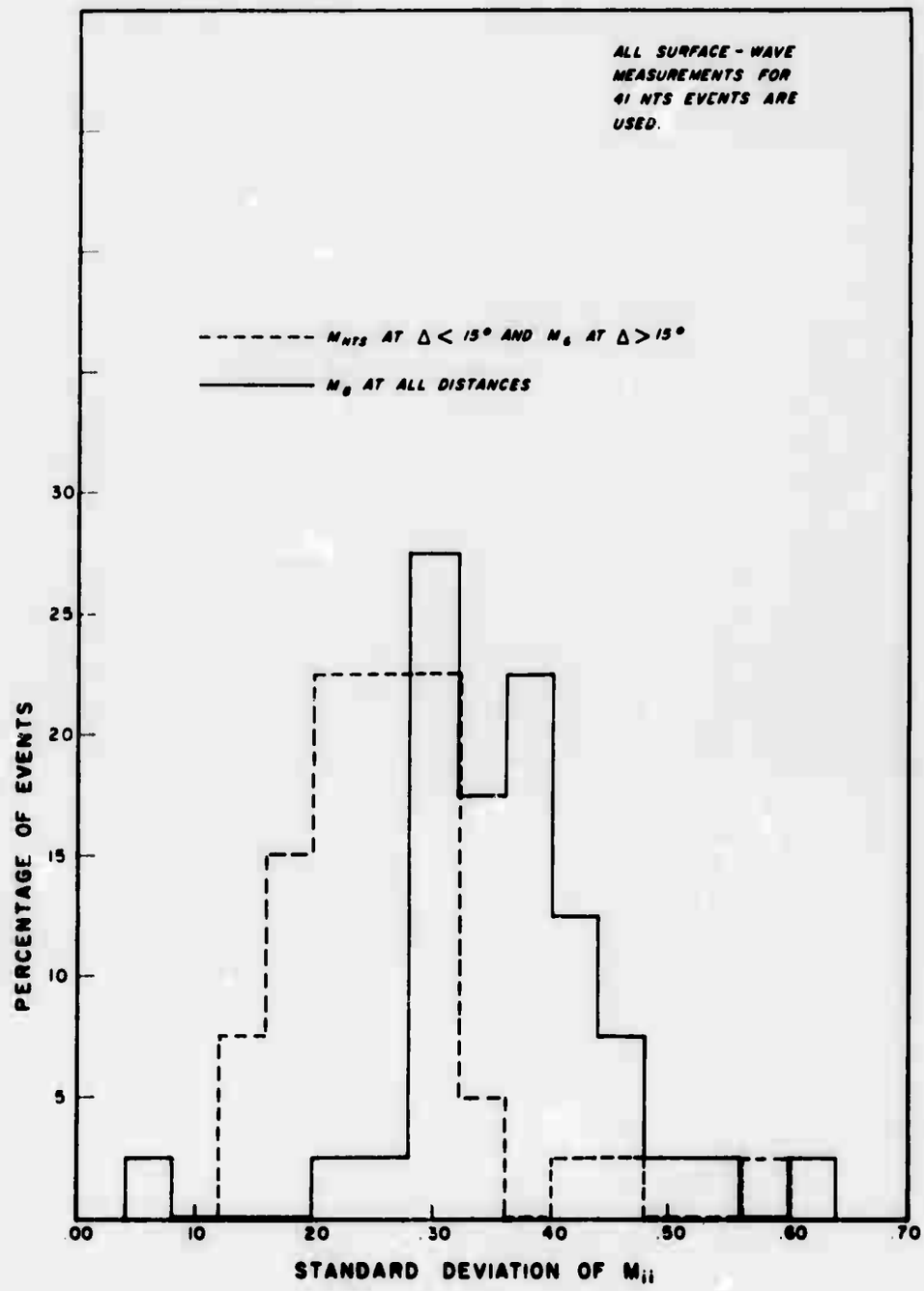

Figure 3. Standard deviations of surface-wave magnitude using NTS and Gutenberg "B" factors for 41 events.

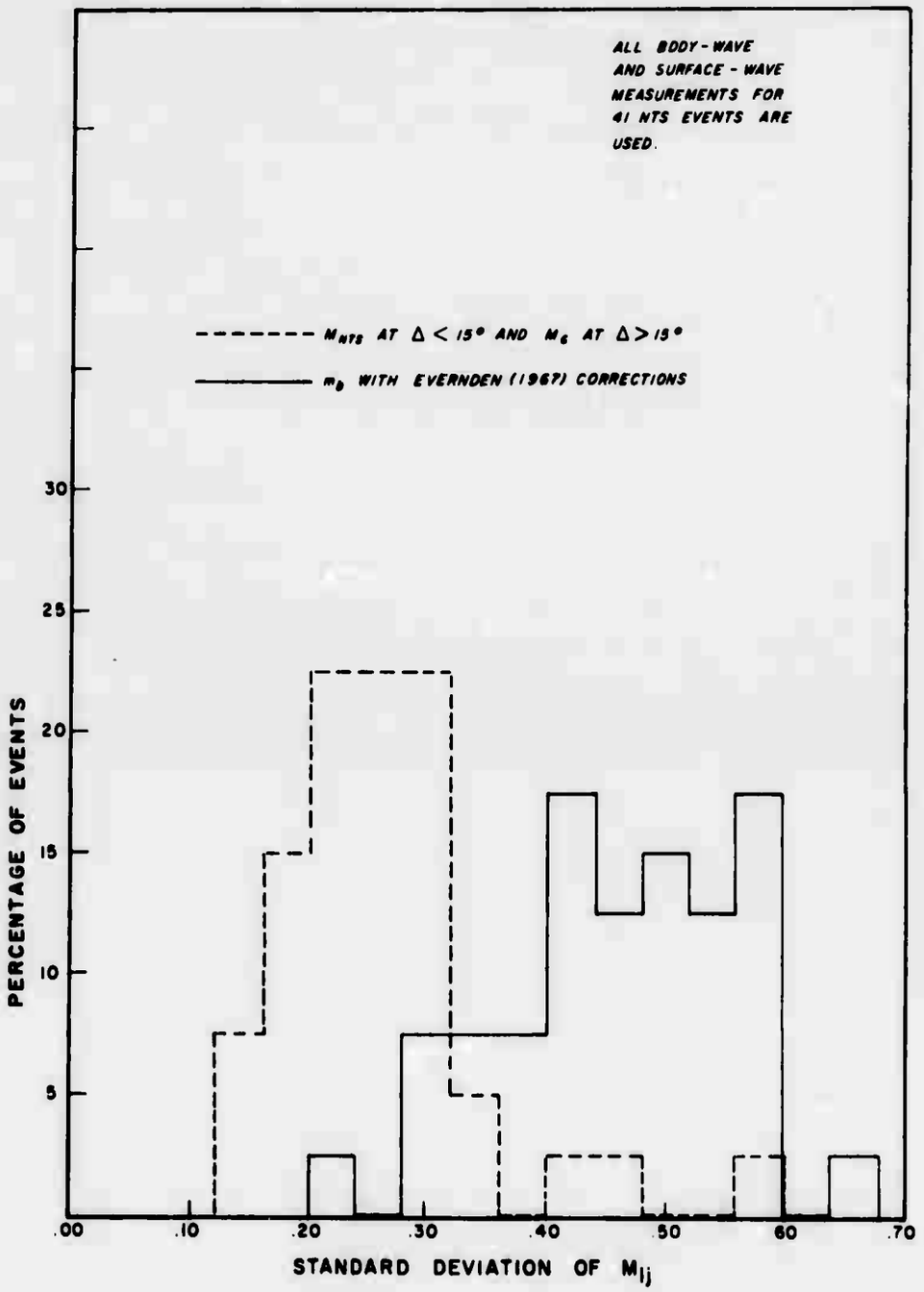

Figure 4. Standard deviations of body-wave magnitudes using Evernden's "B" factor and of surface-wave magnitudes using NTS "B" factor for 41 events.

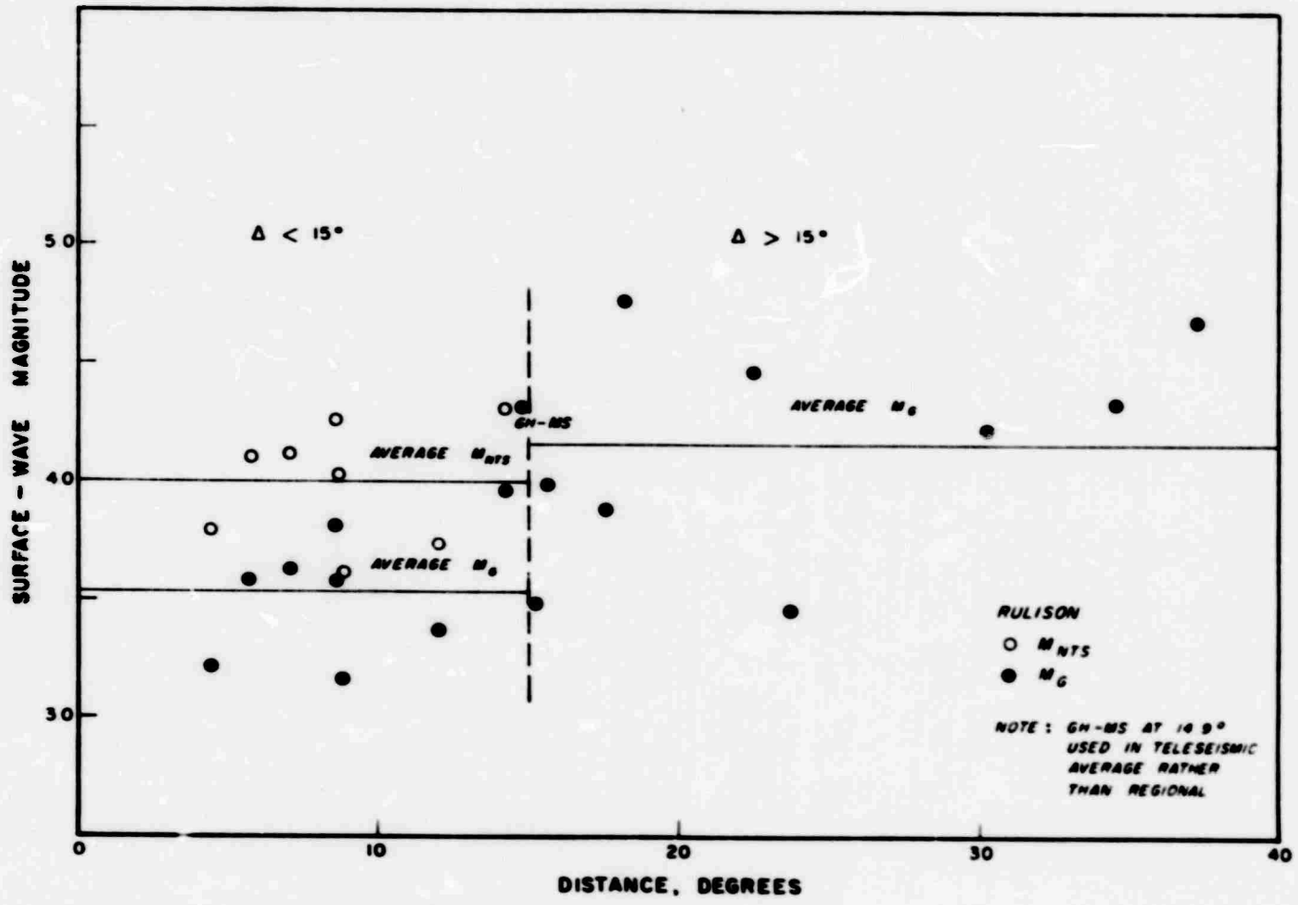

Figure 5. RULISON (Rifle, Colorado) - M_G and M_{NTS}.

SURFACE WAVE RADIATION PATTERNS FOR SOUTHERN NEVADA NUCLEAR EXPLOSIONS AND CAVITY COLLAPSES

By

Robert P. Massé

Seismic Data Laboratory

BLANK PAGE

Source mechanisms of some southern Nevada nuclear explosions and cavity collapses have been studied using the amplitudes of long period Rayleigh waves. The amplitudes were analyzed to determine if they could be represented by the product of an event (source) amplitude factor and a station (total path effect) amplitude factor. This product may be written in the form

$$A_{ij} = E_i S_j$$

where A_{ij} is the measured amplitude (corrected for system response) of a seismic phase recorded at the j'th station for the i'th nuclear explosion, E_i is an event amplitude factor and S_j is a station amplitude factor representing the effect on the measured amplitude of the earth structure along the entire travel path from source to station. Rewriting this equation

$$\ln A_{ij} = \ln E_i + \ln S_j,$$

a least squares solution was found for the factors $\ln E_i$ and $\ln S_j$. For each nuclear explosion and collapse, the adjusted amplitude A'_{ij} was formed, where

$$A'_{ij} = A_{ij}/E_i S_j$$

The A'_{ij} amplitude patterns were then plotted for the explosions and cavity collapses and are shown in Figures 1 through 5. From these figures, it can be seen that, within the measurement error, the patterns are identical. This indicates that the principal factor influencing the Rayleigh wave amplitudes is the earth structure along the travel path from epicenter to station. Furthermore, since cavity collapses are not believed to release tectonic energy, the similarity of the explosion and cavity collapse radiation patterns indicates that less than 20 percent of the Rayleigh wave energy in signals from the nuclear explosions can be attributed to the release of tectonic strain energy.

Employing the above method of analysis, the effect of the travel path on the Rayleigh amplitudes (S_j) may be determined for a given source area. The factors S_j may then be used to remove the effect of structure from the observed amplitudes of Rayleigh waves from an event in order to obtain an accurate source radiation pattern.

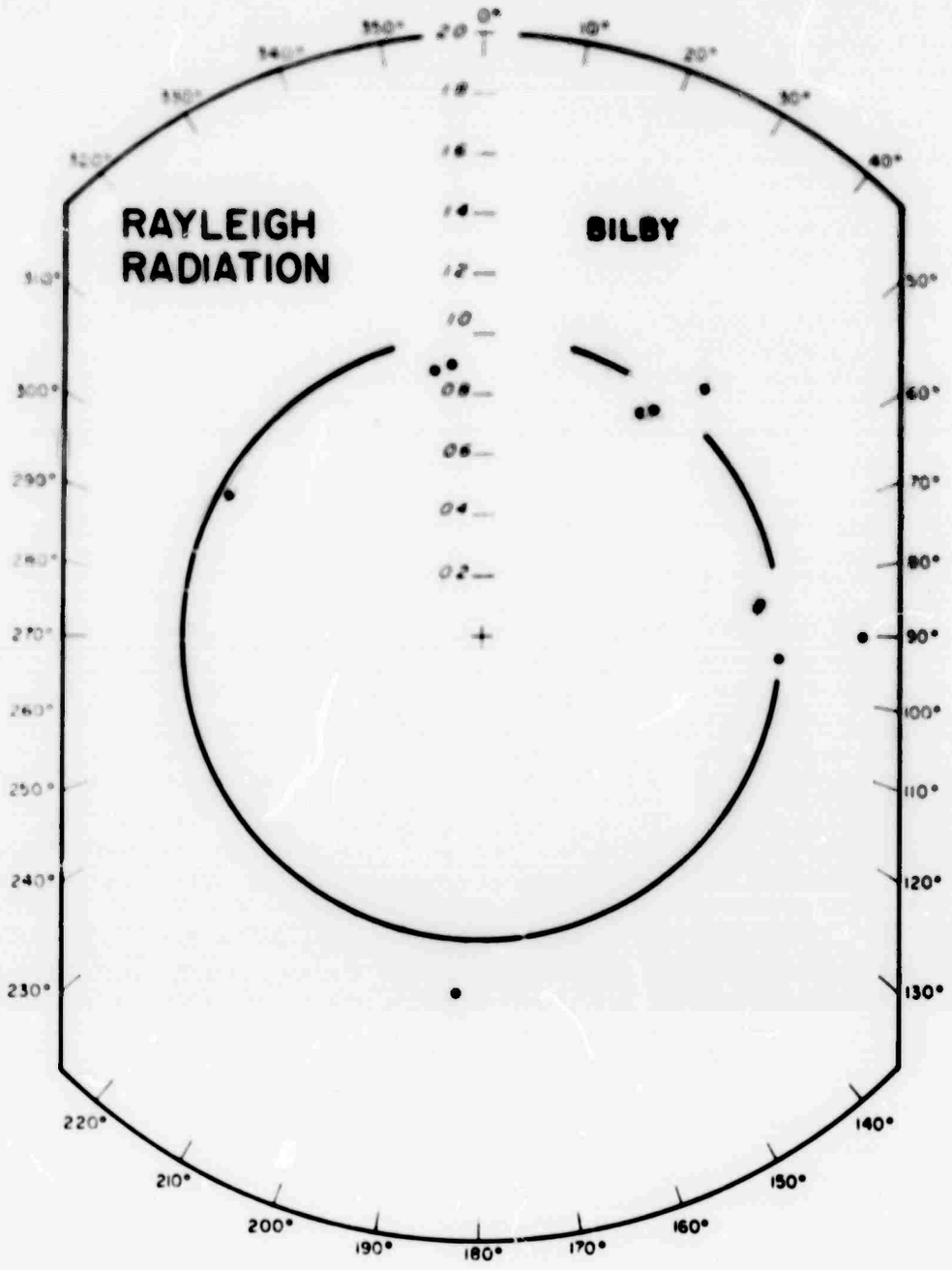
RAYLEIGH
RADIATION
BILBY
0°
10°
20°
30°
40°
50°
60°
70°
80°
90°
100°
110°
120°
130°
140°
150°
160°
170°
180°
190°
200°
210°
220°
230°
240°
250°
260°
270°
280°
290°
300°
310°
320°
330°
340°
350°
20
18
16
14
12
10
08
06
04
02

Figure 1.

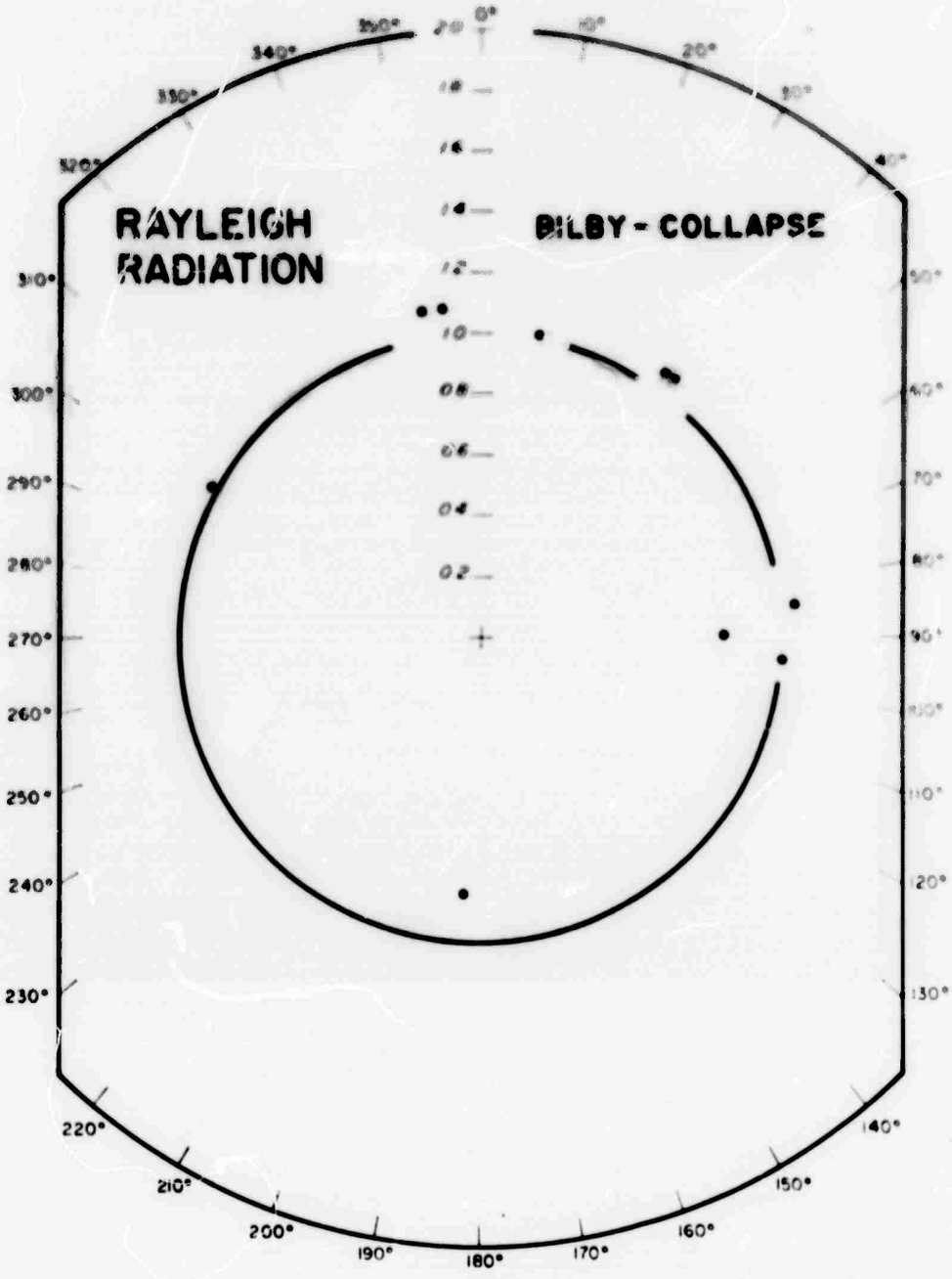
RAYLEIGH
RADIATION
BILBY - COLLAPSE
0°
10°
20°
30°
40°
50°
60°
70°
80°
90°
100°
110°
120°
130°
140°
150°
160°
170°
180°
190°
200°
210°
220°
230°
240°
250°
260°
270°
280°
290°
300°
310°
320°
330°
340°
350°

Figure 2.

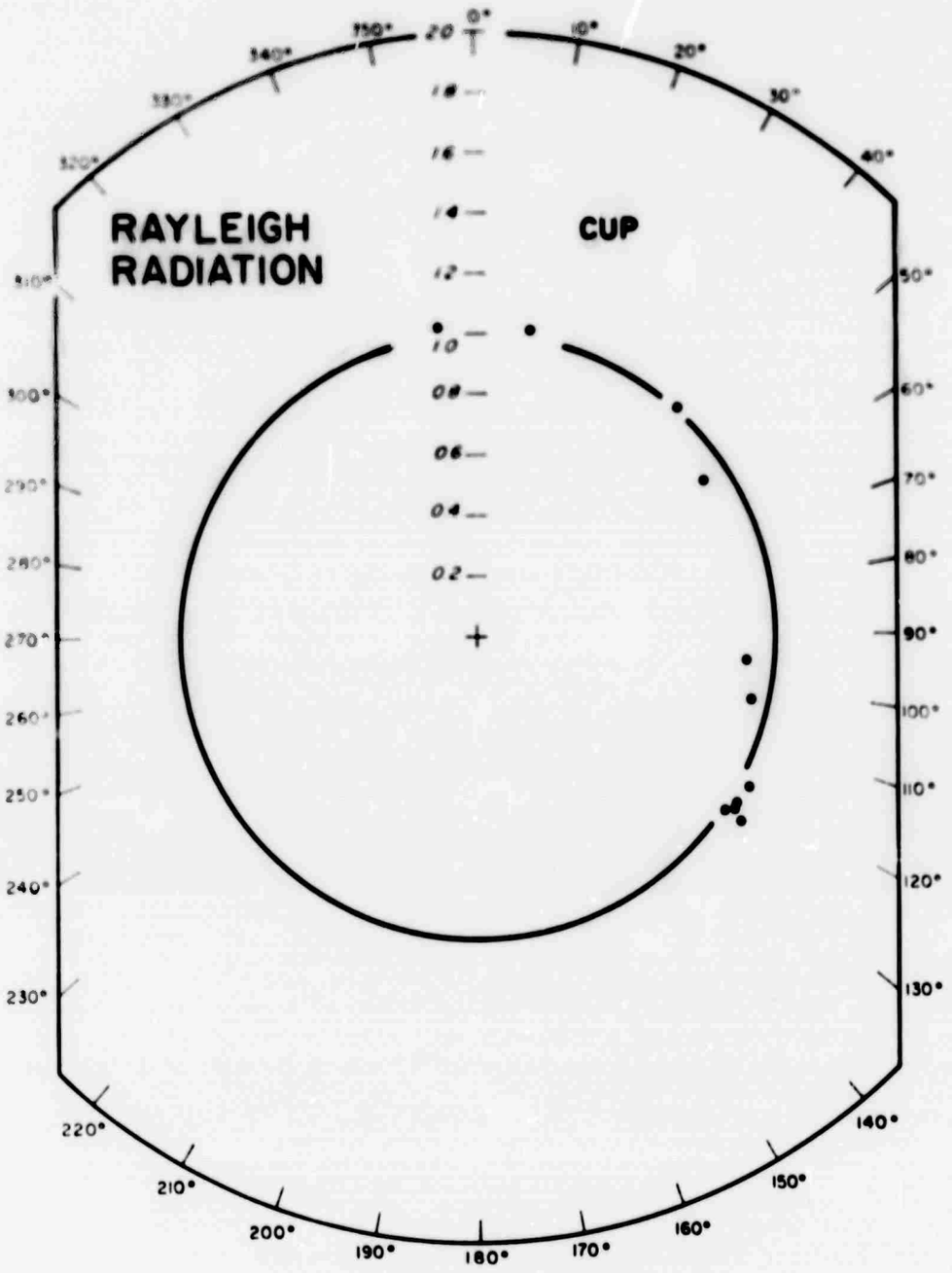
RAYLEIGH
RADIATION
CUP
0°
10°
20°
30°
40°
50°
60°
70°
80°
90°
100°
110°
120°
130°
140°
150°
160°
170°
180°
190°
200°
210°
220°
230°
240°
250°
260°
270°
280°
290°
300°
310°
320°
330°
340°
350°
20
18
16
14
12
10
08
06
04
02

Figure 3.

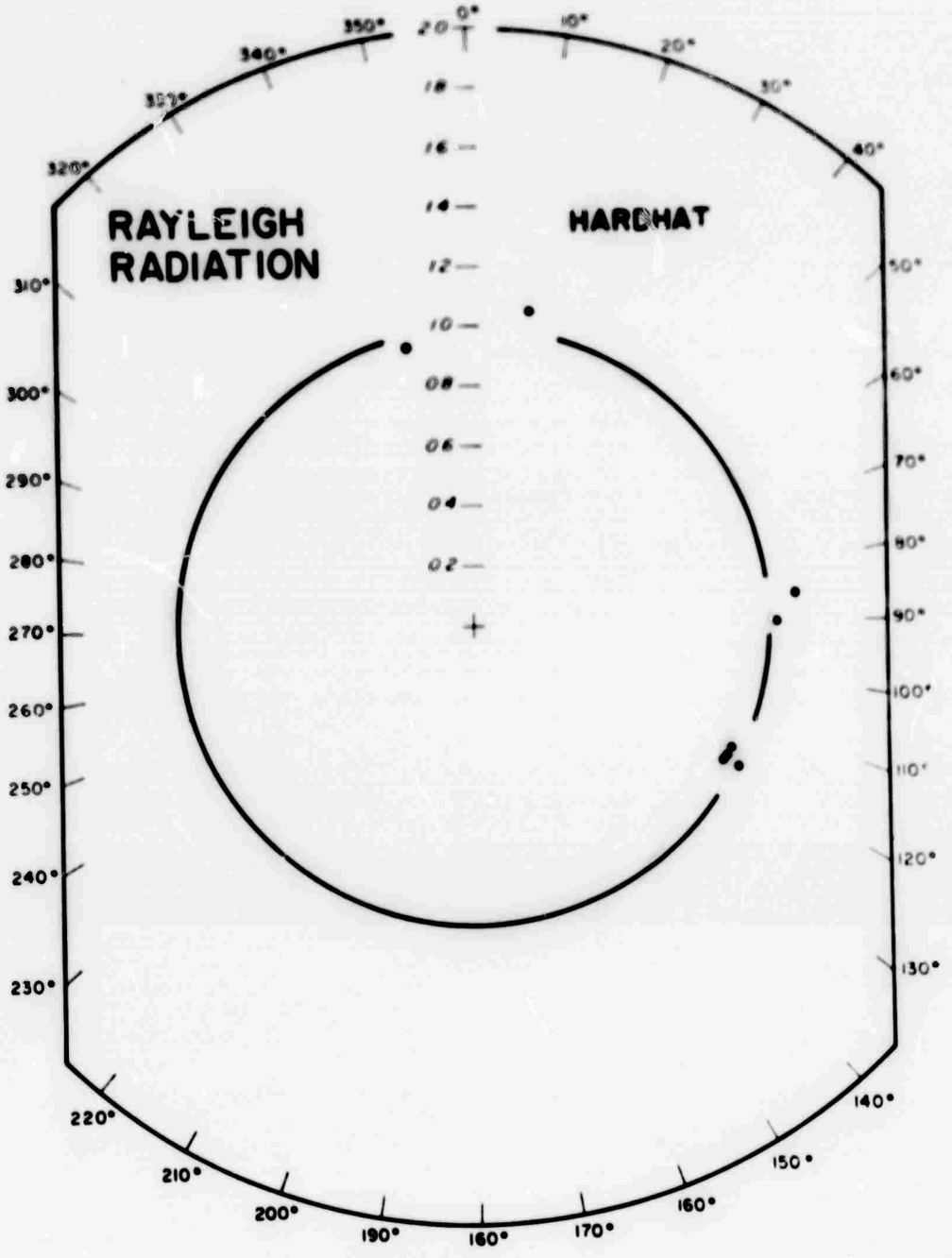
RAYLEIGH
RADIATION
HARDHAT
0°
10°
20°
30°
40°
50°
60°
70°
80°
90°
100°
110°
120°
130°
140°
150°
160°
170°
180°
190°
200°
210°
220°
230°
240°
250°
260°
270°
280°
290°
300°
310°
320°
330°
340°
350°
20
18
16
14
12
10
08
06
04
02

Figure 4.

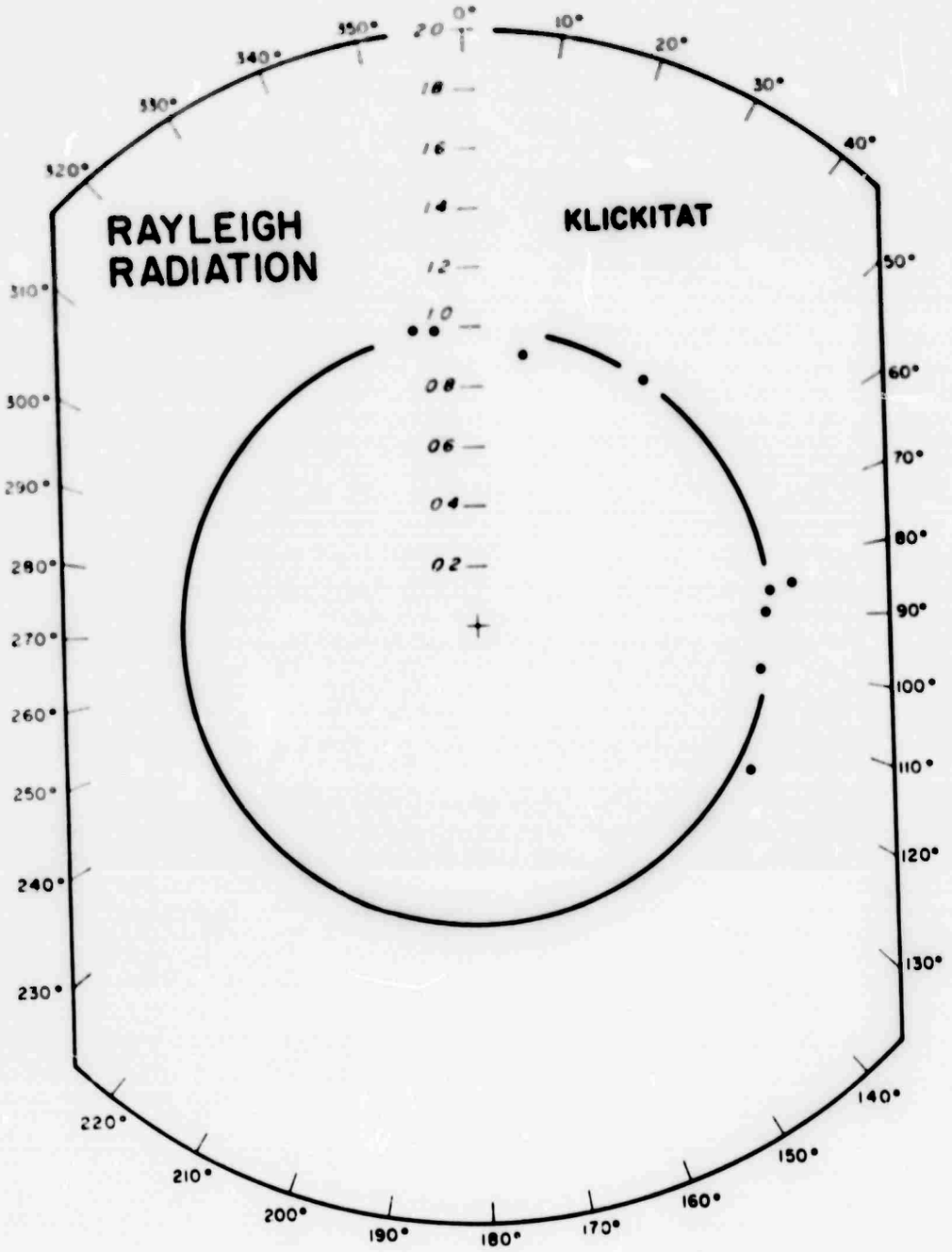
RAYLEIGH
RADIATION
KLICKITAT
0°
10°
20°
30°
40°
50°
60°
70°
80°
90°
100°
110°
120°
130°
140°
150°
160°
170°
180°
190°
200°
210°
220°
230°
240°
250°
260°
270°
280°
290°
300°
310°
320°
330°
340°
350°
20
18
16
14
12
10
08
06
04
02

Figure 5.

ANALYSIS OF SEISMIC EVENTS AS RECORDED BY BOTH WIDE BAND LONG PERIOD AND STANDARD VELA LONG PERIOD SEISMOGRAPH SYSTEMS

By

Robert P. Massé

Seismic Data Laboratory

BLANK PAGE

Since 25 September 1969, two wide band long period vertical seismograph systems (LZX and LZY) have been operating at TFO. These systems have an amplitude response peaked at approximately 40 seconds and have a wider pass band than the standard long period LRSM or VELA instruments (Figure 1).

Seismic events recorded by the wide band (LZX) system and a standard VELA vertical seismometer (LZ1) located at the same site at TFO were analyzed to compare the performance of the two recording systems.

Film recording from the standard and wide band seismograph systems were used to obtain measurements of the longest period observable in the first five minutes of Rayleigh wave signals from seismic events. The longest periods for all events are shown in Figure 2, and the epicenters are given in Figure 3 with the symbol for each epicenter denoting the period range in which the wide band measurement falls.

It can be seen that, for each event, the difference between the periods measured from the standard and the wide band recordings is usually less than five seconds (Figure 2). This indicates that although at the longer periods the amplitude of the signal as recorded by the wide-band system may be larger than that for the signal as recorded by the standard system, the period measurement can still be made from recordings of the standard long period seismograph system. The longest period was found to be less than 70 seconds for most events. The distribution of epicenters shown in Figure 3 indicates that events producing Rayleigh wave energy at periods equal to or greater than 60 seconds (within the first five minutes of the Rayleigh signal) are for the most part located near oceanic trenches and along oceanic ridges.

The spectra of Rayleigh wave signals from several events recorded by the wide band and standard VELA systems were computed. The similarity in the spectra of signals recorded by the two systems can be seen in Figure 4 (calculated using a group velocity window of 3 to 4 km/sec). The differences at low frequency reflect the different response seen in Figure 1.

Signal to noise ratios were computed at selected periods from 20 to 75 seconds (Table 1). These ratios are not less than 2.5 for the wide band recordings indicating that reliable estimates of the signal spectra were obtained for the events processed even at periods as long as 75 seconds.

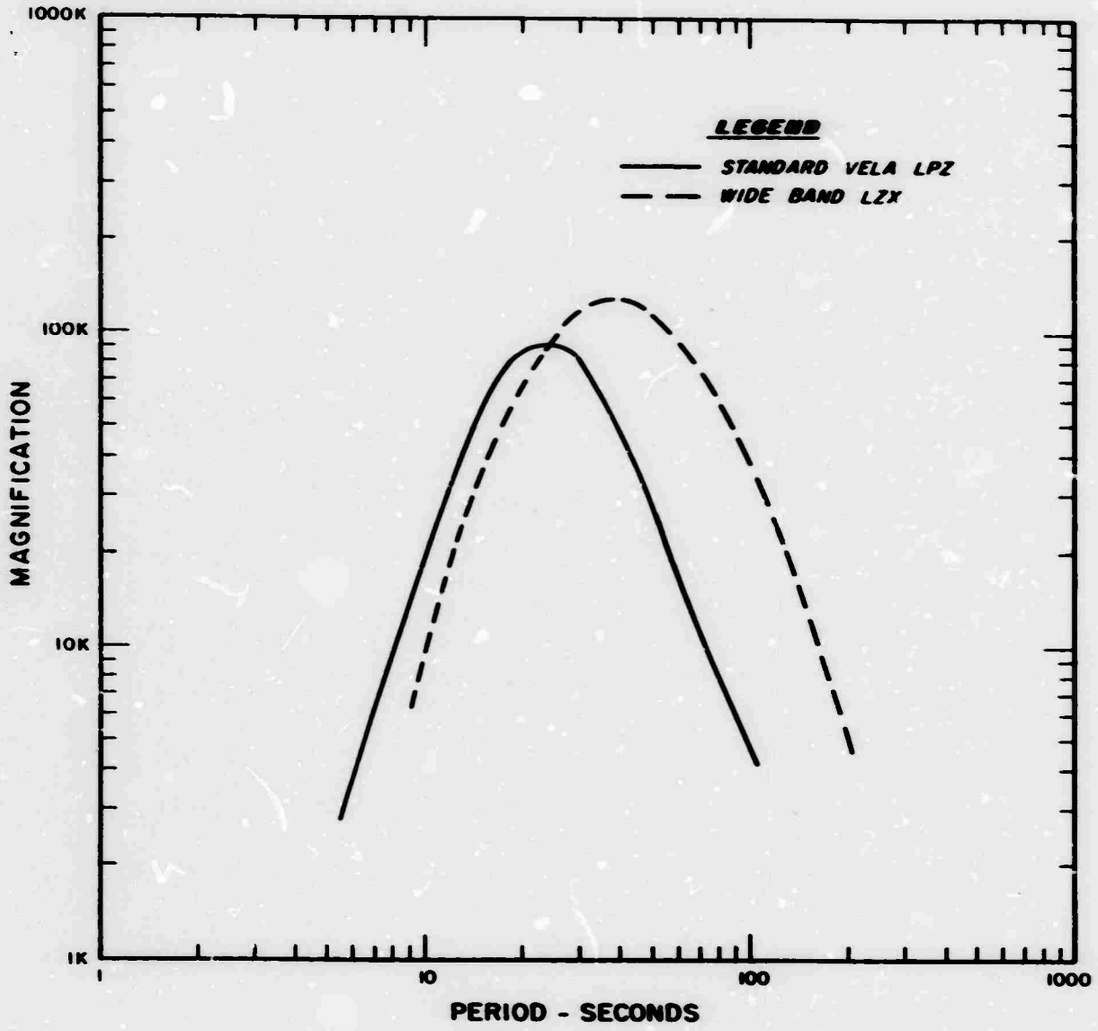

Figure 1. System response of standard Vela long period and of wide band long period seismographs.

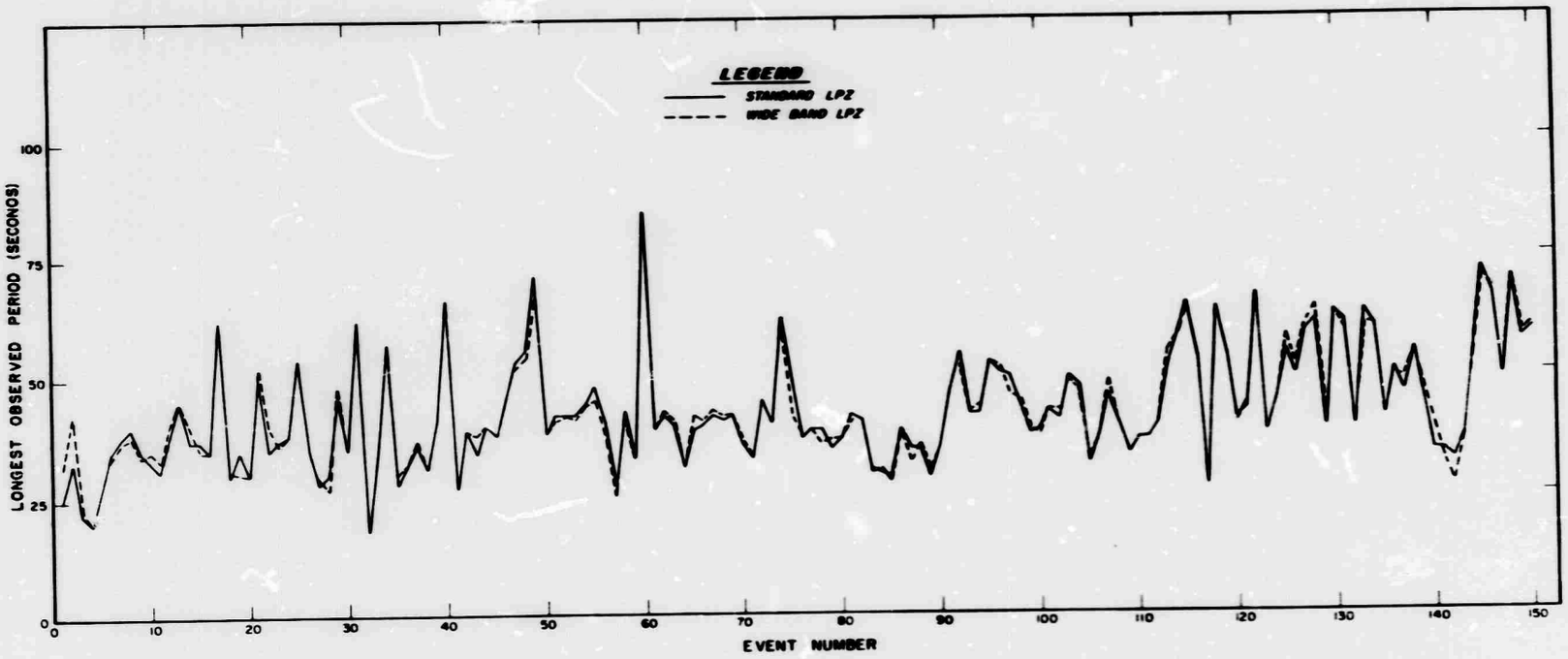

Figure 2. Longest observed periods in Rayleigh wave signals recorded by wide band and standard Vela long period seismograph systems.

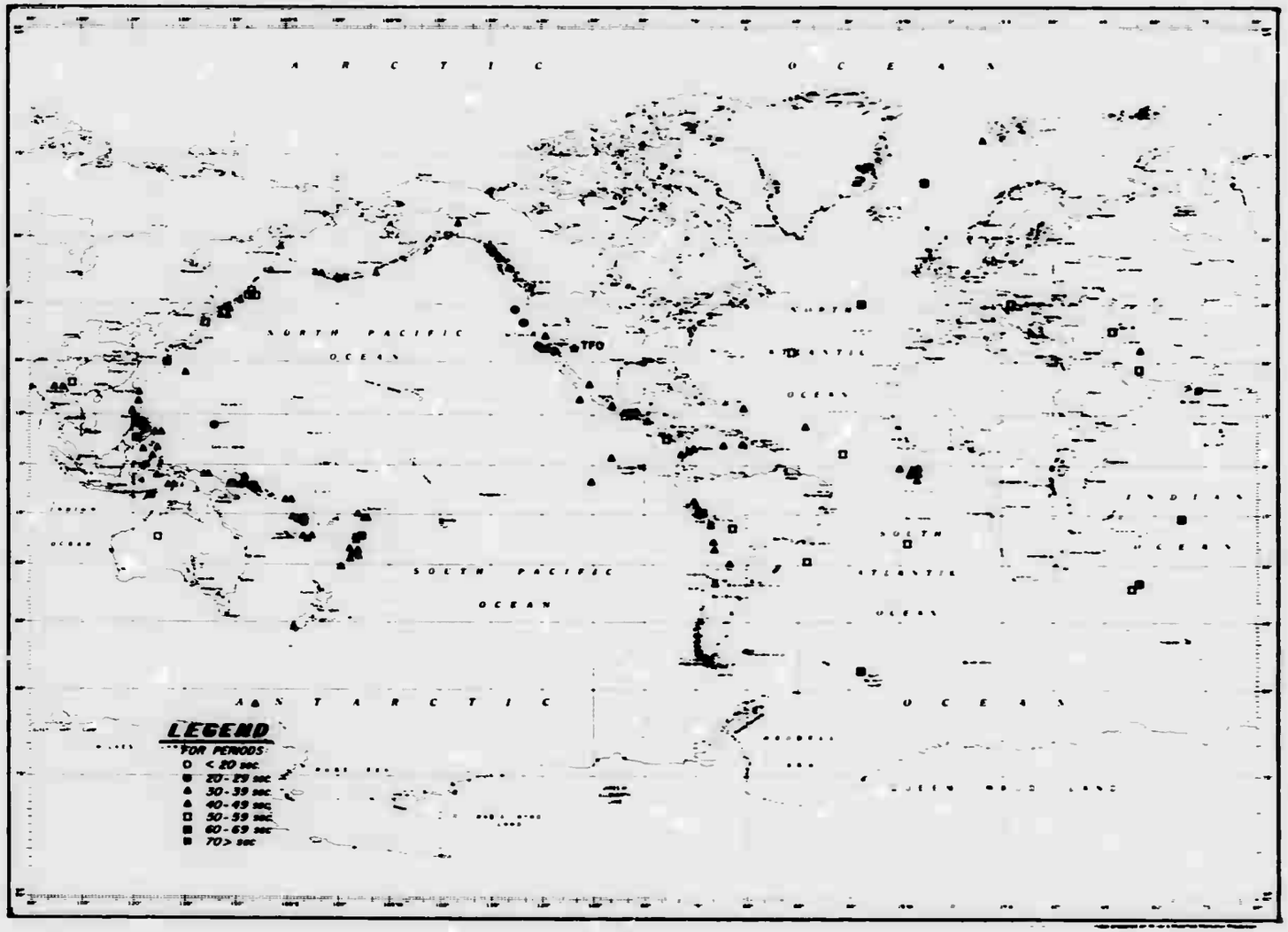

Figure 3. Epicenters and period ranges of events used in film analysis of Rayleigh waves.

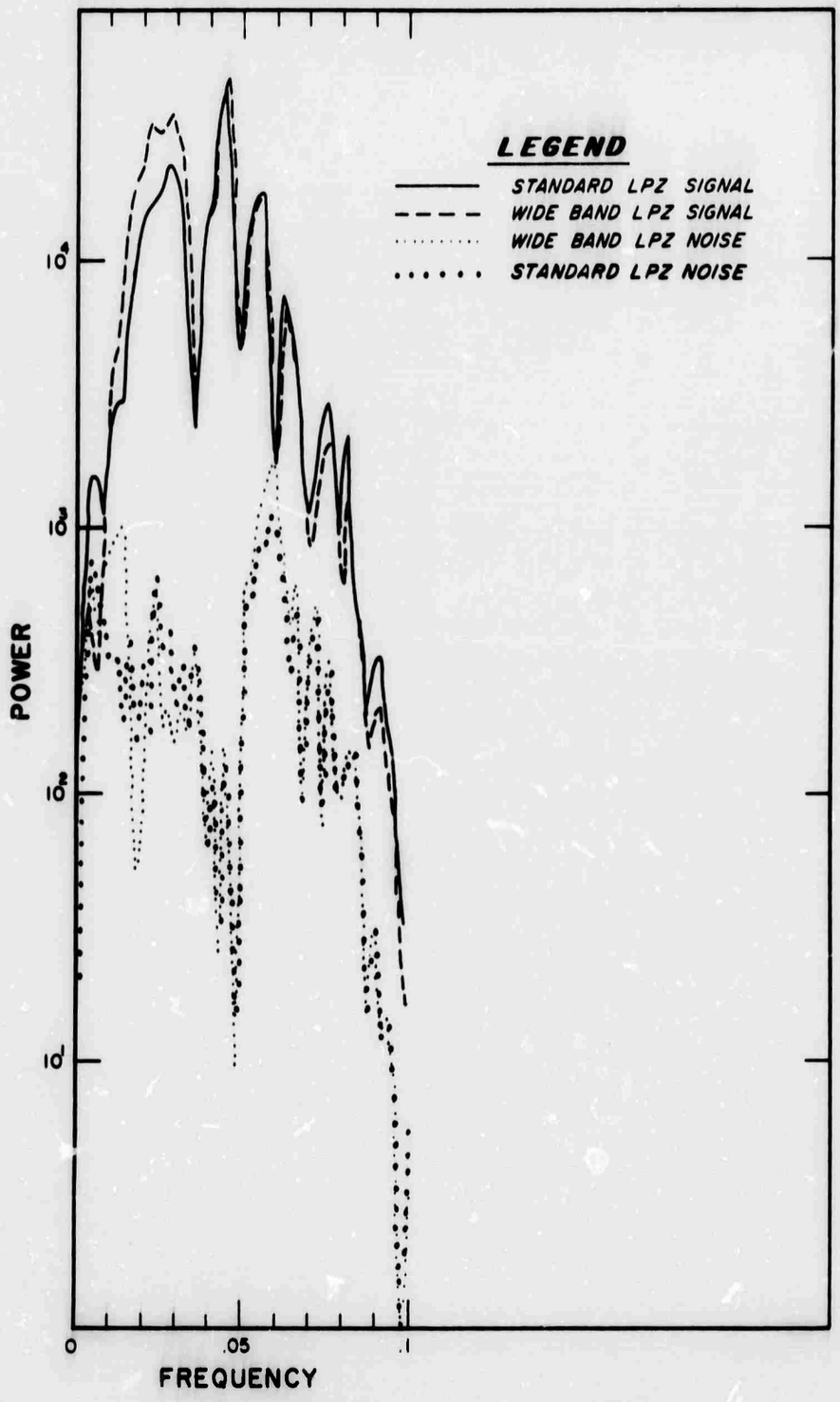

Figure 4. Power spectra of Rayleigh waves from an event in the central Pacific Ocean on 4 November 1969.

TABLE I

Signal to Noise Ratio Determined from Signals
Recorded by a Wide Band Long Period System

EVENT	20.0 Sec	25.0 Sec	33.3 Sec	50.0 Sec	60.0 Sec	75.0 Sec
Philippines	15.1	40.2	17.3	5.8	5.3	2.9
MILROW	17.9	13.4	8.1	5.9	14.1	3.0
Chile	6.7	3.1	5.2	2.5	3.8	4.5
Central Pacific Ocean	5.1	11.5	13.3	14.4	14.9	2.8

THE SPECTRAL RATIO OF P_g AS A DISCRIMINANT FOR EXPLOSIONS

By

William Bakun
Lane Johnson

BLANK PAGE

In this study we have examined the short period spectra of P_g phases recorded at JAS (Jamestown, California) from events in the general area of NTS (Figure 1). In order to limit propagation effects the study has been restricted to events in the same general azimuth and distance range from JAS. The 69 events which have been analyzed to date include the following types: (a) announced underground explosions at NTS, (b) natural earthquakes with epicenters at least 30 km outside the NTS boundary, (c) afterevents of explosions, (d) collapses of explosions, and unidentified events with epicenters on NTS. A limitation of the discrimination aspects of this study has been the small number of natural earthquakes that were available. Examples of the various types of events are shown in Figure 2.

The short period vertical component signals were digitized at a rate of 50 samples per second. The first 8 seconds of the P_g phase was Fourier transformed. These spectra were then corrected for the instrument response and for the effects of attenuation assuming a Q value of 400. The spectral ratio which we have been using is the ratio of the average ground displacement in the 0.6 - 1.25 Hz band to that in the 1.35 - 2.0 Hz band. Calculated values of this spectral ratio are given in Table 1 along with pertinent data about the events. The spectral ratios are plotted in Figure 3.

Of particular interest in Figure 3 is the fact that the convex region containing all known natural earthquakes, field I, does not interesect the convex region containing all known explosions, field II. The two fields are distinctly separate from each other for magnitudes greater than 3.2.

Another point of interest in Figure 3 concerns the afterevents of the large explosions BOXCAR, BENHAM, and JORUM. All 25 of these afterevents lie in the explosion field. In Figure 4 we have compared composite spectra for explosions, natural earthquakes, and BENHAM afterevents. The afterevents appear to be more similar to the explosions than to the natural earthquakes.

The earthquake field of Figure 3 contains 4 unidentified events on NTS, and all 4 of these events occurred 2 - 6 hours after the explosions SCOTCH (magnitude = 5.6). These events could be considered as afterevents of SCOTCH. If this interpretation is accepted, then one must conclude that the spectral behavior of these SCOTCH afterevents is different from that of the afterevents of the larger explosions BOXCAR, BENHAM, and JORUM.

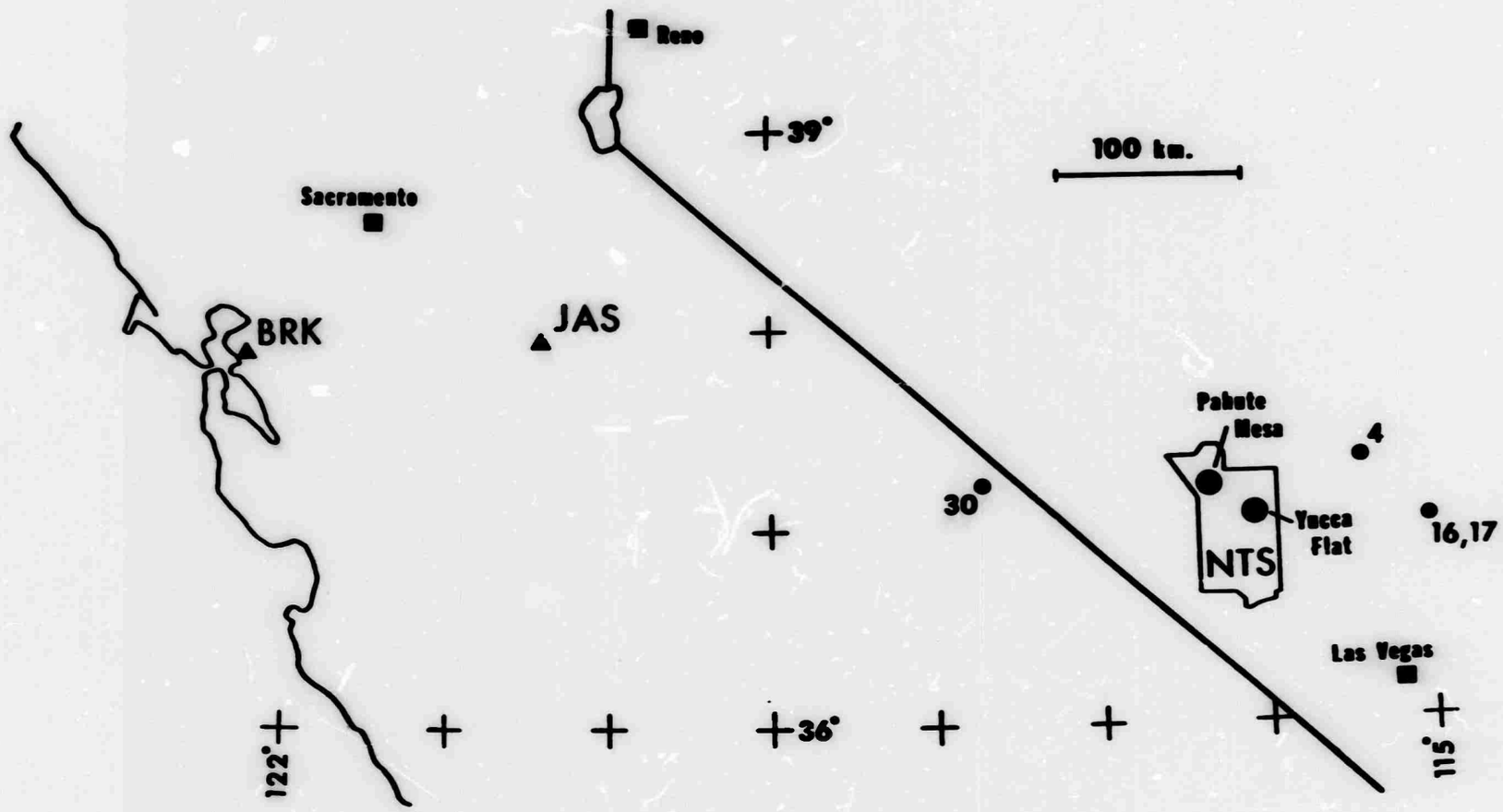

Figure 1. Map of the California-Nevada region showing the relationship of Jamestown (JAS), the Nevada Test Site (NTS), and the natural earthquakes, plotted as small circles, used in this study. The earthquake numbering corresponds to the listing in Table 1.

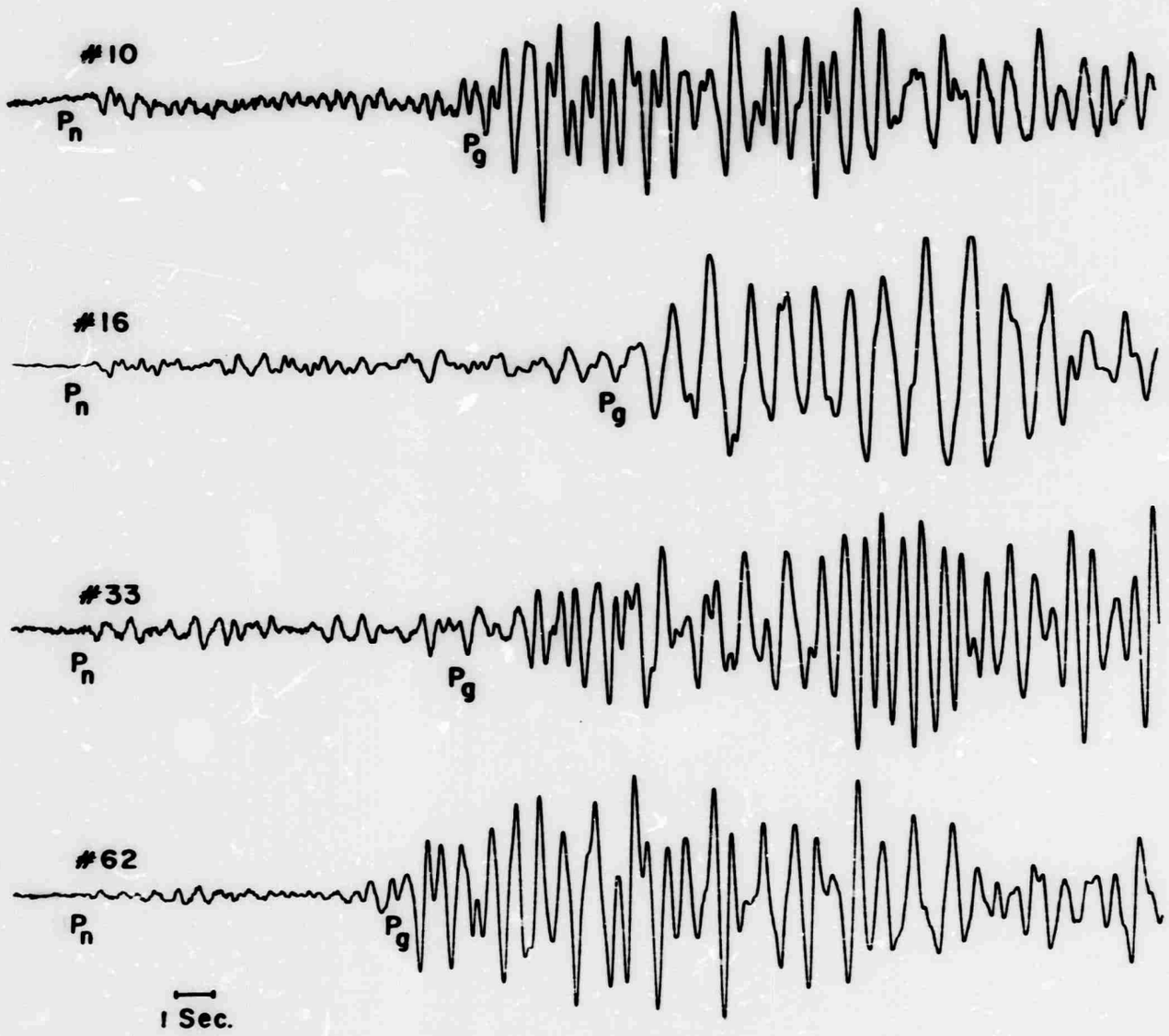

Figure 2. Seismograms recorded on the vertical Benioff at JAS. The traces from top to bottom are an announced NTS explosion, a natural earthquake, an unidentified source, and a BENHAM afterevent, respectively. All of the traces have been normalized to the same maximum amplitude. The numbers refer to the listing in Table I.

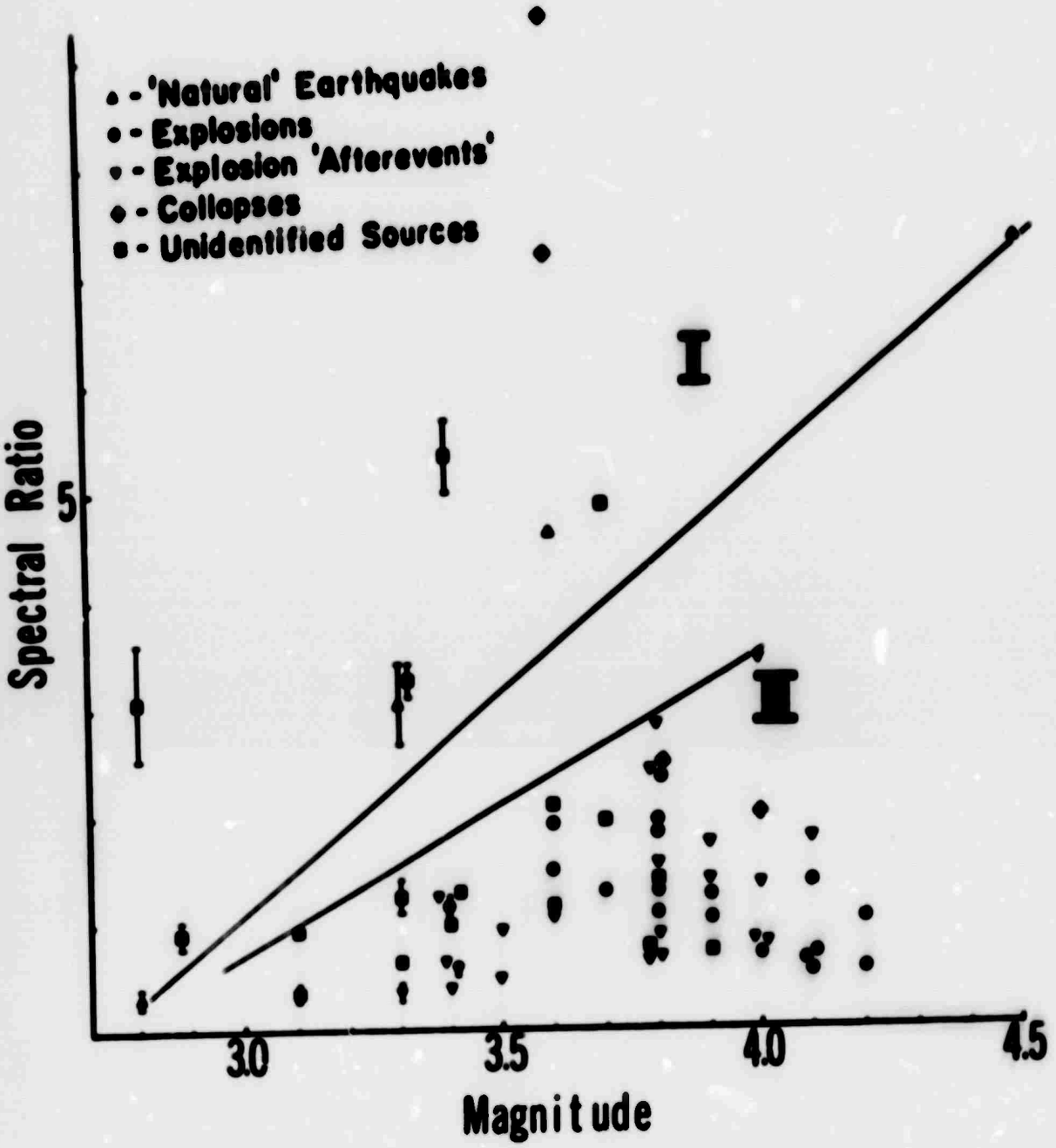

Figure 3. P_g spectral ratio of vertical surface displacement, corrected for attenuation with Q = 400, at JAS for events within 100 km of NTS. I and II denote the earthquake and explosion fields, respectively.

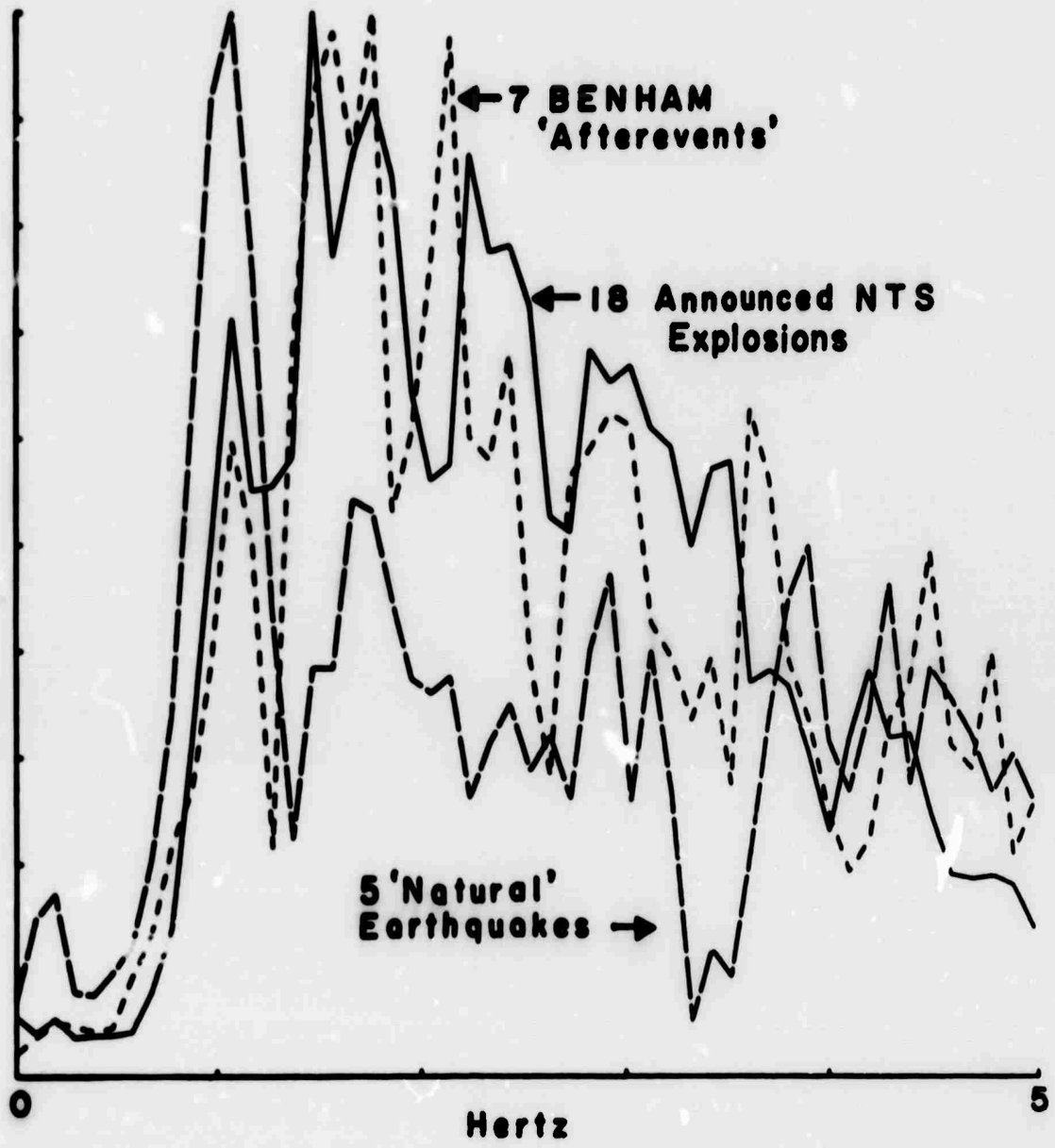

Figure 4. P_g composite spectra at JAS of announced NTS explosions, natural earthquakes, and BENHAM afterevents. Spectra have been corrected for attenuation (Q = 400).

Table 1. Event characteristics

#	Type	Date	OT (GMT)	Lat. (N)	Long. (W)	Δ (km) from JAS	M(1)	Spectral Ratio (P_g)	Comments
1	a	03 Feb. 66	18-17-37.1	37°07'34".7	116°04'10".1	380	4.2	1.00	PLAID II (Y), in alluvium(2)
2	a	01 Apr. 66	18-40-00	37 06 09.7	116 01 11.8	395	3.6	1.90	LIME (Y), in alluvium(2)
3	a	06 Apr. 66	13-57-17.1	37 08 22.3	116 08 27.1	385	4.1	-	STUTZ (Y), in tuff(2)
4	b	06 Apr. 66	17-56-31.7	37.3	115.4	450	3.6	4.60	(3)
5	d	19 May 66	15-37-18	37 06 40.1	116 03 28.5	390	3.8	2.43	DUMONT Collapse (Y)(2)
6	d	1 July 66	01-33-40	37 18 56.9	116 17 56.3	390	4.0	1.99	HALFBEAK Collapse (Y)(2)
7	a	12 Sept.66	15-30-00.5	36 52 37.0	115 57 02.2	410	3.9	1.04	DERRINGER (A5)(2)
8	e	05 Jan. 67	12-15-23.1	37.3	116.5	360	3.6	1.15	(3)
9	d	23 Feb. 67	21-11-35	37 07 36.7	116 03 59.0	390	3.6	7.17	AGILE Collapse (Y)(2)
10	a	02 Mar. 67	15-00-00.0	37 09 57	116 02 55	395	3.6	1.49	RIVET III (Y), in alluvium(2)
11	e	03 Mar. 67	15-19-02	(37.3)	(116.4)	(360)	3.4	0.98	(4)
12	a	07 Apr. 67	15-00-00.0	37 03 15.8	116 01 20	400	3.8	1.91	FAWN (Y), in alluvium(2)
13	a	21 Apr. 67	15-09-00.0	37 01 09.4	116 02 14.7	400	3.7	1.28	CHOCOLATE (Y), in alluvium(2)
14	a	27 Apr. 67	14-45-00.0	37 08 19.6	116 03 47.5	395	4.0	0.69	EFFENDI (Y), in alluvium(2)
15*	e	28 Apr. 67	12-22-58	37.1	116.0	(390)	2.9	0.91	(4)
16	b	07 May 67	18-01-36.1	37.0	115.0	490	4.5	7.22	(3)
17	b	09 May 67	00-42-25.9	37.0	115.0	490	3.3	3.01	(3)
18	e	23 May 67	15-37-47	(37.2)	(116.4)	(360)	3.4	5.34	Assume hypocenter of event at 20-14-06.5
19	e	23 May 67	16-22-08	(37.2)	(116.4)	(360)	2.8	3.07	"

Table 1--page 2

#	Type	Date	OT (GMT)	Lat. (N)	Long. (W)	Δ (km) from JAS	M(1)	Spectral Ratio (P_g)	Comments
20	e	23 May 67	17-52-04.1	37.3	116.4	360	3.3	3.26	(3)
21	e	23 May 67	20-14-06.5	37.2	116.4	360	3.7	4.88	(3)
22	a	22 June 67	13-10-00.0	37°02'32"	116°01'43"2	400	3.8	2.34	SWITCH (Y), in tuff(2)
23	a	29 June 67	11-25-00.4	37 01 43	116 01 24	400	3.8	1.08	UMBER (Y), in alluvium(2)
24	a	27 July 67	13-00-00	37 08 55.4	116 02 54.7	395	4.3	-	STANLEY (Y), in tuff(2)
25	e	08 Aug. 67	17-52-13.8	37.2	116.5	360	3.3	1.24	(3)
26	e	09 Aug. 67	06-45-05.3	37.2	116.7	340	3.4	1.24	(3)
27	a	10 Aug. 67	14-10-00.0	37 09 24.1	116 02 50.2	395	3.9	1.23	WASHER (Y), in tuff(2)
28	e	24 Aug. 67	13-30-00	(37.3)	(116.4)	(360)	3.9	0.70	(4)
29	d	07 Sept.67	14-24-50	37 09 11.4	116 03 10.0	390	3.6	9.37	YARD Collapse (Y)(2)
30	b	27 Oct. 67	01-42-26	(37.2)	(117.7)	(260)	2.8	0.31	White Mountains Earthquake
31	a	18 Jan. 68	16-30-00.0	37 08 44.1	116 03 56.4	395	4.2	0.55	HUPMOBILE (Y)(2)
32	a	26 Jan. 68	16-00-00.1	37 16 51.1	116 30 52	350	3.8	1.80	CABRIOLET (P), in rhyolite(2)
33	e	31 Jan. 68	15-30-00	(37.3)	(116.4)	(360)	3.7	1.92	(4)
34	a	12 Mar. 68	17-04-00.1	37 00 27	116 22 11.9	350	4.1	0.66	BUGGY (R), in basalt(2)
35	a	14 Mar. 68	15-19-00.1	37 02 51.8	116 00 38.9	400	3.4	1.15	POMMARD (Y), in alluvium(2)
36	a	23 Apr. 68	17-01-30.0	37 20 15.8	116 22 32.1	345	4.1	0.54	SCROLL (P), in tuff(2)
37	c	26 Apr. 68	15-14-52.0	37.1	116.2	(360)	4.0	0.82	(3)-BOXCAR 'Afterevent' in Rayleigh wave
38	c	"	15-24-00	(37.2)	(116.4)	(360)	4.0	0.78	BOXCAR 'Afterevent'
39	c	"	15-32-21.0	37.2	116.5	360	4.3	0.93	(3)-BOXCAR 'Afterevent' (collapse?)

Table 1--page 3

#	Type	Date	OT (GMT)	Lat. (N)	Long (W)	Δ (km) from JAS	M(1)	Spectral Ratio (P_g)	Comments
40	c	26 Apr. 68	16-08-00	(37.2)	(116.4)	(360)	3.5	0.93	BOXC R 'Afterevent'
41	c	"	16-12-50	(37.2)	(116.4)	(360)	3.4	0.65	"
42	c	"	16-35-17.0	37.3	116.4	360	4.1	1.77	(3)-BOXCAR 'Afterevent'
43	c	"	16-45-30	(37.2)	(116.4)	(360)	4.0	1.35	BOXCAR 'Afterevent'
44	c	"	20-42-19.0	37.2	116.4	360	3.4	0.63	(3)-BOXCAR 'Afterevent'
45	c	"	21-50-15	(37.2)	(116.4)	(360)	3.3	0.37	BOXCAR 'Afterevent'
46	c	27 Apr. 68	09-06-33	(37.2)	(116.4)	(360)	3.8	0.66	"
47	e	04 May 68	23-28-45.0	37.2	116.4	360	3.1	0.35	(3)
48	e	15 May 68	16-01-11.0	37.2	116.3	360	3.3	0.63	(3)
49	e	30 June 68	21-21-22.0	37.2	116.6	360	3.1	0.93	(3)
50	a	30 July 68	13-00-00.0	37°08'00"	116°04'56"	390	4.1	0.46	TANYA (Y)(2)
51	e	15 Nov. 68	15-30-00	(37.1)	(116.0)	(390)	3.6	2.09	(4)
52	a	15 Nov. 68	15-45-00.4	37 01 34	116 02 00	400	3.8	1.27	KNIFE B (Y)(2)
53	a	22 Nov. 68	16-19-00.2	37 08 24	116 02 32	395	4.1	1.35	TINDERBOX (Y)(2)
54	e	12 Dec. 68	15-20-00	(37.1)	(116.0)	(390)	3.8	1.36	(4)
55	c	19 Dec. 68	17-30-22.8	37.2	116.5	360	3.4	1.24	(3)-BENHAM 'Afterevent'
56	c	"	19-18-19.6	37.3	116.4	360	3.5	0.48	"
57	c	"	19-54-01.2	37.2	116.5	360	3.4	0.39	"
58	c	"	22-23-26.3	37.2	116.5	360	3.6	1.06	" (collapse?)

Table 1 - page 4

#	Type	Date	OT (GMT)	Lat. (N)	Long. (W)	Δ (km) from JAS	M(1)	Spectral Ratio (P_g)	Comments
59	c	20 Dec. 68	20-08-20.4	37.2	116.5	360	3.8	0.61	(3)-BENHAM 'Afterevent'
60	c	21 Dec. 68	00-14-25.2	37.3	116.5	360	4.3	-	"
61	c	06 Jan. 69	06-34-14.5	37.3	116.5	360	4.2	-	"
62	c	10 Jan. 69	09-41-21.5	37.2	116.5	360	3.9	1.72	"
63	c	"	17-21-44.5	37.2	116.5	360	3.8	2.82	"
64	c	"	17-14-17.2	37.2	116.5	360	3.8	0.88	"
65	c	18 Mar. 69	14-40-02.7	37.2	116.0	400	3.8	0.69	(3)
66	c	16 Sept.69	15-43-39.2	37.3	116.5	360	3.8	2.38	(3)-JORUM 'afterevent'
67	c	"	16-23-53.8	37.3	116.5	360	3.9	1.39	"
68	c	"	17-31-14.7	37.3	116.5	360	4.0	3.44	"
69	c	"	18-15-39.3	37.3	116.5	360	3.8	1.52	"

(1) Magnitudes based on P_n and P_g amplitudes at JAS. The scale is based on Wood-Anderson magnitudes at BRK for larger events.

(2) Personal communication, Don Springer, 1970. The letter designations (Y) and (P) indicate the test areas Yucca Flat and Pahute Mesa, respectively; (A5) indicates the explosion was detonated in alluvium; (R) indicates an elongated explosive charge was detonated as a "row shot" at Buckboard Mesa.

(3) U. S. C. G. S. hypocenter.

(4) Arrival times at the Berkeley net indicate NTS hypocenter. Δ = 360 or 390 km is assumed for purposes of attenuation and magnitude calculations.

* Arrival times available for this event are inconsistent so that the epicentral distance is uncertain. The magnitude thus may be as large as 3.2 if the epicenter is 500 km from JAS. The error in the attenuation correction due to the epicentral uncertainty is not significant.

A NOTE ON SURFACE WAVE MAGNITUDE DETERMINATION

By

Otto W. Nuttli

The ratio of m_b to M_S has been found to be an effective discriminator for distinguishing explosions from earthquakes. For small magnitude events, however, little energy is present in the 20 second period band and the usual determination of M_S is not possible with data from conventional long-period instrumentation. The use of short period surface waves, 4-10 seconds, in determining magnitude becomes attractive.

USSR and Czechoslovakian seismologists have developed a relation applicable to surface waves of all periods:

$$M = \log \frac{A}{T} + 1.66 \log \Delta + 3.3$$

in which, A, T are the amplitude (microns) and period of the maximum ground displacement on the seismogram, Δ is in degrees.

We applied this relation and the standard procedure using 20 second waves to three events, explosions in Central Asia and the Sahara and an earthquake in southern Illinois.

Event	Date	M_S(20)	M_S(4-10)
Central Asia explosion	July 19, 1964	3.4	4.3
Sahara explosion	Feb 27, 1965	4.3	4.9
Illinois earthquake	Nov 09, 1968	5.2	6.0

The short period surface wave amplitudes were taken from seismograms in the range of 15°-40°. The Soviet formula gave M_S values that are almost one magnitude unit higher than those determined for 20 second waves.

In studying the Illinois earthquake, a new empirical relation was developed to force M_S from the maximum surface waves to be the same as the value from 20 second horizontal surface waves recorded at large distances. The result is

$$M = \log \frac{A}{T} + 1.66 \log \Delta + 2.40.$$

The coefficients turned out to be the same as in the Soviet relation, except for the constant, which is 0.9 less. When this relation is applied to the two explosions studied the discrepancy between the two methods largely disappears.

This relation must be tested for more events and for regional effects because its value in determining surface wave magnitudes for m_b less than 4 is clear. We have applied it to a number of small earthquakes in the mid-continent for which 20 second waves were not detectable with the instrumentation in use.

MULTIPATHING OF RAYLEIGH WAVES GENERATED BY MILROW

By

Harry Mack

ABSTRACT

Frequency wavenumber analysis of Rayleigh waves generated by MILROW shows that multipathing occurs between the source and LASA in the period range 20-25 seconds. No multipathing is detected at longer periods.

The underground nuclear explosion MILROW was detonated on October 2, 1969 in the Aleutian Islands. The body wave magnitude (m_b) was 6.5 and Rayleigh waves were well recorded at LASA. Frequency-wavenumber analysis of the Rayleigh wavetrain showed that significant multipathing occurred at periods in the range 20-25 seconds but none was observed at longer periods.

Figure 2 is a composite of three plots. The upper curve shows the peak wavenumber spectral value versus frequency. The coherency remains high and almost flat from 0.06 Hz to about 0.02 Hz. The values then decrease rapidly towards the lower frequencies. The triangle shows the peak wavenumber spectral value at 0.05 Hz for an arrival which came approximately five minutes after the original wavetrain.

The middle curve shows how the back azimuth of arrival varied with frequency. The angle increases with decreasing period to an asymptotic value of 306° which is close to the true back azimuth. The triangle indicates that the later arrival had a back azimuth of 321°. The value of 300° at 0.06 Hz is difficult to explain except that this value may be the result of averaging over more than one direction of arrival.

The bottom curve shows the phase velocity dispersion curve. The velocity increases with period in an expected manner and then low values appear as the signal disappears at the lower frequencies. This phenomenon is the result of spectral leakage.

Figure 2 shows the wavenumber spectrum at 0.05 Hz at the two time periods indicated on the figure. The main arrival at this frequency is followed by a later arrival five minutes afterwards at a higher angle. Both phase velocities are the same, and this figure illustrates a case of multipathing.

In conclusion, the above results indicate that multipathing of Rayleigh waves may not be a problem at periods greater than 40 seconds.

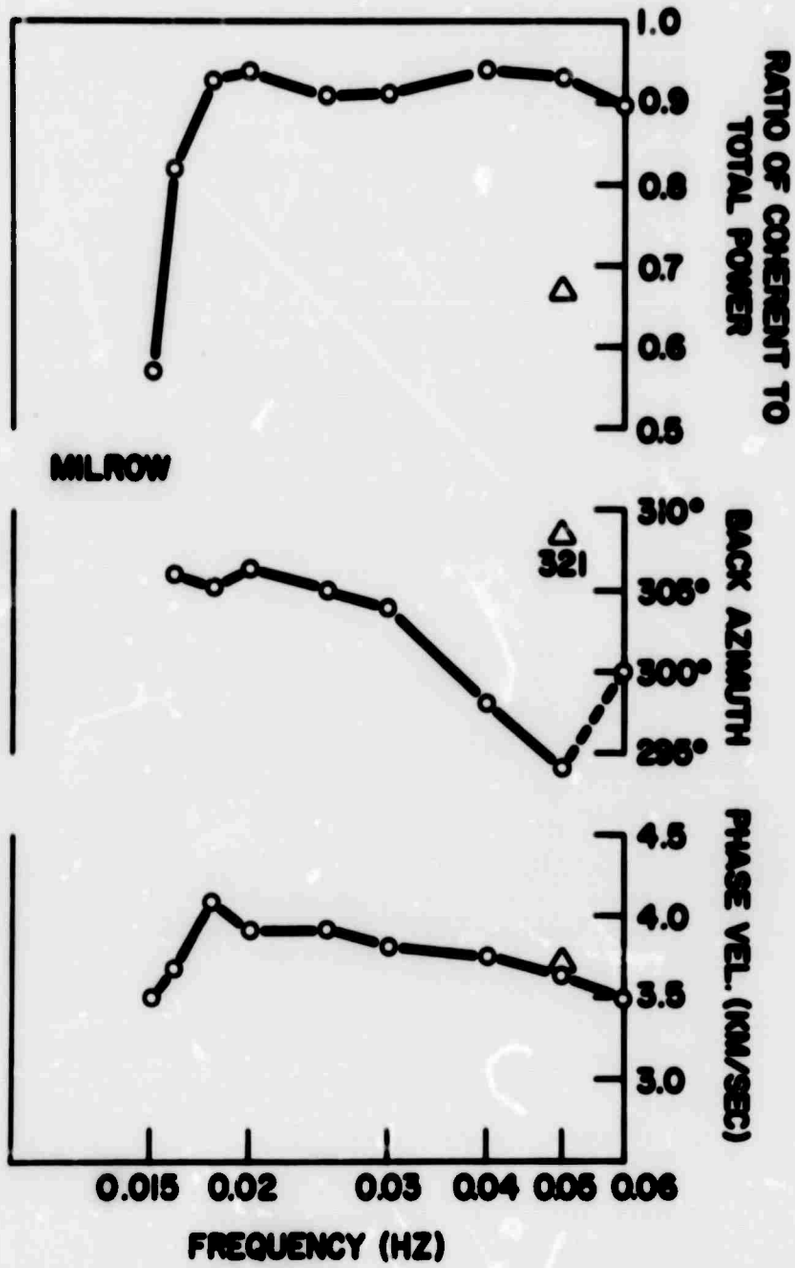

Figure 1. Analysis of Rayleigh waves generated by MILROW recorded at LASA. The top curve is the normalized peak value of the wavenumber spectra versus frequency. The middle curve shows direction of arrival versus frequency. The bottom is the phase velocity dispersion curve. The triangles relate to the later arrival.

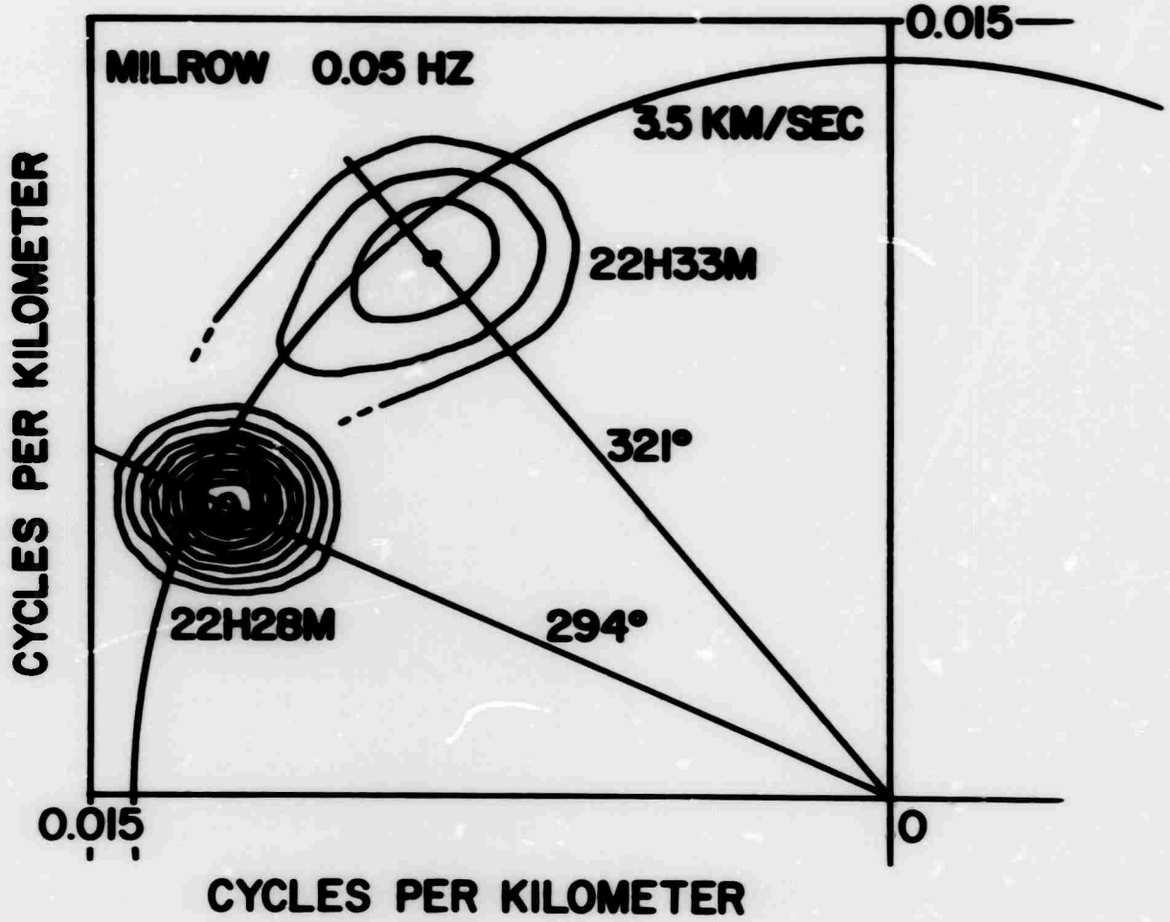

Figure 2. High resolution F-K spectra, at 0.05 Hz, of the Rayleigh wave from MILROW recorded at LASA. The contours (in dB) show the direction and velocity of two separate arrivals at the times shown, illustrating the effects of multipathing.

SEISMIC IDENTIFICATION AT SHORT DISTANCES

By

Alan Ryall

University of Nevada
Mackay School of Mines
Reno, Nevada 89507

INTRODUCTION

During the period the University of Nevada Seismological Laboratory has had AFOSR grant support, we have pursued an orderly development of seismology in the Nevada region, with the idea that a procedure aimed at overall evaluation of blast and earthquake characteristics would prove to be a more fruitful approach to problems of the Vela Uniform program than one based on limited objectives. After working for several years with data from three widely separated outstations, we found ourselves still far from this goal, and in July, 1969 began the construction of a statewide seismic telemetry system. By November, enough stations of this system were installed to permit detailed analysis of seismic events over most of the Nevada region; about a month ago we completed the development of computer programs for epicenter determination, and ran out data for a six-months' period of time. Figure 1 shows the location of earthquakes for part of this period, as well as the location of stations of the telemetry network. From this analysis several characteristics of Nevada seismic events emerged which are pertinent to the discrimination problem, and these are described below.

For the benefit of other workers interested in Nevada earthquakes and explosions, we are presently publishing a Bulletin of the University of Nevada Seismological Laboratory, which lists all of our seismogram readings as well as epicenters, magnitude and other information on events that are large enough to be located by the computer routine. This Bulletin, which will be issued quarterly, can be obtained on request from the Director, Seismological Laboratory.

S_n as a discriminant for earthquakes and explosions

Two years ago, the University of Nevada was involved in an investigation of earthquake activity following large underground explosions. One of the points covered in that study had to do with the difficulty in identifying the same seismic waves for both earthquakes and explosions, and errors in epicenter determination that would result from misidentification of phases. This identification problem is illustrated by Figure 2, which shows records made at Tonopah of a small underground explosion and three aftershocks of a large underground explosion. For Nevada Test Site events the Tonopah station, at a distance of about 110 km, records only P_g and S_g waves for explosions; but recordings of NTS aftershocks have an additional large phase which arrives about three seconds before S_g. For large aftershocks, this phase was usually identified as S_g, with the result that an aftershock would be located about 20 km too close to the Tonopah station. For small aftershocks (Figures 2c and 2d), the P_g phase was often too small to see, and the two later phases were identified as P_g and S_g, placing the epicenter within 20 km of Tonopah.

With improved accuracy in epicentral determination, we are now finding "extra" S phases to be characteristic of earthquakes, and the

lack of such arrivals to be characteristic of explosions. For example, on examination of the list of epicenters and data for six months in 1969 and 1970, we noticed that earthquakes along the Fairview fault zone generate an S wave that arrives at the Battle Mountain station before S_g, while a group of seismic events just east of that zone generate only S_g at Battle Mountain. Based on this observation, inquiries were made of mining companies in the area, and the events with only one S phase were found to be open-pit quarry blasts.

On Figure 3, Battle Mountain recordings are shown for earthquakes and mine explosions at similar distances. At the top of the figure, a blast in the area just mentioned is seen to have only one S phase, while an earthquake on the Fairview fault near Slate Mountain generates two S waves. At the bottom of the figures, an Ely explosion and a Mina earthquake are compared, with only the earthquake having two clear S arrivals.

Figures 4 and 5 show evidence that the early S wave observed for natural earthquakes is probably S_n. Beyond about 140 km distance this wave has apparent velocity of 4.1 km/sec (Figure 4), which is a little low but not unreasonable for S_n in the Basin and Range region. For distances less than 140 km, the earliest of two clear S arrivals for earthquakes has a velocity of 3.6 km/sec, which is appropriate for S_g; interpretation of the double S wave at short distances is still in progress. On Figure 5, the time difference between arrivals of the double S phase is compared with the time difference $P_g - P_n$, for earthquakes more than 140 km for the recording stations. The relationship shown is appropriate for the wave S_n. Based on these very preliminary observations, it would appear that the S_n phase can be used as a discriminant for earthquakes and explosions, up to distance of several hundred kilometers. Work in progress at the present time is aimed at explaining the difference in S-wave generation for earthquakes and blasts, and extending our present observations to larger distances.

$P_g - P_n$ as a discriminant

On Figure 6, the time difference $P_g - P_n$ is shown as a function of distance for 62 earthquake observations and 13 subarray explosions. A line drawn by eye through the points separates all but 2 of the blast points from all but 3 of the earthquake points. This method of discriminating earthquakes and explosions is similar to one proposed several years ago by H.I.S. Thirlaway, in that the events are located using only P_g and S_g readings at several stations, and $P_g - P_n$ time differences are then used together with epicentral distances as an indication of focal depth. As with the S_n observations described above, data currently on hand extends only to about 300 km, and an effort is being made at present to extend the technique to larger distances.

Amplitude ratios

On Figure 7, the ratio of maximum trace amplitude for P_g to maximum trace amplitude for Sg is shown as a function of distance for a number of earthquakes and quarry explosions. In spite of some scatter, the figure indicates that there is a tendency for earthquakes to have a P_g/S_g amplitude ratio less than 1.0, while the ratio is usually greater than 1.0 for blasts. Part of the scatter in Figure 7 is due to azimuthal variation in radiation of seismic waves for the natural earthquakes. For example, in cases where a high P_g/S_g ratio is observed at one location for a natural event, stations in different azimuths from the epicenter almost invariably see a P_g/S_g ratio less than 1.0. On the other hand, the six explosion points on the wrong side of the line at a distance of about 245 km are for three Ely blasts measured at Tonopah and Battle Mountain -- in all cases, the two stations recorded almost identical P_g/S_g ratios in spite of a 65° difference in epicentral azimuth. When radiation patterns for earthquakes and explosions are taken into consideration, the value of amplitude ratios as a discriminant may be better than suggested by Figure 7.

Spectral characteristics

As a first step toward a study of spectral characteristics of small Nevada earthquakes and explosions, a number of mine-blast and earthquake recordings were digitized and subjected to spectral analysis using the Cooley-Tukey algorithm, which is defined in terms of a Fourier transform. The results of this analysis are shown on Figure 8 for three earthquakes, an NTS collapse event, and two mine blasts, all recorded on a short-period vertical instrument at Tonopah. Because of the preliminary nature of this analysis, no attempt was made to correct the spectral amplitudes for effects due to differences in distance, magnitude or instrument response.

Of the six events shown on Figure 8, only one -- the collapse event -- has a simple, relatively monochromatic spectrum. This is not surprising, since hole collapses have a characteristically sinusoidal appearance at the Tonopah station. All of the other events shown on the figure have complicated spectra, with no obvious spectral characteristics that can be ascribed simply to differences between earthquake and blast source. As an example of other parameters which must be taken into account in this kind of study, the two sets of spectra shown at the top left-hand side of the figure are for earthquakes located within a few kilometers of each other, but with focal depths differing by about 10 km. The P-wave spectra for these two events have peaks at the same frequencies but with different amplitudes; however, the two S-wave spectra are quite dissimilar, with the S-spectrum for the shallow earthquake having a number of notches and peaks in common with the spectrum for a nearby (Gabbs) explosion. To extend this study, we are presently operating a tripartite array continuously in the Slate Mountain area, and plan to carry out spectral analysis on events with a range of focal depth, hopefully to separate out spectral characteristics related to specific source parameters.

Finally, on Figure 9 peak spectral frequencies are plotted for P and S waves, for the earthquakes and explosions whose spectra are shown on Figure 8. On this plot there is a clear separation between the two types of events, but the analysis needs to be extended to include a large number of earthquakes and blasts, as well as effects of magnitude, station site characteristics, epicentral distance, focal depth, etc.

Summary

After many years of working with data from a few locally-recording outstations, we have now almost completed the installation of a statewide seismic telemetry system, and this system is already beginning to provide data which will make possible very detailed studies of earthquakes and explosions in the Nevada region. Based on analysis completed only a month ago, we are finding significant differences between local recordings of small earthquakes and mine blasts -- in the relative generation of different seismic waves, amplitude ratios, and peak spectral frequencies.

As an extension of this very preliminary work, we are now compiling data aimed at separating out effects of specific source and station-site characteristics. Then, with a better understanding of relationships between various source parameters (focal depth, mechanism, etc.) and measurable characteristics of local recordings, we hope to be able to predict observable effects at greater epicentral distances for small-magnitude events.

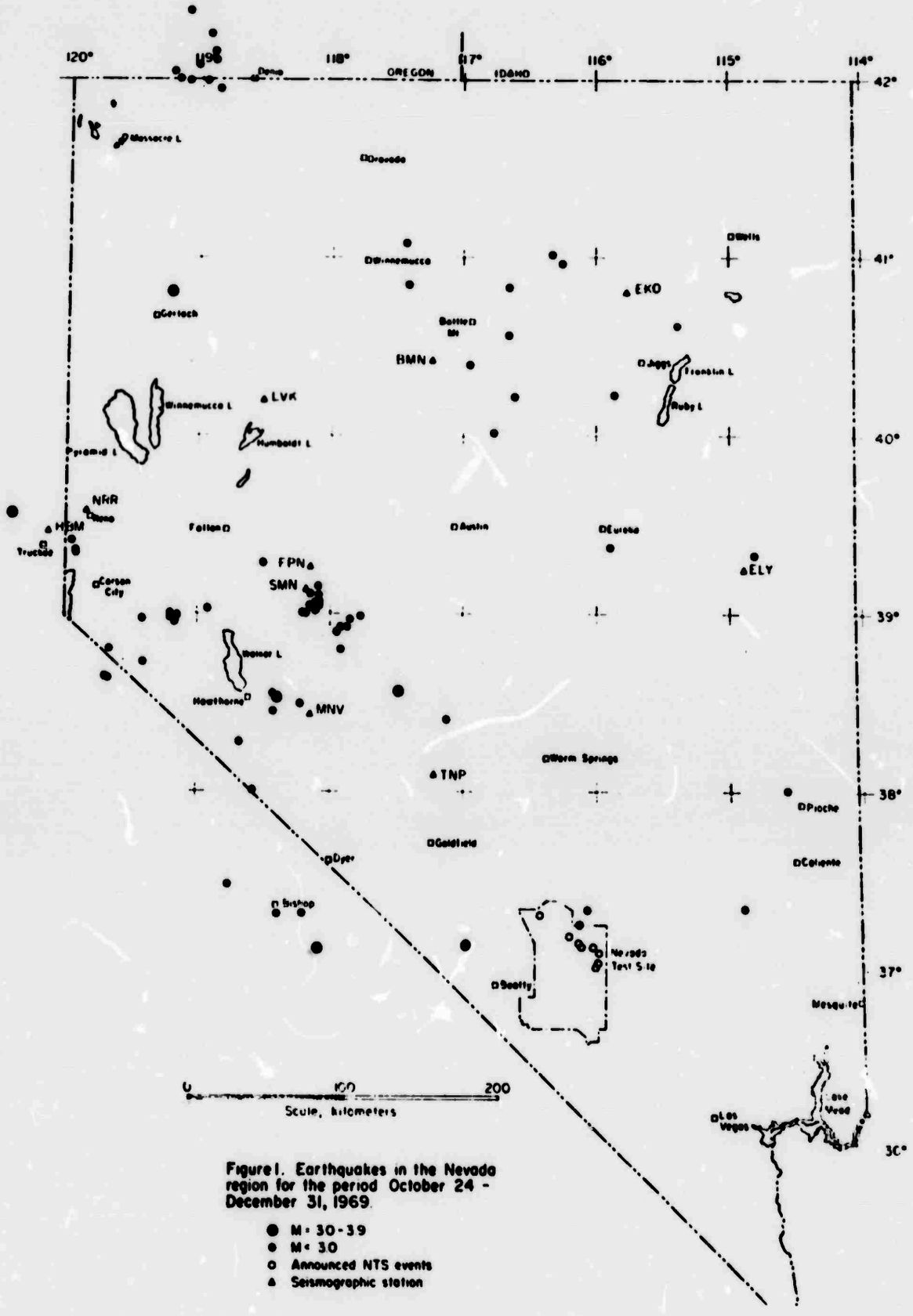

Figure 1. Earthquakes in the Nevada region for the period October 24 - December 31, 1969.

- M = 3.0-3.9
- M < 3.0
- Announced NTS events
- Seismographic station

Figure 1.

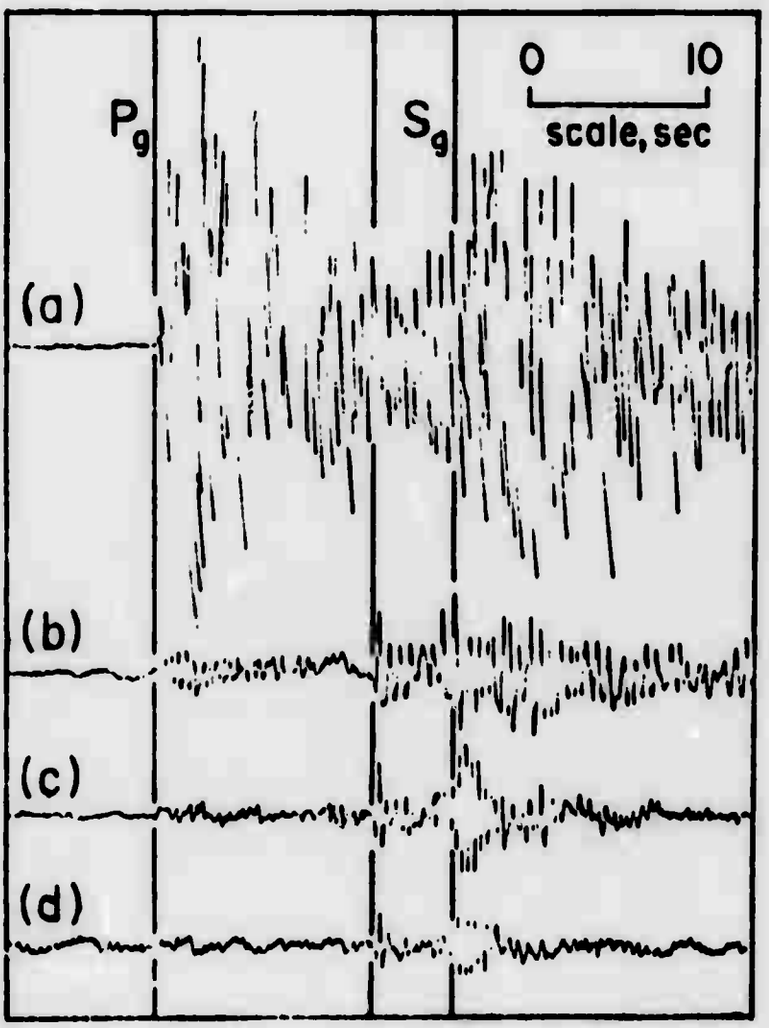

Figure 2.

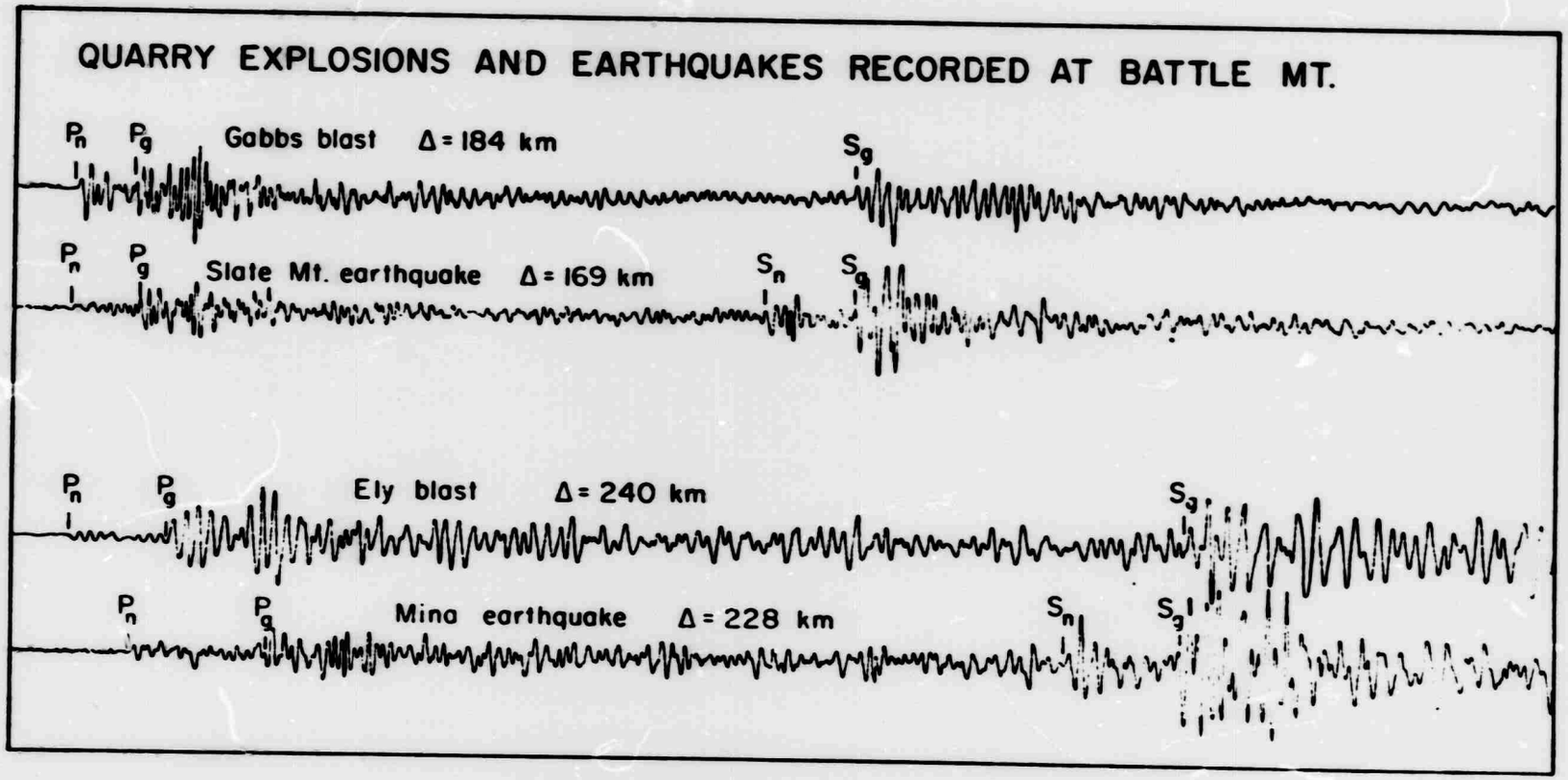
QUARRY EXPLOSIONS AND EARTHQUAKES RECORDED AT BATTLE MT.
Pn
Pg
Gabbs blast Δ = 184 km
Sg
Pn
Pg
Slate Mt. earthquake Δ = 169 km
Sn
Sg
Pn
Pg
Ely blast Δ = 240 km
Sg
Pn
Pg
Mina earthquake Δ = 228 km
Sn
Sg

Figure 3.

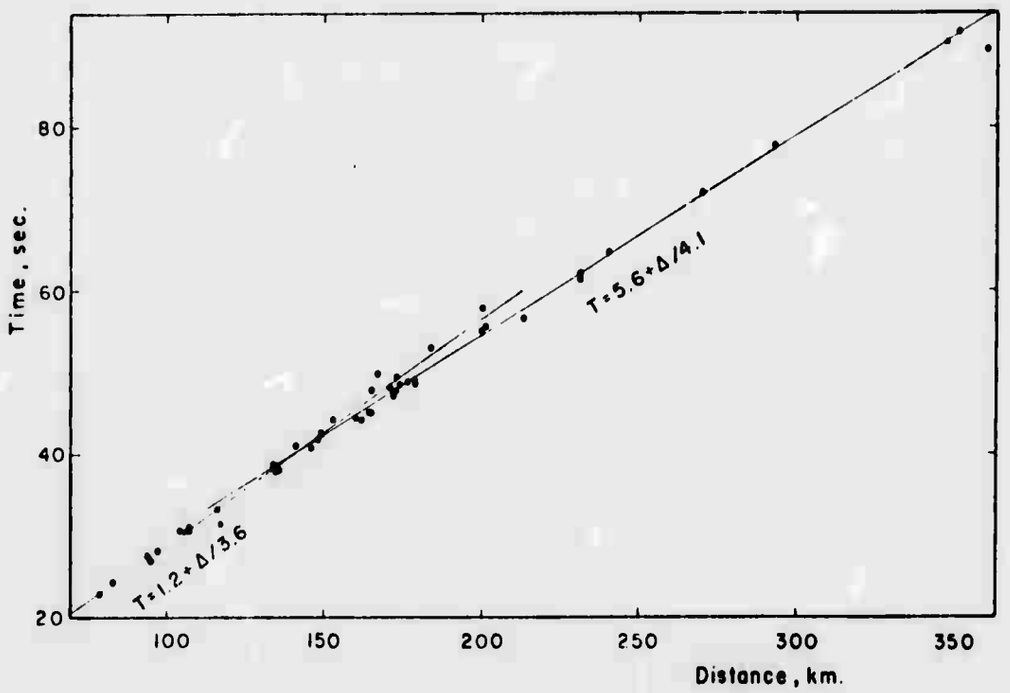

Figure 4.

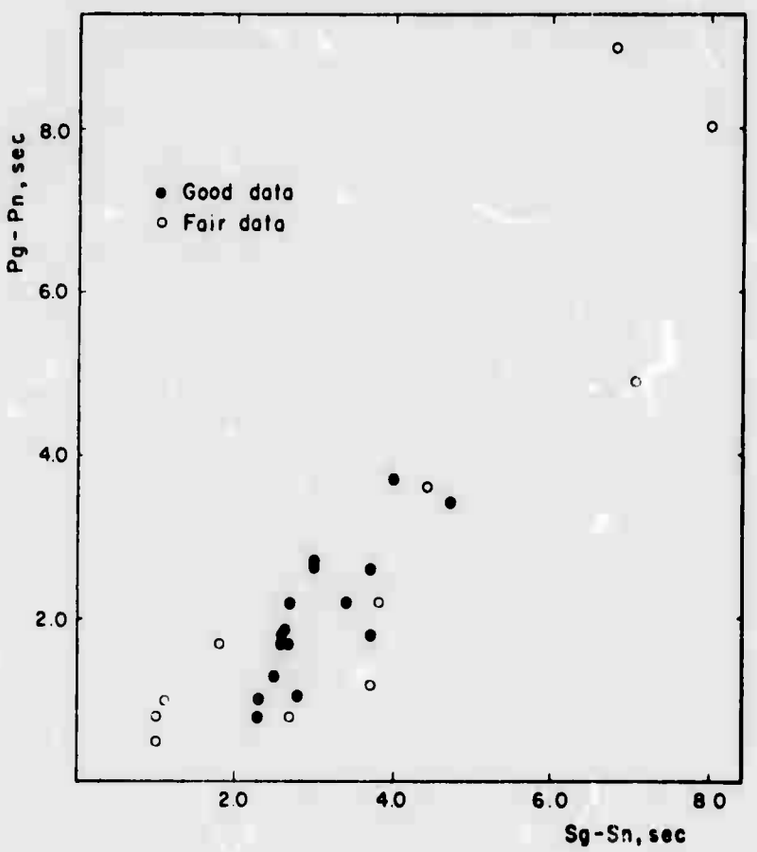

Figure 5.

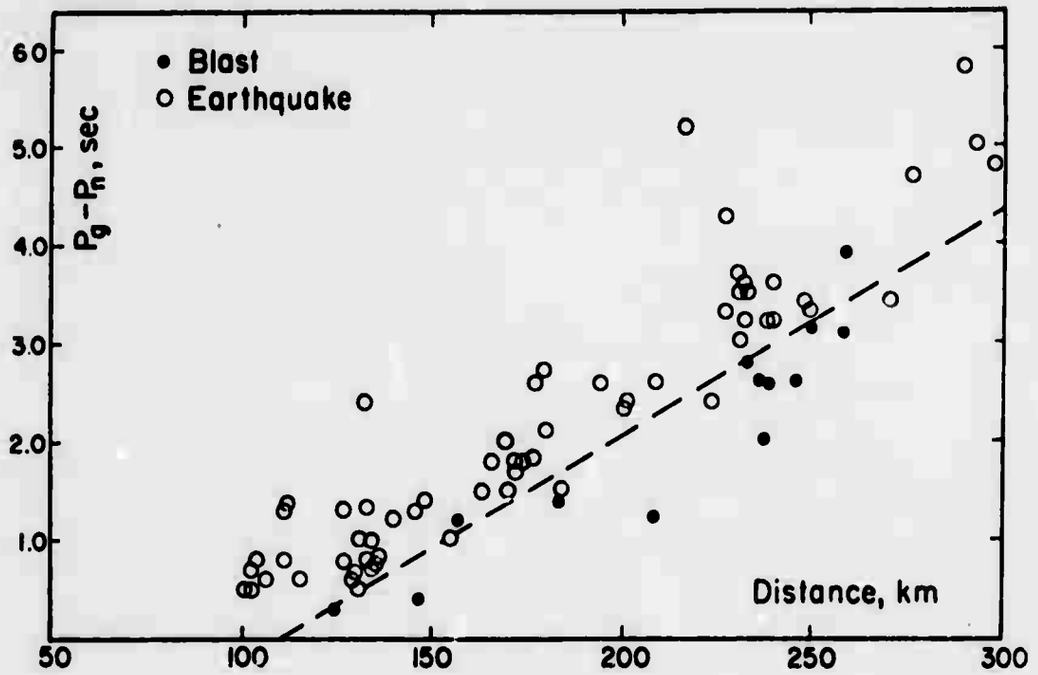

Figure 6.

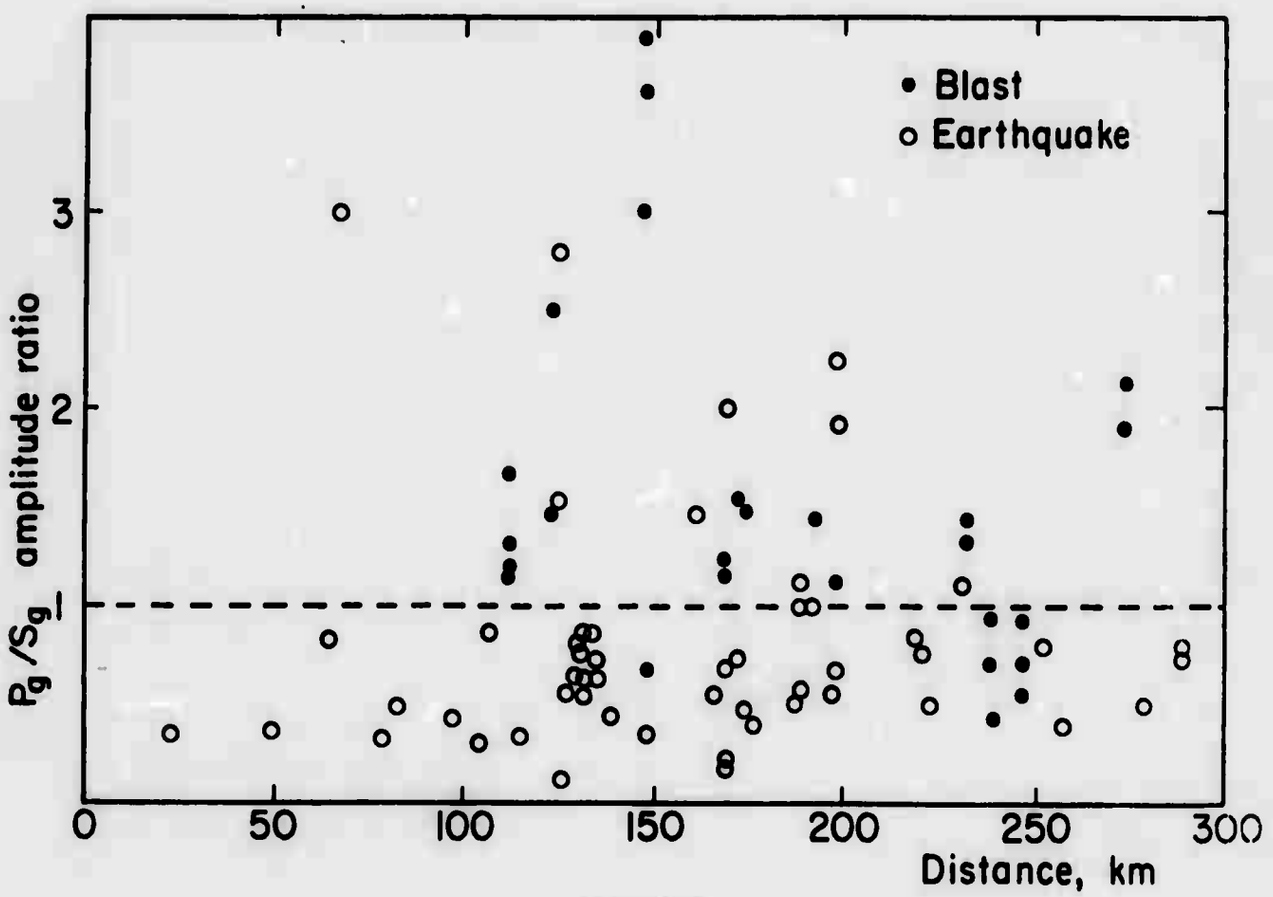

Figure 7.

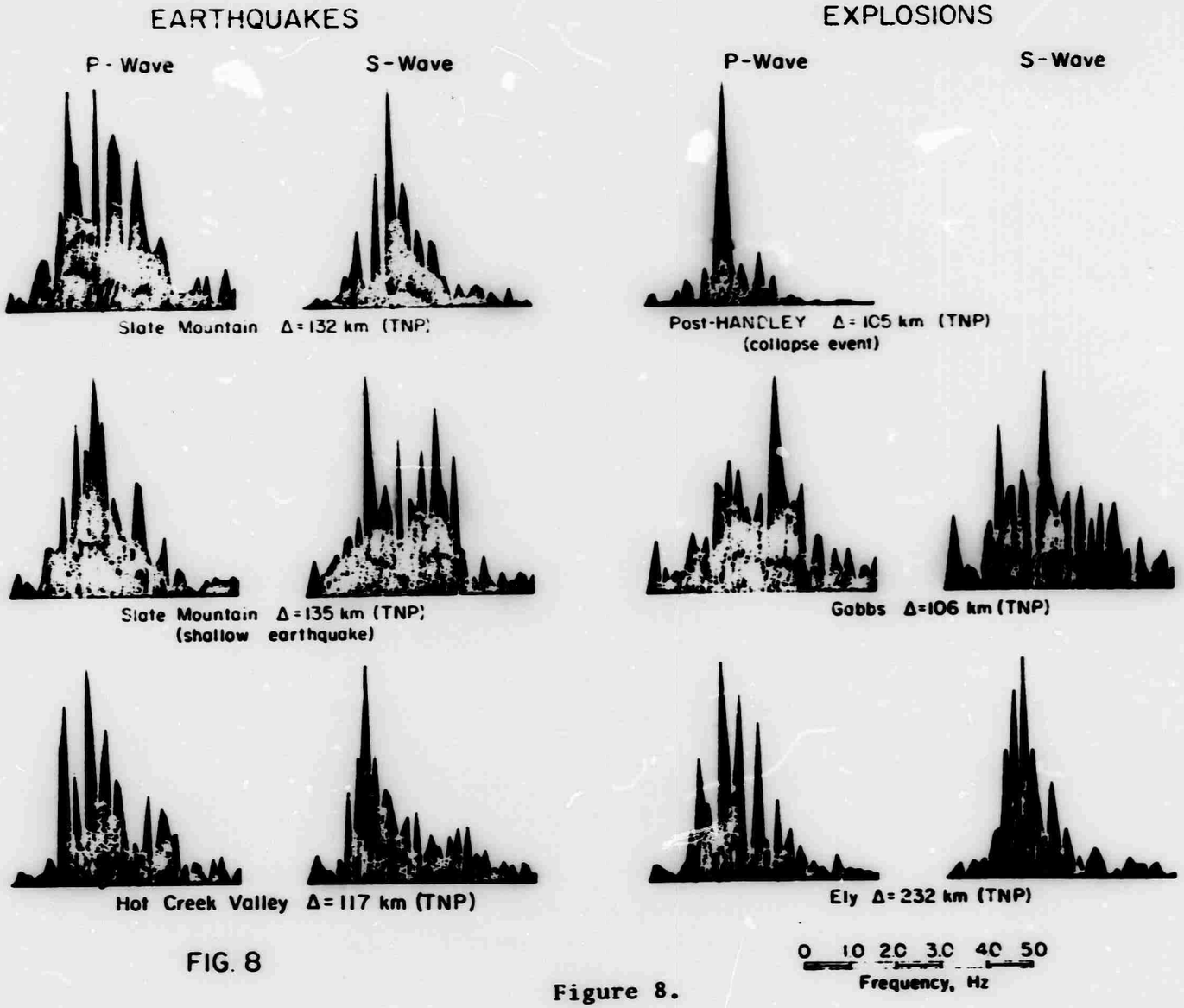

FIG. 8

Figure 8.

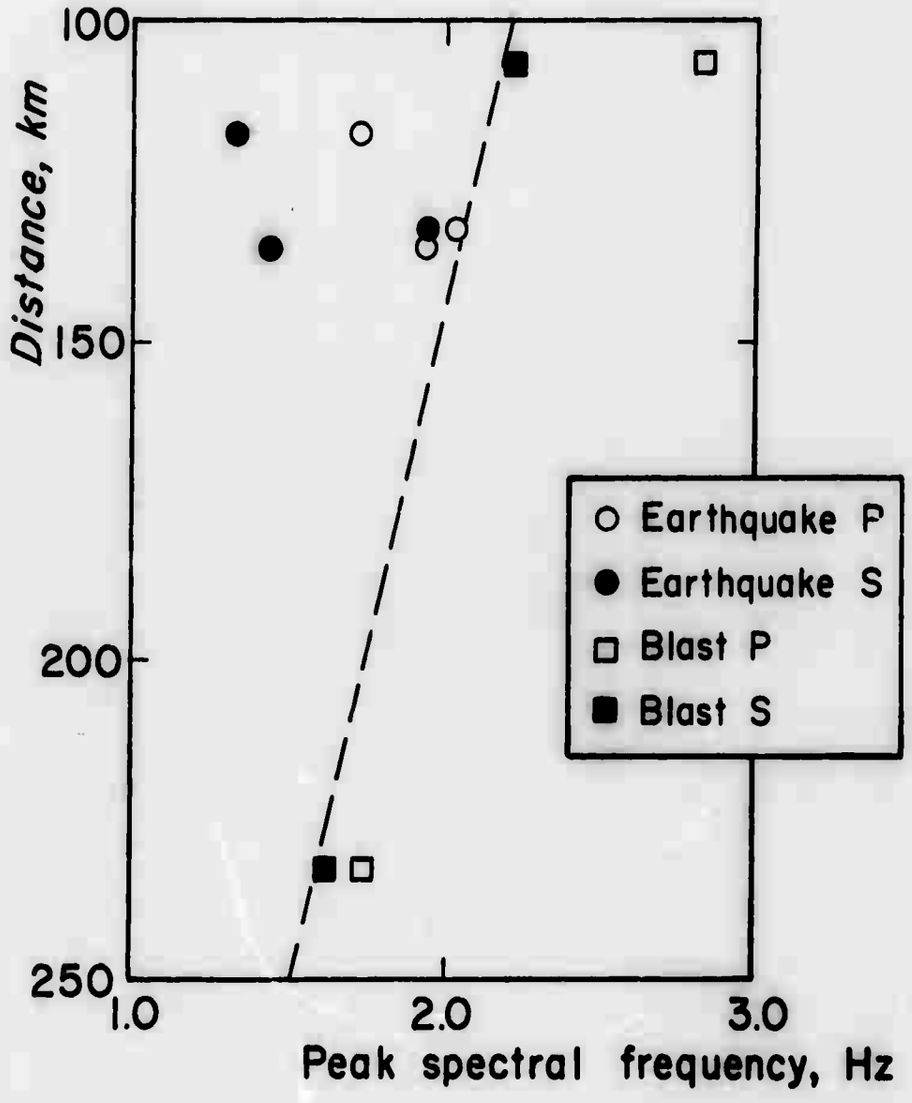
100
150
200
250
Distance, km
1.0
2.0
3.0
Peak spectral frequency, Hz
Earthquake P
Earthquake S
Blast P
Blast S

Figure 9.

SUMMARY OF ARPA SEISMIC DISCRIMINATION MEETING

20 - 23 July 1970 at Woods Hole, Massachusetts

INTRODUCTION

This Conference on Seismic Discrimination was intended to examine criteria for discriminating between the seismic signals arising from earthquakes and explosions, to review our understanding of the processes controlling seismic signatures, and to consider what further research may be required to expand and improve our discrimination capability.

The Conference demonstrated the close connection between the problem of discriminating earthquakes and explosions and the problem of the earthquake mechanism which is receiving much attention. It revealed that many diverse aspects of solid earth geophysics are involved in a complete understanding of the problem. For example, crustal and mantle structure, particularly lateral as well as vertical variations, tectonic release from explosions and earthquakes, and the theory of elastic wave propagation.

It was of interest to note the progress that has been made in the theory of the seismic source to take into account realistic earth models as well as source models. The effect of the initial time function, the source dimension, the symmetry and asymmetry of explosive and earthquake sources respectively, the focal depth and realistic earth structures are taken into account by the theory. It is possible to make synthetic seismograms which match experimental records. The theory for the first time explains the basis of several methods of distinguishing earthquakes from explosions. Thus in the M_S:m_b method it is believed that the source time function affects m_b for earthquakes in a manner different from explosions and the source dimension function results in a more efficient radiation of surface waves for earthquakes than for explosions. In a similar manner the effect of depth of focus, as well as source time and dimension, affect the spectra of surface waves and body waves from explosions and earthquakes. Although the question of why some earthquakes may be high stress-drop events is not fully resolved, the general consensus was that the theory of the seismic source as

it is now understood indicates that the separation of earthquake and explosion populations applies in principle to low-magnitude events. However, it will be necessary to first determine and ultimately allow for regional variations in stress-drop, attenuation, and surface wave propagation to utilize the method. The main problem will be to obtain sufficient signal energy at a sufficient number of stations at appropriate distances and azimuths from the source to apply the diagnostic criteria effectively.

The M_S:m_b Criterion

Data were presented on M_S:m_b values to indicate that the method for discrimination which applies at m_b 5 extends below m_b 4.5, whether discrimination is based on 10, 20, or 40 second Rayleigh waves. It should be noted, however, that there is some overlap of the earthquake and explosion populations, particularly at lower magnitudes, and that the body of M_S data for Rayleigh waves recorded at well distributed stations at teleseismic distances is quite limited. Both of these factors currently limit the effectiveness of M_S:m_b for discriminating between low magnitude earthquakes and explosions at teleseismic distances. Research into this problem continues, particularly with respect to the enhancement of the signal to noise ratio for Rayleigh waves. The long period research arrays recently completed in Norway and Alaska, and the research with very long period seismographs, specially installed at carefully selected, deeply buried, very quiet sites are designed to do this. The Ogdensburg very long period installation is an example of the latter approach to Rayleigh wave signal to noise enhancement and provides data for research in the longer period part of the seismic spectrum. The arrays, and the experimental very long period installations are expected to provide the body of surface wave data, at teleseismic distances, needed to determine the effectiveness of the M_S:m_b discriminant at magnitudes less than m_b=4.5.

Spectral Ratio Criteria

There was considerable discussion of discrimination based upon the amplitude spectra of Rayleigh waves with some attendees claiming that spectral shape itself could be used as a discriminant. Theoretical results make it clear that this is not the case, and that source

orientation has a drastic influence on the shape of the surface wave spectra. For example, a shallow focus dip slip fault will give a spectrum similar to that of an explosion. Clearly a much more sophisticated analysis of observed spectral data is required.

P, S, and Love Wave Criteria

Only limited new data on long period P, S, and Love waves were presented, but two important points did emerge: The ratio of Love to Rayleigh waves may be a useful but as yet undeveloped discriminant since even NTS explosions with their "high" amplitude Love waves do not have enough Love waves commensurate with their observed Rayleigh waves to be indicative of an earthquake mechanism. Also the P wave spectra (3 to 0.03 Hz) of MILROW and LONG SHOT were drastically different from the P wave spectra of Aleutian earthquakes of comparable m_b, the earthquakes having their corner frequency approximately one decade lower in frequency than explosions.

Source Term Theory

The factors of source dimension, source time, depth of focus, and azimuthal variation occur as a product in determining the spectrum of the seismic signal. Although there was some disagreement as to the relative contributions of the separate factors, the general belief was put forward that the product of all factors was essentially different for earthquakes and for explosions at the magnitudes for which data were available.

There was much discussion on tectonic energy release from explosions and earthquakes. There was a difference of opinion as to whether actual tectonic energy is released, or, whether the tectonic fabric in the vicinity of the explosion source was responsible for the generation of Love waves and the azimuthal variation of the surface wave radiation. Tectonic energy release was, in general, thought not to be a problem in the separation of earthquakes and explosions.

Little new work on short range discriminants was reported. An interesting presentation was given on the use of amplitude contours of time versus frequency plots (i.e., standard mode of presentation of hydroacoustic data) for discriminating earthquakes and explosions by use of data taken at ranges of 1,000 to 3,500 kilometers. The high frequency content of P signals and the low amplitude of shear waves of explosions was indicated. This technique should be applied to a larger suite of events to assess its utility.

Signal Enhancement Techniques

Multivariant analysis has lagged due to an inadequate data source. No new ideas on short period discriminants were presented. Only one significant new idea on depth determination was forthcoming: master events and the S-P arrival time differences at distances less than 15^{o} remains the best discriminant when working solely with the P signal. Data presented suggested that the shape of the Rayleigh wave amplitude spectrum may be useful for establishing depth of focus.

Work at several laboratories suggests that virtually all noise of period greater than 25 seconds is non-propagating and is induced by local atmospheric conditions. Its suppression depends on using either arrays of closely spaced long period seismometers(correlation distance of this noise is very short), or deep bore-hole seismometers (Ogdensburg has approximately 30 mμ noise level at 40 seconds), or on optimizing site selection(stable atmosphere). The design details of a long period seismometer which is deployable in deep boreholes were presented. A prototype instrument will soon be placed in the Ogdensburg mine for comparison with the Pomeroy-type installation.

Data on signal enhancement of long period signals by matched filters, band pass filters, and array processing were presented. New results on a seven-element ALPA array indicate gains of 16 db(12 - 20) against coherent 16 - 20 second noise when steering for Asian earthquakes($\sqrt{n}$=7 db). It was also pointed out that multipath problems can severely degrade usefulness of matched filters for some source-station pairs(Kurils to LASA).

Direction of Future Research

A major result of the meeting was a clear impression that much research has yet to be done to resolve the discrimination problem. Depth, source type, corner frequency, stress drop, etc., however, all appear to be determinable.

Future work should be concentrated on devising stations which provide signals at teleseismic distances so that the theoretically predicted separation of earthquake and explosion populations can be tested experimentally. Attention should be given to developing an understanding of those high stress-drop earthquakes which generate less surface wave energy than most earthquakes and thus may be mistaken for explosions. Do these earthquakes exhibit a special pattern in region of occurrence, focal depth, azimuthal variation of spectrum which will lead to their identification as earthquakes? Can the world be regionalized into a reasonable number of blocks each with its own source mechanism and propagation characteristics so that scatter can be reduced and the two populations can be separated further? These are some of the problems considered by the Conference as worthy of special effort.

It should be noted that occasional earthquakes larger than magnitude 4.75 do occur that fail to meet all present criteria for discrimination from explosions. The number of such events increases rapidly at lesser magnitudes. Such events evidently are not randomly distributed in space but possibly are a function of local geological or geophysical conditions. Research which might ultimately lead to understanding of such events is important to the VELA program.

The implementation on a routine basis of a new generation of azimuthal and spectral discriminants would require a major transformation in present data acquisition and analysis procedures.